Natural Balancing of Multicell Converters

Richardt Howard Wilkinson

Dissertation presented for the degree of Doctor of Philosophy in Engineering at the University of Stellenbosch

Supervisor: Prof. H. du T. Mouton

Co-supervisor: Dr T.A. Meynard

April 2004

Natural Balancing of Multicell Converters

Richardt Howard Wilkinson

Dissertation presented for the degree of Doctor of Philosophy in Engineering at the University of Stellenbosch

Supervisor: Prof. H. du T. Mouton

Co-supervisor: Dr T.A. Meynard

April 2004

Declaration

I, the undersigned, hereby declare that the work contained in this dissertation is my own original work, unless otherwise stated, and has not previously, in its entirety or in part, been submitted at any university for a degree.

R.H. Wilkinson
April 2004

Summary

Multilevel converters were developed as a result of a growing need for higher power converters. This dissertation addresses a specific multilevel topology called the multicell topology. A problem associated with this topology is cell capacitor voltage unbalance. This dissertation addresses the issue of natural balancing of multicell converters. The topology is mathematically analysed and a theory is developed to explain the natural balancing mechanism. The study of the natural balancing property includes a detailed harmonic-, steady-state- and time constant analysis. The theory is verified by a comparison between the theoretical-, simulated- and experimental results.

Opsomming

Veelvlakkige omsetters het ontstaan as gevolg van ’n behoefte aan hoër drywing omsetters. Hierdie proefskrif handel spesifiek oor die veelsellige omsetter topologie. ’n Probleem wat met hierdie topologie geassosieer word is selkapasitor onbalans. Hierdie proefskrif ondersoek die natuurlike balansering van veelsellige omsetters. Die topologie word wiskundig geanaliseer en ’n teorie word geformuleer om die natuurlike balanseringsmeganisme te verduidelik. Die ondersoek van die natuurlike balanseringseienskap bevat ’n volledige harmoniese-, bestendige toestand- en tydkonstante analise. Die teorie is gekontroleer deur teoretiese-, simulasie- en eksperimentele resultate te vergelyk.

Acknowledgements

> “To him who sits on the throne and to the Lamb
> be praise and honor and glory and power,
> for ever and ever!”
>
> Revelation 5:13(b) (NIV)

I would like to thank the following people:

My God, Father, Friend, Companion and Saviour: the only living and true God, Father, Son and Holy Spirit for His guidance, support, wisdom and inspiration.

My wife Lize-Marié, for all her love, prayer, understanding and support.

My family for all their prayer and support.

All my pastors, friends and colleagues who played a part in this dissertation.

My two supervisors, Prof. Toit Mouton and Dr Thierry Meynard, for their guidance and support.

The NRF and the CNRS for their financial support.

Contents

List of Figures

List of Tables

Glossary

$\mathbb{C}$	:	the set of complex numbers
C_{bb}	:	capacitance of balance booster tuned to center frequency of λ_1
C_f	:	output filter capacitor
C_i	:	i^{th} cell capacitor
DSP	:	Digital Signal Processor
ε	:	eigenvalue
FPGA	:	Field Programmable Gate Array
f_r	:	reference frequency (Hz)
f_s	:	switching frequency (Hz)
GTO	:	Gate Turn-Off Thyristor
IGBT	:	Insulated Gate Bipolar Transistor
IGCT	:	Integrated Gate Commutated Thyristor
Im	:	Imaginary part of a complex number
L	:	output filter inductor
L_{bb}	:	inductance of balance booster tuned to center frequency of λ_1
$\mathbb{P}$	:	the set of prime numbers
PWM	:	Pulse Width Modulation
Re	:	Real part of a complex number
R	:	load resistor
R_{bb}	:	resistor of balance booster tuned to center frequency of λ_1
s	:	Switching function
s_{d_i}	:	i^{th} difference switching function
s_t	:	total switching function
T_r	:	reference period
T_s	:	switching period
tr	:	trace of a matrix
τ	:	Time constant
V_{d_i}	:	i^{th} difference voltage
V_{C_i}	:	i^{th} cell capacitor voltage
V_t	:	input voltage
ω_r	:	angular reference frequency (rad/s)
ω_s	:	angular switching frequency (rad/s)
Z	:	load impedance
$\mathbb{Z}$	:	the set of integers
Z_{bb}	:	balance booster impedance
Z_{load}	:	load impedance

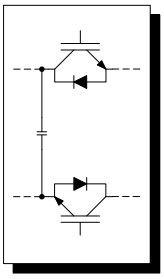

Chapter 1

Multilevel converter topologies and balance theories

1.1 Introduction

Multilevel converters were developed as a result of a growing need for higher power converters. In order to achieve this higher power rating, the voltage and current capabilities of the devices used in the converter need to be increased. Current IGBT technology extends up to $6.5\ kV\ 900\ A$ per switching device [67], while current IGCT technology extends to $6\ kV\ 3\ kA$ per switching device [65].

There are two approaches of addressing the growing need for higher power converters, which are as follows:

(a) By using high voltage switching devices like the latest IGBTs, it is possible to construct converters that can handle a very large dc-bus voltage. These high voltage devices typically have high conduction losses, resulting in relatively low switching frequencies. The large "voltage step" capability of these converters results in high dv/dts due to the full source voltage being switched at every switching instant.

(b) By using established technology, it is possible to construct high power converters with low cost low voltage switching devices using a multilevel topology. These lower voltage switches typically have lower conduction losses and can switch at higher frequencies [63]. Higher switching frequencies and a smaller "voltage step" capability results in these converters being able to produce higher quality switching waveforms.

During the last few years, a number of multilevel topologies were developed, each with its own inherent advantages and disadvantages. These topologies will be discussed briefly in the following section, highlighting the characteristics of each topology and including advantages and disadvantages associated with each one. Comparisons of multilevel topologies can be found in [33] and [43].

A number of these topologies are as follows:

- the plain series connected pseudo multilevel topology [42], [43], [44], [64].
- the neutral-point clamped multilevel topology, also known as the diode-clamped multilevel topology [46], [50].
- the cascaded multilevel topology [52], [54], [55].
- the series-stacked multilevel topology [62].
- the multicell topology, also known as the flying-capacitor multilevel topology [44], [63].

With these topologies came the problem of voltage balance of their clamping or cell capacitors.

This dissertation focuses specifically on the multicell converter topology and the presentation of a theory of the natural balance of these converters [58], [59].

1.2 Multilevel converter topologies

A number of multilevel topologies are briefly discussed in the following sub-sections. This section is not intended as a detailed comparison or analysis of the named topologies. It serves only as an introductory summary.

1.2.1 Plain series connection

The plain series connection of switching devices is the simplest approach to solving the problem of an input dc-bus voltage that is much higher than the blocking-voltage of a single device. This topology is a pseudo multilevel topology as the output voltage is only switched between two levels, although the bus voltage is shared between more devices. For this case, the required switching device is replaced with p switching devices connected in series, where the total of the blocking voltages of the series connected devices can sustain the required total blocking voltage [42], [43], [44]. This topology is shown in Figure 1-1.

An important aspect of this methodology is to ensure that these devices are as similar as possible to avoid device mismatch. It is a physical impossibility for the devices to be exactly the same, therefore the best approach is to ensure that the devices are of the same rating and manufacturing batch. Additional precautions also need to be taken to ensure device protection, e.g. snubbers connected across each device. The purpose of these snubbers is to clamp the voltage as well as the dv/dt across each device to a predetermined maximum voltage [44], [64].

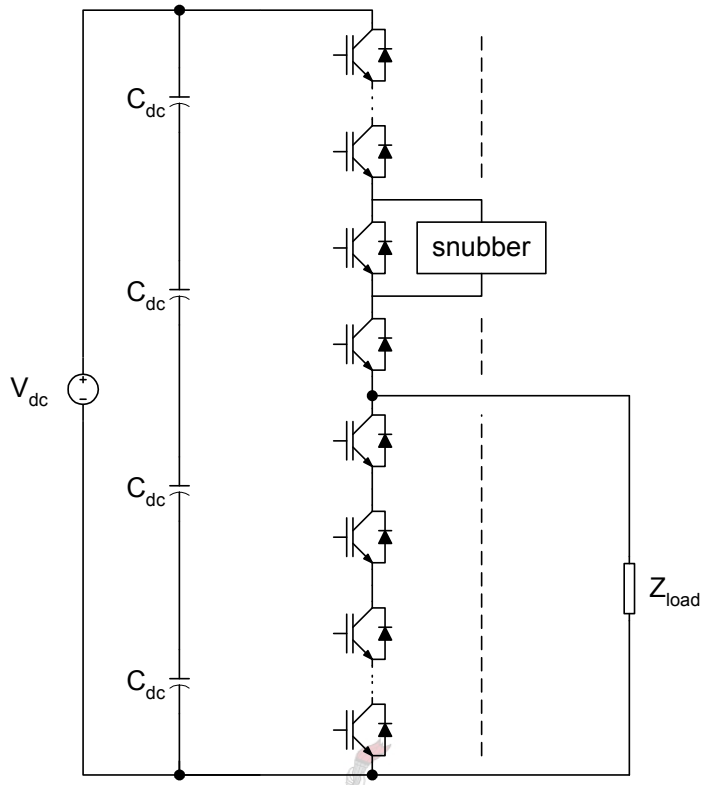

Figure 1-1. *The plain series connected pseudo multilevel topology.*

The advantage of using this topology is that the complexity of the converter is relatively low and the control is simple compared to other multilevel topologies.

A disadvantage associated with this topology include the following:

- high dv/dts due to the full source voltage being switched at every switching instant.

1.2.2 The neutral-point-clamped multilevel topology

The neutral-point-clamped multilevel topology is also sometimes called the diode-clamped multilevel topology. An example of a single phase-arm of this topology is shown in Figure 1-2. It is also possible to configure this topology for three-phase operation by adding another two phase-arms in parallel.

In this topology, all the switches share the same capacitor bus, but are clamped at different voltage levels through diodes. The clamping diodes cause low frequency current harmonics which cancel each other [44].

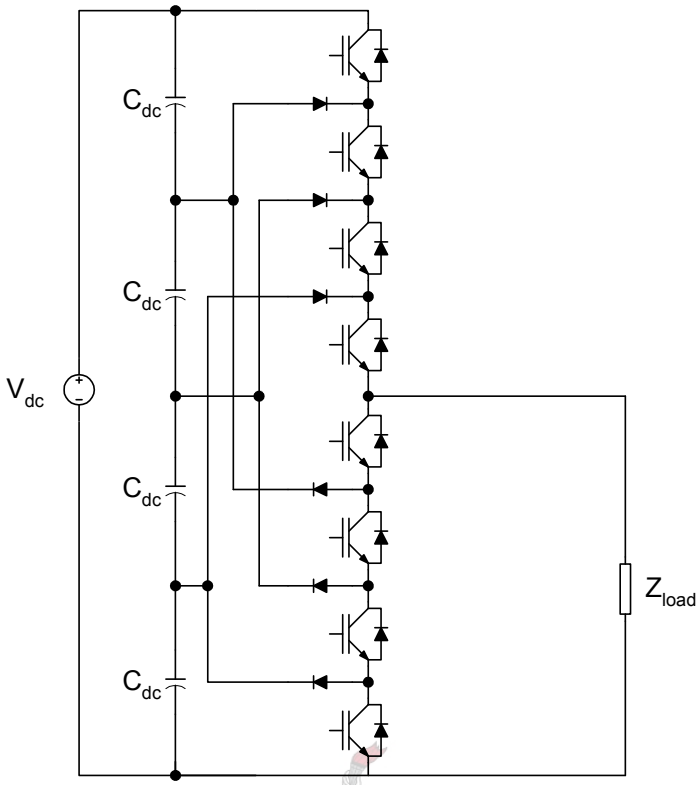

Figure 1-2. *The neutral-point-clamped multilevel topology.*

This topology also suffers from dc-link capacitor voltage unbalance as discussed in [46] and [50].

The natural balance of this topology is discussed in detail in [31].

1.2.3 The series-stacked multilevel topology

The series-stacked multilevel converter topology [32], [49], [62] is formed by connecting the individual dc-bus capacitors of a number of full-bridge converters in series. Each converter has its own output filter. The outputs are connected to matched primary windings of the output transformer. This transformer usually has a single secondary winding providing the output voltage across the load. This topology is shown in Figure 1-3.

This converter topology has excellent steady-state balancing characteristics. One disadvantage of this topology is the requirement of a specially designed transformer.

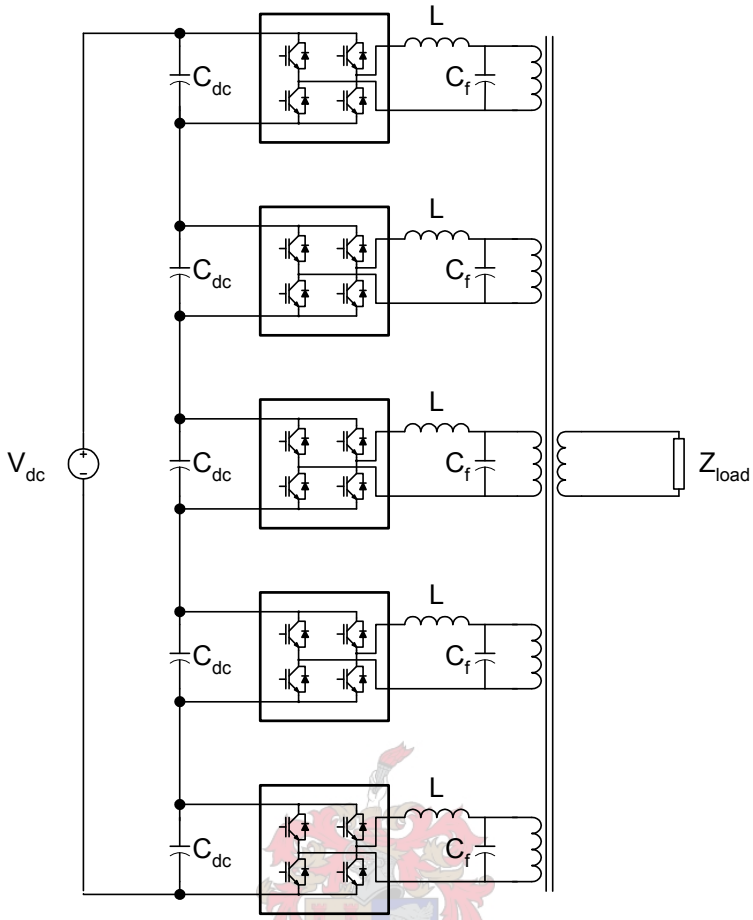

Figure 1-3. *The series-stacked multilevel topology.*

1.2.4 The cascaded multilevel topology

The cascaded multilevel topology [46], [52], [55] is constructed by cascading the outputs of a number of full bridge converters as shown in Figure 1-4.

Each full-bridge converter requires a separate dc capacitor bank. The dc-supply can be made up of batteries, fuel-cells, rectified dc from isolated transformers or even solar cells. When this topology is used purely for reactive compensation, a capacitor bank is sufficient for the dc-supply.

This topology is ideally suited to series voltage injection applications as the need for a series injection transformer is eliminated [54].

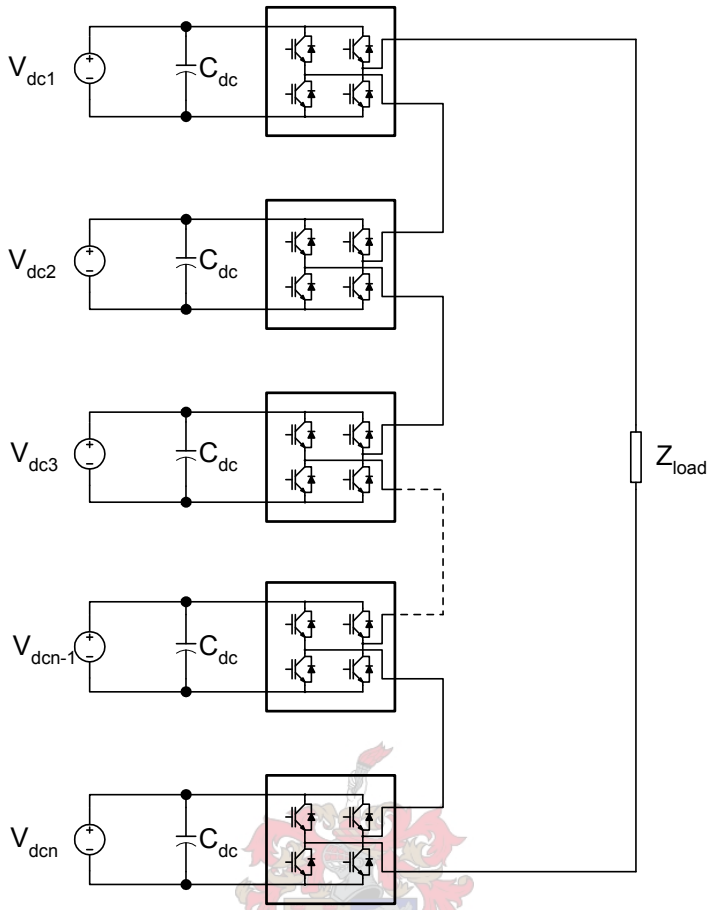

Figure 1-4. *The cascaded multilevel topology.*

1.2.5 The multicell topology

In the multicell topology, commutation cells with voltage ratings of V_{dc}/p are imbricated (overlapped) to form a chopper circuit or inverter leg capable of switching the voltage V_{dc}. A diagram showing an example of the multicell topology is shown in Figure 1-5, in this case a 4-cell topology.

The number of cells can be extended to p cells, depending on the blocking voltage needed. Control signals of the different cells can be interleaved to optimize the output voltage waveform [44]. The output voltage ripple has an amplitude of V_{dc}/p and a frequency that is p times the switching frequency that roughly reduces the output filter inductor by p^2 [44].

The above topology can be applied to choppers (buck-, boost-, buck-boost, $\check{C}$uk-, etc.), voltage-source inverters (half-bridge, full-bridge, three-phase, etc.), current-source inverters, cyclo-converters, etc. Examples of applications listed by Meynard [44] are as follows: a 1.5 kV, 3-cell 4-level sinusoidal rectifier; a 4 kV 300 A, 7-cell 8-level inverter leg switching at 3 kHz, i.e. an output voltage ripple frequency of 21 kHz; an Active Current Filter at 20 kV [44]. For more multicell applications see [20], [27], [28], [30] and [53]. A performance comparison between this topology and a conventional

half-bridge inverter is made in [47].

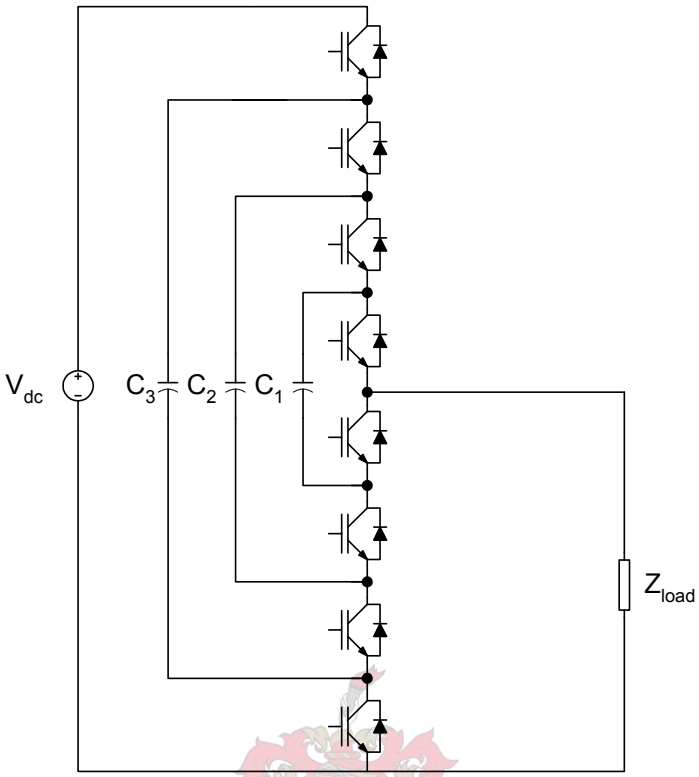

Figure 1-5. *The multicell topology.*

The voltage across a cell capacitor is given by the following equation [63]:

$$V_{C_i} = \frac{i \cdot V_{dc}}{p}, i = 1, \ldots, p-1 \tag{1.1}$$

1.3 The voltage balance problem

This dissertation addresses the issue of natural balance in multicell converters.

In the multicell and other multilevel converter topologies, methods are used to clamp the voltages across each switching element. Capacitors are used as pseudo voltage sources to divide a typically high input voltage into smaller voltage sources that result in lower voltages over the switching elements.

For each topology, a “balanced” capacitor voltage means that each specific capacitor stays at its assigned voltage in steady-state.

As an example, when a 4-cell multicell topology is used and the input voltage is 1000 V, then the first cell capacitor will have 75 % of the total input voltage across it, the next cell capacitor 50 % and the innermost cell capacitor 25 % of the input voltage. For these cell capacitor voltages to be balanced, they are required to stay at these values in steady-state. This topic will be discussed in more detail in Chapter 4 section 4.3.

1.4 Existing balance theories

This section mentions two existing cell capacitor voltage balance theories for the multicell topology. These theories were developed by Meynard et al [26] and Barbi et al [36]. Other theories also exist, but are mostly variants of these theories, i.e. [39] and [40]. The following two subsections briefly examines these theories. In the final section of this Chapter, a new balance theory is proposed for multicell converters.

1.4.1 Meynard et al's voltage balance model

The focus of this natural balancing model is the harmonic content of the cell capacitor currents. The cell capacitor currents are modelled as functions of the duty-cycle over the cells, also taking into account the relative phase-shifts of the switching functions of the cells. A mathematical account of this theory as presented in [26] is repeated in Appendix E for convenience.

An advantage of this theory is that it is valid for the transient behaviour of the cell capacitor voltages and can be used to calculate the time constants of the cell capacitors. The effect of the load impedance on the balancing properties of the converter as well as on the performance of the converter can also be seen in this model. This property lead to the concept of a balance booster circuit, which is discussed in Chapter 2 section 2.2.

This model is also dependent on the type of modulation used. It is also assumed that the load time constants are significantly smaller than each switching period leading to the understanding that the converter voltages and currents are in steady-state after each switching period [26], [62].

This model concluded the following:

- both a static and dynamic model of a multicell converter must take events within a switching period into account.
- a model based on average values cannot effectively represent the characteristics of a multicell converter.
- the harmonic content of the load current is used to calculate the dc current in the cell capacitor currents which is then used to construct equivalent circuits to derive state-equations representing

the converter.

- this model can be used to obtain both the steady-state as well as the dynamic responses of the cell capacitor voltages.

1.4.2 Barbi et al's balance theory

This theory is focussed on the self-balancing of the cell capacitor voltages in a multicell converter and was developed by Barbi et al in [36]. The method which was employed in this derivation, was to derive the spontaneously coupled cell capacitor current control loops inherent to the multicell topology. The self-balancing property is modelled as a built-in control loop.

As in other models, the instantaneous duty-cycles of the cells need to be equal to ensure the steady-state stability of the cell capacitor voltages. The control signals need to be phase-shifted by $\frac{2\pi}{p}$ to optimise the harmonic content of the output voltage waveform [38].

Sub-harmonic modulation, also known as interleaved switching, was used in this model to generate the switching functions. These switching functions were then expressed in their Fourier series form and used to derive an expression for the dc component of the cell capacitor current variation.

The resulting equation was used to derive the cell capacitor voltage transients, as the model includes the time constants of the cell capacitors.

The control diagram of this model is shown in Figure 1-6.

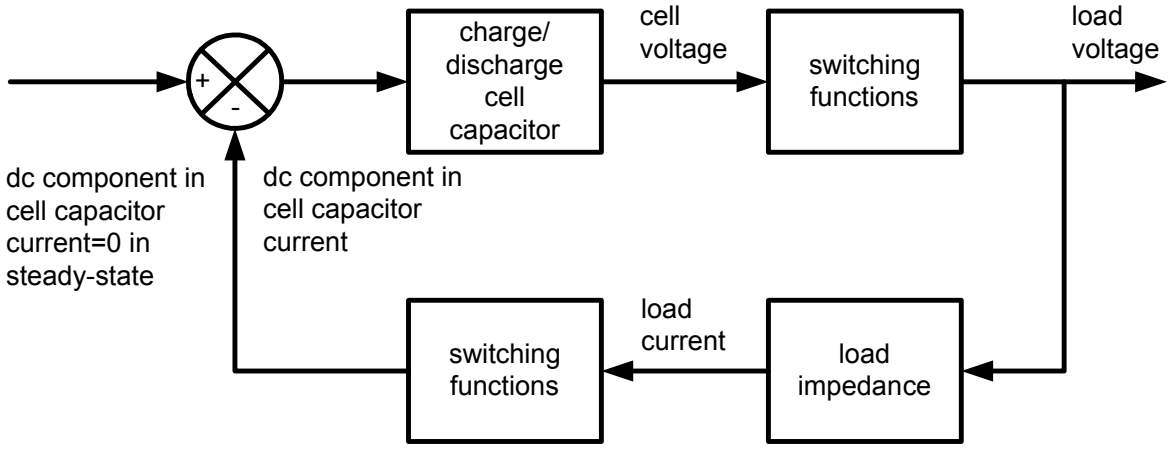

Figure 1-6. *Spontaneous cell capacitor current control loop.*

This model concluded the following:

- the cell capacitor voltages balance under sub-harmonic modulation when the load was not purely reactive.

- the time constant of the cell capacitor voltage transient increases with the capacitance of the cell capacitor, the output impedance amplitude and decreases with modulation index.
- natural balance was observed for the p-cell case under sub-harmonic modulation.
- unbalance was observed for small loads, reactive loads and low modulation indices.
- the need for balance boosters was also highlighted to increase the performance of the natural balance.

It is important to note that this model was only done for the case of sinusoidal modulation and not for fixed duty-cycle switching. This model is discussed in detail in [36].

1.5 New balance theory

The "Natural balance theory for multicell converters" presented in this dissertation, differs from the above theories in the following aspects:

- this theory is not dependent on the type of modulation used.
- it is valid for any type of load.
- it addresses the issue of a prime number of cells.
- this model is implemented in Matlab® as a "Designtool".

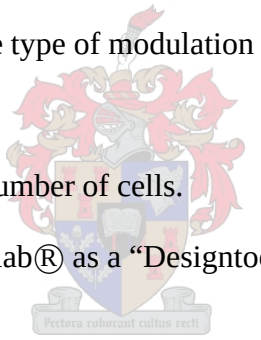

1.6 Summary of contributions

A diagram showing the scope of this dissertation is shown in Figure 1-7. The dissertation starts with a general overview of multilevel topologies and balance theories for the multicell topology. A detailed circuit analysis of the multicell topology starts the mathematical analysis of the dissertation. This circuit analysis is then used to derive equivalent circuits in both the time and frequency domains. The equations describing the relationship between the cell capacitor voltage unbalance and the input voltage result in the balance equations for the multicell topology and are used to prove that the cell capacitor voltages balance naturally. Differential equations are derived for the cell capacitor voltages, which are used to calculate the time constants of the cell capacitors. A Matlab® program was also written to calculate these values for a given multicell converter. The derived model is intuitive in nature and can be used to understand the balancing mechanism of this topology and the effect that the load impedance has on its performance. The use of a balance booster circuit to lower the load impedance at the switching frequency is also discussed. The developed theory is verified through comparing simulations with theoretical results as well as comparing theoretical results with experimental measurements. The dissertation is concluded with a summary of the final conclusions.

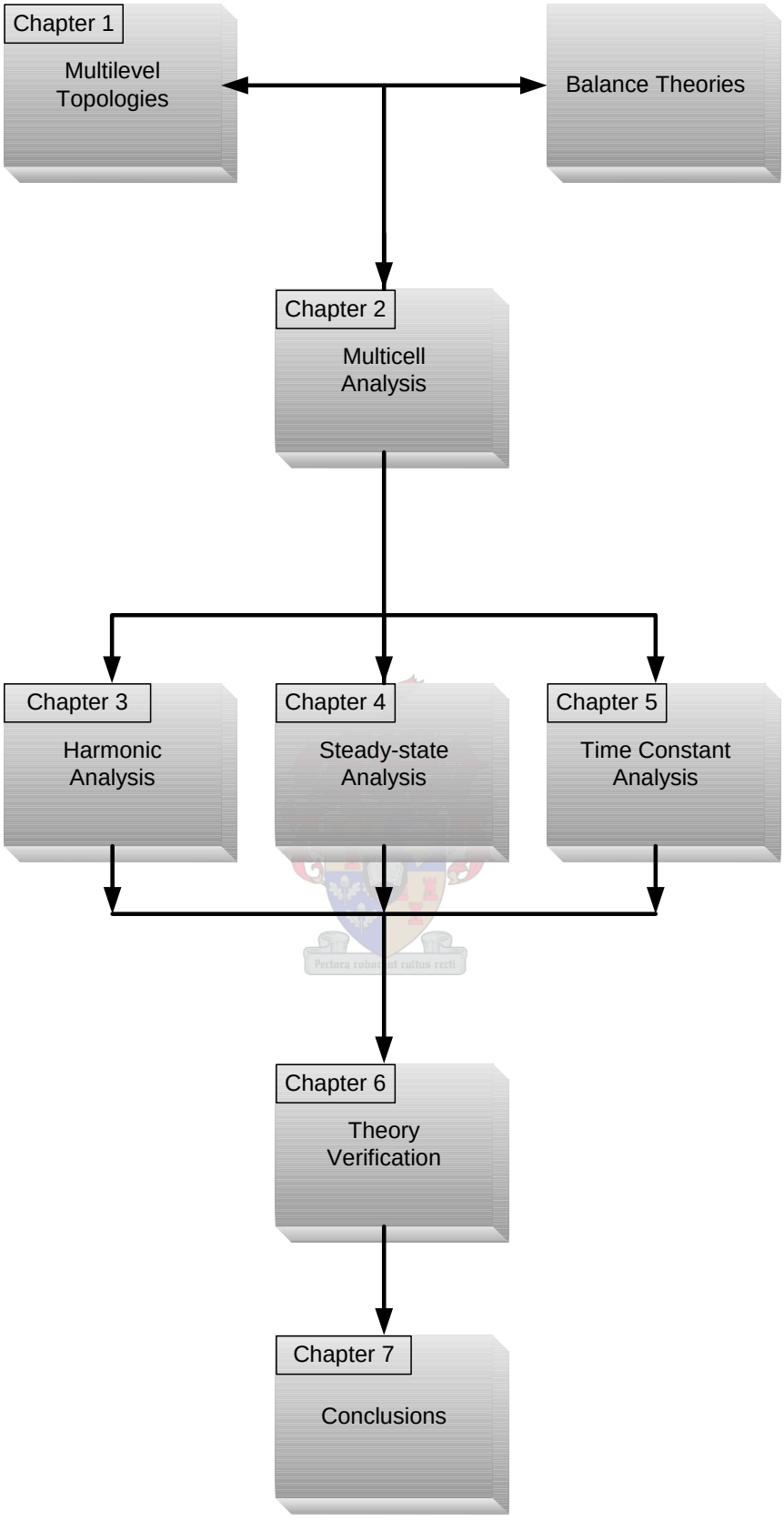

Figure 1-7. *Dissertation layout.*

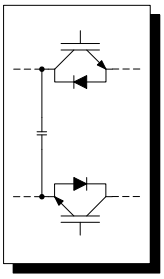

Chapter 2

Analysis of the multicell topology

2.1 Introduction

The focus of this chapter is a time-domain circuit analysis of the multicell topology. This analysis starts with that of a 2-cell topology and then works towards a model for a p-cell topology. The models obtained are then rewritten using 2-port circuits to obtain the final equivalent circuits. These equivalent circuits serve as the foundation to the following chapters, as these models are applied or transformed to fit the relevant analysis of that section.

2.2 Background on the multicell topology

The multicell converter topology is also called the "flying-capacitor multilevel topology", "nested cells multilevel topology" or the "imbricated cells multilevel topology". The last name is derived from the French "convertisseurs à cellules imbriquées" which can be translated literally as "converters with overlapping cells" [64].

The basic operation and characteristics of the multicell topology is briefly discussed in this section. For more information on other characteristics of this topology see [34] and [48].

This topology is formed by connecting a number of semiconductor switches in series and connecting the top- and bottom interconnections with floating capacitors. The multicell topology and circuit layout is shown in Figure 2-1.

As can be seen in Figure 2-1, the floating capacitors act as dc voltage sources that need to be charged to the appropriate voltage for the switching devices not to be destroyed. At this stage it is necessary to define a generic cell in the multicell topology. For this topology, a generic cell is made up of a half-bridge configuration with a capacitor across its input bus and the interconnect between the two switching elements broken. This broken interconnect then serves as the connection point to the next

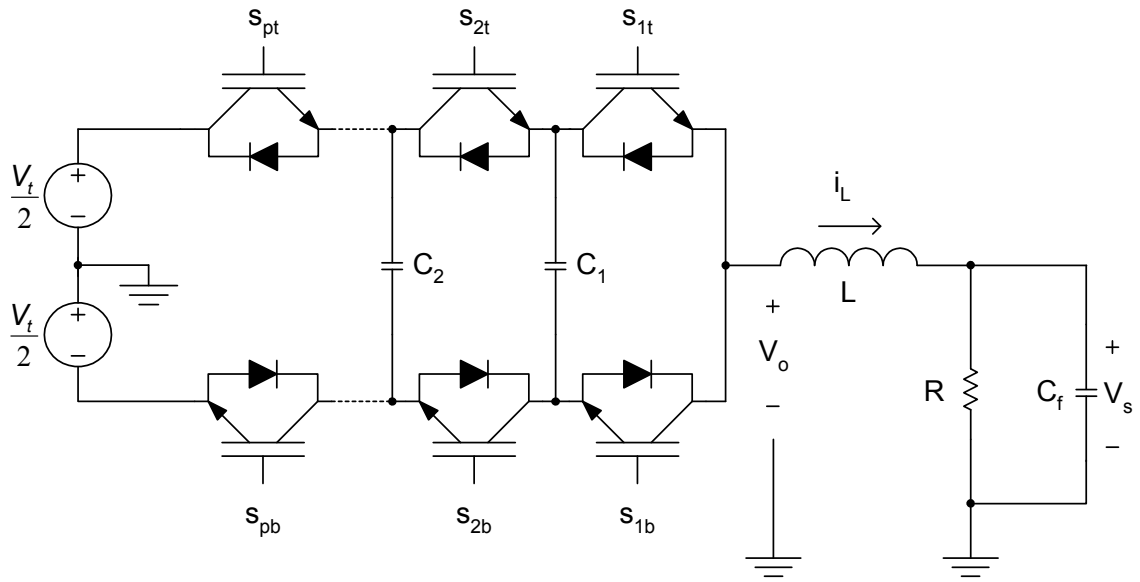

Figure 2-1. *A p-cell multicell inverter.*

cell. A generic cell is shown in Figure 2-2.

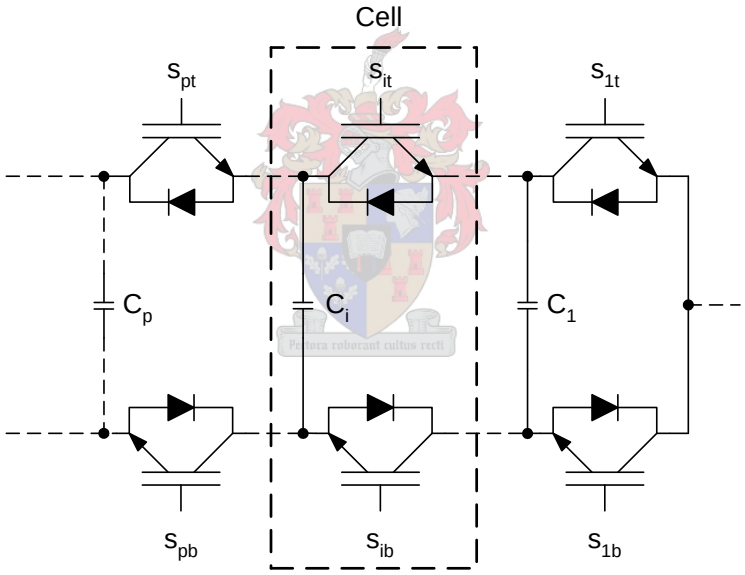

Figure 2-2. *The generic cell structure used in the multicell topology.*

A generic cell can be seen as a standard commutation cell which is obtained when $p = 1$ [26], [42]. It is made up of a top and bottom switching device which should always be in opposite switching states, i.e. when the top switch is conducting, the bottom switch must be blocking. This also implies that the top and bottom devices should never be blocking at the same time, as this can open-circuit an output inductor (current source) when connected. Dead time should also be incorporated in the switching of the devices to compensate for turn-off delays. The switching elements can typically be IGBTs, MOSFETs or GTOs.

An attempt was also made during the course of this study to develop a generic "Powercell" to facilitate a modular approach to the building of multicell converters. This is discussed in [57] and the schematics of the "Powercell" is included in Appendix C.

The ideal voltage across a cell capacitor under balanced conditions is determined by the input voltage V_t and the number of cells p and can be expressed in mathematical terms as follows [26], [42], [63]:

$$V_{C_i} = \frac{i \cdot V_t}{p} \text{ for } i = 1, \ldots, p \tag{2.1}$$

For the case of $i = p$, the cell capacitor is usually replaced with the dc-bus capacitor. When the cell capacitor voltages assume these values, the voltage-drop across each switching element will be equal to $\frac{V_t}{p}$ [26], [42].

The cell capacitors are denoted C_1 through C_{p-1} for the case of p cells. The reason for this is that the p^{th} cell does not have a cell capacitor because it is connected directly to the dc-bus capacitors. As a cell consists of 2 switching devices and a cell capacitor, the top switching device of the i^{th} cell is denoted as S_{it} and the bottom switching device as S_{ib}.

The behaviour of a multicell converter depends strongly on the phase-shift between successive control signals and the duty-cycles of the control signals. It has been shown that when the phase-shift between successive control signals is equal to $\frac{2\pi}{p}$, that cancelling of the harmonics centred at multiples of f_s is allowed up to and including $(p-1)f_s$ [26]. System stability was found to be dependent on whether the control signals had the same duty-cycle and the same phase-shift ($\frac{2\pi}{p}$) relative to each other [26], [42]. The phase-shift between successive control signals are defined as follows:

$$\phi = \frac{2\pi}{p} \tag{2.2}$$

Each control signal's phase-shift can then be defined as follows:

$$\phi_i = (i-1)\phi \text{ for } i = 1, \ldots, p \tag{2.3}$$

The multicell topology has the advantage of redundant voltage levels [43]. As an example, when an output voltage of $\frac{V_t}{4}$ is required for a 4-cell converter with $V_t = 100$, it means that there are four possible switch combinations that will result in the required output voltage. This redundancy can also be utilised to control the individual voltages across the respective cell capacitors. This property has been used in current control strategies in [24]. For other control aspects of this topology see [41], [51] and [56].

A detailed discussion on the design methodology for the cell capacitor and the output filter was developed by Meynard and was published in [35] and [45].

Another important aspect of the multicell topology is the concept of a balance booster. The balance booster was introduced by Carrere [60] and Meynard [26]. It is a notch filter which is connected in parallel with the load. The purpose of this filter is to provide a low impedance at multiples of the switching frequency. A typical implementation is in the form of a series R-L-C circuit. An example of a balance booster circuit is shown in Figure 2-3.

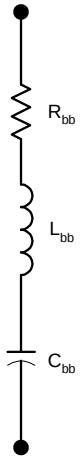

Figure 2-3. *The balance booster.*

The reason for the name balance booster, follows from the effect that this circuit has on the cell capacitor voltage balance. If this circuit is designed to have a low impedance at the switching frequency, it means that the load impedance $Z(\omega)$ is then smaller at the switching frequency due to the parallel combination of the load impedance and the balance booster circuit impedance. The connection of the balance booster in parallel with the load is shown for the 2-cell case in Figure 2-4.

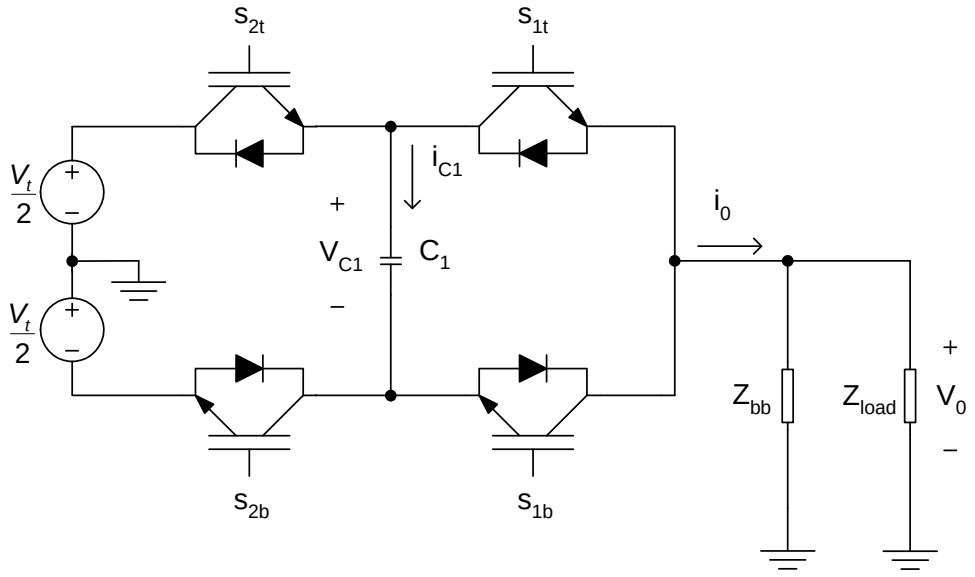

Figure 2-4. *A 2-cell multicell inverter with balance booster in parallel with the load.*

A summary of the notation used in this chapter is listed in Table 2.1. The input dc voltage V_t is shown

Table 2.1. *Summary of multicell circuit notation*

DC-bus voltage	V_t
Unfiltered output voltage	v_o
Filtered output voltage	v_s
i^{th} Cell capacitor current	$i_{C_i}, i = 1, \ldots, p-1$
Filter inductor current	i_L
i^{th} Top switching device	S_{it}
i^{th} Bottom switching device	S_{ib}
i^{th} Cell capacitor	$C_i, i = 1, \ldots, p-1$
Filter inductor	L
Filter capacitor	C_f
Load resistor	R

as a split-supply consisting of 2 series dc sources of $\frac{V_t}{2}$ each, with the centre-point grounded. The models obtained in this chapter are also valid for the case where the centre-point is not grounded, but where the grounding point is moved to the emitter of IGBT S_{pb}. The models need to be adjusted by the change in dc-offset in order for them to be valid for this case.

2.3 Mathematical model

The mathematical model used to represent 2-cell, 3-cell and p-cell multicell converters is derived in this chapter. There are three different mathematical models available to represent a multicell converter. These models are as follows [61], [63]:

- **Direct or instantaneous model:** this model accurately represents the state of each cell during a switching period. All the harmonic phenomena will be present in this model. This model should always be used for the validation of the synthesized control laws when starting from a model with the average values.

- **Average model:** this model is obtained by replacing each switching element with its average value over a switching period T_s. This is a continuous model and can be used to synthesise non-linear control laws to control a multicell converter.

- **Harmonic model:** this model will not be discussed here. This model can be used to obtain a dynamic representation of a multicell converter by taking its harmonic phenomena into account. A detailed discussion of this model can be found in [26].

2.4 Dynamic modelling of a multicell converter

A model of a multicell converter can be obtained by using classical state-space methods. The circuit that will be used as the basis for the following discussion is shown in Figure 2-5. This circuit is a 2-cell multicell converter with a load composed of an inductor, capacitor and resistor. The purpose of this derivation is to obtain an instantaneous model of a multicell converter in order to control the output of the converter as well as ensuring equal cell capacitor voltages.

The following assumptions were taken into account for the instantaneous model [63]:

- Ideal switches were used; implying that the on-state voltage, off-state current, dead-times, delays and switching times were zero [64].
- All passive components are ideal and linear, implying that the equivalent series resistance of capacitors and inductors are not taken into account. It was however found during the experimental verification, that the series resistance of the output filter inductor influenced the balancing times significantly.
- All cell capacitor values are assumed to be equal and of value C unless otherwise stated.
- The dc-bus is assumed to be infinitely stiff and connected to a voltage source V_t. This source is modelled as a split source with a ground connection between the two equal sources of $\frac{V_t}{2}$. The dc-bus capacitor was not included in the circuit analysis of the multicell topology.
- The load is modelled as a pure resistance R, but is later generalised to an impedance Z.

In order to obtain a mathematical model of the multicell topology, it is necessary to start with a basic circuit analysis using the assumptions listed above. Once the circuit differential equations are derived, d and t parameters [62] are introduced in the form of 2-port switching circuits. Two-port switching circuits are discussed in section 2.6.

The d parameter refers to a "difference" contribution, meaning that if a function is defined as f_d, it means that f_d is the difference of two other functions, say f_1 and f_2. This will specifically be used to define a voltage relating to the voltage unbalance in a cell capacitor.

The t parameter refers to a "total" contribution, meaning that if a function is defined as f_t, it means that f_t is the sum of the other functions, say f_1 and f_2.

After defining the above parameters, the differential equations are written for the circuit to be analysed. These differential equations are then rewritten in terms of d and t parameters. An equivalent circuit is then obtained which is then used to quantify the unbalance in the cell capacitors.

The above method was developed in [62]. It was used successfully to model and analyse the natural voltage balance of the dc-bus capacitors of the series-stacked converter topology in [62] and also for a three-level neutral-point-clamped PWM inverter in [31].

2.5 Circuit analysis of a 2-cell multicell converter

The circuit analysis of the multicell topology was started with an analysis of a 2-cell inverter. A circuit diagram used for the analysis of this inverter is shown in Figure 2-5.

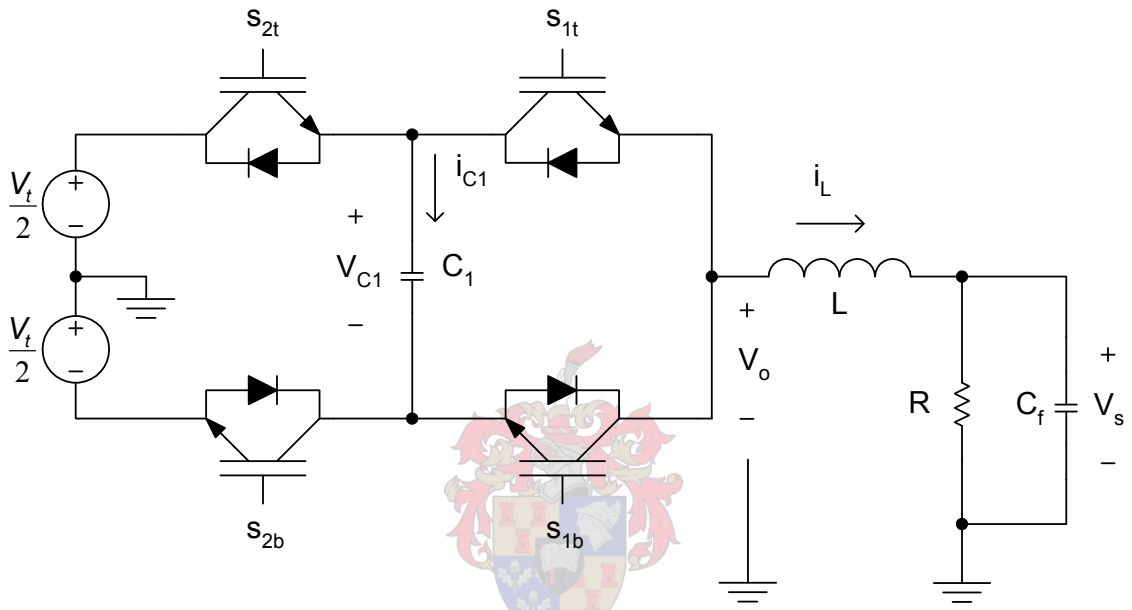

Figure 2-5. *A 2-cell multicell inverter.*

To analyse the circuit shown in Figure 2-5, the switching functions of the 2 cells are chosen as $s_1(t)$ and $s_2(t)$ and are defined as follows:

$$s_1(t) = \begin{cases} 1 & \text{if } S_{1t} \text{ is closed} \\ -1 & \text{if } S_{1b} \text{ is closed} \end{cases} \tag{2.4}$$

$$s_2(t) = \begin{cases} 1 & \text{if } S_{2t} \text{ is closed} \\ -1 & \text{if } S_{2b} \text{ is closed} \end{cases} \tag{2.5}$$

It is easy to see that the unfiltered output voltage v_o is given by the following:

$$v_o = \frac{V_t}{2} \cdot s_2(t) + \frac{1}{2} V_{C_1} \cdot \{s_1(t) - s_2(t)\} \tag{2.6}$$

Note that the cell capacitor current $i_{C_1}(t)$ is given by:

$$i_{C_1}(t) = \frac{1}{2} \cdot \{s_2(t) - s_1(t)\} \cdot i_L(t) \tag{2.7}$$

The differential equations describing the system are:

$$\frac{dV_{C_1}}{dt} = \frac{1}{2C_1} \cdot \{s_2(t) - s_1(t)\} \cdot i_L(t) \tag{2.8}$$

$$\begin{aligned} \frac{di_L}{dt} &= \frac{1}{L} \cdot (v_o(t) - v_s(t)) \\ &= \frac{1}{L} \left\{ \frac{V_t}{2} \cdot s_2(t) + \frac{1}{2} V_{C_1} \cdot \{s_1(t) - s_2(t)\} - v_s(t) \right\} \end{aligned} \tag{2.9}$$

$$\frac{dv_s}{dt} = \frac{1}{C_f} \cdot \left(i_L(t) - \frac{v_s}{R} \right) \tag{2.10}$$

The above equations can be written in matrix form as follows:

$$\begin{bmatrix} \frac{dV_{C_1}}{dt} \\ \frac{di_L}{dt} \\ \frac{dv_s}{dt} \end{bmatrix} = \begin{bmatrix} 0 & \frac{1}{C_1} \cdot \{s_2(t) - s_1(t)\} & 0 \\ \frac{1}{2L} \cdot \{s_1(t) - s_2(t)\} & 0 & -\frac{1}{L} \\ 0 & \frac{1}{C_f} & -\frac{1}{C_f R} \end{bmatrix} \begin{bmatrix} V_{C_1} \\ i_L \\ v_s \end{bmatrix} + \begin{bmatrix} 0 \\ \frac{1}{2L} \cdot s_2(t) \\ 0 \end{bmatrix} V_t \tag{2.11}$$

2.6 Two-port switching circuits

The concept of a two-port switching circuit [62] will be applied throughout the mathematical analysis of the 2-cell, 3-cell and p-cell multicell converter topologies.

The basic 2-port switching circuit is shown in Figure 2-6. This switching circuit is controlled by a switching function $s(t)$. The arrow is pointed from port 1 to port 2. The relationship between the voltages $v_1(t)$ and $v_2(t)$ and the currents $i_1(t)$ and $i_2(t)$ are as follows:

$$v_2(t) = s(t)v_1(t) \tag{2.12}$$

$$i_1(t) = s(t)i_2(t) \tag{2.13}$$

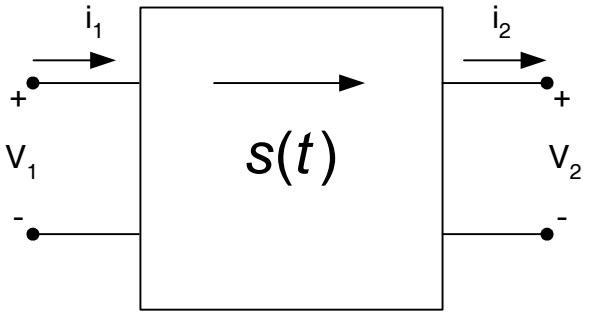

Figure 2-6. *Basic 2-port switching circuit.*

The switching function $s(t)$ can assume any real value.

In the case of a multicell converter, s is the switching state of a cell and assumes the values -1 and 1, depending on the state of a cell.

The switching states could also have been chosen to be 0 and 1 for the respective "off" and "on" states. For this case, the choice of -1 and 1 worked better in obtaining a generic model.

2.7 Deriving an equivalent circuit of a 2-cell multicell converter in terms of *d* and *t* parameters

In order to study the unbalance of a 2-cell multicell converter, it is necessary to define the difference between the required voltage of the cell capacitor and the actual voltage across the cell capacitor. If this voltage difference is defined by V_d, then it follows that:

$$V_d = \frac{V_t}{2} - V_{C_1} \tag{2.14}$$

In the same way, it is possible to define a "difference" switching function, $s_d(t)$ as the scaled difference between the switching function of cell 2 and that of cell 1. The scaling factor depends on the configuration of the source. In this case, a split-source with grounded centre-point is used. This "difference" switching function can be defined as follows:

$$s_d(t) = \frac{1}{2}\{s_2(t) - s_1(t)\} \tag{2.15}$$

Lastly, it is also possible to define a "total" switching function as the scaled sum of all the switching functions. This "total" switching function, $s_t(t)$ can be defined as follows:

$$s_t(t) = \frac{1}{2}\{s_1(t) + s_2(t)\} \tag{2.16}$$

After defining the above equations, they can be used to rewrite $s_1(t)$, $s_2(t)$ and V_{C_1} in terms of $s_d(t)$, $s_t(t)$, V_d and V_t as follows:

$$V_{C_1} = \frac{V_t}{2} - V_d \tag{2.17}$$

$$s_1(t) = s_t(t) - s_d(t) \tag{2.18}$$

$$s_2(t) = s_d(t) + s_t(t) \tag{2.19}$$

The above equations can then be used to rewrite the circuit differential equations in terms of d and t parameters as follows:

$$\frac{dV_d}{dt} = -\frac{1}{C_1} \cdot s_d(t) \cdot i_L(t) \tag{2.20}$$

$$\frac{di_L}{dt} = \frac{1}{L} \cdot \left\{ \frac{V_t}{2} \cdot s_t(t) + V_d \cdot s_d(t) - v_s \right\} \tag{2.21}$$

$$\frac{dv_s}{dt} = \frac{1}{C_f} \cdot \left(i_L(t) - \frac{v_s}{R} \right) \tag{2.22}$$

It is now possible to derive an equivalent circuit in terms of d and t parameters using the differential equations (2.20)-(2.22). This circuit is shown in Figure 2-7.

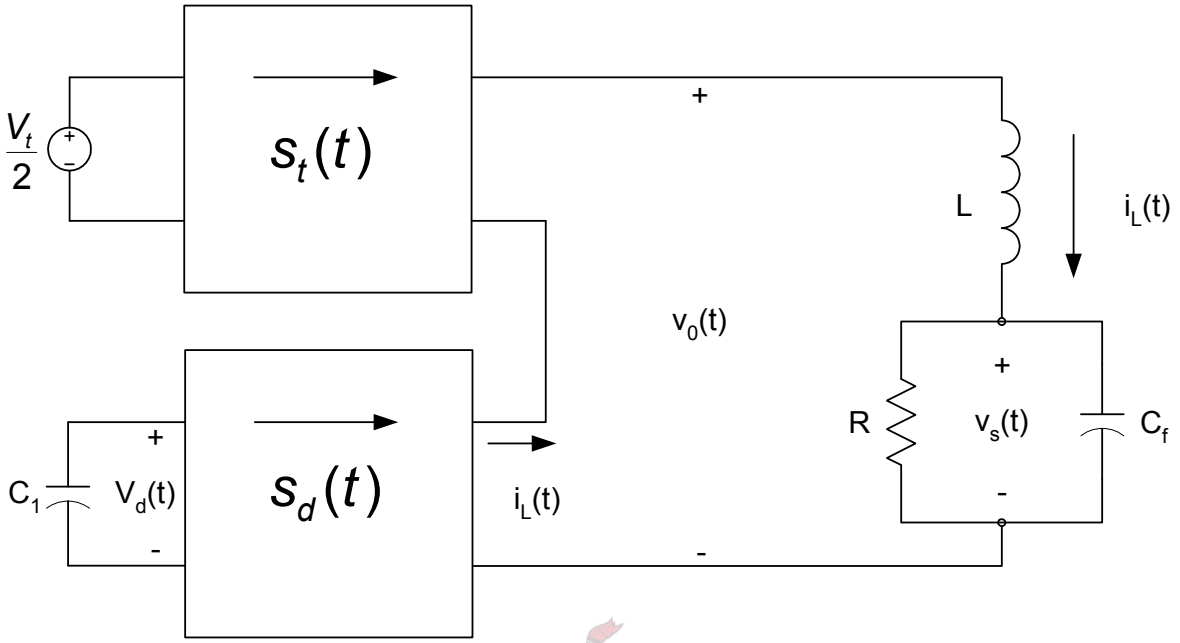

Figure 2-7. *Equivalent circuit in terms of d and t parameters of 2-cell multicell converter.*

2.8 Circuit analysis of a 3-cell multicell converter

The circuit diagram used for the analysis of the 3-cell inverter is shown in Figure 2-8. The same notation was used as summarised in Table 2.1. The same analysis procedure was used as for the 2-cell case discussed in section 2.5, except that it was extended to 3 cells.

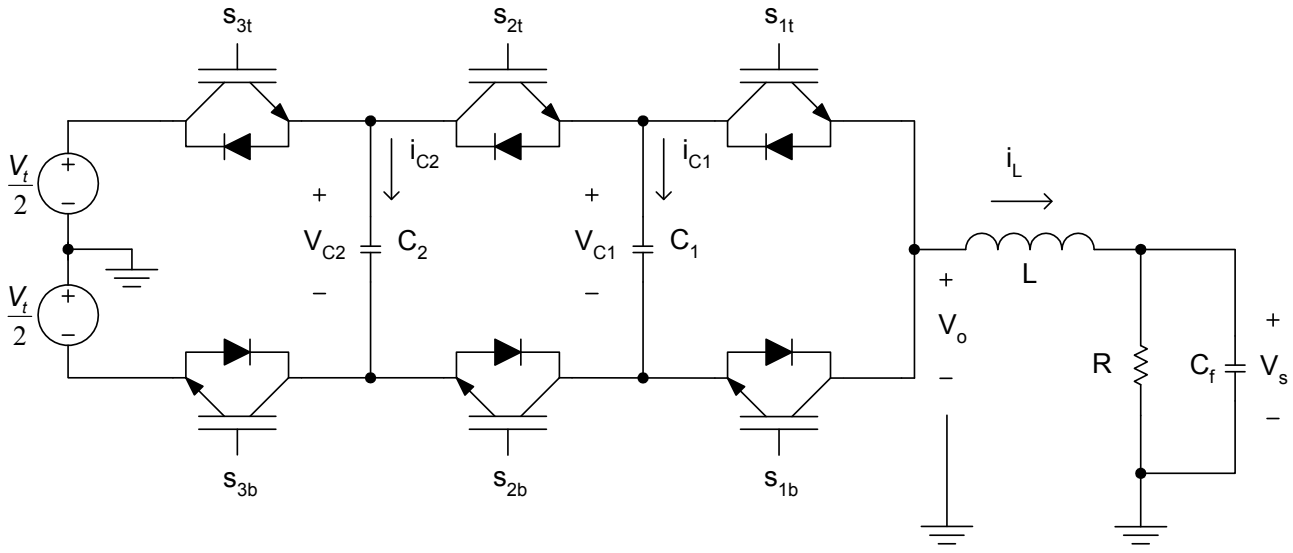

Figure 2-8. *A 3-cell multicell inverter.*

In order to analyse the circuit shown in Figure 2-8 the switching functions $s_1(t)$, $s_2(t)$ and $s_3(t)$ are defined as follows:

$$s_1(t) = \begin{cases} 1 & \text{if } S_{1t} \text{ is closed} \\ -1 & \text{if } S_{1b} \text{ is closed} \end{cases} \tag{2.23}$$

$$s_2(t) = \begin{cases} 1 & \text{if } S_{2t} \text{ is closed} \\ -1 & \text{if } S_{2b} \text{ is closed} \end{cases} \tag{2.24}$$

$$s_3(t) = \begin{cases} 1 & \text{if } S_{3t} \text{ is closed} \\ -1 & \text{if } S_{3b} \text{ is closed} \end{cases} \tag{2.25}$$

It is easy to see that the output voltage $v_o(t)$ is given by the following:

$$v_o = \frac{V_t}{2} \cdot s_3(t) + \frac{1}{2} V_{C_2} \cdot \{s_2(t) - s_3(t)\} + \frac{1}{2} V_{C_1} \cdot \{s_1(t) - s_2(t)\} \tag{2.26}$$

The cell capacitor currents $i_{C_1}(t)$ and $i_{C_2}(t)$ are given by the following:

$$i_{C_1}(t) = \frac{1}{2} \cdot \{s_2(t) - s_1(t)\} \cdot i_L(t) \tag{2.27}$$

$$i_{C_2}(t) = \frac{1}{2} \cdot \{s_3(t) - s_2(t)\} \cdot i_L(t) \tag{2.28}$$

Using equations (2.26)-(2.28), the differential equations describing the system can be calculated as the following:

$$\frac{dV_{C_1}}{dt} = \frac{1}{2C_1} \cdot \{s_2(t) - s_1(t)\} \cdot i_L(t) \tag{2.29}$$

$$\frac{dV_{C_2}}{dt} = \frac{1}{2C_2} \cdot \{s_3(t) - s_2(t)\} \cdot i_L(t) \tag{2.30}$$

$$\begin{aligned} \frac{di_L}{dt} &= \frac{1}{L} \cdot \{v_o - v_s\} \\ &= \frac{1}{L} \cdot \left\{ \frac{V_t}{2} \cdot s_3(t) + \frac{1}{2} V_{C_2} \cdot \{s_2(t) - s_3(t)\} + \frac{1}{2} V_{C_1} \cdot \{s_1(t) - s_2(t)\} - v_s \right\} \end{aligned} \tag{2.31}$$

$$\frac{dv_s}{dt} = \frac{1}{C_f} \cdot \left(i_L(t) - \frac{v_s}{R} \right) \tag{2.32}$$

The above equations will be rewritten in terms of d and t parameters in the next section.

2.9 Deriving an equivalent circuit of a 3-cell multicell converter in terms of *d* and *t* parameters

The study of the balancing properties of the 3-cell circuit can be simplified by defining the following variables:

$$V_{d_1} = \frac{V_t}{3} - V_{C_1} \tag{2.33}$$

$$V_{d_2} = \frac{2V_t}{3} - V_{C_2} \tag{2.34}$$

$$s_{d_1}(t) = \frac{1}{2}\{s_2(t) - s_1(t)\} \tag{2.35}$$

$$s_{d_2}(t) = \frac{1}{2}\{s_3(t) - s_2(t)\} \tag{2.36}$$

$$s_t(t) = \frac{1}{2}\{s_1(t) + s_2(t) + s_3(t)\} \tag{2.37}$$

After defining the above equations, they can be used to write $s_1(t)$, $s_2(t)$, $s_3(t)$, V_{C_1} and V_{C_2} in terms of $s_{d_1}(t)$, $s_{d_2}(t)$ and $s_t(t)$, V_{d_1}, V_{d_2} and V_t as follows:

$$V_{C_1} = \frac{V_t}{3} - V_{d_1} \tag{2.38}$$

$$V_{C_2} = \frac{2V_t}{3} - V_{d_2} \tag{2.39}$$

$$s_1(t) = \frac{2}{3}\{-2s_{d_1}(t) - s_{d_2}(t) + s_t(t)\} \tag{2.40}$$

$$s_2(t) = \frac{2}{3}\{s_{d_1}(t) - s_{d_2}(t) + s_t(t)\} \tag{2.41}$$

$$s_3(t) = \frac{2}{3}\{s_{d_1}(t) + 2s_{d_2}(t) + s_t(t)\} \tag{2.42}$$

The output voltage v_o can now be rewritten in terms of d and t parameters as follows:

$$v_o = \frac{V_t}{3}s_t(t) + V_{d_1}s_{d_1}(t) + V_{d_2}s_{d_2}(t) \tag{2.43}$$

After defining the above equations, the circuit differential equations are rewritten in terms of d and t parameters as follows:

$$\frac{dV_{d_1}}{dt} = -\frac{1}{C_1}\cdot s_{d_1}(t)\cdot i_L(t) = -\frac{1}{C}\cdot s_{d_1}(t)\cdot i_L(t) \tag{2.44}$$

$$\frac{dV_{d_2}}{dt} = -\frac{1}{C_2}\cdot s_{d_2}(t)\cdot i_L(t) = -\frac{1}{C}\cdot s_{d_2}(t)\cdot i_L(t) \tag{2.45}$$

$$\frac{di_L}{dt} = \frac{1}{L}\cdot\left\{\frac{V_t}{3}\cdot s_t(t) + V_{d_1}\cdot s_{d_1}(t) + V_{d_2}\cdot s_{d_2}(t) - v_s\right\} \tag{2.46}$$

$$\frac{dv_s}{dt} = \frac{1}{C_f}\cdot\left(i_L(t) - \frac{v_s}{R}\right) \tag{2.47}$$

It is now possible to derive an equivalent circuit in terms of d and t parameters. This circuit is shown in Figure 2-9.

2.10 Circuit analysis of a p-cell multicell converter

A p-cell multicell circuit is shown in Figure 2-10. The models obtained in the previous sections of this chapter will now be extended to p cells. Again, the same methods will be employed as in previous sections.

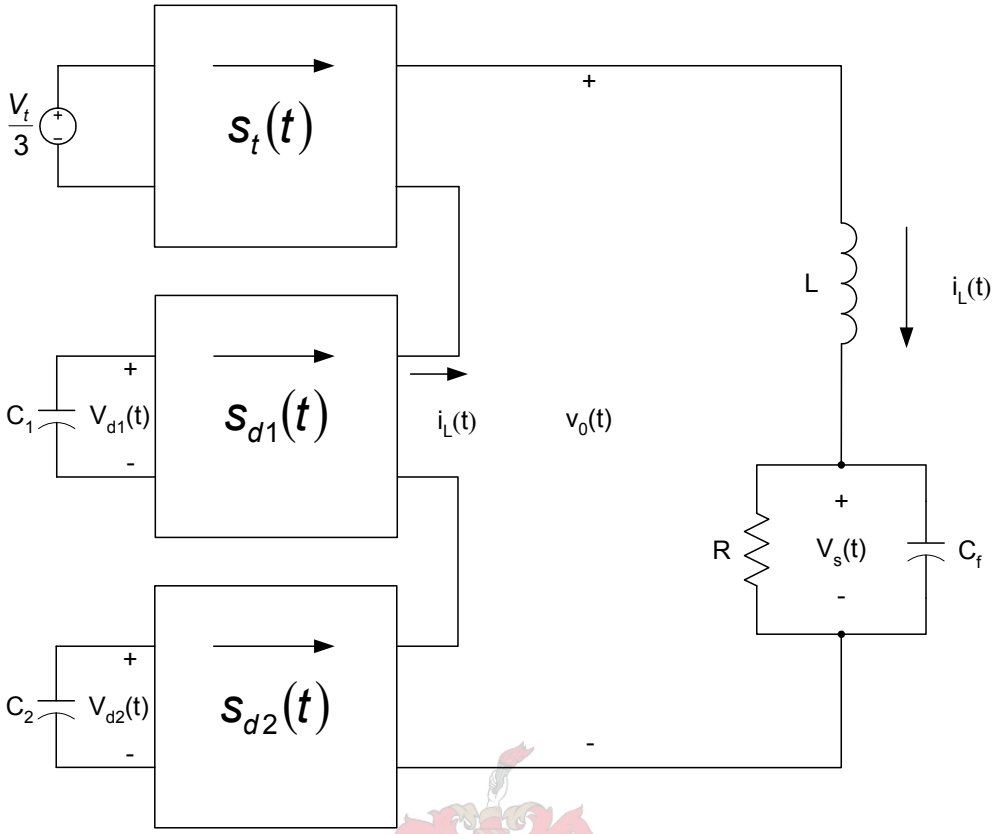

Figure 2-9. *Equivalent circuit in terms of d and t parameters of 3-cell multicell converter.*

The p switching functions needed for p-cells, e.g. $s_1(t), \ldots, s_p(t)$ are defined as follows:

$$s_i(t) = \begin{cases} 1 & \text{if } S_{it} \text{ is closed} \\ -1 & \text{if } S_{ib} \text{ is closed} \end{cases} \quad \text{for } i = 1, \ldots, p \tag{2.48}$$

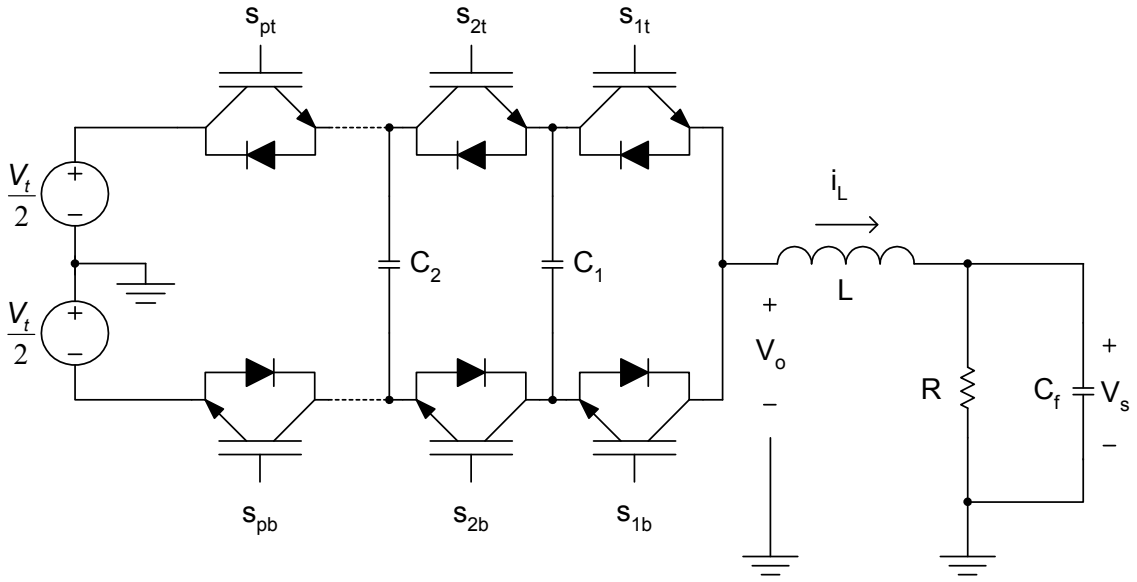

Figure 2-10. *A p-cell multicell converter.*

By inspection, it is possible to see that the output voltage $v_o(t)$ is given by the following:

$$\begin{aligned} v_o = &\frac{V_t}{2} \cdot s_p(t) + \frac{1}{2} V_{C_{p-1}} \cdot \{s_{p-1}(t) - s_p(t)\} + \dots \\ &+ \frac{1}{2} V_{C_2} \cdot \{s_2(t) - s_3(t)\} + \frac{1}{2} V_{C_1} \cdot \{s_1(t) - s_2(t)\} \end{aligned} \tag{2.49}$$

The equation for v_o can be written in a more general form for p cells as follows:

$$v_o = \frac{V_t}{2} \cdot s_p(t) + \frac{1}{2} \sum_{l=1}^{p-1} V_{C_l} \{s_l(t) - s_{l+1}(t)\} \tag{2.50}$$

Note that the currents $i_{C_1}(t), \dots i_{C_{p-1}}(t)$ are given by:

$$i_{C_1}(t) = \frac{1}{2} \cdot \{s_2(t) - s_1(t)\} \cdot i_L(t) \tag{2.51}$$

$$i_{C_2}(t) = \frac{1}{2} \cdot \{s_3(t) - s_2(t)\} \cdot i_L(t) \tag{2.52}$$

$$\vdots \; \vdots \; \vdots$$

$$i_{C_{p-2}}(t) = \frac{1}{2} \cdot \{s_{p-1}(t) - s_{p-2}(t)\} \cdot i_L(t) \tag{2.53}$$

$$i_{C_{p-1}}(t) = \frac{1}{2} \cdot \{s_p(t) - s_{p-1}(t)\} \cdot i_L(t) \tag{2.54}$$

The above equations can be written in a more general form for the i^{th} cell capacitor current as follows:

$$i_{C_i}(t) = \frac{1}{2} \{s_{i+1}(t) - s_i(t)\} \cdot i_L(t) \quad \text{for } i = 1, \dots, p-1 \tag{2.55}$$

The differential equations describing the system are as follows:

$$\frac{dV_{C_1}}{dt} = \frac{1}{2C_1} \cdot \{s_2(t) - s_1(t)\} \cdot i_L(t) = \frac{1}{2C} \cdot \{s_2(t) - s_1(t)\} \cdot i_L(t) \tag{2.56}$$

$$\frac{dV_{C_2}}{dt} = \frac{1}{2C_2} \cdot \{s_3(t) - s_2(t)\} \cdot i_L(t) = \frac{1}{2C} \cdot \{s_3(t) - s_2(t)\} \cdot i_L(t) \tag{2.57}$$

$$\frac{dV_{C_{p-2}}}{dt} = \frac{1}{2C_{p-2}} \cdot \{s_{p-1}(t) - s_{p-2}(t)\} \cdot i_L(t) = \frac{1}{2C} \cdot \{s_{p-1}(t) - s_{p-2}(t)\} \cdot i_L(t) \tag{2.58}$$

$$\frac{dV_{C_{p-1}}}{dt} = \frac{1}{2C_{p-1}} \cdot \{s_p(t) - s_{p-1}(t)\} \cdot i_L(t) = \frac{1}{2C} \cdot \{s_p(t) - s_{p-1}(t)\} \cdot i_L(t) \tag{2.59}$$

$$\begin{aligned} \frac{di_L}{dt} &= \frac{1}{L} \cdot \{v_o - v_s\} \\ &= \frac{1}{L} \cdot \left\{ \frac{V_t}{2} \cdot s_p(t) + \frac{1}{2} V_{C_{p-1}}(t) \cdot \{s_{p-1}(t) - s_p(t)\} + \dots \right. \\ &\qquad \left. + \frac{1}{2} V_{C_2} \cdot \{s_2(t) - s_3(t)\} + \frac{1}{2} V_{C_1} \cdot \{s_1(t) - s_2(t)\} - v_s \right\} \end{aligned}$$

$$= \frac{1}{L} \cdot \left\{ \frac{V_t}{2} \cdot s_p(t) + \frac{1}{2} \sum_{l=1}^{p-1} V_{C_l} \left\{ s_l(t) - s_{l+1} \right\} - v_s \right\} \tag{2.60}$$

$$\frac{dv_s}{dt} = \frac{1}{C_f} \cdot \left(i_L(t) - \frac{v_s}{R} \right) \tag{2.61}$$

2.11 Deriving an equivalent circuit of a p-cell multicell converter in terms of *d* and *t* parameters

To study the balancing properties of p-cell multicell circuit the following variables were defined:

$$V_{d_1} = \frac{V_t}{p} - V_{C_1} \tag{2.62}$$

$$V_{d_2} = \frac{2V_t}{p} - V_{C_2} \tag{2.63}$$

$$V_{d_{p-2}} = \frac{(p-2)V_t}{p} - V_{C_{p-2}} \tag{2.64}$$

$$V_{d_{p-1}} = \frac{(p-1)V_t}{p} - V_{C_{p-1}} \tag{2.65}$$

$$s_{d_1}(t) = \frac{1}{2} \left\{ s_2(t) - s_1(t) \right\} \tag{2.66}$$

$$s_{d_2}(t) = \frac{1}{2} \left\{ s_3(t) - s_2(t) \right\} \tag{2.67}$$

$$\vdots \vdots \vdots$$

$$s_{d_{p-2}}(t) = \frac{1}{2} \left\{ s_{p-1}(t) - s_{p-2}(t) \right\} \tag{2.68}$$

$$s_{d_{p-1}}(t) = \frac{1}{2} \left\{ s_p(t) - s_{p-1}(t) \right\} \tag{2.69}$$

$$s_t(t) = \frac{1}{2} \left\{ s_1(t) + s_2(t) + \ldots + s_{p-1}(t) + s_p(t) \right\} \tag{2.70}$$

A more general form for V_{d_i} can be written as follows:

$$V_{d_i} = \frac{iV_t}{p} - V_{C_i} \quad \text{for } i = 1, \ldots, p-1 \tag{2.71}$$

A more general form for s_{d_i} can be written as follows:

$$s_{d_i} = \frac{1}{2} \left\{ s_{i+1}(t) - s_i(t) \right\} \quad \text{for } i = 1, \ldots, p-1 \tag{2.72}$$

The relationship between s_{d_i} where $i = 1, \ldots, p-1$ and s_t and the switching functions s_i where

$i = 1, \ldots, p$ can be written in matrix form as follows:

$$\begin{bmatrix} s_{d_1}(t) \\ s_{d_2}(t) \\ s_{d_3}(t) \\ \vdots \\ s_{d_{p-1}}(t) \\ s_t(t) \end{bmatrix} = \frac{1}{2} \begin{bmatrix} -1 & 1 & 0 & 0 & \cdots & 0 \\ 0 & -1 & 1 & 0 & \ddots & \vdots \\ 0 & 0 & -1 & 1 & \ddots & \vdots \\ \vdots & \ddots & \ddots & \ddots & \ddots & \vdots \\ 0 & 0 & 0 & \cdots & -1 & 1 \\ 1 & 1 & 1 & 1 & \cdots & 1 \end{bmatrix} \begin{bmatrix} s_1(t) \\ s_2(t) \\ s_3(t) \\ \vdots \\ s_{p-1}(t) \\ s_p(t) \end{bmatrix} \tag{2.73}$$

Inverse the opposite relation in matrix form is as follows:

$$\begin{bmatrix} s_1(t) \\ s_2(t) \\ s_3(t) \\ \vdots \\ s_{p-1}(t) \\ s_p(t) \end{bmatrix} = 2 \begin{bmatrix} -1 & 1 & 0 & 0 & \cdots & 0 \\ 0 & -1 & 1 & 0 & \ddots & \vdots \\ 0 & 0 & -1 & 1 & \ddots & \vdots \\ \vdots & \ddots & \ddots & \ddots & \ddots & \vdots \\ 0 & 0 & 0 & \cdots & -1 & 1 \\ 1 & 1 & 1 & 1 & \cdots & 1 \end{bmatrix}^{-1} \begin{bmatrix} s_{d_1}(t) \\ s_{d_2}(t) \\ s_{d_3}(t) \\ \vdots \\ s_{d_{p-1}}(t) \\ s_t(t) \end{bmatrix} \tag{2.74}$$

The relationship between V_{d_i} where $i = 1, \ldots, p-1$ and V_t and V_{C_i} where $i = 1, \ldots, p-1$ can be written in matrix form as follows:

$$\begin{bmatrix} V_{d_1} \\ V_{d_2} \\ \vdots \\ V_{d_{p-2}} \\ V_{d_{p-1}} \end{bmatrix} = \begin{bmatrix} \frac{1}{p} & -1 & 0 & \cdots & 0 & 0 \\ \frac{2}{p} & 0 & -1 & 0 & \ldots & 0 \\ \vdots & \ddots & \ddots & \ddots & \ddots & \vdots \\ \frac{p-2}{p} & 0 & 0 & \cdots & -1 & 0 \\ \frac{p-1}{p} & 0 & 0 & \cdots & 0 & -1 \end{bmatrix} \begin{bmatrix} V_t \\ V_{C_1} \\ \vdots \\ V_{C_{p-2}} \\ V_{C_{p-1}} \end{bmatrix} \tag{2.75}$$

The equation for $v_o(t)$ can be written in a more general form for p cells in terms of d and t parameters as follows:

$$v_o = \frac{V_t}{p} s_t(t) + \sum_{l=1}^{p-1} V_{d_l} s_{d_l}(t) \tag{2.76}$$

The differential equations for the p-cell multicell converter can be written in terms of d and t parameters as follows:

$$\begin{aligned} \frac{dV_{d_i}}{dt} &= \frac{d}{dt}\left\{\frac{iV_t}{p}\right\} - \frac{dV_{C_i}}{dt} \\ &= -\frac{dV_{C_i}}{dt} \\ &= -\frac{1}{2C_i}\left\{s_{i+1}(t) - s_i(t)\right\} \cdot i_L(t) \\ &= -\frac{1}{C_i} s_{d_i}(t) \cdot i_L(t) \quad \text{for } i = 1, \ldots, p-1 \end{aligned} \tag{2.77}$$

$$\frac{di_L}{dt} = \frac{1}{L} \cdot \{v_o - v_s\}$$
$$= \frac{1}{L} \cdot \left\{ \frac{V_t}{p} s_t(t) + \sum_{l=1}^{p-1} V_{d_l} s_{d_l}(t) - v_s \right\} \quad (2.78)$$

$$\frac{dv_s}{dt} = \frac{1}{C_f} \cdot \left(i_L(t) - \frac{v_s}{R} \right) \quad (2.79)$$

An equivalent circuit in terms of d and t parameters can now be obtained from the above equations. This circuit is shown in Figure 2-11.

2.12 Summary

A mathematical model was developed in this chapter, using circuit analysis techniques as well as applying d and t parameters. The final model differential equations were used to derive equivalent circuits of the multicell topology in terms of d and t parameters.

This model is the foundation upon which the remainder of this balance theory will be built. The above-mentioned equivalent circuits will be converted to the frequency domain for the steady-state analysis in Chapter 4 and will also be used in the time constant analysis in Chapter 5.

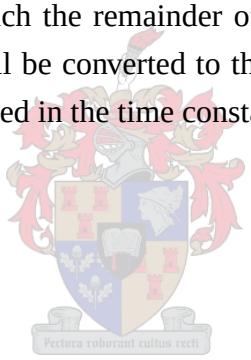

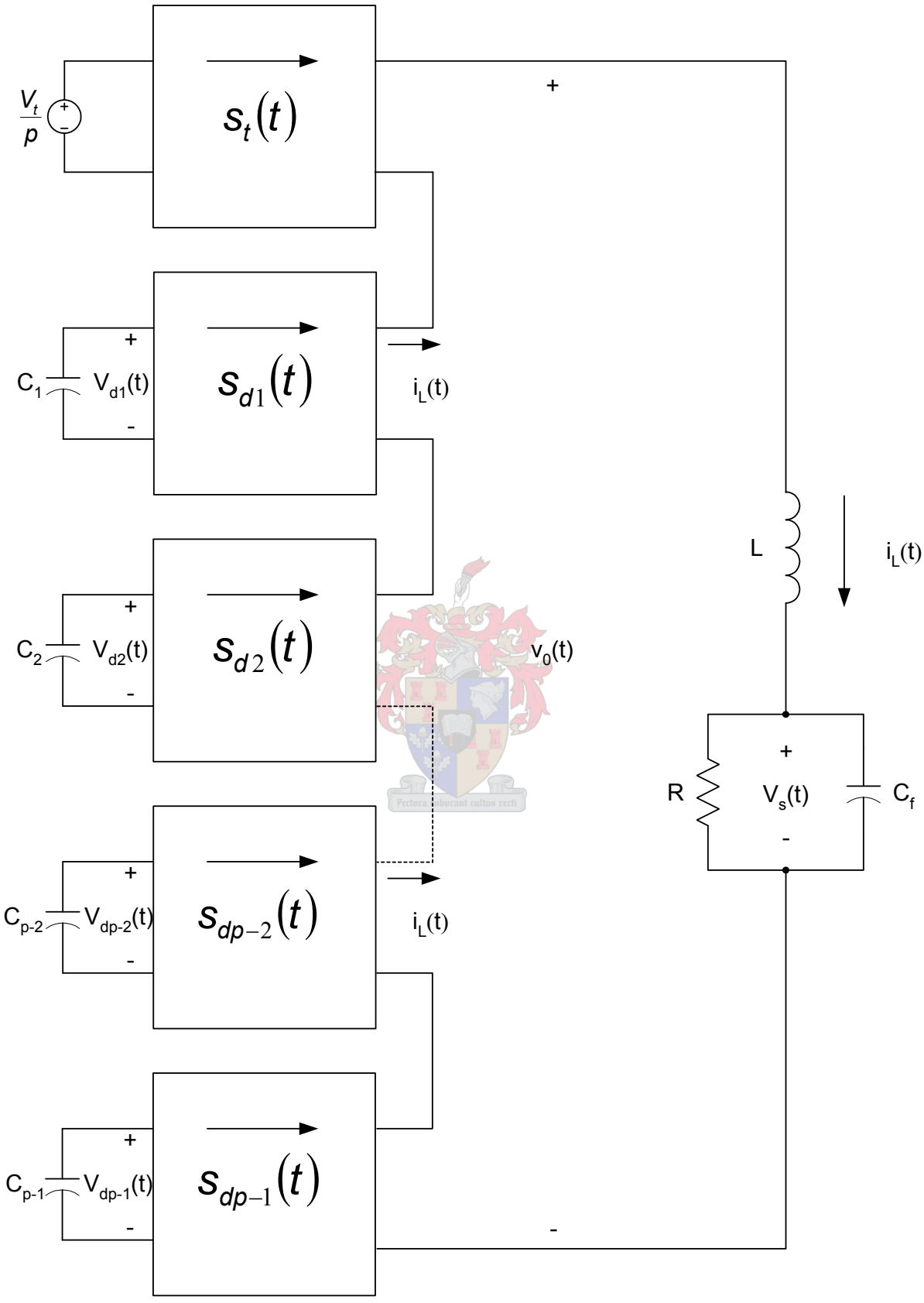

Figure 2-11. *Equivalent circuit in terms of d and t parameters of p-cell multicell converter.*

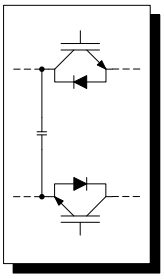

Chapter 3

Harmonic analysis

3.1 Introduction

The previous chapter focussed on the circuit analysis of the multicell converter topology and resulted in a mathematical model for this topology. This model is dependent on the switching functions of the converter.

This chapter focusses on the determination of the switching functions and the characteristics thereof. Switching functions are calculated using interleaved switching for both sinusoidal modulation as well as fixed duty-cycle modulation. Interleaved switching is used to ensure that the switching functions of the respective cells are phase-shifted with the appropriate value, i.e. $\frac{2\pi}{p}$, as discussed in Chapter 2 section 2.2.

The switching functions are calculated using Fourier methods developed by W.R. Bennet [21] and H.S. Black [5]. Switching functions are first calculated for the 2- and 3-cell cases under sinusoidal modulation after which the switching functions for the general case of p-cells are also calculated. This is followed by the calculation of the switching functions for the 2-, 3- and p-cell cases for the fixed duty-cycle case where the same duty-cycle is imposed on each cell.

It is shown in this chapter that the natural balance of the cell capacitor voltages in a multicell converter is promoted when the converter switching frequency is chosen to be significantly higher than the maximum frequency content of the reference signal.

The harmonics are shown to appear in groups around multiples of the switching frequency. It is shown that as long as the harmonic spectra of these groups are non-zero and do not overlap, the conditions are favourable for natural balance to occur in the converter.

The choice of the number of cells is also shown to have a drastic effect on the amplitude spectra of

the switching functions obtained for the fixed duty-cycle modulation case. Conditions that can lead to natural balance as well as unbalance are discussed.

In this section it is assumed that the gating signals of the converter are periodic, with a frequency equal to the reference frequency (denoted f_r in Hz and ω_r in radians per second) except for the fixed duty-cycle case where the gating signals are periodic with a frequency equal to the switching frequency (denoted f_s in Hz and ω_s in radians per second).

As a starting point, an example of PWM is given, which is followed by an introduction to Double Fourier series analysis. This is followed by a discussion of the harmonics of interleaved switching which addresses both sinusoidal modulation as well as fixed duty-cycle switching for specific numbers of cells, modulation indices and duty-cycles.

Example 3.1

As an example, Figure 3-1 shows the switching function generated using a triangle carrier with $f_s = 250\ Hz$ and a sinusoidal reference with $f_r = 50\ Hz$ and a dc offset of 0.5. The reference signal $f_r(t)$ can be written as follows:

$$f_r(t) = 0.5 + 0.8\sin(2\pi \cdot 50t) \tag{3.1}$$

and the carrier $f_c(t)$ as follows [61], [63]:

$$f_c(t) = \frac{2}{\pi}\arcsin\left[\sin(2\pi \cdot 250t)\right]. \tag{3.2}$$

The switching function is as defined in Chapter 2 and is as follows:

$$s(t) = \begin{cases} 1 & \text{if } f_c(t) < f_r(t) \\ -1 & \text{if } f_r(t) < f_c(t) \end{cases} \tag{3.3}$$

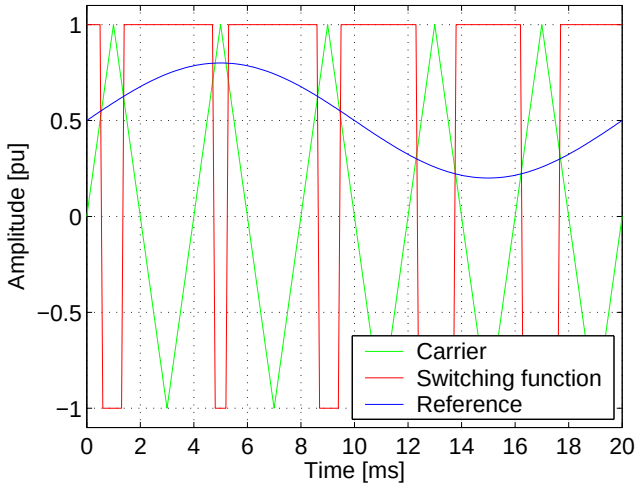

Figure 3-1. *Generation of a switching function from a sinusoidal reference and triangle carrier.*

3.2 Double integral representation of a switched waveform

The harmonic content of a time varying periodic waveform, say $f(t)$ can be determined analytically through Fourier decomposition. This information can then be used to represent $f(t)$ as an infinite series of sinusoidal components as follows:

$$f(t) = \sum_{\kappa=-\infty}^{\kappa=\infty} c_\kappa e^{j\kappa\omega t} \tag{3.4}$$

where

$$c(\kappa) = \frac{1}{T}\int_{-\frac{T}{2}}^{\frac{T}{2}} f(t)e^{-j\kappa\omega t}dt \tag{3.5}$$

The switched waveform $f(t)$ generated with carrier-based PWM is generally not periodic in time and therefore the above technique cannot be used directly. W.R. Bennet [21] was the first person to resolve this problem, followed by H.S. Black [5] and finally S.R. Bowes [22], [23]. S.R. Bowes' study was with specific application to switching power converters.

The switched waveform $f(t)$ can be represented with a double summation series of sinusoids (double Fourier series) arranged around the carrier and fundamental as shown in equation (3.6). The harmonic coefficients are given by the double Fourier integral shown in equation (3.7) [25].

$$\begin{aligned} f(t) &= F(h,t) \\ &= \frac{A_{00}}{2} + \sum_{n=1}^{\infty}\{A_{0n}\cos(n\omega_r t) + B_{0n}\sin(n\omega_r t)\} + \\ &\quad \sum_{m=1}^{\infty}\{A_{m0}\cos(m\omega_s t) + B_{m0}\sin(m\omega_s t)\} + \\ &\quad \sum_{m=1}^{\infty}\sum_{n=\pm1}^{\pm\infty}\{A_{mn}\cos(m\omega_s t + n\omega_r t) + B_{mn}\sin(m\omega_s t + n\omega_r t)\} \end{aligned} \tag{3.6}$$

where

$$\begin{aligned} C_{mn} &= A_{mn} + jB_{mn} \\ &= \frac{1}{2\pi^2}\int_{-\pi}^{\pi}\int_{-\pi}^{\pi} F(h,t)e^{j(m\omega_r t + n\omega_s t)}dhdt \end{aligned} \tag{3.7}$$

This section served as a brief introduction to the double integral representation of a switched waveform. The definition of the function $F(h,t)$ in equation (3.7) will be given later in this chapter when the switching functions are calculated for each respective case.

3.3 Harmonics of interleaved switching

Interleaved switching was chosen as the method for generating the PWM gating signals of the respective cells of a multicell converter. The reason for this choice is that for this topology the switching frequency is effectively multiplied by the number of cells in the converter, i.e. for a p-cell converter the switching frequency will be pf_s [64]. Another reason for this decision is that natural balance of the cell capacitor voltages of the multicell converter is promoted when the gating signals of each successive cell is phase-shifted by $\frac{2\pi}{p}$ radians [26]. This is accomplished with interleaved switching.

Interleaved switching is used for switching the converter under sinusoidal modulation as well as for the fixed duty-cycle case.

In order study the behaviour of multicell converters under interleaved switching it is essential to study the harmonics of the PWM switching functions. The approach that is used for this study is similar to that done in [62] which is based on the use of a double Fourier series approach. This approach was originally used by W.R. Bennett in a study of the spectra of rectified waves in [21]. This technique was developed further by H.S. Black [5] and has been used in several applications which can be found in the literature, e.g. [22], [23], [25] and [31].

This double Fourier method is first applied to a half-bridge or "single"-cell converter after which this result is used and applied for the different multicell cases. Only interleaved PWM with natural sampled modulations is analysed. The techniques are general and can be applied to any modulation strategy and sampling methods.

This harmonic study is in two parts: the first part starts off with calculating and analysing the switching functions of a "single"-cell converter under sinusoidal modulation and then works progressively towards the general case of p cells by starting with the 2-cell case. The second part is dedicated to calculating the same switching functions as in the first part, except that this time it deals with the converter under fixed duty-cycle switching.

3.3.1 Sinusoidal modulation

This section focusses on the calculation of the switching functions of a "single"-, 2-, 3- and p-cell multicell converters using interleaved switching under sinusoidal modulation. The double Fourier series method is used for all the cases discussed in this section, unless otherwise stated.

The graphical method used to construct the background function $F(h,t)$ is the same as the method used in [62]. It is only shown in detail for the first case, after which the result is re-applied for the subsequent cases.

3.3.1.1 Switching functions of a “single”-cell converter

The “single”-cell or half-bridge converter is chosen as the starting point for this analysis as the analysis is simplest for this case. Other subsequent cases are all based on the results found for this case.

Pulse width modulation (PWM) as applied to a half-bridge or “single”-cell converter is shown in Figure 3-2. This figure only shows the first cycle of the reference $f_r(t)$, but it continues periodically along the t-axis for all $t \geq 0$. The reference function, shown in Figure 3-2(a) has a frequency of ω_r and a modulation index m_a and is written as follows:

$$f_r(t) = m_a \sin(\omega_r t) \tag{3.8}$$

The function $f_c(t)$, also shown in Figure 3-2(a), is the triangular carrier with frequency ω_s, which is the switching frequency of each switching device in the half-bridge converter. The carrier can be written as follows [61], [63]:

$$f_c(t) = \frac{2}{\pi} \arcsin\left[\sin(\omega_s t)\right]. \tag{3.9}$$

For simplicity, it is assumed that ω_s is an integer multiple of ω_r for the remainder of this chapter, although the theory still applies when it is not the case.

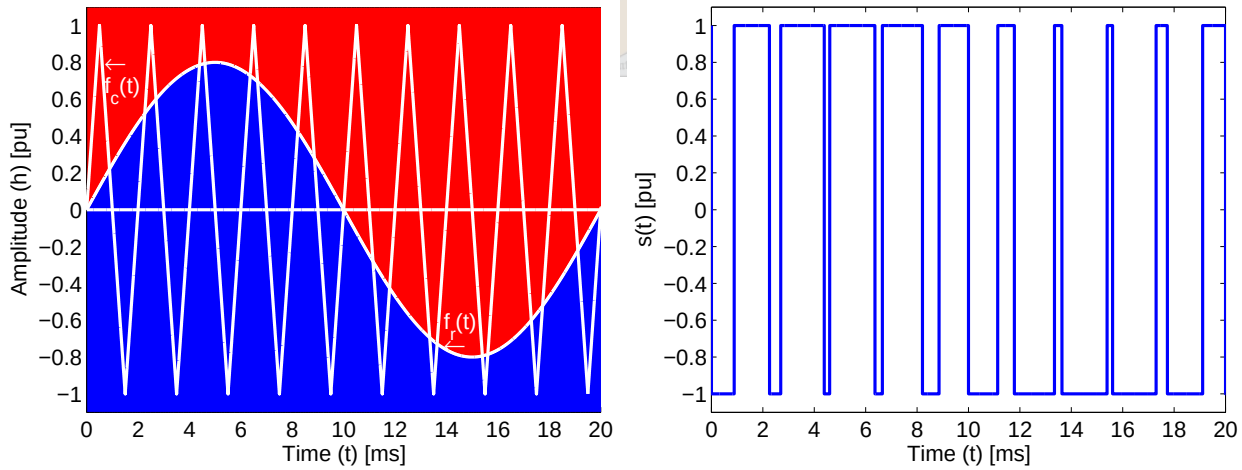

(a) (b)

Figure 3-2. *Switching function generation for a “single”-cell inverter using interleaved switching.*

In Figure 3-2(a), the area between $f_r(t)$ and -1 is coloured blue and is where $s(t) = 1$, while the area above, between $f_r(t)$ and $+1$ is coloured red is where $s(t) = -1$. The amplitudes of the blue and red areas in the $F(h,t)$-axis represent the state of the switching function. The resulting switching

function $s(t)$ is shown in Figure 3-2(b) and is defined as follows:

$$s(t) = \begin{cases} 1 & \text{for the blue region} \\ -1 & \text{for the red region} \end{cases} \tag{3.10}$$

To find the Fourier series representation of the switching function, it is necessary to define a background function $F(h,t)$ for the switching. The first step in obtaining the background function is to modify the original PWM generation figure, shown in Figure 3-2(a), graphically. Arrows are added onto the triangular carrier wave $f_c(t)$ to show the direction of the carrier, i.e. whether it is moving up or down. This is shown in Figure 3-3(a).

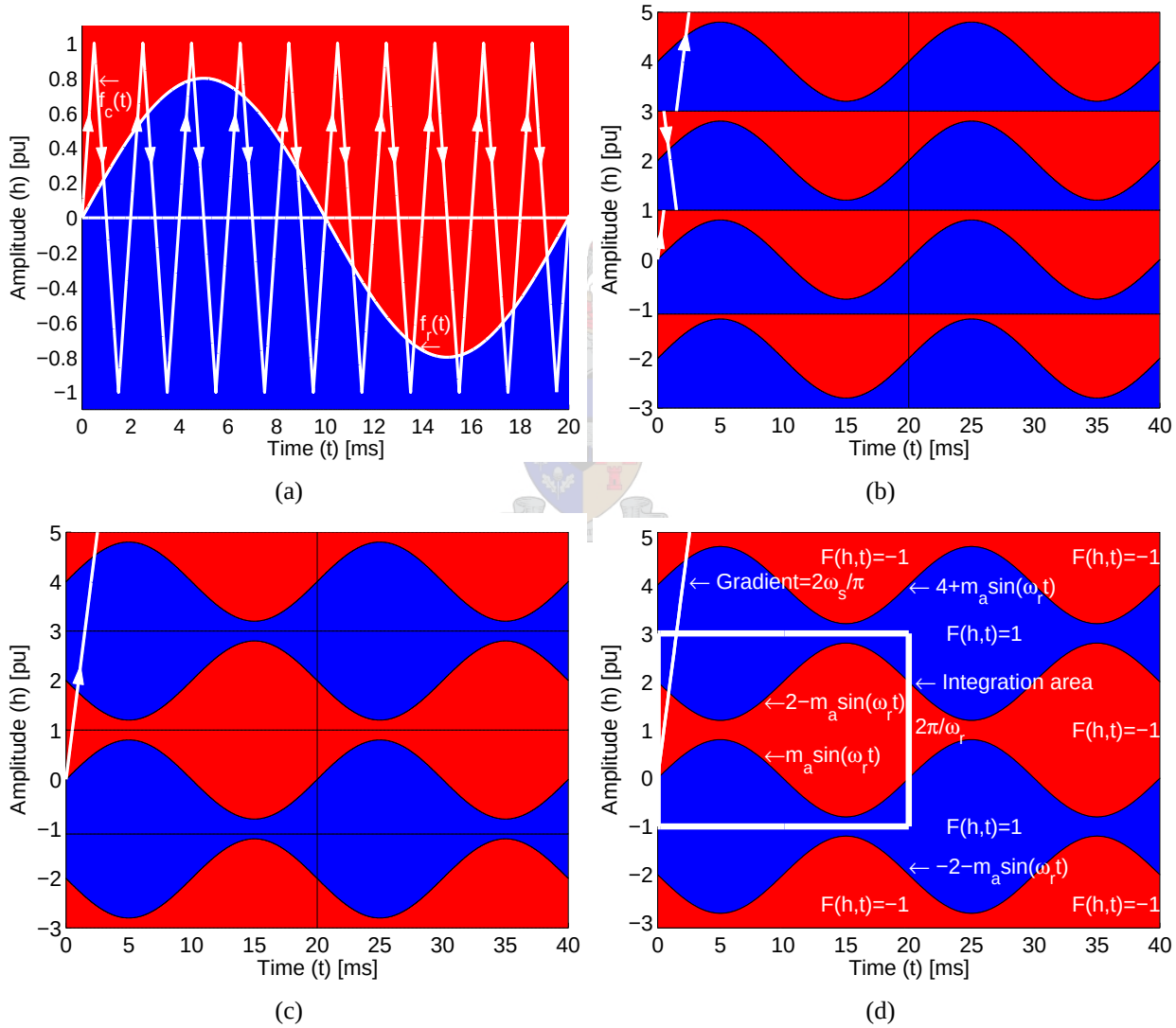

Figure 3-3. *The graphical method used to obtain $F(h,t)$ for a "single"-cell.*

The next step is to separate the triangular carrier wave into segments of a quarter of its period. These segments are then drawn separately, but placed one on top of the other to form a new graph. This is

shown in Figure 3-3(b).

The final step is to fit the segments obtained in the previous step onto a straight line. This is done by flipping around the segments that are not showing in the right direction. The right direction is chosen as "up" and the resulting figure is shown in Figure 3-3(c). It can now be seen that this background function is periodic in both the h- and t directions, therefore it can be represented with a double Fourier series [5]. An area of integration is chosen over one period in both the h- and t directions and is indicated in Figure 3-3(d). Figure 3-3(d) also contains the expressions for the periodic sinusoidal walls between the red and blue areas. Figure 3-3(d) is in fact the top view of a three-dimensional space. A three-dimensional view of this space is shown in Figure 3-4 where the line constructed with the carrier segments is a plane in a three-dimensional space.

The two-dimensional function, $F(h,t)$ is defined as follows:

$$F(h,t) = \begin{cases} \quad 1 & \text{if } -2 - f_r(t) < f_c(t) \leq f_r(t) \\ - \quad 1 & \text{if } f_r(t) < f_c(t) \leq -2 - f_r(t) \end{cases} \tag{3.11}$$

The switching function of the cell is then given by the value of $F(h,t)$ when following the line:

$$(h,t) = \left(\frac{2\omega_s}{\pi}t, t\right) \tag{3.12}$$

in the TOH-plane. This line is shown in Figure 3-3(d). When looking at the three-dimensional representation shown in Figure 3-4, this line is shown as a plane. The expression for the switching function $s(t)$ is then as follows:

$$s(t) = F\left(\frac{2\omega_s}{\pi}t, t\right) \tag{3.13}$$

For any reference, this function $F(h,t)$ can be expanded as follows [5]:

$$\begin{aligned} F(h,t) = \frac{1}{2}A_{00} + \sum_{n=1}^{\infty}(A_{0n}\cos(n\omega_r t) + B_{0n}\sin(n\omega_r t)) + \\ \sum_{m=1}^{\infty}\left(A_{m0}\cos\left(\frac{m\pi h}{2}\right) + B_{m0}\sin\left(\frac{m\pi h}{2}\right)\right) + \\ \sum_{m=1}^{\infty}\sum_{n=\pm 1}^{\pm\infty}\left(A_{mn}\cos\left(\frac{m\pi h}{2} + n\omega_r t\right) + B_{mn}\sin\left(\frac{m\pi h}{2} + n\omega_r t\right)\right) \end{aligned} \tag{3.14}$$

where the coefficients A_{mn} and B_{mn} are as follows:

$$A_{mn} + jB_{mn} = \frac{\omega_r}{4\pi}\int_0^{\frac{2\pi}{\omega_r}}\int_{-1}^{3} F(h,t)e^{j(\frac{m\pi h}{2} + n\omega_r t)}dhdt \tag{3.15}$$

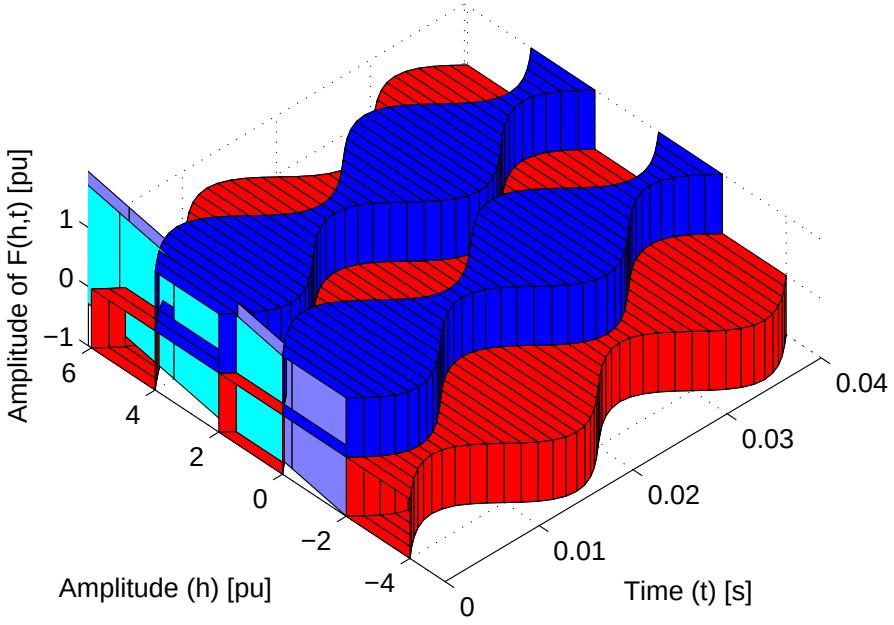

Figure 3-4. *Three dimensional view of* $F(h,t)$ *for* $s(t)$.

The $\frac{\omega_r}{4\pi}$ term is obtained by calculating $\frac{2}{Area}$ where $Area$ is the area of integration as shown in Figure 3-3(d). For the above case h is given as follows:

$$h = \frac{2\omega_s}{\pi}t \tag{3.16}$$

Substituting equation (3.16) into the term $\frac{m\pi h}{2}$ yields the following:

$$\frac{m\pi h}{2} = m\omega_s t \tag{3.17}$$

Substituting equation (3.17) into equation (3.14) results in $s(t)$ as follows:

$$\begin{aligned} s(t) = \frac{1}{2}A_{00} + \sum_{n=1}^{\infty}(A_{0n}\cos(n\omega_r t) + B_{0n}\sin(n\omega_r t)) + \\ \sum_{m=1}^{\infty}(A_{m0}\cos(m\omega_s t) + B_{m0}\sin(m\omega_s t)) + \\ \sum_{m=1}^{\infty}\sum_{n=\pm 1}^{\pm\infty}(A_{mn}\cos(m\omega_s t + n\omega_r t) + B_{mn}\sin(m\omega_s t + n\omega_r t)) \end{aligned} \tag{3.18}$$

In the above expression for $s(t)$ it is important to look at the characteristics of the Fourier coefficients. The coefficients A_{mn} and B_{mn} can be calculated with equation (3.15). Using the area of integration as shown in Figure 3-3(d) the coefficients are calculated in Appendix A section A.1.1 for sinusoidal modulation with a modulation index m_a and these results are repeated here for convenience as follows:

- $m \neq 0$ and n odd:

$$A_{mn} + jB_{mn} = \frac{2j}{m\pi} J_n\left(\frac{m\pi m_a}{2}\right)\left(1 + e^{jm\pi}\right) \tag{3.19}$$

- $m \neq 0$ and n even:

$$A_{mn} + jB_{mn} = \frac{2}{jm\pi} J_n\left(\frac{m\pi m_a}{2}\right)\left(1 - e^{jm\pi}\right) \tag{3.20}$$

- $m = 0$ and $n = 1$:

$$A_{01} + jB_{01} = jm_a \tag{3.21}$$

- $m = 0$ and $n \neq 1$:

$$A_{0n} + jB_{0n} = 0 \tag{3.22}$$

where J_n denotes the Bessel function of the first kind [11], [68].

The characteristics of the above coefficients can be summed up as follows:

- A_{00}**:** this coefficient is the dc-component of $s(t)$ which is zero.
- $A_{0n} + jB_{0n}$**:** these coefficients are the Fourier series coefficients of the reference signal $f_r(t)$.
- $A_{m0} + jB_{m0}$**:** these coefficients are components at the switching frequency ω_s and integer multiples thereof.
- $A_{mn}+jB_{mn}$**:** these coefficients are harmonic side-bands around integer multiples of the switching frequency.

The remainder of this section is devoted to a study of the properties of the above coefficients. These properties are derived in the same way as in [62].

- When $m \neq 0$ equation (3.15) can be rewritten as follows:

$$\begin{aligned}
A_{mn} + jB_{mn} &= \frac{\omega_r}{2\pi} \int_0^{\frac{2\pi}{\omega_r}} \int_{-f_r(t)}^{f_r(t)} e^{j(m\pi h + n\omega_r t)} dh dt \\
&= \frac{\omega_r}{2\pi} \int_0^{\frac{2\pi}{\omega_r}} \left(\int_{-f_r(t)}^{f_r(t)} e^{jm\pi h} dh \right) e^{jn\omega_r t} dt \\
&= \frac{\omega_r}{2\pi} \int_0^{\frac{2\pi}{\omega_r}} \left(\frac{1}{jm\pi} e^{jm\pi h} \Big|_{-f_r(t)}^{f_r(t)} \right) e^{jn\omega_r t} dt \\
&= \frac{\omega_r}{2jm\pi^2} \int_0^{\frac{2\pi}{\omega_r}} \left(e^{jm\pi f_r(t)} - e^{-jm\pi f_r(t)} \right) e^{jn\omega_r t} dt \\
&= \frac{\omega_r}{m\pi^2} \int_0^{\frac{2\pi}{\omega_r}} \sin(m\pi f_r(t)) e^{jn\omega_r t} dt
\end{aligned} \tag{3.23}$$

- When $m = 0$, equation (3.15) is evaluated as follows:

$$\begin{aligned} A_{mn} + jB_{mn} &= \frac{\omega_r}{2\pi} \int_0^{\frac{2\pi}{\omega_r}} \int_{-f_r(t)}^{f_r(t)} e^{jn\omega_r t} dh dt \\ &= \frac{\omega_r}{2\pi} \int_0^{\frac{2\pi}{\omega_r}} \left(h|_{-f_r(t)}^{f_r(t)} \right) e^{jn\omega_r t} dt \\ &= \frac{\omega_r}{2\pi} \int_0^{\frac{2\pi}{\omega_r}} \left(f_r(t) + f_r(t) \right) e^{jn\omega_r t} dt \\ &= \frac{\omega_r}{2\pi} \int_0^{\frac{2\pi}{\omega_r}} 2 f_r(t) e^{jn\omega_r t} dt \\ &= \frac{\omega_r}{\pi} \int_0^{\frac{2\pi}{\omega_r}} f_r(t) e^{jn\omega_r t} dt \end{aligned} \tag{3.24}$$

From equations (3.23) and (3.24) the following properties can be deduced:

(a) Following from equation (3.23) it is important to determine $|A_{mn} + jB_{mn}|$. From the above calculation, this can be calculated as follows:

$$\begin{aligned} |A_{mn} + jB_{mn}| &= \left| \frac{\omega_r}{m\pi^2} \int_0^{\frac{2\pi}{\omega_r}} \sin(m\pi f_r(t)) e^{jn\omega_r t} dt \right| \\ &\leq \frac{\omega_r}{m\pi^2} \int_0^{\frac{2\pi}{\omega_r}} \left| \sin(m\pi f_r(t)) e^{jn\omega_r t} \right| dt \\ &= \frac{\omega_r}{m\pi^2} \int_0^{\frac{2\pi}{\omega_r}} \left| \sin(m\pi f_r(t)) \right| dt \\ &\leq \frac{\omega_r}{m\pi^2} \cdot \frac{2\pi}{\omega_r} \\ &= \frac{2}{m\pi} \end{aligned} \tag{3.25}$$

Equation (3.25) proves that $|A_{mn} + jB_{mn}| \to 0$ as $m \to \infty$.

(b) For the case where $m \neq 0$ and $n \neq 0$, equation (3.23) can be integrated by parts as follows:

$$\begin{aligned} A_{mn} + jB_{mn} &= \frac{\omega_r}{m\pi^2} \int_0^{\frac{2\pi}{\omega_r}} \sin(m\pi f_r(t)) e^{jn\omega_r t} dt \\ &= \frac{\omega_r}{m\pi^2} \left(\left[\sin(m\pi f_r(t)) \frac{1}{jn\omega_r} e^{jn\omega_r t} \right]_0^{\frac{2\pi}{\omega_r}} - \right. \\ &\qquad \left. \frac{1}{jn\omega_r} \int_0^{\frac{2\pi}{\omega_r}} e^{jn\omega_r t} \cos(m\pi f_r(t)) m\pi \frac{df_r(t)}{dt} dt \right) \end{aligned} \tag{3.26}$$

Seeing that $f_r(t)$ is periodic with ω_r, the first term in equation (3.26) is 0. Therefore,

$$\begin{aligned}
|A_{mn} + jB_{mn}| &= \left| \frac{1}{jmn\pi^2} \int_0^{\frac{2\pi}{\omega_r}} e^{jn\omega_r t} \cos(m\pi f_r(t)) m\pi \frac{df_r(t)}{dt} dt \right| \\
&= \left| \frac{-j}{n\pi} \int_0^{\frac{2\pi}{\omega_r}} e^{jn\omega_r t} \cos(m\pi f_r(t)) \frac{df_r(t)}{dt} dt \right| \\
&\leq \frac{1}{|n|\pi} \int_0^{\frac{2\pi}{\omega_r}} \left| e^{jn\omega_r t} \cos(m\pi f_r(t)) \frac{df_r(t)}{dt} \right| dt \\
&= \frac{1}{|n|\pi} \int_0^{\frac{2\pi}{\omega_r}} \left| \frac{df_r(t)}{dt} \right| dt
\end{aligned} \tag{3.27}$$

Knowing that $\int_0^{\frac{2\pi}{\omega_r}} \left| \frac{df_r(t)}{dt} \right| dt$ is a constant, it is clear that $|A_{mn} + jB_{mn}| \to 0$ as $n \to \infty$.

(c) Combining the above results into a single result yields the following expression:

$$|A_{mn} + jB_{mn}| \leq \min \left(\frac{2}{m\pi}, \frac{1}{|n|\pi} \int_0^{\frac{2\pi}{\omega_r}} \left| \frac{df_r(t)}{dt} \right| dt \right) \tag{3.28}$$

Equation (3.28) can be interpreted as follows:

- The magnitude of the Fourier coefficients, e.g. $|A_{mn} + jB_{mn}|$, is less than or equal to the smallest value of either $\frac{2}{m\pi}$ or $\frac{1}{|n|\pi} \int_0^{\frac{2\pi}{\omega_r}} \left| \frac{df_r(t)}{dt} \right| dt$.
- From property (b), this means that if the switching frequency ω_s is chosen much higher than the highest frequency harmonic of $f_r(t)$, that the harmonics of $s(t)$ appear in clusters around integer multiples of $m\omega_s$. For values of $m > 0$, the clusters consist of harmonics at frequencies of $m\omega_s + n\omega_r$, where $n = \pm 1, \pm 2, \ldots$. The magnitude of the clusters of harmonics decay as the magnitude of n increases. The magnitude of the harmonics found in these clusters can be calculated by $\int_0^{\frac{2\pi}{\omega_r}} \left| \frac{df_r(t)}{dt} \right|$. When the value of this integral is small, the magnitude of the side-band harmonics attenuates quickly as $|n|$ increases and these side-bands do not overlap with neighbouring clusters. This proves that when the switching frequency is chosen much higher than the highest frequency component of $f_r(t)$ that the clusters of harmonics do not overlap.

Example 3.2

Consider the following reference function:

$$f_r(t) = \sin(2\pi 50t) \tag{3.29}$$

When using a switching frequency of $5\ kHz$, the magnitude of the Fourier series coefficients of $f_r(t)$ is calculated and shown in Figure 3-5. The estimate given by equation (3.28) is plotted on the same

figure for convenience. The results shown in Figure 3-5 proves the interpretation mentioned earlier

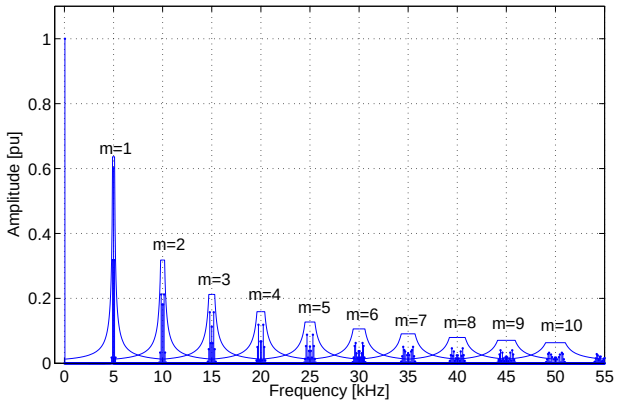

Figure 3-5. *Example of the harmonics of interleaved switching.*

and show that equation (3.28) is valid when $\omega_s >> \omega_r$. It also shows that the clusters of harmonics are around integer multiples of the switching frequency.

3.3.1.2 Switching functions of 2-cell interleaved switching

The switching functions are defined per switching cell in a multicell converter, meaning that for a 2-cell converter there are two switching functions. These switching functions contain the state of both switching elements in a switching cell, as the switches in a cell work as complimentary pairs, i.e. when the one switch conducts, the other blocks and vice versa. The states that the switching functions can assume were defined in Chapter 2 section 2.4 and are repeated here for convenience as follows:

$$s_1(t) = \begin{cases} \quad 1 & \text{if } f_{c_1}(t) < f_r(t) \\ -\quad 1 & \text{if } f_r(t) < f_{c_1}(t) \end{cases} \tag{3.30}$$

$$s_2(t) = \begin{cases} \quad 1 & \text{if } f_{c_2}(t) < f_r(t) \\ -\quad 1 & \text{if } f_r(t) < f_{c_2}(t) \end{cases} \tag{3.31}$$

The reference signal is again chosen to be sinusoidal with an angular frequency of ω_r and the carrier signal is chosen to be triangular with an angular frequency of ω_s.

For the 2-cell case, interleaved PWM is generated by using 2 carrier signals that are phase-shifted by $180°$. Each carrier is used to generate the PWM of each respective cell by comparing it with the same reference signal. These two carriers can be written as follows:

$$f_{c_1}(t) = \frac{2}{\pi} \arcsin\left[\sin(\omega_s t)\right] \tag{3.32}$$

$$f_{c_2}(t) = \frac{2}{\pi} \arcsin\left[\sin(\omega_s t - \pi)\right] \tag{3.33}$$

Interleaved switching for a 2-cell multicell converter is illustrated in the following example.

Example 3.3

A 2-cell multicell converter is switched using interleaved PWM under sinusoidal modulation. The sinusoidal reference signal $f_r(t)$ has a frequency of $50\ Hz$, a modulation index of 0.8 and is defined as follows:

$$f_r(t) = 0.8 \sin(\omega_r t) \tag{3.34}$$

where $\omega_r = 2\pi \cdot 50$ and the switching frequency $f_s = 250\ Hz$.

In order to generate the switching functions, two triangular carriers are used. The two carriers are 180° out of phase. The generation of the switching function of the first cell, i.e. $s_1(t)$ is shown in Figure 3-6(a). The carrier signal of the first cell is denoted by $f_c(t)$ and shown in green, while the reference signal is shown in blue.

The generation of the switching function of the second cell, i.e. $s_2(t)$ is shown in Figure 3-6(b). The carrier signal of this cell is denoted as $-f_c(t)$ and shown in green, while the reference signal is shown in blue.

The "difference" switching function $s_d(t)$ and the "total" switching function $s_t(t)$ are shown respectively in Figures 3-6(c) and 3-6(d). These switching functions were defined in equations (2.15) and (2.16) in Chapter 2 section 2.7 and are repeated here for convenience as follows:

$$s_d(t) = \frac{1}{2}\left\{s_2(t) - s_1(t)\right\} \tag{3.35}$$

$$s_t(t) = \frac{1}{2}\left\{s_1(t) + s_2(t)\right\} \tag{3.36}$$

The figures shown in Figure 3-6 only show the first cycle of the reference signal $f_r(t)$, but these signals continue for all $t \geq 0$.

Using the same arguments as applied in the previous section and using the same graphical methods, the frequency spectra can be obtained for both switching functions. Due to interleaved switching, the carriers of the two cells are π radians out of phase, i.e. the carrier of cell 2 lags that of cell 1 by π radians. The first line in the TOH-plane is the same as for the "single"-cell case discussed in the previous section. The second line is parallel to the first line, but with an h-axis intersection at $h = -2$. This can be calculated from the fact that the gradient of the line is $\frac{2\omega_s}{\pi}$ and knowing that the second

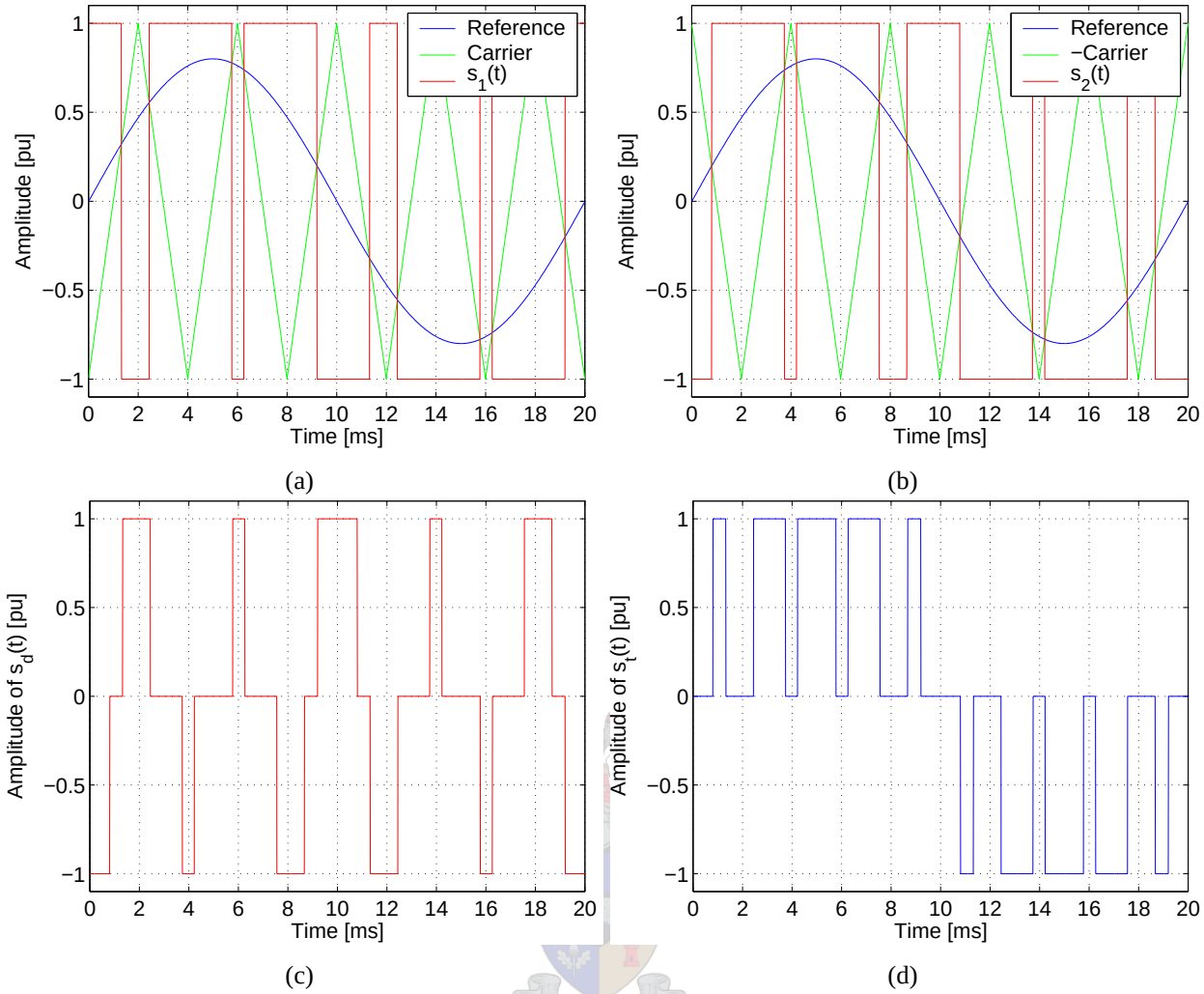

Figure 3-6. *Switching function generation for a 2-cell multicell inverter using interleaved switching.*

line lags the first by π radians. Substituting this information into the equation for a straight line yields the h-axis intersection. This results in the following two lines in the TOH-plane:

$$\left(\frac{2\omega_s}{\pi}t, t\right) \quad \text{and} \quad \left(\frac{2\omega_s}{\pi}t - 2, t\right) \tag{3.37}$$

to generate $s_1(t)$ and $s_2(t)$ respectively. Therefore it follows that the two switching functions can be written as follows:

$$s_1(t) = F\left(\frac{2\omega_s}{\pi}t, t\right) \quad \text{and} \quad s_2(t) = F\left(\frac{2\omega_s}{\pi}t - 2, t\right) \tag{3.38}$$

These two lines are shown in Figure 3-7.

In order to write an expression for the switching function $s_1(t)$, the value of h in $F(h, t)$ is substituted

into equation (3.14). The value of h for this case is as follows:

$$h = \frac{2\omega_s}{\pi}t \tag{3.39}$$

Substituting equation (3.39) into the term $\frac{m\pi h}{2}$ yields the following:

$$\frac{m\pi h}{2} = m\omega_s t \tag{3.40}$$

Substituting equation (3.40) into equation (3.14) results in $s_1(t)$ as follows:

$$\begin{aligned} s_1(t) = \frac{1}{2}A_{00} + \sum_{n=1}^{\infty}(A_{0n}\cos(n\omega_r t) + B_{0n}\sin(n\omega_r t)) + \\ \sum_{m=1}^{\infty}(A_{m0}\cos(m\omega_s t) + B_{m0}\sin(m\omega_s t)) + \\ \sum_{m=1}^{\infty}\sum_{n=\pm 1}^{\pm\infty}(A_{mn}\cos(m\omega_s t + n\omega_r t) + B_{mn}\sin(m\omega_s t + n\omega_r t)) \end{aligned} \tag{3.41}$$

In the same way an expression for the switching function $s_2(t)$ can be written by substituting the value of h in $F(h,t)$ in equation (3.14). The value of h for this case is as follows:

$$h = \frac{2\omega_s}{\pi}t - 2 \tag{3.42}$$

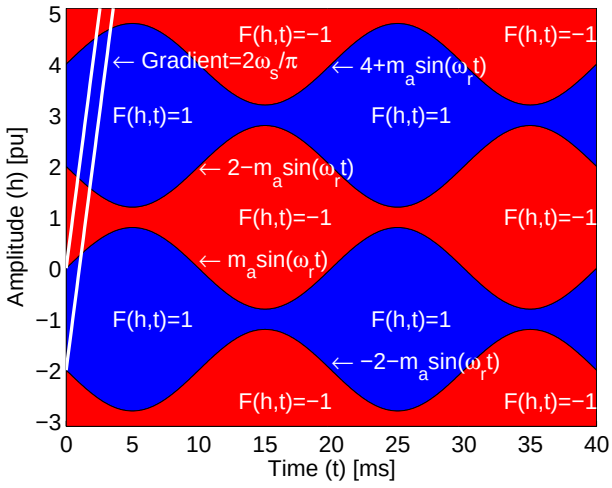

Figure 3-7. *Top view of the background functions for $s_1(t)$ and $s_2(t)$.*

Substituting equation (3.42) into the term $\frac{m\pi h}{2}$ yields the following:

$$\frac{m\pi h}{2} = m\omega_s t - m\pi \tag{3.43}$$

Substituting equation (3.43) into equation (3.14) results in $s_2(t)$ as follows:

$$\begin{aligned} s_2(t) = \frac{1}{2}A_{00} + \sum_{n=1}^{\infty}(A_{0n}\cos(n\omega_r t) + B_{0n}\sin(n\omega_r t)) + \\ \sum_{m=1}^{\infty}(A_{m0}\cos(m\omega_s t - m\pi) + B_{m0}\sin(m\omega_s t - m\pi)) + \\ \sum_{m=1}^{\infty}\sum_{n=\pm 1}^{\pm\infty}(A_{mn}\cos(m\omega_s t + n\omega_r t - m\pi) + B_{mn}\sin(m\omega_s t + n\omega_r t - m\pi)) \end{aligned} \tag{3.44}$$

Attention should be given to the trigonometric terms in equation (3.44) containing the term $-m\pi$. This term has the following effect on the trigonometric terms' signs in equation (3.44):

$$\cos(m\omega_s t - m\pi) = \begin{cases} \cos(m\omega_s t) & \text{if } m \text{ even} \\ -\cos(m\omega_s t) & \text{if } m \text{ odd} \end{cases} \tag{3.45}$$

$$\sin(m\omega_s t - m\pi) = \begin{cases} \sin(m\omega_s t) & \text{if } m \text{ even} \\ -\sin(m\omega_s t) & \text{if } m \text{ odd} \end{cases} \tag{3.46}$$

$$\cos(m\omega_s t + n\omega_r t - m\pi) = \begin{cases} \cos(m\omega_s t + n\omega_r t) & \text{if } m \text{ even} \\ -\cos(m\omega_s t + n\omega_r t) & \text{if } m \text{ odd} \end{cases} \tag{3.47}$$

$$\sin(m\omega_s t + n\omega_r t - m\pi) = \begin{cases} \sin(m\omega_s t + n\omega_r t) & \text{if } m \text{ even} \\ -\sin(m\omega_s t + n\omega_r t) & \text{if } m \text{ odd} \end{cases} \tag{3.48}$$

Using the above trigonometric identities, the expression for $s_2(t)$ can be rewritten as follows:

$$\begin{aligned} s_2(t) = \frac{1}{2}A_{00} + \sum_{n=1}^{\infty}(A_{0n}\cos(n\omega_r t) + B_{0n}\sin(n\omega_r t)) + \\ \sum_{m=2,4,\cdots}^{\infty}(A_{m0}\cos(m\omega_s t) + B_{m0}\sin(m\omega_s t)) - \\ \sum_{m=1,3,\cdots}^{\infty}(A_{m0}\cos(m\omega_s t) + B_{m0}\sin(m\omega_s t)) + \\ \sum_{m=2,4,\cdots}^{\infty}\sum_{n=\pm 1}^{\pm\infty}(A_{mn}\cos(m\omega_s t + n\omega_r t) + B_{mn}\sin(m\omega_s t + n\omega_r t)) - \\ \sum_{m=1,3,\cdots}^{\infty}\sum_{n=\pm 1}^{\pm\infty}(A_{mn}\cos(m\omega_s t + n\omega_r t) + B_{mn}\sin(m\omega_s t + n\omega_r t)) \end{aligned} \tag{3.49}$$

From the above expressions for $s_1(t)$ and $s_2(t)$ it is clear that their coefficients are of equal magnitude for all values of m, while they are of equal phase only around even multiples of the switching frequency. The phases of $s_1(t)$ and $s_2(t)$ differ by π radians around odd multiples of the switching frequency.

It is assumed throughout this chapter that the switching frequency (f_s) is chosen higher than the highest frequency component of the reference signal $f_r(t)$ so that the harmonics of the groups associated with the different values of m do not overlap. Therefore, using this assumption, the Fourier series components of $s_1(t)$ and $s_2(t)$ can be separated into two groups made up of different clusters of harmonics. Following this description, the harmonics of the switching functions can be classified into classes. Harmonics of *class zero* of a switching function are the set of Fourier series components for which $m = 2k$. In the same way, harmonics of *class one* are the set of Fourier series components for which $m = 2k + 1$.

Choosing $\omega = m\omega_s + n\omega_r \geq 0$, the following observations can be made about the Fourier series components and the Fourier transform of $s_1(t)$ and $s_2(t)$:

(a) Harmonics of *class zero*: these are harmonics of $s_1(t)$ and $s_2(t)$ which are equal in magnitude and in phase. In terms of the Fourier transforms of $s_1(t)$ and $s_2(t)$ the following is implied when $m = 2k$:

$$S_1(\omega) = S_2(\omega) \tag{3.50}$$

and

$$S_1(-\omega) = S_2(-\omega) \tag{3.51}$$

(b) Harmonics of *class one*: these are harmonics of $s_1(t)$ and $s_2(t)$ where the Fourier series components of $s_2(t)$ lag those of $s_1(t)$ by π radians. In terms of the Fourier transforms of $s_1(t)$ and $s_2(t)$, this can be written for $m = 2k + 1$ as follows:

$$S_2(\omega) = S_1(\omega)e^{-j\pi} \tag{3.52}$$

and

$$S_2(-\omega) = S_1(-\omega)e^{j\pi} \tag{3.53}$$

The phasor representations of $S_1(\omega)$ and $S_2(\omega)$ are shown in Figure 3-8.

The above observations in conjunction with the phasors shown in Figure 3-8 can also be used to deduce the following properties regarding the switching functions $s_d(t)$ and $s_t(t)$:

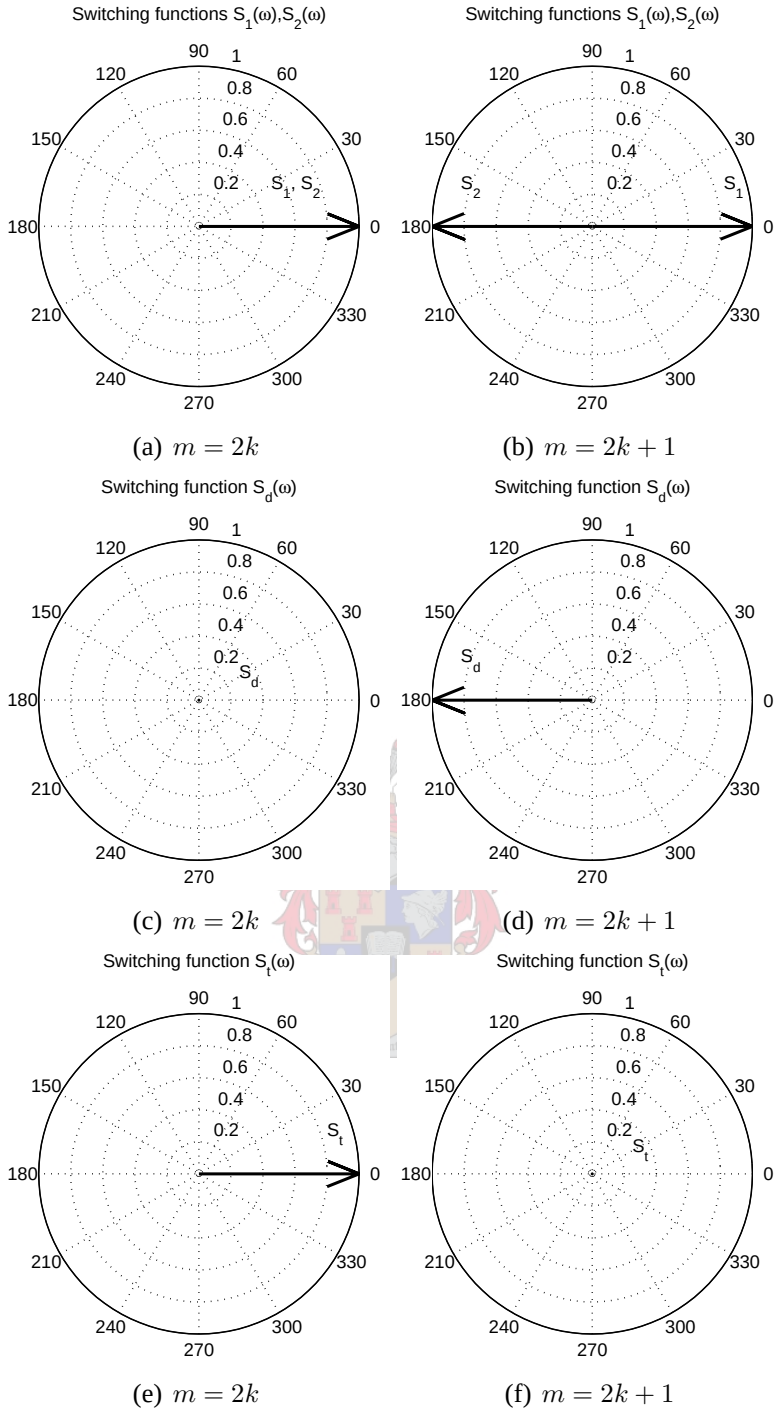

(a) $m = 2k$ (b) $m = 2k + 1$

(c) $m = 2k$ (d) $m = 2k + 1$

(e) $m = 2k$ (f) $m = 2k + 1$

Figure 3-8. *Phasor representation of the switching functions for a 2-cell inverter.*

(a) The "total" switching function contains only harmonics of *class zero*. This means that $s_t(t)$ contains the frequency components of the reference signal as well as the harmonic components of $s_1(t)$ around even multiples of the switching frequency, whereas the harmonics around odd multiples of the switching frequency are cancelled out. This can be seen by comparing $S_t(\omega)$ shown in Figure 3-8(e) with Figure 3-8(f). Therefore, it can be said that the remaining

harmonics of $s_t(t)$ are equal in magnitude and phase to the corresponding components of $s_1(t)$, with the exception of the additional harmonic content of the reference signal $f_r(t)$.

(b) The "difference" switching function contains only harmonics of *class one*, which means that it contains only the harmonic components of $s_1(t)$ around odd multiples of the switching frequency, while the harmonics around even multiples cancel out. There is no additional harmonic content in $s_d(t)$ due to the reference signal, as these components cancel each other out. Thus, the harmonic content of $s_d(t)$ are equal in magnitude and phase to that of the corresponding harmonics of $s_1(t)$. This can be seen by comparing $S_d(\omega)$ shown in Figure 3-8(c) with Figure 3-8(d).

(c) The above two conclusions lead to the following important conclusion:

$$|S_d(\omega)|\,|S_t(\omega)| \approx 0 \tag{3.54}$$

This property will be used extensively in the following sections.

In the above expressions for $s_1(t)$ and $s_2(t)$ it is important to look at the characteristics of the Fourier coefficients. The coefficients A_{mn} and B_{mn} are the same as that for the "single"-cell case which were calculated in the previous section.

The functions $s_d(t)$ and $s_t(t)$ were defined in the previous chapter and repeated earlier in this section as equations (3.35) and (3.36).

Substituting $s_1(t)$ and $s_2(t)$ into (3.35) and (3.36) results in the following expressions for the "difference" and "total" switching functions:

$$\begin{aligned} s_d(t) = &- \sum_{m=1,3,\cdots}^{\infty} (A_{m0}\cos(m\omega_s t) + B_{m0}\sin(m\omega_s t)) - \\ &\sum_{m=1,3,\cdots}^{\infty} \sum_{n=\pm 1}^{\pm\infty} (A_{mn}\cos(m\omega_s t + n\omega_r t) + B_{mn}\sin(m\omega_s t + n\omega_r t)) \end{aligned} \tag{3.55}$$

$$\begin{aligned} s_t(t) = &\frac{1}{2}A_{00} + \sum_{n=1}^{\infty}(A_{0n}\cos(n\omega_r t) + B_{0n}\sin(n\omega_r t)) + \\ &\sum_{m=2,4,\cdots}^{\infty} (A_{m0}\cos(m\omega_s t) + B_{m0}\sin(m\omega_s t)) + \\ &\sum_{m=2,4,\cdots}^{\infty} \sum_{n=\pm 1}^{\pm\infty} (A_{mn}\cos(m\omega_s t + n\omega_r t) + B_{mn}\sin(m\omega_s t + n\omega_r t)) \end{aligned} \tag{3.56}$$

The frequency spectra of $|S_1(\omega)|$, $|S_d(\omega)|$, $|S_t(\omega)|$ and $|S_d(\omega)||S_t(\omega)|$ for different modulation indices are plotted and compared in the following example.

Example 3.4

In this example, $f_r(t)$ is defined as follows:

$$f_r(t) = m_a \sin(\omega_r t) \tag{3.57}$$

The switching frequency $f_s = 5\ kHz$ and the reference frequency $f_r = 50\ Hz$. Three different values are used for the modulation index m_a. These values are as follows: $1.0, 0.8$ and 0.6.

- For $m_a = 1.0$, $f_r(t) = \sin(\omega_r t)$. The spectra of $|S_1(\omega)|$, $|S_d(\omega)|$, $|S_t(\omega)|$ and of $|S_d(\omega)||S_t(\omega)|$ for this case are shown in Figure 3-9.

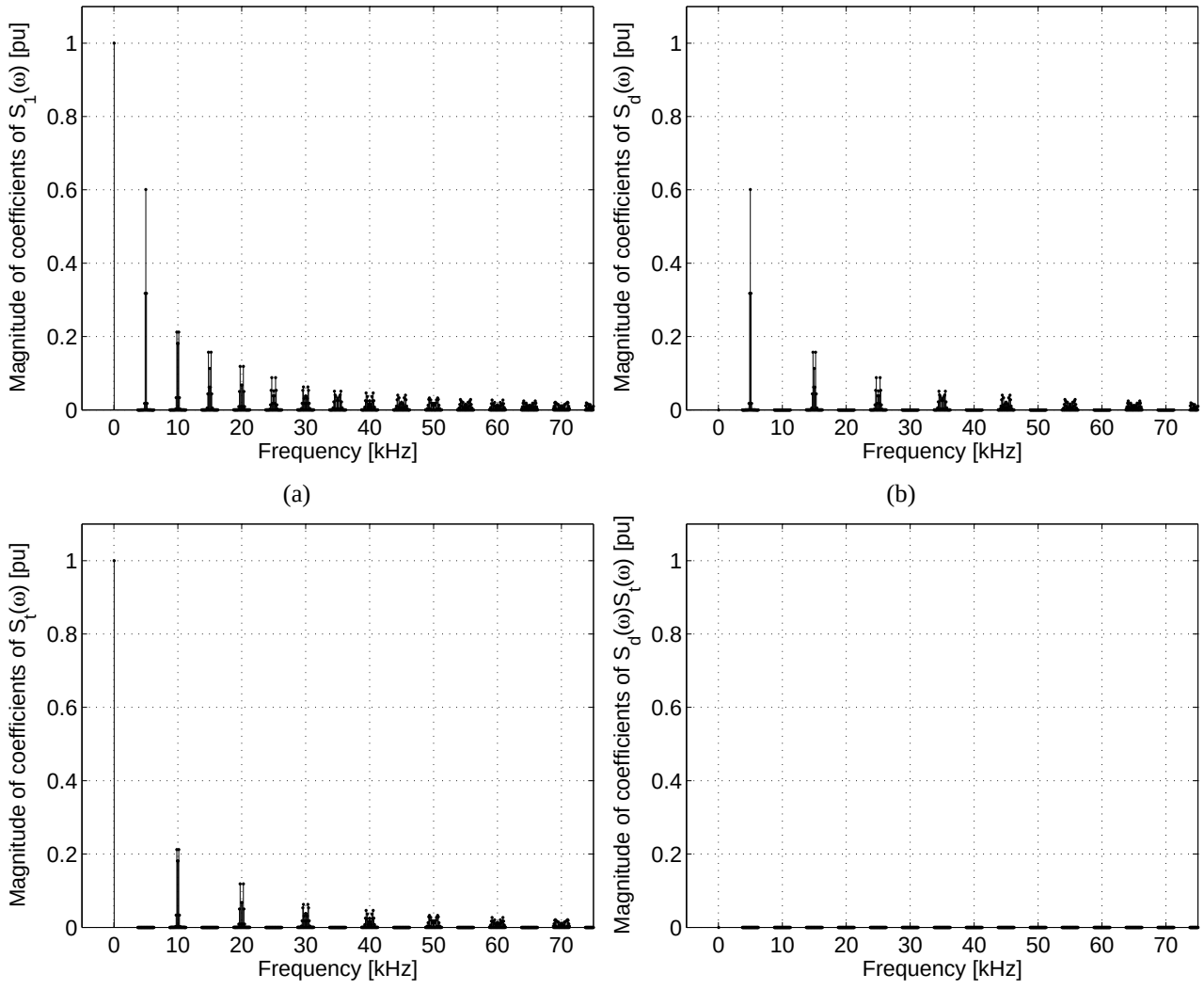

Figure 3-9. *Harmonics of 2-cell switching with* $m_a = 1.0$, $f_r = 50\ Hz$ *and* $f_s = 5\ kHz$.

The spectra of $S_d(\omega)$ are centred around odd multiples of the switching frequency f_s, while the spectra of $S_t(\omega)$ are centred around even multiples thereof. The harmonic at the fundamental frequency is cancelled out in $S_d(\omega)$, while it remains in $S_t(\omega)$. It is clear from Figure 3-9 that the spectra of $S_d(\omega)$ and $S_t(\omega)$ do not overlap, due to the fact that the spectra of $|S_d(\omega)||S_t(\omega)| \approx 0$ in Figure 3-9(d).

- For $m_a = 0.8$, $f_r(t) = 0.8\sin(\omega_r t)$. The spectra of $|S_1(\omega)|$, $|S_d(\omega)|$, $|S_t(\omega)|$ and of $|S_d(\omega)||S_t(\omega)|$ for this case are shown in Figure 3-10.

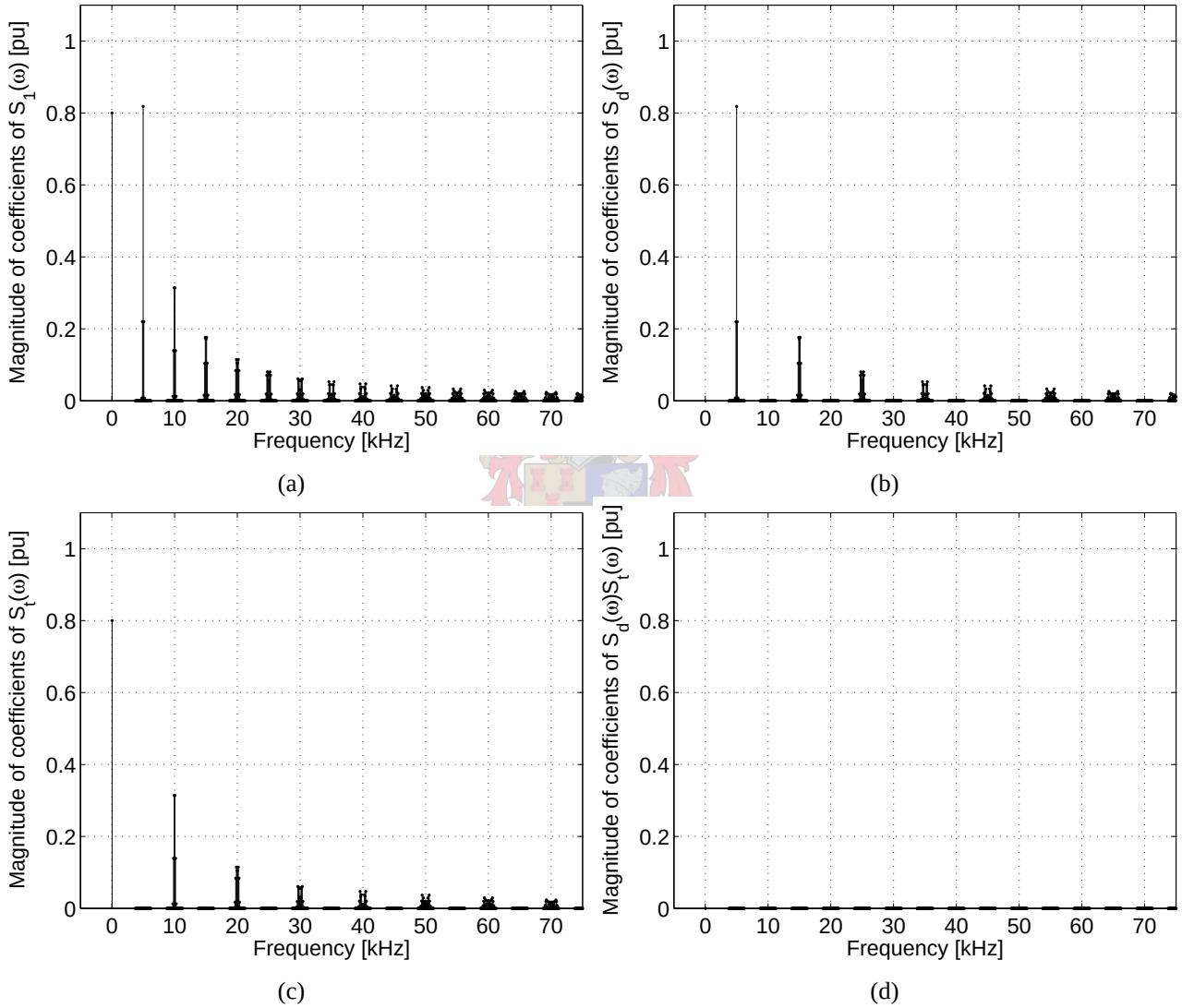

Figure 3-10. *Harmonics of* 2*-cell switching with* $m_a = 0.8$, $f_r = 50\ Hz$ *and* $f_s = 5\ kHz$.

Again, the spectra of $S_d(\omega)$ are centred around odd multiples of the switching frequency f_s, while the spectra of $S_t(\omega)$ are centred around even multiples thereof. The harmonic at the fundamental frequency is also cancelled out in $S_d(\omega)$, while it remains in $S_t(\omega)$. As for the $m_a = 1.0$ case, it is clear from Figure 3-10 that the spectra of $S_d(\omega)$ and $S_t(\omega)$ do not overlap, due to the fact that the spectra of $|S_d(\omega)||S_t(\omega)| \approx 0$ in Figure 3-10(d). When comparing Figures 3-9 and 3-10, it can be seen that the magnitude of the harmonics at both odd and even

multiples of f_s increase when m_a is decreased. This will be confirmed if this trend is repeated for $m_a = 0.6$.

- For $m_a = 0.6$, $f_r(t) = 0.6\sin(\omega_r t)$. The spectra of $|S_1(\omega)|$, $|S_d(\omega)|$, $|S_t(\omega)|$ and of $|S_d(\omega)||S_t(\omega)|$ for this case are shown in Figure 3-11.

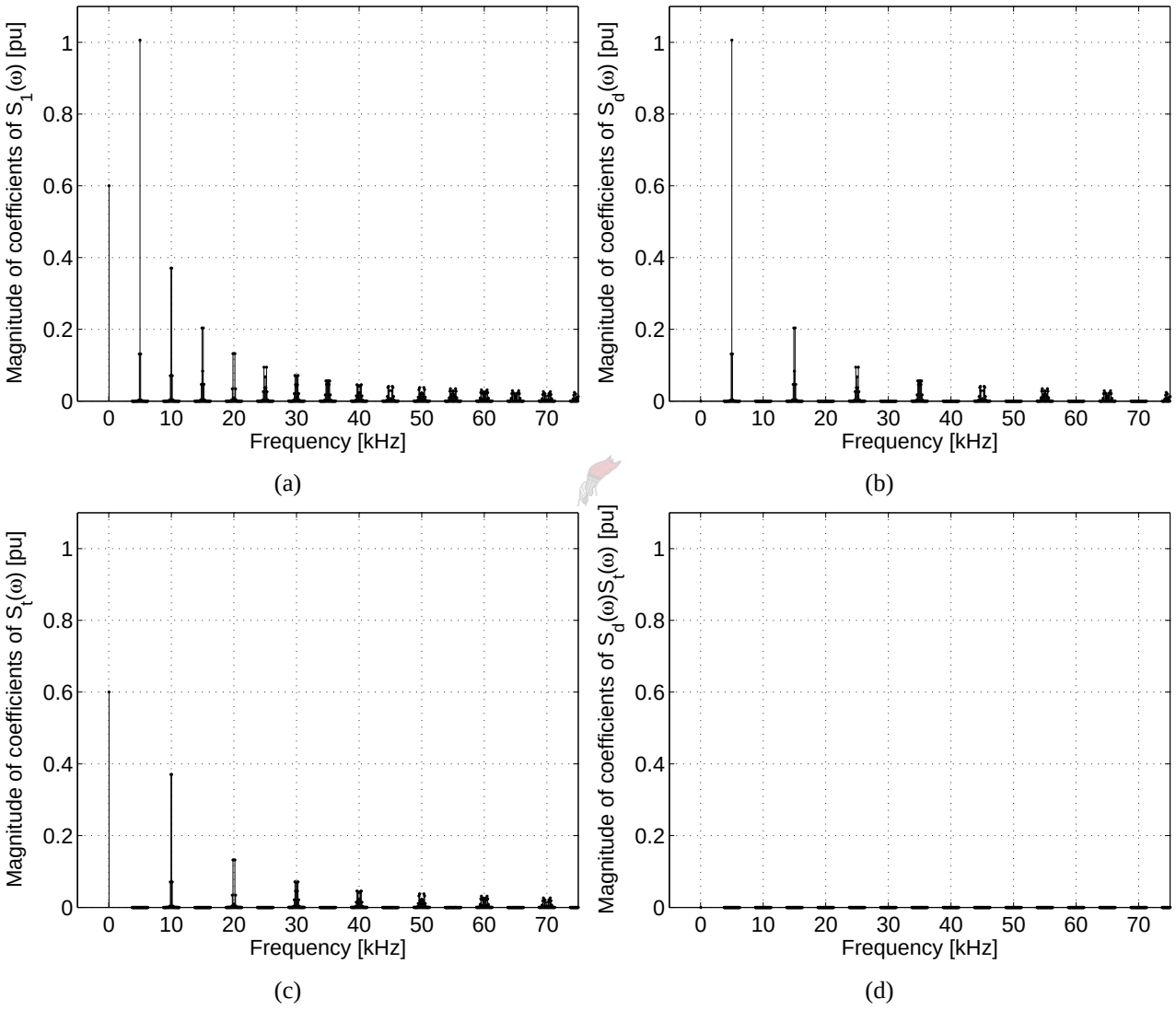

Figure 3-11. *Harmonics of* 2*-cell switching with* $m_a = 0.6$*,* $f_r = 50\ Hz$ *and* $f_s = 5\ kHz$*.*

For this final case, the spectra of $S_d(\omega)$ and $S_t(\omega)$ exhibit the same characteristics as seen in the previous two cases. As for the previous cases of $m_a = 1.0$ and $m_a = 0.8$, it is clear from Figure 3-11 that the spectra of $S_d(\omega)$ and $S_t(\omega)$ do not overlap. This proves that $|S_d(\omega)||S_t(\omega)| \approx 0$. When comparing Figures 3-9, 3-10 and 3-11, it can be seen that the magnitude of the harmonics at both odd and even multiples of f_s increase as m_a is decreased. From the above-mentioned cases it can also be seen in Figures 3-9(a) through 3-11(a) that the magnitude of the harmonic of the reference at the fundamental frequency of $S_1(\omega)$ is a maximum for $m_a = 1.0$ and decreases as m_a is decreased.

3.3.1.3 Switching functions of 3-cell interleaved switching

The switching functions are defined in the same way as for the 2-cell case, except that there are 3 switching functions in this case. The states that the switching functions can assume were defined in Chapter 2 section 2.4 and are repeated here for convenience as follows:

$$s_1(t) = \begin{cases} 1 & \text{if } f_{c_1}(t) < f_r(t) \\ -1 & \text{if } f_r(t) < f_{c_1}(t) \end{cases} \tag{3.58}$$

$$s_2(t) = \begin{cases} 1 & \text{if } f_{c_2}(t) < f_r(t) \\ -1 & \text{if } f_r(t) < f_{c_3}(t) \end{cases} \tag{3.59}$$

$$s_3(t) = \begin{cases} 1 & \text{if } f_{c_3}(t) < f_r(t) \\ -1 & \text{if } f_r(t) < f_{c_3}(t) \end{cases} \tag{3.60}$$

The reference signal is again chosen to be sinusoidal with an angular frequency of ω_r and the carrier signal is chosen to be triangular with an angular frequency of ω_s.

For the 3-cell case, interleaved PWM is generated by using 3 carrier waves that are phase-shifted by 120°. One carrier is used to generate the PWM of each respective cell by comparing it with the same reference signal. These three carriers can be written as follows:

$$f_{c_1}(t) = \frac{2}{\pi}\arcsin\left[\sin\left(\omega_s t\right)\right] \tag{3.61}$$

$$f_{c_2}(t) = \frac{2}{\pi}\arcsin\left[\sin\left(\omega_s t - \frac{2\pi}{3}\right)\right] \tag{3.62}$$

$$f_{c_3}(t) = \frac{2}{\pi}\arcsin\left[\sin\left(\omega_s t - \frac{4\pi}{3}\right)\right] \tag{3.63}$$

Interleaved switching for a 3-cell multicell converter is illustrated in the following example.

Example 3.5

A 3-cell multicell converter is switched using interleaved PWM under sinusoidal modulation. The sinusoidal reference signal $f_r(t)$ has a frequency of $50\ Hz$, a modulation index of 0.8 and is defined as follows:

$$f_r(t) = 0.8\sin(\omega_r t) \tag{3.64}$$

where $\omega_r = 2\pi \cdot 50$ and the switching frequency $f_s = 500\ Hz$.

In order to generate the switching functions, three triangular carriers are used. Each of the three carriers are successively 120° out of phase. The generation of the switching function of the first cell, i.e. $s_1(t)$ is shown in Figure 3-12(a). The carrier signal of the first cell is denoted by $f_{c_1}(t)$ and shown

in green, while the reference signal is shown in blue.

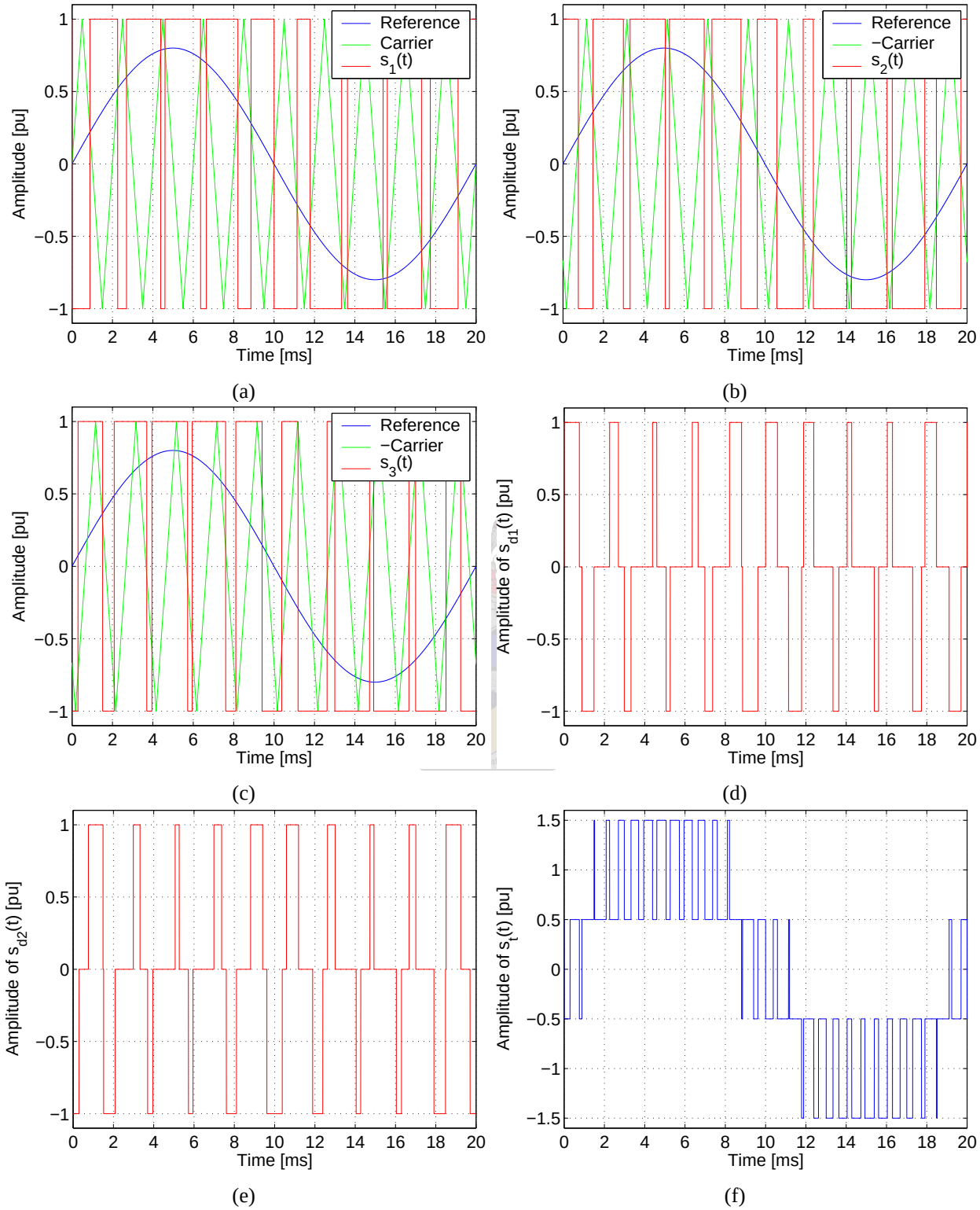

Figure 3-12. *Switching function generation for a 3-cell multicell inverter using interleaved switching.*

The generation of the switching function of the second cell, i.e. $s_2(t)$ is shown in Figure 3-12(b). The

switching function $s_3(t)$ is shown in Figure 3-12(c). The carrier signals of all the cells are shown in green, while the reference signal is shown in blue.

The two "difference" switching functions $s_{d_1}(t)$ and $s_{d_2}(t)$ and the "total" switching function $s_t(t)$ are shown respectively in Figures 3-12(d) through 3-12(f). These switching functions were defined in equations (2.35), (2.36) and (2.37) in Chapter 2 section 2.9 and are repeated here for convenience as follows:

$$s_{d_1}(t) = \frac{1}{2}\{s_2(t) - s_1(t)\} \tag{3.65}$$

$$s_{d_2}(t) = \frac{1}{2}\{s_3(t) - s_2(t)\} \tag{3.66}$$

$$s_t(t) = \frac{1}{2}\{s_1(t) + s_2(t) + s_3(t)\} \tag{3.67}$$

The figures shown in Figure 3-12 only show the first cycle of the reference signal $f_r(t)$, but these signals continue for all $t \geq 0$.

The same approach used for the "single"- and 2-cell multicell converters is now used for the 3-cell case. For a 3-cell multicell converter under interleaved switching, the three switching functions are denoted by $s_1(t)$, $s_2(t)$ and $s_3(t)$. Due to interleaved switching, the carriers of the three cells are $\frac{2\pi}{3}$ radians out of phase, i.e. the carrier of cell 2 lags that of cell 1 by $\frac{2\pi}{3}$ radians and the carrier of cell 3 lags that of cell 2 by $\frac{2\pi}{3}$ radians. The first line in the TOH-plane is again the same as that for the "single"-cell case discussed in an earlier section. This line is given by the following straight line equation in the TOH-plane:

$$h = \frac{2\omega_s}{\pi}t \tag{3.68}$$

The second line is parallel to the first line, which means that it has the same gradient as the first line and an h-axis intersection of c_1. This line can be written as follows:

$$h = \frac{2\omega_s}{\pi}t + c_1 \tag{3.69}$$

The intersection c_1 can be determined by substituting the t-axis intersection, i.e. the point where $h = 0$ and $t = \frac{2\pi}{3\omega_s}$, into equation (3.69). This results in $c_1 = -\frac{4}{3}$. The second line can thus be written as follows:

$$h = \frac{2\omega_s}{\pi}t - \frac{4}{3} \tag{3.70}$$

The third line is again parallel to the first line, which means that it has the same gradient as the first line and an h-axis intersection of c_2. This line can be written as follows:

$$h = \frac{2\omega_s}{\pi}t + c_2 \tag{3.71}$$

The intersection c_2 can be determined by substituting the t-axis intersection, i.e. the point where $h = 0$ and $t = \frac{4\pi}{3\omega_s}$, into equation (3.71). This results in $c_2 = -\frac{8}{3}$. The third line can be written as follows:

$$h = \frac{2\omega_s}{\pi}t - \frac{8}{3} \tag{3.72}$$

This results in the following three lines in the TOH-plane:

$$\left(\frac{2\omega_s}{\pi}t, t\right) \quad , \quad \left(\frac{2\omega_s}{\pi}t - \frac{4}{3}, t\right) \quad \text{and} \quad \left(\frac{2\omega_s}{\pi}t - \frac{8}{3}, t\right) \tag{3.73}$$

to generate $s_1(t)$, $s_2(t)$ and $s_3(t)$ respectively. The three switching functions can therefore be written as follows:

$$s_1(t) = F\left(\frac{2\omega_s}{\pi}t, t\right) \quad , \quad s_2(t) = F\left(\frac{2\omega_s}{\pi}t - \frac{4}{3}, t\right) \quad \text{and} \quad s_3(t) = F\left(\frac{2\omega_s}{\pi}t - \frac{8}{3}, t\right) \tag{3.74}$$

The above three lines are shown in Figure 3-13.

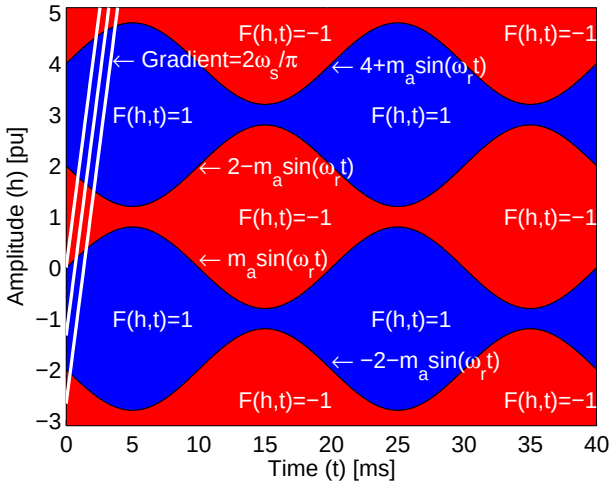

Figure 3-13. *Top view of the background functions for $s_1(t)$, $s_2(t)$ and $s_3(t)$.*

The expression for the switching function $s_1(t)$ is exactly the same as for the 2-cell case which was calculated as equation (3.41). This result is repeated here for convenience as follows:

$$\begin{aligned} s_1(t) = \frac{1}{2}A_{00} + \sum_{n=1}^{\infty}(A_{0n}\cos(n\omega_r t) + B_{0n}\sin(n\omega_r t)) + \\ \sum_{m=1}^{\infty}(A_{m0}\cos(m\omega_s t) + B_{m0}\sin(m\omega_s t)) + \\ \sum_{m=1}^{\infty}\sum_{n=\pm 1}^{\pm\infty}(A_{mn}\cos(m\omega_s t + n\omega_r t) + B_{mn}\sin(m\omega_s t + n\omega_r t)) \end{aligned} \tag{3.75}$$

An expression for the switching function $s_2(t)$ can be written by substituting the value of h in $F(h,t)$

in equation (3.14). The value of h for this case is as follows:

$$h = \frac{2\omega_s}{\pi}t - \frac{4}{3} \tag{3.76}$$

Substituting equation (3.76) into the term $\frac{m\pi h}{2}$ yields the following:

$$\frac{m\pi h}{2} = m\omega_s t - \frac{2m\pi}{3} \tag{3.77}$$

Substituting equation (3.77) into equation (3.14) results in $s_2(t)$ as follows:

$$\begin{aligned} s_2(t) = \frac{1}{2}A_{00} + \sum_{n=1}^{\infty}(A_{0n}\cos(n\omega_r t) + B_{0n}\sin(n\omega_r t)) + \\ \sum_{m=1}^{\infty}\left\{A_{m0}\cos\left(m\omega_s t - \frac{2m\pi}{3}\right) + B_{m0}\sin\left(m\omega_s t - \frac{2m\pi}{3}\right)\right\} + \\ \sum_{m=1}^{\infty}\sum_{n=\pm 1}^{\pm\infty}\left\{A_{mn}\cos\left(m\omega_s t + n\omega_r t - \frac{2m\pi}{3}\right) + B_{mn}\sin\left(m\omega_s t + n\omega_r t - \frac{2m\pi}{3}\right)\right\} \end{aligned} \tag{3.78}$$

In the same way an expression for the switching function $s_3(t)$ can be written by substituting the value of h in $F(h,t)$ in equation (3.14). The value of h for this case is as follows:

$$h = \frac{2\omega_s}{\pi}t - \frac{8}{3} \tag{3.79}$$

Substituting equation (3.79) into the term $\frac{m\pi h}{2}$ yields the following:

$$\frac{m\pi h}{2} = m\omega_s t - \frac{4m\pi}{3} \tag{3.80}$$

Substituting equation (3.80) into equation (3.14) results in $s_3(t)$ as follows:

$$\begin{aligned} s_3(t) = \frac{1}{2}A_{00} + \sum_{n=1}^{\infty}(A_{0n}\cos(n\omega_r t) + B_{0n}\sin(n\omega_r t)) + \\ \sum_{m=1}^{\infty}\left\{A_{m0}\cos\left(m\omega_s t - \frac{4m\pi}{3}\right) + B_{m0}\sin\left(m\omega_s t - \frac{4m\pi}{3}\right)\right\} + \\ \sum_{m=1}^{\infty}\sum_{n=\pm 1}^{\pm\infty}\left\{A_{mn}\cos\left(m\omega_s t + n\omega_r t - \frac{4m\pi}{3}\right) + B_{mn}\sin\left(m\omega_s t + n\omega_r t - \frac{4m\pi}{3}\right)\right\} \end{aligned}$$

$$
\begin{aligned}
&= \frac{1}{2}A_{00} + \sum_{n=1}^{\infty}(A_{0n}\cos(n\omega_r t) + B_{0n}\sin(n\omega_r t)) + \\
&\sum_{m=1}^{\infty}\left\{A_{m0}\cos\left(m\omega_s t + \frac{2m\pi}{3}\right) + B_{m0}\sin\left(m\omega_s t + \frac{2m\pi}{3}\right)\right\} + \\
&\sum_{m=1}^{\infty}\sum_{n=\pm 1}^{\pm\infty}\left\{A_{mn}\cos\left(m\omega_s t + n\omega_r t + \frac{2m\pi}{3}\right) + B_{mn}\sin\left(m\omega_s t + n\omega_r t + \frac{2m\pi}{3}\right)\right\}
\end{aligned}
\tag{3.81}
$$

Attention should be given to the trigonometric terms in equations (3.78) and (3.81) containing the terms $\pm\frac{2m\pi}{3}$. These terms have the following effect on the trigonometric terms' signs:

$$
\cos\left(m\omega_s t + n\omega_r t - \frac{2m\pi}{3}\right) = \begin{cases} \cos(m\omega_s t + n\omega_r t) & \text{for } m = 3k \\ \cos\left(m\omega_s t + n\omega_r t - \frac{2\pi}{3}\right) & \text{for } m = 3k+1 \\ \cos\left(m\omega_s t + n\omega_r t + \frac{2\pi}{3}\right) & \text{for } m = 3k+2 \end{cases} \tag{3.82}
$$

and

$$
\sin\left(m\omega_s t + n\omega_r t - \frac{2m\pi}{3}\right) = \begin{cases} \sin(m\omega_s t + n\omega_r t) & \text{for } m = 3k \\ \sin\left(m\omega_s t + n\omega_r t - \frac{2\pi}{3}\right) & \text{for } m = 3k+1 \\ \sin\left(m\omega_s t + n\omega_r t + \frac{2\pi}{3}\right) & \text{for } m = 3k+2 \end{cases} \tag{3.83}
$$

where $k = 0, \pm 1, \pm 2, \ldots$. For the same values of k the following is also true:

$$
\cos\left(m\omega_s t + n\omega_r t + \frac{2m\pi}{3}\right) = \begin{cases} \cos(m\omega_s t + n\omega_r t) & \text{for } m = 3k \\ \cos\left(m\omega_s t + n\omega_r t + \frac{2\pi}{3}\right) & \text{for } m = 3k+1 \\ \cos\left(m\omega_s t + n\omega_r t - \frac{2\pi}{3}\right) & \text{for } m = 3k+2 \end{cases} \tag{3.84}
$$

and

$$
\sin\left(m\omega_s t + n\omega_r t + \frac{2m\pi}{3}\right) = \begin{cases} \sin(m\omega_s t + n\omega_r t) & \text{for } m = 3k \\ \sin(m\omega_s t + n\omega_r t + \frac{2\pi}{3}) & \text{for } m = 3k+1 \\ \sin(m\omega_s t + n\omega_r t - \frac{2\pi}{3}) & \text{for } m = 3k+2 \end{cases} \tag{3.85}
$$

From the above expressions for $s_1(t)$, $s_2(t)$ and $s_3(t)$ it is clear that their coefficients are of equal magnitude for all values of m, while they are of equal phase only around multiples of three times the switching frequency. The phases of $s_1(t)$, $s_2(t)$ and $s_3(t)$ differ by $\pm\frac{2\pi}{3}$ radians around multiples m of the switching frequency where $m = 3k+1$ and $m = 3k+2$ for $k = 0, \pm 1, \pm 2, \ldots$.

It was mentioned earlier in this chapter that the switching frequency f_s is chosen higher than the highest frequency component of the reference signal $f_r(t)$ so that the harmonics of the groups associated with the different values of m do not overlap. Therefore, using this assumption, the Fourier series

components of $s_1(t)$, $s_2(t)$ and $s_3(t)$ can be separated into three groups made up of different clusters of harmonics. As in the previous section, the harmonics of the switching functions are also classified into classes. Harmonics of *class zero* of a switching function are the set of Fourier series components for which $m = 3k$. In the same way, harmonics of *class one* are the set of Fourier series components for which $m = 3k + 1$ and the harmonics of *class two* are the set of Fourier series components for which $m = 3k + 2$.

As in the previous section, ω is chosen so that $\omega = m\omega_s + n\omega_r \geq 0$. Therefore, the following observations can be made about the Fourier series components and the Fourier transforms of $s_1(t)$, $s_2(t)$ and $s_3(t)$:

(a) Harmonics of *class zero*: these are harmonics of $s_1(t)$, $s_2(t)$ and $s_3(t)$ which are equal in magnitude and in phase. In terms of the Fourier transforms of $s_1(t)$, $s_2(t)$ and $s_3(t)$ the following is implied when $m = 3k$:

$$S_1(\omega) = S_2(\omega) = S_3(\omega) \tag{3.86}$$

and

$$S_1(-\omega) = S_2(-\omega) = S_3(-\omega) \tag{3.87}$$

(b) Harmonics of *class one*: these are harmonics of $s_1(t)$, $s_2(t)$ and $s_3(t)$ where the Fourier series components of $s_2(t)$ lag those of $s_1(t)$ by $\frac{2\pi}{3}$ radians and that of $s_3(t)$ lead those of $s_1(t)$ by $\frac{2\pi}{3}$ radians. In terms of the Fourier transforms of $s_1(t)$, $s_2(t)$ and $s_3(t)$, this can be written for $m = 3k + 1$ as follows:

$$S_2(\omega) = S_1(\omega)e^{-j\frac{2\pi}{3}} \text{ and } S_3(\omega) = S_1(\omega)e^{j\frac{2\pi}{3}} \tag{3.88}$$

and

$$S_2(-\omega) = S_1(-\omega)e^{j\frac{2\pi}{3}} \text{ and } S_3(-\omega) = S_1(-\omega)e^{-j\frac{2\pi}{3}} \tag{3.89}$$

(c) Harmonics of *class two*: these are harmonics of $s_1(t)$, $s_2(t)$ and $s_3(t)$ where the Fourier series components of $s_2(t)$ lead those of $s_1(t)$ by $\frac{2\pi}{3}$ radians and that of $s_3(t)$ lag those of $s_1(t)$ by $\frac{2\pi}{3}$ radians. In terms of the Fourier transforms of $s_1(t)$, $s_2(t)$ and $s_3(t)$, this can be written for $m = 3k + 2$ as follows:

$$S_2(\omega) = S_1(\omega)e^{j\frac{2\pi}{3}} \text{ and } S_3(\omega) = S_1(\omega)e^{-j\frac{2\pi}{3}} \tag{3.90}$$

and

$$S_2(-\omega) = S_1(-\omega)e^{-j\frac{2\pi}{3}} \text{ and } S_3(-\omega) = S_1(-\omega)e^{j\frac{2\pi}{3}} \tag{3.91}$$

The phasor representations of $S_1(\omega)$, $S_2(\omega)$ and $S_3(\omega)$ for the above-mentioned cases are shown in Figures 3-14(a) through 3-14(c). Phasor representations of $S_{d_1}(\omega)$, $S_{d_2}(\omega)$ and $S_t(\omega)$ are obtained using relationships previously mentioned and are shown in Figures 3-14(d) through 3-14(i).

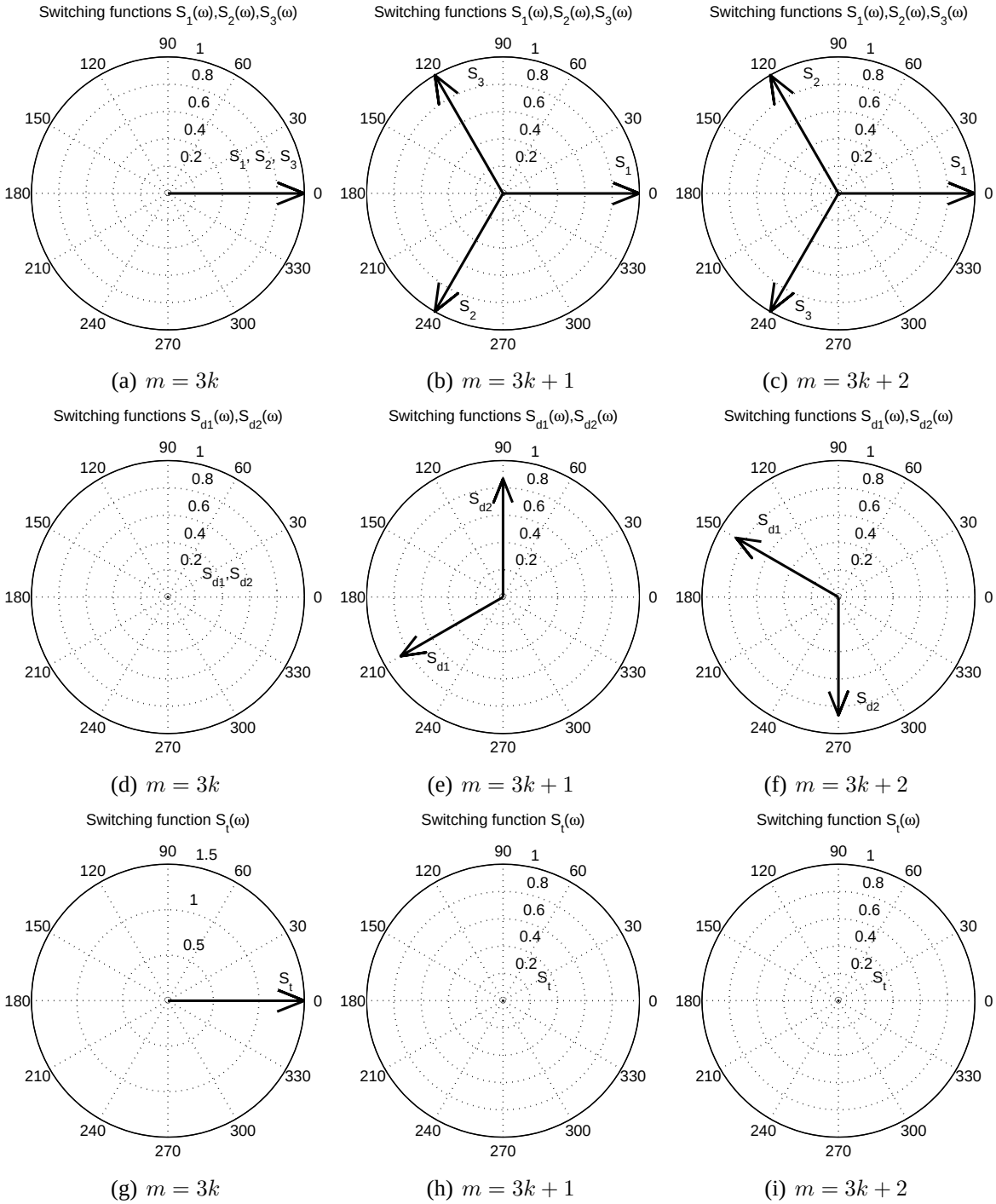

(a) $m = 3k$ (b) $m = 3k + 1$ (c) $m = 3k + 2$

(d) $m = 3k$ (e) $m = 3k + 1$ (f) $m = 3k + 2$

(g) $m = 3k$ (h) $m = 3k + 1$ (i) $m = 3k + 2$

Figure 3-14. *Phasor representation of the switching functions for a* 3*-cell inverter.*

The above observations as well as that of the phasors shown in Figure 3-14 can be used to deduce the following properties regarding the switching functions $s_{d_1}(t)$, $s_{d_2}(t)$ and $s_t(t)$:

(a) The "total" switching function contains only harmonics of *class zero*. This means that $s_t(t)$ contains the frequency components of the reference signal as well as the harmonic components of $s_1(t)$ around integer multiples of three times the switching frequency. This can be seen in Figures 3-14(g) through 3-14(i).

(b) The "difference" switching functions $s_{d_1}(t)$ and $s_{d_2}(t)$ contain harmonics of *class one* and *class two*, which means that it contains only the harmonic components of $s_1(t)$ around multiples m of the switching frequency where $m = 3k + 1$ and $m = 3k + 2$ for $k = 0, \pm 1, \pm 2, \ldots$. This can be seen in Figures 3-14(d) through 3-14(f). The following relationships between S_{d_2} and S_{d_1} can be concluded from Figures 3-14(d) through 3-14(i):

$$S_{d_2}(\omega) = \begin{cases} S_{d_1}(\omega)e^{-j\frac{2\pi}{3}} & \text{if } m = 3k+1 \\ S_{d_1}(\omega)e^{j\frac{2\pi}{3}} & \text{if } m = 3k+2 \end{cases} \tag{3.92}$$

and

$$S_{d_2}(-\omega) = \begin{cases} S_{d_1}(-\omega)e^{j\frac{2\pi}{3}} & \text{if } m = 3k+1 \\ S_{d_1}(-\omega)e^{-j\frac{2\pi}{3}} & \text{if } m = 3k+2 \end{cases} \tag{3.93}$$

(c) The above two conclusions lead to the following important conclusions:

$$|S_{d_1}(\omega)|\,|S_t(\omega)| \approx 0 \tag{3.94}$$

and

$$|S_{d_2}(\omega)|\,|S_t(\omega)| \approx 0 \tag{3.95}$$

These properties will also be used extensively in the next chapter. The frequency spectra of $|S_1(\omega)|$, $|S_{d_1}(\omega)|$, $|S_t(\omega)|$ and $|S_{d_1}(\omega)||S_t(\omega)|$ for different modulation indices are plotted and compared in the following example.

Example 3.6

The previous example shown for the 2-cell case is repeated here for the 3-cell case. The reference $f_r(t)$ is defined as follows:

$$f_r(t) = m_a \sin(\omega_r t) \tag{3.96}$$

The switching frequency $f_s = 5\ kHz$ and the reference frequency $f_r = 50\ Hz$. Three different values are used for the modulation index m_a. These values are as follows: $1.0, 0.8$ and 0.6.

- For $m_a = 1.0$, $f_r(t) = \sin(\omega_r t)$. The spectra of $|S_1(\omega)|$, $|S_{d_1}(\omega)|$, $|S_t(\omega)|$ and of $|S_{d_1}(\omega)||S_t(\omega)|$ for this case are shown in Figure 3-15.

  The spectra of $S_{d_1}(\omega)$ are centred around multiples m of the switching frequency f_s where $m = 3k + 1$ and $m = 3k + 2$ for $k = 0, \pm 1, \pm 2, \ldots$. However, the spectra of $S_t(\omega)$ are centred

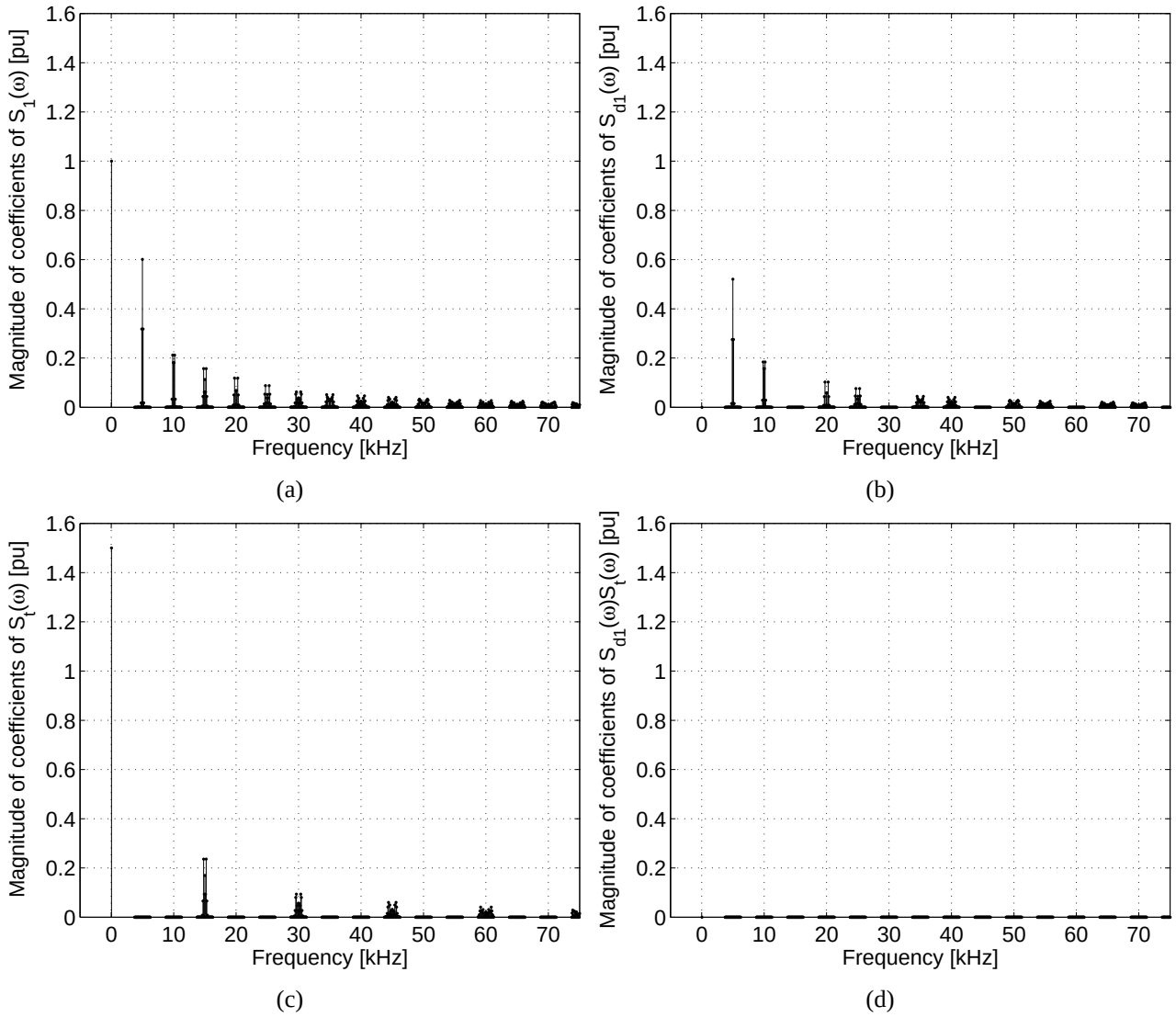

Figure 3-15. *Harmonics of* 3*-cell switching with* $m_a = 1.0$*,* $f_r = 50\ Hz$ *and* $f_s = 5\ kHz$*.*

around multiples of three times the switching frequency. As in the 2-cell case, the harmonic at the fundamental frequency is cancelled out in $S_{d_1}(\omega)$, while it remains in $S_t(\omega)$. It is clear from Figure 3-15 that the spectra of $S_{d_1}(\omega)$ and $S_t(\omega)$ do not overlap, due to the fact that the spectra of $|S_{d_1}(\omega)||S_t(\omega)| \approx 0$ in Figure 3-15(d).

- For $m_a = 0.8$, $f_r(t) = 0.8\sin(\omega_r t)$. The spectra of $|S_1(\omega)|$, $|S_{d_1}(\omega)|$, $|S_t(\omega)|$ and of $|S_{d_1}(\omega)||S_t(\omega)|$ for this case are shown in Figure 3-16.

  The spectra of $S_{d_1}(\omega)$ and $S_t(\omega)$ are centred around the same multiples of the switching frequency f_s as for the case where $m_a = 1.0$. The harmonic at the fundamental frequency is again cancelled out in $S_{d_1}(\omega)$, while it remains in $S_t(\omega)$. As for the $m_a = 1.0$ case, it is clear from Figure 3-16 that the spectra of $S_{d_1}(\omega)$ and $S_t(\omega)$ do not overlap in Figure 3-16(d). When comparing Figures 3-15 and 3-16, it can be seen that the magnitude of the harmonics at

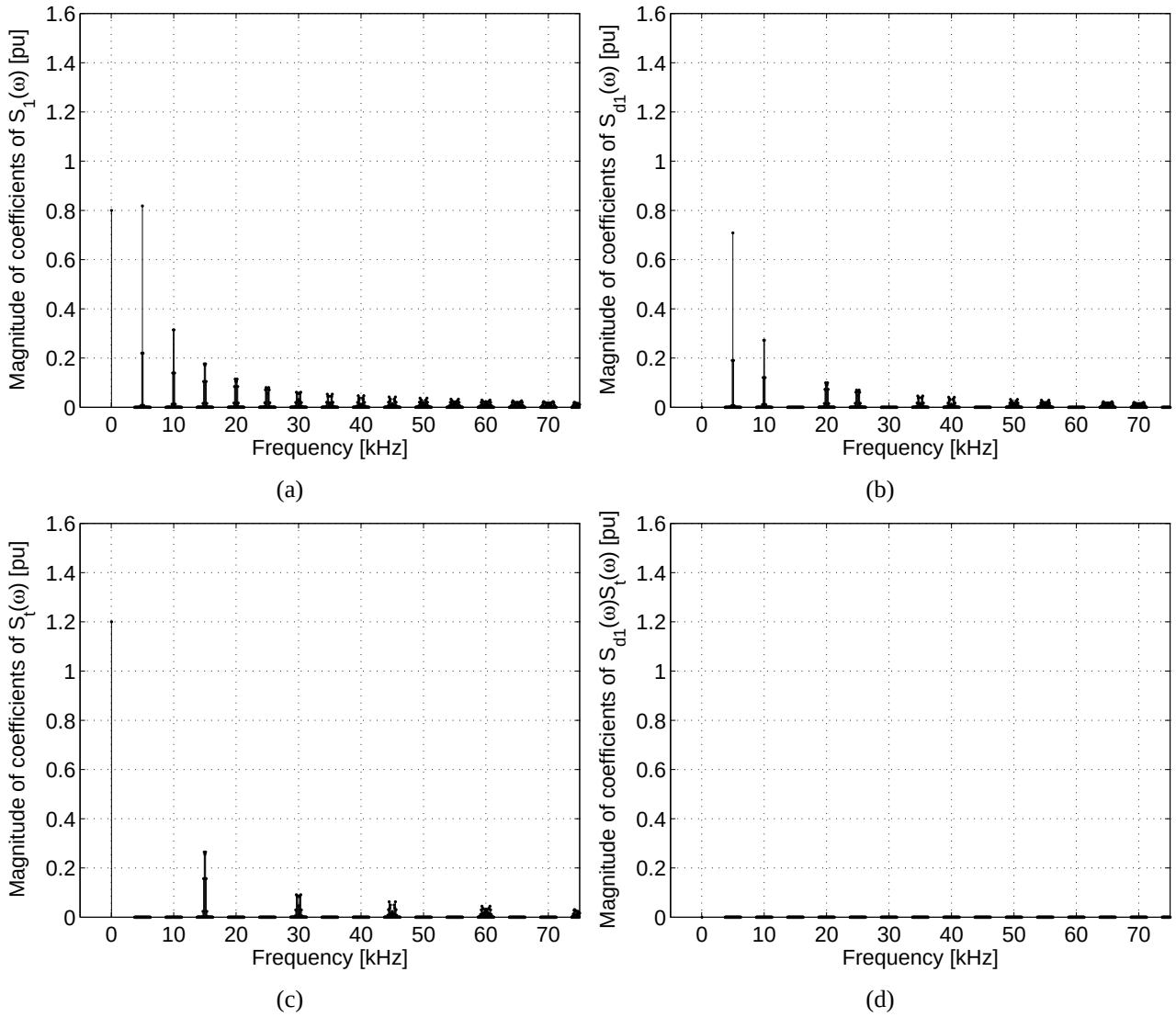

Figure 3-16. *Harmonics of* 3*-cell switching with* $m_a = 0.8$*,* $f_r = 50\ Hz$ *and* $f_s = 5\ kHz$*.*

multiples m of f_s where $m = 3k + 1$ and $m = 3k + 2$ for $k = 0, \pm 1, \pm 2, \ldots$ increase when m_a is decreased. This will be confirmed if this trend is repeated for $m_a = 0.6$.

- For $m_a = 0.6$, $f_r(t) = 0.6 \sin(\omega_r t)$. The spectra of $|S_1(\omega)|$, $|S_{d_1}(\omega)|$, $|S_t(\omega)|$ and of $|S_{d_1}(\omega)||S_t(\omega)|$ for this case are shown in Figure 3-17.

  For this final case, the spectra of $S_{d_1}(\omega)$ and $S_t(\omega)$ also exhibit the same characteristics as seen in the previous two cases. As for the previous cases of $m_a = 1.0$ and $m_a = 0.8$, it is clear from Figure 3-17 that the spectra of $S_{d_1}(\omega)$ and $S_t(\omega)$ do not overlap. This proves that $|S_{d_1}(\omega)||S_t(\omega)| \approx 0$. When comparing Figures 3-15, 3-16 and 3-17, it can be seen that the magnitude of the harmonics at multiples m of f_s where $m = 3k + 1$ and $m = 3k + 2$ for $k = 0, \pm 1, \pm 2, \ldots$ increase as m_a is decreased. From the above-mentioned cases it can also be seen in Figures 3-15(a) through 3-17(a) that the magnitude of the harmonic of the reference at the fundamental frequency of $S_1(\omega)$ is a maximum for $m_a = 1.0$ and decreases as m_a

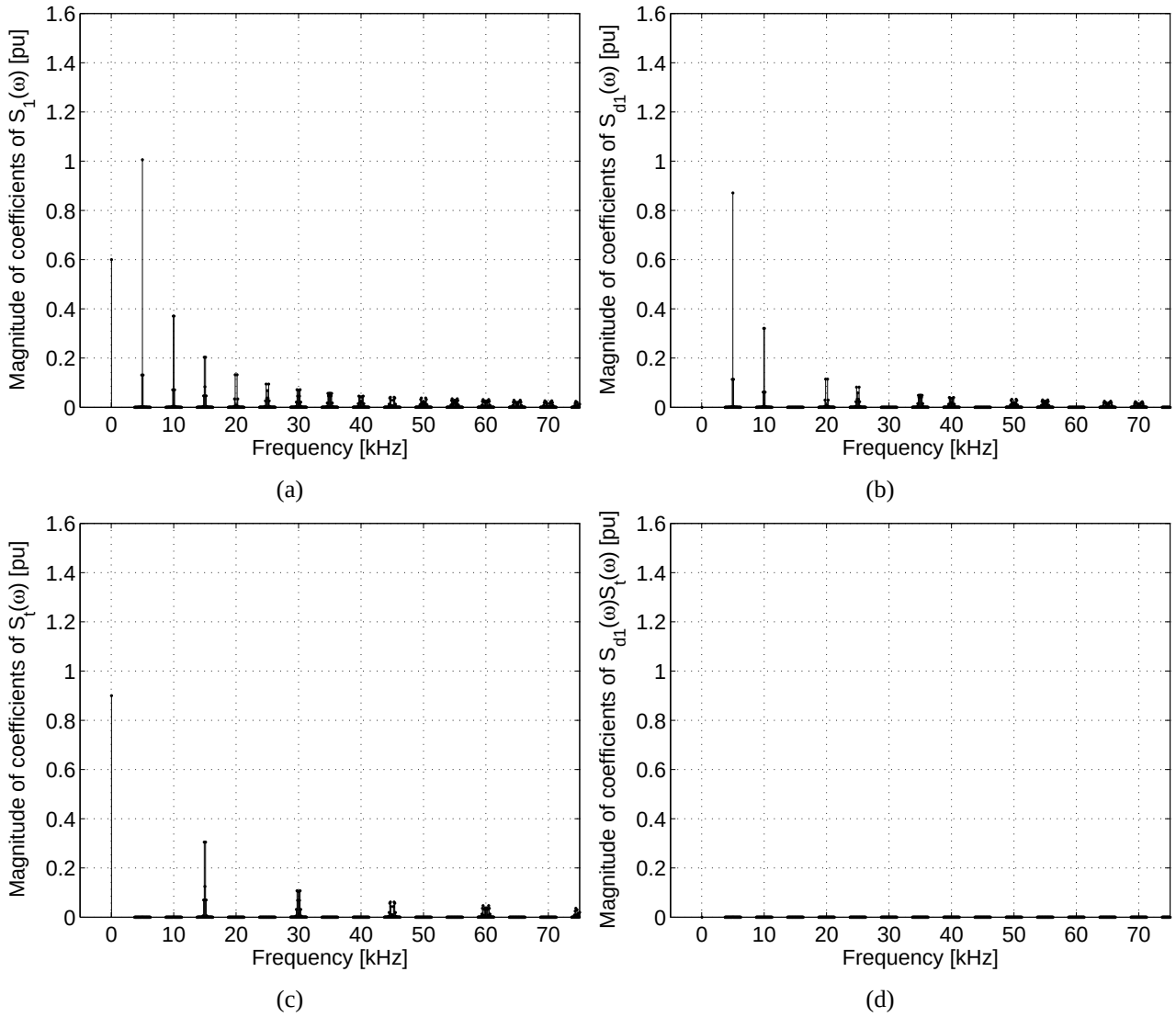

Figure 3-17. *Harmonics of* 3*-cell switching with* $m_a = 0.6$*,* $f_r = 50\ Hz$ *and* $f_s = 5\ kHz$*.*

is decreased. The same properties that are valid for the spectra of $S_{d_1}(\omega)$ are also valid for $S_{d_2}(\omega)$. This is because $S_{d_1}(\omega)$ and $S_{d_2}(\omega)$ are equal in magnitude and different in phase as shown earlier.

3.3.1.4 Switching functions of p-cell interleaved switching

The switching functions are defined in the same way as for the 2- and 3-cell cases, except that there are p switching functions in this case. The states that the switching functions can assume were defined

in Chapter 2 section 2.10 and are repeated here for convenience as follows:

$$s_i(t) = \begin{cases} \quad 1 & \text{if } f_{c_i}(t) < f_r(t) \\ -\quad 1 & \text{if } f_r(t) < f_{c_i}(t) \end{cases} \text{ for } i = 1, \ldots, p \tag{3.97}$$

Due to interleaved switching, the carriers of the p cells are $\frac{2\pi}{p}$ radians out of phase, i.e. the carrier of cell 2 lags that of cell 1 by $\frac{2\pi}{p}$ radians and the carrier of cell 3 lags that of cell 2 by $\frac{2\pi}{p}$ radians. In the same way, the carrier of the p^{th} cell also lags that of the $(p-1)^{th}$ cell by $\frac{2\pi}{p}$ radians. These carriers can be written as follows:

$$f_{c_i}(t) = \frac{2}{\pi} \arcsin\left[\sin(\omega_s t - (i-1)\frac{2\pi}{p})\right] \tag{3.98}$$

The first line in the TOH-plane is again the same as that for the previous cases discussed in the preceding sections. This line is given by the following straight line equation in the TOH-plane:

$$h = \frac{2\omega_s}{\pi} t \tag{3.99}$$

The second line is parallel to the first line, which means that it has the same gradient as the first line and an h-axis intersection of c_1. This line can be written as follows:

$$h = \frac{2\omega_s}{\pi} t + c_1 \tag{3.100}$$

The intersection c_1 can be determined by substituting the t-axis intersection, i.e. the point where $h = 0$ and $t = \frac{2\pi}{p\omega_s}$, into equation (3.100). This results in $c_1 = -\frac{4}{p}$. The second line can thus be written as follows:

$$h = \frac{2\omega_s}{\pi} t - \frac{4}{p} \tag{3.101}$$

The third line is again parallel to the first line, which means that it has the same gradient as the first line and an h-axis intersection of c_2. This line can be written as follows:

$$h = \frac{2\omega_s}{\pi} t + c_2 \tag{3.102}$$

The intersection c_2 can be determined by substituting the t-axis intersection, i.e. the point where $h = 0$ and $t = \frac{4\pi}{p\omega_s}$, into equation (3.102). This results in $c_2 = -\frac{8}{p}$. The third line can be written as follows:

$$h = \frac{2\omega_s}{\pi} t - \frac{8}{p} \tag{3.103}$$

The p^{th} line is again parallel to the previous lines, which means that it has the same gradient as the previous lines and an h-axis intersection of c_p. This line can be written as follows:

$$h = \frac{2\omega_s}{\pi} t + c_p \tag{3.104}$$

The intersection c_p can be determined by substituting the t-axis intersection, i.e. the point where $h = 0$ and $t = \frac{2\pi(p-1)}{p\omega_s}$, into equation (3.104). This results in $c_p = -\frac{4(p-1)}{p}$. The p^{th} line can be written as follows:

$$h = \frac{2\omega_s}{\pi}t - \frac{4(p-1)}{p} \tag{3.105}$$

This results in the following p lines in the TOH-plane:

$$\left(\frac{2\omega_s}{\pi}t, t\right) \ , \ \left(\frac{2\omega_s}{\pi}t - \frac{4}{p}, t\right) \tag{3.106}$$

$$\left(\frac{2\omega_s}{\pi}t - \frac{8}{p}, t\right) \ , \ldots , \ \left(\frac{2\omega_s}{\pi}t - \frac{4(p-1)}{p}, t\right) \tag{3.107}$$

to generate $s_1(t), s_2(t), s_3(t), \ldots, s_p(t)$ respectively. These p switching functions can therefore be written as follows:

$$s_1(t) = F\left(\frac{2\omega_s}{\pi}t, t\right) \ , \ s_2(t) = F\left(\frac{2\omega_s}{\pi}t - \frac{4}{p}, t\right) \tag{3.108}$$

$$s_3(t) = F\left(\frac{2\omega_s}{\pi}t - \frac{8}{p}, t\right) \ , \ldots , \ s_p(t) = F\left(\frac{2\omega_s}{\pi}t - \frac{4(p-1)}{p}, t\right) \tag{3.109}$$

For the case of a p-cell multicell converter, the first switching function is exactly the same as that for the previous cases. This switching function is repeated here for convenience as follows:

$$\begin{aligned} s_1(t) = \frac{1}{2}A_{00} + \sum_{n=1}^{\infty}(A_{0n}\cos(n\omega_r t) + B_{0n}\sin(n\omega_r t)) + \\ \sum_{m=1}^{\infty}(A_{m0}\cos(m\omega_s t) + B_{m0}\sin(m\omega_s t)) + \\ \sum_{m=1}^{\infty}\sum_{n=\pm 1}^{\pm\infty}(A_{mn}\cos(m\omega_s t + n\omega_r t) + B_{mn}\sin(m\omega_s t + n\omega_r t)) \end{aligned} \tag{3.110}$$

An expression for the switching function $s_2(t)$ can be written by substituting the value of h in $F(h,t)$ in equation (3.14). The value of h for this case is as follows:

$$h = \frac{2\omega_s}{\pi}t - \frac{4}{p} \tag{3.111}$$

Substituting equation (3.111) into the term $\frac{m\pi h}{2}$ yields the following:

$$\frac{m\pi h}{2} = m\omega_s t - \frac{2m\pi}{p} \tag{3.112}$$

Substituting equation (3.112) into equation (3.14) results in $s_2(t)$ as follows:

$$\begin{aligned} s_2(t) = \frac{1}{2}A_{00} + \sum_{n=1}^{\infty}(A_{0n}\cos(n\omega_r t) + B_{0n}\sin(n\omega_r t)) + \\ \sum_{m=1}^{\infty}\left\{A_{m0}\cos\left(m\omega_s t - \frac{2m\pi}{p}\right) + B_{m0}\sin\left(m\omega_s t - \frac{2m\pi}{p}\right)\right\} + \\ \sum_{m=1}^{\infty}\sum_{n=\pm 1}^{\pm\infty}\left\{A_{mn}\cos\left(m\omega_s t + n\omega_r t - \frac{2m\pi}{p}\right) + B_{mn}\sin\left(m\omega_s t + n\omega_r t - \frac{2m\pi}{p}\right)\right\} \end{aligned} \tag{3.113}$$

In the same way an expression for the switching function $s_3(t)$ can be written by substituting the value of h in $F(h,t)$ in equation (3.14). The value of h for this case is as follows:

$$h = \frac{2\omega_s}{\pi}t - \frac{8}{p} \tag{3.114}$$

Substituting equation (3.114) into the term $\frac{m\pi h}{2}$ yields the following:

$$\frac{m\pi h}{2} = m\omega_s t - \frac{4m\pi}{p} \tag{3.115}$$

Substituting equation (3.115) into equation (3.14) results in $s_3(t)$ as follows:

$$\begin{aligned} s_3(t) = \frac{1}{2}A_{00} + \sum_{n=1}^{\infty}(A_{0n}\cos(n\omega_r t) + B_{0n}\sin(n\omega_r t)) + \\ \sum_{m=1}^{\infty}\left\{A_{m0}\cos\left(m\omega_s t - \frac{4m\pi}{p}\right) + B_{m0}\sin\left(m\omega_s t - \frac{4m\pi}{p}\right)\right\} + \\ \sum_{m=1}^{\infty}\sum_{n=\pm 1}^{\pm\infty}\left\{A_{mn}\cos\left(m\omega_s t + n\omega_r t - \frac{4m\pi}{p}\right) + B_{mn}\sin\left(m\omega_s t + n\omega_r t - \frac{4m\pi}{p}\right)\right\} \end{aligned} \tag{3.116}$$

The same process can be used as above to find expressions for the remaining $p-3$ lines. The expression for the switching function $s_p(t)$ can also be written by substituting the value of h in $F(h,t)$ in equation (3.14). The value of h for this case is as follows:

$$h = \frac{2\omega_s}{\pi}t - \frac{4(p-1)}{p} \tag{3.117}$$

Substituting equation (3.117) into the term $\frac{m\pi h}{2}$ yields the following:

$$\frac{m\pi h}{2} = m\omega_s t - \frac{2m\pi(p-1)}{p} \tag{3.118}$$

Substituting equation (3.118) into equation (3.14) results in $s_p(t)$ as follows:

$$\begin{aligned} s_p(t) = \frac{1}{2}A_{00} + \sum_{n=1}^{\infty}(A_{0n}\cos(n\omega_r t) + B_{0n}\sin(n\omega_r t)) + \\ \sum_{m=1}^{\infty}\left\{A_{m0}\cos\left(m\omega_s t - \frac{2m\pi(p-1)}{p}\right) + B_{m0}\sin\left(m\omega_s t - \frac{2m\pi(p-1)}{p}\right)\right\} + \\ \sum_{m=1}^{\infty}\sum_{n=\pm 1}^{\pm\infty}\left\{A_{mn}\cos\left(m\omega_s t + n\omega_r t - \frac{2m\pi(p-1)}{p}\right) + \right. \\ \left. B_{mn}\sin\left(m\omega_s t + n\omega_r t - \frac{2m\pi(p-1)}{p}\right)\right\} \end{aligned} \tag{3.119}$$

From the above expressions for $s_1(t)$, $s_2(t)$, $s_3(t)$ and $s_p(t)$ it is clear that their coefficients are of equal magnitude for all values of m, while they are of equal phase only around multiples m of the switching frequency, where $m = pk$ and $k = 0, \pm 1, \pm 2, \ldots$. The phases of $s_1(t),\ s_2(t),\ s_3(t), \ldots,\ s_p(t)$ differ by $\frac{2\pi}{p}$ radians around multiples m of the switching frequency where $m = pk + 1$, $m = pk + 2$ up to $m = pk + (p - 1)$.

Again, the switching frequency (f_s) is chosen higher than the highest frequency component of the reference signal $f_r(t)$ so that the harmonics of the groups associated with the different values of m do not overlap. Therefore, using this assumption, the Fourier series components of $s_1(t)$, $s_2(t),\ s_3(t)$ up to $s_p(t)$ can be separated into p groups made up of different clusters of harmonics. As in the previous section, the harmonics of the switching functions are also classified into classes. Harmonics of *class zero* of a switching function are the set of Fourier series components for which $m = pk$. In the same way, harmonics of *class one* are the set of Fourier series components for which $m = pk + 1$ up to the harmonics of *class p-1* which are the set of Fourier series components for which $m = pk + (p - 1)$, where $k = 0, \pm 1, \pm 2, \ldots$.

As in the previous sections, ω is chosen so that $\omega = m\omega_s + n\omega_r \geq 0$. Therefore, the following observations can be made about the Fourier series components and the Fourier transforms of $s_1(t)$, $s_2(t),\ s_3(t), \ldots,\ s_p(t)$:

(a) Harmonics of *class zero*: these are harmonics of $s_1(t),\ s_2(t),\ s_3(t), \ldots, s_p(t)$ which are equal in magnitude and in phase. In terms of the Fourier transforms of $s_1(t),\ s_2(t),\ s_3(t), \ldots,\ s_p(t)$ the following is implied when $m = pk$, where $k = 0, \pm 1, \pm 2, \ldots$ as follows:

$$S_1(\omega) = S_2(\omega) = S_3(\omega) = \ldots = S_p(\omega) \tag{3.120}$$

and

$$S_1(-\omega) = S_2(-\omega) = S_3(-\omega) = \ldots = S_p(-\omega) \tag{3.121}$$

(b) Harmonics of *class one*: these are harmonics of $s_1(t),\ s_2(t),\ s_3(t), \ldots, s_p(t)$ where the Fourier series components of the i^{th} cell $s_i(t)$ lag those of $s_{i-1}(t)$ by $\frac{2\pi}{p}$ radians for $i = 2, \ldots, p$. In terms of the Fourier transforms of $s_1(t),\ s_2(t),\ s_3(t), \ldots, s_p(t)$, this can be written for $m = pk + 1$, where $k = 0, \pm 1, \pm 2, \ldots$ as follows:

$$S_2(\omega) = S_1(\omega)e^{-j\frac{2\pi}{p}} \text{ and } S_p(\omega) = S_{p-1}(\omega)e^{-j\frac{2\pi}{p}} \tag{3.122}$$

and

$$S_2(-\omega) = S_1(-\omega)e^{j\frac{2\pi}{p}} \text{ and } S_p(-\omega) = S_{p-1}(-\omega)e^{j\frac{2\pi}{p}} \tag{3.123}$$

(c) Harmonics of *class two*: these are harmonics of $s_1(t),\ s_2(t),\ s_3(t), \ldots, s_p(t)$ where the Fourier series components of the i^{th} cell $s_i(t)$ lag those of $s_{i-1}(t)$ by $\frac{4\pi}{p}$ radians for $i = 2, \ldots, p$. In terms of the Fourier transforms of $s_1(t),\ s_2(t),\ s_3(t), \ldots, s_p(t)$, this can be written for $m = pk + 2$, where $k = 0, \pm 1, \pm 2, \ldots$ as follows:

$$S_2(\omega) = S_1(\omega)e^{-j\frac{4\pi}{p}} \text{ and } S_p(\omega) = S_{p-1}(\omega)e^{-j\frac{4\pi}{p}} \tag{3.124}$$

and

$$S_2(-\omega) = S_1(-\omega)e^{j\frac{4\pi}{p}} \text{ and } S_p(-\omega) = S_{p-1}(-\omega)e^{j\frac{4\pi}{p}} \tag{3.125}$$

(d) Harmonics of *class three*: these are harmonics of $s_1(t),\ s_2(t),\ s_3(t), \ldots, s_p(t)$ where the Fourier series components of the i^{th} cell $s_i(t)$ lag those of $s_{i-1}(t)$ by $\frac{6\pi}{p}$ radians for $i = 2, \ldots, p$. In terms of the Fourier transforms of $s_1(t),\ s_2(t),\ s_3(t), \ldots, s_p(t)$, this can be written for $m = pk + 3$, where $k = 0, \pm 1, \pm 2, \ldots$ as follows:

$$S_2(\omega) = S_1(\omega)e^{-j\frac{6\pi}{p}} \text{ and } S_p(\omega) = S_{p-1}(\omega)e^{-j\frac{6\pi}{p}} \tag{3.126}$$

and

$$S_2(-\omega) = S_1(-\omega)e^{j\frac{6\pi}{p}} \text{ and } S_p(-\omega) = S_{p-1}(-\omega)e^{j\frac{6\pi}{p}} \tag{3.127}$$

(e) $\vdots$

(f) Harmonics of *class p-1*: these are harmonics of $s_1(t),\ s_2(t),\ s_3(t), \ldots, s_p(t)$ where the Fourier series components of the i^{th} cell $s_i(t)$ lag those of $s_{i-1}(t)$ by $\frac{2\pi(p-1)}{p}$ radians for $i = 2, \ldots, p$. In terms of the Fourier transforms of $s_1(t),\ s_2(t),\ s_3(t), \ldots, s_p(t)$, this can be written for $m = (p-1)k + p$, where $k = 0, \pm 1, \pm 2, \ldots$ as follows:

$$S_2(\omega) = S_1(\omega)e^{-j\frac{2\pi(p-1)}{p}} \text{ and } S_p(\omega) = S_{p-1}(\omega)e^{-j\frac{2\pi(p-1)}{p}} \tag{3.128}$$

and

$$S_2(-\omega) = S_1(-\omega)e^{j\frac{2\pi(p-1)}{p}} \text{ and } S_p(-\omega) = S_{p-1}(-\omega)e^{j\frac{2\pi(p-1)}{p}} \tag{3.129}$$

Phasor representations of the switching functions for 4- and 5 cells are included in Appendix A section A.2 in Figures A-2 and A-3. These figures verify that the above-mentioned observations are correct for p cells.

The above observations as well as that of the phasors shown in Figures A-2 and A-3 can now be used to deduce the following properties regarding the switching functions $s_{d_1}(t)$, $s_{d_2}(t), \ldots,\ s_{d_{p-1}}(t)$ and $s_t(t)$:

(a) The "total" switching function contains only harmonics of *class zero*. This means that $s_t(t)$ contains the frequency components of the reference signal as well as the harmonic components of $s_1(t)$ around integer multiples of p times the switching frequency. This can be seen in Figures A-2(e) through A-2(l) as well as in Figures A-3(g) through A-3(o).

(b) The "difference" switching functions $s_{d_1}(t),\ s_{d_2}(t), \ldots,\ s_{d_{p-1}}(t)$ contain harmonics of *class one*, *class two* up to and including *class p-1*. This can be seen in Figures A-2(c) through A-2(j) as well as in Figures A-3(d) through A-3(m). The following relationships between S_{d_i} and $S_{d_{i-1}}$ can be concluded from Figures A-2(c) through 3-14(i):

$$S_{d_i}(\omega) = \begin{cases} S_{d_{i-1}}(\omega)e^{-j\frac{2\pi}{p}} & \text{if } m = pk+1 \\ S_{d_{i-1}}(\omega)e^{-j\frac{4\pi}{p}} & \text{if } m = pk+2 \\ \vdots & \vdots \\ S_{d_{i-1}}(\omega)e^{-j\frac{2\pi(p-1)}{p}} & \text{if } m = pk+(p-1) \end{cases} \tag{3.130}$$

and

$$S_{d_i}(-\omega) = \begin{cases} S_{d_{i-1}}(-\omega)e^{j\frac{2\pi}{p}} & \text{if } m = pk+1 \\ S_{d_{i-1}}(-\omega)e^{j\frac{4\pi}{p}} & \text{if } m = pk+2 \\ \vdots & \vdots \\ S_{d_{i-1}}(-\omega)e^{j\frac{2\pi(p-1)}{p}} & \text{if } m = pk+(p-1) \end{cases} \tag{3.131}$$

where $i = 2, \ldots,\ p$ and $k = 0, \pm 1, \pm 2, \ldots$.

(c) The above two conclusions lead to the following important conclusions:

$$|S_{d_1}(\omega)|\,|S_t(\omega)| \approx 0 \tag{3.132}$$

$$|S_{d_2}(\omega)|\,|S_t(\omega)| \approx 0 \tag{3.133}$$

$$\vdots\ \vdots\ \vdots$$

$$\left|S_{d_{p-1}}(\omega)\right|\,|S_t(\omega)| \approx 0 \tag{3.134}$$

The frequency spectra of $|S_1(\omega)|$, $|S_{d_1}(\omega)|$, $|S_t(\omega)|$ and $|S_{d_1}(\omega)||S_t(\omega)|$ for the same modulation index, but for the 4- and 5-cell cases are plotted and compared in the following example.

Example 3.7

The previous example shown for the 2-cell case is repeated here for the 4- and 5-cell cases. The reference $f_r(t)$ is defined as follows:

$$f_r(t) = 0.8\sin(\omega_r t) \tag{3.135}$$

The switching frequency $f_s = 5\ kHz$ and the reference frequency $f_r = 50\ Hz$.

- For the 4-cell case, the spectra of $|S_1(\omega)|$, $|S_{d_1}(\omega)|$, $|S_t(\omega)|$ and of $|S_{d_1}(\omega)||S_t(\omega)|$ are shown in Figure 3-18.

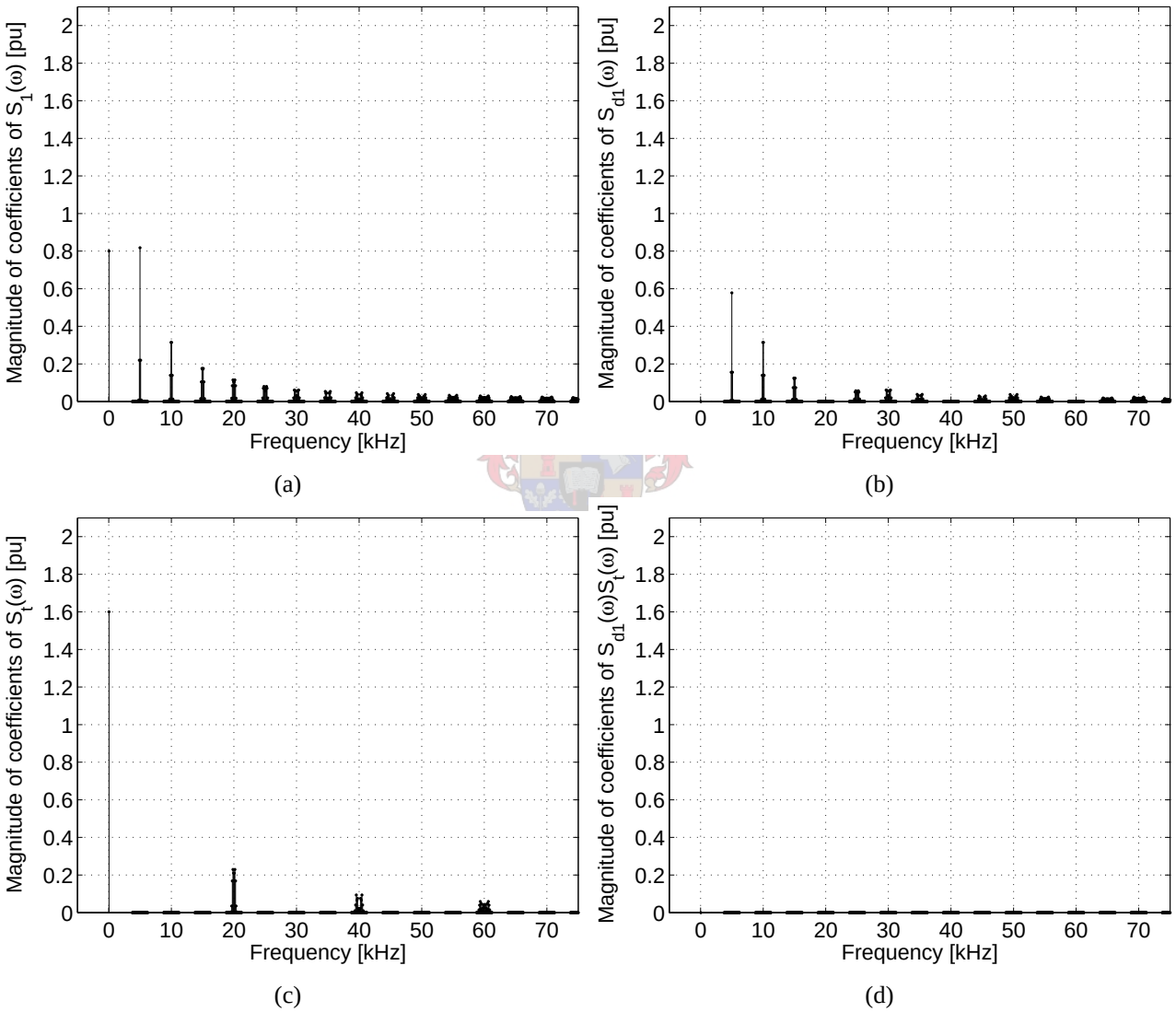

Figure 3-18. *Harmonics of 4-cell switching with $m_a = 0.8$, $f_r = 50\ Hz$ and $f_s = 5\ kHz$.*

The spectra of $S_{d_1}(\omega)$ are centred around multiples m of the switching frequency f_s where $m = 4k+1$, $m = 4k+2$ and $m = 4k+3$ for $k = 0, \pm1, \pm2, \ldots$. However, the spectra of $S_t(\omega)$ are centred around multiples of four times the switching frequency. As in the 2- and 3-cell cases, the harmonic at the fundamental frequency is cancelled out in $S_{d_1}(\omega)$, while it remains

in $S_t(\omega)$. It is clear from Figure 3-18 that the spectra of $S_{d_1}(\omega)$ and $S_t(\omega)$ do not overlap, due to the fact that the spectra of $|S_{d_1}(\omega)||S_t(\omega)| \approx 0$ in Figure 3-18(d).

- For the 5-cell case, the spectra of $|S_1(\omega)|$, $|S_{d_1}(\omega)|$, $|S_t(\omega)|$ and of $|S_{d_1}(\omega)||S_t(\omega)|$ are shown in Figure 3-19.

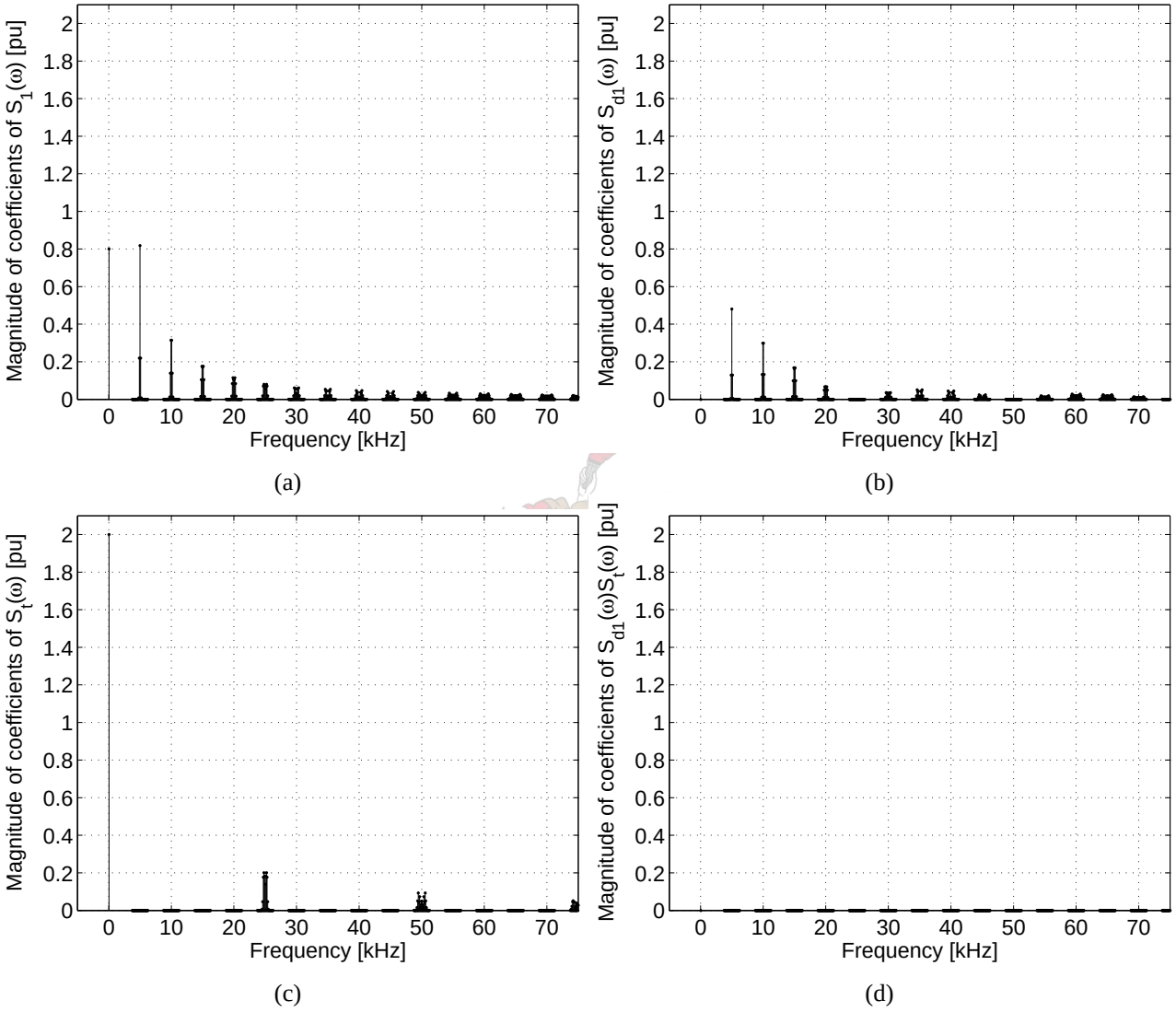

Figure 3-19. *Harmonics of* 5*-cell switching with* $m_a = 0.8$*,* $f_r = 50\ Hz$ *and* $f_s = 5\ kHz$*.*

For this final case, the spectra of $S_{d_1}(\omega)$ are centred around multiples m of the switching frequency f_s where $m = 5k{+}1$, $m = 5k{+}2$, $m = 5k{+}3$ and $m = 5k{+}4$ for $k = 0, \pm1, \pm2, \ldots$. The spectra of $S_t(\omega)$ are centred around multiples of five times the switching frequency. As for the previous cases of 2-, 3- and 4-cells, it is clear from Figure 3-19 that the spectra of $S_{d_1}(\omega)$ and $S_t(\omega)$ do not overlap. This proves that $|S_{d_1}(\omega)||S_t(\omega)| \approx 0$. The same properties that are valid for the spectra of $S_{d_1}(\omega)$ are also valid for $S_{d_2}(\omega)$, $S_{d_3}(\omega)$ and $S_{d_4}(\omega)$, because they are equal in magnitude and different in phase as shown earlier.

3.3.2 Fixed duty-cycle analysis

This section focusses on the special case where the reference is fixed, which results in a switching waveform with a fixed duty-cycle. The same analysis methods as applied in the previous section are valid for this case unless otherwise stated. The reason for this section is to find out if there are any cases where the value of the duty-cycle or the number of cells can cause unbalance in a multicell converter.

The switching functions of a "single"-, 2-, 3- and p-cell multicell converters using interleaved switching with a fixed reference signal is calculated and analysed in this section. The switched waveform resulting from this type of PWM is already periodical. Therefore, the normal Fourier series expansion will be used in the analyses of all the cases discussed in this section.

3.3.2.1 Switching functions of a "single"-cell converter

The "single"-cell or half-bridge converter is chosen as the starting point for this analysis as the analysis is simplest for this case. Other subsequent cases are all based on the results found for this case.

Pulse width modulation (PWM) as applied to a half-bridge or "single"-cell converter using natural sampling is shown in Figure 3-20. This figure shows the fixed reference $f_r(t)$. The value of the reference, A is not equal to the duty-cycle D of the top switch, due to the fact that the switching function is defined between -1 and 1. If it was defined between 0 and 1, the reference would have been equal to the duty-cycle. Therefore, the relationship between the duty-cycle, D and the amplitude, A of the reference can be written as follows:

$$D = \frac{1}{2}A + \frac{1}{2} \tag{3.136}$$

The reference can be written as follows:

$$f_r(t) = A = 2D - 1 \tag{3.137}$$

The function $f_c(t)$, also shown in Figure 3-20(a), is the triangular carrier with frequency ω_s, which is the switching frequency of each switching device in the half-bridge converter. Again, the carrier can be written as follows [61], [63]:

$$f_c(t) = \frac{2}{\pi}\arcsin\left[\sin(\omega_s t)\right]. \tag{3.138}$$

In Figure 3-20(a), the area between $f_r(t)$ and -1 is coloured blue and represents the area in which $s(t)$ has a value of 1, while the area above, between $f_r(t)$ and $+1$ is coloured red and represents the area in which $s(t)$ has a value of -1. The resulting switching function $s(t)$ is shown in Figure 3-20(b)

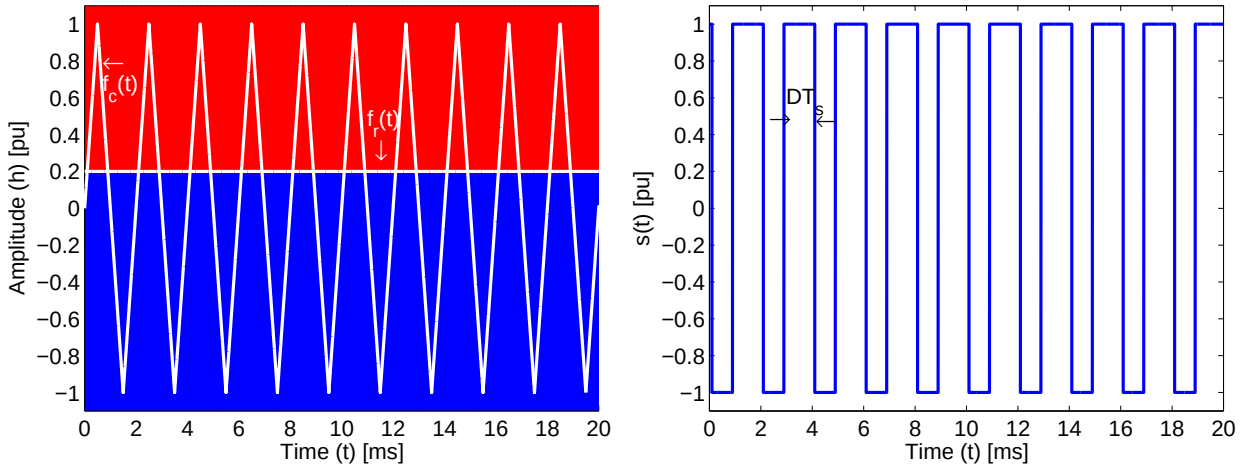

(a) (b)

Figure 3-20. *Switching function generation for a "single"-cell inverter using interleaved switching.*

and is defined as follows:

$$s(t) = \begin{cases} 1 & \text{if } f_c(t) < 2D - 1 \\ -1 & \text{if } 2D - 1 < f_c(t) \end{cases} \tag{3.139}$$

The switching function $s(t)$ is periodic with a period equal to the switching period of the converter, i.e. T_s. Therefore, the switching function $s(t)$ can be represented with a Fourier series. The Fourier series representation of $s(t)$ is of the following form [15]:

$$s(t) = A_0 + \sum_{m=1}^{\infty} (A_m \cos(m\omega_s t) + B_m \sin(m\omega_s t)) \tag{3.140}$$

where the dc-component A_0 is defined in [15] as follows:

$$A_0 = \frac{1}{T_s} \int_0^{T_s} f(t)dt. \tag{3.141}$$

The coefficients A_m and B_m are also defined in [15] and are as follows:

$$A_m = \frac{2}{T_s} \int_0^{T_s} f(t) \cos(m\omega_s t)dt \tag{3.142}$$

and

$$B_m = \frac{2}{T_s} \int_0^{T_s} f(t) \sin(m\omega_s t)dt. \tag{3.143}$$

The above coefficients can be calculated for $s(t)$ using the graphic representations thereof as shown in Figures 3-20(b) and 3-21. The switching period $T_s = \frac{2\pi}{\omega_s}$ can be taken from the start of the first 1-state, with its length equal to the duty-cycle times the switching period, i.e. $D \cdot T_s$, until the end of its corresponding -1-state, i.e. the end of the period T_s. Using this information for the boundaries of the integrals in equations (3.141)-(3.143) the coefficients can be calculated.

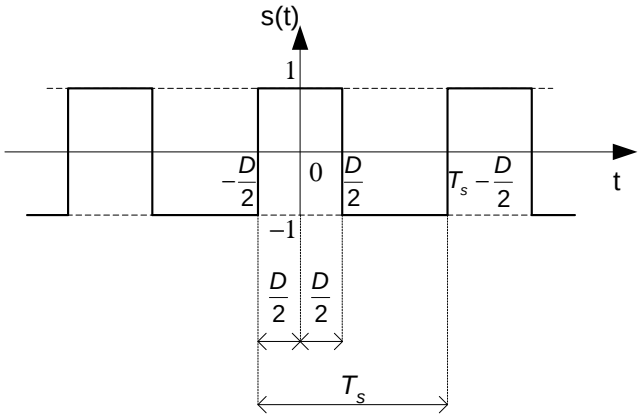

Figure 3-21. *Switching function diagram for Fourier coefficient calculation.*

Using Figure 3-21 the dc-component, A_0 can be calculated as follows:

$$\begin{aligned}
A_0 &= \frac{\omega_s}{2\pi}\int_{-\frac{D}{2}\cdot\frac{2\pi}{\omega_s}}^{\frac{2\pi}{\omega_s}-\frac{D}{2}\cdot\frac{2\pi}{\omega_s}} f(t)dt \\
&= \frac{\omega_s}{2\pi}\left[\int_{-\frac{\pi D}{\omega_s}}^{\frac{\pi D}{\omega_s}}(1)dt + \int_{\frac{\pi D}{\omega_s}}^{\frac{2\pi}{\omega_s}(1-\frac{D}{2}}(-1)dt\right] \\
&= \frac{\omega_s}{2\pi}\left[[t]_{-\frac{\pi D}{\omega_s}}^{\frac{\pi D}{\omega_s}} - [t]_{\frac{\pi D}{\omega_s}}^{\frac{2\pi}{\omega_s}(1-\frac{D}{2}}\right] \\
&= \frac{\omega_s}{2\pi}\left[\frac{\pi D}{\omega_s} + \frac{\pi D}{\omega_s} - \left(\frac{2\pi}{\omega_s}\left(1-\frac{D}{2}\right) - \frac{\pi D}{\omega_s}\right)\right] \\
&= \frac{\omega_s}{2\pi}\left[\frac{2\pi D}{\omega_s} - \frac{2\pi}{\omega_s} + \frac{\pi D}{\omega_s} + \frac{\pi D}{\omega_s}\right] \\
&= \frac{\omega_s}{2\pi}\left[\frac{4\pi D}{\omega_s} - \frac{2\pi}{\omega_s}\right] \\
&= 2D - 1
\end{aligned} \tag{3.144}$$

The coefficient A_m can be calculated using equation (3.142) as follows:

$$\begin{aligned}
A_m &= \frac{2\omega_s}{2\pi}\int_{-\frac{D}{2}\cdot\frac{2\pi}{\omega_s}}^{\frac{2\pi}{\omega_s}-\frac{D}{2}\cdot\frac{2\pi}{\omega_s}} f(t)\cos(m\omega_s t)dt \\
&= \frac{\omega_s}{\pi}\left[\int_{-\frac{\pi D}{\omega_s}}^{\frac{\pi D}{\omega_s}}\cos(m\omega_s t)dt - \int_{\frac{\pi D}{\omega_s}}^{\frac{2\pi}{\omega_s}(1-\frac{D}{2})}\cos(m\omega_s t)dt\right] \\
&= \frac{\omega_s}{\pi}\left[\left[\frac{1}{m\omega_s}\sin(m\omega_s t)\right]_{-\frac{\pi D}{\omega_s}}^{\frac{\pi D}{\omega_s}} - \left[\frac{1}{m\omega_s}\sin(m\omega_s t)\right]_{\frac{\pi D}{\omega_s}}^{\frac{2\pi}{\omega_s}(1-\frac{D}{2})}\right] \\
&= \frac{1}{m\pi}\left[\sin(m\pi D) - \sin(-m\pi D) - \sin\left(2m\pi\left(1-\frac{D}{2}\right)\right) + \sin(m\pi D)\right] \\
&= \frac{4}{m\pi}\sin(m\pi D)
\end{aligned} \tag{3.145}$$

The coefficient B_m can be calculated using equation (3.143) as follows:

$$\begin{aligned}
B_m &= \frac{2\omega_s}{2\pi}\int_{-\frac{D}{2}\cdot\frac{2\pi}{\omega_s}}^{\frac{2\pi}{\omega_s}-\frac{D}{2}\cdot\frac{2\pi}{\omega_s}} f(t)\sin(m\omega_s t)dt \\
&= \frac{\omega_s}{\pi}\left[\int_{-\frac{\pi D}{\omega_s}}^{\frac{\pi D}{\omega_s}}\sin(m\omega_s t)dt - \int_{\frac{\pi D}{\omega_s}}^{\frac{2\pi}{\omega_s}(1-\frac{D}{2})}\sin(m\omega_s t)dt\right] \\
&= \frac{\omega_s}{\pi}\left[\left[-\frac{1}{m\omega_s}\cos(m\omega_s t)\right]_{-\frac{\pi D}{\omega_s}}^{\frac{\pi D}{\omega_s}} + \left[\frac{1}{m\omega_s}\cos(m\omega_s t)\right]_{\frac{\pi D}{\omega_s}}^{\frac{2\pi}{\omega_s}(1-\frac{D}{2})}\right] \\
&= \frac{1}{m\pi}\left[-\cos(m\pi D)+\cos(m\pi D)+\cos(2m\pi - m\pi D)-\cos(m\pi)\right] \\
&= \frac{1}{m\pi}\left[-\cos(m\pi D)+\cos(\pi D)+\cos(m\pi D)-\cos(m\pi D)\right] \\
&= 0
\end{aligned} \tag{3.146}$$

These coefficients can be calculated exactly with the appropriate values of m and D. Certain values of D can cause a coefficient to be zero. It will be shown later in this chapter that these values together with specific numbers of cells may lead to unbalance.

The resulting Fourier series representation of the switching function $s(t)$ is as follows:

$$s(t) = 2D - 1 + \frac{4}{\pi}\sum_{m=1}^{\infty}\frac{1}{m}\sin(m\pi D)\cos(m\omega_s t) \tag{3.147}$$

This Fourier series representation can be used to obtain the amplitude spectra of the switching function. This is done by using the exponential form of the Fourier series, which is as follows [15]:

$$s(t) = \sum_{m=-\infty}^{\infty} C_m e^{jm\omega_s t} \tag{3.148}$$

where $C_0 = A_0$ and C_m is defined in [15] as follows:

$$C_m = \frac{1}{2}\{A_m - jB_m\} \text{ for } m > 0 \tag{3.149}$$

$$C_{-m} = \frac{1}{2}\{A_m + jB_m\} \text{ for } m < 0 \tag{3.150}$$

The spectra of the switching function of a “single”-cell converter is shown in the following example.

Example 3.8

In this example, the amplitude spectra are shown for the switching function $s(t)$ of a “single”-cell converter for the following values of the duty-cycle D:

$$D = \{0.2,\ 0.25,\ 0.5,\ 0.75,\ 0.8,\ 1.0\} \tag{3.151}$$

The switching frequency is chosen as: $f_s = 5\ kHz$. The spectra of $|S(\omega)|$ for these values of D are shown in Figure 3-22.

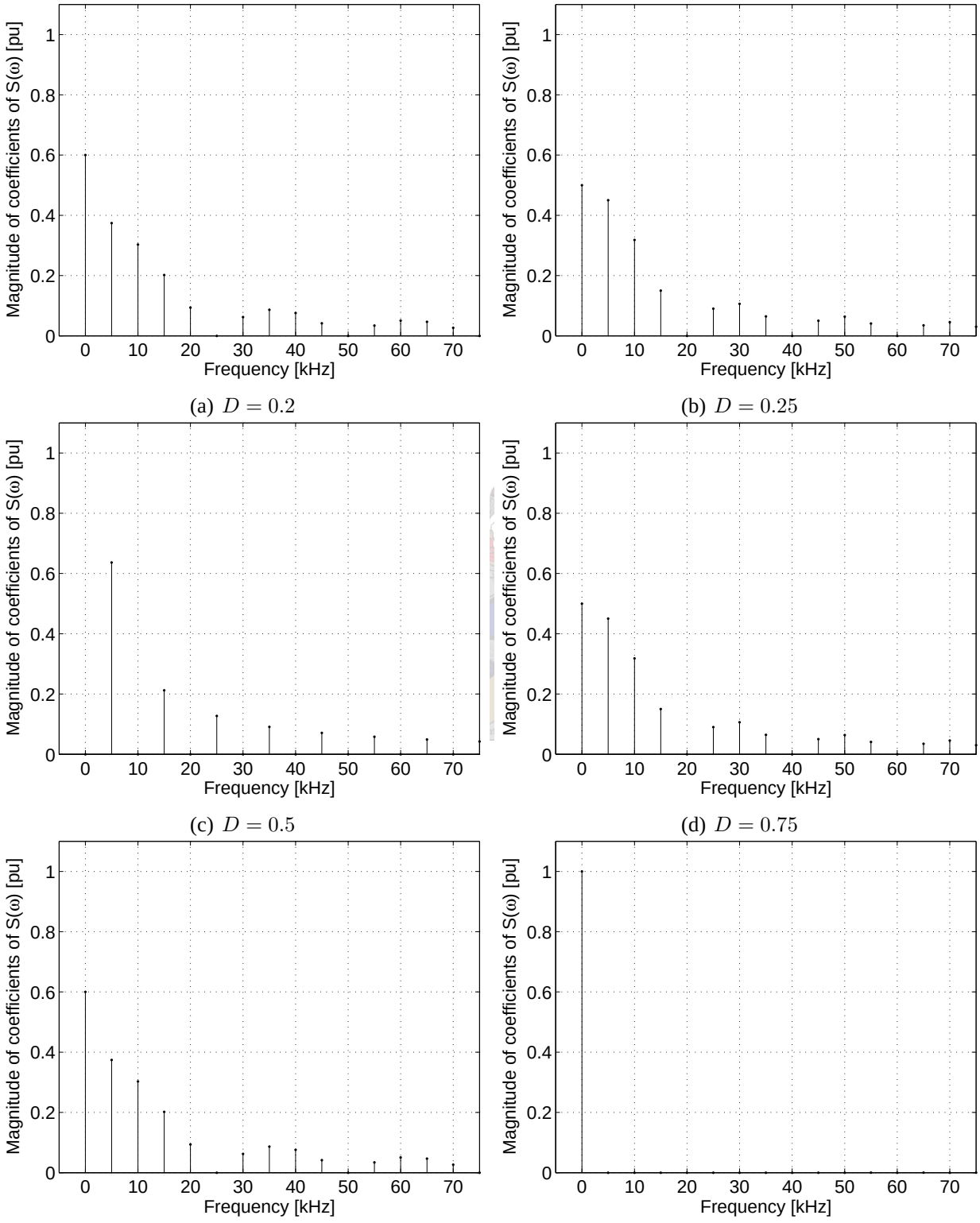

(a) $D = 0.2$ (b) $D = 0.25$

(c) $D = 0.5$ (d) $D = 0.75$

(e) $D = 0.8$ (f) $D = 1.0$

Figure 3-22. *Spectra of $s(t)$ for a "single"-cell with different values of D and $f_s = 5\ kHz$.*

The spectra of $|S(\omega)|$ for these values of D are at integer multiples of the switching frequency f_s except where the value of $m\pi D$ results in a zero magnitude.

- $D = 0.2$: The spectra of $|S(\omega)|$ for $D = 0.2$ are at integer multiples of the switching frequency f_s except where the value of m in $\frac{m\pi}{5}$ is a multiple of 5, which means that the harmonics are zero for multiples of 5 times the switching frequency.
- $D = 0.25$: The spectra of $|S(\omega)|$ for $D = 0.25$ are at integer multiples of the switching frequency f_s except where the value of m in $\frac{m\pi}{4}$ is a multiple of 4, which means that the harmonics are zero for multiples of 4 times the switching frequency.
- $D = 0.5$: The spectra of $|S(\omega)|$ for $D = 0.5$ are at integer multiples of the switching frequency f_s except where the value of m in $\frac{m\pi}{2}$ is even, which means that the harmonics are zero for all even multiples of the switching frequency.
- $D = 0.75$: The spectra of $|S(\omega)|$ for $D = 0.75$ are at integer multiples of the switching frequency f_s except where the value of m in $\frac{3m\pi}{4}$ is a multiple of 4, which means that the harmonics are zero for multiples of 4 times the switching frequency.
- $D = 0.8$: The spectra of $|S(\omega)|$ for $D = 0.8$ are at integer multiples of the switching frequency f_s except where the value of m in $\frac{4m\pi}{5}$ is a multiple of 5, which means that the harmonics are zero for multiples of 5 times the switching frequency.
- $D = 1.0$: The spectra of $|S(\omega)|$ for $D = 1.0$ are all zero except for the dc harmonic component. The reason for this is that the coefficients A_m and B_m are zero for all integer values of m.

3.3.2.2 Switching functions of 2-cell fixed duty-cycle switching

The switching functions for this case are defined exactly the same as in section 3.3.1.2 earlier in this chapter, except for the fact that the reference signal is a dc-signal. The duty-cycle is defined in the same way as discussed in the previous section. It is also assumed that the duty-cycle D is the same for each cell for a given switching cycle. Therefore, the switching functions can be defined as follows:

$$s_1(t) = \begin{cases} \quad 1 & \text{if } f_{c_1}(t) < 2D - 1 \\ -\quad 1 & \text{if } 2D - 1 < f_{c_1}(t) \end{cases} \tag{3.152}$$

$$s_2(t) = \begin{cases} \quad 1 & \text{if } f_{c_2}(t) < 2D - 1 \\ -\quad 1 & \text{if } 2D - 1 < f_{c_2}(t) \end{cases} \tag{3.153}$$

The carrier signal is chosen to be triangular with an angular frequency of ω_s equal to the switching frequency.

For this case, interleaved PWM is again used and generated by using 2 carrier signals that are phase-shifted by $180°$. These two carriers are the same as defined in earlier sections and can be written as follows:

$$f_{c_1}(t) = \frac{2}{\pi} \arcsin\left[\sin(\omega_s t)\right] \tag{3.154}$$

$$f_{c_2}(t) = \frac{2}{\pi} \arcsin\left[\sin(\omega_s t - \pi)\right] \tag{3.155}$$

Interleaved switching using a fixed duty-cycle for a 2-cell multicell converter is illustrated in the following example.

Example 3.9
A 2-cell multicell converter is switched using interleaved PWM with a fixed duty-cycle of $D = 0.6$. The dc reference signal $f_r(t)$ is defined as follows:

$$f_r(t) = A = 2D - 1 = 0.2 \tag{3.156}$$

where the switching frequency $f_s = 500\ Hz$.

In order to generate the switching functions, two triangular carriers are used. The two carriers are $180°$ out of phase. The generation of the switching function of the first cell, i.e. $s_1(t)$ is shown in Figure 3-23(a). The carrier signal of the first cell is denoted by $f_c(t)$ and shown in green, while the reference signal is shown in blue.

The generation of the switching function of the second cell, i.e. $s_2(t)$ is shown in Figure 3-23(b). The carrier signal of this cell is denoted as $-f_c(t)$ and shown in green, while the reference signal is shown in blue.

The "difference" switching function $s_d(t)$ and the "total" switching function $s_t(t)$ are shown respectively in Figures 3-23(c) and 3-23(d). These switching functions were defined earlier in equations (2.15) and (2.16) in Chapter 2 section 2.7 and were repeated in equations (3.35) and (3.36).

The figures shown in Figure 3-23 only show the first cycle of the reference signal $f_r(t)$, but these signals continue for all $t \geq 0$. The switching functions for the fixed duty-cycle 2-cell case have the same coefficients as those for the "single"-cell case. The only difference is that the switching function of cell 2 is phase-shifted by π radians. The switching function of the first cell is the same as for the previous case and was calculated in equation (3.147) to be the following:

$$s_1(t) = 2D - 1 + \frac{4}{\pi} \sum_{m=1}^{\infty} \frac{1}{m} \sin(m\pi D) \cos(m\omega_s t) \tag{3.157}$$

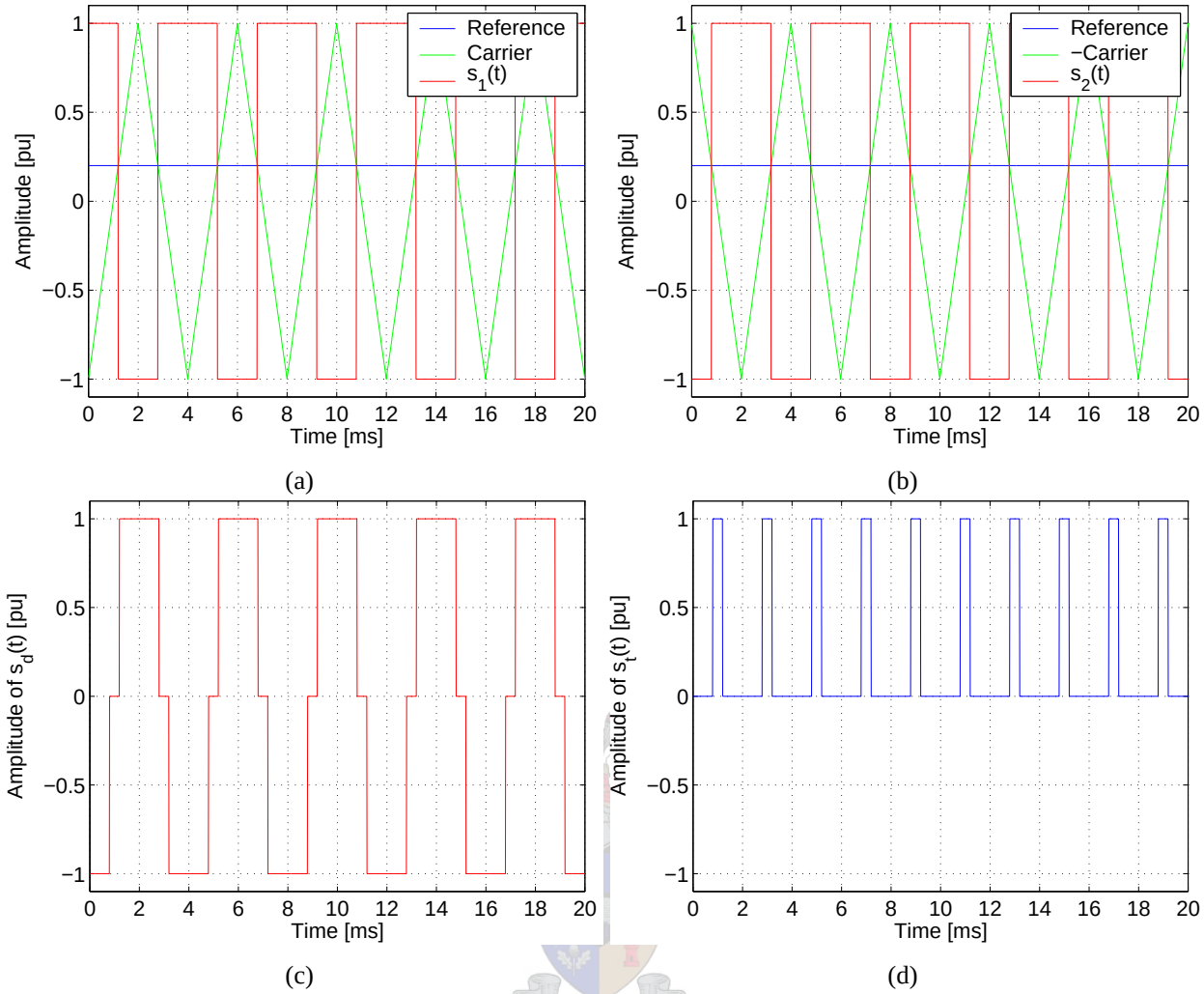

Figure 3-23. *2-cell multicell interleaved switching using a fixed duty-cycle of* $D = 0.6$.

Due to interleaved switching, it is known that the switching function of cell 2 lags that of cell 1 by π radians. The switching function for $s_2(t)$ can therefore be written directly as follows:

$$s_2(t) = 2D - 1 + \frac{4}{\pi}\sum_{m=1}^{\infty}\frac{1}{m}\sin(m\pi D)\cos(m\omega_s t - m\pi) \tag{3.158}$$

Attention should be given to the trigonometric term in equation (3.158) containing $-m\pi$. This term has the following effect on the trigonometric term's sign:

$$\cos(m\omega_s t - m\pi) = \begin{cases} \cos(m\omega_s t) & \text{if } m \text{ even} \\ -\cos(m\omega_s t) & \text{if } m \text{ odd} \end{cases} \tag{3.159}$$

Using the above trigonometric identities, the expression for $s_2(t)$ can be rewritten as follows:

$$s_2(t) = 2D - 1 + \sum_{m=2,4,\ldots}^{\infty} A_m \cos(m\omega_s t) - \sum_{m=1,3,\ldots}^{\infty} A_m \cos(m\omega_s t) \tag{3.160}$$

From the above expressions for $s_1(t)$ and $s_2(t)$ it is clear that their coefficients are of equal magnitude for all values of m, while they are of equal phase only around even multiples of the switching frequency. The phases of $s_1(t)$ and $s_2(t)$ differ by π radians around odd multiples of the switching frequency.

The Fourier series components of $s_1(t)$ and $s_2(t)$ for the fixed duty-cycle case have the same characteristics as for the sinusoidal reference case, except that there are no side-bands present around the harmonics. Therefore, the groups made up of clusters of harmonics reduce to single harmonics. The same classes and phasor representations can be used for these harmonics as discussed for the corresponding sinusoidal reference case. The phasor representations of $S_1(\omega)$ and $S_2(\omega)$ were shown in Figure 3-8.

These observations in conjunction with the phasors shown in Figure 3-8 can also be used to deduce the following properties regarding the switching functions $s_d(t)$ and $s_t(t)$:

(a) The "total" switching function contains only harmonics of *class zero*. This means that $s_t(t)$ contains the harmonic components of $s_1(t)$ at even multiples of the switching frequency. This can be seen by comparing $S_t(\omega)$ shown in Figure 3-8(e) with Figure 3-8(f)

(b) The "difference" switching function contains contains only harmonics of *class one*, which means that it contains only the harmonics of $s_1(t)$ at odd multiples of the switching frequency. This can be seen by comparing $S_d(\omega)$ shown in Figure 3-8(c) with Figure 3-8(d)

In the above expressions for $s_1(t)$ and $s_2(t)$ it is important to look at the characteristics of the Fourier coefficients. The coefficients A_m and B_m are the same as that for the "single"-cell case which were calculated in the previous section.

Previously, $s_d(t)$ and $s_t(t)$ were defined in (2.15) and (2.16) as follows:

$$s_d(t) = \frac{1}{2}\left\{s_2(t) - s_1(t)\right\} \tag{3.161}$$

$$s_t(t) = \frac{1}{2}\left\{s_1(t) + s_2(t)\right\} \tag{3.162}$$

Substituting $s_1(t)$ and $s_2(t)$ into (3.161) and (3.162) results in the expressions for the switching functions $s_d(t)$ and $s_t(t)$ as follows:

$$s_d(t) = -\sum_{m=1,3,\ldots}^{\infty} A_m \cos(m\omega_s t) \tag{3.163}$$

$$s_t(t) = A_{00} + \sum_{m=2,4,\ldots}^{\infty} A_m \cos(m\omega_s t) \tag{3.164}$$

The following conclusions can be made from the above switching functions:

(a) The "total" switching function $s_t(t)$ contains the dc harmonic component as well as harmonics at even multiples of the switching frequency, whereas the harmonics at odd multiples of the switching frequency are cancelled out. Therefore, it can be said that the remaining harmonics of $s_t(t)$ are equal in magnitude and phase to the corresponding components of $s_1(t)$.

(b) The "difference" switching function $s_d(t)$ contains harmonics only at odd multiples of the switching frequency, while the harmonics at even multiples cancel out. Thus, the harmonic content of $s_d(t)$ are equal in magnitude and phase to that of the corresponding harmonics of $s_1(t)$.

(c) The above two conclusions lead to the following important conclusion, which was also shown for the sinusoidal modulation case:

$$|S_d(\omega)|\,|S_t(\omega)| \approx 0 \tag{3.165}$$

The frequency spectra of $|S_1(\omega)|$, $|S_d(\omega)|$, $|S_t(\omega)|$ and $|S_d(\omega)||S_t(\omega)|$ for different duty-cycles are plotted and compared in the following example.

Example 3.10

In this example, $f_r(t)$ is defined as follows:

$$f_r(t) = A = 2D - 1 \tag{3.166}$$

The switching frequency $f_s = 5\ kHz$ and the duty-cycle $D = \{0.2,\ 0.5\}$. These values translate to the following values of A: $A = \{-0.6,\ 0.0\}$.

- For $D = 0.2$, $f_r(t) = A = -0.6$. The spectra of $|S_1(\omega)|$, $|S_d(\omega)|$, $|S_t(\omega)|$ and of $|S_d(\omega)||S_t(\omega)|$ for this case are shown in Figure 3-24.

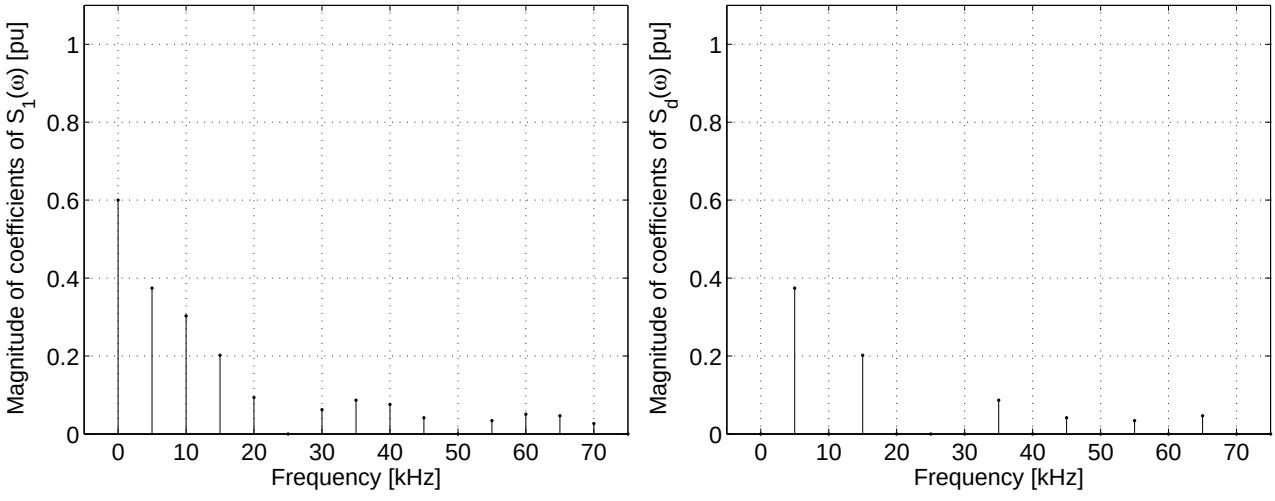

(a) (b)

Figure 3-24. *Spectra of switching functions for 2 cells with $D = 0.2$ and $f_s = 5\ kHz$.*

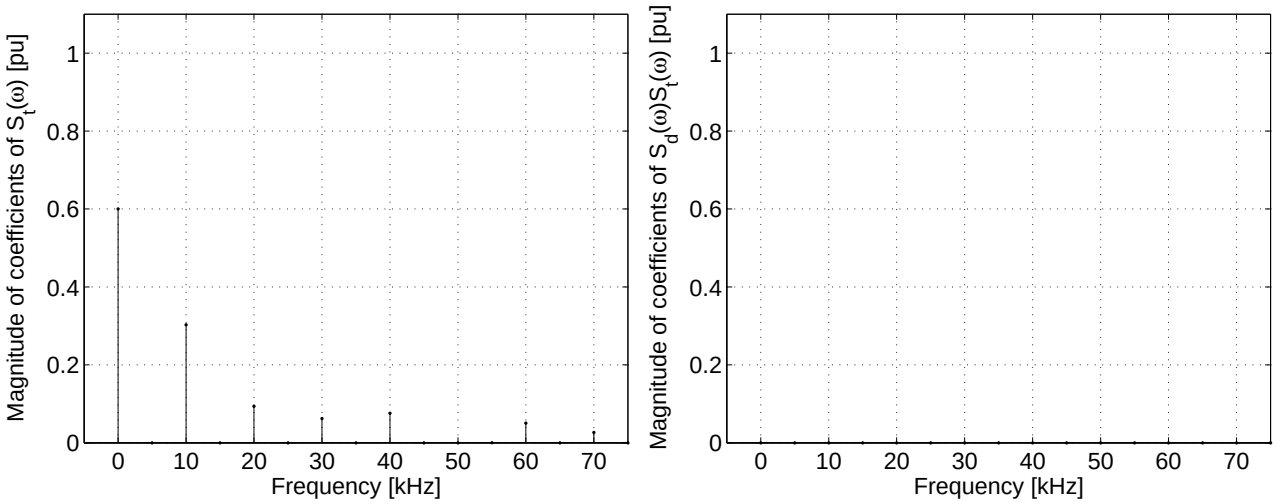

(c) (d)

Figure 3-24. *Spectra of switching functions for* 2 *cells with* $D = 0.2$ *and* $f_s = 5\ kHz$ *(cont.).*

The spectra of $S_d(\omega)$ are at odd multiples of the switching frequency f_s. These harmonics are zero when m is a multiple of 5. In contrast to that, the spectra of $S_t(\omega)$ are at even multiples of the switching frequency. These harmonics are also zero when m is a multiple of 5. The dc harmonic component is cancelled out in $S_d(\omega)$, while it remains in $S_t(\omega)$. It is clear from Figure 3-24 that the spectra of $S_d(\omega)$ and $S_t(\omega)$ do not overlap, due to the fact that the spectra of $|S_d(\omega)||S_t(\omega)| \approx 0$ in Figure 3-24(d).

- For $D = 0.5$, $f_r(t) = A = 0$. The spectra of $|S_1(\omega)|$, $|S_d(\omega)|$, $|S_t(\omega)|$ and of $|S_d(\omega)||S_t(\omega)|$ for this case are shown in Figure 3-25.

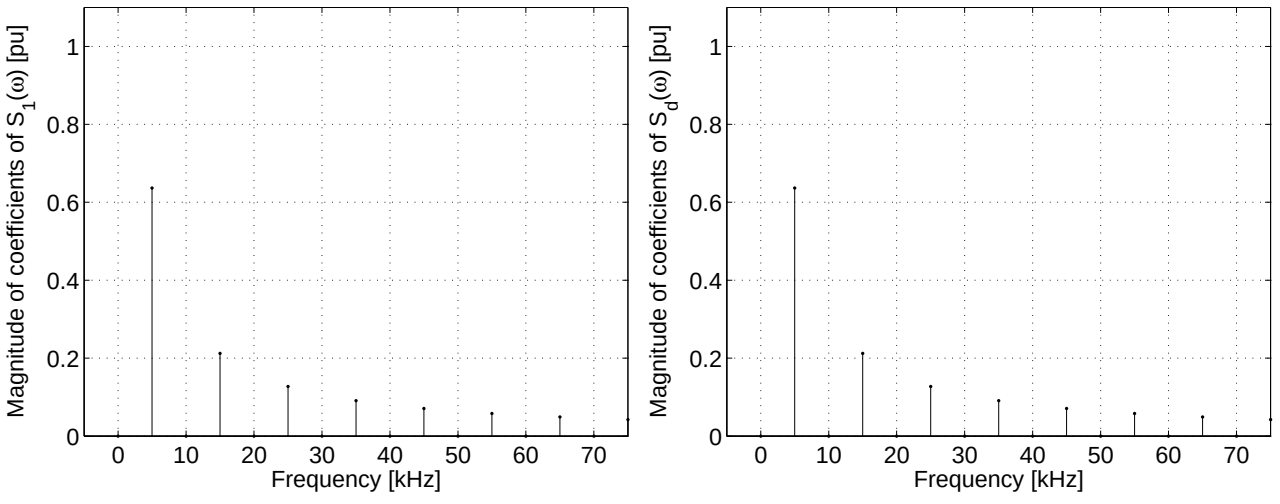

(a) (b)

Figure 3-25. *Spectra of switching functions for* 2 *cells with* $D = 0.5$ *and* $f_s = 5\ kHz$.

Again, the spectra of $S_d(\omega)$ are at odd multiples of the switching frequency f_s, while the spectra of $S_t(\omega)$ are all zero for this case. The reason for this follows from equation (3.164) and

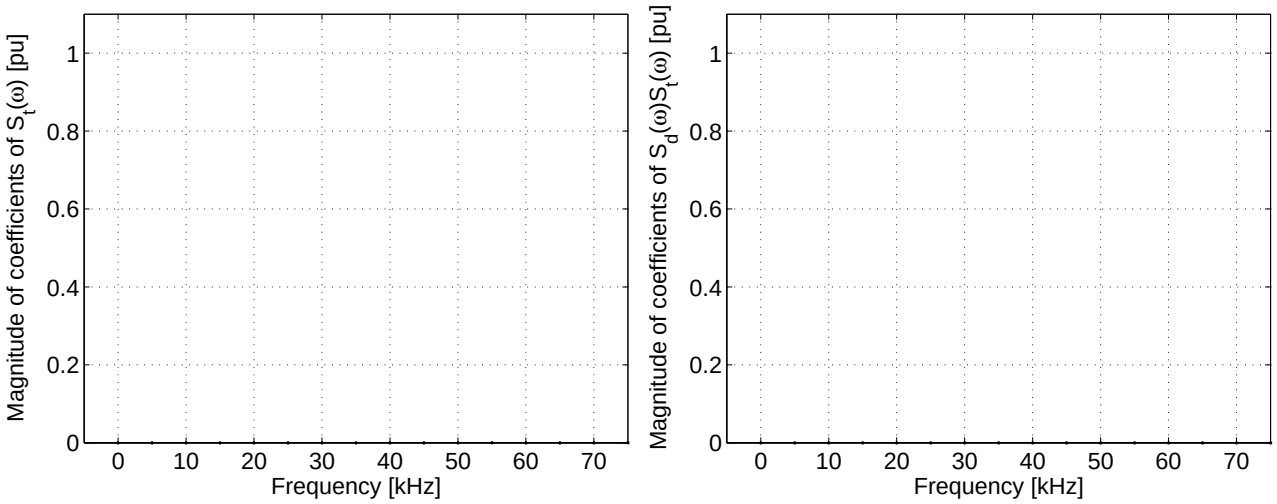

(c) (d)

Figure 3-25. *Spectra of switching functions for* 2 *cells with* $D = 0.5$ *and* $f_s = 5\ kHz$ *(cont.).*

the behaviour of the coefficients. From equation (3.164) it is clear that $S_t(\omega)$ contains only harmonics at even multiples m of the switching frequency. Due to the fact that the duty-cycle $D = \frac{1}{2}$, the coefficient $A_m = \sin(\frac{m\pi}{2}) = 0$ for even m. The dc harmonic component is zero for this case. It is also clear from Figure 3-25 that the spectra of $S_d(\omega)$ and $S_t(\omega)$ do not overlap, because the spectra of $|S_t(\omega)|$ are zero. Therefore, $|S_d(\omega)||S_t(\omega)| \approx 0$ in Figure 3-25(d).

3.3.2.3 Switching functions of 3-cell fixed duty-cycle switching

For this case the switching functions are again exactly the same as in section 3.3.1.3 earlier in this chapter, except for the fact that the reference signal is a dc-signal. The duty-cycle is defined in the same way as discussed in the previous section and is also the same for each cell for a given switching cycle. Therefore, the switching functions can again be defined as follows:

$$s_1(t) = \begin{cases} \quad 1 & \text{if } f_{c_1}(t) < 2D - 1 \\ -\quad 1 & \text{if } 2D - 1 < f_{c_1}(t) \end{cases} \tag{3.167}$$

$$s_2(t) = \begin{cases} \quad 1 & \text{if } f_{c_2}(t) < 2D - 1 \\ -\quad 1 & \text{if } 2D - 1 < f_{c_2}(t) \end{cases} \tag{3.168}$$

$$s_3(t) = \begin{cases} \quad 1 & \text{if } f_{c_3}(t) < 2D - 1 \\ -\quad 1 & \text{if } 2D - 1 < f_{c_3}(t) \end{cases} \tag{3.169}$$

A triangular carrier signal is again used with an angular frequency of ω_s equal to the switching frequency. Interleaved PWM is again used and generated by using 3 carrier signals that are phase-shifted by $120°$. These two carriers are the same as defined in earlier sections and can be written as

follows:

$$f_{c_1}(t) = \frac{2}{\pi} \arcsin\left[\sin\left(\omega_s t\right)\right] \tag{3.170}$$

$$f_{c_2}(t) = \frac{2}{\pi} \arcsin\left[\sin\left(\omega_s t - \frac{2\pi}{3}\right)\right] \tag{3.171}$$

$$f_{c_3}(t) = \frac{2}{\pi} \arcsin\left[\sin\left(\omega_s t - \frac{4\pi}{3}\right)\right] \tag{3.172}$$

Interleaved switching using a fixed duty-cycle is illustrated for a 3-cell multicell converter in the following example.

Example 3.11
A 3-cell multicell converter is switched using interleaved PWM with a fixed duty-cycle of $D = 0.6$. The dc reference signal $f_r(t)$ is defined as follows:

$$f_r(t) = A = 2D - 1 = 0.2 \tag{3.173}$$

where the switching frequency $f_s = 500\ Hz$.

In order to generate the switching functions, 3 triangular carriers are used. The 3 carriers are respectively 120° out of phase. The generation of the switching function of the first cell, i.e. $s_1(t)$ is shown in Figure 3-26(a). The carrier signal of the first cell is denoted by $f_c(t)$ and shown in green, while the reference signal is shown in blue.

The generation of the switching functions of the second and third cells, i.e. $s_2(t)$ and $s_3(t)$ are shown in Figures 3-26(b) and 3-26(c). The respective carrier signals of these cells are both shown in green, while the dc references are shown in blue.

The "difference" switching functions $s_{d_1}(t)$ and $s_{d_2}(t)$ and the "total" switching function $s_t(t)$ are shown respectively in Figures 3-26(d), 3-26(e) and 3-26(f). These switching functions were defined earlier in equations (2.35), (2.36) and (2.37) in Chapter 2 section 2.9 and were repeated in equations (3.65), (3.66) and (3.67).

The switching functions for the fixed duty-cycle 3-cell case also have the same coefficients as those for the "single"- and 2-cell cases. The differences are that the switching function of cell 2 is phase-shifted by $\frac{2\pi}{3}$ radians and that of cell 3 by $\frac{4\pi}{3}$ radians respectively from that of the first cell. The switching function of the first cell is the same as for the previous cases and was calculated in equation

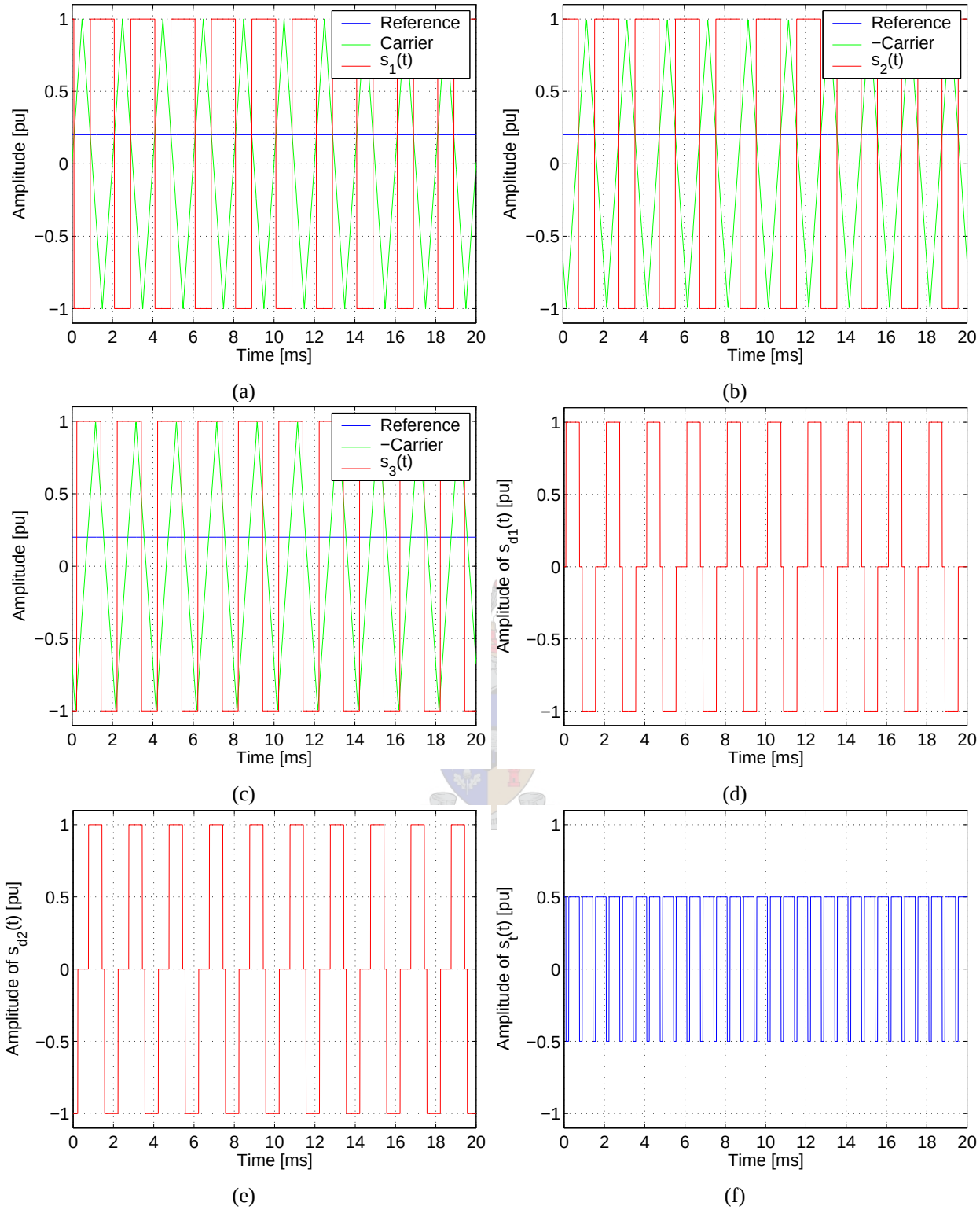

Figure 3-26. *3-cell multicell interleaved switching using a fixed duty-cycle of* $D = 0.6$.

(3.147) to be the following:

$$s_1(t) = 2D - 1 + \frac{4}{\pi}\sum_{m=1}^{\infty}\frac{1}{m}\sin(m\pi D)\cos(m\omega_s t) \tag{3.174}$$

Due to interleaved switching, the switching function of cell 2 lags that of cell 1 by $\frac{2\pi}{3}$ radians. The switching function for $s_2(t)$ can therefore be written directly as follows:

$$s_2(t) = 2D - 1 + \frac{4}{\pi}\sum_{m=1}^{\infty}\frac{1}{m}\sin(m\pi D)\cos\left(m\omega_s t - \frac{2m\pi}{3}\right) \tag{3.175}$$

Interleaved switching as described earlier for this case implies that the switching function of cell 3 lags that of cell 1 by $\frac{4\pi}{3}$ radians. The switching function for $s_3(t)$ can therefore also be written directly as follows:

$$\begin{aligned} s_3(t) &= 2D - 1 + \frac{4}{\pi}\sum_{m=1}^{\infty}\frac{1}{m}\sin(m\pi D)\cos\left(m\omega_s t - \frac{4m\pi}{3}\right) \\ &= 2D - 1 + \frac{4}{\pi}\sum_{m=1}^{\infty}\frac{1}{m}\sin(m\pi D)\cos\left(m\omega_s t + \frac{2m\pi}{3}\right) \end{aligned} \tag{3.176}$$

Attention should be given to the trigonometric terms in equations (3.175) and (3.176) containing $\pm\frac{2m\pi}{3}$. This term has the following effect on the trigonometric terms' signs:

$$\cos\left(m\omega_s t - \frac{2m\pi}{3}\right) = \begin{cases} \cos(m\omega_s t) & \text{for } m = 3k \\ \cos\left(m\omega_s t - \frac{2\pi}{3}\right) & \text{for } m = 3k+1 \\ \cos\left(m\omega_s t + \frac{2\pi}{3}\right) & \text{for } m = 3k+2 \end{cases} \tag{3.177}$$

$$\cos\left(m\omega_s t + \frac{2m\pi}{3}\right) = \begin{cases} \cos\left(m\omega_s t\right) & \text{for } m = 3k \\ \cos\left(m\omega_s t + \frac{2\pi}{3}\right) & \text{for } m = 3k+1 \\ \cos\left(m\omega_s t - \frac{2\pi}{3}\right) & \text{for } m = 3k+2 \end{cases} \tag{3.178}$$

As in the 2-cell case, the Fourier series components of $s_1(t)$, $s_2(t)$ and $s_3(t)$ for the fixed duty-cycle case have the same characteristics as for sinusoidal reference case, except that there are no side-bands present around the harmonics. Therefore, the groups made up of clusters of harmonics reduce to single harmonics. The same classes and phasor representations can be used for these harmonics as discussed for the corresponding sinusoidal reference case. The phasor representations of $S_1(\omega)$, $S_2(\omega)$ and $S_3(\omega)$ were shown in Figure 3-14.

These observations in conjunction with the phasors shown in Figure 3-14 can also be used to deduce similar properties as discussed for the corresponding sinusoidal modulation case regarding the switching functions $s_{d_1}(t)$, $s_{d_2}(t)$ and $s_t(t)$ as follows:

(a) The "total" switching function contains only harmonics of *class zero*. This means that $s_t(t)$ contains the harmonic components of $s_1(t)$ at integer multiples of three times the switching frequency. This can be seen in Figures 3-14(g) through 3-14(i).

(b) The "difference" switching functions $s_{d_1}(t)$ and $s_{d_2}(t)$ contain harmonics of *class one* and *class two*, which means that they contain only the harmonic components of $s_1(t)$ around multiples m

of the switching frequency where $m = 3k + 1$ and $m = 3k + 2$ for $k = 0, \pm 1, \pm 2, \ldots$. This can be seen in Figures 3-14(d) through 3-14(f).

(c) These two conclusions lead to the following important conclusions:

$$|S_{d_1}(\omega)|\,|S_t(\omega)| \approx 0 \tag{3.179}$$

and

$$|S_{d_2}(\omega)|\,|S_t(\omega)| \approx 0 \tag{3.180}$$

The frequency spectra of $|S_1(\omega)|$, $|S_{d_1}(\omega)|$, $|S_t(\omega)|$ and $|S_{d_1}(\omega)||S_t(\omega)|$ for different modulation indices are plotted and compared in the following example.

Example 3.12

In this example, $f_r(t)$ is again defined as follows:

$$f_r(t) = A = 2D - 1 \tag{3.181}$$

The switching frequency $f_s = 5\ kHz$ and the duty-cycle $D = \{0.2,\ 0.33,\ 0.5\}$. These values translate to the following values of A: $A = \{-0.6,\ -0.33,\ 0.0\}$.

- For $D = 0.2$, $f_r(t) = A = -0.6$. The spectra of $|S_1(\omega)|$, $|S_{d_1}(\omega)|$, $|S_t(\omega)|$ and of $|S_{d_1}(\omega)||S_t(\omega)|$ for this case are shown in Figure 3-27.

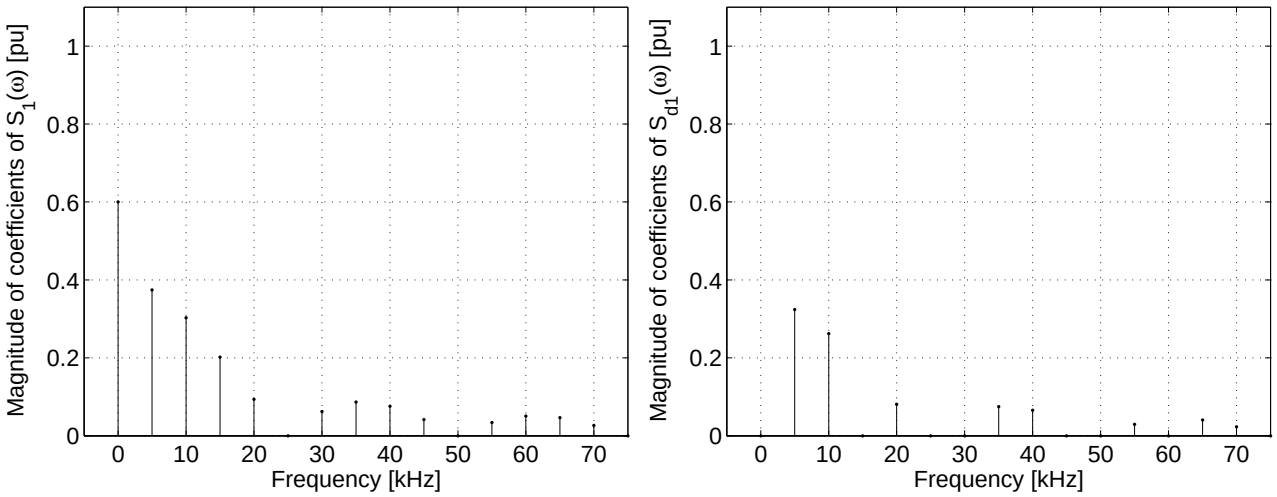

(a) (b)

Figure 3-27. *Spectra of switching functions for* 3 *cells with* $D = 0.2$ *and* $f_s = 5\ kHz$.

The spectra of $S_{d_1}(\omega)$ are at multiples m of the switching frequency f_s where $m = 3k + 1$ and $m = 3k + 2$ for $k = 0, \pm 1, \pm 2, \ldots$. These harmonics are zero when m is a multiple of 5. This is a result of the coefficient A_m containing the term $\frac{m\pi}{5}$. The spectra of $S_t(\omega)$ are at

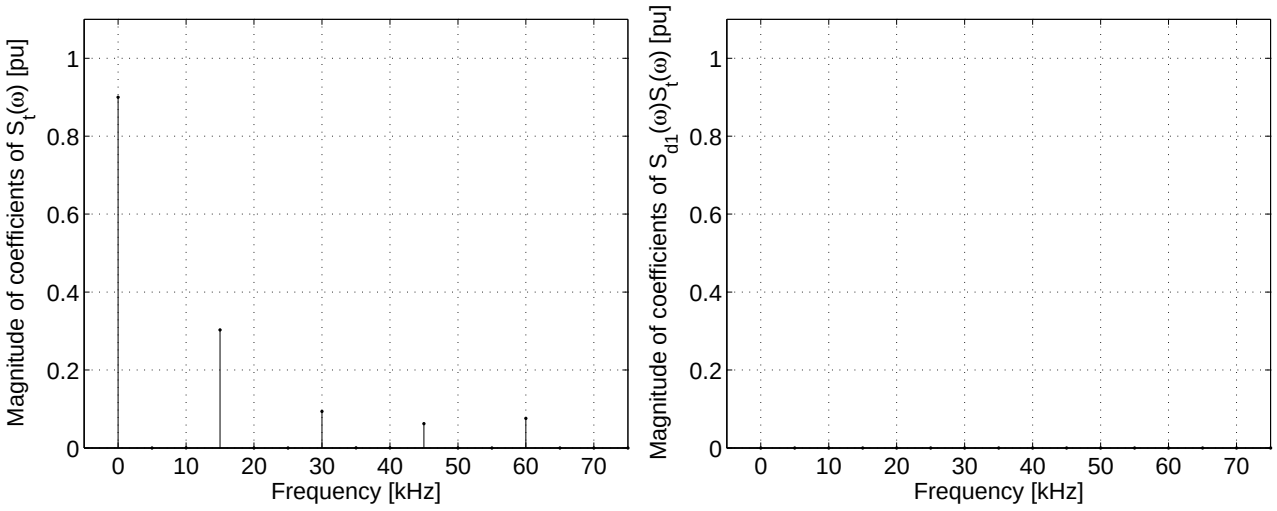

(c) (d)

Figure 3-27. *Spectra of switching functions for* 3 *cells with* $D = 0.2$ *and* $f_s = 5\ kHz$ *(cont.).*

multiples of 3 times the switching frequency. As in the 2-cell case, the dc harmonic component is cancelled out in $S_{d_1}(\omega)$, while it remains in $S_t(\omega)$. It is clear from Figure 3-27 that the spectra of $S_{d_1}(\omega)$ and $S_t(\omega)$ do not overlap, due to the fact that the spectra of $|S_{d_1}(\omega)||S_t(\omega)| \approx 0$ in Figure 3-27(d).

- For $D = 0.33$, $f_r(t) = A = -0.33$. The spectra of $|S_1(\omega)|$, $|S_{d_1}(\omega)|$, $|S_t(\omega)|$ as well as for $|S_{d_1}(\omega)||S_t(\omega)|$ are shown for this case in Figure 3-28.

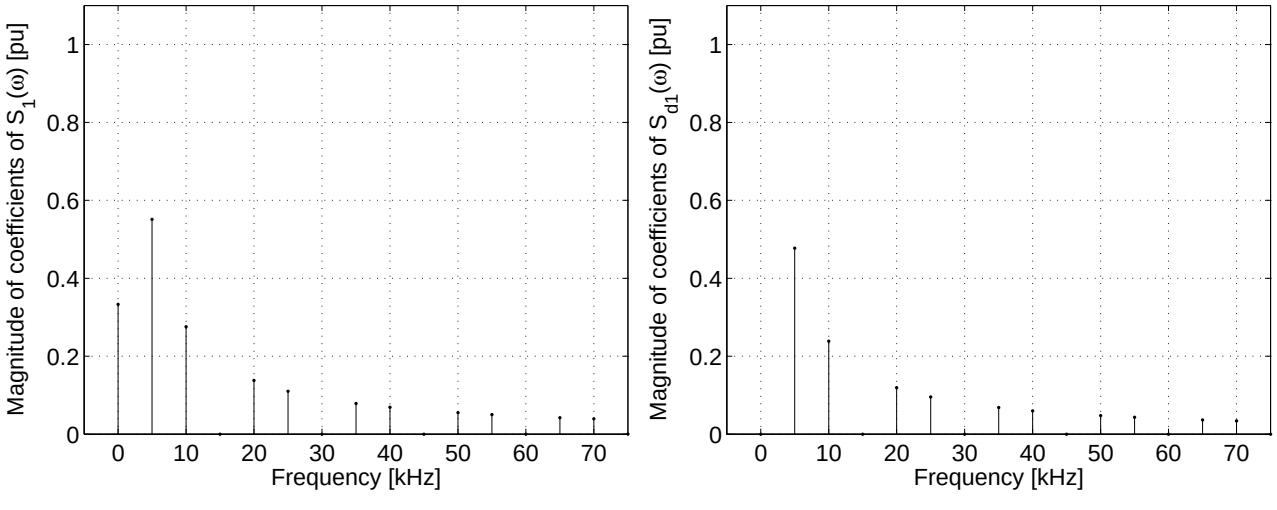

(a) (b)

Figure 3-28. *Spectra of switching functions for* 3 *cells with* $D = 0.33$ *and* $f_s = 5\ kHz$.

The spectra of $S_{d_1}(\omega)$ are at multiples m of the switching frequency where $m = 3k + 1$ and

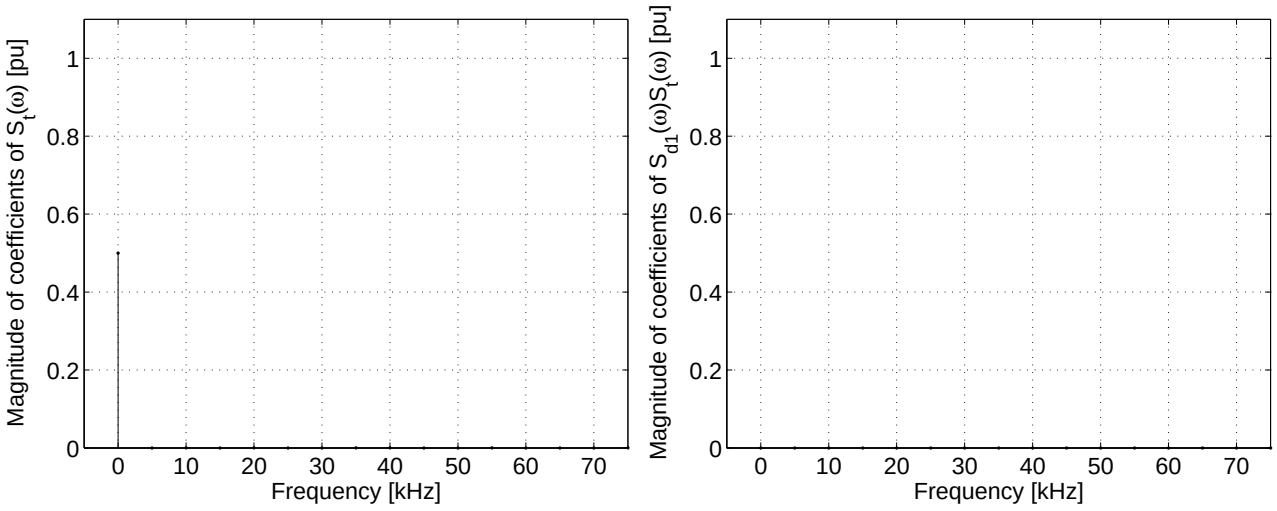

(c) (d)

Figure 3-28. *Spectra of switching functions for* 3 *cells with* $D = 0.33$ *and* $f_s = 5\ kHz$ *(cont.).*

$m = 3k+2$ for $k = 0, \pm1, \pm2, \ldots$. As in the previous case, the spectra of $S_t(\omega)$ are at multiples of 3 times the switching frequency f_s. The dc harmonic component is again cancelled out in $S_{d_1}(\omega)$, while it remains in $S_t(\omega)$. As for the previous case, it is clear from Figure 3-28 that the spectra of $S_{d_1}(\omega)$ and $S_t(\omega)$ do not overlap in Figure 3-28(d).

- For $D = 0.5$, $f_r(t) = A = 0$. The spectra of $|S_1(\omega)|$, $|S_{d_1}(\omega)|$, $|S_t(\omega)|$ and of $|S_{d_1}(\omega)||S_t(\omega)|$ for this case are shown in Figure 3-29.

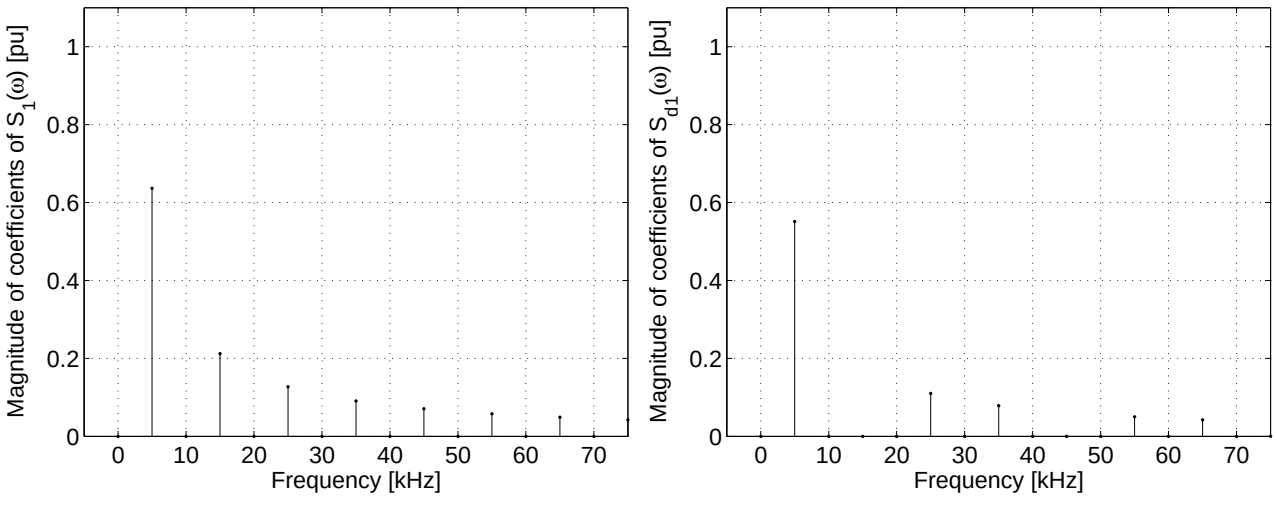

(a) (b)

Figure 3-29. *Spectra of switching functions for* 3 *cells with* $D = 0.5$ *and* $f_s = 5\ kHz$.

For this final case, the dc harmonic component is zero from the definition in equation (3.144). The spectra of $S_{d_1}(\omega)$ are at multiples m of the switching frequency where $m = 3k + 1$ and

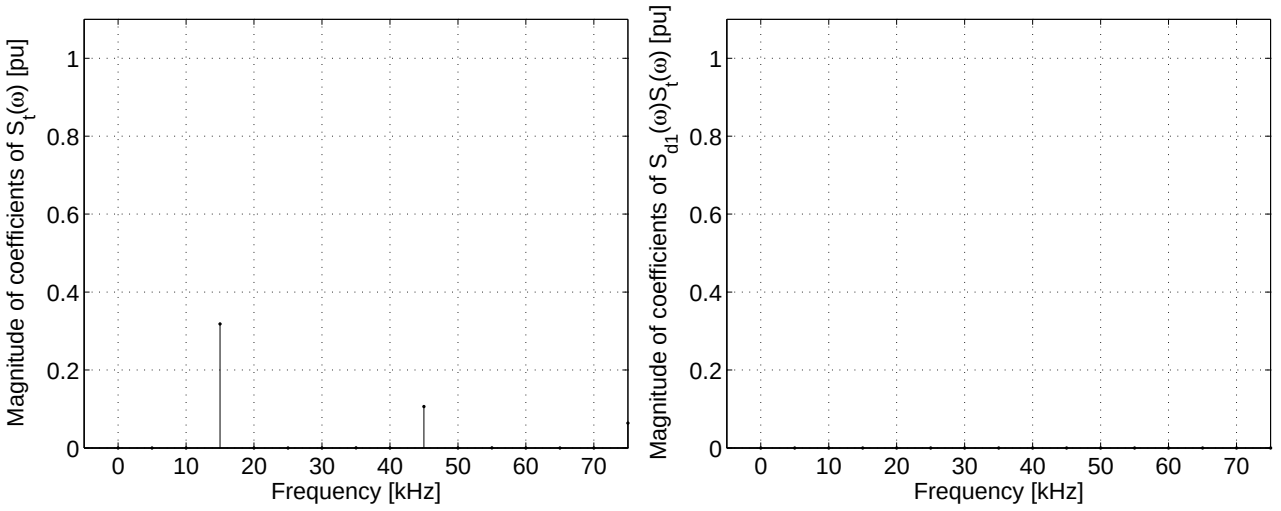

(c) (d)

Figure 3-29. *Spectra of switching functions for* 3 *cells with* $D = 0.5$ *and* $f_s = 5\ kHz$ *(cont.).*

$m = 3k + 2$ where $k = 0, \pm1, \pm2, \ldots$. These harmonics are zero when m is a multiple of 2. $S_t(\omega)$ has harmonics at multiples of 3 times the switching frequency, except where m is a multiple of 2. As in the previous cases it is clear from Figure 3-29 that the spectra of $S_{d_1}(\omega)$ and $S_t(\omega)$ do not overlap. This proves that $|S_{d_1}(\omega)||S_t(\omega)| \approx 0$ as seen in Figure 3-29(d). The same properties that are valid for the spectra of $S_{d_1}(\omega)$ are also valid for $S_{d_2}(\omega)$. This is because $S_{d_1}(\omega)$ and $S_{d_2}(\omega)$ are equal in magnitude and different in phase as shown earlier.

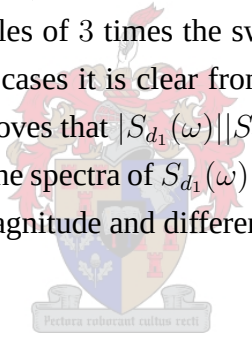

3.3.2.4 Switching functions of *p*-cell fixed duty-cycle switching

For the p-cell case, the switching functions are defined in the same way as in section 3.3.1.4 earlier in this chapter, except that a dc-signal is used as the reference. The duty-cycle is again defined as in the previous sections and is also the same for each successive cell for a given switching period. These switching functions can therefore be defined in general for the i^{th} case as follows:

$$s_i(t) = \begin{cases} \quad 1 & \text{if } f_{c_i}(t) < 2D - 1 \\ -\quad 1 & \text{if } 2D - 1 < f_{c_i}(t) \end{cases} \quad \text{for } i = 1, \ldots, p \tag{3.182}$$

As mentioned earlier, as a result of using interleaved switching, the carriers of the p cells are $\frac{2\pi}{p}$ radians out of phase, i.e. the carrier of cell 1 lags that of cell 1 by $\frac{2\pi}{p}$ radians and the carrier of cell 3 lags that of cell 2 by $\frac{2\pi}{p}$ radians. In the same way, the carrier of the p^{th} cell also lags that of the $(p-1)^{th}$ cell by $\frac{2\pi}{p}$ radians. These carriers can be written for the i^{th} cell as follows:

$$f_{c_i}(t) = \frac{2}{\pi} \arcsin\left[\sin\left(\omega_s t - (i-1)\frac{2\pi}{p}\right)\right] \tag{3.183}$$

For the case of a p-cell multicell converter, the first switching function is exactly the same as for the previous cases. This switching function is repeated here for convenience as follows:

$$s_1(t) = 2D - 1 + \frac{4}{\pi}\sum_{m=1}^{\infty}\frac{1}{m}\sin(m\pi D)\cos(m\omega_s t) \tag{3.184}$$

The second switching function can be obtained by phase-shifting the first switching function by $\frac{2\pi}{p}$ radians. The resulting switching function is as follows:

$$s_2(t) = 2D - 1 + \frac{4}{\pi}\sum_{m=1}^{\infty}\frac{1}{m}\sin(m\pi D)\cos\left(m\omega_s t - \frac{2m\pi}{p}\right) \tag{3.185}$$

In the same way an expression for the switching function $s_3(t)$ can be obtained by phase-shifting $s_1(t)$ by $\frac{4\pi}{p}$ radians as follows:

$$s_3(t) = 2D - 1 + \frac{4}{\pi}\sum_{m=1}^{\infty}\frac{1}{m}\sin(m\pi D)\cos\left(m\omega_s t - \frac{4m\pi}{p}\right) \tag{3.186}$$

Using the same method as used to obtain the previous switching functions, the switching function $s_p(t)$ can be obtained and is as follows:

$$s_p(t) = 2D - 1 + \frac{4}{\pi}\sum_{m=1}^{\infty}\frac{1}{m}\sin(m\pi D)\cos\left(m\omega_s t - \frac{2m\pi(p-1)}{p}\right) \tag{3.187}$$

As for the sinusoidal modulation case it is clear that the coefficients for $s_1(t)$, $s_2(t)$, $s_3(t), \ldots, s_p(t)$ are of equal magnitude for all values of m, while they are of equal phase only around multiples m of the switching frequency, where $m = pk$ and $k = 0, \pm1, \pm2, \ldots$. The phases of $s_1(t),\ s_2(t),\ s_3(t), \ldots,$ $s_p(t)$ differ by $\frac{2\pi}{p}$ radians around multiples m of the switching frequency where $m = pk + 1$, $m = pk + 2$ up to $m = pk + (p - 1)$.

As in the 2- and 3-cell cases, the Fourier series components of $s_1(t)$, $s_2(t)$, $s_3(t), \ldots, s_p(t)$ for the fixed duty-cycle case have the same characteristics as for the sinusoidal reference case, except that there are no side-bands present around the harmonics. Therefore, the groups made up of clusters of harmonics reduce to single harmonics. The same classes and phasor representations can be used for these harmonics as discussed for the corresponding sinusoidal reference case. Phasor representations of the switching functions for 4- and 5 cells are included in Appendix A section A.2 in Figures A-2 and A-3 for reference.

These observations in conjunction with the phasors shown in Figure A-2 and A-3 can also be used to deduce similar properties as discussed for the corresponding sinusoidal modulation case regarding the switching functions $s_{d_1}(t)$, $s_{d_2}(t)$ up to $s_{d_{p-1}}(t)$ and $s_t(t)$ as follows:

(a) The "total" switching function contains only harmonics of *class zero*. This means that $s_t(t)$ contains the frequency components of the reference signal as well as the harmonic components of $s_1(t)$ around integer multiples of p times the switching frequency. This can be seen in Figures A-2(e) through A-2(l) as well as in Figures A-3(g) through A-3(o).

(b) The "difference" switching functions $s_{d_1}(t),\ s_{d_2}(t), \ldots,\ s_{d_{p-1}}(t)$ contain harmonics of *class one*, *class two* up to and including *class p-1*. This can be seen in Figures A-2(c) through A-2(j) as well as in Figures A-3(d) through A-3(m). The same relationships between S_{d_i} and $S_{d_{i-1}}$ are valid as discussed in the corresponding sinusoidal modulation section.

(c) These 2 conclusions lead to same conclusions found for the sinusoidal modulation case:

$$|S_{d_1}(\omega)|\,|S_t(\omega)| \approx 0 \tag{3.188}$$

$$|S_{d_2}(\omega)|\,|S_t(\omega)| \approx 0 \tag{3.189}$$

$$\vdots\ \vdots\ \vdots$$

$$\left|S_{d_{p-1}}(\omega)\right|\,|S_t(\omega)| \approx 0 \tag{3.190}$$

The frequency spectra of $|S_1(\omega)|$, $|S_{d_1}(\omega)|$, $|S_t(\omega)|$ and $|S_{d_1}(\omega)||S_t(\omega)|$ for the same duty-cycles, but for the 4- and 5-cell cases are plotted and compared in the following examples.

Example 3.13

In this example, the reference $f_r(t)$ is defined in the same way as in the previous example. The switching frequency $f_s = 5\ kHz$ and the duty-cycle $D = \{0.2\}$. This value of D translate to the following value of A: $A = \{-0.6\}$.

- For the 4-cell case, where $D = 0.2$ the spectra of $|S_1(\omega)|$, $|S_{d_1}(\omega)|$, $|S_t(\omega)|$ and of $|S_{d_1}(\omega)||S_t(\omega)|$ are shown in Figure 3-30.

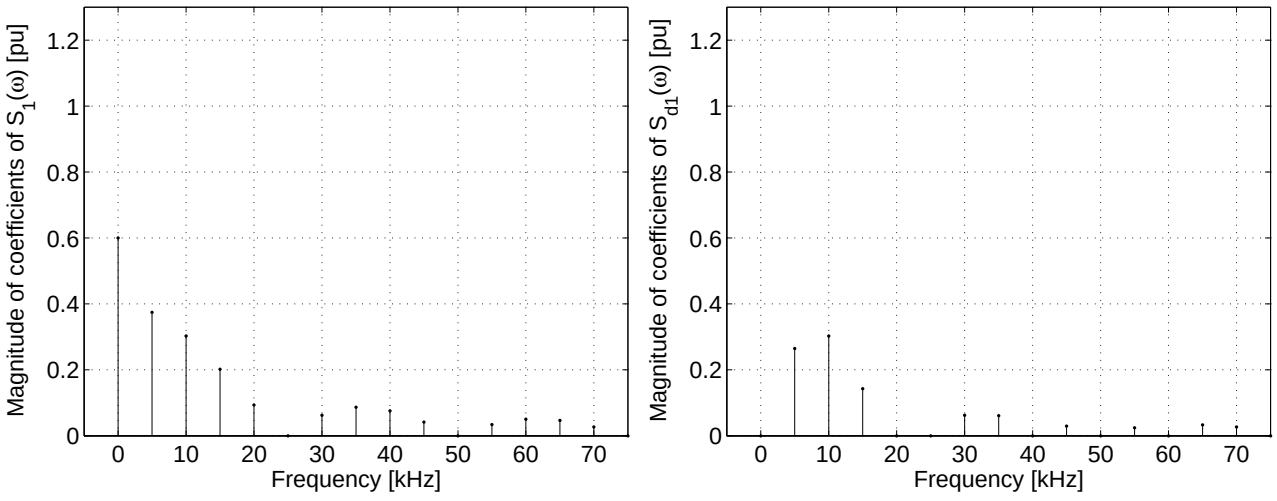

(a) (b)

Figure 3-30. *Harmonics of* 4*-cell switching with* $D = 0.2$ *and* $f_s = 5\ kHz$.

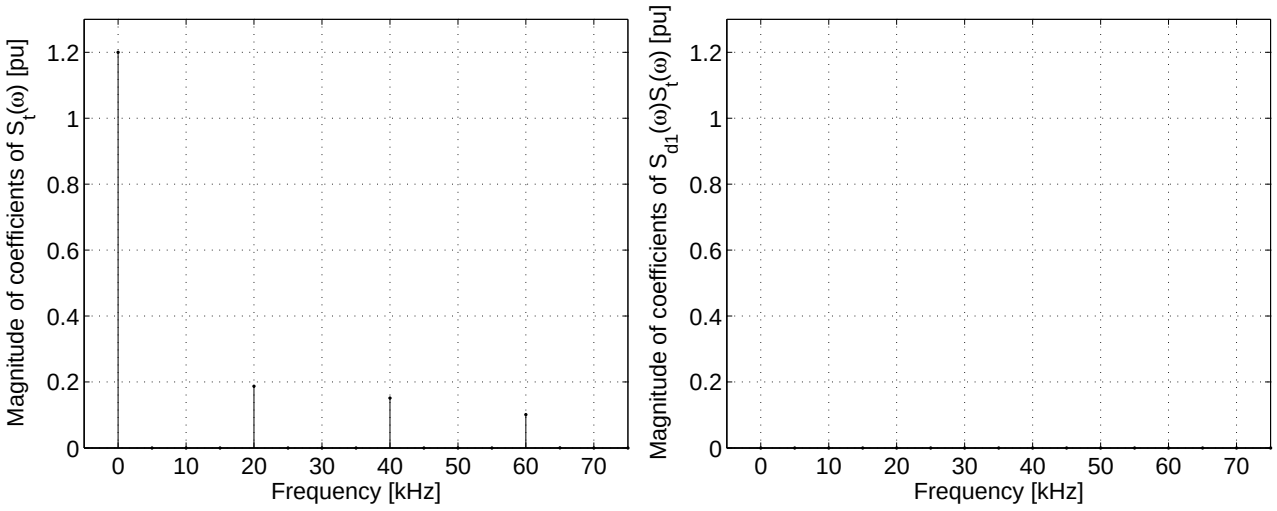

(c) (d)

Figure 3-30. *Harmonics of* 4*-cell switching with* $D = 0.2$ *and* $f_s = 5\ kHz$ *(cont.).*

The spectra of $S_{d_1}(\omega)$ are at multiples m of the switching frequency f_s where $m = 4k + 1$, $m = 4k + 2$ and $m = 4k + 3$ for $k = 0, \pm1, \pm2, \ldots$. These harmonics are zero when m is a multiple of 5. The spectra of $S_t(\omega)$ are at multiples of 4 times the switching frequency. As in the 2- and 3-cell cases, the dc harmonic component is cancelled out in $S_{d_1}(\omega)$, while it remains in $S_t(\omega)$. It is clear from Figure 3-30 that the spectra of $S_{d_1}(\omega)$ and $S_t(\omega)$ do not overlap, due to the fact that the spectra of $|S_{d_1}(\omega)||S_t(\omega)| \approx 0$ in Figure 3-30(d).

- For the 5-cell case where $D = 0.2$ the spectra of $|S_1(\omega)|$, $|S_{d_1}(\omega)|$, $|S_t(\omega)|$ and of $|S_{d_1}(\omega)||S_t(\omega)|$ are shown in Figure 3-31.

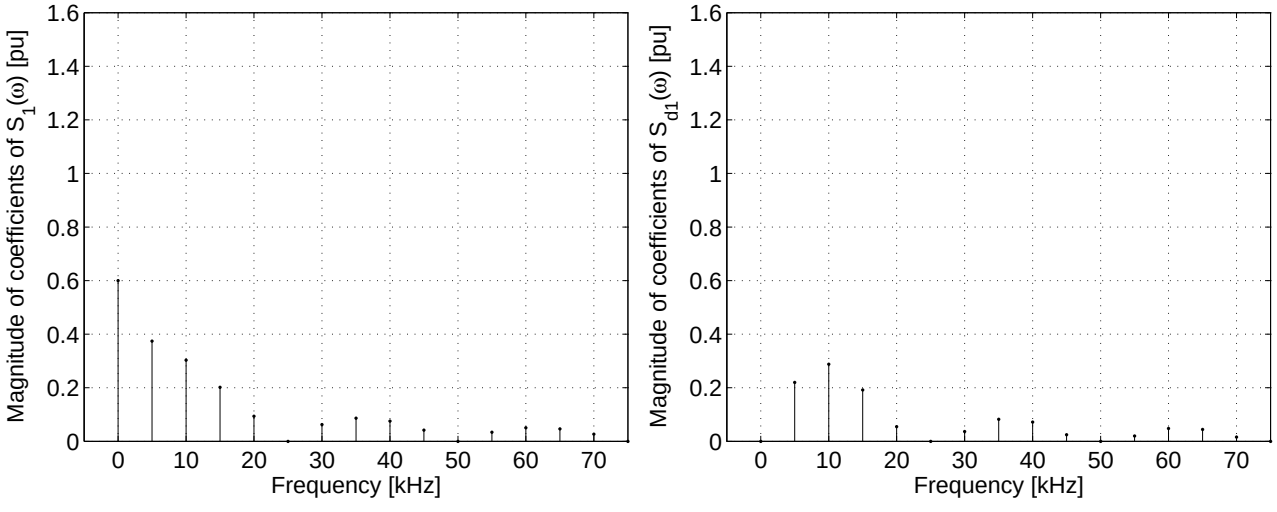

(a) (b)

Figure 3-31. *Harmonics of* 5*-cell switching with* $D = 0.2$ *and* $f_s = 5\ kHz$.

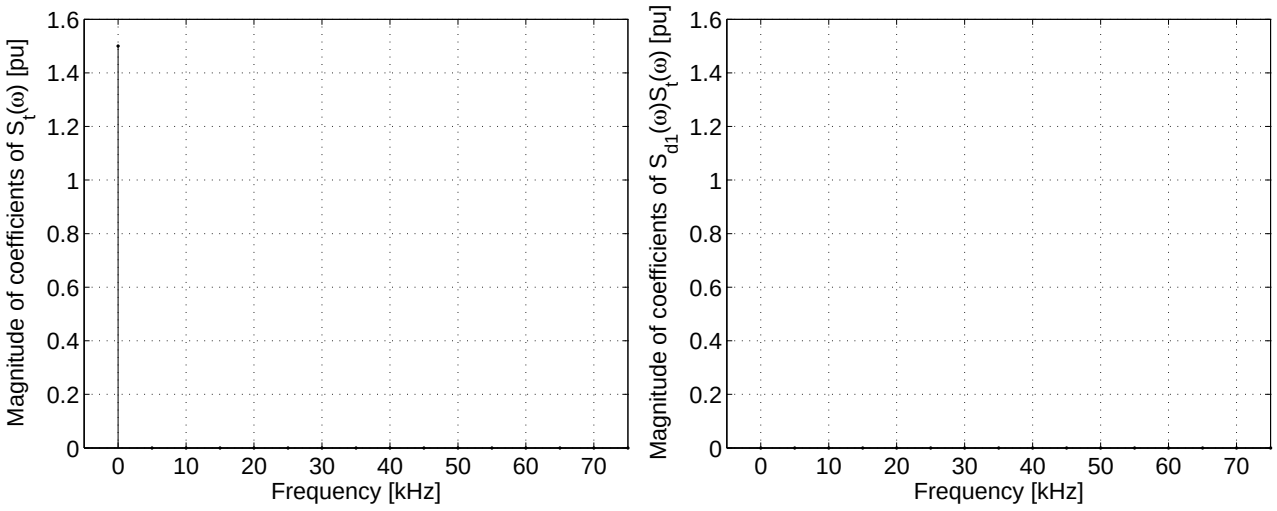

(c) (d)

Figure 3-31. *Harmonics of* 5*-cell switching with* $D = 0.2$ *and* $f_s = 5\ kHz$ *(cont.).*

For this case, the spectra of $S_{d_1}(\omega)$ are at multiples m of the switching frequency f_s where $m = 5k + 1$, $m = 5k + 2$, $m = 5k + 3$ and $m = 5k + 4$ for $k = 0, \pm1, \pm2, \ldots$. The spectra of $S_t(\omega)$ are all zero, except for the dc harmonic component. This can be seen in the phasor representations shown in Figure A-3. The remaining harmonics at $m = 5k$ are also cancelled out as the coefficients are zero when m is a multiple of 5. As for the previous cases of 2-, 3- and 4-cells, it is clear from Figure 3-31 that the spectra of $S_{d_1}(\omega)$ and $S_t(\omega)$ do not overlap. This proves that $|S_{d_1}(\omega)||S_t(\omega)| \approx 0$. The same properties that are valid for the spectra of $S_{d_1}(\omega)$ are also valid for $S_{d_2}(\omega)$, $S_{d_3}(\omega)$ and $S_{d_4}(\omega)$, because they are equal in magnitude and different in phase as shown earlier.

Example 3.14

In this example, the reference $f_r(t)$ is again defined as follows:

$$f_r(t) = A = 2D - 1 \tag{3.191}$$

The switching frequency $f_s = 5\ kHz$ and the duty-cycle $D = 0.25$. This value of D translates to the following value of A: $A = -0.5$.

- For the 4-cell case, where $D = 0.25$ the spectra of $|S_1(\omega)|$, $|S_{d_1}(\omega)|$, $|S_t(\omega)|$ and of $|S_{d_1}(\omega)||S_t(\omega)|$ are shown in Figure 3-32.

  The spectra of $S_{d_1}(\omega)$ are at multiples m of the switching frequency f_s where $m = 4k + 1$, $m = 4k + 2$ and $m = 4k + 3$ for $k = 0, \pm1, \pm2, \ldots$. As in the 2- and 3-cell cases, the dc harmonic component is cancelled out in $S_{d_1}(\omega)$, while it remains in $S_t(\omega)$. The spectra of $S_t(\omega)$ consist only of the dc harmonic component as all the other harmonics are cancelled out. This can be seen in the phasor representations shown in Figure A-2. The remaining harmonics

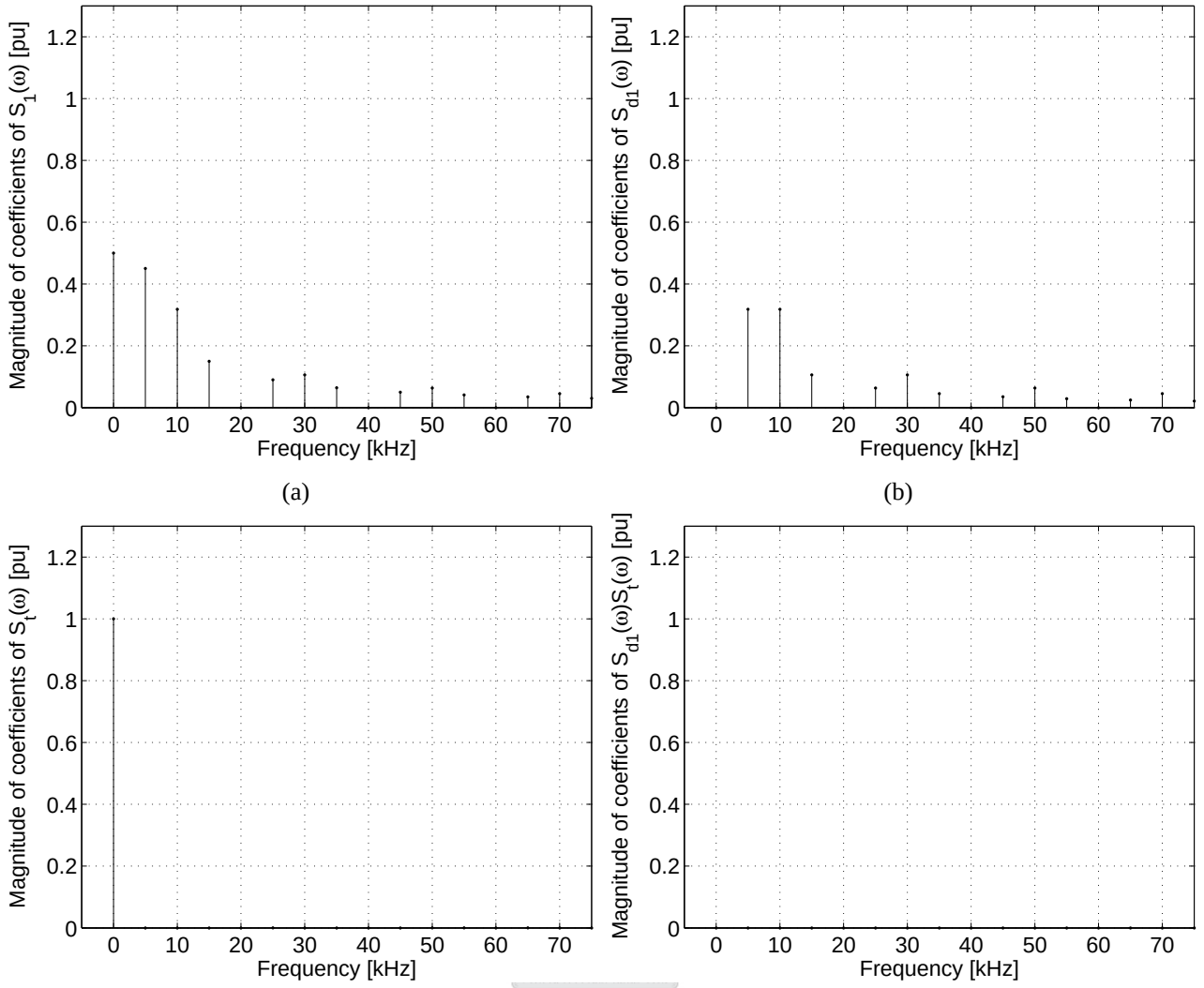

Figure 3-32. *Harmonics of* 4*-cell switching with* $D = 0.25$ *and* $f_s = 5\ kHz$.

at $m = 4k$ are also cancelled out as the coefficients are zero when m is a multiple of 4. It is clear from Figure 3-32 that the spectra of $S_{d_1}(\omega)$ and $S_t(\omega)$ do not overlap, due to the fact that the spectra of $|S_{d_1}(\omega)||S_t(\omega)| \approx 0$ in Figure 3-32(d).

- For the 5-cell case, where $D = 0.25$ the spectra of $|S_1(\omega)|$, $|S_{d_1}(\omega)|$, $|S_t(\omega)|$ and of $|S_{d_1}(\omega)||S_t(\omega)|$ are shown in Figure 3-33.

  For this final case, the spectra of $S_{d_1}(\omega)$ are at multiples m of the switching frequency f_s where $m = 5k+1$, $m = 5k+2$, $m = 5k+3$ and $m = 5k+4$ for $k = 0, \pm1, \pm2, \ldots$. These harmonics are zero when m is a multiple of 4. The spectra of $S_t(\omega)$ are at multiples of 5 times the switching frequency. As for the previous cases of 2-, 3- and 4-cells, it is clear from Figure 3-33 that the spectra of $S_{d_1}(\omega)$ and $S_t(\omega)$ do not overlap. This proves that $|S_{d_1}(\omega)||S_t(\omega)| \approx 0$. The same properties that are valid for the spectra of $S_{d_1}(\omega)$ are also valid for $S_{d_2}(\omega)$, $S_{d_3}(\omega)$ and $S_{d_4}(\omega)$, because they are equal in magnitude and different in phase as shown earlier.

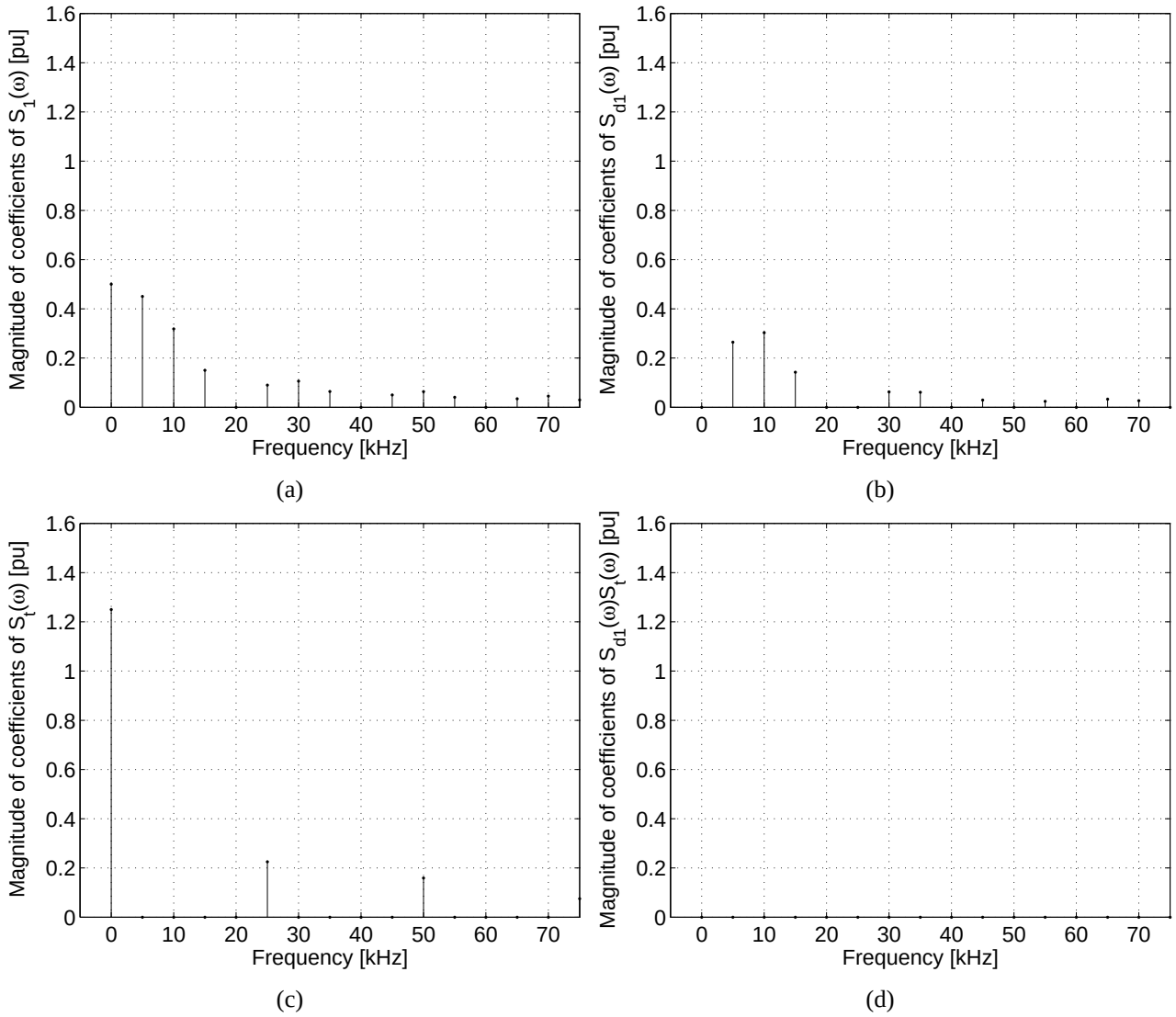

Figure 3-33. *Harmonics of* 5*-cell switching with* $D = 0.25$ *and* $f_s = 5\ kHz$.

3.3.3 Special cases

In the harmonic analysis done in this chapter there exists a number of special cases that need to be mentioned. These cases are not guaranteed to result in unbalance, but caution needs to be taken when dealing with them.

The number of cells as well as the value of the duty-cycle D can also have a dramatic effect on the spectra of the switching functions and will be discussed later in this section.

It has been shown before that for a p-cell multicell converter, there are p switching functions and $p-1$ "difference" switching functions.

It was shown for both the sinusoidal modulation- and fixed duty-cycle cases that the harmonics of $S_{d_i}(\omega)$ appear in groups around multiples of the switching frequency, where the group is a single harmonic for the fixed duty-cycle case. For a p-cell multicell converter there are $p-1$ groups. Examples of this are shown in Figure 3-34. The groups/single harmonics are denoted by ⌒ symbols. It can also be seen that some of these single harmonics are zero for the fixed duty-cycle case. This is true for every case where m is a prime factor of the denominator of the duty-cycle D, when D is expressed as a fraction, i.e. $D = \frac{numerator}{denominator}$.

Example 3.15

As an example, the harmonics of $|S_{d_1}(\omega)|$ for 2-,3- and 4-cell converters are compared for sinusoidal modulation and fixed duty-cycle PWM. The switching frequency $f_s = 5\ kHz$ for both types of modulation and $f_r = 50\ Hz$ and $m_a = 0.8$ for the sinusoidal modulation case.

(a) 2-cell case: The harmonics for the sinusoidal modulation case are shown in Figure 3-34(a). None of the groups of harmonics are zero for this case. For the fixed duty-cycle case, with $D = \frac{8}{10} = \frac{4}{5}$, it can be seen that $|S_{d_1}(\omega)| = 0$ where $m = 2k+1$ is a multiple of 5. Such an example is at $m = 5$ at $25\ kHz$. This is shown in Figure 3-34(b).

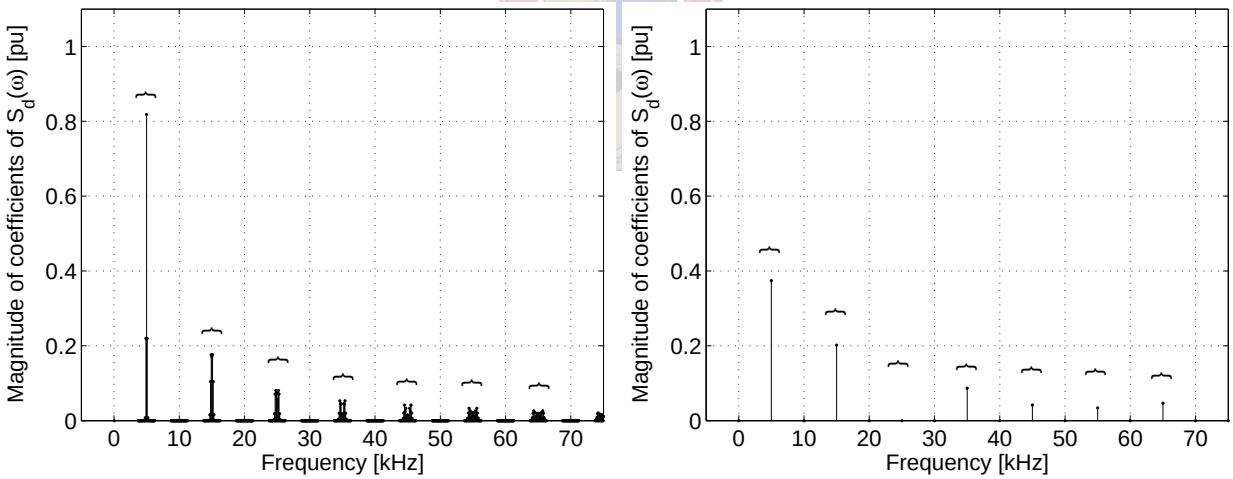

(a) $m_a = 0.8,\ p = 2$ (b) $D = 0.8,\ p = 2$

Figure 3-34. *Comparison of harmonics of sinusoidal modulation and fixed duty-cycle PWM for* $p = 2$ *with* $f_s = 5\ kHz$.

(b) 3-cell case: The harmonics for the sinusoidal modulation case are shown in Figure 3-35(a). Again, none of the groups of harmonics are zero for this case. For the fixed duty-cycle case, with $D = \frac{8}{10} = \frac{4}{5}$, it can be seen that $|S_{d_1}(\omega)| = 0$ where $m = 3k+1$ or $m = 3k+2$ is a multiple of 5. Examples of this can be seen at $m = 5$ at $25\ kHz$ and at $m = 10$ at $50\ kHz$. This is shown in Figure 3-35(b).

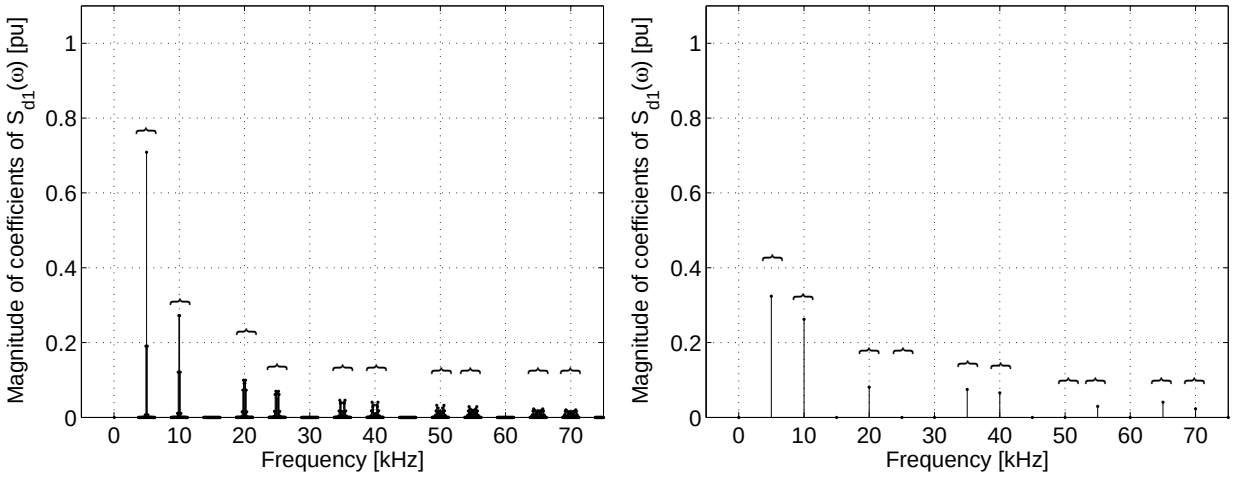

(a) $m_a = 0.8,\ p = 3$ (b) $D = 0.8,\ p = 3$

Figure 3-35. *Comparison of harmonics of sinusoidal modulation and fixed duty-cycle PWM for* $p = 2$ *with* $f_s = 5\ kHz$.

(c) 4-cell case: The harmonics for the sinusoidal modulation case are shown in Figure 3-36(a). Again, none of the groups of harmonics are zero for this case. For the fixed duty-cycle case, with $D = \frac{8}{10} = \frac{4}{5}$, it can be seen that $|S_{d_1}(\omega)| = 0$ where $m = 4k + 1$ or $m = 4k + 2$ or $m = 4k + 3$ is a multiple of 5. Examples of this can be seen at $m = 5$ at $25\ kHz$, at $m = 10$ at $50\ kHz$ and at $m = 15$ at $75\ kHz$. This is shown in Figure 3-36(b).

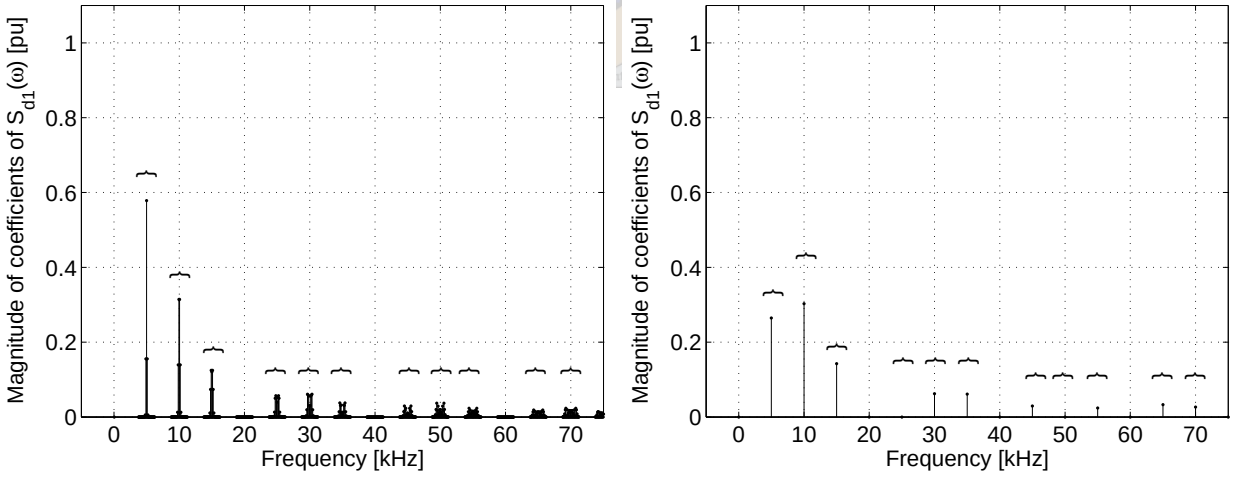

(a) $m_a = 0.8,\ p = 4$ (b) $D = 0.8,\ p = 4$

Figure 3-36. *Comparison of harmonics of sinusoidal modulation and fixed duty-cycle PWM for* $p = 4$ *with* $f_s = 5\ kHz$.

Example 3.16

In this example, the harmonics of $|S_{d_1}(\omega)|$ and $|S_t(\omega)|$ are compared for the fixed duty-cycle PWM case for $p = 2,\ 3, \ldots,\ 7$ cells for $D = \{\frac{1}{p}, \frac{1}{2}\}$. The switching frequency is again chosen as $f_s =$

$5\ kHz$.

(a) 2-cell case: The harmonics of $|S_d(\omega)|$ for $D = 0.5$ are shown in Figure 3-37(a). None of the harmonics at $m = 2k + 1$ are zero for this case.

The harmonics of $|S_t(\omega)|$ for $D = 0.5$ are shown in Figure 3-38(a). All the harmonics of $|S_t(\omega)|$ are zero for this case.

The harmonics of $|S_d(\omega)|$ for $D = \frac{1}{p}$ are shown in Figure 3-39(a). This is exactly the same case as shown in Figure 3-37(a).

(b) 3-cell case: The harmonics of $|S_{d_1}(\omega)|$ for $D = 0.5$ are shown in Figure 3-37(b). The harmonics are zero where $m = 3k + 1$ or $m = 3k + 2$ are multiples of 2.

The harmonics of $|S_t(\omega)|$ for $D = 0.5$ are shown in Figure 3-38(b). The harmonics of $|S_t(\omega)|$ are at multiples of 3 and 9 times the switching frequency.

The harmonics of $|S_d(\omega)|$ for $D = \frac{1}{p}$ are shown in Figure 3-39(b). None of the harmonics of $|S_{d_1}(\omega)|$ for $m = 3k + 1$ or $m = 3k + 2$ are zero.

(c) 4-cell case: The harmonics of $|S_{d_1}(\omega)|$ for $D = 0.5$ are shown in Figure 3-37(c). The harmonics are zero where $m = 4k + 2$ is even.

The harmonics of $|S_t(\omega)|$ for $D = 0.5$ are shown in Figure 3-38(c). All the harmonics of $|S_t(\omega)|$ are zero for this case.

The harmonics of $|S_d(\omega)|$ for $D = \frac{1}{p}$ are shown in Figure 3-39(c). None of the harmonics at $m = 4k + 1$, $m = 4k + 2$ or $m = 4k + 3$ are zero for this case.

(d) 5-cell case: The harmonics of $|S_{d_1}(\omega)|$ for $D = 0.5$ are shown in Figure 3-37(d). The harmonics are zero where $m = 5k + 1$, $m = 5k + 2$, $m = 5k + 3$ or $m = 5k + 4$ are even.

The harmonics of $|S_t(\omega)|$ for $D = 0.5$ are shown in Figure 3-38(d). The harmonics of $|S_t(\omega)|$ are at multiples of 5 and 25 times the switching frequency.

The harmonics of $|S_d(\omega)|$ for $D = \frac{1}{p}$ are shown in Figure 3-39(d). None of the harmonics of $|S_{d_1}(\omega)|$ for $m = 5k + 1$, $m = 5k + 2$, $m = 5k + 3$ or $m = 5k + 4$ are zero.

(e) 6-cell case: The harmonics of $|S_{d_1}(\omega)|$ for $D = 0.5$ are shown in Figure 3-37(e). The harmonics are zero where $m = 6k + 2$ and $m = 6k + 4$ are even.

The harmonics of $|S_t(\omega)|$ for $D = 0.5$ are shown in Figure 3-38(e). All the harmonics of $|S_t(\omega)|$ are zero for this case.

The harmonics of $|S_d(\omega)|$ for $D = \frac{1}{p}$ are shown in Figure 3-39(e). None of the harmonics at $m = 6k + 1$, $m = 6k + 2$,$m = 6k + 3$, $m = 6k + 4$ or $m = 6k + 5$ are zero for this case.

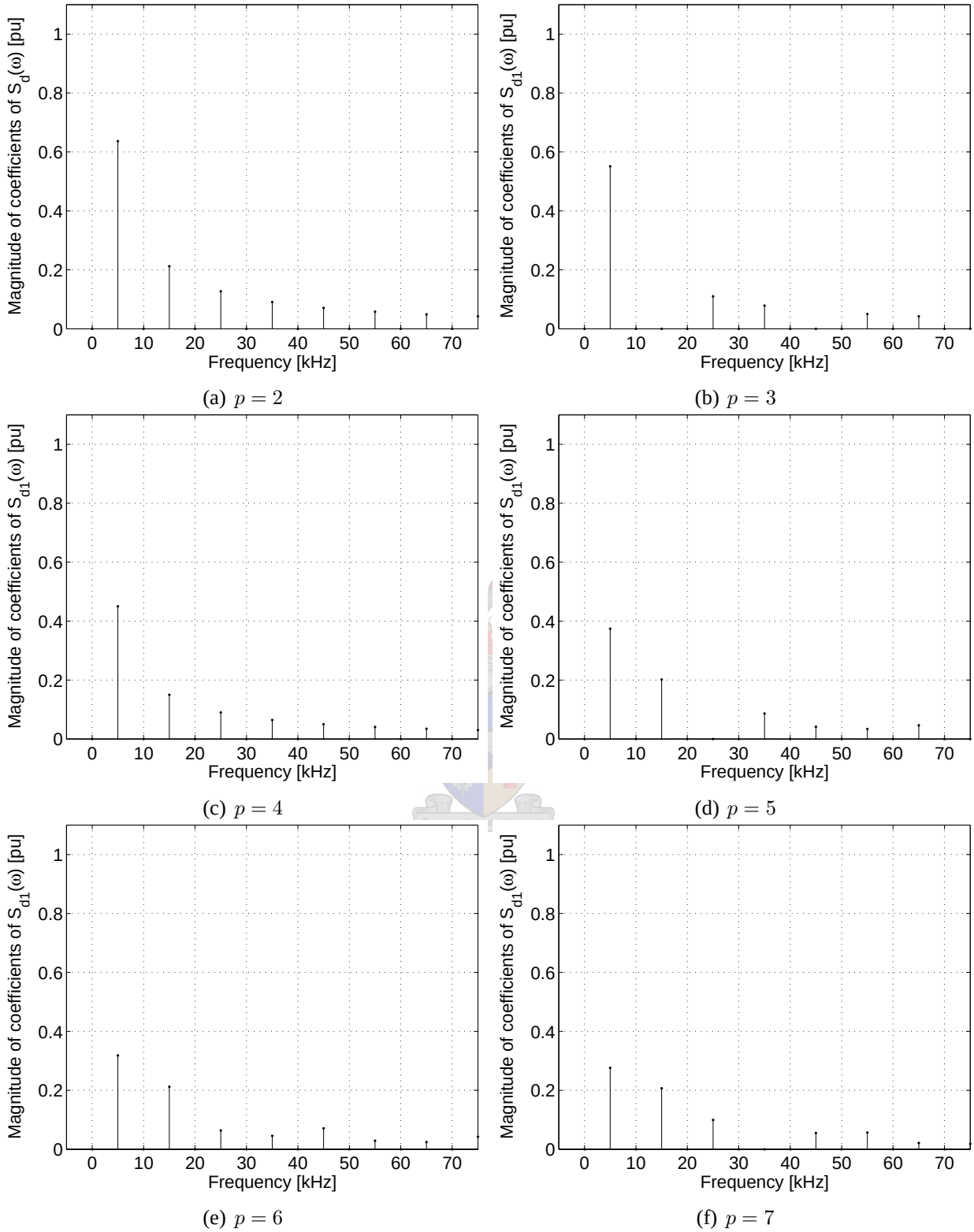

(a) $p = 2$ (b) $p = 3$

(c) $p = 4$ (d) $p = 5$

(e) $p = 6$ (f) $p = 7$

Figure 3-37. *Comparison of harmonics of* $|S_{d_1}(\omega)|$ *for fixed duty-cycle PWM with* $D = 0.5$ *and* $f_s = 5\ kHz$.

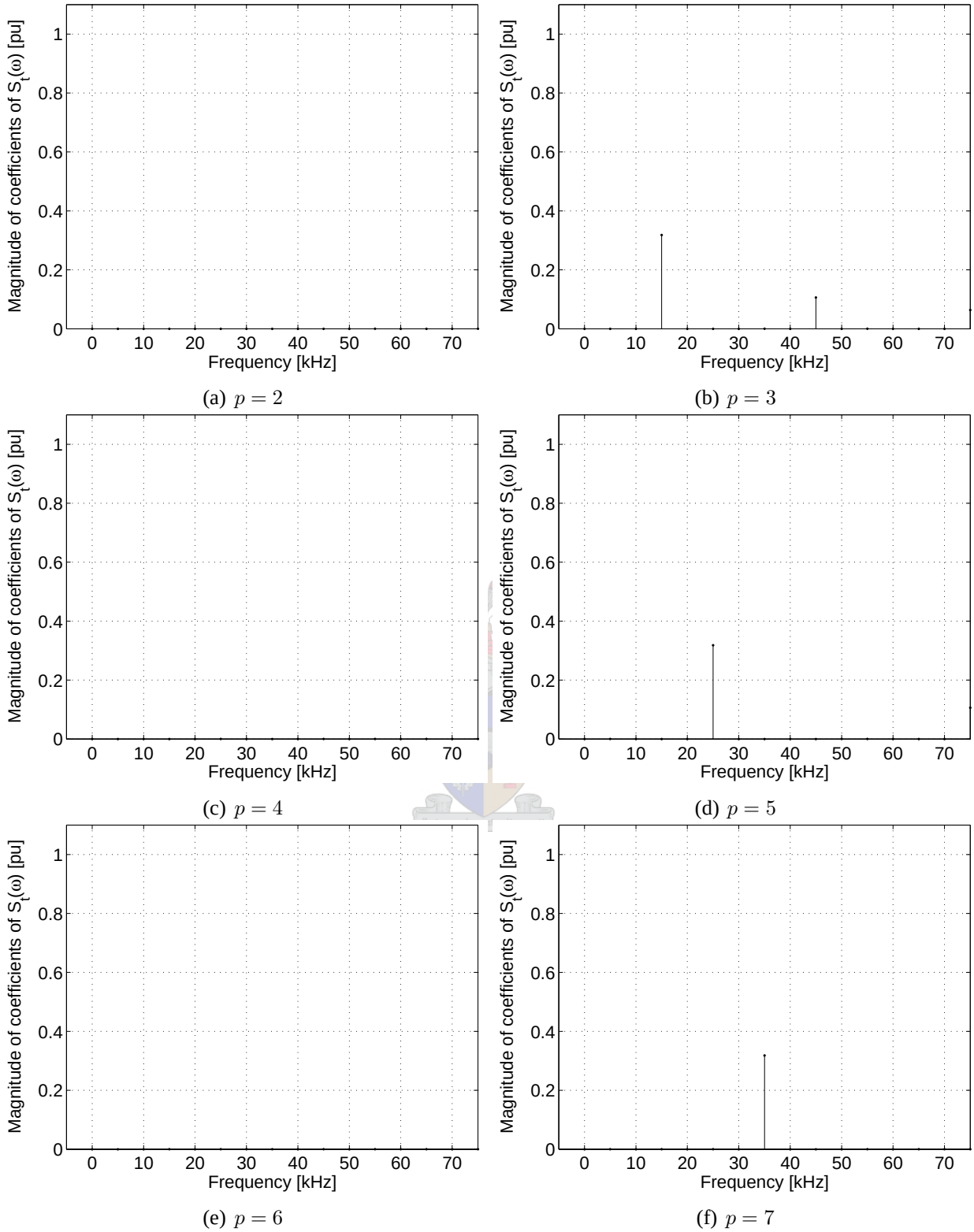

(a) $p = 2$ (b) $p = 3$

(c) $p = 4$ (d) $p = 5$

(e) $p = 6$ (f) $p = 7$

Figure 3-38. *Comparison of harmonics of* $|S_t(\omega)|$ *for fixed duty-cycle PWM with* $D = 0.5$ *and* $f_s = 5\ kHz$.

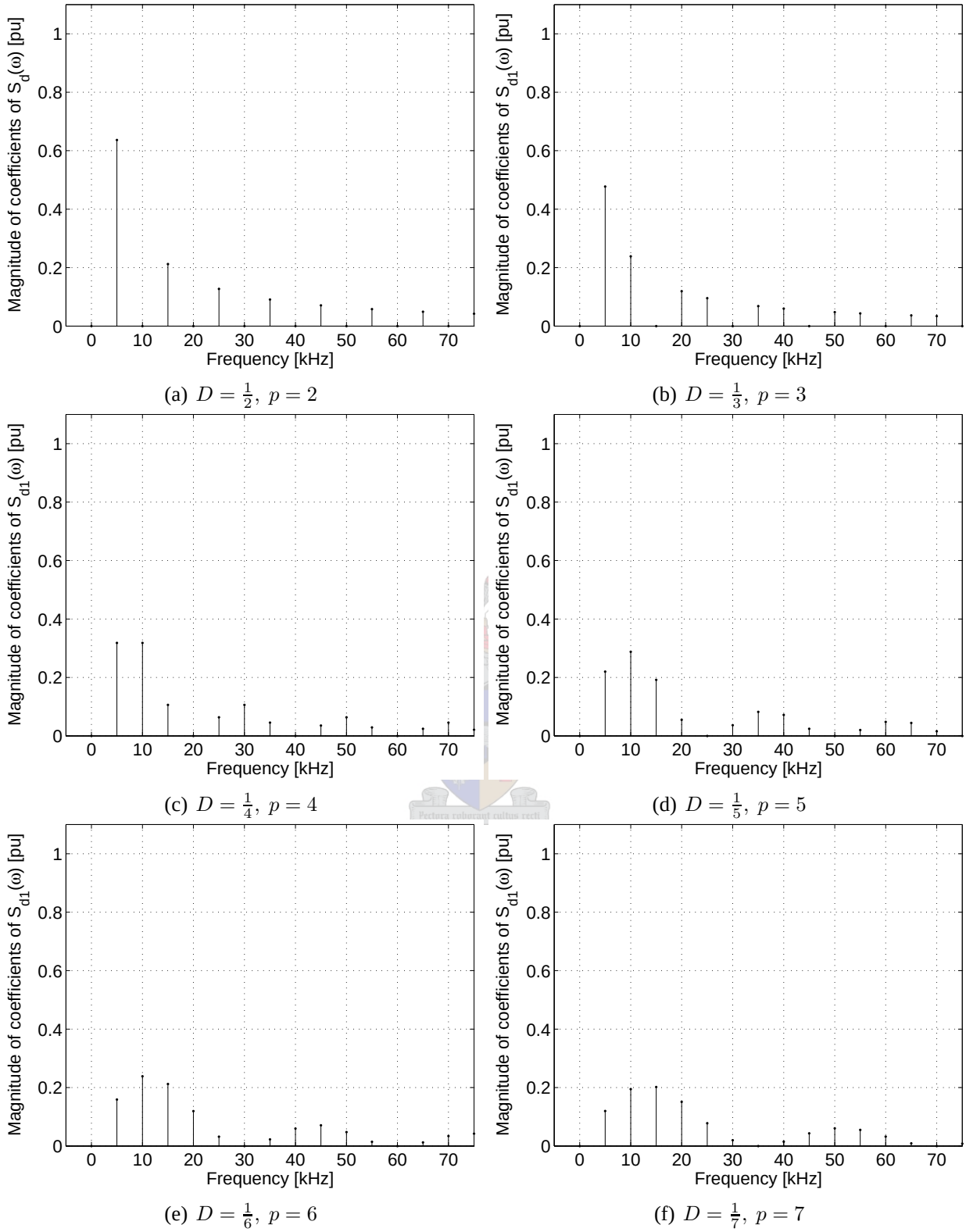

(a) $D = \frac{1}{2},\ p = 2$ (b) $D = \frac{1}{3},\ p = 3$

(c) $D = \frac{1}{4},\ p = 4$ (d) $D = \frac{1}{5},\ p = 5$

(e) $D = \frac{1}{6},\ p = 6$ (f) $D = \frac{1}{7},\ p = 7$

Figure 3-39. *Comparison of harmonics of* $|S_{d_1}(\omega)|$ *for fixed duty-cycle PWM with* $D = \frac{1}{p}$ *and* $f_s = 5\ kHz$.

(f) 7-cell case: The harmonics of $|S_{d_1}(\omega)|$ for $D = 0.5$ are shown in Figure 3-37(f). The harmonics are zero where $m = 7k+1$, $m = 7k+2$, $m = 7k+3$, $m = 7k+4$, $m = 7k+5$ or $m = 7k+6$ are even.

The harmonics of $|S_t(\omega)|$ for $D = 0.5$ are shown in Figure 3-38(f). The harmonics of $|S_t(\omega)|$ are at multiples of 7 and 49 times the switching frequency.

The harmonics of $|S_d(\omega)|$ for $D = \frac{1}{p}$ are shown in Figure 3-39(f). None of the harmonics of $|S_{d_1}(\omega)|$ for $m = 7k+1$, $m = 7k+2$, $m = 7k+3$, $m = 7k+4$, $m = 7k+5$ or $m = 7k+6$ are zero.

For the sinusoidal modulation case, there exists the possibility of overlap between the groups of harmonic clusters. This may lead to $|S_d(\omega)||S_t(\omega)| \neq 0$. This topic is discussed in the next chapter.

Earlier in this chapter, in section 3.3.2, the Fourier coefficients of the switching functions $s_i(t)$ where $i = 1, \ldots, p-1$ for the fixed duty-cycle case were determined. The expressions for these coefficients are repeated for convenience as follows:

$$A_0 = 2D - 1 \tag{3.192}$$

$$A_m = \frac{4}{m\pi}\sin(m\pi D) \tag{3.193}$$

where D is the duty-cycle.

In order to find out what the effect of the duty-cycle is on the harmonics of the switching functions, it is important to note the following:

$$\frac{\sin(m\pi D)}{m\pi} = 0 \tag{3.194}$$

if and only if $m\pi D = v\pi$, where $v \in \mathbb{Z}$ which is only true if $mD \in \mathbb{Z}$. This means that the duty-cycle D can be written as the following fraction:

$$D = \frac{v}{m} \tag{3.195}$$

Equation (3.195) implies that when v is a factor of m, the harmonics will be zero for that value of m. This means that for the fixed duty-cycle case there may exist values of D for a case of p cells where the harmonics may be zero. It will later be shown that single harmonics being zero is not a problem, as seen in Figures 3-37(d) and 3-37(f) where the harmonics that are zero alternate with every k. When the same multiple harmonic, e.g. $m = 4k+2$ in Figure 3-37(c) or $m = 6k+2$ in Figure 3-37(e) is zero for every k, the sum of the harmonics over that group m will be zero. This may cause unbalance. This topic is discussed in more detail in the next chapter when it will become clear why this last case may cause unbalance.

3.4 Summary

This chapter focussed on the harmonic analysis of the switching functions of a multicell converter. The analysis included interleaved switching for both sinusoidal modulation as well as for fixed duty-cycle PWM. This analysis was done for a “single-”, 2-, 3- and p-cell cases.

The switching functions for the sinusoidal modulation cases were calculated using Fourier methods developed by W.R. Bennet [21] and H.S. Black [5]. Switching functions for the fixed duty-cycle PWM case were calculated using conventional Fourier methods.

Several examples were included which demonstrated the generation of the switching functions for both modulation methods. Most of the other examples deal with the spectral analysis of the switching functions for specific values of modulation index and duty-cycle.

The Fourier methods used in this chapter can be modified to include sampling effects for the case of digital modulators [25].

The characteristics of the switching functions derived in this chapter is used extensively in the following 2 chapters.

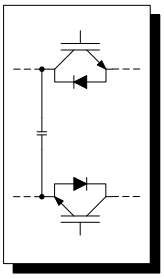

Chapter 4

Steady-state analysis

4.1 Introduction

In this chapter it will be shown that the cell capacitor voltages of 2-cell, 3-cell and eventually p-cell multicell converters will balance naturally under certain conditions. These conditions are mentioned and discussed. Due to the characteristics of this topology as discussed in Chapter 2 and the requirement of the switching functions to be phase-shifted by $\frac{2\pi}{p}$ radians, the switching functions are generated by interleaved switching. It will be shown that as long as the switching frequency of the converter is significantly higher than the highest frequency harmonic of the reference signal, the cell capacitor voltages will balance naturally. The possibility also exists to force the cell capacitor voltages to balance through active control, but this topic is beyond the scope of this dissertation as the focus of this dissertation is to analyse the natural balance property of this topology.

The focus of this chapter is to use the instantaneous model and equivalent circuits of the multicell topology in the time domain derived in Chapter 2 and derive the steady-state equations for these converters. These steady-state equations are then used to derive equations describing the cell capacitor voltage balance.

For this analysis the following is assumed:

- the cell capacitors are very large.
- the cell capacitor voltages change much slower than the rest of the system so that in comparison it appears as if the rest of the system is in steady-state.
- set $\omega = 0$ in order to calculate the dc cell capacitor currents.

The effect of a balance booster circuit, introduced in Chapter 2 section 2.2, on the natural balancing mechanism is also discussed after the balancing equations are formulated.

4.2 Two-port circuits in the frequency domain

The concept of a 2-port switching circuit was introduced in Chapter 2 section 2.6 and applied throughout the rest of that chapter. For that case, the 2-port circuits were in the time domain. In this chapter the concept of a 2-port circuit is applied in the frequency domain. A 2-port circuit in the frequency domain is shown in Figure 4-1.

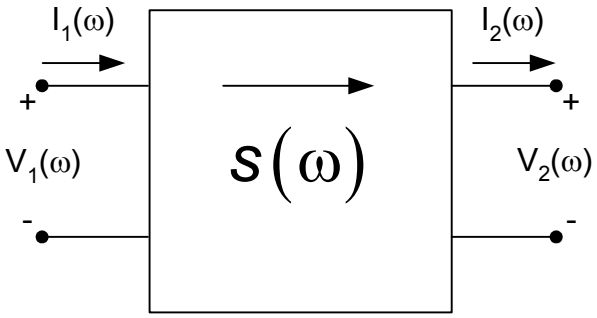

Figure 4-1. *Basic 2-port switching circuit in the frequency domain.*

For this case, the switching function, $S(\omega)$ is shown in the frequency domain. For the frequency domain case, the relationship between the voltages $V_1(\omega)$ and $V_2(\omega)$ and the currents $I_1(\omega)$ and $I_2(\omega)$ are as follows:

$$V_2(\omega) = S(\omega) \star V_1(\omega) \tag{4.1}$$

$$I_1(\omega) = S(\omega) \star I_2(\omega) \tag{4.2}$$

where the symbol "$\star$" represents convolution in the frequency domain. Using the definition of convolution in the frequency domain, the above equations can be rewritten in the following form:

$$V_2(\omega) = \int_{-\infty}^{\infty} S(\xi) V_1(\omega - \xi) d\xi \tag{4.3}$$

$$I_1(\omega) = \int_{-\infty}^{\infty} S(\xi) I_2(\omega - \xi) d\xi \tag{4.4}$$

The principles of equations (4.1)-(4.4) will be used frequently in the remainder of this chapter.

4.3 The 2-cell multicell converter

The first steady-state analysis is that of the 2-cell multicell converter. The equivalent circuit of the 2-cell multicell converter in terms of d and t parameters was derived in Chapter 2 section 2.7 for the time domain case and shown in Figure 2-7. This circuit will be used here for the steady-state analysis in the frequency domain. The equivalent circuit in terms of d and t parameters is repeated here in the frequency domain and is shown in Figure 4-2.

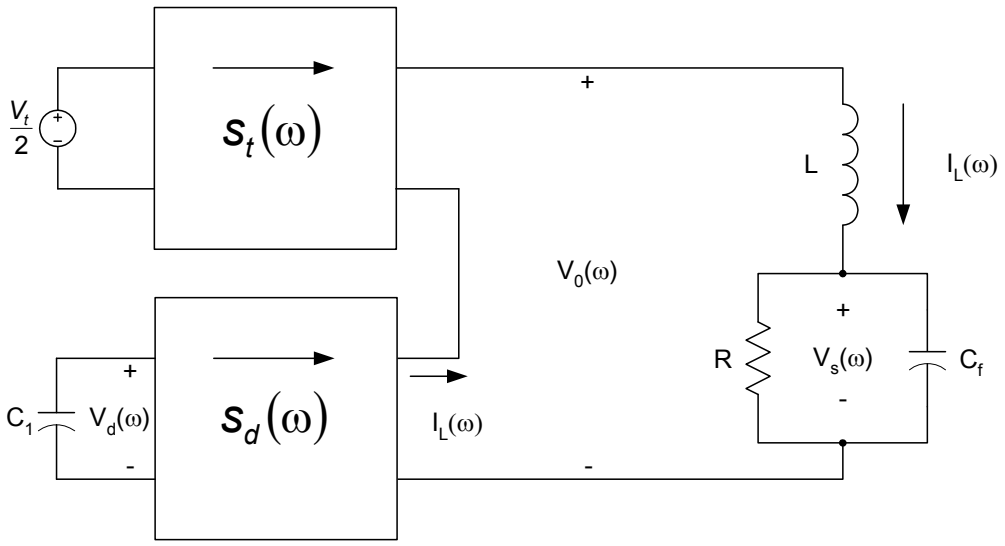

Figure 4-2. *Equivalent circuit in the frequency domain in terms of d and t parameters of a 2-cell multicell converter.*

From Figure 4-2, the expression for the inductor current $I_L(\omega)$ in the frequency domain can be written as follows:

$$\begin{aligned} I_L(\omega) &= \frac{V_0(\omega)}{Z(\omega)} \\ &= \frac{(\frac{V_t}{2} \cdot S_t)(\omega)}{Z(\omega)} + \frac{V_d(\omega) \cdot S_d(\omega)}{Z(\omega)} \end{aligned} \tag{4.5}$$

The expression for the cell capacitor current $I_{C_1}(\omega)$ can then be found by applying equation (4.2):

$$\begin{aligned} I_{C_1}(\omega) &= -I_L(\omega) \star S_d(\omega) \\ &= -\left(\frac{\frac{V_t}{2} \cdot S_t(\omega)}{Z(\omega)} + \frac{V_d(\omega) \cdot S_d(\omega)}{Z(\omega)} \right) \star S_d(\omega) \\ &= -\left[\left(\frac{\frac{V_t}{2} \cdot S_t(\omega)}{Z(\omega)} \right) \star S_d(\omega) + \left(\frac{V_d(\omega) \cdot S_d(\omega)}{Z(\omega)} \right) \star S_d(\omega) \right] \\ &= -\left[\frac{V_t}{2} \int_{-\infty}^{\infty} \frac{S_t(\xi)}{Z(\xi)} S_d(\omega - \xi) d\xi + V_d \int_{-\infty}^{\infty} \frac{S_d(\xi)}{Z(\xi)} S_d(\omega - \xi) d\xi \right] \end{aligned} \tag{4.6}$$

It is well known that in the steady-state the average current through each capacitor in a power electronic circuit is zero, i.e. $I_{C_1}(\omega)|_{\omega=0} = 0$. Therefore, equation (4.6) can be rewritten as follows:

$$\begin{aligned} I_{C_1}(\omega)|_{\omega=0} &= -\left[\frac{V_t}{2} \int_{-\infty}^{\infty} \frac{S_t(\xi)}{Z(\xi)} S_d(-\xi) d\xi + V_d \int_{-\infty}^{\infty} \frac{S_d(\xi)}{Z(\xi)} S_d(-\xi) d\xi \right] \\ 0 &= -\left[\frac{V_t}{2} \int_{-\infty}^{\infty} \frac{S_t(\xi)}{Z(\xi)} \overline{S_d(\xi)} d\xi + V_d \int_{-\infty}^{\infty} \frac{S_d(\xi)}{Z(\xi)} \overline{S_d(\xi)} d\xi \right] \\ &= -\left[\frac{V_t}{2} \int_{-\infty}^{\infty} \frac{S_t(\xi)}{Z(\xi)} \overline{S_d(\xi)} d\xi + V_d \int_{-\infty}^{\infty} \frac{|S_d(\xi)|^2}{Z(\xi)} d\xi \right] \end{aligned} \tag{4.7}$$

In the analysis discussed here, $\overline{S_d(\xi)}$ represents the complex conjugate of $S_d(\xi)$. Therefore, knowing that the switching functions are real valued functions (see [17] p. 171), the following is true:

$$\overline{S_d(\xi)} = S_d(-\xi)\,. \tag{4.8}$$

This definition will be used in the remainder of this chapter, but in a more general form. This general form is defined as follows:

$$\overline{S_{d_i}(\xi)} = S_{d_i}(-\xi) \;\text{ for } i = 1, \ldots, p-1. \tag{4.9}$$

Equation (4.7) can be rearranged into the following expression:

$$V_d \int_{-\infty}^{\infty} \frac{|S_d(\xi)|^2}{Z(\xi)} d\xi = -\left[\frac{V_t}{2} \int_{-\infty}^{\infty} \frac{S_t(\xi)}{Z(\xi)} \overline{S_d(\xi)} d\xi\right] \tag{4.10}$$

Using the additive property of the definite integral, an integral with an interval of $(-\infty, \infty)$ can be split into the sum of 2 integrals, one over an interval of $(-\infty, 0)$ and the other over an interval $[0, \infty)$, for example:

$$\int_{-\infty}^{\infty} \frac{|S_d(\xi)|^2}{Z(\xi)} d\xi = \int_{-\infty}^{0} \frac{|S_d(\xi)|^2}{Z(\xi)} d\xi + \int_{0}^{\infty} \frac{|S_d(\xi)|^2}{Z(\xi)} d\xi \tag{4.11}$$

Using the property shown in (4.11), (4.10) can be simplified further as follows:

$$V_d \left[\int_{-\infty}^{0} \frac{|S_d(\xi)|^2}{Z(\xi)} d\xi + \int_{0}^{\infty} \frac{|S_d(\xi)|^2}{Z(\xi)} d\xi\right] = -\frac{V_t}{2} \left[\int_{-\infty}^{0} \frac{S_t(\xi)}{Z(\xi)} \overline{S_d(\xi)} d\xi + \int_{0}^{\infty} \frac{S_t(\xi)}{Z(\xi)} \overline{S_d(\xi)} d\xi\right] \tag{4.12}$$

Equation (4.12) can now be rearranged further by converting the $(-\infty, 0)$ intervals to $[0, \infty)$ as follows:

$$V_d \left[\int_{0}^{\infty} \frac{|S_d(-\xi)|^2}{Z(-\xi)} d\xi + \int_{0}^{\infty} \frac{|S_d(\xi)|^2}{Z(\xi)} d\xi\right] = -\frac{V_t}{2} \left[\int_{0}^{\infty} \frac{S_t(-\xi)}{Z(-\xi)} \overline{S_d(-\xi)} d\xi + \int_{0}^{\infty} \frac{S_t(\xi)}{Z(\xi)} \overline{S_d(\xi)} d\xi\right] \tag{4.13}$$

The next step is to rewrite variables in (4.13) that represent conjugates using (4.8) as follows:

$$V_d \left[\int_{0}^{\infty} \frac{\left|\overline{S_d(\xi)}\right|^2}{\overline{Z(\xi)}} d\xi + \int_{0}^{\infty} \frac{|S_d(\xi)|^2}{Z(\xi)} d\xi\right] = -\frac{V_t}{2} \left[\int_{0}^{\infty} \frac{\overline{S_t(\xi)}}{\overline{Z(\xi)}} S_d(\xi) d\xi + \int_{0}^{\infty} \frac{S_t(\xi)}{Z(\xi)} \overline{S_d(\xi)} d\xi\right] \tag{4.14}$$

The following step is to see that the integrals that are summed on each side of (4.14) are each the other's conjugate, which means that (4.14) can be rewritten as follows:

$$V_d\left[2Re\left\{\int_0^\infty \frac{|S_d(\xi)|^2}{Z(\xi)}d\xi\right\}\right] = -\frac{V_t}{2}\left[2Re\left\{\int_0^\infty \frac{S_t(\xi)}{Z(\xi)}\overline{S_d(\xi)}d\xi\right\}\right] \tag{4.15}$$

The relationship between V_d and V_t can now be determined and written as follows:

$$\frac{V_d}{V_t} = -\frac{Re\left\{\int_0^\infty \frac{S_t(\xi)}{Z(\xi)}\overline{S_d(\xi)}d\xi\right\}}{2Re\left\{\int_0^\infty \frac{|S_d(\xi)|^2}{Z(\xi)}d\xi\right\}} \tag{4.16}$$

Equation (4.16) represents the relationship of the unbalance of the cell capacitor voltage relative to the input voltage. This equation shows that the relative unbalance is influenced by two factors:

(a) The characteristics of the load impedance $Z(\omega)$.

(b) Overlapping of the harmonics of $S_d(\omega)$ and $S_t(\omega)$, determined by $|S_d(\omega)\,||\,S_t(\omega)|$.

Before these factors are discussed, another definition will be introduced to simplify the analysis. In Chapter 3 it was shown that when using PWM, the harmonics appear in groups around integer multiples (denoted by m) of the switching frequency. For sinusoidal modulation, side-bands appear at integer multiples (denoted by n) of the reference frequency around these harmonics of the switching frequency. With this property it is possible to rewrite the above integrals in terms of integrals over groups of harmonics by using the "Summation Rule of Integrals". Using this rule the integrals in (4.16) can be split into a sum of integrals over the relevant frequency groups as follows:

$$\int_0^\infty \frac{S_t(\xi)}{Z(\xi)}\overline{S_d(\xi)}d\xi = \int_{m=2k} \frac{S_t(\xi)}{Z(\xi)}\overline{S_d(\xi)}d\xi + \int_{m=2k+1} \frac{S_t(\xi)}{Z(\xi)}\overline{S_d(\xi)}d\xi \tag{4.17}$$

and

$$\int_0^\infty \frac{|S_d(\xi)|^2}{Z(\xi)}d\xi = \int_{m=2k} \frac{|S_d(\xi)|^2}{Z(\xi)}d\xi + \int_{m=2k+1} \frac{|S_d(\xi)|^2}{Z(\xi)}d\xi \tag{4.18}$$

To make the analysis easier, new variables are defined that depict these integrals over frequency groups. In the following mathematical definitions m is used as the number of the group of harmonics over which an integral is taken, where the group includes the side-band harmonics. For convenience, the following variables are defined: λ_0 and λ_1, where $k = 0, 1, \ldots, \infty$:

$$\lambda_0 = \int_{m=2k} \frac{|S_d(\xi)|^2}{Z(\xi)}d\xi \tag{4.19}$$

$$\lambda_1 = \int_{m=2k+1} \frac{|S_d(\xi)|^2}{Z(\xi)}d\xi \tag{4.20}$$

and α_0 and α_1, where $k = 0, 1, \ldots, \infty$:

$$\alpha_0 = \int_{m=2k} \frac{S_t(\xi)\overline{S_d(\xi)}}{Z(\xi)} d\xi \tag{4.21}$$

$$\alpha_1 = \int_{m=2k+1} \frac{S_t(\xi)\overline{S_d(\xi)}}{Z(\xi)} d\xi \tag{4.22}$$

The conjugates of the above variables are defined: $\overline{\lambda_0}$ and $\overline{\lambda_1}$, where $k = -\infty, \ldots, -1$:

$$\overline{\lambda_0} = \int_{m=2k} \frac{|S_d(\xi)|^2}{\overline{Z(\xi)}} d\xi \tag{4.23}$$

$$\overline{\lambda_1} = \int_{m=2k+1} \frac{|S_d(\xi)|^2}{\overline{Z(\xi)}} d\xi \tag{4.24}$$

and $\overline{\alpha_0}$ and $\overline{\alpha_1}$, where $k = -\infty, \ldots, -1$:

$$\overline{\alpha_0} = \int_{m=2k} \frac{\overline{S_t(\xi)}S_d(\xi)}{\overline{Z(\xi)}} d\xi \tag{4.25}$$

$$\overline{\alpha_1} = \int_{m=2k+1} \frac{\overline{S_t(\xi)}S_d(\xi)}{\overline{Z(\xi)}} d\xi \tag{4.26}$$

Equations (4.17) and (4.18) can now be rewritten in terms of λ and α using (4.19)-(4.26) as follows:

$$\int_0^\infty \frac{S_t(\xi)}{Z(\xi)} \overline{S_d(\xi)} d\xi = \alpha_0 + \alpha_1 \tag{4.27}$$

and

$$\int_0^\infty \frac{|S_d(\xi)|^2}{Z(\xi)} d\xi = \lambda_0 + \lambda_1 \tag{4.28}$$

The values of λ and α depend on the properties of the harmonic content of the switching functions $S_d(\omega)$ and $S_t(\omega)$. These properties were proven in the previous chapter and are summarised in Table 4.1 for convenience.

Table 4.1. *Summary of* 2*-cell switching function properties*

Conditions	Properties
$m = 2k$, for all $k = 0, 1, \ldots$	$S_d(\xi) = 0$
	$\lvert S_t \rvert \geq 0$
$m = 2k+1$, for all $k = 0, 1, \ldots$	$\lvert S_d(\xi) \rvert > 0$
	$S_t = 0$

From the properties listed in Table 4.1, it can be seen that for the harmonic group $m = 2k$ $S_d(\xi) = 0$,

which implies that both λ_0 and α_0 are zero. Equation (4.16) can finally be simplified to the following:

$$\frac{V_d}{V_t} = -\frac{Re\{\alpha_1\}}{2Re\{\lambda_1\}} = -\frac{1}{2}\frac{\alpha_1 + \overline{\alpha_1}}{\lambda_1 + \overline{\lambda_1}} \tag{4.29}$$

A harmonic analysis of interleaved switching was discussed in Chapter 3. For the 2-cell case it was found that the harmonics of $S_d(\omega)$ were centred around odd multiples of the switching frequency ω_s and that the harmonics of $S_t(\omega)$ were centred around even multiples of the switching frequency ω_s. An example of the harmonics of interleaved switching for the balanced case of a 2-cell multicell inverter switching at $5\ kHz$ with a $50\ Hz$ sinusoidal reference with $m_a = 0.6$ is shown in Figure 4-3.

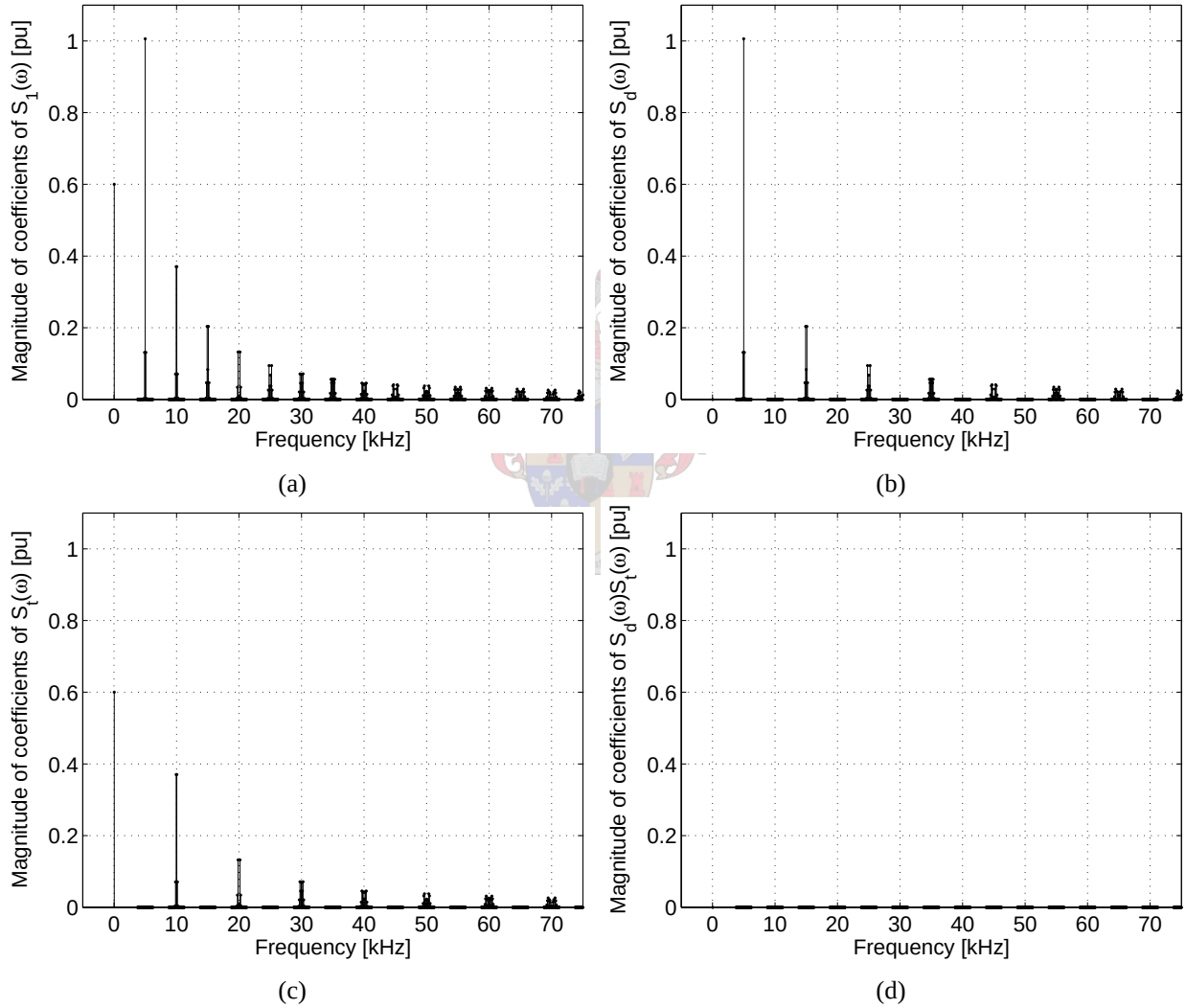

Figure 4-3. *Harmonics of 2-cell switching* $m_a = 0.6$, $f_r = 50\ Hz$ *and* $f_s = 5\ kHz$.

In the previous chapter, in sections 3.3.1.2 and 3.3.2.2 it was shown respectively that for both sinusoidal modulation and fixed duty-cycle PWM that when the harmonics of $S_d(\omega)$ and $S_t(\omega)$ do not overlap, that equations (3.54) and (3.165) are true. These equations are the same equation, only for different types of modulation. This equation is repeated here for convenience as follows:

$$|S_d(\omega)||S_t(\omega)| \approx 0 \tag{4.30}$$

This property can be seen clearly when examining the plots of $|S_d(\omega)|$, $|S_t(\omega)|$ and $|S_d(\omega)\,||\,S_t(\omega)|$ in Figure 4-3. Following from equation (4.30) it can be seen that the top expression in equation (4.29), i.e. α_1, approximates to zero resulting in the following:

$$\frac{V_d}{V_t} \approx \frac{0}{2Re\{\lambda_1\}} = 0 \tag{4.31}$$

From the definition of V_d, it follows that as it tends to zero, the unbalance tends to zero. Therefore, from equation (4.31) it follows that the voltage across cell capacitor C_1 balances in steady-state when the harmonics of $S_t(\omega)$ and $S_d(\omega)$ do not overlap. This is only valid as long as the load impedance $Z(\omega)$ is not purely inductive. When the load impedance is purely inductive, $Re\{Z(\omega)\} = 0$, which means that $\frac{V_d}{V_t}$ will tend towards infinity, causing unbalance.

Two cases were found in which $|S_d(\omega)||S_t(\omega)| > 0$, causing unbalance of the cell capacitor voltage. These two cases are as follows:

- when the switching frequency (ω_s) is higher than the frequency of the reference signal (ω_r), but not high enough to avoid aliasing of the side-bands of the harmonic multiples thereof. An example showing this case is shown in Figure 4-4 where the switching frequency is $250\ Hz$ and the reference frequency $50\ Hz$. The groups of harmonics are at multiples of the switching frequency, but due to the low switching frequency the side-bands around the multiples of the switching frequency overlap. This can be seen in Figure 4-4(b). It can also be seen in Figure 4-4(d) that the harmonics of $S_d(\omega)$ and $S_t(\omega)$ overlap resulting in $|S_d(\omega)||S_t(\omega)| > 0$. This can result in cell capacitor voltage unbalance.

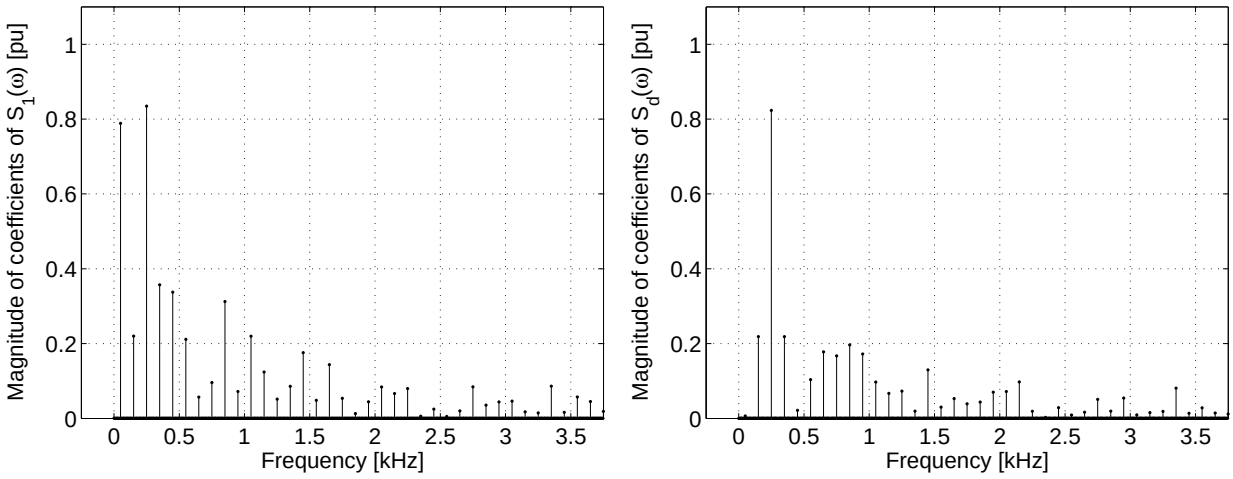

(a) (b)

Figure 4-4. *Overlapping harmonics:* $m_a = 0.8$, $f_r = 50\ Hz$ *and* $f_s = 250\ Hz$.

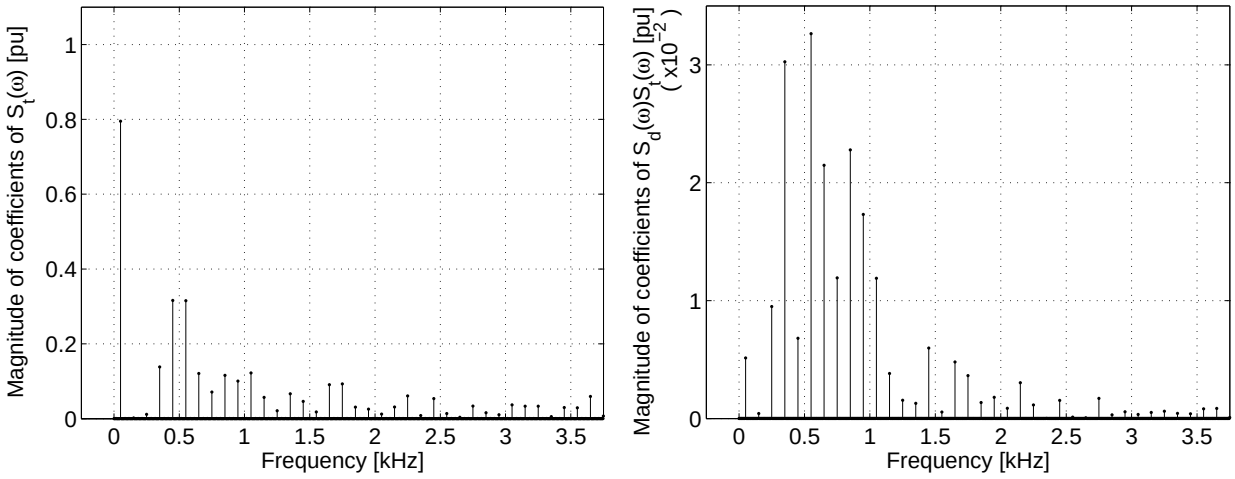

(c) (d)

Figure 4-4. *Overlapping harmonics:* $m_a = 0.8$*,* $f_r = 50\ Hz$ *and* $f_s = 250\ Hz$ *(cont.).*

- when the reference signal contains high frequency components, high enough so that there is aliasing of the side-bands of the harmonic multiples thereof. An example showing this case is shown in Figure 4-5 where the switching frequency is $5\ kHz$ and the reference is a triangular wave with a frequency of $550\ Hz$. The groups of harmonics are at multiples of the switching frequency, but due to the high frequency content of the reference the high frequency side-bands overlap with harmonics around neighbouring groups of harmonics. This can be seen in Figure 4-5(b). It can also be seen in Figure 4-5(d) that the harmonics of $S_d(\omega)$ and $S_t(\omega)$ overlap resulting in $|S_d(\omega)||S_t(\omega)| > 0$. This can also result in cell capacitor voltage unbalance.

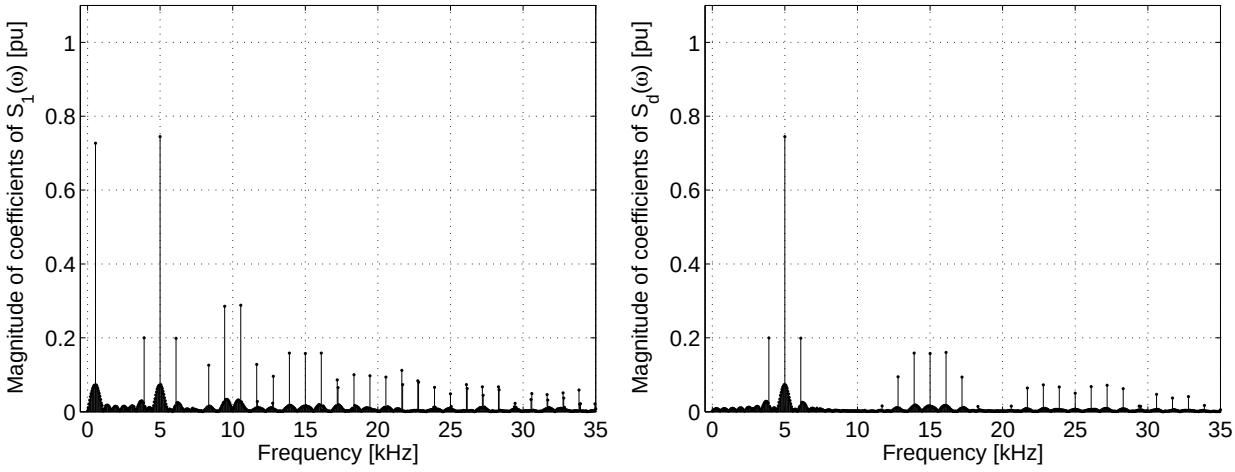

(a) (b)

Figure 4-5. *Overlapping harmonics: triangular reference with* $f_r = 550\ Hz$ *and* $f_s = 5\ kHz$*.*

For a detailed discussion of the above switching function properties refer back to Chapter 3.

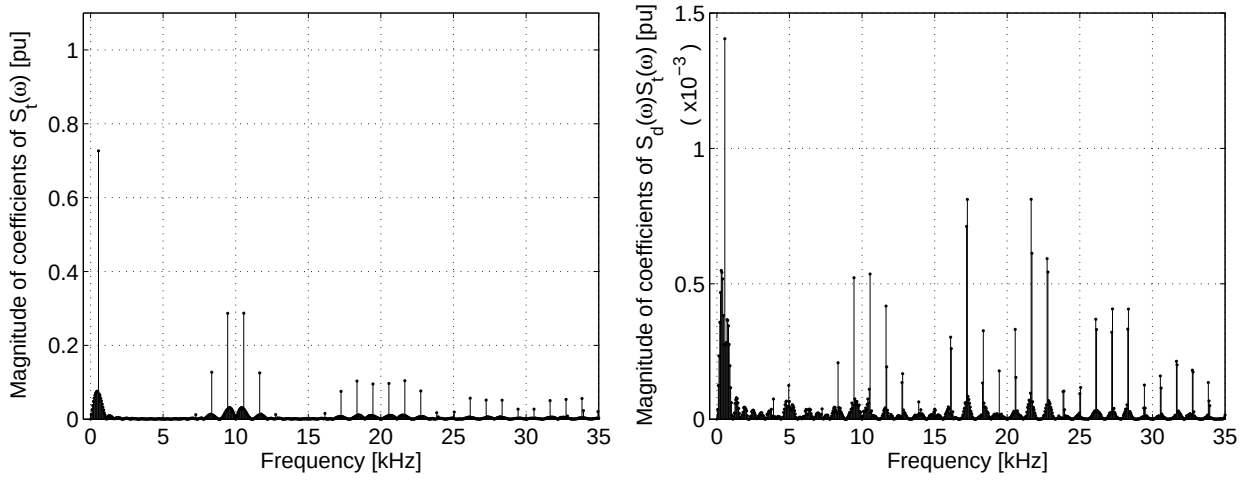

(c) (d)

Figure 4-5. *Overlapping harmonics: triangular reference with $f_r = 550\ Hz$ and $f_s = 5\ kHz$ (cont.).*

It was shown in [26], [29] and [60] that the connection of a balance booster circuit in parallel with the load can improve the balancing of the cell capacitor voltages. The balance booster is designed to have a low impedance at the switching frequency of the converter.

The balancing equation for the 2-cell converter case is repeated here for convenience as follows:

$$\frac{V_d}{V_t} = -\frac{Re\{\alpha_1\}}{2Re\{\lambda_1\}} \tag{4.32}$$

In order to improve the cell capacitor voltage balance, it can be seen from equation (4.29) that $\frac{V_d}{V_t}$ becomes smaller when λ_1 is increased. From the definition of λ_1 in equation (4.20), repeated here as equation (4.33), it is clear that when $Z(\omega)$ becomes smaller, λ_1 increases.

$$\lambda_1 = \int_{m=2k+1} \frac{|S_d(\xi)|^2}{Z(\xi)} d\xi \tag{4.33}$$

From equation (4.33), λ_1 is defined over the harmonic groups $m = 2k + 1$ where $k = 0, \ldots, \infty$, which are all the odd multiples of the switching frequency. Thus, if the balance booster is designed to have a low impedance at the switching frequency, it will increase the value of λ_1 and $\frac{V_d}{V_t}$ will decrease.

4.4 The 3-cell multicell converter

This section focusses on the steady-state analysis of a 3-cell multicell converter. This is the next step in the progression of the analysis towards the analysis of the p-cell multicell converter. This analysis starts in the same way as in the previous section, but becomes more complicated early in the analysis.

The time domain equivalent circuit in terms of d and t parameters of a 3-cell multicell converter was shown in Figure 2-9. For the steady-state analysis of this converter, it is necessary to convert this circuit to the frequency domain. The equivalent circuit in terms of d and t parameters in the frequency domain is shown in Figure 4-6.

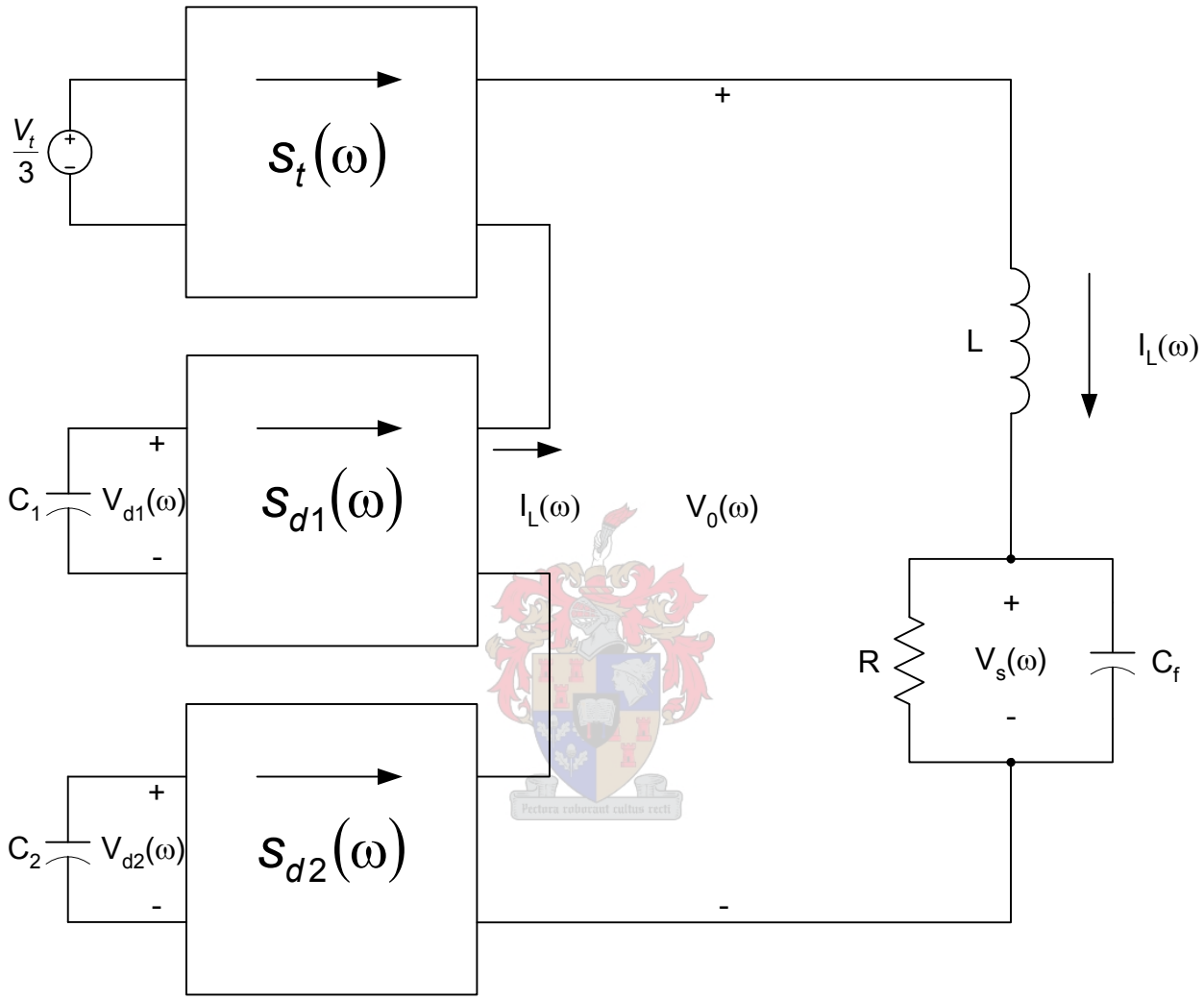

Figure 4-6. *Equivalent circuit in the frequency domain in terms of d and t parameters of a 3-cell multicell converter.*

In the frequency domain, the expression for the inductor current $I_L(\omega)$ can be written as follows:

$$I_L(\omega) = \frac{V_0(\omega)}{Z(\omega)} = \frac{\frac{V_t}{3} \cdot S_t(\omega)}{Z(\omega)} + \frac{V_{d_1}(\omega) \cdot S_{d_1}(\omega)}{Z(\omega)} + \frac{V_{d_2}(\omega) \cdot S_{d_2}(\omega)}{Z(\omega)} \tag{4.34}$$

The expression for the cell capacitor current $I_{C_1}(\omega)$ can then be found by applying equation (4.2) and the definition of convolution in the frequency domain:

$$
\begin{aligned}
I_{C_1}(\omega) &= -I_L(\omega) \star S_{d_1}(\omega) \\
&= -\left(\frac{\frac{V_t}{3} \cdot S_t(\omega)}{Z(\omega)} + \frac{V_{d_1}(\omega) \cdot S_{d_1}(\omega)}{Z(\omega)} + \frac{V_{d_2}(\omega) \cdot S_{d_2}(\omega)}{Z(\omega)} \right) \star S_{d_1}(\omega) \\
&= -\left[\left(\frac{\frac{V_t}{3} \cdot S_t(\omega)}{Z(\omega)} \right) \star S_{d_1}(\omega) + \left(\frac{V_{d_1}(\omega) \cdot S_{d_1}(\omega)}{Z(\omega)} \right) \star S_{d_1}(\omega) + \left(\frac{V_{d_2}(\omega) \cdot S_{d_2}(\omega)}{Z(\omega)} \right) \star S_{d_1}(\omega) \right] \\
&= -\left[\frac{V_t}{3} \int_{-\infty}^{\infty} \frac{S_t(\xi)}{Z(\xi)} S_{d_1}(\omega - \xi) d\xi + V_{d_1} \int_{-\infty}^{\infty} \frac{S_{d_1}(\xi)}{Z(\xi)} S_{d_1}(\omega - \xi) d\xi + V_{d_2} \int_{-\infty}^{\infty} \frac{S_{d_2}(\xi)}{Z(\xi)} S_{d_1}(\omega - \xi) d\xi \right]
\end{aligned}
\tag{4.35}
$$

If in steady-state, $I_{C_1}(\omega)|_{\omega=0} = 0$, then the following is true:

$$
\begin{aligned}
I_{C_1}(\omega)|_{\omega=0} &= -\left[\frac{V_t}{3} \int_{-\infty}^{\infty} \frac{S_t(\xi)}{Z(\xi)} S_{d_1}(-\xi) d\xi + V_{d_1} \int_{-\infty}^{\infty} \frac{S_{d_1}(\xi)}{Z(\xi)} S_{d_1}(-\xi) d\xi + V_{d_2} \int_{-\infty}^{\infty} \frac{S_{d_2}(\xi)}{Z(\xi)} S_{d_1}(-\xi) d\xi \right] \\
0 &= -\left[\frac{V_t}{3} \int_{-\infty}^{\infty} \frac{S_t(\xi)}{Z(\xi)} \overline{S_{d_1}(\xi)} d\xi + V_{d_1} \int_{-\infty}^{\infty} \frac{S_{d_1}(\xi)}{Z(\xi)} \overline{S_{d_1}(\xi)} d\xi + V_{d_2} \int_{-\infty}^{\infty} \frac{S_{d_2}(\xi)}{Z(\xi)} \overline{S_{d_1}(\xi)} d\xi \right]
\end{aligned}
\tag{4.36}
$$

Using the same method as used to write an expression for $I_{C_1}(\omega)$ shown in equation (4.35), the expression for $I_{C_2}(\omega)$ can be written as follows:

$$
\begin{aligned}
I_{C_2}(\omega) &= -I_L(\omega) \star S_{d_2}(\omega) \\
&= -\left(\frac{\frac{V_t}{3} \cdot S_t(\omega)}{Z(\omega)} + \frac{V_{d_1}(\omega) \cdot S_{d_1}(\omega)}{Z(\omega)} + \frac{V_{d_2}(\omega) \cdot S_{d_2}(\omega)}{Z(\omega)} \right) \star S_{d_2}(\omega) \\
&= -\left[\left(\frac{\frac{V_t}{3} \cdot S_t(\omega)}{Z(\omega)} \right) \star S_{d_2}(\omega) + \left(\frac{V_{d_1}(\omega) \cdot S_{d_1}(\omega)}{Z(\omega)} \right) \star S_{d_2}(\omega) + \left(\frac{V_{d_2}(\omega) \cdot S_{d_2}(\omega)}{Z(\omega)} \right) \star S_{d_2}(\omega) \right] \\
&= -\left[\frac{V_t}{3} \int_{-\infty}^{\infty} \frac{S_t(\xi)}{Z(\xi)} S_{d_2}(\omega - \xi) d\xi + V_{d_1} \int_{-\infty}^{\infty} \frac{S_{d_1}(\xi)}{Z(\xi)} S_{d_2}(\omega - \xi) d\xi + V_{d_2} \int_{-\infty}^{\infty} \frac{S_{d_2}(\xi)}{Z(\xi)} S_{d_2}(\omega - \xi) d\xi \right]
\end{aligned}
\tag{4.37}
$$

If in steady-state, $I_{C_2}(\omega)|_{\omega=0} = 0$, then the following is true:

$$
\begin{aligned}
I_{C_2}(\omega)|_{\omega=0} &= -\left[\frac{V_t}{3} \int_{-\infty}^{\infty} \frac{S_t(\xi)}{Z(\xi)} S_{d_2}(-\xi) d\xi + V_{d_1} \int_{-\infty}^{\infty} \frac{S_{d_1}(\xi)}{Z(\xi)} S_{d_2}(-\xi) d\xi + V_{d_2} \int_{-\infty}^{\infty} \frac{S_{d_2}(\xi)}{Z(\xi)} S_{d_2}(-\xi) d\xi \right] \\
0 &= -\left[\frac{V_t}{3} \int_{-\infty}^{\infty} \frac{S_t(\xi)}{Z(\xi)} \overline{S_{d_2}(\xi)} d\xi + V_{d_1} \int_{-\infty}^{\infty} \frac{S_{d_1}(\xi)}{Z(\xi)} \overline{S_{d_2}(\xi)} d\xi + V_{d_2} \int_{-\infty}^{\infty} \frac{S_{d_2}(\xi)}{Z(\xi)} \overline{S_{d_2}(\xi)} d\xi \right]
\end{aligned}
\tag{4.38}
$$

The equations (4.36) and (4.38) form the following system of equations that need to be solved:

$$\frac{V_t}{3}\int_{-\infty}^{\infty}\frac{S_t(\xi)\overline{S_{d_1}(\xi)}}{Z(\xi)}d\xi + V_{d_1}\int_{-\infty}^{\infty}\frac{S_{d_1}(\xi)\overline{S_{d_1}(\xi)}}{Z(\xi)}d\xi + V_{d_2}\int_{-\infty}^{\infty}\frac{S_{d_2}(\xi)\overline{S_{d_1}(\xi)}}{Z(\xi)}d\xi = 0 \tag{4.39}$$

$$\frac{V_t}{3}\int_{-\infty}^{\infty}\frac{S_t(\xi)\overline{S_{d_2}(\xi)}}{Z(\xi)}d\xi + V_{d_1}\int_{-\infty}^{\infty}\frac{S_{d_1}(\xi)\overline{S_{d_2}(\xi)}}{Z(\xi)}d\xi + V_{d_2}\int_{-\infty}^{\infty}\frac{S_{d_2}(\xi)\overline{S_{d_2}(\xi)}}{Z(\xi)}d\xi = 0 \tag{4.40}$$

The above equations can be rewritten using the following properties of the definite integral: the additive property as shown in equation (4.11) and the property that the sum of two integrals, the one the conjugate of the other, results in twice the real part of one of the integrals, as shown in equation (4.15). Equations (4.39) and (4.40) can thus be rewritten as follows:

$$V_{d_1}\cdot 2Re\left\{\int_0^{\infty}\frac{S_{d_1}(\xi)\overline{S_{d_1}(\xi)}}{Z(\xi)}d\xi\right\} + V_{d_2}\cdot 2Re\left\{\int_0^{\infty}\frac{S_{d_2}(\xi)\overline{S_{d_1}(\xi)}}{Z(\xi)}d\xi\right\} = \frac{V_t}{3}\cdot 2Re\left\{\int_0^{\infty}\frac{S_t(\xi)\overline{S_{d_1}(\xi)}}{Z(\xi)}d\xi\right\} \tag{4.41}$$

$$V_{d_1}\cdot 2Re\left\{\int_0^{\infty}\frac{S_{d_1}(\xi)\overline{S_{d_2}(\xi)}}{Z(\xi)}d\xi\right\} + V_{d_2}\cdot 2Re\left\{\int_0^{\infty}\frac{S_{d_2}(\xi)\overline{S_{d_2}(\xi)}}{Z(\xi)}d\xi\right\} = \frac{V_t}{3}\cdot 2Re\left\{\int_0^{\infty}\frac{S_t(\xi)\overline{S_{d_2}(\xi)}}{Z(\xi)}d\xi\right\} \tag{4.42}$$

In the previous section it was mentioned that it was shown in Chapter 3 that when using PWM, the harmonics appear in groups around integer multiples (denoted by m) of the switching frequency. For sinusoidal modulation, side-bands appear at integer multiples (denoted by n) of the reference frequency around these harmonics of the switching frequency. Using this property it is possible to rewrite the integrals in the above system of equations in terms of integrals over groups of harmonics by using the "Summation Rule of Integrals". These groups were defined and discussed in section 3.3.1.3.

The properties of the switching functions $S_{d_1}(\omega)$, $S_{d_2}(\omega)$ and $S_t(\omega)$ were proven in section 3.3.1.3 of the previous chapter, but are repeated here for convenience in Table 4.2. These properties will be used to rewrite the switching functions in terms of $S_{d_1}(\omega)$ and also to simplify the equations where possible.

The above-mentioned "Summation Rule of Integrals" will now be applied on each of the integrals in equations (4.41) and (4.42). The decomposition of these integrals are summarised in Table 4.3.

As in the previous section, the integrals over harmonic groups can be simplified by using new variables. In the following mathematical definitions m is used as the number of the group of harmonics over which an integral is taken, where the group includes the side-band harmonics.

Table 4.2. *Summary of* 3*-cell switching function properties*

Conditions	Properties
all m	$\lvert S_{d_1}(\xi)\rvert = \lvert S_{d_2}(\xi)\rvert$
$m = 3k$, for all $k = 0, 1, \ldots$	$S_{d_1}(\xi) = S_{d_2}(\xi) = 0$ $\lvert S_t\rvert \geq 0$
$m = 3k+1$, for all $k = 0, 1, \ldots$	$S_{d_1}(\xi) = S_{d_2}(\xi)e^{-j\frac{2\pi}{3}}$ $\Rightarrow S_{d_2}(\xi)\overline{S_{d_1}(\xi)} = S_{d_2}(\xi)\overline{S_{d_2}(\xi)}e^{j\frac{2\pi}{3}}$ $S_t = 0$
$m = 3k+2$, for all $k = 0, 1, \ldots$	$S_{d_1}(\xi) = S_{d_2}(\xi)e^{j\frac{2\pi}{3}}$ $\Rightarrow S_{d_2}(\xi)\overline{S_{d_1}(\xi)} = S_{d_2}(\xi)\overline{S_{d_2}(\xi)}e^{-j\frac{2\pi}{3}}$ $S_t = 0$

For convenience, the following variables are defined: $\lambda_0, \lambda_1, \lambda_2$, where $k = 0, 1, \ldots, \infty$:

$$\lambda_0 = \int_{m=3k} \frac{|S_{d_1}(\xi)|^2}{Z(\xi)} d\xi \tag{4.43}$$

$$\lambda_1 = \int_{m=3k+1} \frac{|S_{d_1}(\xi)|^2}{Z(\xi)} d\xi \tag{4.44}$$

$$\lambda_2 = \int_{m=3k+2} \frac{|S_{d_1}(\xi)|^2}{Z(\xi)} d\xi \tag{4.45}$$

and $\alpha_0, \alpha_1, \alpha_2$, where $k = 0, 1, \ldots, \infty$:

$$\alpha_0 = \int_{m=3k} \frac{S_t(\xi)\overline{S_{d_1}(\xi)}}{Z(\xi)} d\xi \tag{4.46}$$

$$\alpha_1 = \int_{m=3k+1} \frac{S_t(\xi)\overline{S_{d_1}(\xi)}}{Z(\xi)} d\xi \tag{4.47}$$

$$\alpha_2 = \int_{m=3k+2} \frac{S_t(\xi)\overline{S_{d_1}(\xi)}}{Z(\xi)} d\xi \tag{4.48}$$

The conjugates of the above variables are defined: $\overline{\lambda_0}$, $\overline{\lambda_1}$, $\overline{\lambda_2}$, where $k = -\infty, \ldots, -1$:

$$\overline{\lambda_0} = \int_{m=3k} \frac{|S_{d_1}(\xi)|^2}{\overline{Z(\xi)}} d\xi \tag{4.49}$$

$$\overline{\lambda_1} = \int_{m=3k+1} \frac{|S_{d_1}(\xi)|^2}{\overline{Z(\xi)}} d\xi \tag{4.50}$$

$$\overline{\lambda_2} = \int_{m=3k+2} \frac{|S_{d_1}(\xi)|^2}{\overline{Z(\xi)}} d\xi \tag{4.51}$$

and $\overline{\alpha_0}, \overline{\alpha_1}, \overline{\alpha_2}$, where $k = -\infty, \ldots, -1$:

$$\overline{\alpha_0} = \int_{m=3k} \frac{\overline{S_t(\xi)} S_{d_1}(\xi)}{\overline{Z(\xi)}} d\xi \tag{4.52}$$

$$\overline{\alpha_1} = \int_{m=3k+1} \frac{\overline{S_t(\xi)} S_{d_1}(\xi)}{\overline{Z(\xi)}} d\xi \tag{4.53}$$

$$\overline{\alpha_2} = \int_{m=3k+2} \frac{\overline{S_t(\xi)} S_{d_1}(\xi)}{\overline{Z(\xi)}} d\xi \tag{4.54}$$

The integrals summarised in Table 4.3 have to be rewritten in terms of λ and α using (4.43)-(4.54). Before this can be done, integrals that contain S_{d_2} terms need to be rewritten in terms of S_{d_1} using the switching function harmonic properties listed in Table 4.2. At this point it is also important to note that for $m = 3k$: $S_{d_1}(\xi) = S_{d_2}(\xi) = 0$, which implies that the integrals over harmonic groups $m = 3k$ are zero, i.e. λ_0 and α_0 are zero. The resulting expressions are also summarised in Table 4.3 (a)-(f).

The results listed in Table 4.3 (a)-(f) can be used to write equations (4.41) and (4.42) in matrix form as follows:

$$2Re\{\mathbf{\Lambda}\}\mathbf{V_d} = -\frac{V_t}{3} 2Re\{\mathbf{A}\} \tag{4.55}$$

where the matrix $\mathbf{\Lambda}$ and the vectors $\mathbf{V_d}$ and $\mathbf{A}$ are defined as follows:

$$\mathbf{\Lambda} = \begin{bmatrix} \lambda_1 + \lambda_2 & e^{j\frac{2\pi}{3}}\lambda_1 + e^{-j\frac{2\pi}{3}}\lambda_2 \\ e^{-j\frac{2\pi}{3}}\lambda_1 + e^{j\frac{2\pi}{3}}\lambda_2 & \lambda_1 + \lambda_2 \end{bmatrix} \tag{4.56}$$

$$\mathbf{V_d} = \begin{bmatrix} V_{d_1} \\ V_{d_2} \end{bmatrix} \tag{4.57}$$

$$\mathbf{A} = \begin{bmatrix} \alpha_1 + \alpha_2 \\ e^{-j\frac{2\pi}{3}}\alpha_1 + e^{j\frac{2\pi}{3}}\alpha_2 \end{bmatrix} \tag{4.58}$$

The matrix $2Re\{\mathbf{\Lambda}\}$ was rewritten in Appendix B section B.3 equation (B.22) to be the following:

$$\begin{aligned} 2Re\{\mathbf{\Lambda}\} &= \mathbf{\Lambda} + \overline{\mathbf{\Lambda}} \\ &= \begin{bmatrix} 1 & 1 \\ e^{-j\frac{2\pi}{3}} & e^{j\frac{2\pi}{3}} \end{bmatrix} \begin{bmatrix} \lambda_1 & 0 \\ 0 & \lambda_2 \end{bmatrix} \begin{bmatrix} 1 & e^{j\frac{2\pi}{3}} \\ 1 & e^{-j\frac{2\pi}{3}} \end{bmatrix} + \end{aligned}$$

Table 4.3. *Integrals rewritten in terms of groups of harmonics*

Integral	Integrals over groups	
$\int_0^\infty \frac{S_t(\xi)\overline{S_{d_1}(\xi)}}{Z(\xi)}d\xi$	$\int_{m=3k} \frac{S_t(\xi)\overline{S_{d_1}(\xi)}}{Z(\xi)}d\xi + \int_{m=3k+1} \frac{S_t(\xi)\overline{S_{d_1}(\xi)}}{Z(\xi)}d\xi + \int_{m=3k+2} \frac{S_t(\xi)\overline{S_{d_1}(\xi)}}{Z(\xi)}d\xi$ $=\alpha_1 + \alpha_2$	(a)
$\int_0^\infty \frac{S_{d_1}(\xi)\overline{S_{d_1}(\xi)}}{Z(\xi)}d\xi$	$\int_{m=3k} \frac{S_{d_1}(\xi)\overline{S_{d_1}(\xi)}}{Z(\xi)}d\xi + \int_{m=3k+1} \frac{S_{d_1}(\xi)\overline{S_{d_1}(\xi)}}{Z(\xi)}d\xi + \int_{m=3k+2} \frac{S_{d_1}(\xi)\overline{S_{d_1}(\xi)}}{Z(\xi)}d\xi$ $=\lambda_1 + \lambda_2$	(b)
$\int_0^\infty \frac{S_{d_2}(\xi)\overline{S_{d_1}(\xi)}}{Z(\xi)}d\xi$	$\int_{m=3k} \frac{S_{d_2}(\xi)\overline{S_{d_1}(\xi)}}{Z(\xi)}d\xi + \int_{m=3k+1} \frac{S_{d_2}(\xi)\overline{S_{d_1}(\xi)}}{Z(\xi)}d\xi + \int_{m=3k+2} \frac{S_{d_2}(\xi)\overline{S_{d_1}(\xi)}}{Z(\xi)}d\xi$ $=e^{j\frac{2\pi}{3}}\lambda_1 + e^{-j\frac{2\pi}{3}}\lambda_2$	(c)
$\int_0^\infty \frac{S_t(\xi)\overline{S_{d_2}(\xi)}}{Z(\xi)}d\xi$	$\int_{m=3k} \frac{S_t(\xi)\overline{S_{d_2}(\xi)}}{Z(\xi)}d\xi + \int_{m=3k+1} \frac{S_t(\xi)\overline{S_{d_2}(\xi)}}{Z(\xi)}d\xi + \int_{m=3k+2} \frac{S_t(\xi)\overline{S_{d_2}(\xi)}}{Z(\xi)}d\xi$ $=e^{-j\frac{2\pi}{3}}\alpha_1 + e^{j\frac{2\pi}{3}}\alpha_2$	(d)
$\int_0^\infty \frac{S_{d_1}(\xi)\overline{S_{d_2}(\xi)}}{Z(\xi)}d\xi$	$\int_{m=3k} \frac{S_{d_1}(\xi)\overline{S_{d_2}(\xi)}}{Z(\xi)}d\xi + \int_{m=3k+1} \frac{S_{d_1}(\xi)\overline{S_{d_2}(\xi)}}{Z(\xi)}d\xi + \int_{m=3k+2} \frac{S_{d_1}(\xi)\overline{S_{d_2}(\xi)}}{Z(\xi)}d\xi$ $=e^{-j\frac{2\pi}{3}}\lambda_1 + e^{j\frac{2\pi}{3}}\lambda_2$	(e)
$\int_0^\infty \frac{S_{d_2}(\xi)\overline{S_{d_2}(\xi)}}{Z(\xi)}d\xi$	$\int_{m=3k} \frac{S_{d_2}(\xi)\overline{S_{d_2}(\xi)}}{Z(\xi)}d\xi + \int_{m=3k+1} \frac{S_{d_2}(\xi)\overline{S_{d_2}(\xi)}}{Z(\xi)}d\xi + \int_{m=3k+2} \frac{S_{d_2}(\xi)\overline{S_{d_2}(\xi)}}{Z(\xi)}d\xi$ $=\lambda_1 + \lambda_2$	(f)

$$\begin{aligned} &\begin{bmatrix} 1 & 1 \\ e^{-j\frac{2\pi}{3}} & e^{j\frac{2\pi}{3}} \end{bmatrix} \begin{bmatrix} \overline{\lambda_2} & 0 \\ 0 & \overline{\lambda_1} \end{bmatrix} \begin{bmatrix} 1 & e^{j\frac{2\pi}{3}} \\ 1 & e^{-j\frac{2\pi}{3}} \end{bmatrix} \\ &= \begin{bmatrix} 1 & 1 \\ e^{-j\frac{2\pi}{3}} & e^{j\frac{2\pi}{3}} \end{bmatrix} \begin{bmatrix} \lambda_1 + \overline{\lambda_2} & 0 \\ 0 & \lambda_2 + \overline{\lambda_1} \end{bmatrix} \begin{bmatrix} 1 & e^{j\frac{2\pi}{3}} \\ 1 & e^{-j\frac{2\pi}{3}} \end{bmatrix} \end{aligned} \tag{4.59}$$

Equation (4.55) can be manipulated so that $\frac{\mathbf{V_d}}{V_t}$ is the subject as follows:

$$\frac{\mathbf{V_d}}{V_t} = -\frac{1}{3}(2Re\{\mathbf{\Lambda}\})^{-1}2Re\{\mathbf{A}\} \tag{4.60}$$

To analyse (4.60) it needs to be shown that $(2Re\{\mathbf{\Lambda}\})^{-1}$ exists. This is done by calculating the determinant of $2Re\{\mathbf{\Lambda}\}$. This determinant was calculated in Appendix B section B.3 equation (B.34) and the answer is repeated here for convenience as follows:

$$\det(2Re\{\mathbf{\Lambda}\}) = 3(\lambda_1 + \overline{\lambda_2})(\lambda_2 + \overline{\lambda_1}) \tag{4.61}$$

Equation (4.61) proves that $\det(2Re\{\mathbf{\Lambda}\})$ is nonzero if the following conditions are true:

- $\lambda_1 \neq 0$ and $\lambda_2 \neq 0$. It was shown in Chapter 3 section 3.3.1.3 that $S_{d_1}(\omega) \neq 0$ and $S_{d_2}(\omega) \neq 0$ for both $m = 3k+1$ and $m = 3k+2$. From the properties of $S_{d_1}(\omega)$ and $S_{d_2}(\omega)$ listed in Table 4.2 and the definitions of λ_1 and λ_2, shown respectively in equations (4.44) and (4.45) it is clear that $\lambda_1 \neq 0$ and $\lambda_2 \neq 0$

- $\lambda_1 \neq \lambda_2$. It was shown in Chapter 3 section 3.3.1.3 and listed in Table 4.2 that $S_{d_1}(\omega)$ and $S_{d_2}(\omega)$ differ by $e^{\mp\frac{2\pi}{3}}$ for $m = 3k+1$ and $m = 3k+2$. Therefore, from the definitions of λ_1 and λ_2 it follows that $\lambda_1 \neq \lambda_2$.

As the above conditions are true, $\det(2Re\{\mathbf{\Lambda}\}) \neq 0$ and equation (4.60) has a unique solution.

In order to solve the relationships of $\frac{V_{d_1}}{V_t}$ and $\frac{V_{d_2}}{V_t}$ as described in equation (4.60), the respective matrices and inverse matrices can be substituted as follows:

$$\begin{aligned}
\begin{bmatrix} \frac{V_{d_1}}{V_t} \\ \frac{V_{d_2}}{V_t} \end{bmatrix} &= -\frac{1}{3}\begin{bmatrix} 2Re\{\lambda_1+\lambda_2\} & 2Re\{e^{j\frac{2\pi}{3}}\lambda_1 + e^{-j\frac{2\pi}{3}}\lambda_2\} \\ 2Re\{e^{-j\frac{2\pi}{3}}\lambda_1 + e^{j\frac{2\pi}{3}}\lambda_2\} & 2Re\{\lambda_1+\lambda_2\} \end{bmatrix}^{-1}\begin{bmatrix} 2Re\{\alpha_1+\alpha_2\} \\ 2Re\{e^{-j\frac{2\pi}{3}}\alpha_1 + e^{j\frac{2\pi}{3}}\alpha_2\} \end{bmatrix} \\
&= \begin{bmatrix} -\frac{(\lambda_1+\overline{\lambda_2})+(\lambda_2+\overline{\lambda_1})}{9(\lambda_1+\overline{\lambda_2})(\lambda_2+\overline{\lambda_1})} & \frac{e^{j\frac{2\pi}{3}}(\lambda_1+\overline{\lambda_2})+e^{-j\frac{2\pi}{3}}(\lambda_2+\overline{\lambda_1})}{9(\lambda_1+\overline{\lambda_2})(\lambda_2+\overline{\lambda_1})} \\ \frac{e^{-j\frac{2\pi}{3}}(\lambda_1+\overline{\lambda_2})+e^{j\frac{2\pi}{3}}(\lambda_2+\overline{\lambda_1})}{9(\lambda_1+\overline{\lambda_2})(\lambda_2+\overline{\lambda_1})} & -\frac{(\lambda_1+\overline{\lambda_2})+(\lambda_2+\overline{\lambda_1})}{9(\lambda_1+\overline{\lambda_2})(\lambda_2+\overline{\lambda_1})} \end{bmatrix}\begin{bmatrix} 2Re\{\alpha_1+\alpha_2\} \\ 2Re\{e^{-j\frac{2\pi}{3}}\alpha_1 + e^{j\frac{2\pi}{3}}\alpha_2\} \end{bmatrix} \\
&= \begin{bmatrix} -\frac{2Re\{\lambda_1+\lambda_2\}}{9(\lambda_1+\overline{\lambda_2})(\lambda_2+\overline{\lambda_1})} & \frac{2Re\{e^{j\frac{2\pi}{3}}\lambda_1+e^{-j\frac{2\pi}{3}}\lambda_2\}}{9(\lambda_1+\overline{\lambda_2})(\lambda_2+\overline{\lambda_1})} \\ \frac{2Re\{e^{-j\frac{2\pi}{3}}\lambda_1+e^{j\frac{2\pi}{3}}\lambda_2\}}{9(\lambda_1+\overline{\lambda_2})(\lambda_2+\overline{\lambda_1})} & -\frac{2Re\{\lambda_1+\lambda_2\}}{9(\lambda_1+\overline{\lambda_2})(\lambda_2+\overline{\lambda_1})} \end{bmatrix}\begin{bmatrix} 2Re\{\alpha_1+\alpha_2\} \\ 2Re\{e^{j\frac{-2\pi}{3}}\alpha_1 + e^{j\frac{2\pi}{3}}\alpha_2\} \end{bmatrix}
\end{aligned} \tag{4.62}$$

Equation (4.62) contains the two unbalance equations for the two cell capacitor voltages in a 3-cell multicell converter. These two unbalance equations can be written separately as follows:

$$\frac{V_{d_1}}{V_t} = -\frac{2Re\{\lambda_1+\lambda_2\}2Re\{\alpha_1+\alpha_2\} - 2Re\{e^{j\frac{2\pi}{3}}\lambda_1 + e^{-j\frac{2\pi}{3}}\lambda_2\}2Re\{e^{-j\frac{2\pi}{3}}\alpha_1 + e^{j\frac{2\pi}{3}}\alpha_2\}}{9(\lambda_1+\overline{\lambda_2})(\lambda_2+\overline{\lambda 1})} \tag{4.63}$$

$$\frac{V_{d_2}}{V_t} = -\frac{-2Re\{e^{-j\frac{2\pi}{3}}\lambda_1 + e^{j\frac{2\pi}{3}}\lambda_2\}2Re\{\alpha_1+\alpha_2\} + 2Re\{\lambda_1+\lambda_2\}2Re\{e^{-j\frac{2\pi}{3}}\alpha_1 + e^{j\frac{2\pi}{3}}\alpha_2\}}{9(\lambda_1+\overline{\lambda_2})(\lambda_2+\overline{\lambda 1})} \tag{4.64}$$

To prove that the cell capacitor voltages balance naturally, both the unbalance equations must tend to zero. For this proof, α_1 and α_2 need to be examined more closely. The defining equations (4.47) and (4.48) of α_1 and α_2 are repeated here for convenience:

$$\alpha_1 = \int_{m=3k+1} \frac{S_t(\xi)\overline{S_{d_1}(\xi)}}{Z(\xi)} d\xi \tag{4.65}$$

$$\alpha_2 = \int_{m=3k+2} \frac{S_t(\xi)\overline{S_{d_1}(\xi)}}{Z(\xi)} d\xi \tag{4.66}$$

According to Table 4.2, $S_t = 0$ for $m = 3k + 1$ as well as $m = 3k + 2$. This means that $\alpha_1 = 0$ and $\alpha_2 = 0$ when $S_{d_1}(\omega)$ and $S_t(\omega)$ do not overlap, which are the same conditions that applied in section 4.3. The resulting balance equations are as follows:

$$\frac{V_{d_1}}{V_t} = \frac{0}{9(\lambda_1 + \overline{\lambda_2})(\lambda_2 + \overline{\lambda_1})} \tag{4.67}$$

$$\frac{V_{d_2}}{V_t} = \frac{0}{9(\lambda_1 + \overline{\lambda_2})(\lambda_2 + \overline{\lambda_1})} \tag{4.68}$$

The denominator in equations (4.67) and (4.68) is the determinant of $2Re\{\mathbf{\Lambda}\}$ scaled with a constant. It was proved in equation (4.61) that the determinant is nonzero.

From the definitions of V_{d_1} and V_{d_2}, it follows that as they tend to zero, the unbalance tends to zero. Therefore, from equations (4.67) and (4.68) it follows that the respective voltages across cell capacitors C_1 and C_2 balance in steady-state when the harmonics of $S_t(\omega)$ and $S_{d_1}(\omega)$ do not overlap. Again, as stated in the previous section, this is only valid as long as the load impedance $Z(\omega)$ is not purely inductive or purely imaginary. When the load impedance is purely inductive, $Re\{Z(\omega)\} = 0$, which means that $\frac{V_{d_1}}{V_t}$ and $\frac{V_{d_2}}{V_t}$ will tend towards infinity, causing unbalanced cell capacitor voltages. The same cases that caused unbalance for the 2-cell case is also valid for this case.

It was shown in the previous section that the connection of a balance booster circuit in parallel with the load can improve the balancing of the cell capacitor voltages when the balance booster is designed to have a low impedance at the switching frequency of the converter. It will now be shown that a balance booster tuned to resonate at the switching frequency also improves the balancing of the cell capacitor voltages for the 3-cell case.

The balancing equations for the 3-cell converter case are repeated here for convenience as follows:

$$\frac{V_{d_1}}{V_t} = -\frac{2Re\{\lambda_1 + \lambda_2\}2Re\{\alpha_1 + \alpha_2\} - 2Re\{e^{j\frac{2\pi}{3}}\lambda_1 + e^{-j\frac{2\pi}{3}}\lambda_2\}2Re\{e^{-j\frac{2\pi}{3}}\alpha_1 + e^{j\frac{2\pi}{3}}\alpha_2\}}{9(\lambda_1 + \overline{\lambda_2})(\lambda_2 + \overline{\lambda 1})} \tag{4.69}$$

$$\frac{V_{d_2}}{V_t} = -\frac{-2Re\{e^{-j\frac{2\pi}{3}}\lambda_1 + e^{j\frac{2\pi}{3}}\lambda_2\}2Re\{\alpha_1+\alpha_2\} + 2Re\{\lambda_1+\lambda_2\}2Re\{e^{-j\frac{2\pi}{3}}\alpha_1 + e^{j\frac{2\pi}{3}}\alpha_2\}}{9(\lambda_1+\overline{\lambda_2})(\lambda_2+\overline{\lambda 1})} \tag{4.70}$$

In order to improve the cell capacitor voltage balance, it can be seen from equations (4.69) and (4.70) that $\frac{V_{d_1}}{V_t}$ and $\frac{V_{d_2}}{V_t}$ decrease when λ_1 is increased. When λ_1 is increased, $\overline{\lambda_1}$ is also increased. From the definition of λ_1 in equation (4.44), repeated here as equation (4.71), it is clear that when $Z(\omega)$ becomes smaller, λ_1 increases.

$$\lambda_1 = \int_{m=3k+1} \frac{|S_{d_1}(\xi)|^2}{Z(\xi)} d\xi \tag{4.71}$$

From equation (4.71), λ_1 is defined over the harmonic groups $m = 3k+1$ where $k = 0, \ldots, \infty$, which are all the multiples m of the switching frequency. Thus, if the balance booster is designed to have a low impedance at the switching frequency, it will increase the value of λ_1 and both $\frac{V_{d_1}}{V_t}$ and $\frac{V_{d_2}}{V_t}$ will decrease.

4.5 The p-cell multicell converter

This section focusses on the steady-state analysis of a p-cell multicell converter. This is the final step in the progression of the analysis that started with the analysis of the 2-cell multicell converter. This analysis starts in the same way as in the previous section, but uses matrix analysis in the later stages. The reader is referred to Appendix B for the detailed matrix analysis.

The time domain equivalent circuit in terms of d and t parameters of a p-cell multicell converter was shown in Figure 2-11. For the steady-state analysis of this converter, this circuit is converted to the frequency domain. The equivalent circuit in terms of d and t parameters in the frequency domain is shown in Figure 4-7.

Looking at the equivalent circuit shown in Figure 4-7, an expression for the inductor current in the frequency domain can be written. Using Ohm's Law, $I_L(\omega)$ can be written as follows:

$$I_L(\omega) = \frac{V_0(\omega)}{Z(\omega)} = \frac{\frac{V_t}{p}\cdot S_t(\omega)}{Z(\omega)} + \frac{\sum_{l=1}^{p-1} V_{d_l} S_{d_l}(\omega)}{Z(\omega)} \tag{4.72}$$

The expression for the cell capacitor current $I_{C_1}(\omega)$ can then be found by using convolution in the

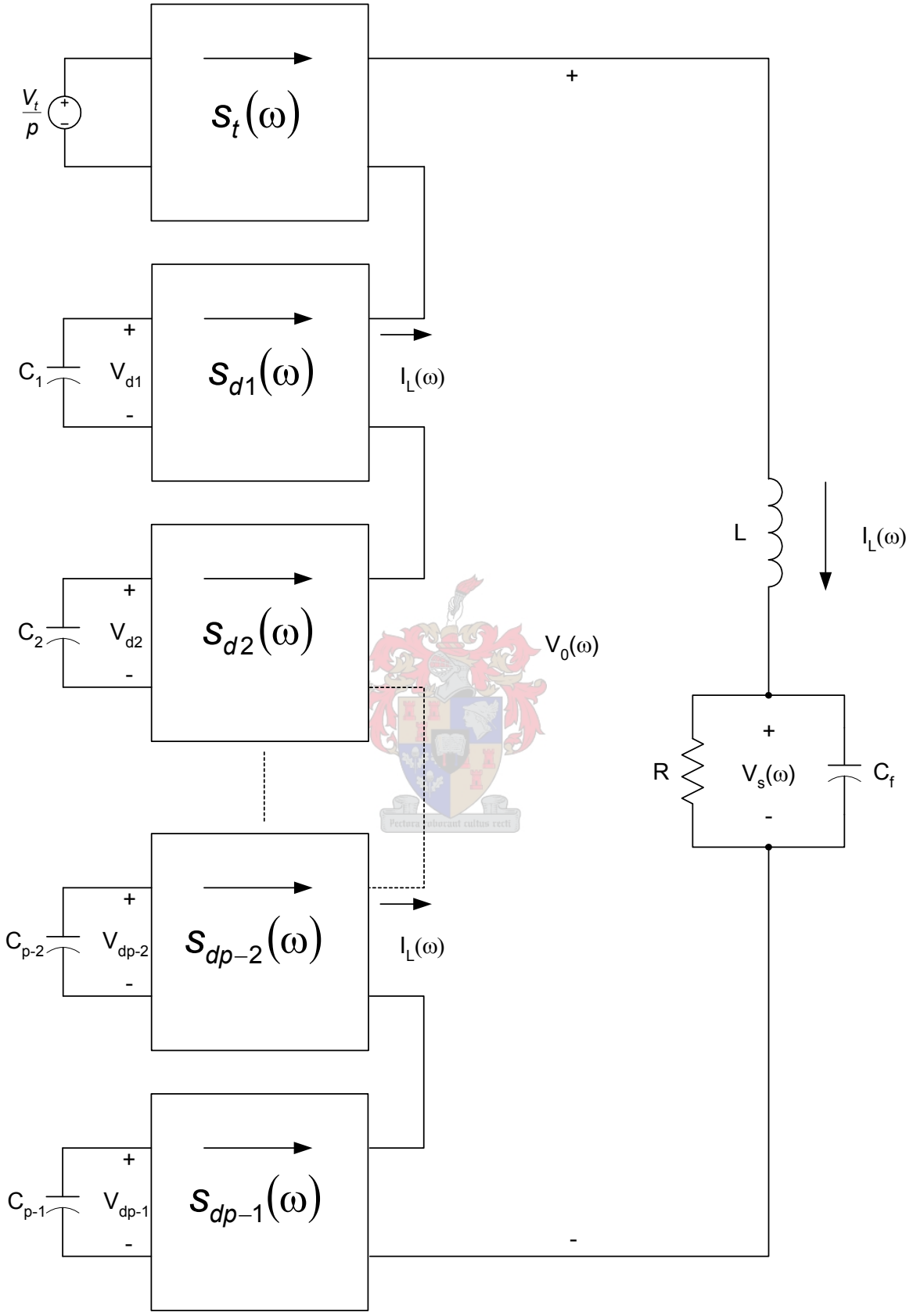

Figure 4-7. *Equivalent circuit in the frequency domain in terms of d and t parameters of a p-cell multicell converter.*

frequency domain, i.e. applying equation (4.2):

$$\begin{aligned} I_{C_1}(\omega) &= -I_L(\omega) \star S_{d_1}(\omega) \\ &= -\left(\frac{\frac{V_t}{p} \cdot S_t(\omega)}{Z(\omega)} + \frac{\sum_{l=1}^{p-1} V_{d_l} S_{d_l}(\omega)}{Z(\omega)} \right) \star S_{d_1}(\omega) \\ &= -\left[\left(\frac{\frac{V_t}{p} \cdot S_t(\omega)}{Z(\omega)} \right) \star S_{d_1}(\omega) + \left(\frac{\sum_{l=1}^{p-1} V_{d_l} S_{d_l}(\omega)}{Z(\omega)} \right) \star S_{d_1}(\omega) \right] \\ &= -\left[\frac{V_t}{p} \int_{-\infty}^{\infty} \frac{S_t(\xi)}{Z(\xi)} S_{d_1}(\omega - \xi) d\xi + \int_{-\infty}^{\infty} \frac{\sum_{l=1}^{p-1} V_{d_l} S_{d_l}(\xi)}{Z(\xi)} S_{d_1}(\omega - \xi) d\xi \right] \end{aligned} \tag{4.73}$$

In the same way, an expression for the cell capacitor current $I_{C_i}(\omega)$, where $I_{C_i}(\omega)$ refers to the i^{th} cell capacitor current in the frequency domain, can then be found by applying equation (4.2):

$$\begin{aligned} I_{C_i}(\omega) &= -I_L(\omega) \star S_{d_i}(\omega) \\ &= -\left(\frac{\frac{V_t}{p} \cdot S_t(\omega)}{Z(\omega)} + \frac{\sum_{l=1}^{p-1} V_{d_l} S_{d_l}(\omega)}{Z(\omega)} \right) \star S_{d_i}(\omega) \\ &= -\left[\left(\frac{\frac{V_t}{p} \cdot S_t(\omega)}{Z(\omega)} \right) \star S_{d_i}(\omega) + \left(\frac{\sum_{l=1}^{p-1} V_{d_l} S_{d_l}(\omega)}{Z(\omega)} \right) \star S_{d_i}(\omega) \right] \\ &= -\left[\frac{V_t}{p} \int_{-\infty}^{\infty} \frac{S_t(\xi)}{Z(\xi)} S_{d_i}(\omega - \xi) d\xi + \int_{-\infty}^{\infty} \frac{\sum_{l=1}^{p-1} V_{d_l} S_{d_l}(\xi)}{Z(\xi)} S_{d_i}(\omega - \xi) d\xi \right] \end{aligned} \tag{4.74}$$

If in steady-state, $I_{C_i}(\omega)|_{\omega=0} = 0$, where $i = 1, \ldots, p-1$, then the following is true:

$$\begin{aligned} I_{C_i}(\omega)|_{\omega=0} &= -\left[\frac{V_t}{p} \int_{-\infty}^{\infty} \frac{S_t(\xi)}{Z(\xi)} S_{d_i}(-\xi) d\xi + \int_{-\infty}^{\infty} \frac{\sum_{l=1}^{p-1} V_{d_l} S_{d_l}(\xi)}{Z(\xi)} S_{d_i}(-\xi) d\xi \right] \\ 0 &= -\left[\frac{V_t}{p} \int_{-\infty}^{\infty} \frac{S_t(\xi)}{Z(\xi)} \overline{S_{d_i}(\xi)} d\xi + \int_{-\infty}^{\infty} \frac{\sum_{l=1}^{p-1} V_{d_l} S_{d_l}(\xi)}{Z(\xi)} \overline{S_{d_i}(\xi)} d\xi \right] \\ &= -\left[\frac{V_t}{p} \int_{-\infty}^{\infty} \frac{S_t(\xi)}{Z(\xi)} \overline{S_{d_i}(\xi)} d\xi + \sum_{l=1}^{p-1} V_{d_l} \int_{-\infty}^{\infty} \frac{S_{d_l}(\xi)}{Z(\xi)} \overline{S_{d_i}(\xi)} d\xi \right] \end{aligned} \tag{4.75}$$

Equation (4.75) can be rewritten as follows:

$$\sum_{l=1}^{p-1} V_{d_l} \int_{-\infty}^{\infty} \frac{S_{d_l}(\xi)}{Z(\xi)} \overline{S_{d_i}(\xi)} d\xi = -\frac{V_t}{p} \int_{-\infty}^{\infty} \frac{S_t(\xi)}{Z(\xi)} \overline{S_{d_i}(\xi)} d\xi \tag{4.76}$$

Using the same properties of the definite integral as used in sections 4.3 and 4.4, it is possible to

rewrite equation (4.76) as follows:

$$\sum_{l=1}^{p-1} V_{d_l} 2Re\left\{\int_0^\infty \frac{S_{d_l}(\xi)}{Z(\xi)}\overline{S_{d_i}(\xi)}d\xi\right\} = -\frac{V_t}{p}2Re\left\{\int_0^\infty \frac{S_t(\xi)}{Z(\xi)}\overline{S_{d_i}(\xi)}d\xi\right\} \tag{4.77}$$

Rewriting equation (4.77) in matrix form results in the following:

$$\begin{bmatrix} \sum_{l=1}^{p-1} V_{d_l} 2Re\{\int_0^\infty \frac{S_{d_l}(\xi)}{Z(\xi)}\overline{S_{d_1}(\xi)}d\xi\} \\ \vdots \\ \sum_{l=1}^{p-1} V_{d_l} 2Re\{\int_0^\infty \frac{S_{d_l}(\xi)}{Z(\xi)}\overline{S_{d_{p-1}}(\xi)}d\xi\} \end{bmatrix} = -\frac{V_t}{p}\begin{bmatrix} 2Re\{\int_0^\infty \frac{S_t(\xi)}{Z(\xi)}\overline{S_{d_1}(\xi)}d\xi\} \\ \vdots \\ 2Re\{\int_0^\infty \frac{S_t(\xi)}{Z(\xi)}\overline{S_{d_{p-1}}(\xi)}d\xi\} \end{bmatrix}$$

$$\begin{bmatrix} \sum_{l=1}^{p-1} 2Re\{\int_0^\infty \frac{S_{d_l}(\xi)}{Z(\xi)}\overline{S_{d_1}(\xi)}d\xi\} \\ \vdots \\ \sum_{l=1}^{p-1} 2Re\{\int_0^\infty \frac{S_{d_l}(\xi)}{Z(\xi)}\overline{S_{d_{p-1}}(\xi)}d\xi\} \end{bmatrix}\begin{bmatrix} V_{d_1} \\ \vdots \\ V_{d_{p-1}} \end{bmatrix} = -\frac{V_t}{p}\begin{bmatrix} 2Re\{\int_0^\infty \frac{S_t(\xi)}{Z(\xi)}\overline{S_{d_1}(\xi)}d\xi\} \\ \vdots \\ 2Re\{\int_0^\infty \frac{S_t(\xi)}{Z(\xi)}\overline{S_{d_{p-1}}(\xi)}d\xi\} \end{bmatrix}$$

$$\begin{bmatrix} 2Re\{\sum_{l=1}^{p-1} \int_0^\infty \frac{S_{d_l}(\xi)}{Z(\xi)}\overline{S_{d_1}(\xi)}d\xi\} \\ \vdots \\ 2Re\{\sum_{l=1}^{p-1} \int_0^\infty \frac{S_{d_l}(\xi)}{Z(\xi)}\overline{S_{d_{p-1}}(\xi)}d\xi\} \end{bmatrix}\begin{bmatrix} V_{d_1} \\ \vdots \\ V_{d_{p-1}} \end{bmatrix} = -\frac{V_t}{p}\begin{bmatrix} 2Re\{\int_0^\infty \frac{S_t(\xi)}{Z(\xi)}\overline{S_{d_1}(\xi)}d\xi\} \\ \vdots \\ 2Re\{\int_0^\infty \frac{S_t(\xi)}{Z(\xi)}\overline{S_{d_{p-1}}(\xi)}d\xi\} \end{bmatrix}$$

$$2Re\{\mathbf{\Lambda}\}\mathbf{V_d} = -\frac{V_t}{p}2Re\{\mathbf{A}\} \tag{4.78}$$

where the matrix $\mathbf{\Lambda}$ and the vectors $\mathbf{V_d}$ and $\mathbf{A}$ are defined as follows:

$$\begin{aligned}\mathbf{\Lambda} &= \begin{bmatrix} \sum_{l=1}^{p-1} \int_0^\infty \frac{S_{d_l}(\xi)}{Z(\xi)}\overline{S_{d_1}(\xi)}d\xi \\ \vdots \\ \sum_{l=1}^{p-1} \int_0^\infty \frac{S_{d_l}(\xi)}{Z(\xi)}\overline{S_{d_{p-1}}(\xi)}d\xi \end{bmatrix} \\ &= \begin{bmatrix} \int_0^\infty \frac{S_{d_1}(\xi)}{Z(\xi)}\overline{S_{d_1}(\xi)}d\xi & \dots & \int_0^\infty \frac{S_{d_{p-1}}(\xi)}{Z(\xi)}\overline{S_{d_1}(\xi)}d\xi \\ \vdots & \ddots & \vdots \\ \int_0^\infty \frac{S_{d_1}(\xi)}{Z(\xi)}\overline{S_{d_{p-1}}(\xi)}d\xi & \dots & \int_0^\infty \frac{S_{d_{p-1}}(\xi)}{Z(\xi)}\overline{S_{d_{p-1}}(\xi)}d\xi \end{bmatrix}\end{aligned} \tag{4.79}$$

$$\mathbf{V_d} = \begin{bmatrix} V_{d_1} \\ \vdots \\ V_{d_{p-1}} \end{bmatrix} \tag{4.80}$$

$$\mathbf{A} = \begin{bmatrix} \int_0^\infty \frac{S_t(\xi)}{Z(\xi)}\overline{S_{d_1}(\xi)}d\xi \\ \vdots \\ \int_0^\infty \frac{S_t(\xi)}{Z(\xi)}\overline{S_{d_{p-1}}(\xi)}d\xi \end{bmatrix} \tag{4.81}$$

A general term of the matrix $\mathbf{\Lambda}$ can be written as follows:

$$[\mathbf{\Lambda}]_{rs} = \int_0^{\infty} \frac{S_{d_s}(\xi)\overline{S_{d_r}(\xi)}}{Z(\xi)} d\xi \tag{4.82}$$

where $1 \leq r \leq p-1$ and $1 \leq s \leq p-1$.

A general term of the vector $\mathbf{A}$ can be written as follows:

$$[\mathbf{A}]_{r1} = \int_0^{\infty} \frac{S_t(\xi)\overline{S_{d_r}(\xi)}}{Z(\xi)} d\xi \tag{4.83}$$

where $1 \leq r \leq p-1$. The same techniques will be now be used for this analysis as used in sections 4.3 and 4.4.

Again as in the previous sections, the integral terms in equations (4.82) and (4.83) can be split into integrals over the harmonic groups by using the "Summation Rule of Integrals". These harmonic groups were discussed for both sinusoidal modulation as well as fixed duty-cycle PWM respectively in Chapter 3 sections 3.3.1.4 and 3.3.2.4. In the following mathematical definitions the variable m is used as the number of the group of harmonics over which an integral is taken, where the group includes the side-band harmonics. Equations (4.82) and (4.83) are rewritten as follows:

$$\begin{aligned}
[\mathbf{\Lambda}]_{rs} = & \int_{m=pk} \frac{S_{d_s}(\xi)\overline{S_{d_r}(\xi)}}{Z(\xi)} d\xi + \\
& \int_{m=pk+1} \frac{S_{d_s}(\xi)\overline{S_{d_r}(\xi)}}{Z(\xi)} d\xi + \\
& \int_{m=pk+2} \frac{S_{d_s}(\xi)\overline{S_{d_r}(\xi)}}{Z(\xi)} d\xi + \ldots + \\
& \int_{m=pk+(p-1)} \frac{S_{d_s}(\xi)\overline{S_{d_r}(\xi)}}{Z(\xi)} d\xi
\end{aligned} \tag{4.84}$$

$$\begin{aligned}
[\mathbf{A}]_{r1} = & \int_{m=pk} \frac{S_t(\xi)\overline{S_{d_r}(\xi)}}{Z(\xi)} d\xi + \\
& \int_{m=pk+1} \frac{S_t(\xi)\overline{S_{d_r}(\xi)}}{Z(\xi)} d\xi + \\
& \int_{m=pk+2} \frac{S_t(\xi)\overline{S_{d_r}(\xi)}}{Z(\xi)} d\xi + \ldots + \\
& \int_{m=pk+(p-1)} \frac{S_t(\xi)\overline{S_{d_r}(\xi)}}{Z(\xi)} d\xi
\end{aligned} \tag{4.85}$$

The properties of the switching functions $S_{d_1}(\omega),\ S_{d_2}(\omega), \ldots,\ S_{d_{p-1}}(\omega)$ and $S_t(\omega)$ were proven in Chapter 3 sections 3.3.1.4 and 3.3.2.4 and are summarised in Table 4.4 for convenience. These properties can be used to rewrite all the switching functions in terms of S_{d_1} and also to simplify the equations where possible.

Using the properties listed in Table 4.4, the S_{d_s} and $\overline{S_{d_r}}$ terms in equations (4.84) and (4.85) can be rewritten in terms of S_{d_1} and $\overline{S_{d_1}}$ as follows:

$$\begin{aligned}[\mathbf{\Lambda}]_{rs} = &\int_{m=pk+1} \frac{e^{j\frac{2\pi(s-1)}{p}} S_{d_1}(\xi) e^{-j\frac{2\pi(r-1)}{p}} \overline{S_{d_1}(\xi)}}{Z(\xi)} d\xi + \\ &\int_{m=pk+2} \frac{e^{j\frac{4\pi(s-1)}{p}} S_{d_1}(\xi) e^{-j\frac{4\pi(r-1)}{p}} \overline{S_{d_1}(\xi)}}{Z(\xi)} + \ldots + \\ &\int_{m=pk+(p-1)} \frac{e^{j\frac{2\pi(p-1)(s-1)}{p}} S_{d_1}(\xi) e^{-j\frac{2\pi(p-1)(r-1)}{p}} \overline{S_{d_1}(\xi)}}{Z(\xi)}\end{aligned} \tag{4.86}$$

$$\begin{aligned}[\mathbf{A}]_{r1} = &\int_{m=pk+1} \frac{S_t(\xi) e^{-j\frac{2\pi(r-1)}{p}} \overline{S_{d_1}(\xi)}}{Z(\xi)} d\xi + \\ &\int_{m=pk+2} \frac{S_t(\xi) e^{-j\frac{4\pi(r-1)}{p}} \overline{S_{d_1}(\xi)}}{Z(\xi)} d\xi + \ldots + \\ &\int_{m=pk+(p-1)} \frac{S_t(\xi) e^{-j\frac{2\pi(p-1)(r-1)}{p}} \overline{S_{d_1}(\xi)}}{Z(\xi)} d\xi\end{aligned} \tag{4.87}$$

Again as in sections 4.3 and 4.4, the integrals over harmonic groups of equations (4.86) and (4.87) can be simplified by using new variables. The λ and α terms used in equations (4.103)-(4.106) are defined in the same way as in the previous cases and are as follows: $\lambda_0, \ldots, \lambda_{p-1}$, where $k = 0, 1, \ldots, \infty$:

$$\lambda_0 = \int_{m=pk} \frac{|S_{d_1}(\xi)|^2}{Z(\xi)} d\xi = 0 \tag{4.88}$$

$$\lambda_1 = \int_{m=pk+1} \frac{|S_{d_1}(\xi)|^2}{Z(\xi)} d\xi \tag{4.89}$$

$$\vdots \vdots \vdots$$

$$\lambda_{p-1} = \int_{m=pk+(p-1)} \frac{|S_{d_1}(\xi)|^2}{Z(\xi)} d\xi \tag{4.90}$$

and $\alpha_0, \ldots, \alpha_{p-1}$, where $k = 0, 1, \ldots, \infty$:

$$\alpha_0 = \int_{m=pk} \frac{S_t(\xi)\overline{S_{d_1}(\xi)}}{Z(\xi)} d\xi = 0 \tag{4.91}$$

Table 4.4. *Summary of p-cell switching function properties*

Conditions	Properties
all m	$\lvert S_{d_1}(\xi)\rvert = \lvert S_{d_2}(\xi)\rvert = \lvert S_{d_3}(\xi)\rvert$
$m = pk$, for all $k = 0, 1, \ldots$	$S_{d_1}(\xi) = 0$ $S_{d_2}(\xi) = 0$ $\vdots$ $S_{d_{p-2}}(\xi) = 0$ $S_{d_{p-1}}(\xi) = 0$ $\lvert S_t\rvert \geq 0$
$m = pk + 1$, for all $k = 0, 1, \ldots$	$S_{d_1}(\xi) = S_{d_2}(\xi)e^{-j\frac{2\pi}{p}}$ $S_{d_2}(\xi) = S_{d_3}(\xi)e^{-j\frac{2\pi}{p}}$ $\vdots$ $S_{d_{p-2}}(\xi) = S_{d_{p-1}}(\xi)e^{-j\frac{2\pi}{p}}$ $S_t = 0$ $\Rightarrow S_{d_2}(\xi)\overline{S_{d_1}(\xi)} = S_{d_2}(\xi)\overline{S_{d_2}(\xi)}e^{j\frac{2\pi}{p}}$ $\Rightarrow S_{d_3}(\xi)\overline{S_{d_2}(\xi)} = S_{d_3}(\xi)\overline{S_{d_3}(\xi)}e^{j\frac{2\pi}{p}}$ $\vdots$ $\Rightarrow S_{d_{p-1}}(\xi)\overline{S_{d_{p-2}}(\xi)} = S_{d_{p-1}}(\xi)\overline{S_{d_{p-1}}(\xi)}e^{j\frac{2\pi}{p}}$
$m = pk + 2$, for all $k = 0, 1, \ldots$	$S_{d_1}(\xi) = S_{d_2}(\xi)e^{-j\frac{4\pi}{p}}$ $S_{d_2}(\xi) = S_{d_3}(\xi)e^{-j\frac{4\pi}{p}}$ $\vdots$ $S_{d_{p-2}}(\xi) = S_{d_{p-1}}(\xi)e^{-j\frac{4\pi}{p}}$ $S_t = 0$ $\Rightarrow S_{d_2}(\xi)\overline{S_{d_1}(\xi)} = S_{d_2}(\xi)\overline{S_{d_2}(\xi)}e^{j\frac{4\pi}{p}}$ $\Rightarrow S_{d_3}(\xi)\overline{S_{d_2}(\xi)} = S_{d_3}(\xi)\overline{S_{d_3}(\xi)}e^{j\frac{4\pi}{p}}$ $\vdots$ $\Rightarrow S_{d_{p-1}}(\xi)\overline{S_{d_{p-2}}(\xi)} = S_{d_{p-1}}(\xi)\overline{S_{d_{p-1}}(\xi)}e^{j\frac{4\pi}{p}}$
$\vdots$	$\vdots$
$m = pk + (p-1)$, for all $k = 0, 1, \ldots$	$S_{d_1}(\xi) = S_{d_2}(\xi)e^{-j\frac{2\pi(p-1)}{p}}$ $S_{d_2}(\xi) = S_{d_3}(\xi)e^{-j\frac{2(p-1)\pi}{p}}$ $\vdots$ $S_{d_{p-2}}(\xi) = S_{d_{p-1}}(\xi)e^{-j\frac{2(p-1)\pi}{p}}$ $S_t = 0$ $\Rightarrow S_{d_2}(\xi)\overline{S_{d_1}(\xi)} = S_{d_2}(\xi)\overline{S_{d_2}(\xi)}e^{j\frac{2\pi(p-1)}{p}}$ $\Rightarrow S_{d_3}(\xi)\overline{S_{d_2}(\xi)} = S_{d_3}(\xi)\overline{S_{d_3}(\xi)}e^{j\frac{2\pi(p-1)}{p}}$ $\vdots$ $\Rightarrow S_{d_{p-1}}(\xi)\overline{S_{d_{p-2}}(\xi)} = S_{d_{p-1}}(\xi)\overline{S_{d_{p-1}}(\xi)}e^{j\frac{2\pi(p-1)}{p}}$

$$\alpha_1 = \int_{m=pk+1} \frac{S_t(\xi)\overline{S_{d_1}(\xi)}}{Z(\xi)} d\xi \tag{4.92}$$

$$\vdots \vdots \vdots$$

$$\alpha_{p-1} = \int_{m=pk+(p-1)} \frac{S_t(\xi)\overline{S_{d_1}(\xi)}}{Z(\xi)} d\xi \tag{4.93}$$

The conjugates of the above variables are defined: $\overline{\lambda_0}$, $\overline{\lambda_1}$,..., $\overline{\lambda_{p-1}}$, where $k = -\infty, \ldots, -1$:

$$\overline{\lambda_0} = \int_{m=pk} \frac{|S_{d_1}(\xi)|^2}{\overline{Z(\xi)}} d\xi \tag{4.94}$$

$$\overline{\lambda_1} = \int_{m=pk+1} \frac{|S_{d_1}(\xi)|^2}{\overline{Z(\xi)}} d\xi \tag{4.95}$$

$$\vdots \vdots \vdots$$

$$\overline{\lambda_{p-1}} = \int_{m=pk+(p-1)} \frac{|S_{d_1}(\xi)|^2}{\overline{Z(\xi)}} d\xi \tag{4.96}$$

and $\overline{\alpha_0}, \overline{\alpha_1}, \ldots, \overline{\alpha_{p-1}}$, where $k = -\infty, \ldots, -1$:

$$\overline{\alpha_0} = \int_{m=pk} \frac{\overline{S_t(\xi)}S_{d_1}(\xi)}{\overline{Z(\xi)}} d\xi \tag{4.97}$$

$$\overline{\alpha_1} = \int_{m=pk+1} \frac{\overline{S_t(\xi)}S_{d_1}(\xi)}{\overline{Z(\xi)}} d\xi \tag{4.98}$$

$$\vdots \vdots \vdots$$

$$\overline{\alpha_{p-1}} = \int_{m=pk+(p-1)} \frac{\overline{S_t(\xi)}S_{d_1}(\xi)}{\overline{Z(\xi)}} d\xi \tag{4.99}$$

Using equations (4.88)-(4.90), equation (4.86) can now be written in terms of λ as follows:

$$\begin{aligned}[\mathbf{\Lambda}]_{rs} = & e^{j\frac{2\pi(s-r)}{p}}\lambda_1 + \\ & e^{j\frac{4\pi(s-r)}{p}}\lambda_2 + \ldots + \\ & e^{j\frac{2\pi(p-1)(s-r)}{p}}\lambda_{p-1} \\ = & \sum_{l=1}^{p-1} e^{j\frac{2\pi r(s-l)}{p}}\lambda_l \end{aligned} \tag{4.100}$$

It is important to recognise that for all $[\mathbf{\Lambda}]_{rs}$ with $r \neq s$, the matrix elements consist of sums of the principal p^{th} roots of unity, excluding 1 itself. The diagonal elements, $[\mathbf{\Lambda}]_{rr}$ can be described as follows:

$$[\mathbf{\Lambda}]_{rr} = \sum_{l=1}^{p-1} \lambda_l \tag{4.101}$$

In the same way, using equations (4.88)-(4.90), equation (4.87) can now be written in terms of α as

follows:

$$[\mathbf{A}]_{r1} = e^{-j\frac{2\pi(r-1)}{p}}\alpha_1 + e^{-j\frac{4\pi(r-1)}{p}}\alpha_2 + \ldots + e^{-j\frac{2\pi(p-1)(r-1)}{p}}\alpha_{p-1} \tag{4.102}$$

The system of balance equations for the p-cell case can be written in the same form as (4.55) and is as follows:

$$\frac{\mathbf{V_d}}{V_t} = -\frac{1}{p}(2Re\{\mathbf{\Lambda}\})^{-1}2Re\{\mathbf{A}\} \tag{4.103}$$

The matrix $\mathbf{\Lambda}$ can now be written using equation (4.100) as follows:

$$\mathbf{\Lambda} = \begin{bmatrix} \sum_{l=1}^{p-1}\lambda_l & \sum_{l=1}^{p-1}e^{j\frac{2\pi l}{p}}\lambda_l & \ldots & \sum_{l=1}^{p-1}e^{j\frac{2\pi l(p-2)}{p}}\lambda_l \\ \sum_{l=1}^{p-1}e^{j\frac{-2\pi l}{p}}\lambda_l & \sum_{l=1}^{p-1}\lambda_l & \ldots & \sum_{l=1}^{p-1}e^{j\frac{2\pi l(p-3)}{p}}\lambda_l \\ \vdots & \vdots & \ddots & \vdots \\ \sum_{l=1}^{p-1}e^{j\frac{-2\pi l(p-2)}{p}}\lambda_l & \sum_{l=1}^{p-1}e^{j\frac{2\pi l(p-3)}{p}}\lambda_l & \ldots & \sum_{l=1}^{p-1}\lambda_l \end{bmatrix} \tag{4.104}$$

The vector $\mathbf{V_d}$ in (4.103) is as follows:

$$\mathbf{V_d} = \begin{bmatrix} V_{d_1} \\ V_{d_2} \\ \vdots \\ V_{d_{p-1}} \end{bmatrix} \tag{4.105}$$

The vector $\mathbf{A}$ in (4.103) can be written using equation (4.102) as follows:

$$\mathbf{A} = \begin{bmatrix} \alpha_1 + \alpha_2 + \cdots + \alpha_{p-1} \\ e^{-j\frac{2\pi}{p}}\alpha_1 + e^{-j\frac{4\pi}{p}}\alpha_2 + \cdots + e^{-j\frac{2\pi(p-1)}{p}}\alpha_{p-1} \\ \vdots \\ e^{-j\frac{2\pi(p-2)}{p}}\alpha_1 + e^{-j\frac{4\pi(p-2)}{p}}\alpha_2 + \cdots + e^{-j\frac{2\pi(p-1)(p-2)}{p}}\alpha_{p-1} \end{bmatrix} = \begin{bmatrix} \sum_{l=1}^{p-1}\alpha_l \\ \sum_{l=1}^{p-1}e^{-j\frac{2\pi l}{p}}\alpha_l \\ \vdots \\ \sum_{l=1}^{p-1}e^{-j\frac{2\pi l(p-2)}{p}}\alpha_l \end{bmatrix} \tag{4.106}$$

The unbalance equations describing the relationships between $\frac{V_{d_1}}{V_t}$, $\frac{V_{d_2}}{V_t}$, ..., $\frac{V_{d_{p-1}}}{V_t}$ are as follows:

$$\begin{bmatrix} \frac{V_{d_1}}{V_t} \\ \frac{V_{d_2}}{V_t} \\ \vdots \\ \frac{V_{d_{p-1}}}{V_t} \end{bmatrix} = -\frac{1}{p} \begin{bmatrix} 2Re\{\sum_{l=1}^{p-1} \lambda_l\} & 2Re\{\sum_{l=1}^{p-1} e^{j\frac{2\pi l}{p}} \lambda_l\} & \dots & 2Re\{\sum_{l=1}^{p-1} e^{j\frac{2\pi l(p-2)}{p}} \lambda_l\} \\ 2Re\{\sum_{l=1}^{p-1} e^{j\frac{-2\pi l}{p}} \lambda_l\} & 2Re\{\sum_{l=1}^{p-1} \lambda_l\} & \dots & 2Re\{\sum_{l=1}^{p-1} e^{j\frac{2\pi l(p-3)}{p}} \lambda_l\} \\ \vdots & \vdots & \ddots & \vdots \\ 2Re\{\sum_{l=1}^{p-1} e^{j\frac{-2\pi l(p-2)}{p}} \lambda_l\} & 2Re\{\sum_{l=1}^{p-1} e^{j\frac{2\pi l(p-3)}{p}} \lambda_l\} & \dots & 2Re\{\sum_{l=1}^{p-1} \lambda_l\} \end{bmatrix}^{-1} \begin{bmatrix} 2Re\{\sum_{l=1}^{p-1} \alpha_l\} \\ 2Re\{\sum_{l=1}^{p-1} e^{-j\frac{2\pi l}{p}} \alpha_l\} \\ \vdots \\ 2Re\{\sum_{l=1}^{p-1} e^{-j\frac{2\pi l(p-2)}{p}} \alpha_l\} \end{bmatrix} \tag{4.107}$$

In order to solve the unbalance equations for the p-cell case, it is necessary to determine the inverse of the matrix $2Re\{\mathbf{\Lambda}\}$, i.e. $(2Re\{\mathbf{\Lambda}\})^{-1}$. Due to the need to calculate $(2Re\{\mathbf{\Lambda}\})^{-1}$, it is necessary to first calculate the determinant of $2Re\{\mathbf{\Lambda}\}$ to determine if $(2Re\{\mathbf{\Lambda}\})^{-1}$ exists. The determinant of $2Re\{\mathbf{\Lambda}\}$ was calculated in Appendix B section B.5 and the result was shown as equation (B.136). This result is repeated here for convenience as follows:

$$\begin{aligned} \det(2Re\{\mathbf{\Lambda}\}) &= p^{p-2}(\lambda_1 + \overline{\lambda_{p-1}})(\lambda_2 + \overline{\lambda_{p-2}}) \dots (\lambda_{p-1} + \overline{\lambda_1}) \\ &= p^{p-2} \prod_{l=1}^{p-1} (\lambda_l + \overline{\lambda_{p-l}}) \end{aligned} \tag{4.108}$$

From equation (4.108), it follows that the determinant of $2Re\{\mathbf{\Lambda}\}$ is nonzero if the following conditions are true:

- $\lambda_1,\ \lambda_2, \dots,\ \lambda_{p-1} \neq 0$. It was shown in Chapter 3 sections 3.3.1.4 and 3.3.2.4 that $S_{d_1}(\omega)$, $S_{d_2}(\omega)$, ..., $S_{d_{p-1}}(\omega) \neq 0$ for $m = pk+1$, $m = pk+2$, ..., $m = pk+(p-1)$. From the properties of $S_{d_1}(\omega)$, $S_{d_2}(\omega)$, ..., $S_{d_{p-1}}(\omega)$ listed in Table 4.4 and the definitions of λ_1, λ_2, ..., λ_{p-1} shown in equations (4.89) through (4.90) it is clear that $\lambda_1,\ \lambda_2, \dots,\ \lambda_{p-1} \neq 0$.
- $\lambda_1 \neq \lambda_2 \neq \dots \neq \lambda_{p-1}$. It was shown in Chapter 3 sections 3.3.1.4 and 3.3.2.4 and listed in Table 4.4 that $S_{d_1}(\omega)$, $S_{d_2}(\omega)$, ..., $S_{d_{p-1}}(\omega)$ differ respectively by $e^{\mp\frac{2\pi}{p}}$ for $m = pk+1$, $m = pk+2$, ..., $m = pk+(p-1)$. Therefore, from the definitions of λ_1, λ_2, ..., λ_{p-1} it follows that $\lambda_1 \neq \lambda_2 \neq \dots \neq \lambda_{p-1}$.

As the above conditions are true, $\det(2Re\{\mathbf{\Lambda}\}) \neq 0$ and equation (4.103) has a unique solution. This shows that equation (4.107) has a unique solution.

To solve equation (4.107), is not trivial. The inverse of $2Re\{\mathbf{\Lambda}\}$ must be calculated to solve equation

(4.107). This cannot be calculated directly and a method was developed to approximate the inverse of $2Re\{\mathbf{\Lambda}\}$ indirectly. These calculations are shown in Appendix B section B.5. Using this indirect method does not deliver the exact matrix $(2Re\{\mathbf{\Lambda}\})^{-1}$, but rather an approximation of the elements of this matrix. This approximation is done by calculating the norm of $(2Re\{\mathbf{\Lambda}\})^{-1}$, i.e. $\|(2Re\{\mathbf{\Lambda}\})^{-1}\|$. The matrix norm is defined in Appendix B section B.2 Theorem B.5.

From equation (B.148), the operator norm of $(2Re\{\mathbf{\Lambda}\})^{-1}$ is repeated for convenience:

$$\begin{aligned}\left\|(2Re\{\mathbf{\Lambda}\})^{-1}\right\| &\leq \left\| \begin{array}{cccc} \frac{1}{\lambda_1+\overline{\lambda_{p-1}}} & 0 & \cdots & 0 \\ 0 & \frac{1}{\lambda_2+\overline{\lambda_{p-2}}} & \cdots & 0 \\ \vdots & \ddots & \ddots & \vdots \\ 0 & 0 & \cdots & \frac{1}{\lambda_{p-1}+\overline{\lambda_1}} \end{array} \right\| \\ &= \max\left\{ \frac{1}{\left|\lambda_1+\overline{\lambda_{p-1}}\right|}, \frac{1}{\left|\lambda_2+\overline{\lambda_{p-2}}\right|}, \ldots, \frac{1}{\left|\lambda_{p-1}+\overline{\lambda_1}\right|} \right\} \end{aligned} \tag{4.109}$$

Equation (4.109) means that the norm of the inverse of $2Re\{\mathbf{\Lambda}\}$ is less than or equal to the inverse of the absolute value of the smallest eigenvalue of $2Re\{\mathbf{\Lambda}\}$.

In the 2- and 3-cell cases it was shown that the denominators of the unbalance equations consist of the determinant of $2Re\{\mathbf{\Lambda}\}$. It was also shown that the numerator consists of product terms that each contain an α term. Since it has already been shown that the determinant of $2Re\{\mathbf{\Lambda}\}$ is nonzero, the numerator needs to be examined to determine if natural balance exists for the p-cell case.

Examining the switching function properties listed in Table 4.4, it can be seen that all the α_i where $i = 1, \ldots, p-1$ in equation (4.107) evaluate to zero as follows:

$$\begin{aligned}\alpha_1 &= \int_0^\infty \frac{S_t(\xi)\overline{S_{d_1}(\xi)}}{Z(\xi)}d\xi \\ &= \int_{m=pk} \frac{S_t(\xi)\overline{S_{d_1}(\xi)}}{Z(\xi)}d\xi + \int_{m=pk+1} \frac{S_t(\xi)\overline{S_{d_1}(\xi)}}{Z(\xi)}d\xi + \ldots + \int_{m=pk+(p-1)} \frac{S_t(\xi)\overline{S_{d_1}(\xi)}}{Z(\xi)}d\xi \\ &= \int_{m=pk} \frac{S_t(\xi)\cdot 0}{Z(\xi)}d\xi + \int_{m=pk+1} \frac{0\cdot\overline{S_{d_1}(\xi)}}{Z(\xi)}d\xi + \ldots + \int_{m=pk+(p-1)} \frac{0\cdot\overline{S_{d_1}(\xi)}}{Z(\xi)}d\xi \\ &= 0 \end{aligned} \tag{4.110}$$

In the same way it can be shown that $\alpha_2 = 0$ for all $k = 0, 1, \ldots, \infty$ as follows:

$$\begin{aligned}
\alpha_2 &= \int_0^{\infty} \frac{S_t(\xi)\overline{S_{d_2}(\xi)}}{Z(\xi)} d\xi \\
&= \int_{m=pk} \frac{S_t(\xi)\overline{S_{d_2}(\xi)}}{Z(\xi)} d\xi + \int_{m=pk+1} \frac{S_t(\xi)\overline{S_{d_2}(\xi)}}{Z(\xi)} d\xi + \ldots + \int_{m=pk+(p-1)} \frac{S_t(\xi)\overline{S_{d_2}(\xi)}}{Z(\xi)} d\xi \\
&= \int_{m=pk} \frac{S_t(\xi)\cdot 0}{Z(\xi)} d\xi + \int_{m=pk+1} \frac{0\cdot\overline{S_{d_2}(\xi)}}{Z(\xi)} d\xi + \ldots + \int_{m=pk+(p-1)} \frac{0\cdot\overline{S_{d_2}(\xi)}}{Z(\xi)} d\xi \\
&= 0
\end{aligned} \tag{4.111}$$

In general, these integrals can be written as follows:

$$\begin{aligned}
\alpha_i &= \int_0^{\infty} \frac{S_t(\xi)\overline{S_{d_i}(\xi)}}{Z(\xi)} d\xi \\
&= \sum_{l=0}^{p-1} \int_{m=pk+l} \frac{S_t(\xi)\overline{S_{d_i}(\xi)}}{Z(\xi)} d\xi \\
&= 0 \quad \text{for all } k = 0, 1, \ldots, \infty
\end{aligned} \tag{4.112}$$

The above results can be used to simplify equation (4.107) further. Knowing the determinant of $2Re\{\mathbf{\Lambda}\}$ and that all $\alpha_i = 0$, the solutions to the system of balance equations are as follows:

$$\frac{1}{V_t} \|\mathbf{V_d}\| \leq -\frac{1}{p} \left\| (2Re\{\mathbf{\Lambda}\})^{-1} \right\| \|2Re\{\mathbf{A}\}\| \tag{4.113}$$

Knowing that $\|2Re\{\mathbf{A}\}\| = 0$ it follows from equation (4.113) that $\|\mathbf{V_d}\| = 0$. Therefore, it follows that:

$$\frac{V_{d_1}}{V_t} = 0 \ , \ \frac{V_{d_2}}{V_t} = 0 \ , \ \ldots \ , \ \frac{V_{d_{p-1}}}{V_t} = 0 \tag{4.114}$$

From the definitions of $V_{d_1}, \ldots, V_{d_{p-1}}$, it follows that as V_{d_i} tend to zero, the unbalance tends to zero. Therefore, from the equations listed in (4.114) it follows that the respective voltages across cell capacitors $C_1, \ldots, C_{p-1}$ balance in steady-state. These voltages across cell capacitors $C_1, \ldots, C_{p-1}$ balance in steady-state when the harmonics of $S_t(\omega)$ and $S_{d_1}(\omega)$ do not overlap. Again, as stated in the previous sections, this is only valid as long as the load impedance $Z(\omega)$ is not purely inductive. When the load impedance is purely inductive or purely imaginary, i.e. $Re\{Z(\omega)\} = 0$, which means that $\frac{V_{d_1}}{V_t}$, $\frac{V_{d_2}}{V_t}, \ldots, \frac{V_{d_{p-1}}}{V_t}$ will each tend towards infinity, causing unbalanced cell capacitor voltages. The same cases that caused unbalance for the 2- and 3-cell cases are also valid for this case.

It was shown in the previous sections that the connection of a balance booster circuit in parallel with the load can improve the balancing of the cell capacitor voltages when the balance booster is designed to have a low impedance at the switching frequency of the converter. It will now be shown that a balance booster tuned to resonate at the switching frequency also improves the balancing of the

cell capacitor voltages for the p-cell case.

The balancing equations for the p-cell converter case were written in matrix form in equation (4.107). As the inverse of the matrix $2Re\{\mathbf{\Lambda}\}$ contains the determinant thereof in the denominator it can be seen that λ_1 affects the denominator when its value changes. The determinant was shown in equation (4.108) and is repeated here for convenience as follows:

$$\begin{aligned}\det(2Re\{\mathbf{\Lambda}\}) &= p^{p-2}(\lambda_1 + \overline{\lambda_{p-1}})(\lambda_2 + \overline{\lambda_{p-2}})\dots(\lambda_{p-1} + \overline{\lambda_1}) \\ &= p^{p-2}\prod_{l=1}^{p-1}(\lambda_l + \overline{\lambda_{p-l}}) \end{aligned} \tag{4.115}$$

As equation (4.115) includes products of pairs of the form $\lambda_i + \overline{\lambda_{p-i}}$ where $i = 1, \dots, p-1$ it is clear that there will always be 2 terms containing a λ_1-term: one with λ_1 and the other $\overline{\lambda_1}$. From the definition of λ_1 in equation (4.89), repeated here as equation (4.116), the groups of harmonics over which λ_1 is defined always include the switching frequency. Thus, if $Z(\omega)$ is decreased at the switching frequency by using a balance booster, then λ_1 will increase which will have a decreasing effect on $\det(2Re\{\mathbf{\Lambda}\})$ resulting in $\frac{V_{d_1}}{V_t}, \frac{V_{d_2}}{V_t}, \dots, \frac{V_{d_{p-1}}}{V_t}$ decreasing as λ_1 increases.

$$\lambda_1 = \int_{m=pk+1} \frac{|S_{d_1}(\xi)|^2}{Z(\xi)} d\xi \tag{4.116}$$

Furthermore, the same arguments can be used to design balance boosters that affect $\lambda_2, \dots, \lambda_{p-1}$, by designing them to resonate at $2f_s, \dots, (p-1)f_s$. In this way, $\lambda_2, \dots, \lambda_{p-1}$ will be increased, which will decrease $\frac{V_{d_1}}{V_t}, \frac{V_{d_2}}{V_t}, \dots, \frac{V_{d_{p-1}}}{V_t}$ even more drastically. The use of multiple balance boosters resonating at multiples of the switching frequency was shown in [60].

4.6 Special case

In Chapter 3 section 3.3.2, the Fourier coefficients of the switching functions $s_i(t)$ where $i = 1, \dots, p-1$ for the fixed duty-cycle case were determined. The expressions for these coefficients are repeated for convenience as follows:

$$A_0 = 2D - 1 \tag{4.117}$$

$$A_m = \frac{4}{m\pi}\sin(m\pi D) \tag{4.118}$$

where D is the duty-cycle and m the index of the Fourier series.

In order to find out what the effect of the duty-cycle is on the harmonics of the switching functions, it

is important to note the following:

$$\frac{\sin(m\pi D)}{m\pi} = 0 \tag{4.119}$$

if and only if $m\pi D = v\pi$, where $v \in \mathbb{Z}$ and $v = 0, \pm 1, \pm 2, \ldots, \pm\infty$ which is only true if $mD \in \mathbb{Z}$. This means that the duty-cycle D can be written as the following fraction:

$$D = \frac{v}{m} \tag{4.120}$$

Equation (4.120) implies that when v is a factor of m, the coefficients will be zero resulting in zero magnitude harmonics.

The next part of this discussion focusses on values of the duty-cycle D that can result in unbalance. For unbalance to occur, it is necessary for $\det(2Re\{\mathbf{\Lambda}\})$ to be zero. This can only happen if one or all of the λ-sums on the diagonal of the matrix $\mathbf{L}$ are zero. The matrix $\mathbf{L}$ is introduced in Appendix B sections B.3 through B.5. The next sections will each discuss a specific number of cells and the corresponding values of D that can cause unbalance for that case.

4.6.1 The 2-cell case

This section focusses on the trivial case for 2 cells. For this case there is only one λ-term, which is defined for the group of harmonics $m = 2k + 1$, where $k = 0, 1, 2, \ldots, \infty$. The $\mathbf{L}$-matrix reduces to a single element for the 2-cell case. The only term in $\mathbf{L}$ is $\lambda_1 + \overline{\lambda_1}$, which is zero if and only if $\lambda_1 = 0$. This implies the following:

$$\lambda_1 = 0 \Leftrightarrow (2k+1)D \in \mathbb{Z} \text{ for all } k \tag{4.121}$$

The values of D that satisfy equation (4.121) can be determined by evaluating this expression for values of k as follows:

(a) $k = 0$:

$$D \in \mathbb{Z} \Leftrightarrow D \in \{0, 1\} \tag{4.122}$$

This means that $\lambda_1 = 0$ if and only if:

$$D \in \{0, 1\} \tag{4.123}$$

(b) $k = 1$:

$$3D \in \mathbb{Z} \Leftrightarrow D \in \left\{0, \frac{1}{3}, \frac{2}{3}, 1\right\} \tag{4.124}$$

This means that $\lambda_1 = 0$ if and only if:

$$D \in \left\{0, \frac{1}{3}, \frac{2}{3}, 1\right\} \tag{4.125}$$

(c) $k = 2$:

$$5D \in \mathbb{Z} \Leftrightarrow D \in \left\{0, \frac{1}{5}, \frac{2}{5}, \frac{3}{5}, \frac{4}{5}, 1\right\} \tag{4.126}$$

This means that $\lambda_1 = 0$ if and only if:

$$D \in \left\{0, \frac{1}{5}, \frac{2}{5}, \frac{3}{5}, \frac{4}{5}, 1\right\} \tag{4.127}$$

(d) $k = u$:

$$(2u+1)D \in \mathbb{Z} \Leftrightarrow D \in \left\{0, \frac{1}{2u+1}, \frac{2}{2u+1}, \ldots, \frac{2u}{2u+1}, 1\right\} \tag{4.128}$$

This means that $\lambda_1 = 0$ if and only if:

$$D \in \left\{0, \frac{1}{2u+1}, \frac{2}{2u+1}, \ldots, \frac{2u}{2u+1}, 1\right\} \tag{4.129}$$

At this stage it is clear that the intersection of the values of D between equations (4.122)-(4.128) is $D \in \{0, 1\}$. This means that unbalance can only occur in a 2-cell multicell converter for the trivial case of a cell being either in the "off"-state or the "on"-state all the time. This is not practical as a converter is not designed to remain in either of these states all the time.

4.6.2 The 3-cell case

This section focusses on the case for 3 cells. For this case there are two λ-terms, which are defined for the groups of harmonics $m = 3k + 1$ and $m = 3k + 2$, where $k = 0, 1, 2, \ldots, \infty$. The matrix $\mathbf{L}$ for the 3-cell case is repeated from Appendix B section B.3 equation (B.24) and is as follows:

$$\mathbf{L} = \begin{bmatrix} \lambda_1 + \overline{\lambda_2} & 0 \\ 0 & \lambda_2 + \overline{\lambda_1} \end{bmatrix} \tag{4.130}$$

The only terms in $\mathbf{L}$ are $\lambda_1 + \overline{\lambda_2}$, which are zero if and only if $\lambda_1 + \overline{\lambda_2} = 0$, which is only true if $\lambda_1 = \lambda_2 = 0$. This implies the following:

$$\lambda_1 = 0 \Leftrightarrow (3k+1)D \in \mathbb{Z} \text{ for all } k \text{ and} \tag{4.131}$$

$$\lambda_2 = 0 \Leftrightarrow (3k+2)D \in \mathbb{Z} \text{ for all } k \tag{4.132}$$

The values of D that satisfy equations (4.131) and (4.132) can be determined by evaluating these

expressions for values of k as follows:

(a) $k = 0$:

$$D \in \mathbb{Z} \Leftrightarrow D \in \{0, 1\} \tag{4.133}$$

$$2D \in \mathbb{Z} \Leftrightarrow D \in \left\{0, \frac{1}{2}, 1\right\} \tag{4.134}$$

This means that $\lambda_1 = \lambda_2 = 0$ if and only if:

$$D \in \{0, 1\} \tag{4.135}$$

(b) $k = 1$:

$$4D \in \mathbb{Z} \Leftrightarrow D \in \left\{0, \frac{1}{4}, \frac{1}{2}, \frac{3}{4}, 1\right\} \tag{4.136}$$

$$5D \in \mathbb{Z} \Leftrightarrow D \in \left\{0, \frac{1}{5}, \frac{2}{5}, \frac{3}{5}, \frac{4}{5}, 1\right\} \tag{4.137}$$

This means that $\lambda_1 = \lambda_2 = 0$ if and only if:

$$D \in \{0, 1\} \tag{4.138}$$

(c) $k = 2$:

$$7D \in \mathbb{Z} \Leftrightarrow D \in \left\{0, \frac{1}{7}, \frac{2}{7}, \frac{3}{7}, \frac{4}{7}, \frac{5}{7}, \frac{6}{7}, 1\right\} \tag{4.139}$$

$$8D \in \mathbb{Z} \Leftrightarrow D \in \left\{0, \frac{1}{8}, \frac{1}{4}, \frac{3}{8}, \frac{1}{2}, \frac{5}{8}, \frac{3}{4}, \frac{7}{8}, 1\right\} \tag{4.140}$$

This means that $\lambda_1 = \lambda_2 = 0$ if and only if:

$$D \in \{0, 1\} \tag{4.141}$$

(d) $k = u$:

$$(3u + 1)D \in \mathbb{Z} \Leftrightarrow D \in \left\{0, \frac{1}{3u+1}, \frac{2}{3u+1}, \ldots, \frac{3u}{3u+1}, 1\right\} \tag{4.142}$$

$$(3u + 2)D \in \mathbb{Z} \Leftrightarrow D \in \left\{0, \frac{1}{3u+2}, \frac{2}{3u+2}, \ldots, \frac{3u+1}{3u+2}, 1\right\} \tag{4.143}$$

This means that $\lambda_1 = \lambda_2 = 0$ if and only if:

$$D \in \{0, 1\} \tag{4.144}$$

except if there exists a β_1 and β_2 so that $\frac{\beta_1}{3u+1} = \frac{\beta_2}{3u+2}$, which will result in these fractions being included in the set of D.

At this stage it is clear from equations (4.133)-(4.143) that the intersection of all the possible values of D that can cause $\lambda_1 = \lambda_2 = 0$ is $D \in \{0, 1\}$. Thus, unbalance can only occur in a 3-cell multicell converter if the duty-cycle $D \in \{0, 1\}$.

4.6.3 The 4-cell case

This section focusses on the case for 4 cells. For this case there are 3 λ-terms, which are defined for the groups of harmonics $m = 4k + 1$, $m = 4k + 2$ and $m = 4k + 3$, where $k = 0, 1, 2, \ldots, \infty$. The matrix $\mathbf{L}$ for the 4-cell case is repeated from Appendix B section B.4 equation (B.73) and is as follows:

$$\mathbf{L} = \begin{bmatrix} \lambda_1 + \overline{\lambda_3} & 0 & 0 \\ 0 & \lambda_2 + \overline{\lambda_2} & 0 \\ 0 & 0 & \lambda_3 + \overline{\lambda_1} \end{bmatrix} \tag{4.145}$$

The only terms in $\mathbf{L}$ are $\lambda_1 + \overline{\lambda_3}$ and $\lambda_2 + \overline{\lambda_2}$, which are zero if and only if $\lambda_1 + \overline{\lambda_3} = 0$ or if $\lambda_2 + \overline{\lambda_2} = 0$, which is only true if $\lambda_1 = \lambda_3 = 0$ or when $\lambda_2 = 0$. This implies the following:

$$\lambda_1 = 0 \Leftrightarrow (4k + 1)D \in \mathbb{Z} \text{ for all } k \tag{4.146}$$

$$\lambda_2 = 0 \Leftrightarrow (4k + 2)D \in \mathbb{Z} \text{ for all } k \tag{4.147}$$

$$\lambda_3 = 0 \Leftrightarrow (4k + 3)D \in \mathbb{Z} \text{ for all } k \tag{4.148}$$

The values of D that satisfy equations (4.146) to (4.148) can be determined by evaluating these expressions for values of k as follows:

(a) $k = 0$:

- $\lambda_1 = \lambda_3 = 0$ when:

$$D \in \mathbb{Z} \Leftrightarrow D \in \{0, 1\} \tag{4.149}$$

$$3D \in \mathbb{Z} \Leftrightarrow D \in \left\{0, \frac{1}{3}, \frac{2}{3}, 1\right\} \tag{4.150}$$

The intersection of the 2 sets in (4.149) and (4.150) results in $\lambda_1 = \lambda_3 = 0$ if and only if:

$$D \in \{0, 1\}. \tag{4.151}$$

- $\lambda_2 = 0$ when:

$$2D \in \mathbb{Z} \Leftrightarrow D \in \left\{0, \frac{1}{2}, 1\right\} \tag{4.152}$$

From equation (4.152) it is clear that $\lambda_2 = 0$ if and only if:

$$D \in \left\{0, \frac{1}{2}, 1\right\}. \tag{4.153}$$

(b) $k = 1$:

- $\lambda_1 = \lambda_3 = 0$ when:

$$5D \in \mathbb{Z} \Leftrightarrow D \in \left\{0, \frac{1}{5}, \frac{2}{5}, \frac{3}{5}, \frac{4}{5}, 1\right\} \tag{4.154}$$

$$7D \in \mathbb{Z} \Leftrightarrow D \in \left\{0, \frac{1}{7}, \frac{2}{7}, \frac{3}{7}, \frac{4}{7}, \frac{5}{7}, \frac{6}{7}, 1\right\} \tag{4.155}$$

The intersection of the 2 sets in (4.154) and (4.155) results in $\lambda_1 = \lambda_3 = 0$ if and only if:

$$D \in \{0, 1\}. \tag{4.156}$$

- $\lambda_2 = 0$ when:

$$6D \in \mathbb{Z} \Leftrightarrow D \in \left\{0, \frac{1}{6}, \frac{1}{3}, \frac{1}{2}, \frac{2}{3}, \frac{5}{6}, 1\right\} \tag{4.157}$$

From equation (4.157) it is clear that $\lambda_2 = 0$ if and only if:

$$D \in \left\{0, \frac{1}{6}, \frac{1}{3}, \frac{1}{2}, \frac{2}{3}, \frac{5}{6}, 1\right\}. \tag{4.158}$$

(c) $k = 2$:

- $\lambda_1 = \lambda_3 = 0$ when:

$$9D \in \mathbb{Z} \Leftrightarrow D \in \left\{0, \frac{1}{9}, \frac{2}{9}, \frac{1}{3}, \frac{4}{9}, \frac{5}{9}, \frac{2}{3}, \frac{7}{9}, \frac{8}{9}, 1\right\} \tag{4.159}$$

$$11D \in \mathbb{Z} \Leftrightarrow D \in \left\{0, \frac{1}{11}, \frac{2}{11}, \frac{3}{11}, \frac{4}{11}, \frac{5}{11}, \frac{6}{11}, \frac{7}{11}, \frac{8}{11}, \frac{9}{11}, \frac{10}{11}, 1\right\} \tag{4.160}$$

The intersection of the 2 sets in (4.159) and (4.160) results in $\lambda_1 = \lambda_3 = 0$ if and only if:

$$D \in \{0, 1\}. \tag{4.161}$$

- $\lambda_2 = 0$ when:

$$10D \in \mathbb{Z} \Leftrightarrow D \in \left\{0, \frac{1}{10}, \frac{1}{5}, \frac{3}{10}, \frac{2}{5}, \frac{1}{2}, \frac{3}{5}, \frac{7}{10}, \frac{4}{5}, \frac{9}{10}, 1\right\} \tag{4.162}$$

From equation (4.162) it is clear that $\lambda_2 = 0$ if and only if:

$$D \in \left\{0, \frac{1}{10}, \frac{1}{5}, \frac{3}{10}, \frac{2}{5}, \frac{1}{2}, \frac{3}{5}, \frac{7}{10}, \frac{4}{5}, \frac{9}{10}, 1\right\}. \tag{4.163}$$

(d) $k = u$:

- $\lambda_1 = \lambda_3 = 0$ when:

$$(4u+1)D \in \mathbb{Z} \Leftrightarrow D \in \left\{0, \frac{1}{4u+1}, \frac{2}{4u+1}, \ldots, \frac{4u}{4u+1}, 1\right\} \tag{4.164}$$

$$(4u+3)D \in \mathbb{Z} \Leftrightarrow D \in \left\{0, \frac{1}{4u+3}, \frac{2}{4u+3}, \ldots, \frac{4u+2}{4u+3}, 1\right\} \tag{4.165}$$

The intersection of the 2 sets in (4.164) and (4.165) results in $\lambda_1 = \lambda_3 = 0$ if and only if:

$$D \in \{0, 1\}. \tag{4.166}$$

- $\lambda_2 = 0$ when:

$$(4u+2)D \in \mathbb{Z} \Leftrightarrow D \in \left\{0, \frac{1}{4u+2}, \frac{2}{4u+2}, \ldots, \frac{4u+1}{4u+2}, 1\right\} \tag{4.167}$$

From equation (4.167) it is clear that $\lambda_2 = 0$ if and only if:

$$D \in \left\{0, \frac{1}{4u+2}, \frac{2}{4u+2}, \ldots, \frac{4u+1}{4u+2}, 1\right\} \tag{4.168}$$

except if there exists a β_1 and β_2 so that $\frac{\beta_1}{4u+1} = \frac{\beta_2}{4u+2}$, which will result in these fractions being included in the set of D.

Taking the intersections of the values of D for each case for different values of k it is possible to see which values of D can cause unbalance. These conditions and the corresponding values of D that can result in unbalance are as follows:

(a) $\lambda_1 = \lambda_3 = 0$: This is only possible when $D \in \{0, 1\}$. This is the trivial case which is not practical.

(b) $\lambda_2 = 0$: This is only possible when $D \in \left\{0, \frac{1}{2}, 1\right\}$. This case does affect practical systems, as it means that $D = \frac{1}{2}$ can cause unbalance in a 4-cell multicell converter under fixed duty-cycle PWM.

4.6.4 The 5-cell case

This section focusses on the case for 5 cells. For this case there are 4 λ-terms, which are defined for the groups of harmonics $m = 5k + 1$, $m = 5k + 2$, $m = 5k + 3$ and $m = 5k + 4$, where $k = 0, 1, 2, \ldots, \infty$. The matrix $\mathbf{L}$ for the 5-cell case is constructed from Appendix B section B.5 equation (B.116) and is as follows:

$$\mathbf{L} = \begin{bmatrix} \lambda_1 + \overline{\lambda_4} & 0 & 0 & 0 \\ 0 & \lambda_2 + \overline{\lambda_3} & 0 & 0 \\ 0 & 0 & \lambda_3 + \overline{\lambda_2} & 0 \\ 0 & 0 & 0 & \lambda_4 + \overline{\lambda_1} \end{bmatrix} \tag{4.169}$$

The only terms in $\mathbf{L}$ are $\lambda_1 + \overline{\lambda_4}$ and $\lambda_2 + \overline{\lambda_3}$, which are zero if and only if $\lambda_1 + \overline{\lambda_4} = 0$ or if $\lambda_2 + \overline{\lambda_3} = 0$, which is only true if $\lambda_1 = \lambda_4 = 0$ or when $\lambda_2 = \lambda_3 = 0$. This implies the following:

$$\lambda_1 = 0 \Leftrightarrow (5k + 1)D \in \mathbb{Z} \text{ for all } k \tag{4.170}$$

$$\lambda_2 = 0 \Leftrightarrow (5k + 2)D \in \mathbb{Z} \text{ for all } k \tag{4.171}$$

$$\lambda_3 = 0 \Leftrightarrow (5k + 3)D \in \mathbb{Z} \text{ for all } k \tag{4.172}$$

$$\lambda_4 = 0 \Leftrightarrow (5k + 4)D \in \mathbb{Z} \text{ for all } k \tag{4.173}$$

The values of D that satisfy equations (4.170) to (4.173) can be determined by evaluating these expressions for values of k as follows:

(a) $k = 0$:

- $\lambda_1 = \lambda_4 = 0$ when:

$$D \in \mathbb{Z} \Leftrightarrow D \in \{0, 1\} \tag{4.174}$$

$$4D \in \mathbb{Z} \Leftrightarrow D \in \left\{0, \frac{1}{4}, \frac{1}{2}, \frac{3}{4}, 1\right\} \tag{4.175}$$

The intersection of the 2 sets in (4.174) and (4.175) results in $\lambda_1 = \lambda_4 = 0$ if and only if:

$$D \in \{0, 1\}. \tag{4.176}$$

- $\lambda_2 = \lambda_3 = 0$ when:

$$2D \in \mathbb{Z} \Leftrightarrow D \in \left\{0, \frac{1}{2}, 1\right\} \tag{4.177}$$

$$3D \in \mathbb{Z} \Leftrightarrow D \in \left\{0, \frac{1}{3}, \frac{2}{3}, 1\right\} \tag{4.178}$$

The intersection of the 2 sets in (4.177) and (4.178) results in $\lambda_2 = \lambda_3 = 0$ if and only if:

$$D \in \{0, 1\}. \tag{4.179}$$

(b) $k = 1$:

- $\lambda_1 = \lambda_4 = 0$ when:

$$6D \in \mathbb{Z} \Leftrightarrow D \in \left\{0, \frac{1}{6}, \frac{1}{3}, \frac{1}{2}, \frac{2}{3}, \frac{5}{6}, 1\right\} \tag{4.180}$$

$$9D \in \mathbb{Z} \Leftrightarrow D \in \left\{0, \frac{1}{9}, \frac{2}{9}, \frac{1}{3}, \frac{4}{9}, \frac{5}{9}, \frac{2}{3}, \frac{7}{9}, \frac{8}{9}, 1\right\} \tag{4.181}$$

The intersection of the 2 sets in (4.180) and (4.181) results in $\lambda_1 = \lambda_4 = 0$ if and only if:

$$D \in \left\{0, \frac{1}{3}, \frac{2}{3}, 1\right\}. \tag{4.182}$$

- $\lambda_2 = \lambda_3 = 0$ when:

$$7D \in \mathbb{Z} \Leftrightarrow D \in \left\{0, \frac{1}{7}, \frac{2}{7}, \frac{3}{7}, \frac{4}{7}, \frac{5}{7}, \frac{6}{7}, 1\right\} \tag{4.183}$$

$$8D \in \mathbb{Z} \Leftrightarrow D \in \left\{0, \frac{1}{8}, \frac{1}{4}, \frac{3}{8}, \frac{1}{2}, \frac{5}{8}, \frac{3}{4}, \frac{7}{8}, 1\right\} \tag{4.184}$$

The intersection of the 2 sets in (4.183) and (4.184) results in $\lambda_2 = \lambda_3 = 0$ if and only if:

$$D \in \{0, 1\}. \tag{4.185}$$

(c) $k = 2$:

- $\lambda_1 = \lambda_4 = 0$ when:

$$11D \in \mathbb{Z} \Leftrightarrow D \in \left\{0, \frac{1}{11}, \frac{2}{11}, \frac{3}{11}, \frac{4}{11}, \frac{5}{11}, \frac{6}{11}, \frac{7}{11}, \frac{8}{11}, \frac{9}{11}, \frac{10}{11}, 1\right\} \tag{4.186}$$

$$14D \in \mathbb{Z} \Leftrightarrow D \in \left\{0, \frac{1}{14}, \frac{1}{7}, \frac{3}{14}, \frac{2}{7}, \frac{5}{14}, \frac{3}{7}, \frac{7}{14}, \frac{4}{7}, \frac{9}{14}, \frac{5}{7}, \frac{11}{14}, \frac{6}{7}, \frac{13}{14}, 1\right\} \tag{4.187}$$

The intersection of the 2 sets in (4.186) and (4.187) results in $\lambda_1 = \lambda_4 = 0$ if and only if:

$$D \in \{0, 1\}. \tag{4.188}$$

- $\lambda_2 = \lambda_3 = 0$ when:

$$12D \in \mathbb{Z} \Leftrightarrow D \in \left\{0, \frac{1}{12}, \frac{1}{6}, \frac{3}{12}, \frac{1}{3}, \frac{5}{12}, \frac{1}{2}, \frac{7}{12}, \frac{2}{3}, \frac{3}{4}, \frac{5}{6}, 1\right\} \tag{4.189}$$

$$13D \in \mathbb{Z} \Leftrightarrow D \in \left\{0, \frac{1}{13}, \frac{2}{13}, \frac{3}{13}, \frac{4}{13}, \frac{5}{13}, \frac{6}{13}, \frac{7}{13}, \frac{8}{13}, \frac{9}{13}, \frac{10}{13}, \frac{11}{13}, \frac{12}{13}, 1\right\} \tag{4.190}$$

The intersection of the 2 sets in (4.189) and (4.190) results in $\lambda_2 = \lambda_3 = 0$ if and only if:

$$D \in \{0, 1\}. \tag{4.191}$$

(d) $k = u$:

- $\lambda_1 = \lambda_4 = 0$ when:

$$(5u+1)D \in \mathbb{Z} \Leftrightarrow D \in \left\{0, \frac{1}{5u+1}, \frac{2}{5u+1}, \ldots, \frac{5u}{5u+1}, 1\right\} \tag{4.192}$$

$$(5u+4)D \in \mathbb{Z} \Leftrightarrow D \in \left\{0, \frac{1}{5u+4}, \frac{2}{5u+4}, \ldots, \frac{5u+3}{5u+4}, 1\right\} \tag{4.193}$$

The intersection of the 2 sets in (4.192) and (4.193) results in $\lambda_1 = \lambda_4 = 0$ if and only if:

$$D \in \{0, 1\} \tag{4.194}$$

except if there exists a β_1 and β_2 so that $\frac{\beta_1}{5u+1} = \frac{\beta_2}{5u+4}$, which will result in these fractions being included in the set of D.

- $\lambda_2 = \lambda_3 = 0$ when:

$$(5u+2)D \in \mathbb{Z} \Leftrightarrow D \in \left\{0, \frac{1}{5u+2}, \frac{2}{5u+2}, \ldots, \frac{5u+1}{5u+2}, 1\right\} \tag{4.195}$$

$$(5u+3)D \in \mathbb{Z} \Leftrightarrow D \in \left\{0, \frac{1}{5u+3}, \frac{2}{5u+3}, \ldots, \frac{5u+2}{5u+3}, 1\right\} \tag{4.196}$$

The intersection of the 2 sets in (4.195) and (4.196) results in $\lambda_2 = \lambda_3 = 0$ if and only if:

$$D \in \{0, 1\} \tag{4.197}$$

except if there exists a β_1 and β_2 so that $\frac{\beta_1}{5u+2} = \frac{\beta_2}{5u+3}$, which will result in these fractions being included in the set of D.

Taking the intersections of the values of D for each case for different values of k it is possible to see which values of D can cause unbalance. These conditions and the corresponding values of D that can result in unbalance are as follows:

(a) $\lambda_1 = \lambda_4 = 0$: This is only possible when $D \in \{0, 1\}$. This is the trivial case which is not practical.

(b) $\lambda_2 = \lambda_3 = 0$: This is only possible when $D \in \{0, 1\}$. This is also the trivial case.

From these results it is possible to say that a 5-cell multicell converter under fixed duty-cycle PWM will balance for practical values of D. With practical values, it is implied that $0 < D < 1$.

4.6.5 The 6-cell case

This section focusses on the case for 6 cells. For this case there are 5 λ-terms, which are defined for the groups of harmonics $m = 6k + 1$, $m = 6k + 2$, $m = 6k + 3$, $6k + 4$ and $m = 6k + 5$, where $k = 0, 1, 2, \ldots, \infty$. The matrix $\mathbf{L}$ for the 6-cell case is constructed from Appendix B section B.5 equation (B.116) and is as follows:

$$\mathbf{L} = \begin{bmatrix} \lambda_1 + \overline{\lambda_5} & 0 & 0 & 0 & 0 \\ 0 & \lambda_2 + \overline{\lambda_4} & 0 & 0 & 0 \\ 0 & 0 & \lambda_3 + \overline{\lambda_3} & 0 & 0 \\ 0 & 0 & 0 & \lambda_4 + \overline{\lambda_2} & 0 \\ 0 & 0 & 0 & 0 & \lambda_5 + \overline{\lambda_1} \end{bmatrix} \tag{4.198}$$

The only terms in $\mathbf{L}$ are $\lambda_1 + \overline{\lambda_5}$, $\lambda_2 + \overline{\lambda_4}$ and $\lambda_3 + \overline{\lambda_3}$, which are zero if and only if $\lambda_1 + \overline{\lambda_5} = 0$ or if $\lambda_2 + \overline{\lambda_4} = 0$ or if $\lambda_3 + \overline{\lambda_3} = 0$, which is only true if $\lambda_1 = \lambda_5 = 0$ or when $\lambda_2 = \lambda_4 = 0$ or when $\lambda_3 = 0$. This implies the following:

$$\lambda_1 = 0 \Leftrightarrow (6k + 1)D \in \mathbb{Z} \text{ for all } k \tag{4.199}$$

$$\lambda_2 = 0 \Leftrightarrow (6k + 2)D \in \mathbb{Z} \text{ for all } k \tag{4.200}$$

$$\lambda_3 = 0 \Leftrightarrow (6k+3)D \in \mathbb{Z} \text{ for all } k \tag{4.201}$$

$$\lambda_4 = 0 \Leftrightarrow (6k+4)D \in \mathbb{Z} \text{ for all } k \tag{4.202}$$

$$\lambda_5 = 0 \Leftrightarrow (6k+5)D \in \mathbb{Z} \text{ for all } k \tag{4.203}$$

The values of D that satisfy equations (4.199) to (4.203) can be determined by evaluating these expressions for values of k as follows:

(a) $k = 0$:

- $\lambda_1 = \lambda_5 = 0$ when:

$$D \in \mathbb{Z} \Leftrightarrow D \in \{0, 1\} \tag{4.204}$$

$$5D \in \mathbb{Z} \Leftrightarrow D \in \left\{0, \frac{1}{5}, \frac{2}{5}, \frac{3}{5}, \frac{4}{5}, 1\right\} \tag{4.205}$$

The intersection of the 2 sets in (4.204) and (4.205) results in $\lambda_1 = \lambda_5 = 0$ if and only if:

$$D \in \{0, 1\}. \tag{4.206}$$

- $\lambda_2 = \lambda_4 = 0$ when:

$$2D \in \mathbb{Z} \Leftrightarrow D \in \left\{0, \frac{1}{2}, 1\right\} \tag{4.207}$$

$$4D \in \mathbb{Z} \Leftrightarrow D \in \left\{0, \frac{1}{4}, \frac{1}{2}, \frac{3}{4}, 1\right\} \tag{4.208}$$

The intersection of the 2 sets in (4.207) and (4.208) results in $\lambda_2 = \lambda_4 = 0$ if and only if:

$$D \in \left\{0, \frac{1}{2}, 1\right\}. \tag{4.209}$$

- $\lambda_3 = 0$ when:

$$3D \in \mathbb{Z} \Leftrightarrow D \in \left\{0, \frac{1}{3}, \frac{2}{3}, 1\right\} \tag{4.210}$$

From equation (4.210) it is clear that $\lambda_3 = 0$ if and only if:

$$D \in \left\{0, \frac{1}{3}, \frac{2}{3}, 1\right\}. \tag{4.211}$$

(b) $k = 1$:

- $\lambda_1 = \lambda_5 = 0$ when:

$$7D \in \mathbb{Z} \Leftrightarrow D \in \left\{0, \frac{1}{7}, \frac{2}{7}, \frac{3}{7}, \frac{4}{7}, \frac{5}{7}, \frac{6}{7}, 1\right\} \tag{4.212}$$

$$11D \in \mathbb{Z} \Leftrightarrow D \in \left\{0, \frac{1}{11}, \frac{2}{11}, \frac{3}{11}, \frac{4}{11}, \frac{5}{11}, \frac{6}{11}, \frac{7}{11}, \frac{8}{11}, \frac{9}{11}, \frac{10}{11}, 1\right\} \tag{4.213}$$

The intersection of the 2 sets in (4.212) and (4.213) results in $\lambda_1 = \lambda_5 = 0$ if and only if:

$$D \in \{0, 1\}. \tag{4.214}$$

- $\lambda_2 = \lambda_4 = 0$ when:

$$8D \in \mathbb{Z} \Leftrightarrow D \in \left\{0, \frac{1}{8}, \frac{1}{4}, \frac{3}{8}, \frac{1}{2}, \frac{5}{8}, \frac{3}{4}, \frac{7}{8}, 1\right\} \tag{4.215}$$

$$10D \in \mathbb{Z} \Leftrightarrow D \in \left\{0, \frac{1}{10}, \frac{1}{5}, \frac{3}{10}, \frac{2}{5}, \frac{1}{2}, \frac{3}{5}, \frac{7}{10}, \frac{4}{5}, \frac{9}{10}, 1\right\} \tag{4.216}$$

The intersection of the 2 sets in (4.215) and (4.216) results in $\lambda_2 = \lambda_4 = 0$ if and only if:

$$D \in \left\{0, \frac{1}{2}, 1\right\}. \tag{4.217}$$

- $\lambda_3 = 0$ when:

$$9D \in \mathbb{Z} \Leftrightarrow D \in \left\{0, \frac{1}{9}, \frac{2}{9}, \frac{1}{3}, \frac{4}{9}, \frac{5}{9}, \frac{2}{3}, \frac{7}{9}, \frac{8}{9}, 1\right\} \tag{4.218}$$

From equation (4.218) it is clear that $\lambda_3 = 0$ if and only if:

$$D \in \left\{0, \frac{1}{9}, \frac{2}{9}, \frac{1}{3}, \frac{4}{9}, \frac{5}{9}, \frac{2}{3}, \frac{7}{9}, \frac{8}{9}, 1\right\}. \tag{4.219}$$

(c) $k = 2$:

- $\lambda_1 = \lambda_5 = 0$ when:

$$13D \in \mathbb{Z} \Leftrightarrow D \in \left\{0, \frac{1}{13}, \frac{2}{13}, \frac{3}{13}, \frac{4}{13}, \frac{5}{13}, \frac{6}{13}, \frac{7}{13}, \frac{8}{13}, \frac{9}{13}, \frac{10}{13}, \frac{11}{13}, \frac{12}{13}, 1\right\} \tag{4.220}$$

$$17D \in \mathbb{Z} \Leftrightarrow D \in \left\{0, \frac{1}{17}, \frac{2}{17}, \frac{3}{17}, \frac{4}{17}, \frac{5}{17}, \frac{6}{17}, \frac{7}{17}, \frac{8}{17}, \frac{9}{17}, \frac{10}{17}, \frac{11}{17}, \frac{12}{17}, \frac{13}{17}, \frac{14}{17}, \frac{15}{17}, \frac{16}{17}, 1\right\} \tag{4.221}$$

The intersection of the 2 sets in (4.220) and (4.221) results in $\lambda_1 = \lambda_5 = 0$ if and only if:

$$D \in \{0, 1\}. \tag{4.222}$$

- $\lambda_2 = \lambda_4 = 0$ when:

$$14D \in \mathbb{Z} \Leftrightarrow D \in \left\{0, \frac{1}{14}, \frac{1}{7}, \frac{3}{14}, \frac{2}{7}, \frac{5}{14}, \frac{3}{7}, \frac{7}{14}, \frac{4}{7}, \frac{9}{14}, \frac{5}{7}, \frac{11}{14}, \frac{6}{7}, \frac{13}{14}, 1\right\} \tag{4.223}$$

$$16D \in \mathbb{Z} \Leftrightarrow D \in \left\{0, \frac{1}{16}, \frac{1}{8}, \frac{3}{16}, \frac{1}{4}, \frac{5}{16}, \frac{3}{8}, \frac{7}{16}, \frac{1}{2}, \frac{9}{16}, \frac{5}{8}, \frac{11}{16}, \frac{3}{4}, \frac{13}{16}, \frac{7}{8}, \frac{15}{16}, 1\right\} \tag{4.224}$$

The intersection of the 2 sets in (4.223) and (4.224) results in $\lambda_2 = \lambda_4 = 0$ if and only if:

$$D \in \left\{0, \frac{1}{2}, 1\right\}. \tag{4.225}$$

- $\lambda_3 = 0$ when:

$$15D \in \mathbb{Z} \Leftrightarrow D \in \left\{0, \frac{1}{15}, \frac{2}{15}, \frac{1}{5}, \frac{4}{15}, \frac{1}{3}, \frac{2}{5}, \frac{7}{15}, \frac{8}{15}, \frac{3}{5}, \frac{2}{3}, \frac{11}{15}, \frac{4}{5}, \frac{13}{15}, \frac{14}{15}, 1\right\} \tag{4.226}$$

From equation (4.226) it is clear that $\lambda_3 = 0$ if and only if:

$$D \in \left\{0, \frac{1}{15}, \frac{2}{15}, \frac{1}{5}, \frac{4}{15}, \frac{1}{3}, \frac{2}{5}, \frac{7}{15}, \frac{8}{15}, \frac{3}{5}, \frac{2}{3}, \frac{11}{15}, \frac{4}{5}, \frac{13}{15}, \frac{14}{15}, 1\right\}. \tag{4.227}$$

(d) $k = u$:

- $\lambda_1 = \lambda_5 = 0$ when:

$$(6u+1)D \in \mathbb{Z} \Leftrightarrow D \in \left\{0, \frac{1}{6u+1}, \frac{2}{6u+1}, \ldots, \frac{6u}{6u+1}, 1\right\} \tag{4.228}$$

$$(6u+5)D \in \mathbb{Z} \Leftrightarrow D \in \left\{0, \frac{1}{6u+5}, \frac{2}{6u+5}, \ldots, \frac{6u+4}{6u+5}, 1\right\} \tag{4.229}$$

The intersection of the 2 sets in (4.228) and (4.229) results in $\lambda_1 = \lambda_5 = 0$ if and only if:

$$D \in \{0, 1\} \tag{4.230}$$

except if there exists a β_1 and β_2 so that $\frac{\beta_1}{6u+1} = \frac{\beta_2}{6u+5}$, which will result in these fractions being included in the set of D.

- $\lambda_2 = \lambda_4 = 0$ when:

$$(6u+2)D \in \mathbb{Z} \Leftrightarrow D \in \left\{0, \frac{1}{6u+2}, \frac{2}{6u+2}, \ldots, \frac{6u+1}{6u+2}, 1\right\} \tag{4.231}$$

$$(6u+4)D \in \mathbb{Z} \Leftrightarrow D \in \left\{0, \frac{1}{6u+4}, \frac{2}{6u+4}, \ldots, \frac{6u+3}{6u+4}, 1\right\} \tag{4.232}$$

  The intersection of the 2 sets in (4.231) and (4.232) results in $\lambda_2 = \lambda_4 = 0$ if and only if:

$$D \in \left\{0, \frac{1}{2}, 1\right\} \tag{4.233}$$

  as there exists a c_1 and c_2 so that $\frac{c_1}{6u+2} = \frac{c_2}{6u+4} = \frac{1}{2}$. There may also exist a β_1 and β_2 so that $\frac{\beta_1}{6u+2} = \frac{\beta_2}{6u+4}$, which will result in these fractions being included in the set of D.

- $\lambda_3 = 0$ when:

$$(6u+3)D \in \mathbb{Z} \Leftrightarrow D \in \left\{0, \frac{1}{6u+3}, \frac{2}{6u+3}, \ldots, \frac{6u+2}{6u+3}, 1\right\} \tag{4.234}$$

  From equation (4.234) it is clear that $\lambda_3 = 0$ if and only if:

$$D \in \left\{0, \frac{1}{6u+3}, \frac{2}{6u+3}, \ldots, \frac{6u+2}{6u+3}, 1\right\}. \tag{4.235}$$

  From equation (4.235) it follows that there exists a c_1 and c_2 so that $\frac{c_1}{6u+3} = \frac{1}{3}$ and $\frac{c_2}{6u+3} = \frac{2}{3}$. This means that equation (4.235) now becomes:

$$D \in \left\{0, \frac{1}{3}, \frac{2}{3}, 1\right\}. \tag{4.236}$$

Taking the intersections of the values of D for each case for different values of k it is possible to see which values of D can cause unbalance. These conditions and the corresponding values of D that can result in unbalance are listed as follows:

(a) $\lambda_1 = \lambda_5 = 0$: This is only possible when $D \in \{0, 1\}$. This is the trivial case which is not practical.

(b) $\lambda_2 = \lambda_4 = 0$: This is only possible when $D \in \left\{0, \frac{1}{2}, 1\right\}$. This case affects practical systems, as it means that $D = \frac{1}{2}$ can cause unbalance in a 6-cell multicell converter under fixed duty-cycle PWM.

(c) $\lambda_3 = 0$: This is only possible when $D \in \left\{0, \frac{1}{3}, \frac{2}{3}, 1\right\}$. This case also affects practical systems, as it means that $D = \frac{1}{3}$ and $D = \frac{2}{3}$ can cause unbalance in a 6-cell multicell converter under fixed duty-cycle PWM.

From these results it can be seen that duty-cycles $D \in \{\frac{1}{3}, \frac{1}{2}, \frac{2}{3}\}$ cause unbalance in a 6-cell multicell converter under fixed duty-cycle PWM.

4.6.6 The 7-cell case

This section focusses on the case for 7 cells. For this case there are 6 λ-terms, which are defined for the groups of harmonics $m = 7k + 1$, $m = 7k + 2$, $m = 7k + 3$, $7k + 4$, $m = 7k + 5$ and $m = 7k + 6$, where $k = 0, 1, 2, \ldots, \infty$. The matrix $\mathbf{L}$ for the 7-cell case is constructed from Appendix B section B.5 equation (B.116) and is as follows:

$$\mathbf{L} = \begin{bmatrix} \lambda_1 + \overline{\lambda_6} & 0 & 0 & 0 & 0 & 0 \\ 0 & \lambda_2 + \overline{\lambda_5} & 0 & 0 & 0 & 0 \\ 0 & 0 & \lambda_3 + \overline{\lambda_4} & 0 & 0 & 0 \\ 0 & 0 & 0 & \lambda_4 + \overline{\lambda_3} & 0 & 0 \\ 0 & 0 & 0 & 0 & \lambda_5 + \overline{\lambda_2} & 0 \\ 0 & 0 & 0 & 0 & 0 & \lambda_6 + \overline{\lambda_1} \end{bmatrix} \tag{4.237}$$

The only terms in $\mathbf{L}$ are $\lambda_1 + \overline{\lambda_6}$, $\lambda_2 + \overline{\lambda_5}$ and $\lambda_3 + \overline{\lambda_4}$, which are zero if and only if $\lambda_1 + \overline{\lambda_6} = 0$ or if $\lambda_2 + \overline{\lambda_5} = 0$ or if $\lambda_3 + \overline{\lambda_4} = 0$, which is only true if $\lambda_1 = \lambda_6 = 0$ or when $\lambda_2 = \lambda_5 = 0$ or when $\lambda_3 = \lambda_4 = 0$. This implies the following:

$$\lambda_1 = 0 \Leftrightarrow (7k + 1)D \in \mathbb{Z} \text{ for all } k \tag{4.238}$$
$$\lambda_2 = 0 \Leftrightarrow (7k + 2)D \in \mathbb{Z} \text{ for all } k \tag{4.239}$$
$$\lambda_3 = 0 \Leftrightarrow (7k + 3)D \in \mathbb{Z} \text{ for all } k \tag{4.240}$$
$$\lambda_4 = 0 \Leftrightarrow (7k + 4)D \in \mathbb{Z} \text{ for all } k \tag{4.241}$$
$$\lambda_5 = 0 \Leftrightarrow (7k + 5)D \in \mathbb{Z} \text{ for all } k \tag{4.242}$$
$$\lambda_6 = 0 \Leftrightarrow (7k + 6)D \in \mathbb{Z} \text{ for all } k \tag{4.243}$$

The values of D that satisfy equations (4.238) to (4.243) can be determined by evaluating these expressions for values of k as follows:

(a) $k = 0$:

- $\lambda_1 = \lambda_6 = 0$ when:

$$D \in \mathbb{Z} \Leftrightarrow D \in \{0, 1\} \tag{4.244}$$
$$6D \in \mathbb{Z} \Leftrightarrow D \in \left\{0, \frac{1}{6}, \frac{1}{3}, \frac{1}{2}, \frac{2}{3}, \frac{5}{6}, 1\right\} \tag{4.245}$$

The intersection of the 2 sets in (4.244) and (4.245) results in $\lambda_1 = \lambda_6 = 0$ if and only if:

$$D \in \{0, 1\}. \tag{4.246}$$

- $\lambda_2 = \lambda_5 = 0$ when:

$$2D \in \mathbb{Z} \Leftrightarrow D \in \left\{0, \frac{1}{2}, 1\right\} \tag{4.247}$$

$$5D \in \mathbb{Z} \Leftrightarrow D \in \left\{0, \frac{1}{5}, \frac{2}{5}, \frac{3}{5}, \frac{4}{5}, 1\right\} \tag{4.248}$$

The intersection of the 2 sets in (4.247) and (4.248) results in $\lambda_2 = \lambda_5 = 0$ if and only if:

$$D \in \{0, 1\}. \tag{4.249}$$

- $\lambda_3 = \lambda_4 0$ when:

$$3D \in \mathbb{Z} \Leftrightarrow D \in \left\{0, \frac{1}{3}, \frac{2}{3}, 1\right\} \tag{4.250}$$

$$4D \in \mathbb{Z} \Leftrightarrow D \in \left\{0, \frac{1}{4}, \frac{1}{2}, \frac{3}{4}, 1\right\} \tag{4.251}$$

From equations (4.250) and (4.251) it is clear that $\lambda_3 = \lambda_4 = 0$ if and only if:

$$D \in \{0, 1\}. \tag{4.252}$$

(b) $k = 1$:

- $\lambda_1 = \lambda_6 = 0$ when:

$$8D \in \mathbb{Z} \Leftrightarrow D \in \left\{0, \frac{1}{8}, \frac{1}{4}, \frac{3}{8}, \frac{1}{2}, \frac{5}{8}, \frac{3}{4}, \frac{7}{8}, 1\right\} \tag{4.253}$$

$$13D \in \mathbb{Z} \Leftrightarrow D \in \left\{0, \frac{1}{13}, \frac{2}{13}, \frac{3}{13}, \frac{4}{13}, \frac{5}{13}, \frac{6}{13}, \frac{7}{13}, \frac{8}{13}, \frac{9}{13}, \frac{10}{13}, \frac{11}{13}, \frac{12}{13}, 1\right\} \tag{4.254}$$

The intersection of the 2 sets in (4.253) and (4.254) results in $\lambda_1 = \lambda_6 = 0$ if and only if:

$$D \in \{0, 1\}. \tag{4.255}$$

- $\lambda_2 = \lambda_5 = 0$ when:

$$9D \in \mathbb{Z} \Leftrightarrow D \in \left\{0, \frac{1}{9}, \frac{2}{9}, \frac{1}{3}, \frac{4}{9}, \frac{5}{9}, \frac{2}{3}, \frac{7}{9}, \frac{8}{9}, 1\right\} \tag{4.256}$$

$$12D \in \mathbb{Z} \Leftrightarrow D \in \left\{0, \frac{1}{12}, \frac{1}{6}, \frac{1}{4}, \frac{1}{3}, \frac{5}{12}, \frac{1}{2}, \frac{7}{12}, \frac{2}{3}, \frac{3}{4}, \frac{5}{6}, \frac{11}{12}, 1\right\} \tag{4.257}$$

The intersection of the 2 sets in (4.256) and (4.257) results in $\lambda_2 = \lambda_5 = 0$ if and only if:

$$D \in \left\{0, \frac{1}{3}, \frac{2}{3}, 1\right\}. \tag{4.258}$$

- $\lambda_3 = \lambda_4 = 0$ when:

$$10D \in \mathbb{Z} \Leftrightarrow D \in \left\{0, \frac{1}{9}, \frac{2}{9}, \frac{1}{3}, \frac{4}{9}, \frac{5}{9}, \frac{2}{3}, \frac{7}{9}, \frac{8}{9}, 1\right\} \tag{4.259}$$

$$11D \in \mathbb{Z} \Leftrightarrow D \in \left\{0, \frac{1}{11}, \frac{2}{11}, \frac{3}{11}, \frac{4}{11}, \frac{5}{11}, \frac{6}{11}, \frac{7}{11}, \frac{8}{11}, \frac{9}{11}, \frac{10}{11}, 1\right\} \tag{4.260}$$

From equations (4.259) and (4.260) it is clear that $\lambda_3 = \lambda_4 = 0$ if and only if:

$$D \in \{0, 1\}. \tag{4.261}$$

(c) $k = 2$:

- $\lambda_1 = \lambda_6 = 0$ when:

$$15D \in \mathbb{Z} \Leftrightarrow D \in \left\{0, \frac{1}{15}, \frac{2}{15}, \frac{1}{5}, \frac{4}{15}, \frac{1}{3}, \frac{2}{5}, \frac{7}{15}, \frac{8}{15}, \frac{3}{5}, \frac{2}{3}, \frac{11}{15}, \frac{4}{5}, \frac{13}{15}, \frac{14}{15}, 1\right\} \tag{4.262}$$

$$20D \in \mathbb{Z} \Leftrightarrow D \in \left\{0, \frac{1}{20}, \frac{1}{10}, \frac{3}{20}, \frac{1}{5}, \frac{1}{4}, \frac{3}{10}, \frac{7}{20}, \frac{2}{5}, \frac{9}{20}, \frac{1}{2}, \frac{11}{20}, \frac{3}{5}, \frac{13}{20}, \frac{7}{10}, \frac{3}{4}, \frac{4}{5}, \frac{17}{20}, \frac{9}{10}, \frac{19}{20}, 1\right\} \tag{4.263}$$

The intersection of the 2 sets in (4.262) and (4.263) results in $\lambda_1 = \lambda_6 = 0$ if and only if:

$$D \in \left\{0, \frac{1}{5}, \frac{2}{5}, \frac{3}{5}, \frac{4}{5}, 1\right\}. \tag{4.264}$$

- $\lambda_2 = \lambda_5 = 0$ when:

$$16D \in \mathbb{Z} \Leftrightarrow D \in \left\{0, \frac{1}{16}, \frac{1}{8}, \frac{3}{16}, \frac{1}{4}, \frac{5}{16}, \frac{3}{8}, \frac{7}{16}, \frac{1}{2}, \frac{9}{16}, \frac{5}{8}, \frac{11}{16}, \frac{3}{4}, \frac{13}{16}, \frac{7}{8}, \frac{15}{16}, 1\right\} \tag{4.265}$$

$$19D \in \mathbb{Z} \Leftrightarrow D \in \left\{0, \frac{1}{19}, \frac{2}{19}, \frac{3}{19}, \frac{4}{19}, \frac{5}{19}, \frac{6}{19}, \frac{7}{19}, \frac{8}{19}, \frac{9}{19}, \frac{10}{19}, \frac{11}{19}, \frac{12}{19}, \frac{13}{19}, \frac{14}{19}, \frac{15}{19}, \frac{16}{19}, \frac{17}{19}, \frac{18}{19}, 1\right\} \tag{4.266}$$

The intersection of the 2 sets in (4.265) and (4.266) results in $\lambda_2 = \lambda_5 = 0$ if and only if:

$$D \in \{0, 1\}. \tag{4.267}$$

- $\lambda_3 = \lambda_4 = 0$ when:

$$17D \in \mathbb{Z} \Leftrightarrow D \in \left\{0, \frac{1}{17}, \frac{2}{17}, \frac{3}{17}, \frac{4}{17}, \frac{5}{17}, \frac{6}{17}, \frac{7}{17}, \frac{8}{17}, \frac{9}{17}, \frac{10}{17}, \frac{11}{17}, \frac{12}{17}, \frac{13}{17}, \frac{14}{17}, \frac{15}{17}, \frac{16}{17}, 1\right\} \tag{4.268}$$

$$18D \in \mathbb{Z} \Leftrightarrow D \in \left\{0, \frac{1}{18}, \frac{1}{9}, \frac{1}{6}, \frac{2}{9}, \frac{5}{18}, \frac{1}{3}, \frac{7}{18}, \frac{4}{9}, \frac{1}{2}, \frac{5}{9}, \frac{11}{18}, \frac{2}{3}, \frac{13}{18}, \frac{7}{9}, \frac{5}{6}, \frac{8}{9}, \frac{17}{18}, 1\right\} \tag{4.269}$$

From equations (4.268) and (4.269) it is clear that $\lambda_3 = \lambda_4 = 0$ if and only if:

$$D \in \{0, 1\}. \tag{4.270}$$

(d) $k = u$:

- $\lambda_1 = \lambda_6 = 0$ when:

$$(7u+1)D \in \mathbb{Z} \Leftrightarrow D \in \left\{0, \frac{1}{7u+1}, \frac{2}{7u+1}, \ldots, \frac{7u}{7u+1}, 1\right\} \tag{4.271}$$

$$(7u+6)D \in \mathbb{Z} \Leftrightarrow D \in \left\{0, \frac{1}{7u+6}, \frac{2}{7u+6}, \ldots, \frac{7u+5}{7u+6}, 1\right\} \tag{4.272}$$

The intersection of the 2 sets in (4.271) and (4.272) results in $\lambda_1 = \lambda_6 = 0$ if and only if:

$$D \in \{0, 1\} \tag{4.273}$$

except if there exists a β_1 and β_2 so that $\frac{\beta_1}{7u+1} = \frac{\beta_2}{7u+6}$, which will result in these fractions being included in the set of D.

- $\lambda_2 = \lambda_5 = 0$ when:

$$(7u+2)D \in \mathbb{Z} \Leftrightarrow D \in \left\{0, \frac{1}{7u+2}, \frac{2}{7u+2}, \ldots, \frac{7u+1}{7u+2}, 1\right\} \tag{4.274}$$

$$(7u+5)D \in \mathbb{Z} \Leftrightarrow D \in \left\{0, \frac{1}{7u+5}, \frac{2}{7u+5}, \ldots, \frac{7u+4}{7u+5}, 1\right\} \tag{4.275}$$

The intersection of the 2 sets in (4.274) and (4.275) results in $\lambda_2 = \lambda_5 = 0$ if and only if:

$$D \in \{0, 1\} \tag{4.276}$$

except if there exists a β_1 and β_2 so that $\frac{\beta_1}{7u+2} = \frac{\beta_2}{7u+5}$, which will result in these fractions being included in the set of D.

- $\lambda_3 = \lambda_4 = 0$ when:

$$(7u+3)D \in \mathbb{Z} \Leftrightarrow D \in \left\{0, \frac{1}{7u+3}, \frac{2}{7u+3}, \ldots, \frac{7u+2}{7u+3}, 1\right\} \tag{4.277}$$

$$(7u+4)D \in \mathbb{Z} \Leftrightarrow D \in \left\{0, \frac{1}{7u+4}, \frac{2}{7u+4}, \ldots, \frac{7u+3}{7u+4}, 1\right\} \tag{4.278}$$

From equations (4.277) and (4.278) it is clear that $\lambda_3 = \lambda_4 = 0$ if and only if:

$$D \in \{0, 1\} \tag{4.279}$$

except if there exists a β_1 and β_2 so that $\frac{\beta_1}{7u+3} = \frac{\beta_2}{7u+4}$, which will result in these fractions being included in the set of D.

Taking the intersections of the values of D for each case for different values of k it is possible to see which values of D can cause unbalance. These conditions and the corresponding values of D that can result in unbalance are listed as follows:

(a) $\lambda_1 = \lambda_5 = 0$: This is only possible when $D \in \{0, 1\}$. This is the trivial case which is not practical.

(b) $\lambda_2 = \lambda_4 = 0$: This is only possible when $D \in \{0, 1\}$. This is also the trivial case.

(c) $\lambda_3 = \lambda_4 = 0$: This is only possible when $D \in \{0, 1\}$. This is also the trivial case.

From these results it is possible to say that a 7-cell multicell converter under fixed duty-cycle PWM will balance for all practical values of D. Again, with practical values it is implied that $0 < D < 1$.

4.6.7 Conclusion

It was previously thought that multicell converters balanced naturally only for a prime number of cells. This was not proven nor published. It was shown in this section that multicell converters under fixed duty-cycle PWM balance naturally for any practical number of cells, taken in this case to be $p = 2, \ldots, 7$, as long as the duty-cycle D does not assume specific values.

It was found that only the trivial values of D, i.e. 0 and 1 cause unbalance when the number of cells p is a prime number.

If the number of cells is not a prime number, there exists values of D other than the trivial values that also cause unbalance. These values of D are fractions, where the denominators are prime factors of p. A brief list of these values of D are as follows:

(a) 4-cells: $D \in \{\frac{1}{2}\}$ (prime factors: $4 = 2 \times 2$)

(b) 6-cells: $D \in \{\frac{1}{3}, \frac{1}{2}, \frac{2}{3}\}$ (prime factors: $6 = 2 \times 3$)

4.7 Summary

In this chapter it was shown that the cell capacitor voltages of a p-cell multicell converter balance naturally in steady-state under certain conditions. Natural balance is guaranteed for the following circumstances:

- When the switching frequency is sufficiently higher than the reference frequency such that there is no overlapping of the harmonics of $S_{d_1}(\omega)$ and $S_t(\omega)$.
- When the reference signal does not contain high frequency components which result in aliasing of the harmonics of $S_{d_1}(\omega)$ and $S_t(\omega)$.

These circumstances are only valid when the following condition is met:

- The load impedance $Z(\omega)$ is reactive, i.e. $Re\{Z(\omega)\} > 0$.

From the unbalance equations it can also be concluded that the steady-state balancing can be improved if $Z(\omega)$ is made smaller at the switching frequency and harmonic multiples thereof. This will be discussed further in Chapter 5.

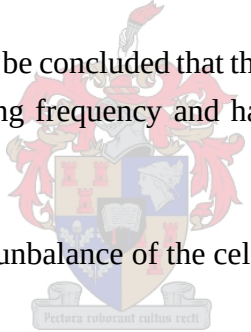

Two cases were found which can cause unbalance of the cell capacitor voltages. These two cases are as follows:

- when the switching frequency (ω_s) is higher than the frequency of the reference signal (ω_r), but not high enough to avoid aliasing of the side-bands of the harmonic multiples thereof. This is when the harmonics of $S_d(\omega)$ and $S_t(\omega)$ overlap resulting in $|S_d(\omega)||S_t(\omega)| > 0$.
- when the reference signal contains high frequency components, $|S_d(\omega)||S_t(\omega)| > 0$ is possible.

The norm, which was used to approximate the inverse of $2Re\{\mathbf{\Lambda}\}$ will be referred to again in Chapter 5 when the balancing time constants will be calculated and discussed.

It was also shown that specific values of the duty-cycle D can cause unbalance in a p-cell multicell converter under fixed duty-cycle PWM when p is not a prime number. In this case p is a practical number of cells which was chosen to be in the range $2 \leq p \leq 7$.

It was also shown that when the number of cells p is a practical prime number, the converter will balance naturally for any duty-cycle where $0 < D < 1$ when using fixed duty-cycle PWM.

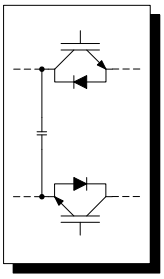

Chapter 5

Time constant analysis

5.1 Introduction

The concept of a time constant is best understood when considering a simple RC circuit. The current in a capacitor can be described by a first-order differential equation, e.g. $I = C\frac{dV}{dt}$. The solution to this differential equation is $V = V_0 e^{-t/RC}$ where V_0 is the initial voltage across the capacitor. The time constant for this case, is defined by the reciprocal of the exponent. In this case, the time constant is defined as follows:

$$\tau = RC \tag{5.1}$$

The physical significance of the time constant is that it represents the time that it will take for the capacitor to discharge to a voltage of $37\ \%$ of its initial value.

This chapter focusses on the determination and calculation of the time constants of p-cell multicell converters, starting with the 2-cell case and then working towards the p-cell case. For this specific case, it is important to quantify the time that it takes for the cell capacitor voltage unbalance to decay to zero. The definition of a voltage balance time constant is therefore the time that it will take for the unbalance to decay to $37\ \%$ of the initial unbalance. In previous chapters, the cell capacitor voltage unbalance was defined as V_{d_i} where i refers to the cell number.

Taking all of the above into consideration, it is expected that it will be possible to characterise the unbalance in the system with a system of differential equations of the following form:

$$\frac{dV_d}{dt} = EV_d \tag{5.2}$$

with a homogeneous solution of the form:

$$V_d = e^{-Et}V_{d_0} \tag{5.3}$$

If the unbalance can be characterised by equation (5.2) and the solution is equation (5.3), it means that for the 2-cell case, the time constant will be $1/E$. For the p-cell case, E will be a matrix and the time constants will be linear combinations of the eigenvalues of the matrix E. Thus, for the p-cell case it will be possible to give an estimation of the worst time constant in the system. The worst time constant in this case means the cell capacitor unbalance that takes the longest to decay to zero.

It is important to know the time constants of a multicell converter, because that determines the natural balancing characteristics of the converter. The user will then be able to decide if natural balancing is sufficient for his/her application. If the natural balancing is not fast enough, the user may want to use active balancing techniques. Active balancing is beyond the theme of this dissertation and further information can be found in [24].

This approach will start with the steady-state approach as used in Chapter 4 with the following assumptions:

- the cell capacitors are very large.
- the cell capacitor voltages change much slower than the rest of the system so that in comparison it appears as if the rest of the system is in steady-state.
- assume that V_t is zero in order to calculate the homogeneous solutions of the differential equations characterising the cell capacitor currents.

The idea behind this approach is to model the system mathematically so that it appears as if the source is changing slowly in comparison with the rest of the converter. If the rest of the converter appears as an impedance, the response of the circuit to the slow-changing source can be calculated. It is assumed that the response of the converter is fast compared to the source. This idea is illustrated in Figure 5-1.

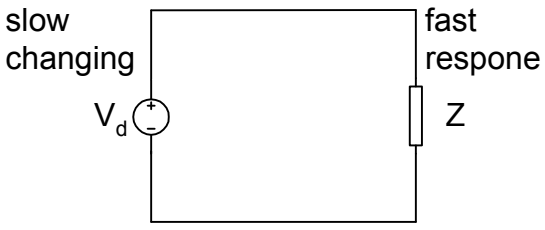

Figure 5-1. *Basic circuit with slow changing source.*

The analyses which follow in the subsequent sections are aided with Matlab® programs which are used to solve the time constant differential equations for specific cases. These cases are included as

Table 5.1. *Multicell converter parameters*

V_t	$50\ V$
C_i, $i = 1, \ldots, p-1$	$40\ \mu F$
L	$200\ \mu H$
C_f	$50\ \mu F$
R	$10\ \Omega$
L_{bb}	$237\ \mu H$
C_{bb}	$4.3\ \mu F$
R_{bb}	$2.2\ \Omega$

examples. The parameters of the converters used in these examples are listed in Table 5.1. These parameters are the same for the 2-, 3- and p-cell cases unless otherwise stated. The only difference is the number of cells used.

5.2 The 2-cell multicell converter

This section deals with calculating the balancing time constant of a 2-cell multicell converter. The equivalent circuit of the 2-cell multicell converter in terms of d and t parameters will be used for the steady-state analysis of the circuit in the frequency domain. This equivalent circuit was shown in Figure 4-2 and is repeated here as Figure 5-2 for convenience.

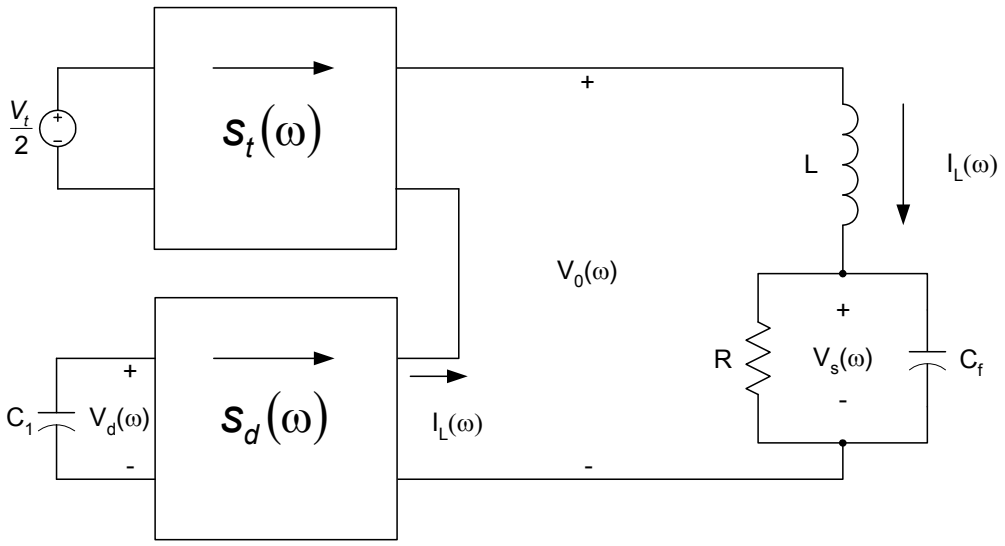

Figure 5-2. *Equivalent circuit in the frequency domain in terms of d and t parameters of a 2-cell multicell converter.*

In the frequency domain, the expression for the inductor current $I_L(\omega)$ can be written as follows:

$$\begin{aligned} I_L(\omega) &= \frac{V_0(\omega)}{Z(\omega)} \\ &= \frac{(\frac{V_t}{2} \cdot S_t)(\omega)}{Z(\omega)} + \frac{V_d(\omega) \cdot S_d(\omega)}{Z(\omega)} \end{aligned} \tag{5.4}$$

The expression for the cell capacitor current $I_{C_1}(\omega)$ was calculated in Chapter 4 and given as equation (4.6). The result is repeated here for convenience as follows:

$$I_{C_1}(\omega) = -\left[\frac{V_t}{2}\int_{-\infty}^{\infty}\frac{S_t(\xi)}{Z(\xi)}S_d(\omega-\xi)d\xi + V_d\int_{-\infty}^{\infty}\frac{S_d(\xi)}{Z(\xi)}S_d(\omega-\xi)d\xi\right] \tag{5.5}$$

In order to calculate the time constants, the converter is observed in a special steady-state. For this special steady-state it is assumed that the cell capacitor voltages change much slower than the rest of the system. This means that the low frequency harmonics are needed to calculate the time constant. These low frequency harmonics can be obtained through:

- Setting $V_t(\omega)|_{\omega=0} = 0$ to calculate the homogeneous solution of the differential equation characterising the cell capacitor current.
- Replacing the cell capacitors with pseudo-dc sources and eliminating all the high frequency components by setting $\omega = 0$ in order to calculate the dc value of $I_{C_1}(\omega)$.

This value of $I_{C_1}(\omega)|_{\omega=0}$ can be seen as a pseudo-dc value, as it contains neither the dc component nor the high frequency components, but only the lower frequency components in-between. Using the same technique as used in equation (4.7), equation (5.5) can be rewritten for this special steady-state as follows:

$$I_{C_1}(\omega)|_{\omega=0} = -\left[\frac{V_t}{2}\int_{-\infty}^{\infty}\frac{S_t(\xi)}{Z(\xi)}\overline{S_d(\xi)}d\xi + V_d\int_{-\infty}^{\infty}\frac{|S_d(\xi)|^2}{Z(\xi)}d\xi\right] \tag{5.6}$$

This special steady-state case is indicated with the use of the "hat"-symbol, e.g. $\widehat{x}$. Equation (5.6) can be simplified by substituting I_{C_1} with $\widehat{I_{C_1}}$, V_d with $\widehat{V}_d$ and V_t with 0, resulting in the following:

$$\begin{aligned} \widehat{I_{C_1}} &= -\left[0 + \widehat{V}_d\int_{-\infty}^{\infty}\frac{|S_d(\xi)|^2}{Z(\xi)}d\xi\right] \\ &= -\left[\widehat{V}_d\int_{-\infty}^{\infty}\frac{|S_d(\xi)|^2}{Z(\xi)}d\xi\right] \end{aligned} \tag{5.7}$$

Using the properties of integrals in the same way as used in Chapter 4 section 4.3, equation (5.7) can be simplified as follows:

$$\begin{aligned}
\widehat{I_{C_1}} &= -\widehat{V}_d \left[\int_{-\infty}^{0} \frac{|S_d(\xi)|^2}{Z(\xi)} d\xi + \int_{0}^{\infty} \frac{|S_d(\xi)|^2}{Z(\xi)} d\xi \right] \\
&= -\widehat{V}_d \left[\int_{0}^{\infty} \frac{|S_d(-\xi)|^2}{Z(-\xi)} d\xi + \int_{0}^{\infty} \frac{|S_d(\xi)|^2}{Z(\xi)} d\xi \right] \\
&= -\widehat{V}_d \left[\int_{0}^{\infty} \frac{\left|\overline{S_d(\xi)}\right|^2}{\overline{Z(\xi)}} d\xi + \int_{0}^{\infty} \frac{|S_d(\xi)|^2}{Z(\xi)} d\xi \right] \\
&= -\widehat{V}_d \left[\int_{0}^{\infty} \frac{|S_d(\xi)|^2}{\overline{Z(\xi)}} d\xi + \int_{0}^{\infty} \frac{|S_d(\xi)|^2}{Z(\xi)} d\xi \right] \\
&= -\widehat{V}_d \left[2Re \left\{ \int_{0}^{\infty} \frac{|S_d(\xi)|^2}{Z(\xi)} d\xi \right\} \right]
\end{aligned} \tag{5.8}$$

Following from equation (5.8), it can be seen that $\widehat{I_{C_1}}$ is real.

Applying the "Summation Rule of Integrals" and the properties of the harmonics of the switching functions as applied in Chapter 4 section 4.3, equation (5.8) can be simplified further in terms of groups of harmonics as follows:

$$\widehat{I_{C_1}} = -\widehat{V}_d \left[2Re \left\{ \int_{m=2k} \frac{|S_d(\xi)|^2}{Z(\xi)} d\xi + \int_{m=2k+1} \frac{|S_d(\xi)|^2}{Z(\xi)} d\xi \right\} \right] \tag{5.9}$$

Equation (5.9) can be rewritten in terms of λ terms as defined in Chapter 4 in equations (4.19)-(4.20) as follows:

$$\widehat{I_{C_1}} = -\widehat{V}_d \left[2Re \left\{ \lambda_0 + \lambda_1 \right\} \right] \tag{5.10}$$

where:

$$\lambda_0 = \int_{m=2k} \frac{|S_d(\xi)|^2}{Z(\xi)} d\xi \tag{5.11}$$

$$\lambda_1 = \int_{m=2k+1} \frac{|S_d(\xi)|^2}{Z(\xi)} d\xi \tag{5.12}$$

The same switching function properties as listed in Table 4.1 are valid for this case as for the case in Chapter 4 section 4.3 and therefore it is known that $\lambda_0 = 0$, which leads to the further simplification

of equation (5.10) as follows:

$$\widehat{I_{C_1}} = -\widehat{V_d}\left[2Re\left\{\lambda_1\right\}\right] \tag{5.13}$$

The fact that $\widehat{I_{C_1}}$ can be represented as a first-order differential equation can be used to simplify equation (5.13). The mentioned differential equation is repeated for convenience as follows:

$$\widehat{I_{C_1}} = C_1\frac{d\widehat{V_d}}{dt} \tag{5.14}$$

Substituting equation (5.14) into equation (5.13) and knowing that all cell capacitors are of equal value C, results in the following differential equation:

$$\begin{aligned} C\frac{d\widehat{V_d}}{dt} &= -\widehat{V_d}\left[2Re\left\{\lambda_1\right\}\right] \\ \frac{d\widehat{V_d}}{dt} &= -\frac{\widehat{V_d}}{C}\left[2Re\left\{\lambda_1\right\}\right] \end{aligned} \tag{5.15}$$

The above equation (5.15) is a system of the form:

$$\dot{x} = \Lambda x \tag{5.16}$$

The homogeneous solution of this system is of the following form [9], [13]:

$$x = e^{\Lambda t}x_0 \tag{5.17}$$

Using equations (5.16) - (5.17), the homogeneous solution of the capacitor voltage $\widehat{V_d}$ can be written as follows:

$$\widehat{V_d} = e^{-\frac{1}{C}[2Re\{\lambda_1\}]t}\widehat{V_{d_0}} \tag{5.18}$$

where $\widehat{V_{d_0}}$ is the initial cell capacitor voltage unbalance.

The time constant of a 2-cell multicell converter is the exponent of equation (5.18).

$$\tau = \frac{C}{2Re\left\{\lambda_1\right\}} \tag{5.19}$$

Equation (5.18) can thus be rewritten in terms of τ as follows:

$$\widehat{V_d} = e^{-\frac{t}{\tau}}\widehat{V_{d_0}} \tag{5.20}$$

In equation (5.19), it is clear that the time constant is affected by the switching function $S_d(\omega)$, the load impedance $Z(\omega)$ and the value of the cell capacitor.

From equation (5.19) it follows that the time constant have the following properties:

- if $\lambda_1 = 0$ the time constant $\tau \to \infty$ which means that $-\frac{t}{\tau} \to 0$ and the cell capacitor voltage unbalance $\widehat{V_d} \to \widehat{V_{d_0}}$. This means that the cell capacitor voltage will not necessarily balance. Conditions that can lead to $\lambda_1 = 0$ are when the load impedance is purely imaginary, i.e. $Re\{Z(\omega)\} = 0$ or when $S_d(\omega) = 0$.

- if $\lambda_1 \to \infty$ the time constant $\tau \to 0$ which means that $-\frac{t}{\tau} \to -\infty$ and the cell capacitor voltage unbalance $\widehat{V_d} \to 0$. This means that the cell capacitor voltage will balance. If $\frac{|S_d(\xi)|^2}{|Z(\xi)|} > 0$ and at least one integral over a group of harmonics exists, then due to the fact that this integral includes all harmonics in the specified group in the interval $(-\infty, \infty)$ it can be concluded that $\lambda_1 \to \infty$. This is not possible in a physical system, as $\tau \to 0$ implies an infinite cell capacitor current.

- if $0 < \lambda_1 < \infty$ the time constant $\tau = \frac{C}{2Re\{\lambda_1\}}$ which means that the cell capacitor voltage unbalance will decay according to $\widehat{V_d} = e^{-\frac{t}{\tau}}\widehat{V_{d_0}}$. This implies that the cell capacitor voltage unbalance will decay to zero in a finite amount of time.

The time constants of 2-cell multicell converters under sinusoidal modulation as well as fixed duty-cycle PWM are calculated in the following example. The parameters of the converter are listed in Table 5.1.

Example 5.1

In this example, a 2-cell multicell converter is switched using both sinusoidal and fixed duty-cycle PWM. Matlab® was used to calculate τ for different values of D and m_a.

- For fixed duty-cycle PWM the switching frequency $f_s = 5\ kHz$ and the duty-cycle $D = 0.5$. The decay of $\widehat{V_d}$ was calculated for this value of D for 2 cases: without a balance booster connected and with a balance booster connected in parallel with the load. The results obtained are shown in Figure 5-3.

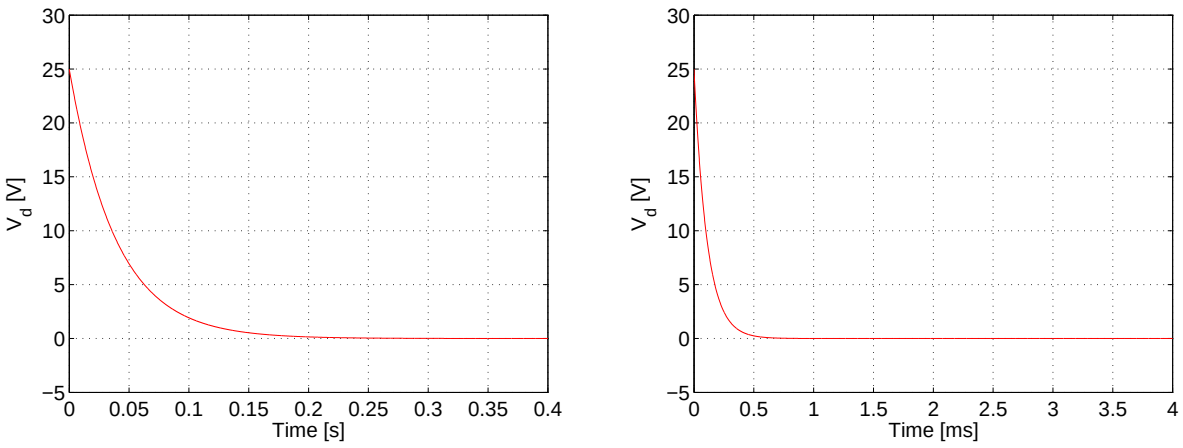

(a) $D = 0.5$: without balance booster (b) $D = 0.5$: with balance booster

Figure 5-3. *Decay of $\widehat{V_d}$ for 2 cells for fixed duty-cycle PWM with $f_s = 5\ kHz$.*

The time constant for the case of $D = 0.5$ without a balance booster is $\tau = 38.97\ ms$, which corresponds with the value of $\widehat{V}_d$ after one time constant in Figure 5-3(a). For the case where a balance booster is connected in parallel with the load, the time constant $\tau = 108.14\ \mu s$. Again, this corresponds with the value of $\widehat{V}_d$ after one time constant in Figure 5-3(b).

- For sinusoidal modulation the switching frequency $f_s = 5\ kHz$, the sinusoidal reference frequency $f_r = 50\ Hz$ and the modulation index $m_a = 0.6$. The decay of $\widehat{V}_d$ was calculated for this value of m_a for 2 cases: without a balance booster connected and with a balance booster connected in parallel with the load. The results obtained are shown in Figure 5-4.

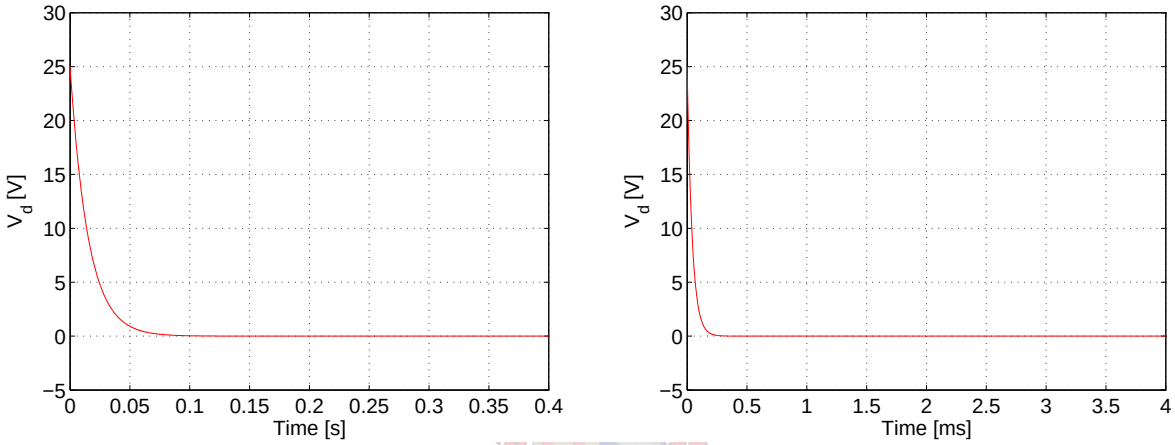

(a) $m_a = 0.6$: without balance booster (b) $m_a = 0.6$: with balance booster

Figure 5-4. *Decay of $\widehat{V}_d$ for 2 cells for sinusoidal modulation with $f_s = 5\ kHz$ and $f_r = 50\ Hz$.*

The time constant for the case of $m_a = 0.6$ without a balance booster is $\tau = 15.10\ ms$, which corresponds with the value of $\widehat{V}_d$ after one time constant in Figure 5-4(a). For the case where a balance booster is connected in parallel with the load, the time constant $\tau = 41.93\ \mu s$. Again, this corresponds with the value of $\widehat{V}_d$ after one time constant in Figure 5-4(b).

5.3 The 3-cell multicell converter

The next step in determining the time constants for a p-cell multicell converter is to determine the time constants for the 3-cell case. The equivalent circuit in terms of d and t parameters of a 3-cell multicell converter in the frequency domain was shown in Figure 4-6 and used in the steady-state analysis of this converter. This figure will also be used in this analysis and is repeated for convenience in Figure 5-5.

In the frequency domain, using Ohm's Law, the expression for the inductor current $I_L(\omega)$ can be written as follows:

$$I_L(\omega) = \frac{V_0(\omega)}{Z(\omega)} = \frac{\frac{V_t}{3} \cdot S_t(\omega)}{Z(\omega)} + \frac{V_{d_1}(\omega) \cdot S_{d_1}(\omega)}{Z(\omega)} + \frac{V_{d_2}(\omega) \cdot S_{d_2}(\omega)}{Z(\omega)} \tag{5.21}$$

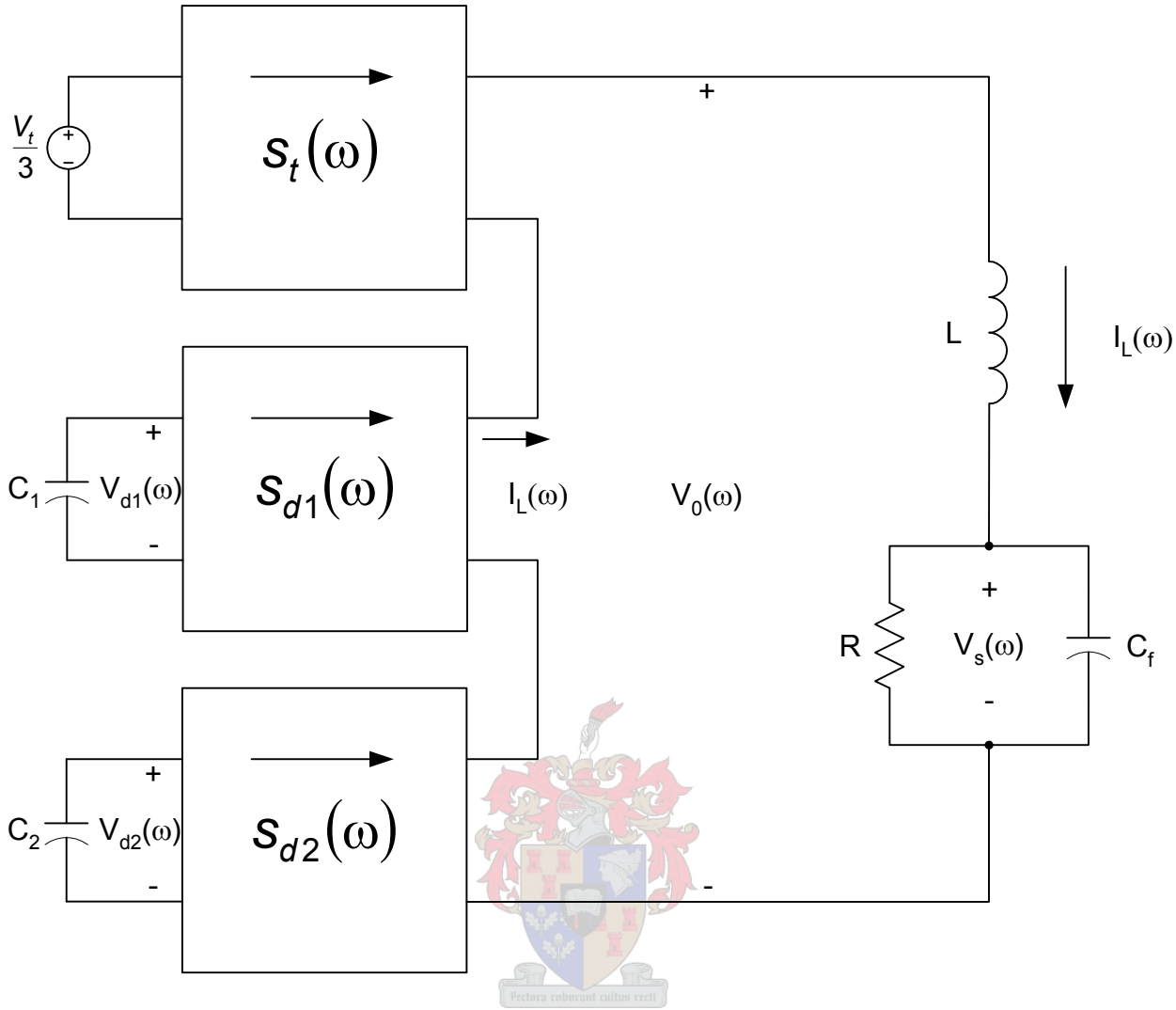

Figure 5-5. *Equivalent circuit in the frequency domain in terms of d and t parameters of a 3-cell multicell converter.*

The expression for the cell capacitor current $I_{C_1}(\omega)$ was calculated in Chapter 4 and given as equation (4.35). The result is repeated here for convenience as follows:

$$I_{C_1}(\omega) = -\left[\frac{V_t}{3}\int_{-\infty}^{\infty}\frac{S_t(\xi)}{Z(\xi)}S_{d_1}(\omega-\xi)d\xi + V_{d_1}\int_{-\infty}^{\infty}\frac{S_{d_1}(\xi)}{Z(\xi)}S_{d_1}(\omega-\xi)d\xi + V_{d_2}\int_{-\infty}^{\infty}\frac{S_{d_2}(\xi)}{Z(\xi)}S_{d_1}(\omega-\xi)d\xi\right] \tag{5.22}$$

Using the same techniques as used in equation (4.36) and knowing that $V_t(\omega)|_{\omega=0} = 0$, equation (5.22) can be rewritten as follows:

$$I_{C_1}(\omega)|_{\omega=0} = -\left[\frac{V_t}{3}\int_{-\infty}^{\infty}\frac{S_t(\xi)}{Z(\xi)}\overline{S_{d_1}(\xi)}d\xi + V_{d_1}\int_{-\infty}^{\infty}\frac{S_{d_1}(\xi)}{Z(\xi)}\overline{S_{d_1}(\xi)}d\xi + V_{d_2}\int_{-\infty}^{\infty}\frac{S_{d_2}(\xi)}{Z(\xi)}\overline{S_{d_1}(\xi)}d\xi\right]$$

$$= - \left[V_{d_1} \int_{-\infty}^{\infty} \frac{S_{d_1}(\xi)}{Z(\xi)} \overline{S_{d_1}(\xi)} d\xi + V_{d_2} \int_{-\infty}^{\infty} \frac{S_{d_2}(\xi)}{Z(\xi)} \overline{S_{d_1}(\xi)} d\xi \right] \tag{5.23}$$

For the remainder of this section, the variables that are in the special steady-state, as defined in the previous section, will be denoted by the "hat" symbol. These variables are as follows:

$$\widehat{I_{C_1}} = I_{C_1}(\omega)|_{\omega=0} \tag{5.24}$$

$$\widehat{I_{C_2}} = I_{C_2}(\omega)|_{\omega=0} \tag{5.25}$$

$$\widehat{V_{d_1}} = V_{d_1}(\omega)|_{\omega=0} \tag{5.26}$$

$$\widehat{V_{d_2}} = V_{d_2}(\omega)|_{\omega=0} \tag{5.27}$$

Using the above symbols, equation (5.23) can be rewritten as follows:

$$\widehat{I_{C_1}} = - \left[\widehat{V_{d_1}} \int_{-\infty}^{\infty} \frac{S_{d_1}(\xi)}{Z(\xi)} \overline{S_{d_1}(\xi)} d\xi + \widehat{V_{d_2}} \int_{-\infty}^{\infty} \frac{S_{d_2}(\xi)}{Z(\xi)} \overline{S_{d_1}(\xi)} d\xi \right] \tag{5.28}$$

The same approach as used in equation (5.8) can now be used again as follows:

$$\widehat{I_{C_1}} = -2 \left[\widehat{V_{d_1}} Re \left\{ \int_0^{\infty} \frac{|S_{d_1}(\xi)|^2}{Z(\xi)} d\xi \right\} + \widehat{V_{d_2}} Re \left\{ \int_0^{\infty} \frac{S_{d_2}(\xi) \overline{S_{d_1}(\xi)}}{Z(\xi)} d\xi \right\} \right] \tag{5.29}$$

Again, in the analysis discussed here, $\overline{S_{d_1}(\xi)}$ represents the complex conjugate of $S_{d_1}(\xi)$. Therefore, the following is true:

$$\overline{S_{d_1}(\xi)} = S_{d_1}(-\xi) \text{ and} \tag{5.30}$$

$$\overline{S_{d_2}(\xi)} = S_{d_2}(-\xi)\,. \tag{5.31}$$

The same method was used to write an expression for $I_{C_2}(\omega)$ in Chapter 4. This result was given as equation (4.35). This equation is repeated here for convenience as follows:

$$I_{C_2}(\omega) = - \left[\frac{V_t}{3} \int_{-\infty}^{\infty} \frac{S_t(\xi)}{Z(\xi)} S_{d_2}(\omega - \xi) d\xi + V_{d_1} \int_{-\infty}^{\infty} \frac{S_{d_1}(\xi)}{Z(\xi)} S_{d_2}(\omega - \xi) d\xi + V_{d_2} \int_{-\infty}^{\infty} \frac{S_{d_2}(\xi)}{Z(\xi)} S_{d_2}(\omega - \xi) d\xi \right] \tag{5.32}$$

Using the same techniques as used in equation (4.38) and knowing that $V_t(\omega)|_{\omega=0} = 0$, equation (5.32) can be rewritten as follows:

$$I_{C_2}(\omega)|_{\omega=0} = - \left[\frac{V_t}{3} \int_{-\infty}^{\infty} \frac{S_t(\xi)}{Z(\xi)} \overline{S_{d_2}(\xi)} d\xi + V_{d_1} \int_{-\infty}^{\infty} \frac{S_{d_1}(\xi)}{Z(\xi)} \overline{S_{d_2}(\xi)} d\xi + V_{d_2} \int_{-\infty}^{\infty} \frac{S_{d_2}(\xi)}{Z(\xi)} \overline{S_{d_2}(\xi)} d\xi \right]$$

$$= - \left[V_{d_1} \int_{-\infty}^{\infty} \frac{S_{d_1}(\xi)}{Z(\xi)} \overline{S_{d_2}(\xi)} d\xi + V_{d_2} \int_{-\infty}^{\infty} \frac{S_{d_2}(\xi)}{Z(\xi)} \overline{S_{d_2}(\xi)} d\xi \right] \tag{5.33}$$

Equation (5.33) can now be rewritten for the special steady-state case using the definitions of equations (5.25)-(5.27), where $I_{C_2}(\omega)|_{\omega=0} \neq 0$ and $V_t(\omega)|_{\omega=0} = 0$, as follows:

$$\widehat{I_{C_2}} = - \left[\widehat{V_{d_1}} \int_{-\infty}^{\infty} \frac{S_{d_1}(\xi)}{Z(\xi)} \overline{S_{d_2}(\xi)} d\xi + \widehat{V_{d_2}} \int_{-\infty}^{\infty} \frac{S_{d_2}(\xi)}{Z(\xi)} \overline{S_{d_2}(\xi)} d\xi \right] \tag{5.34}$$

The same approach as used in equation (5.8) can now be used again as follows:

$$\widehat{I_{C_2}} = -2 \left[\widehat{V_{d_1}} Re \left\{ \int_0^{\infty} \frac{S_{d_1}(\xi) \overline{S_{d_2}(\xi)}}{Z(\xi)} d\xi \right\} + \widehat{V_{d_2}} Re \left\{ \int_0^{\infty} \frac{|S_{d_2}(\xi)|^2}{Z(\xi)} d\xi \right\} \right] \tag{5.35}$$

The same approach can now be used to simplify the integrals in equations (5.29) and (5.35) by using the "Summation Rule of Integrals". Instead of repeating the calculations done in Chapter 4 section 4.4, the relevant results of Table 4.3 are repeated in Table 5.2 and implemented directly afterwards.

Table 5.2. *Integrals rewritten in terms of groups of harmonics*

Integral	Integrals over groups	
$\int_0^{\infty} \frac{S_{d_1}(\xi)\overline{S_{d_1}(\xi)}}{Z(\xi)} d\xi$	$\int_{m=3k} \frac{S_{d_1}(\xi)\overline{S_{d_1}(\xi)}}{Z(\xi)} d\xi + \int_{m=3k+1} \frac{S_{d_1}(\xi)\overline{S_{d_1}(\xi)}}{Z(\xi)} d\xi + \int_{m=3k+2} \frac{S_{d_1}(\xi)\overline{S_{d_1}(\xi)}}{Z(\xi)} d\xi$ $= \lambda_1 + \lambda_2$	(a)
$\int_0^{\infty} \frac{S_{d_2}(\xi)\overline{S_{d_1}(\xi)}}{Z(\xi)} d\xi$	$\int_{m=3k} \frac{S_{d_2}(\xi)\overline{S_{d_1}(\xi)}}{Z(\xi)} d\xi + \int_{m=3k+1} \frac{S_{d_2}(\xi)\overline{S_{d_1}(\xi)}}{Z(\xi)} d\xi + \int_{m=3k+2} \frac{S_{d_2}(\xi)\overline{S_{d_1}(\xi)}}{Z(\xi)} d\xi$ $= e^{j\frac{2\pi}{3}} \lambda_1 + e^{-j\frac{2\pi}{3}} \lambda_2$	(b)
$\int_0^{\infty} \frac{S_{d_1}(\xi)\overline{S_{d_2}(\xi)}}{Z(\xi)} d\xi$	$\int_{m=3k} \frac{S_{d_1}(\xi)\overline{S_{d_2}(\xi)}}{Z(\xi)} d\xi + \int_{m=3k+1} \frac{S_{d_1}(\xi)\overline{S_{d_2}(\xi)}}{Z(\xi)} d\xi + \int_{m=3k+2} \frac{S_{d_1}(\xi)\overline{S_{d_2}(\xi)}}{Z(\xi)} d\xi$ $= e^{-j\frac{2\pi}{3}} \lambda_1 + e^{j\frac{2\pi}{3}} \lambda_2$	(c)
$\int_0^{\infty} \frac{S_{d_2}(\xi)\overline{S_{d_2}(\xi)}}{Z(\xi)} d\xi$	$\int_{m=3k} \frac{S_{d_2}(\xi)\overline{S_{d_2}(\xi)}}{Z(\xi)} d\xi + \int_{m=3k+1} \frac{S_{d_2}(\xi)\overline{S_{d_2}(\xi)}}{Z(\xi)} d\xi + \int_{m=3k+2} \frac{S_{d_2}(\xi)\overline{S_{d_2}(\xi)}}{Z(\xi)} d\xi$ $= \lambda_1 + \lambda_2$	(d)

Equations (5.29) and (5.35) can now be rewritten by substituting the relevant integrals listed in Table 5.2 with their corresponding λ-terms as follows:

$$\widehat{I_{C_1}} = -2\left[Re\left\{\lambda_1+\lambda_2\right\}\widehat{V_{d_1}} + Re\left\{e^{j\frac{2\pi}{3}}\lambda_1 + e^{-j\frac{2\pi}{3}}\lambda_2\right\}\widehat{V_{d_2}}\right] \tag{5.36}$$

$$\widehat{I_{C_2}} = -2\left[Re\left\{e^{-j\frac{2\pi}{3}}\lambda_1 + e^{j\frac{2\pi}{3}}\lambda_2\right\}\widehat{V_{d_1}} + Re\left\{\lambda_1+\lambda_2\right\}\widehat{V_{d_2}}\right] \tag{5.37}$$

The quantities $\widehat{I_{C_1}}$ and $\widehat{I_{C_2}}$ are steady-state averages of frequency-domain quantities at $\omega = 0$, implying dc averages. From this implication, it follows that the derivatives of $\widehat{I_{C_1}}$ and $\widehat{I_{C_2}}$ with respect to time, exists. Therefore, the first-order relationships between the cell capacitor voltages and currents can be used to construct 2 differential equations from equations (5.36) and (5.37). These first-order relationships are as follows:

$$\widehat{I_{C_1}} = C_1\frac{d\widehat{V_{d_1}}}{dt} = C\frac{d\widehat{V_{d_1}}}{dt} \tag{5.38}$$

$$\widehat{I_{C_2}} = C_2\frac{d\widehat{V_{d_2}}}{dt} = C\frac{d\widehat{V_{d_2}}}{dt} \tag{5.39}$$

Substituting $\widehat{I_{C_1}}$ and $\widehat{I_{C_2}}$ in equations (5.36) and (5.37) using equations (5.38) and (5.39), yields the following differential equations: Equations (5.29) and (5.35) can now be rewritten as follows:

$$\begin{aligned} C\frac{d\widehat{V_{d_1}}}{dt} &= -\left[2Re\left\{\lambda_1+\lambda_2\right\}\widehat{V_{d_1}} + 2Re\left\{e^{j\frac{2\pi}{3}}\lambda_1 + e^{-j\frac{2\pi}{3}}\lambda_2\right\}\widehat{V_{d_2}}\right] \\ \frac{d\widehat{V_{d_1}}}{dt} &= -\frac{1}{C}\left[2Re\left\{\lambda_1+\lambda_2\right\}\widehat{V_{d_1}} + 2Re\left\{e^{j\frac{2\pi}{3}}\lambda_1 + e^{-j\frac{2\pi}{3}}\lambda_2\right\}\widehat{V_{d_2}}\right] \end{aligned} \tag{5.40}$$

$$\begin{aligned} C\frac{d\widehat{V_{d_2}}}{dt} &= -\left[2Re\left\{e^{-j\frac{2\pi}{3}}\lambda_1 + e^{j\frac{2\pi}{3}}\lambda_2\right\}\widehat{V_{d_1}} + 2Re\left\{\lambda_1+\lambda_2\right\}\widehat{V_{d_2}}\right] \\ \frac{d\widehat{V_{d_2}}}{dt} &= -\frac{1}{C}\left[2Re\left\{e^{-j\frac{2\pi}{3}}\lambda_1 + e^{j\frac{2\pi}{3}}\lambda_2\right\}\widehat{V_{d_1}} + 2Re\left\{\lambda_1+\lambda_2\right\}\widehat{V_{d_2}}\right] \end{aligned} \tag{5.41}$$

Equations (5.40) and (5.41) can be rewritten in matrix form as follows:

$$\begin{aligned} \begin{bmatrix} \frac{d\widehat{V_{d_1}}}{dt} \\ \frac{d\widehat{V_{d_2}}}{dt} \end{bmatrix} &= -\frac{1}{C}\begin{bmatrix} 2Re\left\{\lambda_1+\lambda_2\right\} & 2Re\left\{e^{j\frac{2\pi}{3}}\lambda_1 + e^{-j\frac{2\pi}{3}}\lambda_2\right\} \\ 2Re\left\{e^{-j\frac{2\pi}{3}}\lambda_1 + e^{j\frac{2\pi}{3}}\lambda_2\right\} & 2Re\left\{\lambda_1+\lambda_2\right\} \end{bmatrix}\begin{bmatrix} \widehat{V_{d_1}} \\ \widehat{V_{d_2}} \end{bmatrix} \\ &= -\frac{1}{C}2Re\left\{\begin{bmatrix} \lambda_1+\lambda_2 & e^{j\frac{2\pi}{3}}\lambda_1 + e^{-j\frac{2\pi}{3}}\lambda_2 \\ e^{-j\frac{2\pi}{3}}\lambda_1 + e^{j\frac{2\pi}{3}}\lambda_2 & \lambda_1+\lambda_2 \end{bmatrix}\right\}\begin{bmatrix} \widehat{V_{d_1}} \\ \widehat{V_{d_2}} \end{bmatrix} \end{aligned} \tag{5.42}$$

The above system of differential equations is of the following form:

$$\dot{\widehat{\mathbf{V_d}}} = -\frac{1}{C}2Re\left\{\mathbf{\Lambda}\right\}\widehat{\mathbf{V_d}} \tag{5.43}$$

where the matrix $\mathbf{\Lambda}$ is the same matrix defined as $\mathbf{\Lambda}$ in Chapter 4 section 4.4 equation (4.56).

The homogeneous solution to the differential equation (5.43) is as follows:

$$\widehat{\mathbf{V_d}} = e^{-\frac{1}{C}2Re\{\mathbf{\Lambda}\}t}\widehat{\mathbf{V_{d_0}}} \tag{5.44}$$

where the matrix $\mathbf{\Lambda}$ and the vectors $\dot{\widehat{\mathbf{V}}}_\mathbf{d}$ and $\widehat{\mathbf{V_d}}$ are defined as follows:

$$\mathbf{\Lambda} = \begin{bmatrix} \lambda_1 + \lambda_2 & e^{j\frac{2\pi}{3}}\lambda_1 + e^{-j\frac{2\pi}{3}}\lambda_2 \\ e^{-j\frac{2\pi}{3}}\lambda_1 + e^{j\frac{2\pi}{3}}\lambda_2 & \lambda_1 + \lambda_2 \end{bmatrix} \tag{5.45}$$

$$\dot{\widehat{\mathbf{V}}}_\mathbf{d} = \begin{bmatrix} \frac{d\widehat{V_{d_1}}}{dt} \\ \frac{d\widehat{V_{d_2}}}{dt} \end{bmatrix} \tag{5.46}$$

$$\widehat{\mathbf{V_d}} = \begin{bmatrix} \widehat{V_{d_1}} \\ \widehat{V_{d_2}} \end{bmatrix} \tag{5.47}$$

The poles of a 3-cell multicell converter are the eigenvalues of the matrix $-\frac{1}{C}2Re\{\mathbf{\Lambda}\}$. These eiegenvalues, denoted ε can be calculated as follows:

$$\varepsilon_{1,2} = \frac{-2Re\{\lambda_1\} - 2Re\{\lambda_2\}}{C} \pm \frac{\sqrt{Re\{\lambda_1\}^2 + 2Re\{\lambda_1\}Re\{\lambda_2\} + Re\{\lambda_2\}^2 - 3Im\{\lambda_1\}^2 - 3Im\{\lambda_2\}^2 + 6Im\{\lambda_1\}Im\{\lambda_2\}}}{C} \tag{5.48}$$

As long as the poles of the system lie on the left-hand side of the complex plane, i.e. $Re\{\varepsilon\} < 0$, the unbalance will decay. If $Re\{\varepsilon\} \geq 0$ the unbalance will not decay.

The time constants of a second-order system can be obtained from the poles as discussed by Ogata in [16] p. 267. The time constants, τ_1 and τ_2 of a 3-cell multicell converter can now be be defined as follows:

$$\tau_1 = -\frac{1}{Re\{\varepsilon_1\}} \quad \text{and} \quad \tau_2 = -\frac{1}{Re\{\varepsilon_2\}} \tag{5.49}$$

where ε_1 and ε_2 are the respective eigenvalues of $-\frac{1}{C}2Re\{\mathbf{\Lambda}\}$.

The equations (5.49) show the relationship between the time constants and the inverse of the eigenvalues of the matrix $-\frac{1}{C}2Re\{\mathbf{\Lambda}\}$. It was shown in Appendix B section B.3 equation (B.68) that the eigenvalues of the matrix $-\frac{1}{C}2Re\{\mathbf{\Lambda}\}$ are less than or equal to $\frac{3}{C}$ times the absolute value of the

largest eigenvalue of $-\frac{1}{C}2Re\{\mathbf{\Lambda}\}$. This means that the eigenvalues of $-\frac{1}{C}2Re\{\mathbf{\Lambda}\}$ lie within a circle with a radius equal to the spectral radius of the matrix. The spectral radius of this matrix is repeated from equation (B.68) as follows:

$$\rho\left(-\frac{1}{C}2Re\{\mathbf{\Lambda}\}\right) \leq \frac{3}{C}\max\left\{\left|\lambda_1+\overline{\lambda_2}\right|,\left|\lambda_2+\overline{\lambda_1}\right|\right\} \tag{5.50}$$

A better approximation of the eigenvalues can be obtained by combining the result of equation (5.50) with Gerschgorin circles. Gerschgorin circles are defined in Appendix B section B.2 Theorem B.8. These 2 methods will be applied in the following example.

Example 5.2

This example is the same as the previous example, except that this example is based on a 3-cell multicell converter. The converter parameters are the same as used in the previous example. The converter is again switched using both sinusoidal and fixed duty-cycle PWM. Matlab® was used to calculate the matrices $-\frac{1}{C}2Re\{\mathbf{\Lambda}\}$ and their respective eigenvalues for different values of D and m_a. The information obtained is then used to draw Gerschgorin circles and the circle obtained using the spectral radius. The eigenvalues are also plotted on these graphs to prove that they fall within these circles.

- For fixed duty-cycle PWM the switching frequency $f_s = 5\ kHz$ and the duty-cycle $D = 0.5$. The decay of $\widehat{V_{d_1}}$ and $\widehat{V_{d_2}}$ was calculated for this value of D for 2 cases: without a balance booster connected and with a balance booster connected in parallel with the load. The results obtained are shown in Figure 5-6.

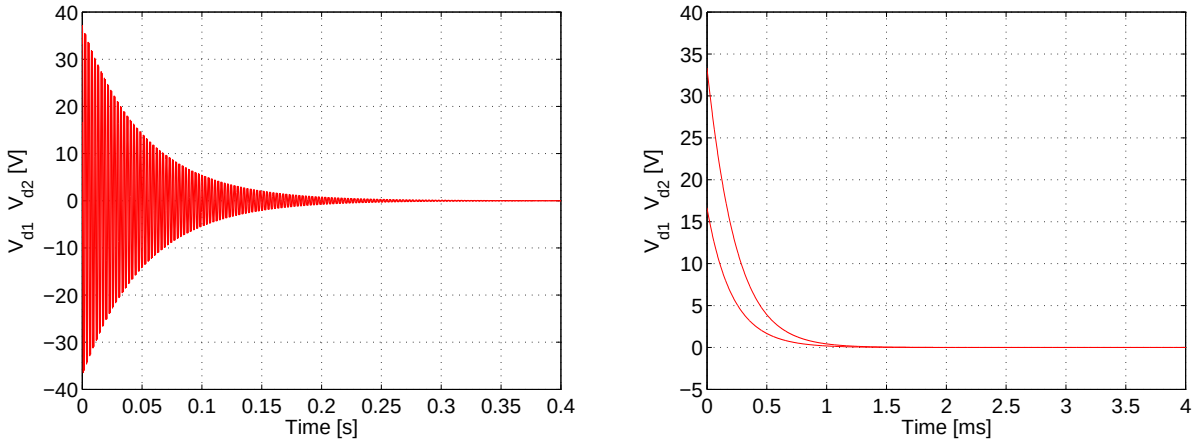

(a) $D = 0.5$: without balance booster (b) $D = 0.5$: with balance booster

Figure 5-6. *Decay of $\widehat{V_d}$ for 3 cells for fixed duty-cycle PWM with $f_s = 5\ kHz$.*

The time constants for the case of $D = 0.5$ without a balance booster are $\tau_{1,2} = 52.02\ ms$, which corresponds roughly with the values of $\widehat{V_{d_1}}$ and $\widehat{V_{d_2}}$ after one time constant in Figure 5-6(a). For the case where a balance booster is connected in parallel with the load, the time constants are as follows: $\tau_1 = 106.40\ \mu s$ and $\tau_2 = 224.52\ \mu s$. Again, this corresponds

with the values of $\widehat{V_{d_1}}$ and $\widehat{V_{d_2}}$ after one time constant in Figure 5-6(b).

The circles obtained using Gerschgorin's theorem and the spectral radii of the matrices are shown in Figure 5-7. Figure 5-7(a) corresponds to the case without a balance booster and Figure 5-7(b) to the case where a balance booster is connected.

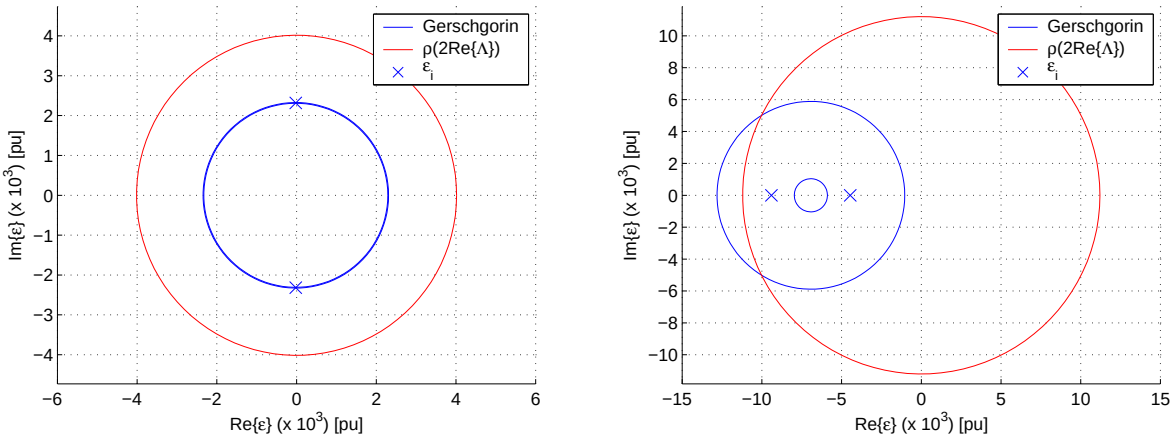

(a) $D = 0.5$: without balance booster (b) $D = 0.5$: with balance booster

Figure 5-7. *Gerschgorin and spectral radii circles with the eigenvalues within them.*

The spectral radii shown in red in Figures 5-7(a) and 5-7(b) depict the largest circle within which the eigenvalues are. The union of the 2 blue Gerschgorin circles depict a smaller circle within which the eigenvalues are. A combination of these results can be made by taking the intersection of the following: the union of the Gerschgorin circles and the circle obtained using the spectral radius. This results in a smaller area in which the eigenvalues are situated. For this example, the values of the respective eigenvalues are as follows:

(a) $D = 0.5$ without balance booster: $\varepsilon_{1,2} = -19.22 \pm j2318.30$.

(b) $D = 0.5$ with balance booster: $\varepsilon_1 = -9398.40$ and $\varepsilon_2 = -4454$.

It is clear that both of these eigenvalues are on the left-hand side of the complex plane, which means that the unbalance will decay. This is verified by the results shown in Figure 5-6. The further a pole lies to the left of the complex plane, the faster the unbalance will decay [8]. This is verified by the values of $\varepsilon_{1,2}$ for the case where a balance booster is connected - these poles lie much more to the left of the complex plane than those of the case where a balance booster is not connected.

The centre-points of the Gerschgorin circles are the diagonal elements of the matrix $-\frac{1}{C}2Re\{\mathbf{\Lambda}\}$ shown in equation (5.42). From the definition of this matrix it is clear that these circles all have the same centre-points, as the diagonal elements of this matrix are all the same, i.e. $-\frac{1}{C}2Re\{\lambda_1 + \lambda_2\}$. The calculated matrix $-\frac{1}{C}2Re\{\mathbf{\Lambda}\}$ for the above 2 cases are shown in the following equations:

(a) $D = 0.5$ without balance booster:

$$-\frac{1}{C}2Re\{\mathbf{\Lambda}\} = \begin{bmatrix} -19.22 & -2308.7 \\ 2327.9 & -19.22 \end{bmatrix} \tag{5.51}$$

(b) $D = 0.5$ with balance booster:

$$-\frac{1}{C}2Re\{\mathbf{\Lambda}\} = \begin{bmatrix} -6926.2 & 1037.9 \\ 5888.3 & -6926.2 \end{bmatrix} \tag{5.52}$$

At this stage it is clear that the values of λ_1 and λ_2 have a significant effect on the positions of the poles of the system. This is discussed briefly at the end of this example.

- For sinusoidal modulation the switching frequency $f_s = 5\ kHz$, the sinusoidal reference frequency $f_r = 50\ Hz$ and the modulation index $m_a = 0.6$. The decay of $\widehat{V_d}$ was calculated for this value of m_a for 2 cases: without a balance booster connected and with a balance booster connected in parallel with the load. The results obtained are shown in Figure 5-8.

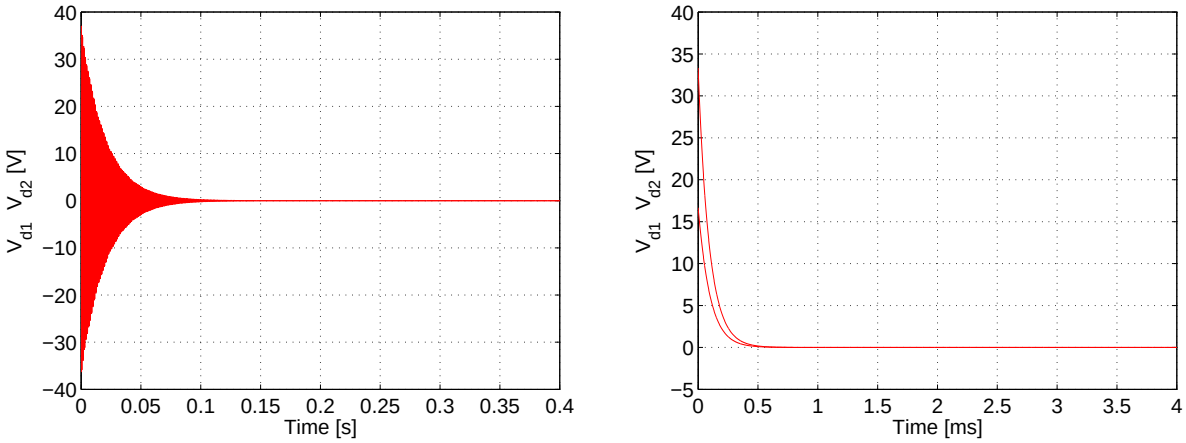

(a) $m_a = 0.6$: without balance booster

(b) $m_a = 0.6$: with balance booster

Figure 5-8. *Decay of $\widehat{V_d}$ for 3 cells for sinusoidal modulation with $f_s = 5\ kHz$ and $f_r = 50\ Hz$.*

The time constants for the case of $m_a = 0.6$ without a balance booster is $\tau_{1,2} = 19.86\ ms$, which corresponds with the values of $\widehat{V_{d_1}}$ and $\widehat{V_{d_2}}$ after one time constant in Figure 5-8(a). For the case where a balance booster is connected in parallel with the load, the time constants are as follows: $\tau_1 = 38.94\ \mu s$ and $\tau_2 = 95.95\ \mu s$. Again, this corresponds with the values of $\widehat{V_{d_1}}$ and $\widehat{V_{d_2}}$ after one time constant in Figure 5-8(b).

Again, the circles obtained using Gerschgorin's theorem and the spectral radii of the matrices are shown in Figure 5-9. Figure 5-9(a) corresponds to the case without a balance booster and Figure 5-9(b) to the case where a balance booster is connected.

The largest circle within which the eigenvalues are situated is defined by the spectral radii

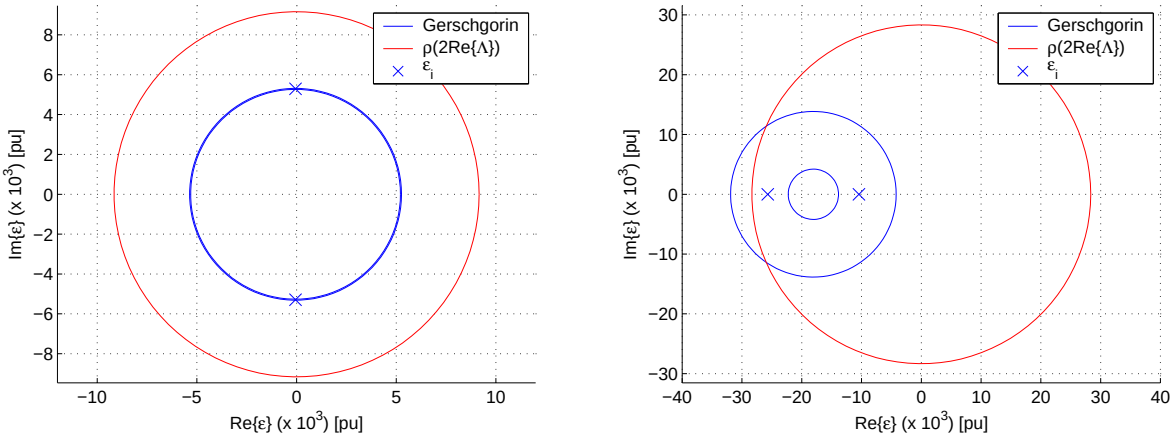

(a) $m_a = 0.6$: without balance booster (b) $m_a = 0.6$: with balance booster

Figure 5-9. *Gerschgorin and spectral radii circles with the eigenvalues within them.*

shown in red in Figures 5-9(a) and 5-9(b). The union of the 2 blue Gerschgorin circles depict a smaller circle within which the eigenvalues are. These results can be combined by taking the intersection of the largest Gerschgorin circle and the spectral circle, which results in a smaller area in which the eigenvalues are. The values of the respective eigenvalues for the cases discussed here are as follows:

(a) $m_a = 0.6$ without balance booster: $\varepsilon_{1,2} = -50.35 \pm j5289.1$.

(b) $m_a = 0.6$ with balance booster: $\varepsilon_1 = -25681$ and $\varepsilon_2 = -10422$.

For the sinusoidal modulation case it is also clear that both of these eigenvalues are on the left-hand side of the complex plane, which means that the unbalance will decay. This is verified by the results shown in Figure 5-8. Again, the values of $\varepsilon_{1,2}$ is much larger for the case where a balance booster is connected - these poles also lie much more to the left of the complex plane than those of the case where a balance booster is not connected.

The same arguments are valid for the centre-points of the Gerschgorin circles and the values of the diagonal elements of the matrix $-\frac{1}{C}2Re\{\mathbf{\Lambda}\}$ as for the fixed duty-cycle case. The calculated matrices $-\frac{1}{C}2Re\{\mathbf{\Lambda}\}$ for the above 2 cases are shown in the following equations:

(a) $m_a = 0.6$ without balance booster:

$$-\frac{1}{C}2Re\{\mathbf{\Lambda}\} = \begin{bmatrix} -50.35 & -5263.9 \\ 5314.3 & -50.35 \end{bmatrix} \tag{5.53}$$

(b) $m_a = 0.6$ with balance booster:

$$-\frac{1}{C}2Re\{\mathbf{\Lambda}\} = \begin{bmatrix} -18051 & 4204 \\ 13847 & -18051 \end{bmatrix} \tag{5.54}$$

From the definitions of λ_1 and λ_2 in Chapter 4 section 4.4 equations (4.44) and (4.45) and the effect of the load impedance on the value of these terms, it can be said that the smaller the load impedance at multiples of the switching frequency, the larger their value. Thus, the larger the values of the λ-terms, the larger their sum, leading to the Gerschgorin circles' centre-points moving further to the left of the complex plane. This corresponds to the difference observed between the case without a balance booster and the case with a balance booster. The unbalance decays much faster for the case with the balance booster than the case without, as the balance booster lowers the load impedance considerably at the switching frequency.

5.4 The p-cell multicell converter

This section is the final step in determining the time constants for a multicell converter for the general case of p cells. The equivalent circuit in terms of d and t parameters of a p-cell multicell converter in the frequency domain was derived in Chapter 4 and shown in Figure 4-7. This figure is repeated for convenience in Figure 5-10 and will be used for the time constant analysis discussed in this section.

In the frequency domain, using Ohm's Law, the expression for the inductor current $I_L(\omega)$ can be written as follows:

$$I_L(\omega) = \frac{V_0(\omega)}{Z(\omega)} = \frac{\frac{V_t}{p} \cdot S_t(\omega)}{Z(\omega)} + \frac{\sum_{l=1}^{p-1} V_{d_l} S_{d_l}(\omega)}{Z(\omega)} \tag{5.55}$$

The expression for the cell capacitor current $I_{C_1}(\omega)$ was calculated in Chapter 4 and given as equation (4.73). The result is repeated here for convenience as follows:

$$I_{C_1}(\omega) = -\left[\frac{V_t}{p}\int_{-\infty}^{\infty} \frac{S_t(\xi)}{Z(\xi)} S_{d_1}(\omega-\xi)d\xi + \int_{-\infty}^{\infty} \frac{\sum_{l=1}^{p-1} V_{d_l} S_{d_l}(\xi)}{Z(\xi)} S_{d_1}(\omega-\xi)d\xi\right] \tag{5.56}$$

The expression for the cell capacitor current $I_{C_i}(\omega)$ was derived in Chapter 4 as equation (4.74) and is repeated here for convenience:

$$I_{C_i}(\omega) = -\left[\frac{V_t}{p}\int_{-\infty}^{\infty} \frac{S_t(\xi)}{Z(\xi)} S_{d_i}(\omega-\xi)d\xi + \int_{-\infty}^{\infty} \frac{\sum_{l=1}^{p-1} V_{d_l} S_{d_l}(\xi)}{Z(\xi)} S_{d_i}(\omega-\xi)d\xi\right] \tag{5.57}$$

Using the same techniques as used in equation (4.75) and knowing that $V_t(\omega)|_{\omega=0} = 0$, equation (5.57) can be rewritten as follows:

$$\begin{aligned} I_{C_i}(\omega)|_{\omega=0} &= -\left[\frac{V_t}{p}\int_{-\infty}^{\infty} \frac{S_t(\xi)}{Z(\xi)} \overline{S_{d_i}(\xi)}d\xi + \int_{-\infty}^{\infty} \frac{\sum_{l=1}^{p-1} V_{d_l} S_{d_l}(\xi)}{Z(\xi)} \overline{S_{d_i}(\xi)}d\xi\right] \\ &= -\left[\int_{-\infty}^{\infty} \frac{\sum_{l=1}^{p-1} V_{d_l} S_{d_l}(\xi)}{Z(\xi)} \overline{S_{d_i}(\xi)}d\xi\right] \\ &= -\left[\sum_{l=1}^{p-1} V_{d_l} \int_{-\infty}^{\infty} \frac{S_{d_l}(\xi)}{Z(\xi)} \overline{S_{d_i}(\xi)}d\xi\right] \end{aligned} \tag{5.58}$$

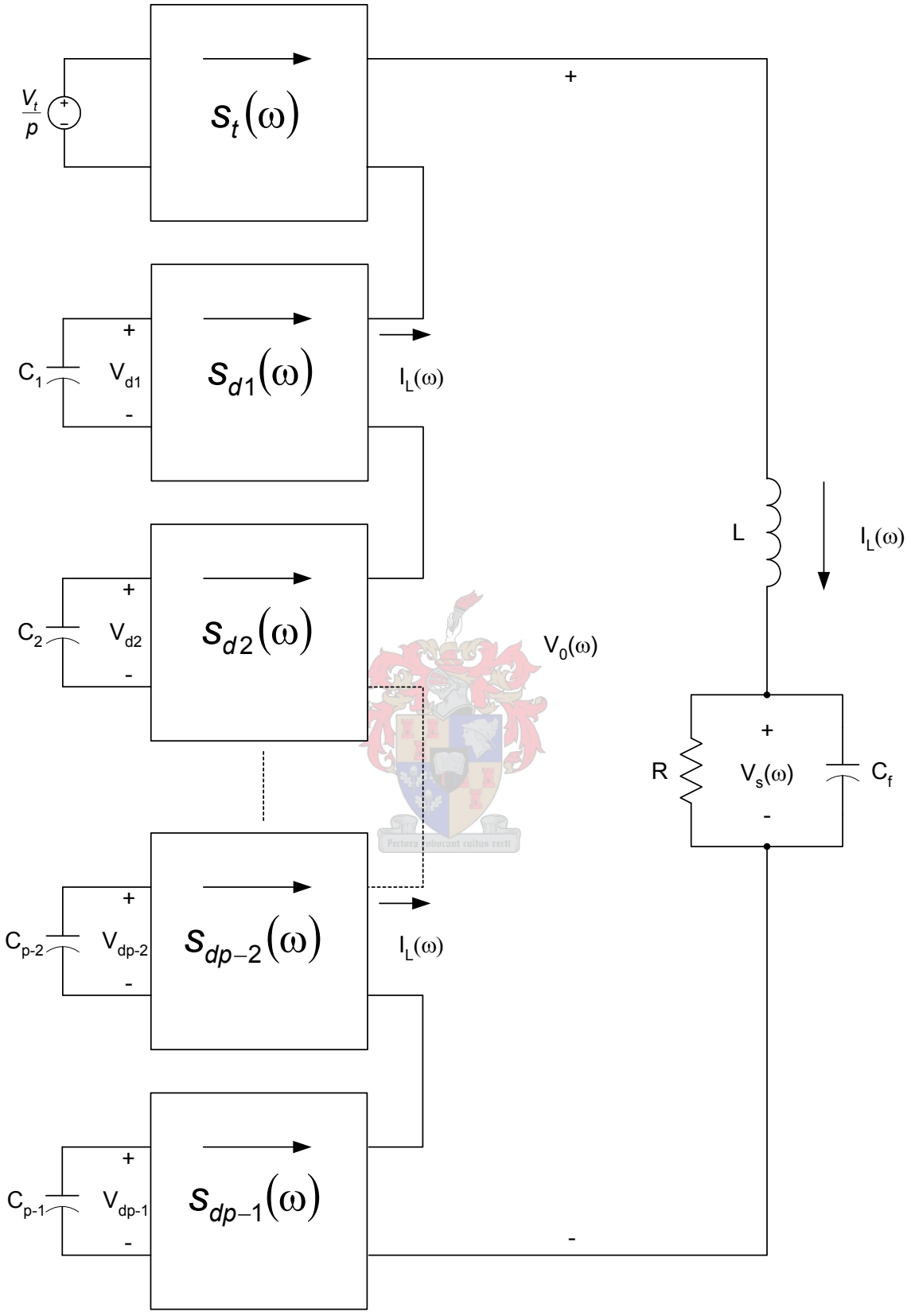

Figure 5-10. *Equivalent circuit in the frequency domain in terms of d and t parameters of a p-cell multicell converter.*

The special steady-state that was defined in section 5.2 will now be used for the remainder of this section. Variables that are in this state will be denoted by the "hat"-symbol, e.g. $\widehat{x}$. These variables are as follows:

$$\widehat{I_{C_i}} = I_{C_i}(\omega)|_{\omega=0} \quad \text{for } i = 1, \cdots, p-1 \tag{5.59}$$

$$\widehat{V_{d_i}} = V_{d_i}(\omega)|_{\omega=0} \quad \text{for } i = 1, \cdots, p-1 \tag{5.60}$$

Using the symbols defined in equations (5.59) and (5.60), equation (5.58) can be rewritten as follows:

$$\widehat{I_{C_i}} = -\left[\sum_{l=1}^{p-1} \widehat{V_{d_l}} \int_{-\infty}^{\infty} \frac{S_{d_l}(\xi)}{Z(\xi)} \overline{S_{d_i}(\xi)} d\xi\right] \tag{5.61}$$

The same approach as used in equation (5.8) can now be used again to rewrite equation (5.61) in the following form:

$$\widehat{I_{C_i}} = -2\left[\sum_{l=1}^{p-1} \widehat{V_{d_l}} Re\left\{\int_{0}^{\infty} \frac{S_{d_l}(\xi)}{Z(\xi)} \overline{S_{d_i}(\xi)} d\xi\right\}\right] \tag{5.62}$$

As mentioned in the previous sections, $\overline{S_{d_i}(\xi)}$ represents the complex conjugate of $S_{d_i}(\xi)$. Therefore, the following is true:

$$\overline{S_{d_i}(\xi)} = S_{d_i}(-\xi) \quad \text{for } i = 1, \ldots, p-1. \tag{5.63}$$

The quantities $\widehat{I_{C_i}}$ for $i = 1, \ldots, p-1$ are steady-state averages of frequency-domain quantities at $\omega = 0$, implying dc averages. From this implication, it follows that the derivatives of $\widehat{I_{C_i}}$ for $i = 1, \ldots, p-1$ with respect to time, exists. Therefore, the first-order relationships between the cell capacitor voltages and currents can be used to construct $p-1$ differential equations from equation (5.62). These first-order relationships are as follows:

$$\widehat{I_{C_i}} = C_i \frac{d\widehat{V_{d_i}}}{dt} = C \frac{d\widehat{V_{d_i}}}{dt} \tag{5.64}$$

Substituting $\widehat{I_{C_i}}$ in equations (5.62) using equations (5.64), yields the following differential equations:

$$\begin{aligned} C\frac{d\widehat{V_{d_i}}}{dt} &= -2\sum_{l=1}^{p-1} \widehat{V_{d_l}} Re\left\{\int_{0}^{\infty} \frac{S_{d_l}(\xi)}{Z(\xi)} \overline{S_{d_i}(\xi)} d\xi\right\} \\ \frac{d\widehat{V_{d_i}}}{dt} &= -\frac{2}{C}\sum_{l=1}^{p-1} \widehat{V_{d_l}} Re\left\{\int_{0}^{\infty} \frac{S_{d_l}(\xi)}{Z(\xi)} \overline{S_{d_i}(\xi)} d\xi\right\} \end{aligned} \tag{5.65}$$

The above system of differential equations are of the following form:

$$\dot{\widehat{\mathbf{V_d}}} = -\frac{1}{C} 2Re\left\{\mathbf{\Lambda}\right\} \widehat{\mathbf{V_d}} \tag{5.66}$$

where the matrix $\mathbf{\Lambda}$ is the same matrix defined as $\mathbf{\Lambda}$ in Chapter 4 section 4.5 equation (4.79). The homogeneous solution to the the differential equation (5.66) is as follows:

$$\widehat{\mathbf{V_d}} = e^{-\frac{1}{C}2Re\{\mathbf{\Lambda}\}t} \widehat{\mathbf{V_{d0}}} \tag{5.67}$$

where the matrix $\mathbf{\Lambda}$ and the vectors $\dot{\widehat{\mathbf{V_d}}}$ and $\widehat{\mathbf{V_d}}$ are defined as follows:

$$\mathbf{\Lambda} = \begin{bmatrix} \sum_{l=1}^{p-1} \lambda_l & \sum_{l=1}^{p-1} e^{j\frac{2\pi l}{p}} \lambda_l & \dots & \sum_{l=1}^{p-1} e^{j\frac{2\pi l(p-2)}{p}} \lambda_l \\ \sum_{l=1}^{p-1} e^{j\frac{-2\pi l}{p}} \lambda_l & \sum_{l=1}^{p-1} \lambda_l & \dots & \sum_{l=1}^{p-1} e^{j\frac{2\pi l(p-3)}{p}} \lambda_l \\ \vdots & \vdots & \ddots & \vdots \\ \sum_{l=1}^{p-1} e^{j\frac{-2\pi l(p-2)}{p}} \lambda_l & \sum_{l=1}^{p-1} e^{j\frac{2\pi l(p-3)}{p}} \lambda_l & \dots & \sum_{l=1}^{p-1} \lambda_l \end{bmatrix} \tag{5.68}$$

$$\dot{\widehat{\mathbf{V_d}}} = \begin{bmatrix} \frac{d\widehat{V_{d_1}}}{dt} \\ \frac{d\widehat{V_{d_2}}}{dt} \\ \vdots \\ \frac{d\widehat{V_{d_{p-1}}}}{dt} \end{bmatrix} \tag{5.69}$$

$$\widehat{\mathbf{V_d}} = \begin{bmatrix} \widehat{V_{d_1}} \\ \widehat{V_{d_2}} \\ \vdots \\ \widehat{V_{d_{p-1}}} \end{bmatrix} \tag{5.70}$$

The eigenvalues of the matrix $-\frac{1}{C}2Re\{\mathbf{\Lambda}\}$ are the poles of a p-cell multicell converter. It is difficult to calculate these eigenvalues analytically, although they can be calculated numerically for specific cases using computer packages like Matlab®, Maple® or Mathematica®.

An approximation of the eigenvalues can be made by calculating the spectral radius of the matrix $-\frac{1}{C}2Re\{\mathbf{\Lambda}\}$.

It was shown in Appendix B section B.5 equation (B.157) that spectral radius of the matrix $-\frac{1}{C}2Re\{\mathbf{\Lambda}\}$ is less than or equal to $\frac{p}{C}$ times the absolute value of the largest eigenvalue of $-\frac{1}{C}2Re\{\mathbf{\Lambda}\}$. This means that the eigenvalues of $-\frac{1}{C}2Re\{\mathbf{\Lambda}\}$ lie within a circle with a radius equal to the spectral radius of the

matrix. The spectral radius of this matrix is repeated from equation (B.157) as follows:

$$\rho\left(-\frac{1}{C}2Re\{\mathbf{\Lambda}\}\right) \leq \frac{p}{C}\max\left\{\left|\lambda_1+\overline{\lambda_{p-1}}\right|,\left|\lambda_2+\overline{\lambda_{p-2}}\right|,\ldots,\left|\lambda_{p-1}+\overline{\lambda_1}\right|\right\} \tag{5.71}$$

As in the previous section, this result can also be improved by combining the result of equation (5.71) with Gerschgorin circles [14]. Gerschgorin circles are defined in Appendix B section B.2 Theorem B.8. The results can be combined by taking the intersection of the spectral circle and the largest Gerschgorin circle. These methods will again be applied in the following example.

Example 5.3

This example is again the same as the previous examples, except that it is based on a 4-cell multicell converter. The converter parameters are the same as used in the previous examples. In this example the converter is switched using both fixed duty-cycle PWM as well as sinusoidal modulation. Matlab® was again used to calculate the matrices $-\frac{1}{C}2Re\{\mathbf{\Lambda}\}$ and their respective eigenvalues for the values of D and m_a. The information obtained is then used to draw Gerschgorin circles and the circle obtained using the spectral radius. The eigenvalues are also plotted on these graphs to prove that they fall within these circles.

- For fixed duty-cycle PWM the switching frequency $f_s = 5\ kHz$ and the duty-cycle $D = 0.5$. The decay of $\widehat{V_{d_1}}$, $\widehat{V_{d_2}}$ and $\widehat{V_{d_3}}$ was calculated for this value of D for 2 cases: without a balance booster connected and with a balance booster connected in parallel with the load. The results obtained are shown in Figure 5-11.

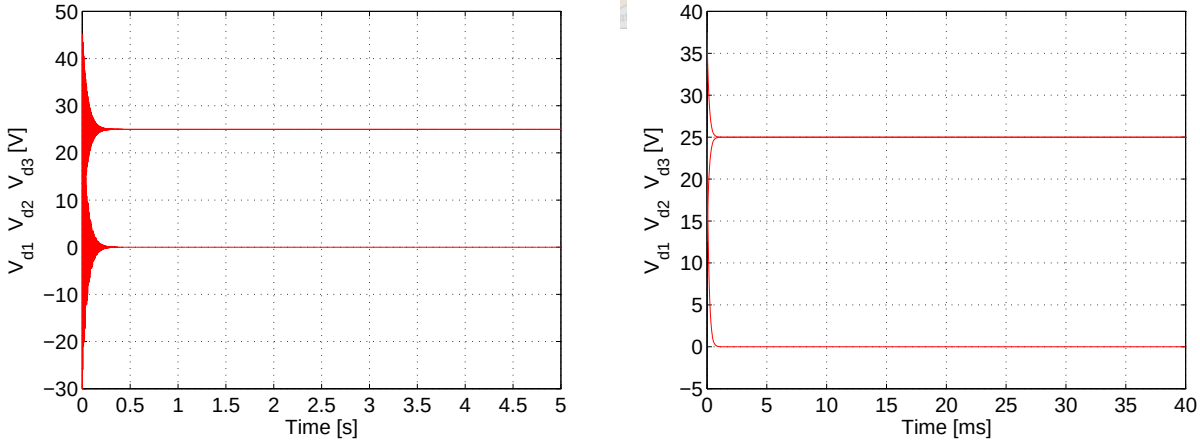

(a) $D = 0.5$: without balance booster (b) $D = 0.5$: with balance booster

Figure 5-11. *Decay of $\widehat{V_d}$ for 4 cells for fixed duty-cycle PWM with $f_s = 5\ kHz$.*

For a larger order system as in this case, the time constants cannot be calculated directly from the poles of the system. It is clear from both Figures 5-11(a) and 5-11(b) that for $D = 0.5$ the unbalance does not decay for all the cell capacitors. Even the addition of a balance booster does not eliminate the unbalance. This case falls under the "Special cases" category discussed in Chapter 3 section 3.3.3 and Chapter 4 section 4.6.

The circles obtained using Gerschgorin's theorem and the spectral radii of the matrices are shown in Figure 5-12. Figure 5-12(a) corresponds to the case without a balance booster and Figure 5-12(b) to the case where a balance booster is connected.

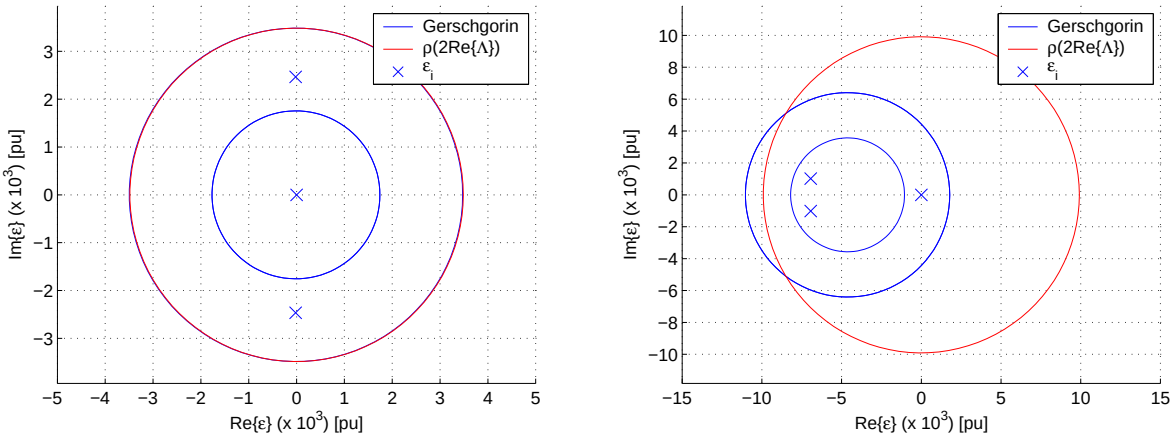

(a) $D = 0.5$: without balance booster

(b) $D = 0.5$: with balance booster

Figure 5-12. *Gerschgorin and spectral radii circles with the eigenvalues within them.*

The spectral radii shown in red in Figures 5-12(a) and 5-12(b) depict the largest circle within which the eigenvalues are. The union of the 2 blue Gerschgorin circles depict a smaller circle within which the eigenvalues are. The values of the respective eigenvalues are as follows:

(a) $D = 0.5$ without balance booster: $\varepsilon_{1,2} = -19.25 \pm j2464.6$ and $\varepsilon_3 = 2.26 \times 10^{-14}$.

(b) $D = 0.5$ with balance booster: $\varepsilon_{1,2} = -6935.7 \pm j1014.6$ and $\varepsilon_3 = 4.22 \times 10^{-13}$.

It is clear that for both of these cases there is an eigenvalue on the right-hand side of the complex plane, which means that the unbalance for one capacitor will not decay. The other 2 eigenvalues correspond to the unbalance of the remaining 2 cell capacitors which decays. This is verified by the results shown in Figure 5-11. The further a pole lies to the left of the complex plane, the faster the unbalance will decay [8]. This is verified by the values of $\varepsilon_{1,2}$ for the case where a balance booster is connected - these poles lie much more to the left of the complex plane than those of the case where a balance booster is not connected.

The centre-points of the Gerschgorin circles are the diagonal elements of the matrix $-\frac{1}{C}2Re\{\mathbf{\Lambda}\}$ shown in equation (5.68). From the definition of this matrix it is clear that these circles all have the same centre-points, as the diagonal elements of this matrix are all the same, i.e. $-\frac{1}{C}2Re\{\lambda_1 + \lambda_2 + \lambda_3\}$. The calculated matrix $-\frac{1}{C}2Re\{\mathbf{\Lambda}\}$ for the above 2 cases are shown in the following equations:

(a) $D = 0.5$ without balance booster:

$$-\frac{1}{C}2Re\{\mathbf{\Lambda}\} = \begin{bmatrix} -12.83 & -1742.7 & 12.83 \\ 1742.7 & -12.83 & -1742.7 \\ 12.83 & 1742.7 & -12.83 \end{bmatrix} \tag{5.72}$$

(b) $D = 0.5$ with balance booster:

$$-\frac{1}{C}2Re\{\mathbf{\Lambda}\} = \begin{bmatrix} -4623.8 & -1785.2 & 4623.8 \\ 1785.2 & -4623.8 & -1785.2 \\ 4623.8 & 1785.2 & -4623.8 \end{bmatrix} \tag{5.73}$$

It was shown in the previous section that the values of the λ-terms have a significant effect on the positions of the poles of the system. This is discussed in more detail at the end of this example. It is also interesting to note that the matrix $-\frac{1}{C}2Re\{\mathbf{\Lambda}\}$ has a Toeplitz structure [14].

- For sinusoidal modulation the switching frequency $f_s = 5\ kHz$, the sinusoidal reference frequency $f_r = 50\ Hz$ and the modulation index $m_a = 0.6$. The decay of $\widehat{V_{d_1}}$, $\widehat{V_{d_2}}$ and $\widehat{V_{d_3}}$ was calculated for this value of m_a for 2 cases: without a balance booster connected and with a balance booster connected in parallel with the load. The results obtained are shown in Figure 5-13.

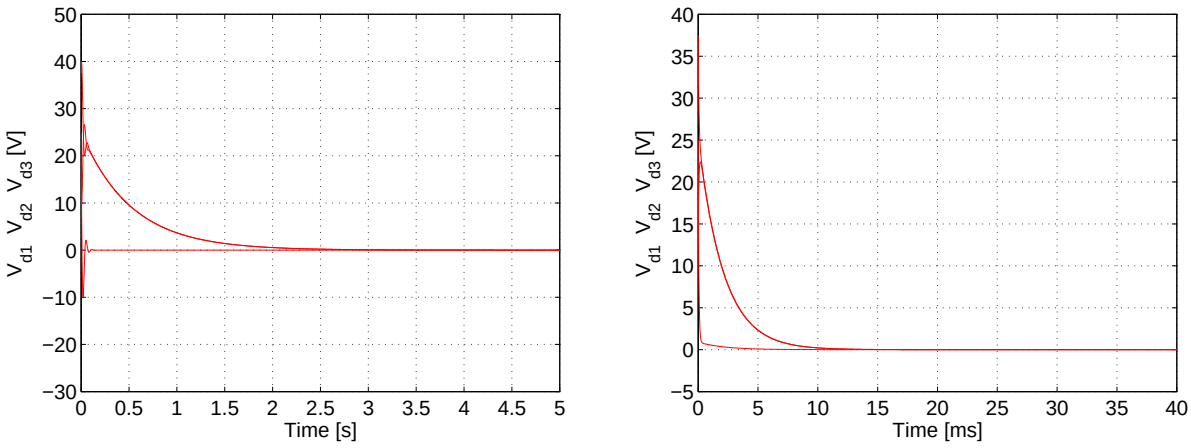

(a) $m_a = 0.6$: without balance booster (b) $m_a = 0.6$: with balance booster

Figure 5-13. *Decay of $\widehat{V_d}$ for 4 cells for sinusoidal modulation with $f_s = 5\ kHz$ and $f_r = 50\ Hz$.*

It is clear from Figure 5-13 that the unbalance decays for the 4-cell converter case under sinusoidal modulation. It is also clear that the unbalance decays much slower than for the cases discussed in the previous sections. The case without a balance booster, shown in Figure 5-13(a) decays the slowest of all the examples considered where the unbalance decays. For the case where a balance booster is connected, the unbalance decays much faster, except for the unbalance across 2 capacitors which decay slower compared to the other capacitor. This is

shown in Figure 5-13(b). The time constants for this case cannot be calculated directly, but the poles can be calculated using Matlab®.

Again, the circles obtained using Gerschgorin's theorem and the spectral radii of the matrices are shown in Figure 5-14. Figure 5-14(a) corresponds to the case without a balance booster and Figure 5-14(b) to the case where a balance booster is connected.

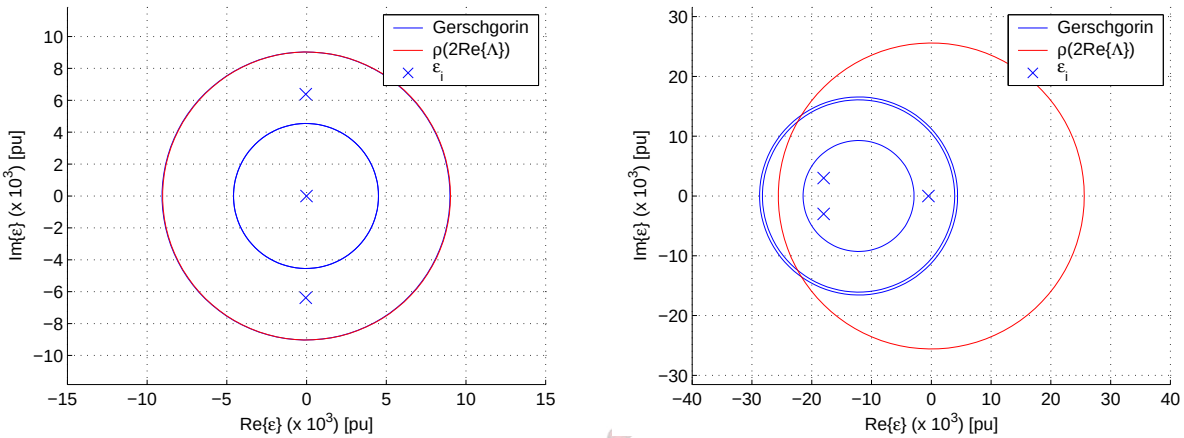

(a) $m_a = 0.6$: without balance booster (b) $m_a = 0.6$: with balance booster

Figure 5-14. *Gerschgorin and spectral radii circles with the eigenvalues within them.*

The largest circle within which the eigenvalues are situated is defined by the spectral radii shown in red in Figures 5-14(a) and 5-14(b). The union of the 2 blue Gerschgorin circles depict a smaller circle within which the eigenvalues are. The values of the respective eigenvalues are as follows:

(a) $m_a = 0.6$ without balance booster: $\varepsilon_{1,2} = -50.15 \pm j6385$ and $\varepsilon_3 = -1.92$.

(b) $m_a = 0.6$ with balance booster: $\varepsilon_{1,2} = -18011 \pm j2996.8$ and $\varepsilon_3 = -477.23$.

For the sinusoidal modulation case it is clear that all the poles are on the left-hand side of the complex plane, which means that the unbalance will decay. This is verified by the results shown in Figure 5-13. Again, the values of $\varepsilon_{1,2,3}$ are much larger for the case where a balance booster is connected - these poles also lie much more to the left of the complex plane than those of the case where a balance booster is not connected. It should also be noted that for both cases there are 2 poles relatively far to the left-hand side of the complex plane and one pole close to the origin of the complex plane, but still on the left-hand side of the plane.

The same arguments are valid for the centre-points of the Gerschgorin circles and the values of the diagonal elements of the matrix $-\frac{1}{C}2Re\{\mathbf{\Lambda}\}$ as for the fixed duty-cycle case. The calculated matrices $-\frac{1}{C}2Re\{\mathbf{\Lambda}\}$ for the above 2 cases are shown in the following equations:

(a) $m_a = 0.6$ without balance booster:

$$-\frac{1}{C}2Re\{\mathbf{\Lambda}\} = \begin{bmatrix} -34.07 & -4513.9 & 32.16 \\ 4515.9 & -34.07 & -4513.9 \\ 32.16 & 4515.9 & -34.07 \end{bmatrix} \tag{5.74}$$

(b) $m_a = 0.6$ with balance booster:

$$-\frac{1}{C}2Re\{\mathbf{\Lambda}\} = \begin{bmatrix} -12167 & -4396.9 & 11681 \\ 4882.8 & -12167 & -4396.9 \\ 11681 & 4882.8 & -12167 \end{bmatrix} \tag{5.75}$$

Again, it is clear that the matrix $-\frac{1}{C}2Re\{\mathbf{\Lambda}\}$ has a Toeplitz structure [14]. More information on the subject of Toeplitz matrices can be found in [6].

From the definitions of λ-terms in general in Chapter 4 section 4.5 equations (4.88) - (4.90) and the effect of the load impedance on the values of these terms, it can be said that the smaller the load impedance at multiples of the switching frequency, the larger their value. Thus, the larger the values of the λ-terms, the larger their sum, leading to the Gerschgorin circles' centre-points moving further to the left of the complex plane. The opposite is also true, i.e. the larger the load impedance at multiples of the switching frequency, the smaller the values of the λ-terms and the smaller their sums. This means that the Gerschgorin circles' centre-points move closer to the origin of the complex plane, i.e. to the right in the left-hand side of the plane. The closer the centre-points of the Gerschgorin circles are to the origin of the complex plane, the higher the probability of the existence of a pole on the right-hand side of the complex plane. Another aspect of the specific case of 4-cells and $D = 0.5$, is that this value of duty-cycle causes the harmonics of the $S_d(\omega)$ terms to be zero at specific multiples of the switching frequency, which results in a smaller corresponding λ-term. This case is discussed in more detail in Chapter 3 section 3.3.3 and Chapter 4 section 4.6.

In comparison, for the case of a 4-cell converter under sinusoidal modulation the unbalance decays. The reason for this is that the groups of harmonics are more spread out resulting in a smaller probability of a λ-term becoming zero. This means that the unbalance in a sinusoidally modulated converter is more probable to decay than for a corresponding number of cells under fixed duty-cycle PWM.

This corresponds to the differences observed between the case without a balance booster and the case with a balance booster. The unbalance decays much faster for the case with the balance booster than the case without, as the balance booster lowers the load impedance considerably at the switching frequency.

5.5 Summary

The time constants of a multicell converter were calculated for the 2- and 3-cell cases. The time constants could not be calculated directly for the p-cell case. However, the poles of the system were approximated by calculating the spectral radius and the Gerschgorin circles of the matrix resulting from the system of differential equations. This was done successfully and applied in the examples shown in sections 5.3 and 5.4.

The time constant of a 2-cell multicell converter was calculated in section 5.2 equation (5.19) to be the following:

$$\tau = \frac{C}{2Re\left\{\lambda_1\right\}} \tag{5.76}$$

The time constants of a 3-cell multicell converter was calculated in section 5.3 equation (5.49) to be the following:

$$\tau_1 = -\frac{1}{Re\{\varepsilon_1\}} \quad \text{and} \quad \tau_2 = -\frac{1}{Re\{\varepsilon_2\}} \tag{5.77}$$

where ε_1 and ε_2 are the respective eigenvalues of $-\frac{1}{C}2Re\{\mathbf{\Lambda}\}$.

The poles of a p-cell multicell converter were approximated in section 5.4 equation (5.71) to lie within the circle defined by the spectral radius of the matrix $-\frac{1}{C}2Re\{\mathbf{\Lambda}\}$ as follows:

$$\rho\left(-\frac{1}{C}2Re\{\mathbf{\Lambda}\}\right) \leq \frac{p}{C}\max\left\{\left|\lambda_1+\overline{\lambda_{p-1}}\right|,\left|\lambda_2+\overline{\lambda_{p-2}}\right|,\ldots,\left|\lambda_{p-1}+\overline{\lambda_1}\right|\right\} \tag{5.78}$$

It was also found that the matrix $-\frac{1}{C}2Re\{\mathbf{\Lambda}\}$ has a Toeplitz structure [6], [14] for $p \geq 4$ which may be used to find an analytical solution of the eigenvalues. This is a topic for future work.

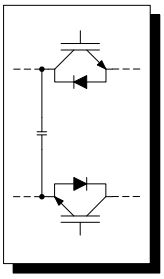

Chapter 6

Theory verification

6.1 Introduction

The aim of this chapter is to verify the theory that was proposed in the previous chapters. A Matlab® "Designtool" was developed by implementing the theory which was developed in the preceding chapters.

A number of multicell converter configurations were simulated in Simplorer® and in Matlab® using the "Designtool". The results obtained are presented and compared in this chapter.

The same converter configurations were also tested experimentally with modular "Powercell" multicell converter building blocks developed by the author. More information on the "Powercell" building blocks is included in Appendix C. A photo showing a "Powercell" is shown in Figure 6-1.

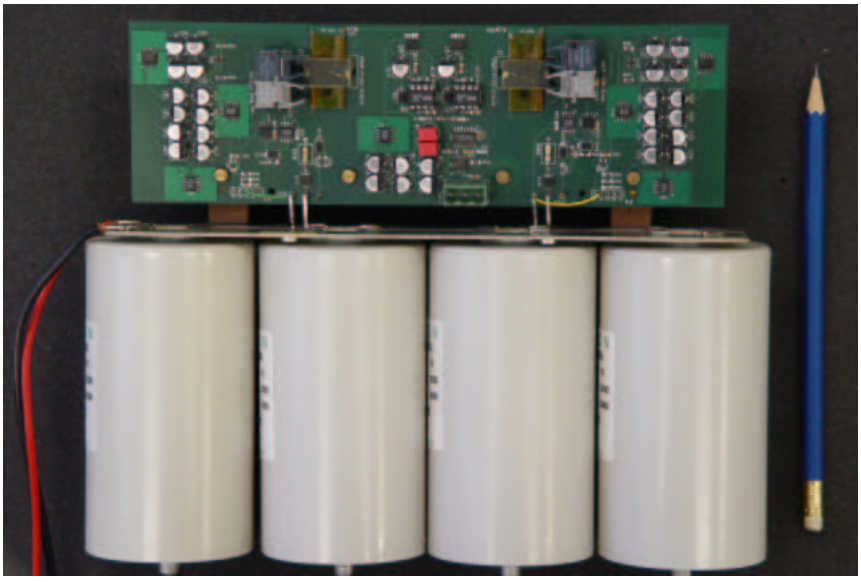

Figure 6-1. *The modular "Powercell" multicell converter building block.*

The same experimental configurations were also simulated in Matlab® using the "Designtool". These results are compared later in this chapter.

The multicell converter used in the simulations as well as in the experimental setup is shown for the general case of p cells in Figure 6-2. The same converter parameters are used for all the cases discussed in this chapter unless otherwise stated. The converter parameters are listed in Table 6.1.

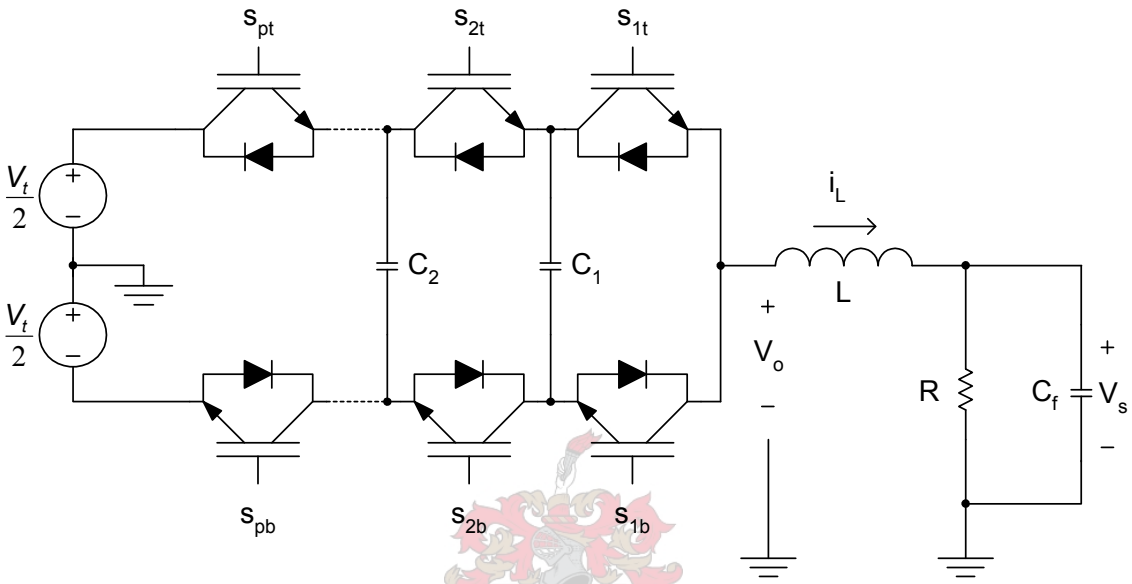

Figure 6-2. *The p-cell multicell converter.*

Table 6.1. *Multicell converter parameters*

V_t	$50\ V$
C_i, $i = 1, \ldots, p-1$	$40\ \mu F$
L	$200\ \mu H$
C_f	$50\ \mu F$
R	$10\ \Omega$
L_{bb}	$237\ \mu H$
C_{bb}	$4.3\ \mu F$
R_{bb}	$2.2\ \Omega$
R_{loss}	$26\ \Omega$
f_s	$5\ kHz$

This chapter is divided into 3 main sections as follows:

(a) Simulation with a current source load: only the 2-cell case is considered in this section.

(b) Simulation of the unbalance decay in a multicell converter: 2-, 3- and 4-cell converters are considered for both the sinusoidal modulation and fixed duty-cycle PWM cases for different values of m_a and D.

(c) Experimental measurements of voltage balance in multicell converters: 2-, 3- and 4-cell converters are considered for both the sinusoidal modulation and fixed duty-cycle PWM cases for different values of m_a and D.

(d) Harmonic measurements of the unfiltered output voltage of multicell converters: 2-, 3- and 4-cell converters are considered for sinusoidal modulation with $m_a = 0.6$ and different load conditions.

6.2 Simulation with a current source load

A 2-cell multicell inverter is configured using the parameters listed in Table 6.1. The load as shown in Figure 6-2 is replaced with a $50\ Hz$ current source load with an amplitude of $15\ A$. The converter is switched using sinusoidal modulation with $m_a = 0.5$ and $f_r = 50\ Hz$. The initial cell capacitor voltage is zero.

The reason for choosing a current source as load is that in theory a current source has infinite impedance. This will not result in natural balancing of the cell capacitor voltage. The results are shown in Figure 6-3 and confirm what was expected.

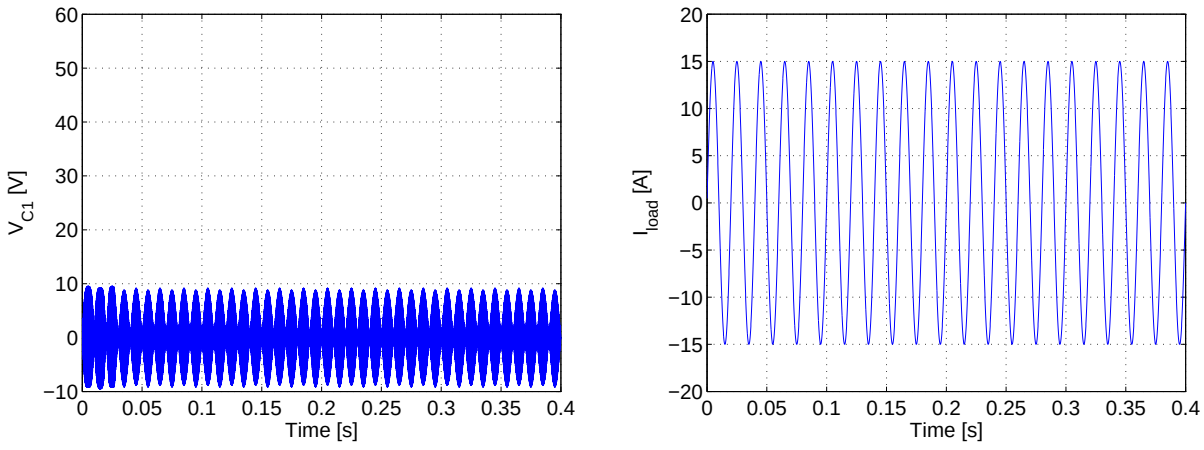

(a) (b)

Figure 6-3. *Simulation results showing the cell capacitor voltage and the current source load of a 2-cell multicell converter.*

The cell capacitor voltage is shown in Figure 6-3(a). This voltage does not charge to its desired voltage, it oscillates around zero as it charges and discharges.

The current of the current source load is shown in Figure 6-3(b).

6.3 Simulation of the unbalance decay in a multicell converter

This section is devoted to the simulation of the unbalance decay in 2-, 3- and 4-cell converters for both sinusoidal modulation and fixed duty-cycle modulation. The converter configuration is as shown in Figure 6-2 with the parameters as in Table 6.1. The same converter configuration is used for all the numbers of cells.

In this section the initial cell capacitor voltages are set according to the following formula:

$$V_{C_{0i}} = \frac{i \cdot V_t}{p} \quad \text{for } i = 1, \ldots, p \tag{6.1}$$

where $V_{C_{0i}}$ is the initial voltage of the i^{th} cell capacitor. After obtaining these values, the input voltage V_t of the converter is set to zero in the simulation package so that the decay of the unbalance can be simulated. Simulation time-steps are set very small in order to minimise numeric losses.

The voltage unbalance decay was simulated in Simplorer® and in Matlab®. Each case was simulated in 2 configurations: one without a balance booster connected and the other with a balance booster circuit connected in parallel with the load, as shown in Chapter 2 section 2.2 Figure 2-3. The balance booster is designed to resonate at the switching frequency and its parameters are listed in Table 6.1. The same balance booster is used whenever mentioned unless otherwise stated.

6.3.1 Unbalance decay of the 2-cell multicell converter

The simulated unbalance decay of a 2-cell multicell converter is shown and compared in this section for both sinusoidal modulation and fixed duty-cycle PWM.

For the 2-cell case the initial cell capacitor voltage is as follows: $V_{C_{01}} = 25\ V$ as $V_t = 50\ V$.

(a) Sinusoidal modulation: the sinusoidal reference frequency is $f_r = 50\ Hz$. Figure 6-4 contains the results for the following values of m_a: 0.6, 0.8 and 1.0.

It can be observed in Figure 6-4 that the unbalance V_d decays slower as the modulation index m_a is increased. This is true with and without a balance booster connected in parallel to the load. The theoretical results obtained with Matlab® are shown in red while the Simplorer® results are shown in blue. The theoretical results are a good approximation for this case.

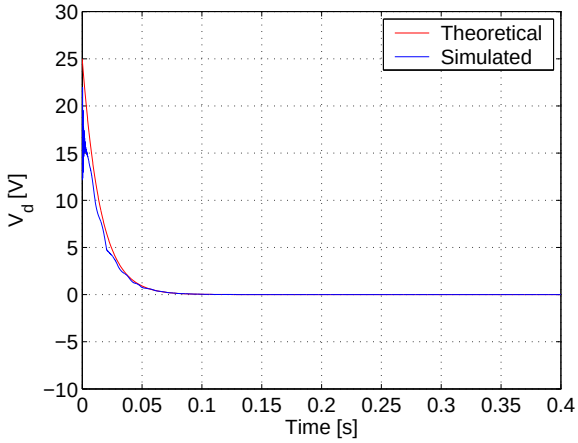

(a) $m_a = 0.6$: without balance booster

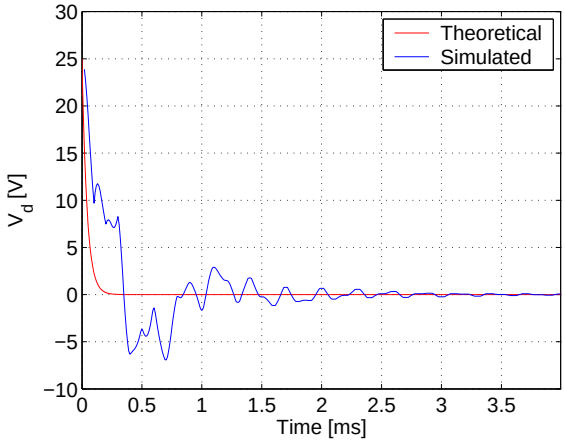

(b) $m_a = 0.6$: with balance booster

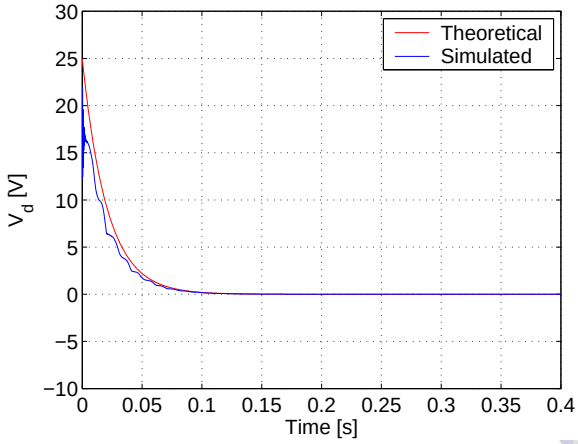

(c) $m_a = 0.8$: without balance booster

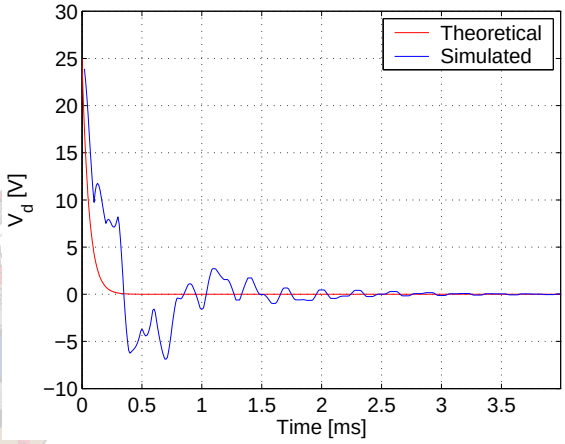

(d) $m_a = 0.8$: with balance booster

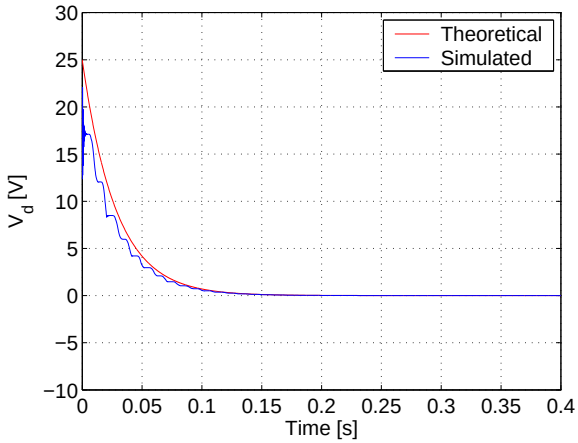

(e) $m_a = 1.0$: without balance booster

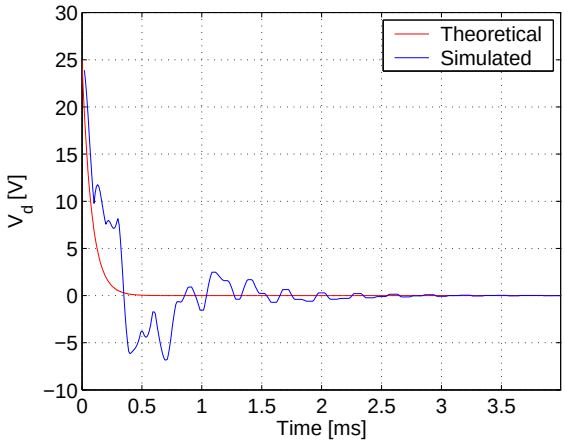

(f) $m_a = 1.0$: with balance booster

Figure 6-4. *The cell voltage unbalance decay of a 2-cell multicell converter with* $f_r = 50\ Hz$ *and* $f_s = 5\ kHz$.

(b) Fixed duty-cycle PWM: the switching frequency is $f_s = 5\ kHz$. Figure 6-5 shows the unbalance decay for the following values of D: 0.25 and 0.5.

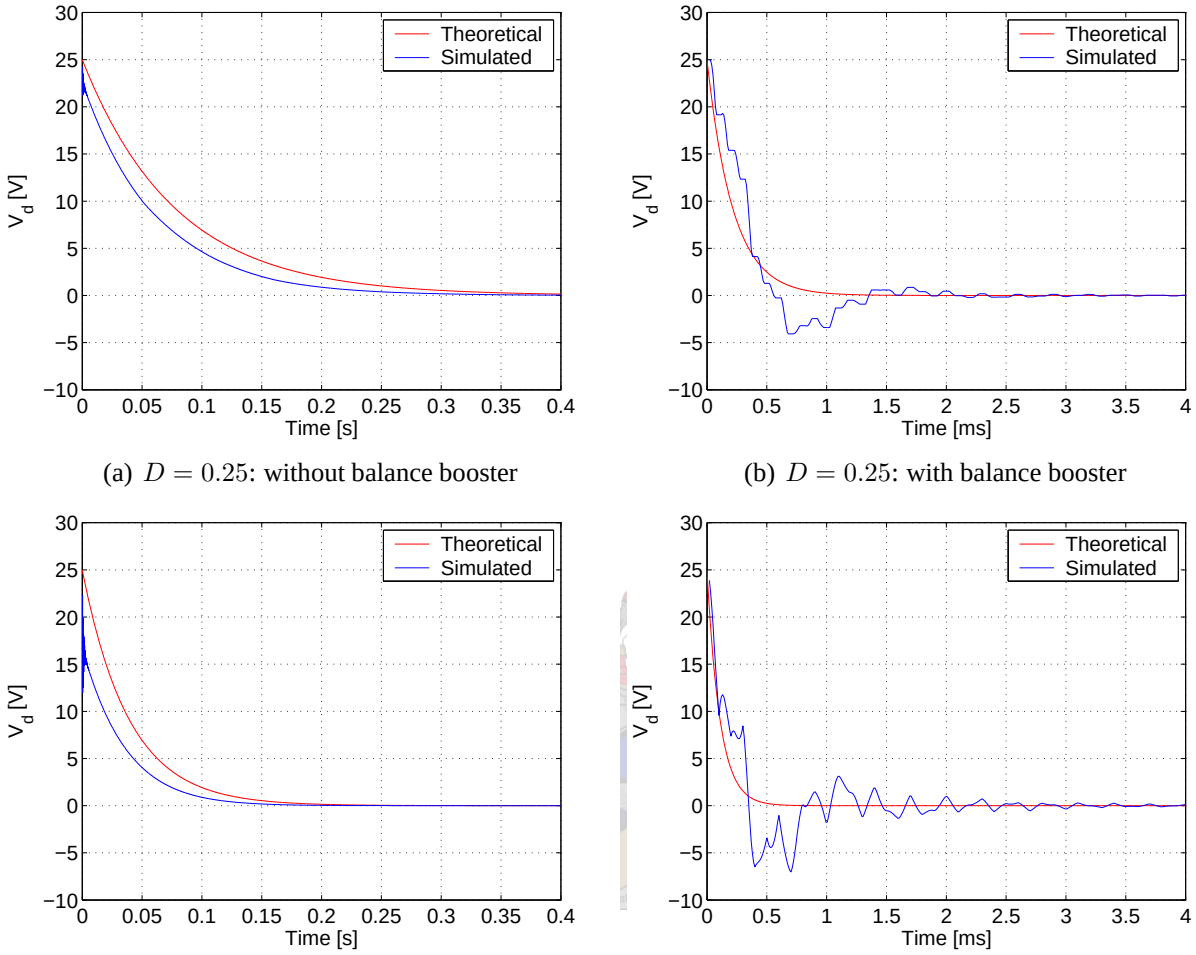

(a) $D = 0.25$: without balance booster

(b) $D = 0.25$: with balance booster

(c) $D = 0.5$: without balance booster

(d) $D = 0.5$: with balance booster

Figure 6-5. *The cell voltage unbalance decay of a 2-cell multicell converter with* $f_s = 5\ kHz$.

It can be seen in Figure 6-5 that the unbalance V_d decays slower as the duty-cycle D is increased. This is true with and without a balance booster connected in parallel to the load. The theoretical results obtained with Matlab® are shown in red while the Simplorer® results are shown in blue. The theoretical results are still a good approximation for this case, but can be improved.

6.3.2 Unbalance decay of the 3-cell multicell converter

The simulated unbalance decay of a 3-cell multicell converter is shown and compared in this section for both sinusoidal modulation and fixed duty-cycle PWM.

For the 3-cell case the initial cell capacitor voltages are as follows: $V_{C_{01}} = 16.67\ V$ and $V_{C_{02}} = 33.33\ V$ as $V_t = 50\ V$.

(a) Sinusoidal modulation: the sinusoidal reference frequency is $f_r = 50\ Hz$. Figure 6-6 shows the results for the following values of m_a: 0.6, 0.8 and 1.0.

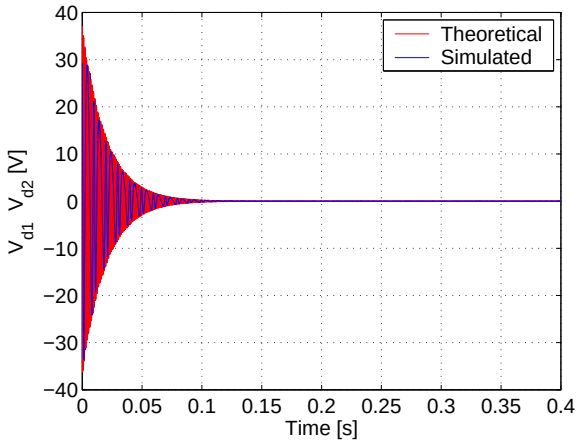

(a) $m_a = 0.6$: without balance booster

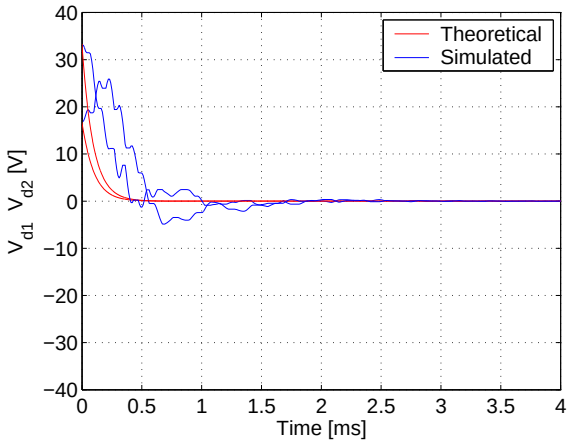

(b) $m_a = 0.6$: with balance booster

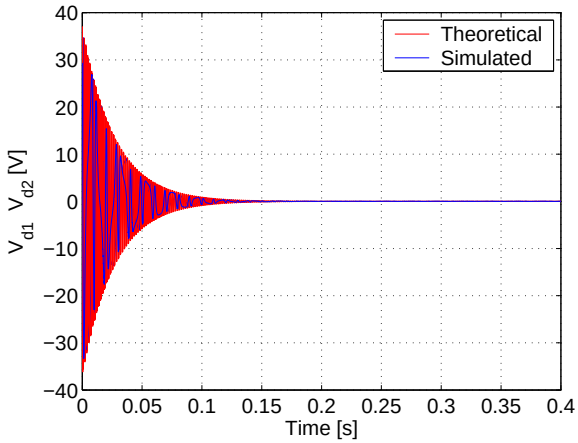

(c) $m_a = 0.8$: without balance booster

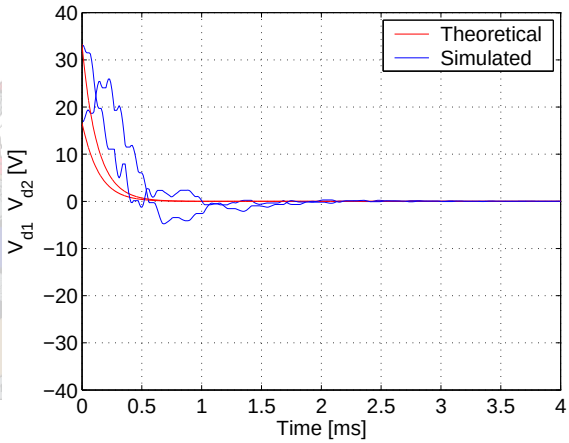

(d) $m_a = 0.8$: with balance booster

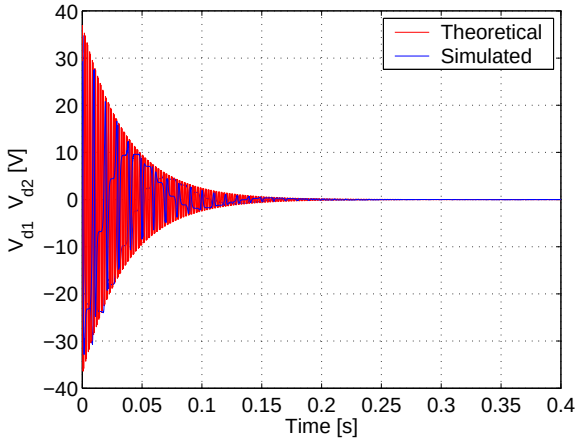

(e) $m_a = 1.0$: without balance booster

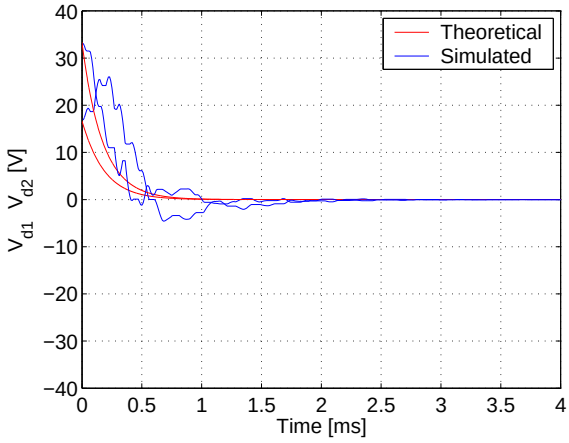

(f) $m_a = 1.0$: with balance booster

Figure 6-6. *The cell voltage unbalance decay of a 3-cell multicell converter with* $f_r = 50\ Hz$ *and* $f_s = 5\ kHz$.

It is clear from Figure 6-6 that the unbalance V_{d_1} and V_{d_2} decay slower as the modulation index m_a is increased. This is also true with and without a balance booster connected in parallel to the load. The theoretical results obtained with Matlab® are shown in red while the Simplorer® results are shown in blue. The theoretical results are a good approximation for the case without a balance booster connected. The approximation is poorer for the case when a balance booster is connected. This is due to the limitations of the model as it was assumed that the unbalance decays slowly compared with the rest of the system.

(b) Fixed duty-cycle PWM: the switching frequency is $f_s = 5\ kHz$. The results shown in Figure 6-7 are for the following values of D: 0.33 and 0.5.

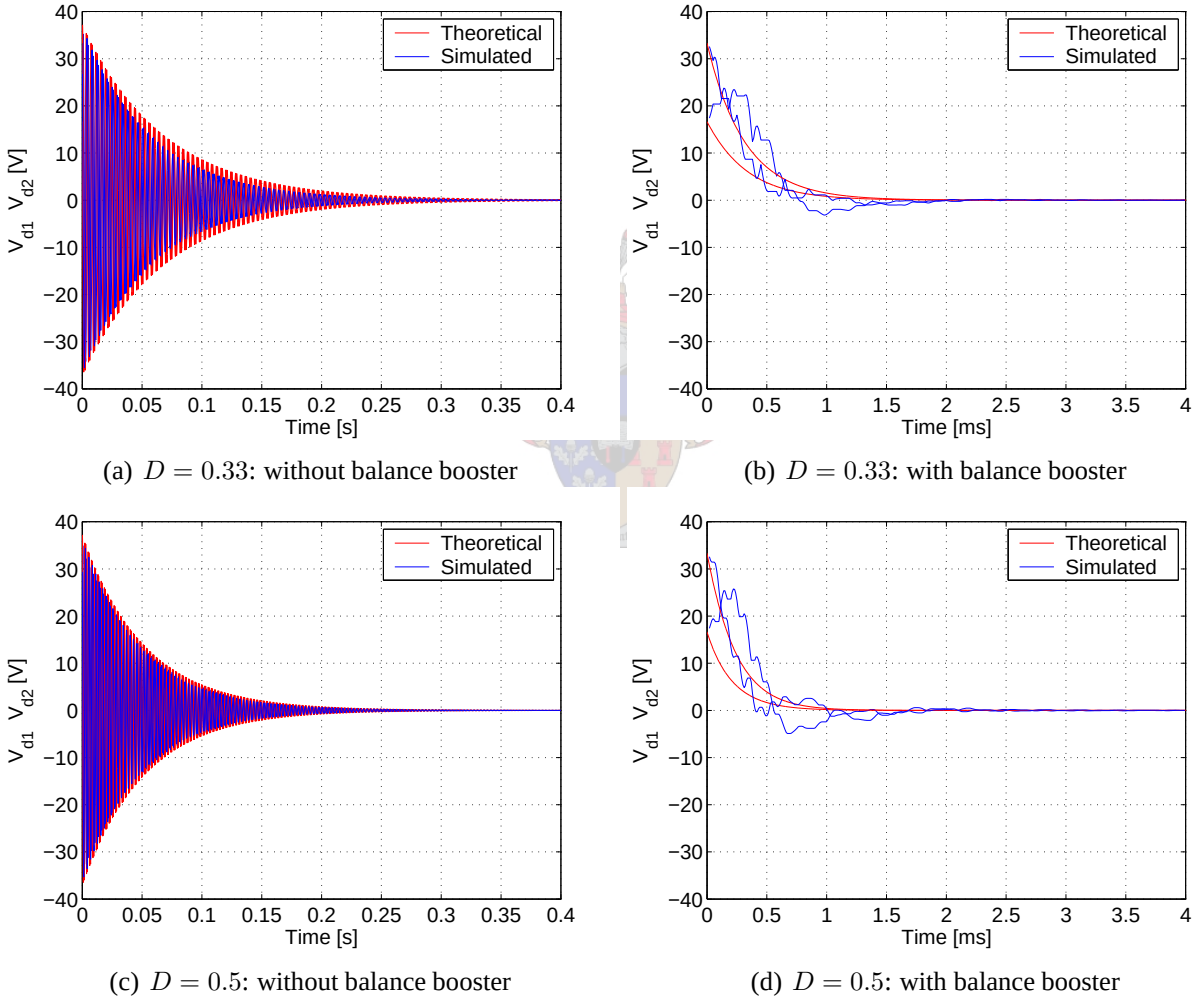

(a) $D = 0.33$: without balance booster

(b) $D = 0.33$: with balance booster

(c) $D = 0.5$: without balance booster

(d) $D = 0.5$: with balance booster

Figure 6-7. *The cell voltage unbalance decay of a 3-cell multicell converter with* $f_s = 5\ kHz$.

For this case it can be seen in Figure 6-7 that the unbalance V_{d_1} and V_{d_2} decay slower as the duty-cycle D is increased. This is true with and without a balance booster connected in parallel to the load. The theoretical results obtained with Matlab® are shown in red while the Simplorer® results are shown in blue. The theoretical results are still a good approximation for the case

without a balance booster, but as for the sinusoidal modulation case, the approximation is poorer when a balance booster is connected. The reason for this is the same as for the sinusoidal modulation case with a balance booster connected.

6.3.3 Unbalance decay of the 4-cell multicell converter

The simulated unbalance decay of a 4-cell multicell converter is shown and compared in this section for both sinusoidal modulation and fixed duty-cycle PWM.

For the 4-cell case the initial cell capacitor voltages are as follows: $V_{C_{01}} = 12.5\ V$, $V_{C_{02}} = 25\ V$ and $V_{C_{03}} = 37.5\ V$ as $V_t = 50\ V$.

(a) Sinusoidal modulation: the sinusoidal reference frequency is $f_r = 50\ Hz$. The results obtained are shown in Figure 6-8 for the following values of m_a: 0.6, 0.8 and 1.0.

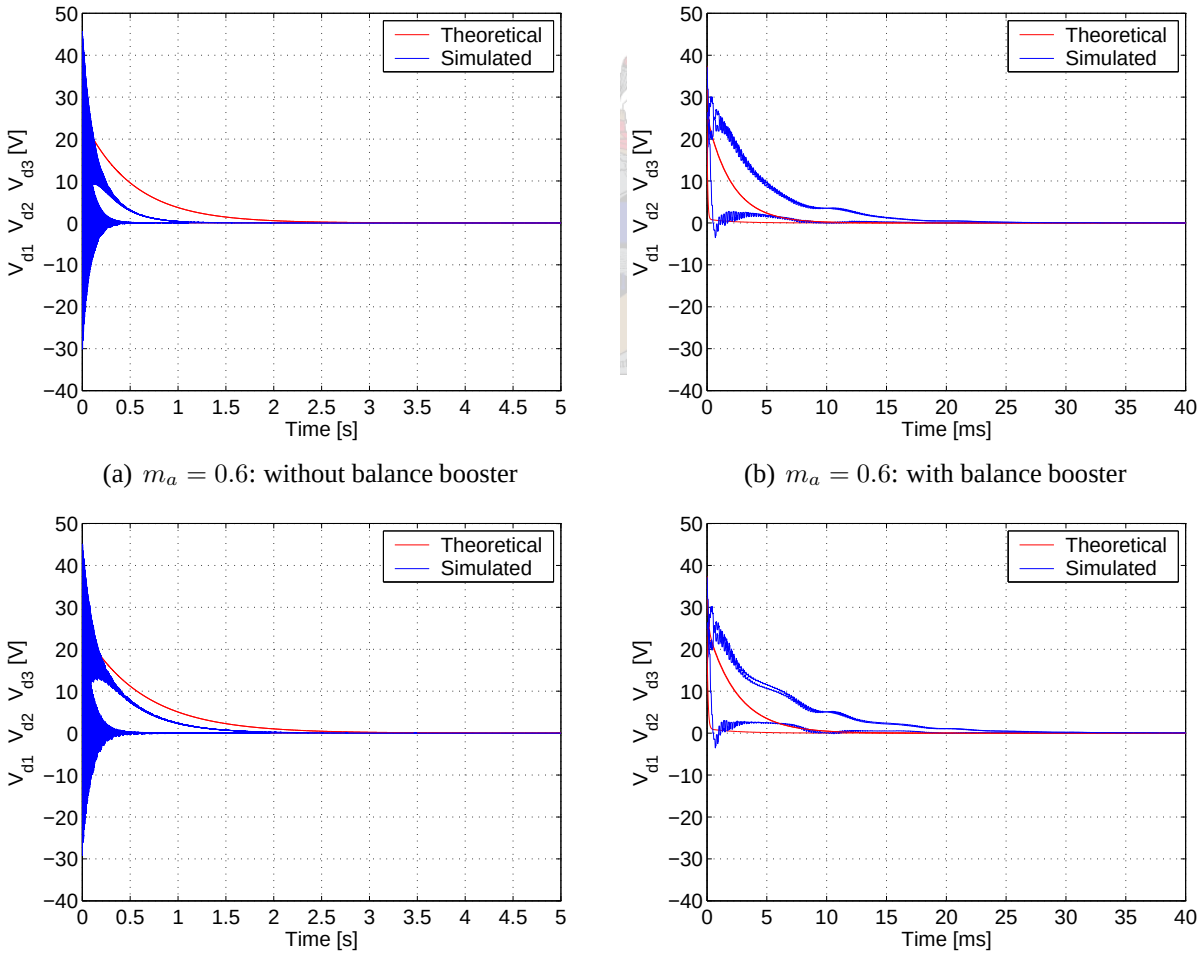

(a) $m_a = 0.6$: without balance booster

(b) $m_a = 0.6$: with balance booster

(c) $m_a = 0.8$: without balance booster

(d) $m_a = 0.8$: with balance booster

Figure 6-8. *The cell voltage unbalance decay of a 4-cell multicell converter with $f_r = 50\ Hz$ and $f_s = 5\ kHz$.*

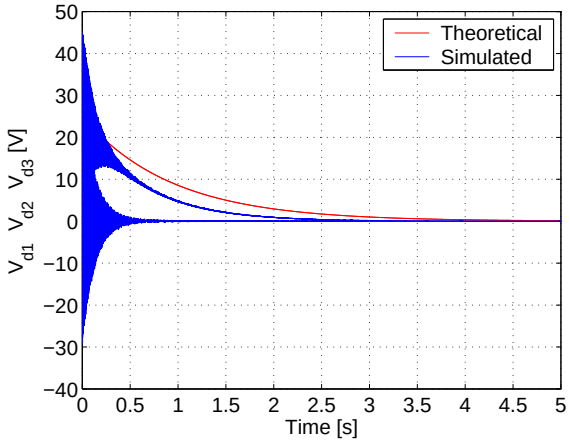

(e) $m_a = 1.0$: without balance booster

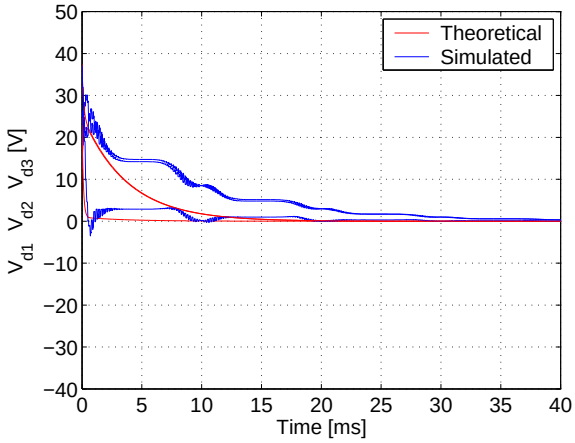

(f) $m_a = 1.0$: with balance booster

Figure 6-8. *The cell voltage unbalance decay of a 4-cell multicell converter with $f_r = 50\ Hz$ and $f_s = 5\ kHz$ (cont.).*

It is clear from Figure 6-8 that the unbalance V_{d_1}, V_{d_2} and V_{d_3} also decay slower as the modulation index m_a is increased. This is true with and without a balance booster connected in parallel to the load. The theoretical results obtained with Matlab® are shown in red while the Simplorer® results are shown in blue. The theoretical results and the simulated results differ even more for the 4-cell case than any of the previous cases discussed so far. The one reason for this can be due to the step sizes used in Simplorer®. It was found that the step sizes can have a significant effect on the simulation results, especially when using Euler integration. It was later found that more consistent results can be obtained by using Trapezoidal integration in Simplorer®. The other reason is that the assumptions of the theoretical model are not true anymore, resulting in a poorer approximation.

(b) Fixed duty-cycle PWM: the switching frequency is $f_s = 5\ kHz$. The results obtained are shown in Figure 6-9 for the following values of D: 0.25 and 0.5.

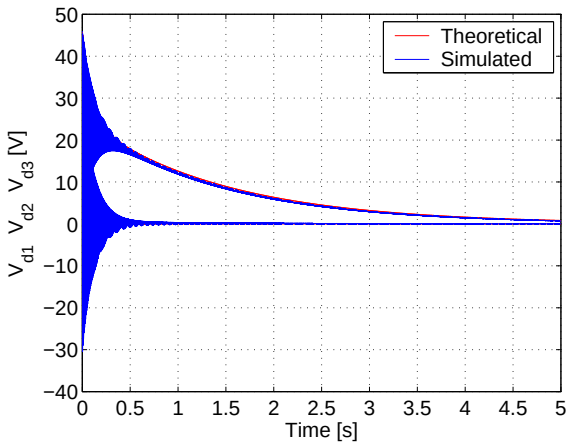

(a) $D = 0.25$: without balance booster

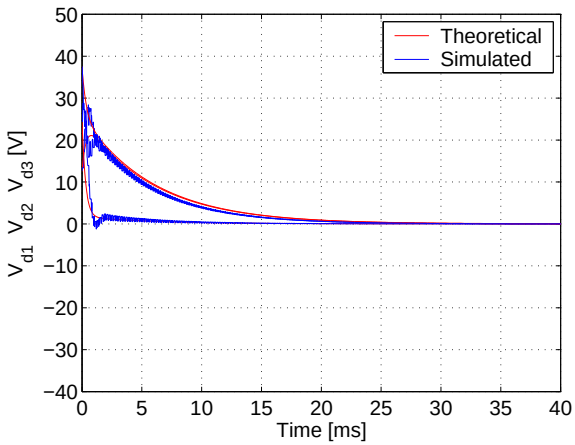

(b) $D = 0.25$: with balance booster

Figure 6-9. *The cell voltage unbalance decay of a 4-cell multicell converter with $f_s = 5\ kHz$.*

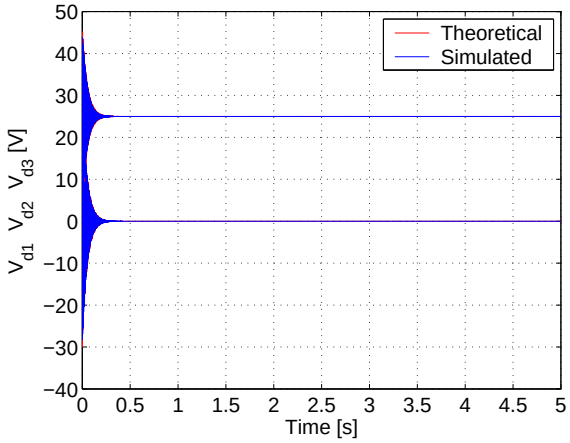

(c) $D = 0.5$: without balance booster

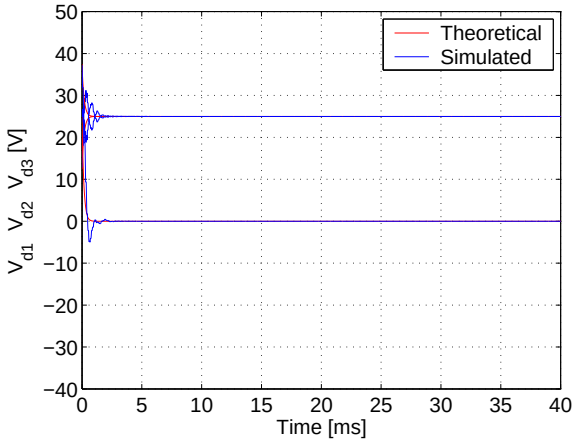

(d) $D = 0.5$: with balance booster

Figure 6-9. *The cell voltage unbalance decay of a 4-cell multicell converter with $f_s = 5\ kHz$ (cont.).*

For this case it can be seen in Figure 6-9(a) that the unbalance V_{d_1}, V_{d_2} and V_{d_3} decay much slower than for the previous cases with fewer cells. This result was obtained using the Trapezoidal integration option in Simplorer® and it is clear that the theoretical and simulated results correspond very well. This is true for the case without a balance booster as well as the case with a balance booster connected. It is clear from Figure 6-9(c) that all the unbalance does not decay and that the unbalance over some of the capacitors remains. It can be seen in Figure 6-9(d) that even the addition of a balance booster does not remove the unbalance. This case for $p = 4$ and $D = 0.5$ is a special case which results in unbalance when $D = 0.5$. This case is discussed in more detail in Chapter 4 section 4.6 and in Chapter 5 section 5.4. The theoretical results obtained with Matlab® are shown in red while the Simplorer® results are shown in blue. The theoretical results for this case are a very good approximation for the cases with and without a balance booster.

6.4 Experimental measurements of voltage balance in multicell converters

This section focusses on measuring the cell capacitor voltage balance in 2-, 3- and 4-cell converters experimentally for both sinusoidal modulation and fixed duty-cycle modulation. The converter configuration is as shown in Figure 6-2 with the parameters as in Table 6.1 except that the inductor has a measured inductance of $L = 219\ \mu H$ and a resistance of $R_{loss} = 26\ \Omega$. These measured values are used in the simulation in Matlab® with the "Designtool". This simulation is compared with the experimental results in order to establish if the results obtained with the "Designtool" can be used as a good approximation of the real results. The gating signals were generated with an FPGA-based modulator on the "PEC31" DSP-based controller board [37]. The modulator was designed and implemented by C.H. Hansmann. The same experimental configuration is used for all the numbers of cells. For the measurements in this section the initial cell capacitor voltages are set to zero by

Table 6.2. *Measurement equipment*

Oscilloscope	Tektronix® TDS 3014B
Voltage probes	Tektronix® P3010
Differential voltage probes	Tektronix® P5205
	Tektronix® P5200
True RMS Multimeter	Fluke® 79III

physically shorting the cell capacitors and opening the short-circuit when the input bus voltage is at the appropriate voltage, i.e. $V_t = 50\ V$. When the cell capacitor voltages reach steady-state, they should be equal to the values determined by the following formula:

$$V_{C_i} = \frac{i \cdot V_t}{p} \quad \text{for } i = 1, \ldots, p \tag{6.2}$$

where V_{C_i} is the i^{th} cell capacitor voltage.

The experimental results were taken for 2 configurations: one without a balance booster connected and the other with a balance booster circuit connected in parallel with the load, as shown in Chapter 2 section 2.2 Figure 2-3. The same balance booster is used here as mentioned in the previous section. The equipment used in obtaining the experimental results are listed in Table 6.2. A photo of the experimental setup is shown in Figure 6-10.

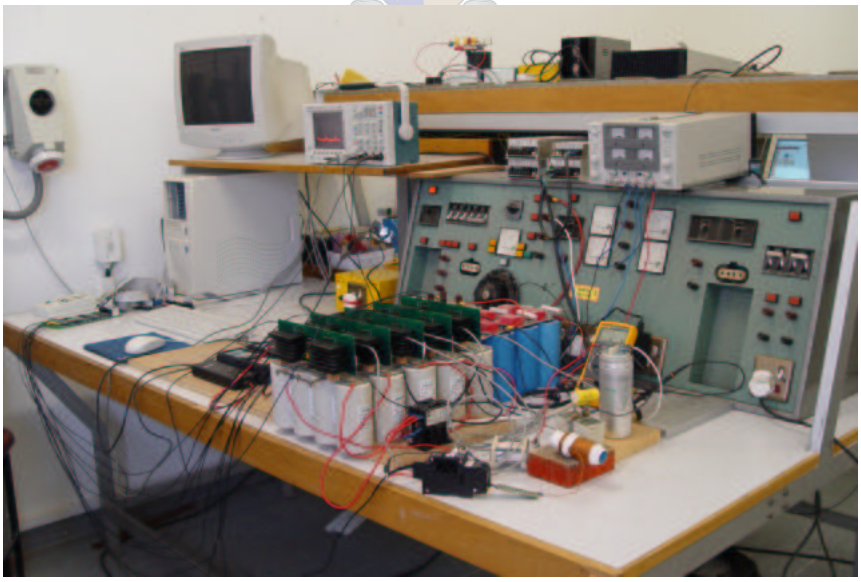

Figure 6-10. *The experimental setup.*

6.4.1 Voltage balance of the 2-cell multicell converter

The measured voltage balance of a 2-cell multicell converter is shown and compared in this section for both sinusoidal modulation and fixed duty-cycle PWM.

(a) Sinusoidal modulation: the sinusoidal reference frequency is $f_r = 50\ Hz$. The measured results are shown in Figure 6-11 for the following values of m_a: 0.6, 0.8 and 1.0.

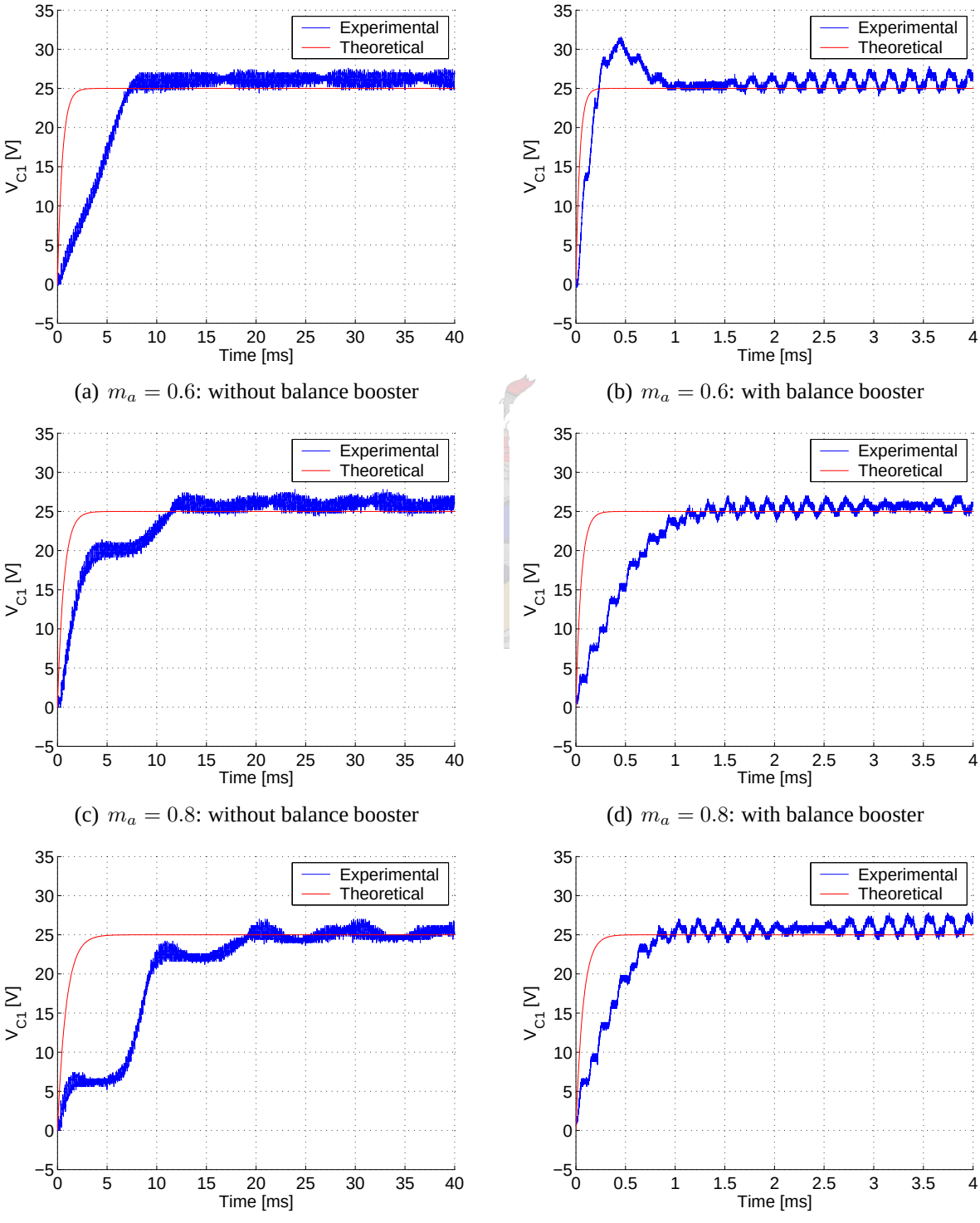

(a) $m_a = 0.6$: without balance booster

(b) $m_a = 0.6$: with balance booster

(c) $m_a = 0.8$: without balance booster

(d) $m_a = 0.8$: with balance booster

(e) $m_a = 1.0$: without balance booster

(f) $m_a = 1.0$: with balance booster

Figure 6-11. *Voltage balance of a 2-cell multicell converter with $f_r = 50\ Hz$ and $f_s = 5\ kHz$.*

It is clear from Figure 6-11 that the cell capacitor voltage V_{C_1} balances. It can also be seen that the voltage balances slower as the modulation index m_a is increased. This is true with and without a balance booster connected in parallel to the load. The theoretical results obtained with Matlab® are shown in red while the experimental results are shown in blue. The theoretical results and the experimental results differ significantly. One of the reasons for this is due to the fact that the sampling effect of the digital modulator used is not taken into account in Matlab®. Another reason is that dead-time is also not taken into account in the "Designtool". The final reason is that the assumption of the theoretical model, i.e. that the cell capacitor voltages change slow with respect to the rest of the circuit is not true anymore.

(b) Fixed duty-cycle PWM: the switching frequency is $f_s = 5\ kHz$. The measured results obtained are shown in Figure 6-12 for the following values of D: 0.25 and 0.5.

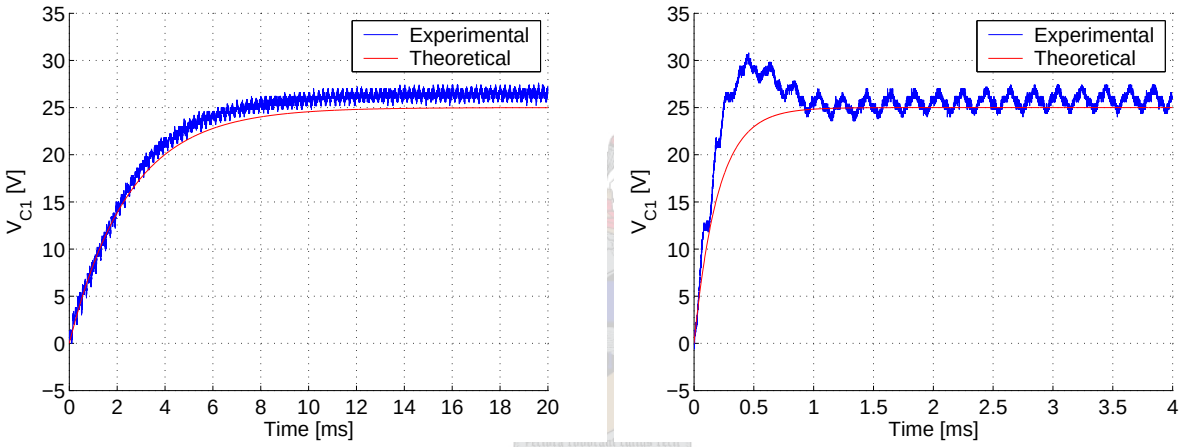

(a) $D = 0.25$: without balance booster

(b) $D = 0.25$: with balance booster

(c) $D = 0.5$: without balance booster

(d) $D = 0.5$: with balance booster

Figure 6-12. *Voltage balance of a 2-cell multicell converter with $f_s = 5\ kHz$.*

For this case it can be seen in Figure 6-12 that cell capacitor voltage V_{C_1} balances faster as the duty-cycle D is increased for the case without a balance booster as well as the case with

a balance booster connected. The theoretical results obtained with Matlab® are shown in red while the measured results are shown in blue. It is clear from Figure 6-12 that the theoretical approximation for the fixed duty-cycle PWM case is much better than for the sinusoidal modulation case. Thus, the "Designtool" gives a good approximation of the cell capacitor voltage balance for the fixed duty-cycle PWM case.

6.4.2 Voltage balance of the 3-cell multicell converter

The measured voltage balance of a 3-cell multicell converter is shown and compared in this section for both sinusoidal modulation and fixed duty-cycle PWM.

(a) Sinusoidal modulation: the sinusoidal reference frequency is $f_r = 50\ Hz$. The measured results obtained are shown in Figure 6-13 for the following values of m_a: 0.6, 0.8 and 1.0.

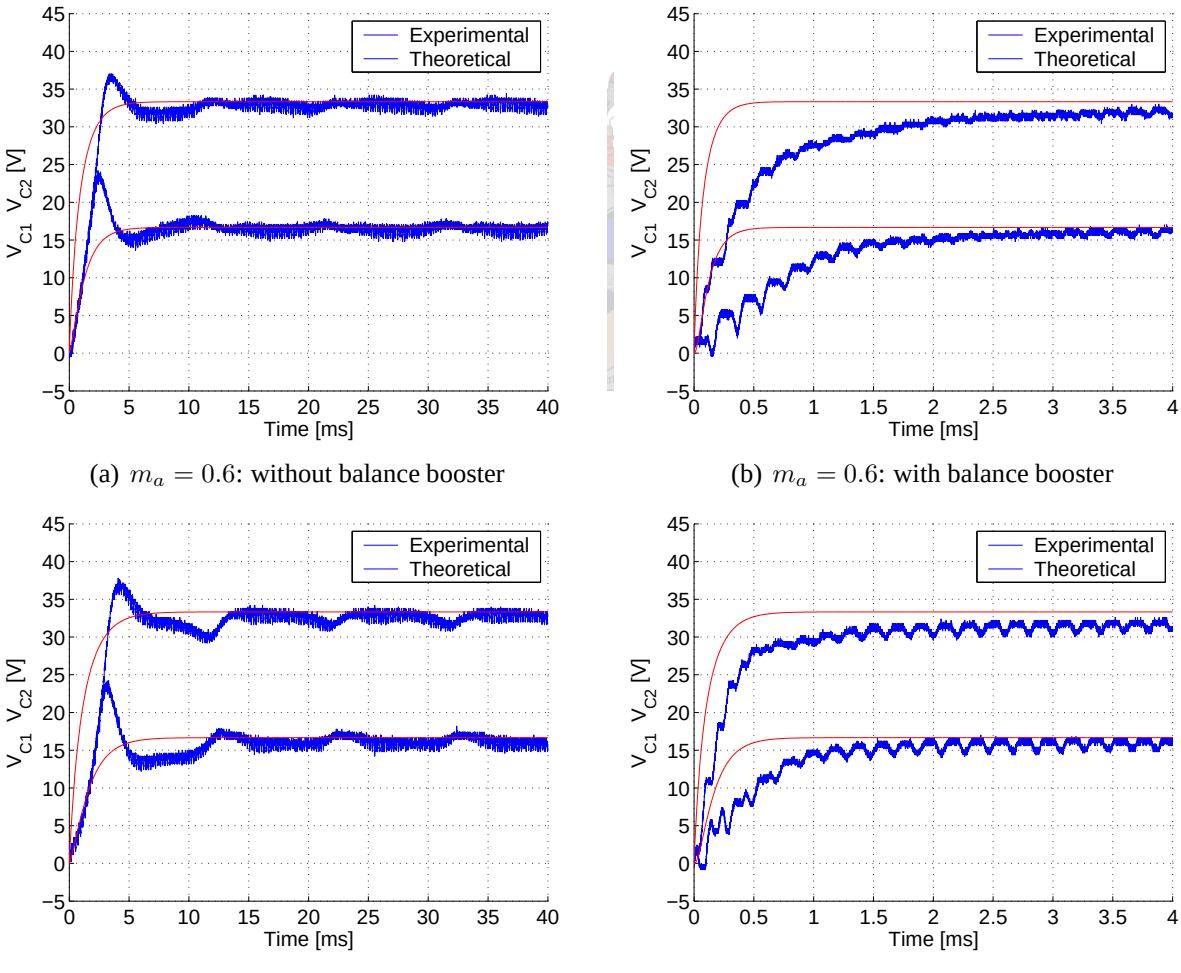

(a) $m_a = 0.6$: without balance booster

(b) $m_a = 0.6$: with balance booster

(c) $m_a = 0.8$: without balance booster

(d) $m_a = 0.8$: with balance booster

Figure 6-13. *Voltage balance of a 3-cell multicell converter with $f_r = 50\ Hz$ and $f_s = 5\ kHz$.*

It is clear from Figure 6-13 that the cell capacitor voltages V_{C_1} and V_{C_2} balance. It can also be seen that the voltage balances slower as the modulation index m_a is increased. This is true

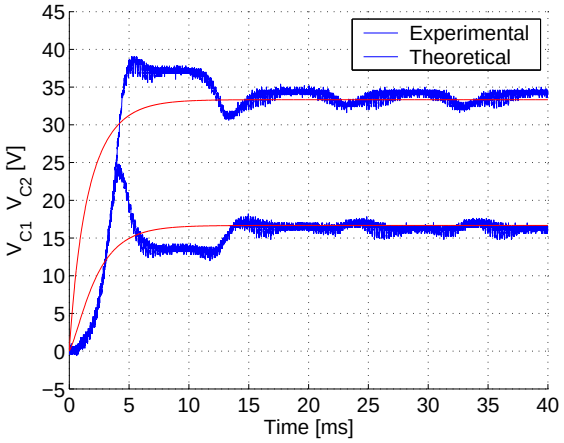

(e) $m_a = 1.0$: without balance booster

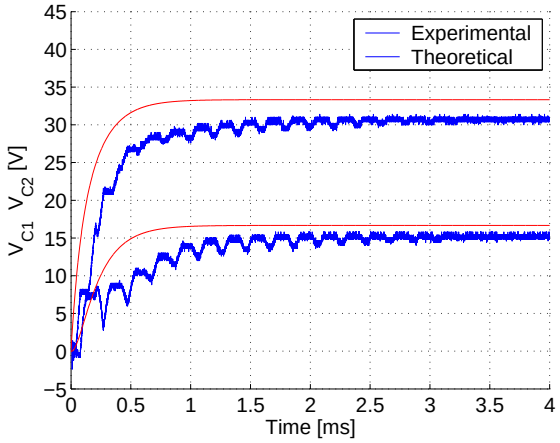

(f) $m_a = 1.0$: with balance booster

Figure 6-13. *Voltage balance of a 3-cell multicell converter with $f_r = 50\ Hz$ and $f_s = 5\ kHz$ (cont.).*

with and without a balance booster connected in parallel to the load. The theoretical results obtained with Matlab® are shown in red while the experimental results are shown in blue. The theoretical results and the experimental results differ significantly, especially for the case where a balance booster is connected in parallel to the load. For the case without a balance booster connected, the results obtained with Matlab® approximates the envelope around which the measured results vary. The reason for the theoretical results following the envelope of the measured result is due to the assumption of the theoretical model, i.e. that the cell capacitor voltages change slowly with respect to the rest of the circuit.

(b) Fixed duty-cycle PWM: the switching frequency is $f_s = 5\ kHz$. The measured results obtained are shown in Figure 6-14 for the following values of D: 0.33 and 0.5.

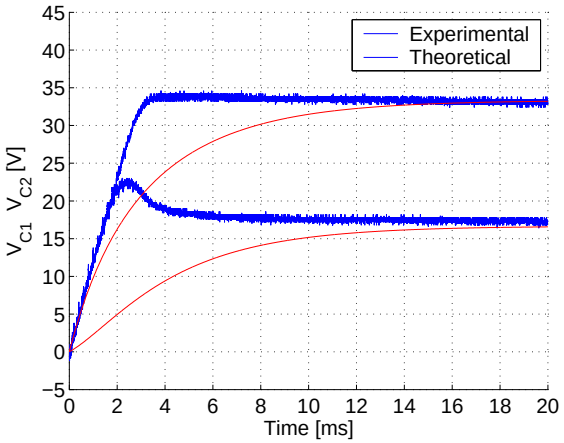

(a) $D = 0.33$: without balance booster

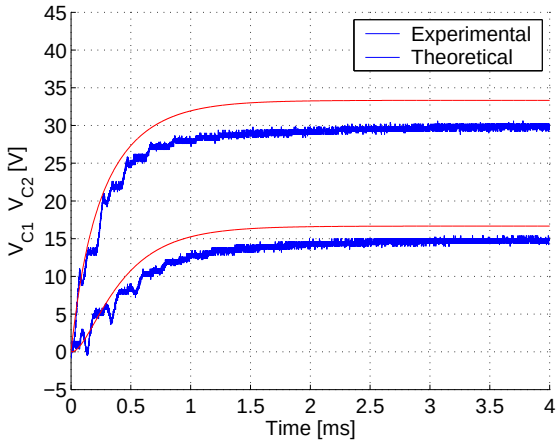

(b) $D = 0.33$: with balance booster

Figure 6-14. *Voltage balance of a 3-cell multicell converter with $f_s = 5\ kHz$.*

From Figure 6-14 it follows that the cell capacitor voltages V_{C_1} and V_{C_2} balance faster as D

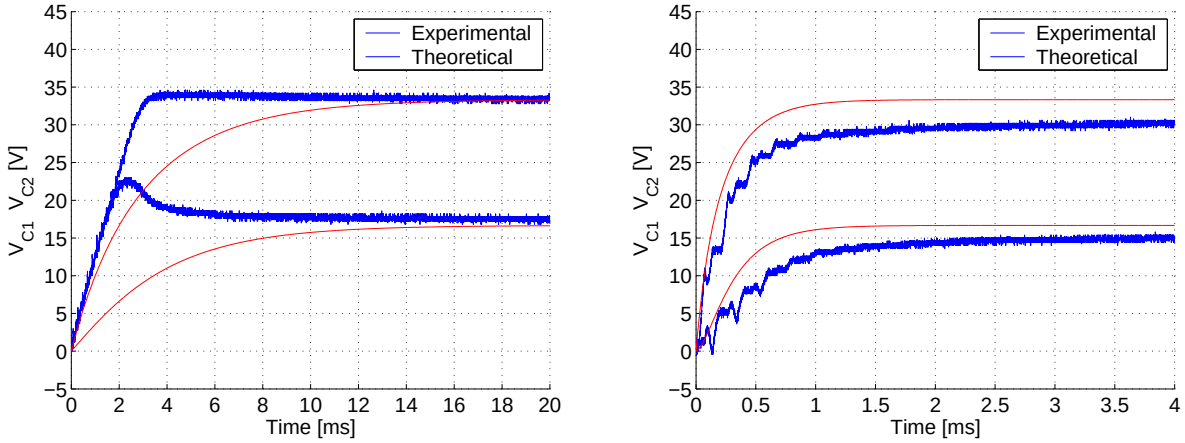

(c) $D = 0.5$: without balance booster (d) $D = 0.5$: with balance booster

Figure 6-14. *Voltage balance of a 3-cell multicell converter with $f_s = 5\ kHz$ (cont.).*

is increased for the case without a balance booster as well as the case with a balance booster connected. The theoretical results obtained are shown in red while the measured results are shown in blue. It is clear from Figure 6-14 that the theoretical results follow the envelope of the measured results. The final values of the measured results and the theoretical results obtained with the balance booster differ with a few volt. This is due to the "on"-state voltages across the IGBT devices in the experimental converter which were not accounted for in the "Designtool".

6.4.3 Voltage balance of the 4-cell multicell converter

The measured voltage balance of a 4-cell multicell converter is shown and compared in this section for both sinusoidal modulation and fixed duty-cycle PWM.

(a) Sinusoidal modulation: the sinusoidal reference frequency is $f_r = 50\ Hz$. The measured results obtained are shown in Figure 6-15 for the following values of m_a: 0.6, 0.8 and 1.0.

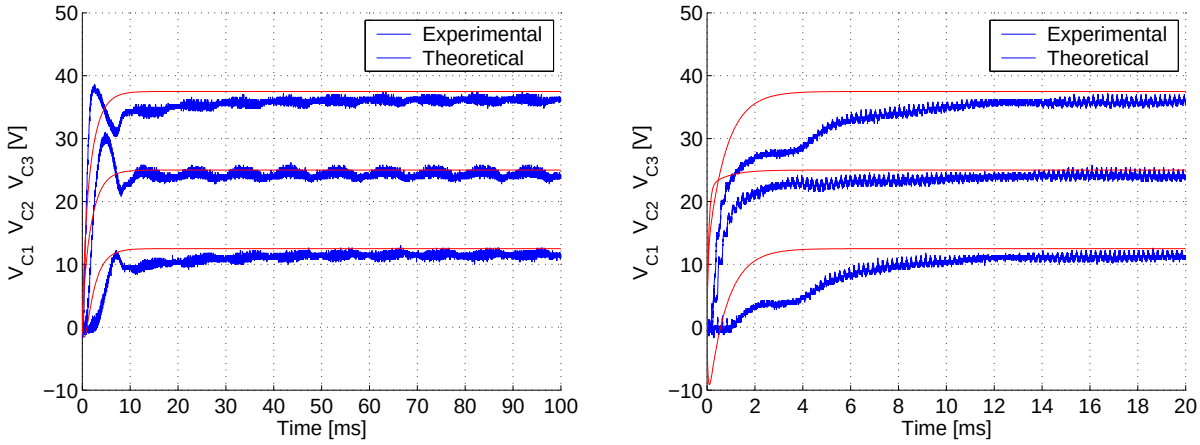

(a) $m_a = 0.6$: without balance booster (b) $m_a = 0.6$: with balance booster

Figure 6-15. *Voltage balance of a 4-cell multicell converter with $f_r = 50\ Hz$ and $f_s = 5\ kHz$.*

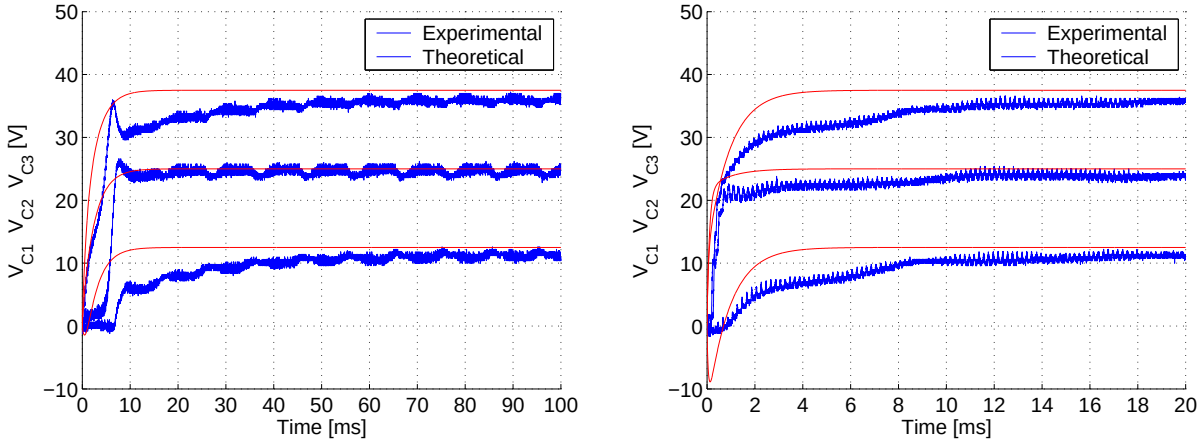

(c) $m_a = 0.8$: without balance booster

(d) $m_a = 0.8$: with balance booster

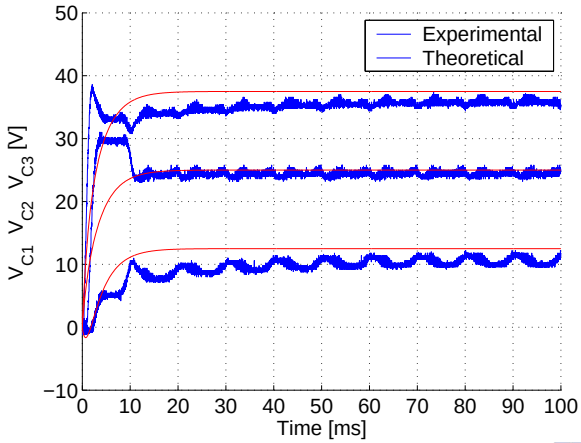

(e) $m_a = 1.0$: without balance booster

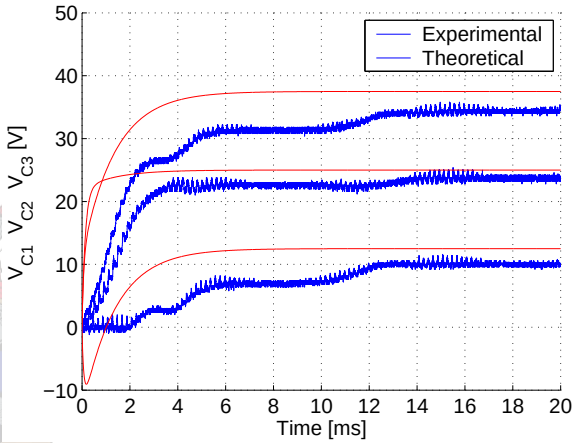

(f) $m_a = 1.0$: with balance booster

Figure 6-15. *Voltage balance of a 4-cell multicell converter with $f_r = 50\ Hz$ and $f_s = 5\ kHz$ (cont.).*

It is clear from Figure 6-15 that the cell capacitor voltages V_{C_1}, V_{C_2} and V_{C_3} balance roughly for the 4-cell case. It can also be seen that the voltage balances slower as the modulation index m_a is increased. This is true with and without a balance booster connected in parallel to the load. The theoretical results are shown in red while the experimental results are shown in blue. The theoretical results and the experimental results differ significantly, especially for the case where a balance booster is connected in parallel to the load. For the case without a balance booster connected, the results obtained with Matlab® approximates the envelope around which the measured results vary. The reason for the theoretical results following the envelope of the measured result is as mentioned in the previous section.

(b) Fixed duty-cycle PWM: the switching frequency is $f_s = 5\ kHz$ and results are shown for the following values of D: 0.25 and 0.5.

From Figure 6-16 it follows that the cell capacitor voltages V_{C_1}, V_{C_2} and V_{C_3} balance faster as D is increased for the case without a balance booster as well as the case with a balance

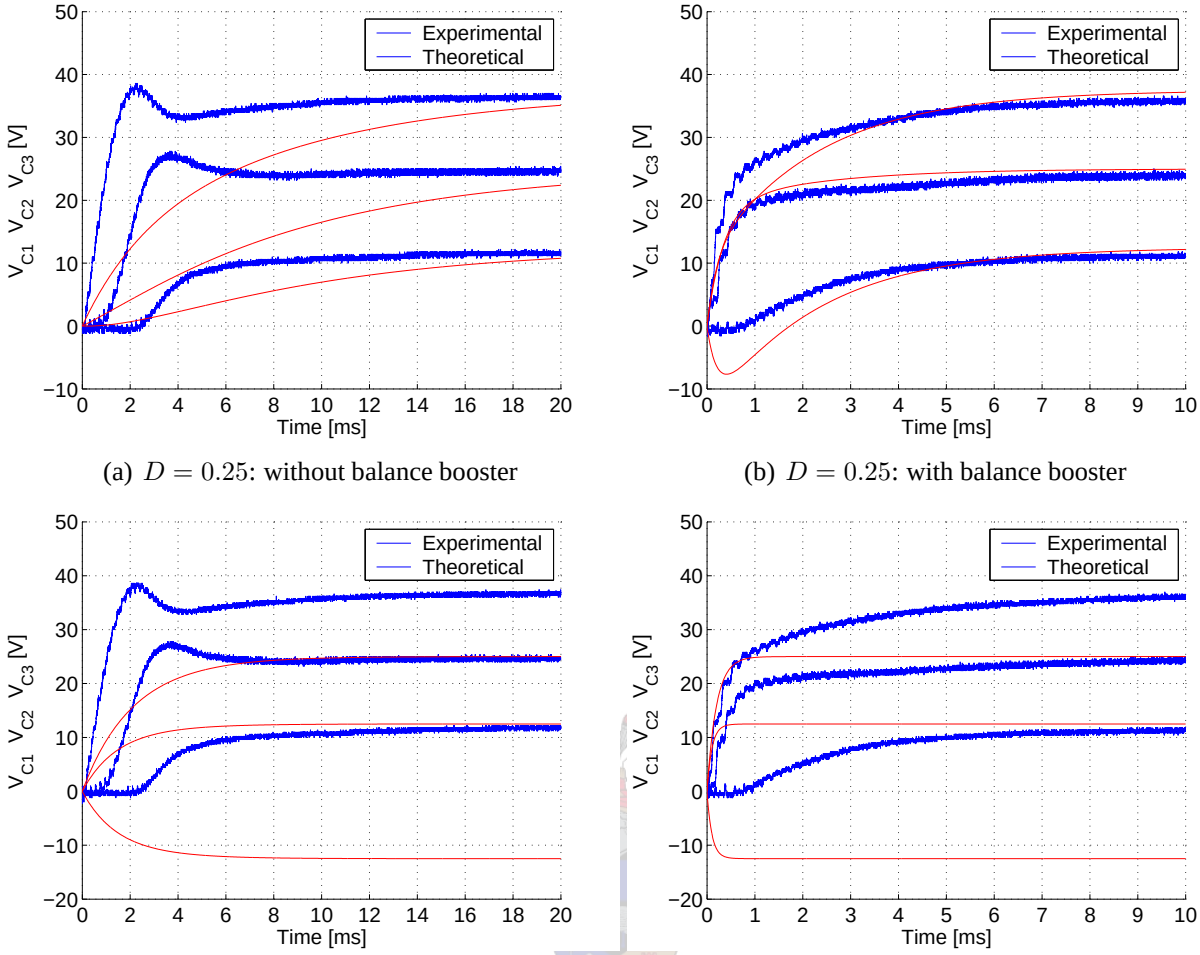

(a) $D = 0.25$: without balance booster

(b) $D = 0.25$: with balance booster

(c) $D = 0.5$: without balance booster

(d) $D = 0.5$: with balance booster

Figure 6-16. *Voltage balance of a 4-cell multicell converter with* $f_s = 5\ kHz$.

booster connected. It is interesting to note that the theoretical results show unbalance for the case of $D = 0.5$, as shown in Figures 6-16(c) and 6-16(d). The cell capacitor voltages of the experimental converter balance. The reason for this is due to the losses in the experimental converter. The theoretical model is based on the assumption that the converter is lossless. Even though the losses were approximated by adding a loss resistor in series with the load inductor, the theoretical results still do not balance. The reason for the unbalance in the theoretical results was mentioned in the previous section for the same case. The theoretical results obtained are shown in red while the measured results are shown in blue. For this case the theoretical results give a design guideline, as it can be used to show possible unbalance conditions which should be avoided.

6.5 Harmonic measurements

This section focusses on harmonic measurements of the unfiltered output voltage of 2-, 3- and 4-cell converters for sinusoidal modulation with $m_a = 0.6$ and $f_r = 50\ Hz$. The converter configuration is as shown in Figure 6-2 with the parameters as in Table 6.1. The same converter configuration is used

for all the numbers of cells.

The unfiltered output voltage is denoted as V_o in Figure 6-2. The harmonic measurements are obtained by performing a Fast Fourier Transform on the unfiltered output voltage. This is done using the built-in FFT-function of the oscilloscope used to take the measurements.

The harmonic measurements were taken for 3 cases for each number of cells:

(a) half-bridge/"single-cell" operation obtained by shorting all the cell capacitors except the bus capacitor of the outermost cell.

(b) multicell operation obtained by opening all the shorted cell capacitors.

(c) forced unbalance obtained by connecting a small resistor in parallel to one cell capacitor.

Each case was also measured in 2 configurations: one without a balance booster connected and the other with a balance booster circuit connected in parallel with the load, as shown in Chapter 2 section 2.2 Figure 2-3. The same balance booster is used as mentioned previously.

6.5.1 Harmonic measurements of the 2-cell multicell converter

The harmonic measurements of the unfiltered output voltage of a 2-cell multicell converter is shown and compared in this section for sinusoidal modulation for 3 types of operation.

(a) Half-bridge/"single-cell" operation: the sinusoidal reference frequency is $f_r = 50\ Hz$. The measured FFT results are shown in Figure 6-17 for $m_a = 0.6$.

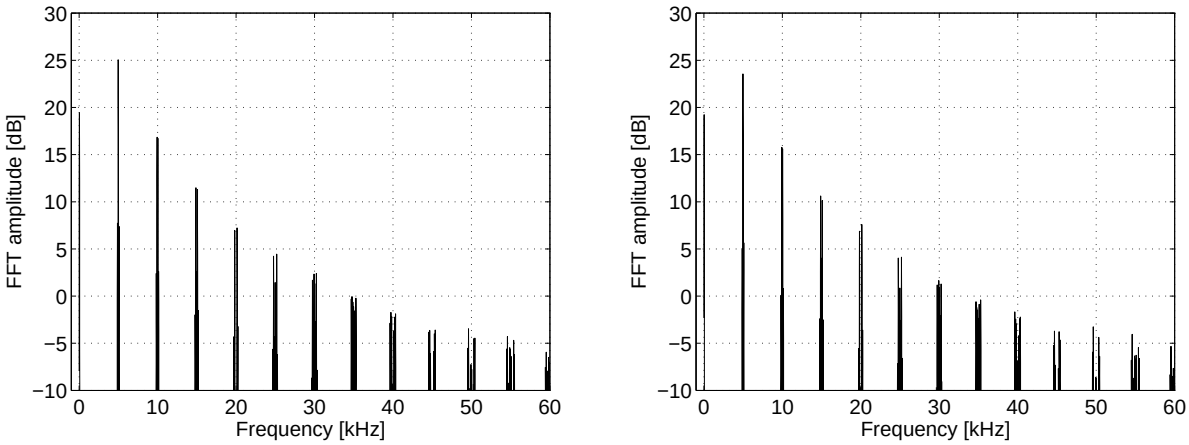

(a) $m_a = 0.6$: without balance booster (b) $m_a = 0.6$: with balance booster

Figure 6-17. *Half-bridge/"single-cell" operation of a 2-cell multicell converter with $f_s = 5\ kHz$.*

When all the cell capacitors are shorted except for the dc-bus capacitor, a 2-cell multicell converter is reduced to a half-bridge converter. This causes the first group of harmonics of the unfiltered output voltage to be centred around the switching frequency, i.e. $f_s = 5\ kHz$. The subsequent groups of harmonics are centred around further integer multiples of the switching frequency. The magnitude of the harmonic at $5\ kHz$ is $25\ dB$ for the case without a balance booster connected. When a balance booster which is designed to resonate at the switching frequency is connected in parallel with the load, the magnitude of this harmonic is reduced to $23.5\ dB$. Thus the addition of a balance booster reduces the main harmonic at $5\ kHz$ by $1.5\ dB$.

(b) Multicell operation: the sinusoidal reference frequency is $f_r = 50\ Hz$. The measured FFT results are shown in Figure 6-18 for $m_a = 0.6$.

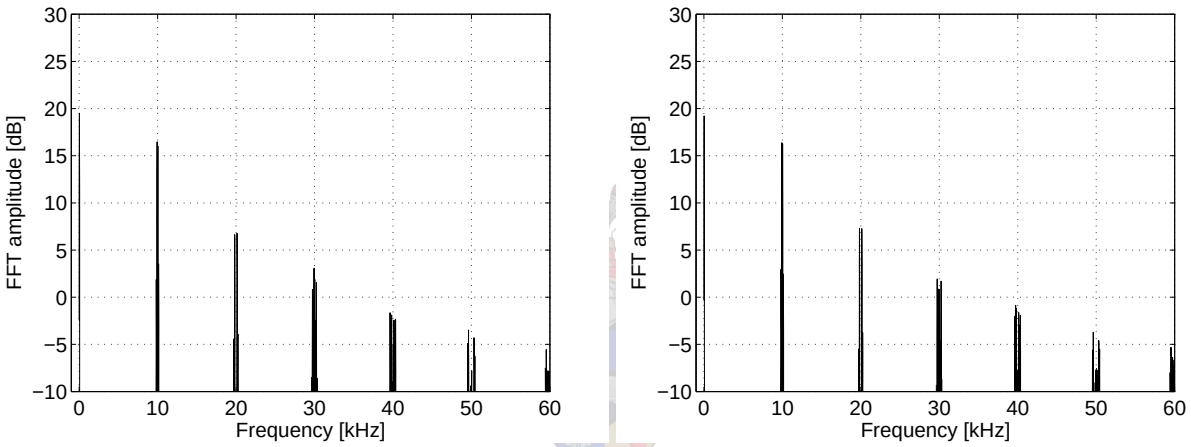

(a) $m_a = 0.6$: without balance booster (b) $m_a = 0.6$: with balance booster

Figure 6-18. *Multicell operation of a 2-cell multicell converter with $f_s = 5\ kHz$.*

When all the cell capacitors are connected the 2-cell multicell converter operates in full multicell operation. The first group of harmonics of the unfiltered output voltage is centred around 2 times the switching frequency, i.e. $2f_s = 10\ kHz$. The subsequent groups of harmonics are centred around further integer multiples of $2f_s$. The magnitude of the largest harmonic at $10\ kHz$ is $16.5\ dB$ for the case without a balance booster connected. When a balance booster which is designed to resonate at f_s is connected in parallel with the load, the magnitude of this harmonic is reduced to $16.4\ dB$. Thus the addition of a balance booster tuned to f_s does not reduce the main harmonic at $10\ kHz$ significantly. This harmonic is only reduced by $0.1\ dB$.

(c) Forced unbalance: the sinusoidal reference frequency is $f_r = 50\ Hz$. The measured FFT results are shown in Figure 6-19 for $m_a = 0.6$.

When a small resistor is connected in parallel to the cell capacitor, the multicell converter is forced into an unbalanced state. A $22\ \Omega$ resistor was used to introduce this unbalance. For the 2-cell case, the converter is effectively forced into a pseudo half-bridge operation. The

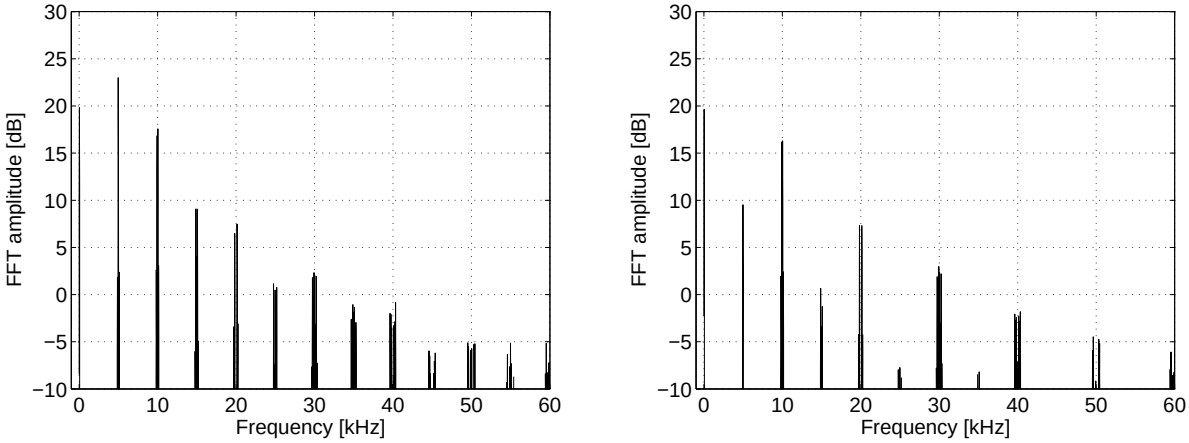

(a) $m_a = 0.6$: without balance booster (b) $m_a = 0.6$: with balance booster

Figure 6-19. *Forced unbalance of a 2-cell multicell converter with $f_s = 5\ kHz$.*

first group of harmonics of the unfiltered output voltage is again centred around the switching frequency, i.e. $f_s = 5\ kHz$ instead of $2f_s$ for conventional multicell operation. The subsequent groups of harmonics are centred around further integer multiples of f_s. The magnitude of the largest harmonic at $5\ kHz$ is $23\ dB$ for the case without a balance booster connected. When a balance booster which is designed to resonate at f_s is connected in parallel with the load, the magnitude of this harmonic is reduced to $9.5\ dB$. Thus the addition of a balance booster tuned to f_s reduces the main harmonic at $5\ kHz$ by $13.5\ dB$. This is a significant reduction, but the unbalance was not eliminated.

6.5.2 Harmonic measurements of the 3-cell multicell converter

The harmonic measurements of the unfiltered output voltage of a 3-cell multicell converter is shown and compared in this section for sinusoidal modulation for 3 types of operation.

(a) Half-bridge/"single-cell" operation: the sinusoidal reference frequency is $f_r = 50\ Hz$. The measured FFT results are shown in Figure 6-20 for $m_a = 0.6$.

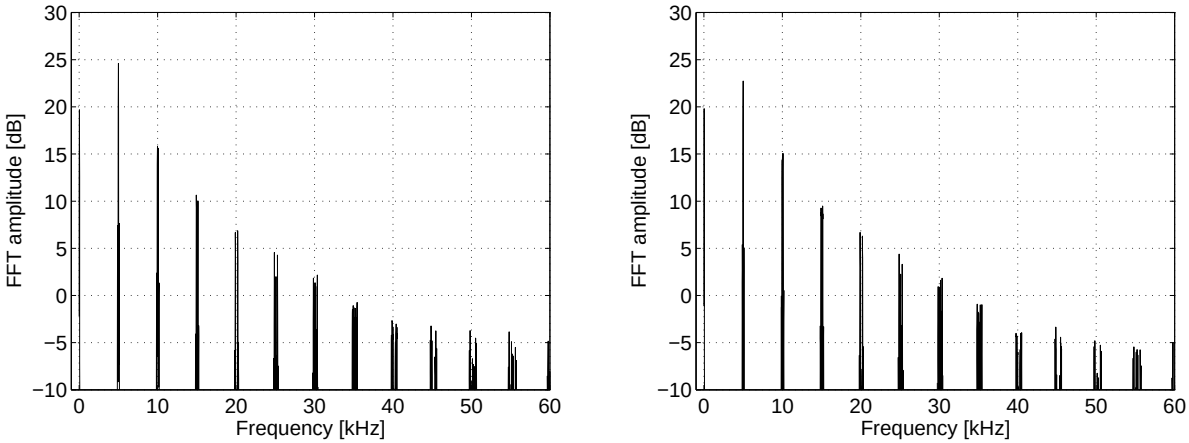

(a) $m_a = 0.6$: without balance booster (b) $m_a = 0.6$: with balance booster

Figure 6-20. *Half-bridge/"single-cell" operation of a 3-cell multicell converter with $f_s = 5\ kHz$.*

When all the cell capacitors are shorted except for the dc-bus capacitor, a 3-cell multicell converter is effectively reduced to a half-bridge converter. This causes the first group of harmonics of the unfiltered output voltage to be centred around the switching frequency, i.e. $f_s = 5\ kHz$. The subsequent groups of harmonics are centred around further integer multiples of the switching frequency. The magnitude of the largest harmonic at $5\ kHz$ is $24.5\ dB$ for the case without a balance booster connected. When a balance booster which is designed to resonate at the switching frequency is connected in parallel with the load, the magnitude of this harmonic is reduced to $22.7\ dB$, which implies a reduction of $1.8\ dB$.

(b) Multicell operation: the sinusoidal reference frequency is $f_r = 50\ Hz$. The measured FFT results are shown in Figure 6-21 for $m_a = 0.6$.

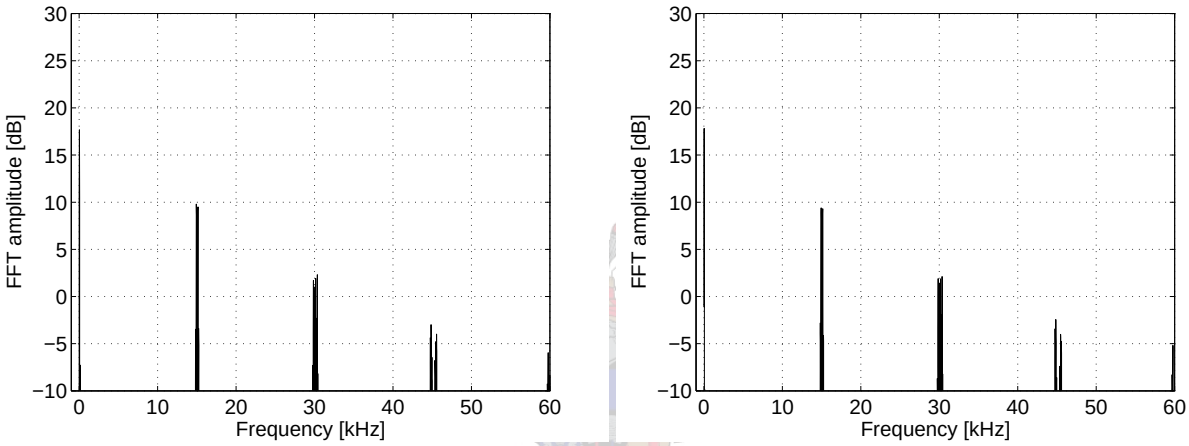

(a) $m_a = 0.6$: without balance booster (b) $m_a = 0.6$: with balance booster

Figure 6-21. *Multicell operation of a 3-cell multicell converter with $f_s = 5\ kHz$.*

When all the cell capacitors are connected the 3-cell multicell converter operates in full multicell operation. The first group of harmonics of the unfiltered output voltage is centred around 3 times the switching frequency, i.e. $3f_s = 15\ kHz$. The subsequent groups of harmonics are centred around further integer multiples of $3f_s$. The magnitude of the largest harmonic at $15\ kHz$ is $9.7\ dB$ for the case without a balance booster connected. When a balance booster which is designed to resonate at f_s is connected in parallel with the load, the magnitude of this harmonic is reduced to $9.4\ dB$. Thus the addition of a balance booster tuned to f_s does not reduce the main harmonic at $15\ kHz$ significantly. This harmonic is only reduced by $0.3\ dB$.

(c) Forced unbalance: the sinusoidal reference frequency is $f_r = 50\ Hz$. The measured FFT results are shown in Figure 6-22 for $m_a = 0.6$.

When a small resistor is connected in parallel to one of the cell capacitors the multicell converter is forced into an unbalanced state. A $22\ \Omega$ resistor was used to introduce this unbalance. For the 3-cell case, the converter is also effectively forced into a pseudo half-bridge operation. The first group of harmonics of the unfiltered output voltage is again centred around the switching

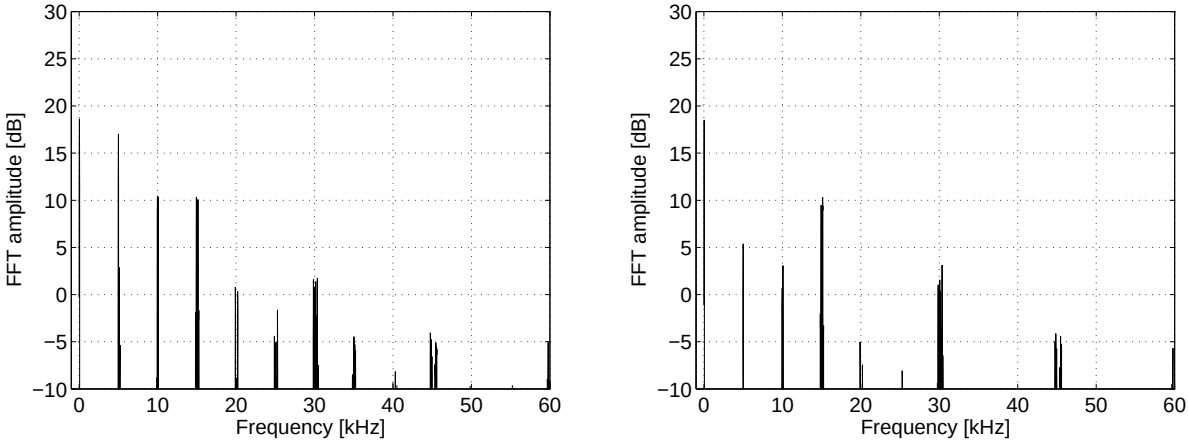

(a) $m_a = 0.6$: without balance booster (b) $m_a = 0.6$: with balance booster

Figure 6-22. *Forced unbalance of a 3-cell multicell converter with $f_s = 5\ kHz$.*

frequency, i.e. $f_s = 5\ kHz$ instead of $3f_s$ for conventional 3-cell multicell operation. The subsequent groups of harmonics are centred around further integer multiples of f_s. The magnitude of the largest harmonic at $5\ kHz$ is $17\ dB$ for the case without a balance booster connected. When a balance booster which is designed to resonate at f_s is connected in parallel with the load, the magnitude of this harmonic is reduced to $5.5\ dB$. Thus the addition of a balance booster tuned to f_s reduces this harmonic at $5\ kHz$ by $11.5\ dB$. This is a significant reduction, but the unbalance was not eliminated.

6.5.3 Harmonic measurements of the 4-cell multicell converter

The harmonic measurements of the unfiltered output voltage of a 4-cell multicell converter is shown and compared in this section for sinusoidal modulation for 4 types of operation.

(a) Half-bridge/"single-cell" operation: the sinusoidal reference frequency is $f_r = 50\ Hz$. The measured FFT results are shown in Figure 6-23 for $m_a = 0.6$.

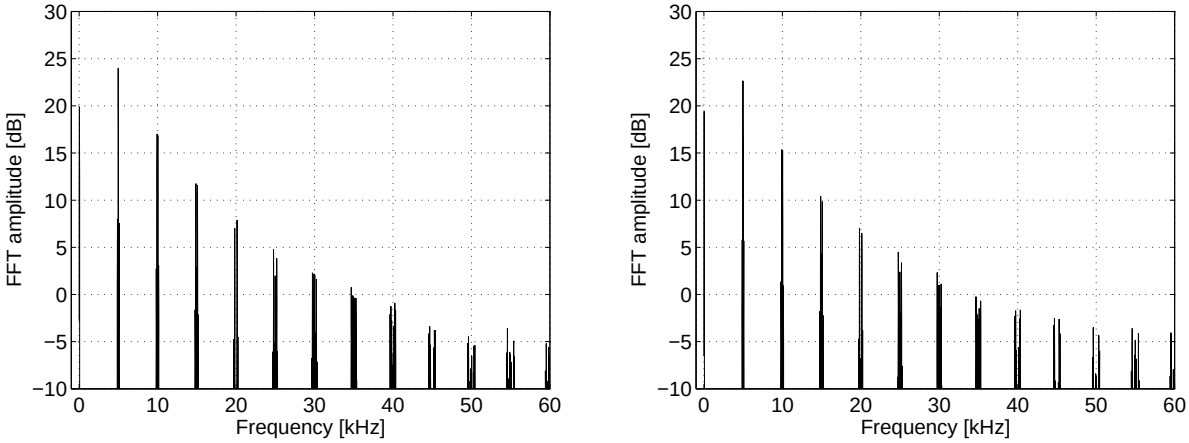

(a) $m_a = 0.6$: without balance booster (b) $m_a = 0.6$: with balance booster

Figure 6-23. *Half-bridge/"single-cell" operation of a 4-cell multicell converter with $f_s = 5\ kHz$.*

When all the cell capacitors are shorted except for the dc-bus capacitor, a 4-cell multicell converter is effectively reduced to a half-bridge converter. This causes the first group of harmonics of the unfiltered output voltage to be centred around the switching frequency, i.e. $f_s = 5\ kHz$. The subsequent groups of harmonics are centred around further integer multiples of the switching frequency. The magnitude of the largest harmonic at $5\ kHz$ is $24\ dB$ for the case without a balance booster connected. When a balance booster which is designed to resonate at the switching frequency is connected in parallel with the load, the magnitude of this harmonic is reduced to $22.5\ dB$, which implies a reduction of $1.5\ dB$.

(b) Multicell operation: the sinusoidal reference frequency is $f_r = 50\ Hz$. The measured FFT results are shown in Figure 6-24 for $m_a = 0.6$.

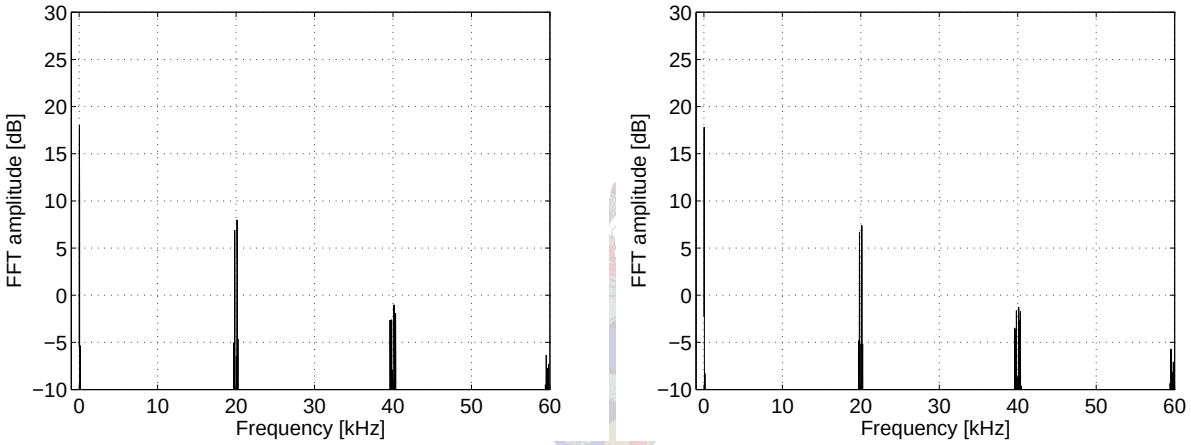

(a) $m_a = 0.6$: without balance booster (b) $m_a = 0.6$: with balance booster

Figure 6-24. *Multicell operation of a 4-cell multicell converter with $f_s = 5\ kHz$.*

When all the cell capacitors are connected the 4-cell multicell converter operates in full multicell operation. The first group of harmonics of the unfiltered output voltage is centred around 4 times the switching frequency, i.e. $4f_s = 20\ kHz$. The subsequent groups of harmonics are centred around further integer multiples of $4f_s$. The magnitude of the largest harmonic at $20\ kHz$ is $8\ dB$ for the case without a balance booster connected. When a balance booster which is designed to resonate at f_s is connected in parallel with the load, the magnitude of this harmonic is reduced to $7\ dB$. Thus the addition of a balance booster tuned to f_s does not reduce this harmonic at $20\ kHz$ significantly. This harmonic is only reduced by $1\ dB$.

(c) Forced unbalance: the sinusoidal reference frequency is $f_r = 50\ Hz$. The measured FFT results are shown in Figure 6-25 for $m_a = 0.6$.

When a small resistor is connected in parallel to one of the cell capacitors the multicell converter is forced into an unbalanced state. A $22\ \Omega$ resistor was used to introduce this unbalance. For the 4-cell case, the converter is also effectively forced into a pseudo 2-cell multicell operation.

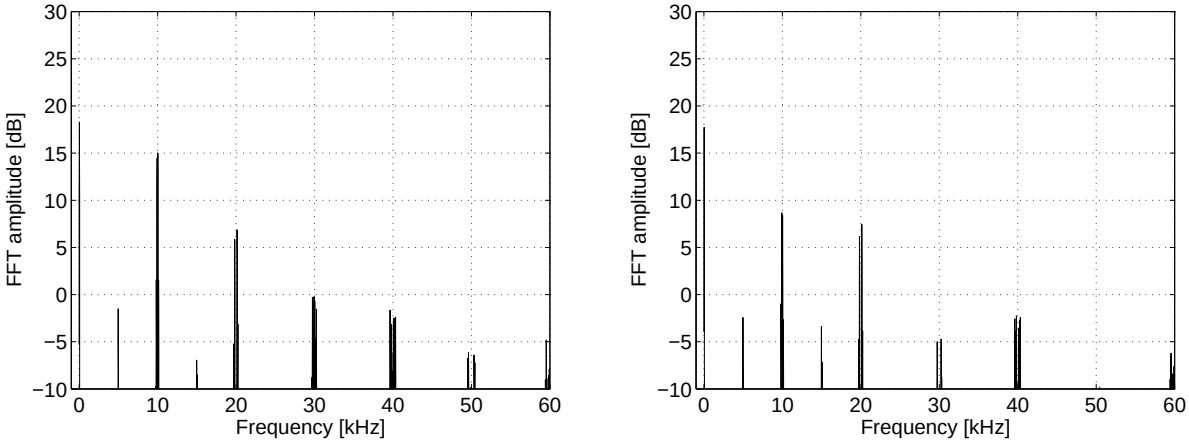

(a) $m_a = 0.6$: without balance booster (b) $m_a = 0.6$: with balance booster

Figure 6-25. *Forced unbalance of a 4-cell multicell converter with $f_s = 5\ kHz$.*

The first group of harmonics of the unfiltered output voltage is centred around 2 times the switching frequency, i.e. $2f_s = 10\ kHz$ instead of $4f_s$ for conventional 4-cell multicell operation. The subsequent groups of harmonics are centred around further integer multiples of $2f_s$. The magnitude of the largest harmonic at $10\ kHz$ is $15\ dB$ for the case without a balance booster connected. When a balance booster which is designed to resonate at f_s is connected in parallel with the load, the magnitude of this harmonic is reduced to $8.5\ dB$. Thus the addition of a balance booster tuned to f_s reduces the this harmonic at $10\ kHz$ by $6.5\ dB$. This is a significant reduction, but the unbalance was not eliminated.

6.6 Summary

The aim of this chapter was to verify the theory that was proposed in the previous chapters. A Matlab® "Designtool" was developed by implementing the theory which was developed in the preceding chapters.

The approximation provided by the theory implemented in the "Designtool" assumes the following:

(a) for sinusoidal modulation: that the cell capacitor voltages remain constant over the sinusoidal reference period T_r.

(b) fixed duty-cycle PWM: that the cell capacitor voltages remain constant over one switching period T_s.

(c) the cell capacitors are in steady-state.

(d) transients are not taken into consideration.

The unbalance decay in a multicell converter was simulated in Simplorer® and in Matlab® using the "Designtool" for 2-, 3- and 4-cell multicell converters for both sinusoidal modulation and fixed duty-cycle PWM cases for different values of m_a and D. The results compared favourably and it can be concluded that the "Designtool" can be used as a good approximation to simulate the decay of the voltage unbalance in a multicell converter. Inaccuracies were found to be as a result of the assumptions of the model not being valid for certain cases, especially transient conditions.

The same converter configurations were also tested experimentally. Experimental measurements of voltage balance in multicell converters were compared with results generated in Matlab® using the "Designtool". The losses in the practical converter were compensated for in the "Designtool" by including a loss resistor in series with the filter inductor. The theoretical results generated in Matlab® using the "Designtool" proved to be good enough to be a good first iteration result when only a rough approximation of the results for a specific converter setup is required.

Harmonic measurements of the unfiltered output voltage of multicell converters were taken for 2-, 3- and 4-cell converters for sinusoidal modulation with $m_a = 0.6$ and different load conditions. The working of the balance booster was shown through these results. It was also seen that the higher the number of cells, the smaller the effect of the balance booster when tuned to the switching frequency.

To conclude, the "Designtool" gives a good and fast approximation of the behaviour of multicell converters which can be used effectively for any number of cells. This is only limited by the computing power of the hardware on which it is executed. The computing time needed to obtain a result using the "Designtool" is much shorter than that needed for a corresponding simulation in Simplorer®, e.g. minutes when using the "Designtool" compared to hours when using Simplorer®.

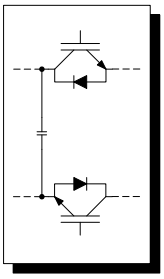

Chapter 7

Conclusions and future work

7.1 Introduction

A theory for the natural balance of multicell converters was developed in this dissertation. This chapter is a brief summary of the findings, contributions and conclusions of the theory which was developed.

7.2 Analysis of the multicell topology

The multicell topology was analysed and a mathematical model was developed in Chapter 2. This analysis was done using circuit analysis techniques as well as applying d and t parameters. The final model differential equations were used to derive equivalent circuits of the multicell topology in terms of d and t parameters.

The model obtained was used as the foundation upon which the remainder of the balance theory was built. The time-domain equivalent circuits derived was used to obtain frequency domain equivalent circuits for the steady-state analysis in Chapter 4 and was also used for the time constant analysis in Chapter 5.

7.3 Harmonic analysis

An extensive harmonic analysis of the switching functions of a multicell converter was done in Chapter 3. This analysis included interleaved switching for both sinusoidal modulation as well as for fixed duty-cycle PWM. The analysis was done for the 2-, 3- and p-cell cases.

The switching functions for the sinusoidal modulation cases were calculated using Fourier methods developed by W.R. Bennet [21] and H.S. Black [5]. Switching functions for the fixed duty-cycle PWM case were calculated using conventional Fourier methods.

Several examples were included which demonstrated the generation of the switching functions for both modulation methods for 2-, 3- and p cells. Other examples included dealt with the spectral analysis of the switching functions for specific values of modulation index and duty-cycle for sinusoidal modulation and fixed duty-cycle PWM respectively.

The results obtained were for natural sampling, the Fourier methods used in this analysis could be modified to include sampling effects as discussed in [25].

The derived characteristics of the switching functions were used extensively in Chapters 4 and 5.

7.4 Steady-state analysis

A steady-state analysis of the multicell converter was done in Chapter 4. It was shown that the cell capacitor voltages of a p-cell multicell converter balance naturally in steady-state under certain conditions.

Conditions that guarantee natural balance were defined. From these conditions it follows that natural balance is guaranteed for the following circumstances :

- When the switching frequency is sufficiently higher than the reference frequency such that there is no overlapping of the harmonics of $S_{d_1}(\omega)$ and $S_t(\omega)$.
- When the reference signal does not contain high frequency components which result in aliasing of the harmonics of $S_{d_1}(\omega)$ and $S_t(\omega)$.

These circumstances are only valid when the following condition is met:

- The load impedance $Z(\omega)$ is reactive, i.e. $Re\{Z(\omega)\} > 0$.

Unbalance equations were derived for the 2-, 3- and p-cell cases. From these unbalance equations it was concluded that the steady-state balancing can be improved when the load impedance $Z(\omega)$ is made smaller at the switching frequency and harmonic multiples thereof.

Two conditions that lead to unbalance of the cell capacitor voltages were also defined. These conditions are as follows:

- when the switching frequency (ω_s) is higher than the frequency of the reference signal (ω_r), but not high enough to avoid aliasing of the side-bands of the harmonic multiples thereof. This is when the harmonics of $S_d(\omega)$ and $S_t(\omega)$ overlap resulting in $|S_d(\omega)||S_t(\omega)| > 0$.
- when the reference signal contains high frequency components, $|S_d(\omega)||S_t(\omega)| > 0$ is possible.

It was also shown that specific values of the duty-cycle D can cause unbalance in a p-cell multicell converter under fixed duty-cycle PWM when p is not a practical prime number, where the largest practical number of cells was chosen to be 7.

It was also shown that when the number of cells p is a practical prime number, i.e. $p \in \{2, 3, 5, 7\}$, the converter will balance naturally for any duty-cycle $0 < D < 1$ when using fixed duty-cycle PWM.

7.5 Time constant analysis

A time constant analysis of a multicell converter was done in Chapter 5. The time constants of a multicell converter were calculated for the 2- and 3-cell cases. The time constants could not be calculated directly for the p-cell case. The poles of the system were approximated by calculating the spectral radius and the Gerschgorin circles of the matrix resulting from the system of differential equations. This was done successfully and applied in the examples shown in Chapter 5 sections 5.3 and 5.4.

The time constant of a 2-cell multicell converter was calculated in Chapter 5 section 5.2 equation (5.19) to be the following:

$$\tau = \frac{C}{2Re\left\{\lambda_1\right\}} \tag{7.1}$$

The time constants of a 3-cell multicell converter was calculated in Chapter 5 section 5.3 equation (5.49) to be the following:

$$\tau_1 \;=\; -\tfrac{1}{Re\{\varepsilon_1\}} \quad \text{and} \quad \tau_2 \;=\; -\tfrac{1}{Re\{\varepsilon_2\}} \tag{7.2}$$

where ε_1 and ε_2 are the respective eigenvalues of $-\frac{1}{C}2Re\{\mathbf{\Lambda}\}$.

The poles of a p-cell multicell converter were approximated in Chapter 5 section 5.4 equation (5.71) to lie within the circle defined by the spectral radius of the matrix $-\frac{1}{C}2Re\{\mathbf{\Lambda}\}$ as follows:

$$\rho\left(-\frac{1}{C}2Re\{\mathbf{\Lambda}\}\right) \leq \frac{p}{C}\max\left\{\left|\lambda_1 + \overline{\lambda_{p-1}}\right|, \left|\lambda_2 + \overline{\lambda_{p-2}}\right|, \ldots, \left|\lambda_{p-1} + \overline{\lambda_1}\right|\right\} \tag{7.3}$$

It was also found that the matrix $-\frac{1}{C}2Re\{\mathbf{\Lambda}\}$ had a Toeplitz structure [6], [14] for $p \geq 4$ which might be used to find an analytical solution of the eigenvalues.

It was also shown that the choice of the number of cells and the value of the duty-cycle D when using

fixed duty-cycle PWM can result in poles on the right-hand side of the complex plane which results in unbalance.

7.6 General conclusion on balance theory

It was found that p-cell multicell converters balance naturally:

(a) when the switching frequency is sufficiently higher than the reference frequency such that there is no overlapping of the groups of harmonics of $S_{d_1}(\omega)$ and $S_t(\omega)$ with the condition that the load impedance $Z(\omega)$ is reactive, i.e. $Re\{Z(\omega)\} > 0$.

(b) when the reference signal does not contain high frequency components which result in aliasing of the harmonics of $S_{d_1}(\omega)$ and $S_t(\omega)$ with the condition that the load impedance $Z(\omega)$ is reactive, i.e. $Re\{Z(\omega)\} > 0$.

(c) when sinusoidal modulation is used.

(d) when fixed duty-cycle PWM is used and p is not a practical prime number, i.e. $p \in \{4, 6\}$, that the denominator of the duty-cycle D (when expressed as a fraction) is not a prime factor of p.

(e) when fixed duty-cycle PWM is used and p is a practical prime number, i.e. $p \in \{2, 3, 5, 7\}$ and $0 < D < 1$.

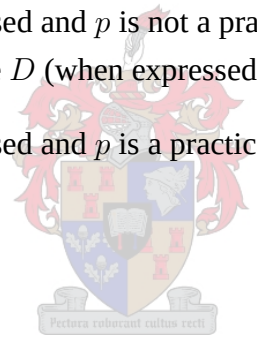

7.7 Future work

The natural balance theory was developed for single-phase multicell converters. The models and the theory which were developed need to be extended to include 3-phase multicell converters.

The harmonic analysis done in Chapter 3 should be extended to include different types of sampling.

It was found that the matrix $-\frac{1}{C}2Re\{\mathbf{\Lambda}\}$ which was derived in Chapter 5 had a Toeplitz structure [6], [14] for $p \geq 4$. This matrix structure should be investigated to determine whether an analytical solution for the eigenvalues of $-\frac{1}{C}2Re\{\mathbf{\Lambda}\}$ is feasible.

Bibliography

Textbooks

[1] H. Anton, *Elementary Linear Algebra*, 5th ed., John Wiley & Sons. Inc., New York, 1987.

[2] B. Aupetit, *A Primer on Spectral Theory*, Springer-Verlag Inc., New York, 1991.

[3] R. Bhatia, *Matrix Analysis*, Springer-Verlag Inc., New York, 1997.

[4] D. Bini and V. Pan, *Polynomial and Matrix Computations, Vol. 1: Fundamental Algorithms*, Birkhäuser, Boston, Massachusetts, 1994.

[5] H.S. Black, *Modulation Theory*, D. van Nostrand Company, Inc., Princeton, New Jersey, 1953.

[6] A. Böttcher and B. Silbermann, *Introduction to Large Truncated Toeplitz Matrices*, Springer-Verlag, New York, 1999.

[7] B. de la Rosa et al, *Inleidende Algebra*, Lexicon Uitgewers, Johannesburg, 1984.

[8] G.F. Franklin, J.D. Powell and A. Emami-Naeini, *Feedback Control of Dynamic Systems*, Addison-Wesley Publishing Company, Reading, Massachusetts, 1994.

[9] M.W. Hirsch and S. Smale, *Differential Equations, Dynamic Systems and Linear Algebra*, Academic Press, New York, 1974.

[10] R.A. Horn and C.R. Johnson, *Matrix Analysis*, Cambridge University Press, Cambridge, 1988.

[11] E. Kreyszig, *Advanced Engineering Mathematics*, John Wiley & Sons. Inc., New York, 1988.

[12] E. Kreyszig, *Introductory Functional Analysis with Applications*, John Wiley & Sons. Inc., New York, 1978.

[13] D.L. Lukes, *Differential Equations: Classical to Controlled*, Academic Press, New York, 1982.

[14] C.D. Meyer, *Matrix Analysis and Applied Linear Algebra*, SIAM, Philadelphia, 2000.

[15] J.W. Nilsson and S.A. Riedel, *Electric Circuits*, Sixth Edition, Prentice-Hall International Inc., New Jersey, 2000.

[16] K. Ogata, *Modern Control Engineering*, Second Edition, Prentice-Hall International Inc., New Jersey, 1990.

[17] J.G. Proakis, D.G. Manolakis, *Digital Signal Processing: Principles, Algorithms and Applications*, Macmillan Publishing Company, USA, 1992.

[18] J.W. Robbin, *Matrix Algebra*, A.K. Peters, Ltd., Wellesley, Massachusetts, 1995.

[19] G. Strang, *Introduction to Linear Algebra*, Wellesley-Cambridge Press, Wellesley, 1993.

Journal papers

[20] N. Aouda, L. Prisse, T.A. Meynard, H. Foch, "A multilevel rectifier with unity power factor and sinusoidal input current for high voltage applications," *EPE Journal*, vol. 6, no. 3 pp. 27-35, December 1996.

[21] W.R. Bennet, "New results in the calculation of modulation products," *Bell Sytems Technical Journal*, vol. 12, pp. 228-243, 1933.

[22] S.R. Bowes, B.M. Bird, "Novel approach to the analysis and synthesis of modulation processes in power converters," *Proc. IEE*, vol. 122, no. 5, pp. 507-513, May 1975.

[23] S.R. Bowes, "New sinusoidal pulse-width modulated inverter," *Proc. IEE*, vol. 122, no. 11, pp. 1279-1285, November 1975.

[24] G. Gateau, M. Fadel, P. Maussion, R. Bensaid, T.A. Meynard, "Multicell converters: active control and observation of flying-capacitor voltages," *IEEE Transactions on Industrial Electronics*, vol. 49, no. 5, pp. 998-1008, October 2002.

[25] B.P. McGrath, D.G. Holmes, "An analytical technique for the determination of spectral components of multilevel carrier-based PWM methods," *IEEE Transactions on Industrial Electronics*, vol. 49, no. 4, pp. 847-857, August 2002.

[26] T.A. Meynard, M. Fadel, N. Aouda, "Modelling of multilevel converters," *IEEE Transactions on Industrial Electronics*, vol. 44, no. 3, pp. 356-364, June 1997.

[27] T.A. Meynard, H. Foch, "Multi-level choppers for high voltage applications," *EPE Journal*, vol. 2, no. 1 pp. 45-50, March 1992.

[28] T.A. Meynard, H. Foch, "Imbricated cells multilevel voltage-source inverters for high voltage applications," *EPE Journal*, vol. 3, no. 2 pp. 99-106, June 1993.

[29] T.A. Meynard, H. Foch, P. Thomas, J. Courault, R. Jakob, M. Nahrstaedt, "Multicell converters: basic concepts and industry applications," *IEEE Transactions on Industrial Electronics*, vol. 49, no. 5, pp. 955-964, October 2002.

[30] T.A. Meynard, H. Foch, F. Forest, C. Turpin, F. Richardeau, L. Delmas, G. Gateau, E. Lefeuvre, "Multicell converters: derived topologies," *IEEE Transactions on Industrial Electronics*, vol. 49, no. 5, pp. 978-987, October 2002.

[31] H. du T. Mouton, "Natural balancing of three-level neutral-point-clamped PWM inverters," *IEEE Transactions on Industrial Electronics*, vol. 49, no. 5, pp. 1017-1025, October 2002.

[32] B. Mwinyiwiwa, Z. Wolanski and B.T. Ooi, "Current equalization in SPWM FACTS controllers at lowest switching rates," *IEEE Transactions on Power Electronics*, vol. 14, no. 5, pp. 900-905, September 1999.

[33] D. Soto, T.C. Green, "A comparison of high-power converter topologies for the implementation of facts controllers," *IEEE Transactions on Industrial Electronics*, vol. 49, no. 5, pp. 1072-1080, October 2002.

[34] C. Turpin, P. Baudesson, F. Richardeau, F. Forest, T.A. Meynard, "Fault management of multicell converters," *IEEE Transactions on Industrial Electronics*, vol. 49, no. 5, pp. 988-997, October 2002.

[35] F. Tourkhani, P. Viarouge, T.A. Meynard, "A simulation-optimization system for the optimal design of a multilevel inverter," *IEEE Transactions on Power Electronics*, vol. 14, no. 6, pp. 1037-1045, November 1999.

[36] X. Yuan, H. Stemmler, I. Barbi, "Self-balancing of the clamping-capacitor-voltages in the multilevel capacitor-clamping-inverter under sub-harmonic PWM modulation," *IEEE Trans. on Power Electronics*, vol. 16, no. 2, pp. 256-263, March 2001.

Conference papers

[37] D.D. Bester, J.A. du Toit, J.H.R. Enslin, "High performance DSP/FPGA controller for implementation of computationally intensive algorithms," in *Proc. IEEE ISIE'98*, vol. 1, Pretoria, South Africa, pp. 240-244, July 1998.

[38] P. Carrere, T.A. Meynard, J.P. Lavieville, "4000V-300A Eight-level IGBT inverter leg," in *Proc. EPE'95*, vol. 1, Seville, Spain, pp. 106-111, September 1995.

[39] S. Delfo, T. Taleb, H. Jacobs, J. Petzoldt, "Analysis and simulation of multilevel converter with self voltage balancing based on flying capacitors topology," in *Proc. EPE-PEMC'02*, Cavtat & Dubrovnik, Croatia, September 2002.

[40] A. Donzel, G. Bornard, "New control law for capacitor voltage balance in multilevel inverter with switching rate control (CVC)," in *Proc. IEEE IAS'00*, vol. 3, Rome, Italy, pp. 2037-2044, October 2000.

[41] G. Gateau, P. Maussion, T.A. Meynard, "Fuzzy phase control of series multicell converters," in *Proc. FUZZ-IEEE'97*, vol. 3, Barcelona, Spain, pp. 1627-1633, July 1997.

[42] F. Hamma, T.A. Meynard, F. Tourkhani, P. Viarouge, "Characteristics and design of multilevel choppers," in *Proc. IEEE PESC'95*, vol. 2, Atlanta, USA, pp. 1208-1214, June 1995.

[43] C. Hochgraf, R. Lasseter, D. Divan, T.A. Lipo, "Comparison of multilevel inverters for static var compensation," in *Proc. IEEE IAS'94*, vol. 2, Denver, USA, pp. 921-928, 1994.

[44] T.A. Meynard, H. Foch, "Multilevel converters and derived topologies for high power conversion," in *Proc. IEEE IECON'95*, vol. 1, Orlando, USA, pp. 21-26, September 1995.

[45] T.A. Meynard, H. Foch, "Multi-level conversion: high voltage choppers and voltage-source inverters," in *Proc. IEEE PESC'92*, vol. 1, Toledo, Spain, pp. 397-403, June 1992.

[46] F.Z. Peng, J.S. Lai, J. McKeever, J. VanCoevering, "A multilevel voltage source converter system with balanced dc voltages," in *Proc. IEEE PESC'95*, vol. 2, Atlanta, USA, pp. 11441150, June 1995.

[47] J. Petzoldt, S. Delfo, H. Jacobs, T. Reimann, "Performance comparison of conventional two-level PWM-VSI and four-level flying capacitor PWM-VSI," in *Proc. IEEE IAS'02*, vol. 1, Pittsburgh, USA, pp. 515-522, October 2002.

[48] F. Richardeau, P. Baudesson, T.A. Meynard, "Failures-tolerance and remedial strategies of a PWM multicell inverter," in *Proc. IEEE PESC'00*, vol. 2, Galway, Ireland, pp. 649-654, June 2000.

[49] J. Rodriguez, L. Moran, A. Gonzalez, C. Silva, "High voltage multilevel converter with regeneration capability," in *Proc. IEEE PESC'99*, vol. 2, Charleston, USA, pp. 1077-1082, June 1999.

[50] G. Sinha, T. Lipo, "A four level inverter based drive with a passive front end," in *Proc. IEEE PESC'97*, vol. 1, St. Louis, USA, pp. 590596, June 1997.

[51] O. Tachon, M. Fadel, T.A. Meynard, "Control of series multicell converters by linear state feedback decoupling," in *Proc. EPE'97*, vol. 1, Trondheim, Norway, pp. 588-593, September 1997.

[52] L.M. Tolbert, F.Z. Peng, "Multilevel converters for large electric drives," in *Proc. IEEE APEC'98*, vol. 2, Anaheim, USA, pp. 530-536, February 1998.

[53] C. Turpin, L. Deprez, F. Forest, F. Richardeau, T.A. Meynard, "A new ZVS imbricated cell multilevel inverter with auxiliary resonant commutated poles," in *Proc. IEEE PESC'01*, vol. 2, Vancouver, Canada, pp. 1159-1164, June 2001.

[54] A.J. Visser, H. du T. Mouton, "250 kW Transformer-less voltage dip compensator," in *Proc. IEEE AFRICON'99*, vol. 2, Cape Town, South Africa, pp. 865-880, September 1999.

[55] A.J. Visser, H. du T. Mouton, J.H.R. Enslin, "Direct-coupled multilevel sag compensator," in *Proc. IEEE PESC'00*, vol. 1, Galway, Ireland, pp. 463-469, June 2000.

[56] R.H. Wilkinson, T.A. Meynard, J.H.R. Enslin, "Dynamic control and voltage balance of multilevel converters," in *Proc. EPE'99*, Lausanne, Switzerland, September 1999.

[57] R.H. Wilkinson, J.A. du Toit, T.A. Meynard, H. du T. Mouton, "Design considerations in creating a generic PowerCell for the multicell topology," in *Proc. SAUPEC'01*, Cape Town, South Africa, pp. 238-241, January 2001.

[58] R.H. Wilkinson, T.A. Meynard, H. du T. Mouton, "Voltage unbalance in the multicell converter topology," in *Proc. IEEE AFRICON'02*, vol. 2, George, South Africa, pp. 759-764, October 2002.

[59] R.H. Wilkinson, T.A. Meynard, H. du T. Mouton, "Natural balance of multicell converters," in *Proc. IEEE PESC'03*, vol. 3, Acapulco, Mexico, pp. 1307-1312, June 2003.

Dissertations

[60] P. Carrere: *Etude et Réalisation de Convertisseurs Multicellulaires Série à IGBT Equilibrage des Condensateurs Flottants*, PhD Thesis, Institut National Polytechnique de Toulouse, Toulouse, France, October 1996.

[61] G. Gateau, *Contribution à la Commande des Convertisseurs Statiques Multicellulaires série: Commande Non Linéaire et Commande Floue*, PhD Thesis, Institut National Polytechnique de Toulouse, Toulouse, France, September 1997.

[62] H. du T. Mouton, *Analysis and synthesis of a 2 MVA series-stacked power-quality conditioner*, PhD Thesis, University of Stellenbosch, Stellenbosch, South Africa, December 1999.

[63] O. Tachon, *Commande des Convertisseurs Multiniveaux*, PhD Thesis, Institut National Polytechnique de Toulouse, Toulouse, France, April 1998.

[64] R.H. Wilkinson, *Topology, control and development of high power multilevel converters*, M.Eng. Thesis, University of Stellenbosch, Stellenbosch, South Africa, December 1997.

Web sites

[65] ABB Ltd, "The ABB Group," http://www.abb.com, 2003.

[66] J. Loy, "Roots of Unity," http://www.jimloy.com/algebra/roots.htm, 1999.

[67] Powerex Inc., "Powerex Power Semiconductors," http://www.pwrx.com, 2003.

[68] E. Weisstein, "Eric Weisstein's World of Mathematics," http://mathworld.wolfram.com, 2003.

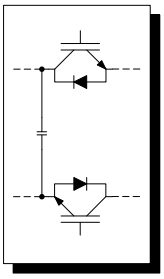

Appendix A

Fourier series calculations

A.1 Double Fourier series coefficient calculations

The double Fourier series coefficients referred to in Chapter 3 section 3.3.1.1 are calculated in this section.

A.1.1 Sinusoidal reference

The following equation can be used to calculate the double Fourier series coefficients:

$$A_{mn} + jB_{mn} = \frac{\omega_r}{4\pi} \int_0^{\frac{2\pi}{\omega_r}} \int_{-1}^{3} F(h,t) e^{j(\frac{m\pi h}{2} + n\omega_r t)} dh dt \tag{A.1}$$

Figure 3-3(d) is repeated here as Figure A-1 to aid in the calculation of the double Fourier series coefficients $A_{mn} + jB_{mn}$ of interleaved switching for sinusoidal modulation as discussed in Chapter 3 section 3.3.1.1.

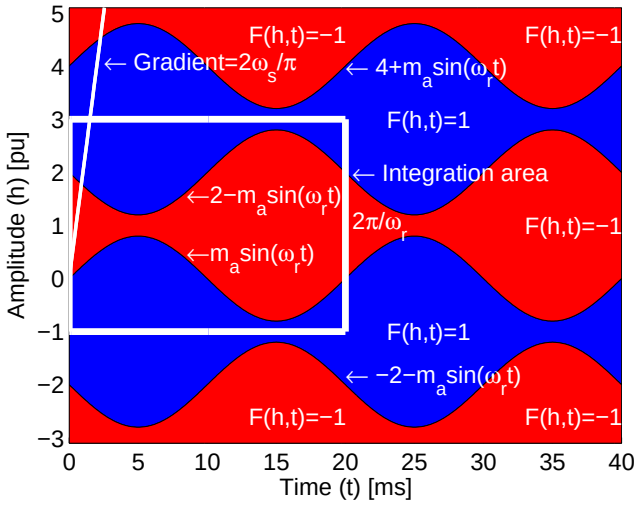

Figure A-1. *Area of integration for the calculation of* $A_{mn} + jB_{mn}$.

Using the area of integration, as shown in Figure A-1, using a sinusoidal reference of the following form:

$$f_r(t) = m_a \sin \omega_r t \tag{A.2}$$

with modulation index of m_a and frequency of ω_r, equation (A.1) can be written as follows:

$$\begin{aligned} A_{mn} + jB_{mn} &= \frac{\omega_r}{4\pi} \int_0^{\frac{2\pi}{\omega_r}} \int_{-1}^{3} F(h,t) e^{j(\frac{m\pi h}{2} + n\omega_r t)} dh dt \\ &= \frac{\omega_r}{4\pi} \int_0^{\frac{2\pi}{\omega_r}} \left\{ \int_{-1}^{m_a \sin \omega_r t} (1) e^{j\frac{m\pi h}{2}} dh + \int_{m_a \sin \omega_r t}^{2-m_a \sin \omega_r t} (-1) e^{j\frac{m\pi h}{2}} dh + \right. \\ &\qquad \left. \int_{2-m_a \sin \omega_r t}^{1} (1) e^{j\frac{m\pi h}{2}} dh \right\} e^{jn\omega_r t} dt \end{aligned} \tag{A.3}$$

This equation has to be calculated for 2 cases, i.e. where $m \neq 0$ and where $m = 0$. These 2 cases are as follows:

- Case 1: $m \neq 0$

$$\begin{aligned} A_{mn} + jB_{mn} &= \frac{2\omega_r}{4jm\pi^2} \int_0^{\frac{2\pi}{\omega_r}} \left\{ e^{j\frac{m\pi h}{2}} \Big|_{-1}^{m_a \sin \omega_r t} - e^{j\frac{m\pi h}{2}} \Big|_{m_a \sin \omega_r t}^{2-m_a \sin \omega_r t} + \right. \\ &\qquad \left. e^{j\frac{m\pi h}{2}} \Big|_{2-m_a \sin \omega_r t}^{1} \right\} e^{jn\omega_r t} dt \\ &= \frac{2\omega_r}{4jm\pi^2} \int_0^{\frac{2\pi}{\omega_r}} \left\{ e^{j\frac{m\pi}{2}(m_a \sin \omega_r t)} - e^{-j\frac{m\pi}{2}} - e^{j\frac{m\pi}{2}(2-m_a \sin \omega_r t)} + e^{j\frac{m\pi}{2}(m_a \sin \omega_r t)} + \right. \\ &\qquad \left. e^{\frac{j3m\pi}{2}} - e^{\frac{jm\pi}{2}(2-m_a \sin \omega_r t)} \right\} e^{jn\omega_r t} dt \\ &= \frac{\omega_r}{2jm\pi^2} \int_0^{\frac{2\pi}{\omega_r}} \left(2e^{j\frac{m\pi}{2}(m_a \sin \omega_r t)} - 2e^{j\frac{m\pi}{2}(2-m_a \sin \omega_r t)} \right) e^{jn\omega_r t} dt \\ &= \frac{\omega_r}{jm\pi^2} \int_0^{\frac{2\pi}{\omega_r}} \left(e^{j\frac{m\pi}{2} m_a \sin \omega_r t + jn\omega_r t} - e^{j\frac{m\pi}{2}(2-m_a \sin \omega_r t) + jn\omega_r t} \right) dt \end{aligned} \tag{A.4}$$

Now, let $\theta = \omega_r t$, thus $d\theta = \omega_r dt$, $dt = \frac{1}{\omega_r} d\theta$. At $t = \frac{2\pi}{\omega_r}$, $\theta = 2\pi$. Changing the variables in equation (A.4) the following is obtained:

$$A_{mn} + jB_{mn} = \frac{1}{jm\pi^2} \int_0^{2\pi} \left(e^{j\frac{m\pi}{2} m_a \sin \theta + jn\theta} - e^{j\frac{m\pi}{2}(2-m_a \sin \theta) + jn\theta} \right) d\theta \tag{A.5}$$

In order to change the boundaries of the integral, another substitution can be made: $\phi = \theta - \pi$

and $d\phi = d\theta$. The integration boundaries change as follows:

$$\phi = \begin{cases} - \quad \pi & \text{if } \theta = 0 \\ \quad \pi & \text{if } \theta = 2\pi. \end{cases} \tag{A.6}$$

Substituting the above boundary values into equation (A.5) results in the following:

$$\begin{aligned} A_{mn} + jB_{mn} &= \frac{1}{jm\pi^2} \int_{-\pi}^{\pi} \left(e^{j\frac{m\pi}{2} m_a \sin(\phi+\pi) + jn(\phi+\pi)} - e^{j\frac{m\pi}{2}(2 - m_a \sin(\phi+\pi)) + jn(\phi+\pi)} \right) d\phi \\ &= \frac{1}{jm\pi^2} \int_{-\pi}^{\pi} \left(e^{j\frac{m\pi}{2}(-m_a \sin\phi) + jn(\phi+\pi)} - e^{-j\frac{m\pi}{2}(2 + m_a \sin\phi) + jn(\phi+\pi)} \right) d\phi \\ &= \frac{1}{jm\pi^2} \int_{-\pi}^{\pi} \left(e^{jn\pi} e^{-j\frac{m\pi}{2} m_a \sin\phi + jn\phi} - e^{j(m+n)\pi} e^{j\frac{m\pi}{2} m_a \sin\phi + jn\phi} \right) d\phi \end{aligned} \tag{A.7}$$

Equation (A.7) can be written in terms of Bessel functions of the first kind using the following properties:

$$J_n(x) = \frac{1}{2\pi} \int_{-\pi}^{\pi} e^{j(x \sin y - ny)} dy \tag{A.8}$$

$$J_n(-x) = (-1)^n J_n(x) \tag{A.9}$$

$$J_{-n}(x) = (-1)^n J_n(x) \tag{A.10}$$

Using the properties of the Bessel function listed in equations (A.8)-(A.10), equation (A.7) can be rewritten as follows:

$$\begin{aligned} A_{mn} + jB_{mn} &= \frac{2}{jm\pi} \left(e^{jn\pi} J_{-n}\left(-\frac{m\pi m_a}{2} \right) - e^{j(m+n)\pi} J_{-n}\left(\frac{m\pi m_a}{2} \right) \right) \\ &= \frac{2}{jm\pi} \left(e^{jn\pi} (-1)^n J_n\left(-\frac{m\pi m_a}{2} \right) - e^{j(m+n)\pi} (-1)^n J_n\left(\frac{m\pi m_a}{2} \right) \right) \\ &= \frac{2}{jm\pi} \left(e^{jn\pi} (-1)^n (-1)^n J_n\left(\frac{m\pi m_a}{2} \right) - e^{j(m+n)\pi} (-1)^n J_n\left(\frac{m\pi m_a}{2} \right) \right) \\ &= \frac{2}{jm\pi} J_n\left(\frac{m\pi m_a}{2} \right) \left(e^{jn\pi} - e^{j(m+n)\pi} (-1)^n \right) \\ &= \frac{2}{jm\pi} J_n\left(\frac{m\pi m_a}{2} \right) \left(e^{jn\pi} - e^{jm\pi + jn\pi} (-1)^n \right) \end{aligned} \tag{A.11}$$

If n is odd, equation (A.11) can be simplified as follows:

$$\begin{aligned} A_{mn} + jB_{mn} &= \frac{2}{jm\pi} J_n\left(\frac{m\pi m_a}{2} \right) \left(e^{jn\pi} - e^{jm\pi + jn\pi} (-1)^n \right) \\ &= \frac{2}{jm\pi} J_n\left(\frac{m\pi m_a}{2} \right) \left(-1 + e^{jm\pi} (-1) \right) \end{aligned}$$

$$= \frac{-2}{jm\pi} J_n\left(\frac{m\pi m_a}{2}\right)\left(1 + e^{jm\pi}\right)$$
$$= \frac{2j}{m\pi} J_n\left(\frac{m\pi m_a}{2}\right)\left(1 + e^{jm\pi}\right) \quad \text{(A.12)}$$

If the h-axis boundaries of the integration area was chosen differently, e.g. from $[-3, -1]$, the above calculation would result in the following:

$$A_{mn} + jB_{mn} = \frac{2j}{m\pi} J_n\left(\frac{m\pi m_a}{2}\right)\left(1 + e^{-jm\pi}\right) \quad \text{(A.13)}$$

which is equal to the result in equation (A.12) because $e^{-jm\pi} = e^{jm\pi}$.

If n is even, equation (A.11) can be simplified as follows:

$$\begin{aligned} A_{mn} + jB_{mn} &= \frac{2}{jm\pi} J_n\left(\frac{m\pi m_a}{2}\right)\left(e^{jn\pi} - e^{jm\pi + jn\pi}(-1)^n\right) \\ &= \frac{2}{jm\pi} J_n\left(\frac{m\pi m_a}{2}\right)\left[e^{jn\pi}\left(1 - e^{jm\pi}(1)\right)\right] \\ &= \frac{2}{jm\pi} J_n\left(\frac{m\pi m_a}{2}\right)\left[1\left(1 - e^{jm\pi}\right)\right] \\ &= \frac{2}{jm\pi} J_n\left(\frac{m\pi m_a}{2}\right)\left(1 - e^{jm\pi}\right) \quad \text{(A.14)} \end{aligned}$$

Again, if the h-axis boundaries of the integration area was chosen differently, as mentioned above, the above calculation would result in the following:

$$A_{mn} + jB_{mn} = \frac{2}{jm\pi} J_n\left(\frac{m\pi m_a}{2}\right)\left(1 - e^{-jm\pi}\right) \quad \text{(A.15)}$$

which is also equal to the result obtained in equation (A.14) because $e^{-jm\pi} = e^{jm\pi}$.

- Case 2: $m = 0$

$$\begin{aligned} A_{0n} + jB_{0n} &= \frac{\omega_r}{4\pi} \int_0^{\frac{2\pi}{\omega_r}} \int_{-1}^{3} F(h,t) e^{j(\frac{m\pi h}{2} + n\omega_r t)} dh dt \\ &= \frac{\omega_r}{4\pi} \int_0^{\frac{2\pi}{\omega_r}} \left\{ \int_{-1}^{m_a \sin\omega_r t} (1) dh + \int_{m_a \sin\omega_r t}^{2 - m_a \sin\omega_r t} (-1) dh + \right. \\ &\qquad \left. \int_{2 - m_a \sin\omega_r t}^{3} (1) dh \right\} e^{jn\omega_r t} dt \\ &= \frac{\omega_r}{4\pi} \int_0^{\frac{2\pi}{\omega_r}} \{ m_a \sin\omega_r t + 1 - 2 + m_a \sin\omega_r t + m_a \sin\omega_r t + 3 - 2 + \\ &\qquad m_a \sin\omega_r t \} e^{jn\omega_r t} dt \\ &= \frac{\omega_r}{\pi} \int_0^{\frac{2\pi}{\omega_r}} m_a \sin(\omega_r t) e^{jn\omega_r t} dt \quad \text{(A.16)} \end{aligned}$$

Let $\theta = \omega_r t$, thus $d\theta = \omega_r dt$. The boundary values change as follows:

$$\theta = \begin{cases} 0 & \text{if } t = 0 \\ 2\pi & \text{if } t = \frac{2\pi}{\omega_r} \end{cases} \tag{A.17}$$

Substituting the above boundary values into equation (A.16) results in the following:

$$A_{0n} + jB_{0n} = \frac{1}{\pi}\int_0^{2\pi} m_a \sin\theta e^{jn\theta} d\theta \tag{A.18}$$

If $n = 1$:

$$\begin{aligned} A_{01} + jB_{01} &= \frac{1}{\pi}\int_0^{2\pi} m_a \sin\theta e^{j\theta} d\theta \\ &= \frac{m_a}{\pi}\int_0^{2\pi} \frac{1}{2j}\left(e^{j\theta} - e^{-j\theta}\right) e^{j\theta} d\theta \\ &= \frac{m_a}{\pi}\left[\int_0^{2\pi} \frac{1}{2j} e^{j2\theta} d\theta - \int_0^{2\pi} \frac{1}{2j} d\theta\right] \\ &= \frac{m_a}{\pi}\left[e^{j2\theta}\Big|_0^{2\pi} - \frac{1}{2j}\theta\Big|_0^{2\pi}\right] \\ &= \frac{m_a}{\pi}\left[e^{j4\pi} - 1 - \frac{1}{2j}(2\pi - 0)\right] \\ &= \frac{m_a}{\pi}\left[1 - 1 - \frac{\pi}{j}\right] \\ &= \frac{-m_a}{j} \cdot \frac{-j}{-j} \\ &= jm_a \end{aligned} \tag{A.19}$$

- For odd values of both n and m:

$$A_{mn} + jB_{mn} = \frac{2j}{m\pi} J_n\left(\frac{m\pi m_a}{2}\right)\left(1 + e^{jm\pi}\right) = 0. \tag{A.20}$$

- For even values of both n and m:

$$A_{mn} + jB_{mn} = \frac{2}{jm\pi} J_n\left(\frac{m\pi m_a}{2}\right)\left(1 - e^{jm\pi}\right) = 0. \tag{A.21}$$

The coefficients can now be summarised as follows:

- $m \neq 0$ and n odd:

$$A_{mn} + jB_{mn} = \frac{2j}{m\pi} J_n\left(\frac{m\pi m_a}{2}\right)\left(1 + e^{jm\pi}\right) \tag{A.22}$$

- $m \neq 0$ and n even:

$$A_{mn} + jB_{mn} = \frac{2}{jm\pi} J_n\left(\frac{m\pi m_a}{2}\right)\left(1 - e^{jm\pi}\right) \tag{A.23}$$

- $m = 0$ and $n = 1$:

$$A_{01} + jB_{01} = jm_a \tag{A.24}$$

- $m = 0$ and $n \neq 1$:

$$A_{0n} + jB_{0n} = 0 \tag{A.25}$$

A.2 Phasor representations

This section contains the phasor representations for both 4- and 5-cell multicell inverters as referred to in Chapter 3 sections 3.3.1.4 and 3.3.2.4.

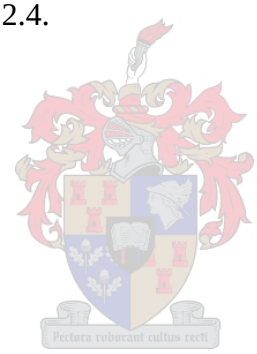

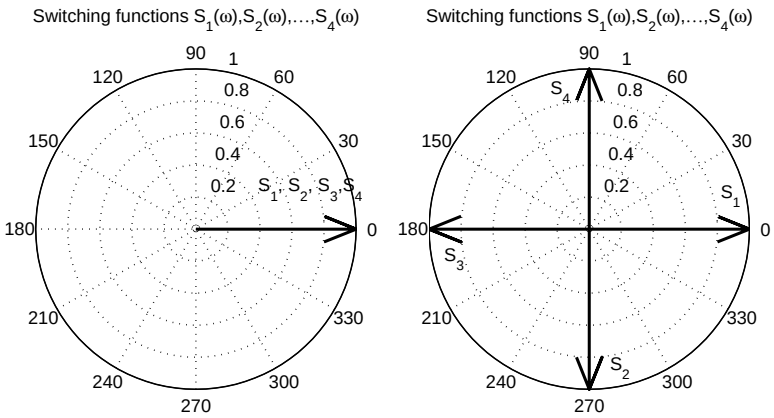

(a) $m = 4k$ (b) $m = 4k + 1$

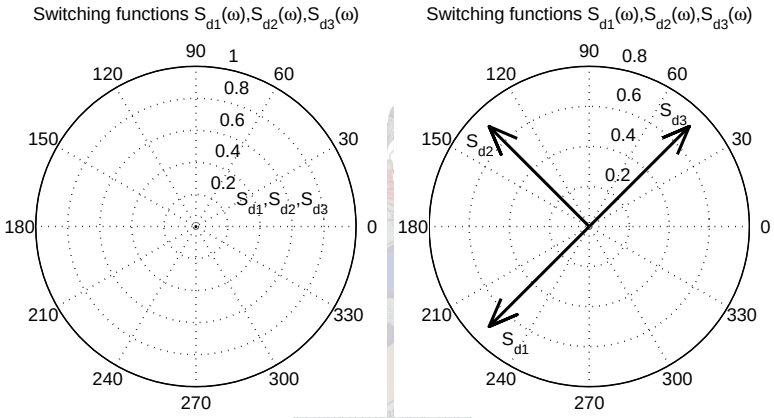

(c) $m = 4k$ (d) $m = 4k + 1$

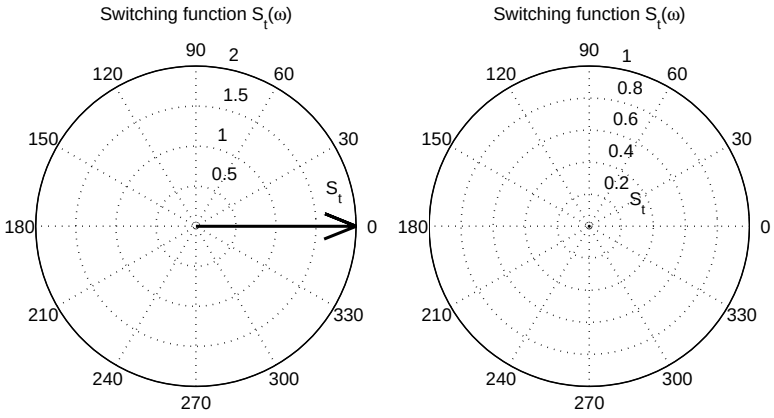

(e) $m = 4k$ (f) $m = 4k + 1$

Figure A-2. *Phasor representation of the switching functions of a* 4*-cell inverter.*

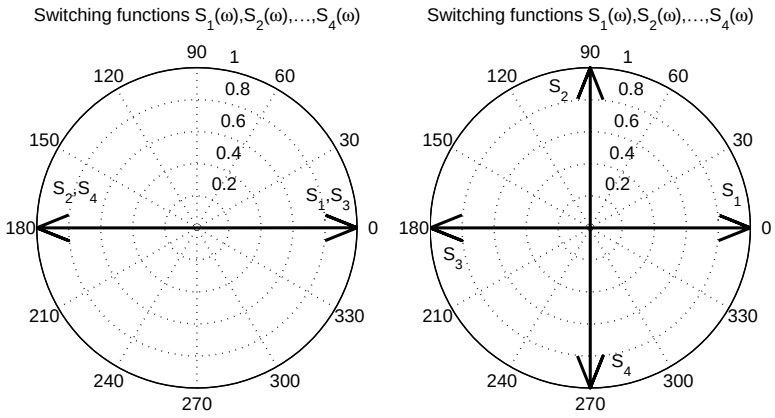

(g) $m = 4k + 2$ (h) $m = 4k + 3$

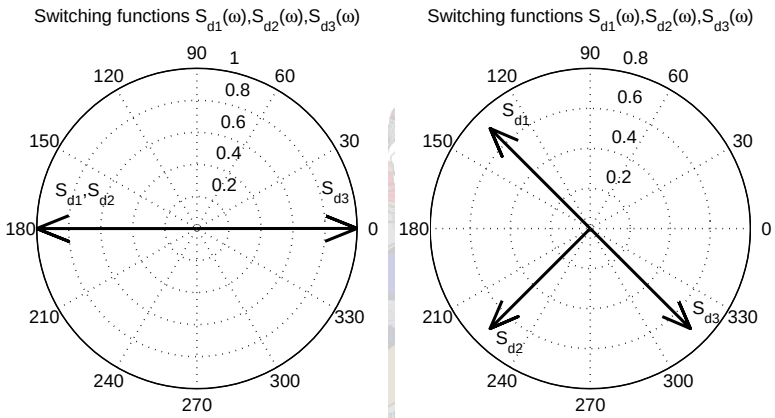

(i) $m = 4k + 2$ (j) $m = 4k + 3$

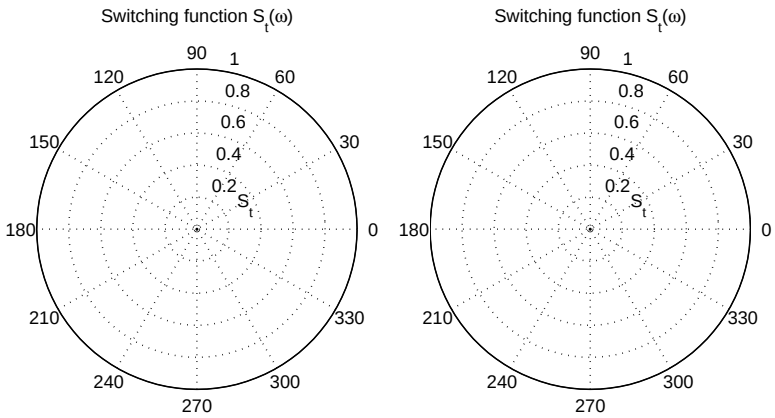

(k) $m = 4k + 2$ (l) $m = 4k + 3$

Figure A-2. *Phasor representation of the switching functions of a* 4*-cell inverter (cont.).*

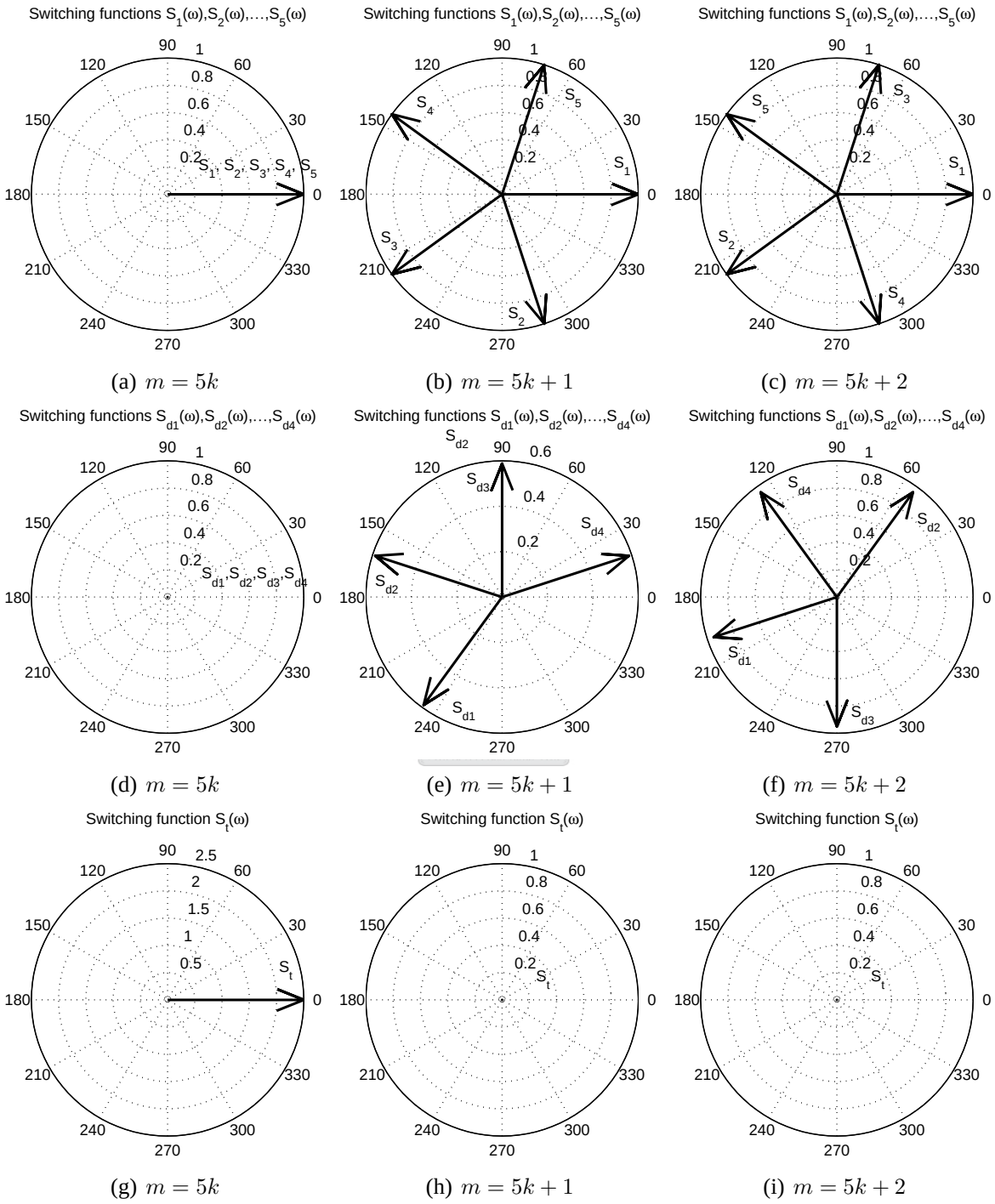

(a) $m = 5k$ (b) $m = 5k + 1$ (c) $m = 5k + 2$

(d) $m = 5k$ (e) $m = 5k + 1$ (f) $m = 5k + 2$

(g) $m = 5k$ (h) $m = 5k + 1$ (i) $m = 5k + 2$

Figure A-3. *Phasor representation of the switching functions of a* 5*-cell inverter.*

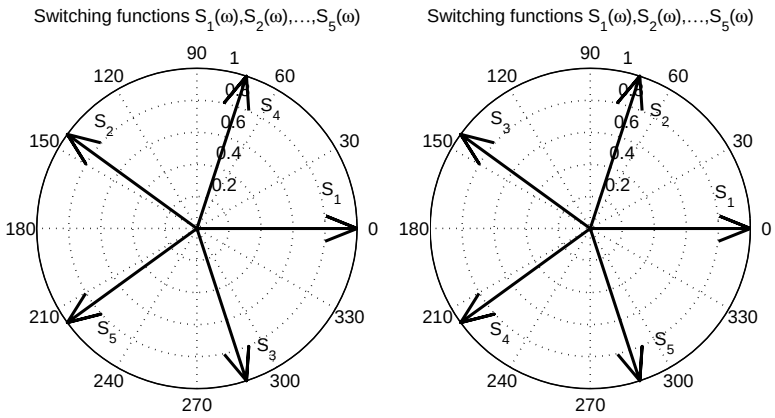

(j) $m = 5k + 3$ (k) $m = 5k + 4$

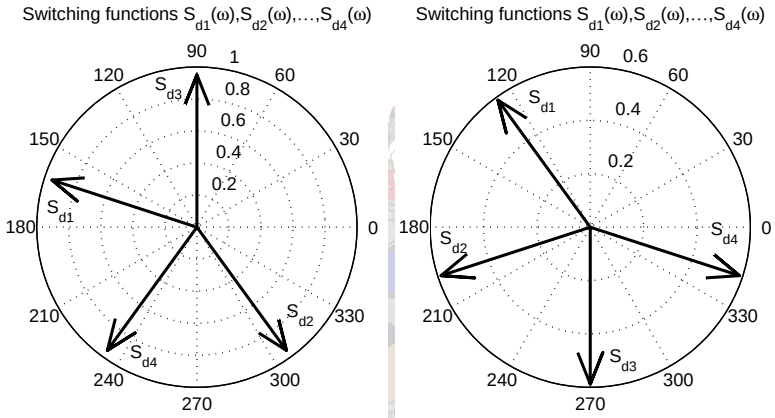

(l) $m = 5k + 3$ (m) $m = 5k + 4$

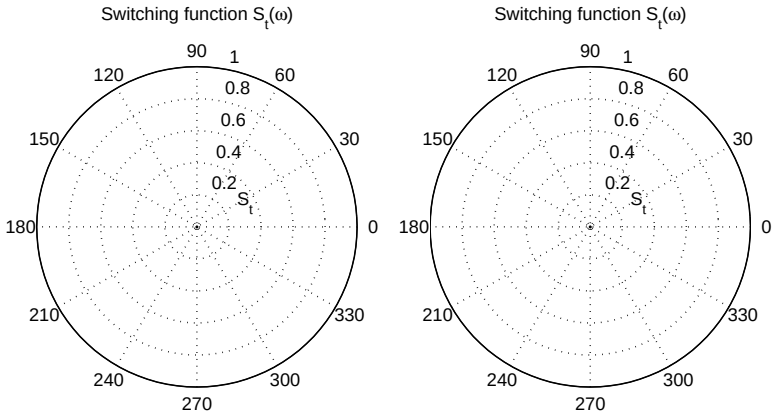

(n) $m = 5k + 3$ (o) $m = 5k + 4$

Figure A-3. *Phasor representation of the switching functions of a* 5*-cell inverter (cont.).*

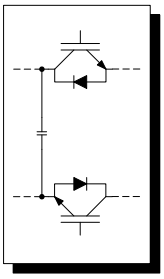

Appendix B

Matrix calculations

B.1 Introduction

This appendix aims at describing in detail the calculations in obtaining the determinants and inverses of the characteristic matrices discussed in Chapter 4.

In the following sections, it will be shown that for a p-cell multicell converter:

$$\det(2Re\{\mathbf{\Lambda}\}) = p^{p-2}\prod_{l=1}^{p-1}(\lambda_l + \overline{\lambda_{p-l}}) \tag{B.1}$$

$$\left\|(2Re\{\mathbf{\Lambda}\})^{-1}\right\| \leq \max\left\{\frac{1}{\left|\lambda_1 + \overline{\lambda_{p-1}}\right|}, \frac{1}{\left|\lambda_2 + \overline{\lambda_{p-2}}\right|}, \ldots, \frac{1}{\left|\lambda_{p-1} + \overline{\lambda_1}\right|}\right\} \tag{B.2}$$

which means that the norm of the inverse of the matrix $(2Re\{\mathbf{\Lambda}\})^{-1}$ is less than or equal to the inverse of the absolute value of the smallest eigenvalue of $2Re\{\mathbf{\Lambda}\}$.

$$\rho\left(2Re\{\mathbf{\Lambda}\}\right) \leq \max\left\{\left|\lambda_1 + \overline{\lambda_{p-1}}\right|, \left|\lambda_2 + \overline{\lambda_{p-2}}\right|, \ldots, \left|\lambda_{p-1} + \overline{\lambda_1}\right|\right\} \tag{B.3}$$

which means that the spectral radius of the matrix $2Re\{\mathbf{\Lambda}\}$ is less than or equal to the absolute value of the largest eigenvalue of $2Re\{\mathbf{\Lambda}\}$.

These results will be used in Chapter 4 in the steady-state analysis of p-cell multicell converters. The above results were also used in Chapter 5, but in a modified form. The following equations are the modified forms of (B.1) to (B.3) which will be shown in these sections:

$$\det\left(-\frac{1}{C}2Re\{\mathbf{\Lambda}\}\right) = \left(-\frac{1}{C}\right)^{p-1} p^{p-2}\prod_{l=1}^{p-1}(\lambda_l + \overline{\lambda_{p-l}}) \tag{B.4}$$

$$\left\| \left(-\frac{1}{C} 2Re\{\mathbf{\Lambda}\} \right)^{-1} \right\| \leq |C| \max \left\{ \frac{1}{\left|\lambda_1 + \overline{\lambda_{p-1}}\right|}, \frac{1}{\left|\lambda_2 + \overline{\lambda_{p-2}}\right|}, \ldots, \frac{1}{\left|\lambda_{p-1} + \overline{\lambda_1}\right|} \right\} \tag{B.5}$$

$$\rho \left(-\frac{1}{C} 2Re\{\mathbf{\Lambda}\} \right) \leq \frac{p}{C} \max \left\{ \left|\lambda_1 + \overline{\lambda_{p-1}}\right|, \left|\lambda_2 + \overline{\lambda_{p-2}}\right|, \ldots, \left|\lambda_{p-1} + \overline{\lambda_1}\right| \right\} \tag{B.6}$$

B.2 Preliminaries

This section includes and lists the mathematical theories and definitions used for the calculations contained in this Appendix. In most cases, only the material relevant to this study has been repeated. References are included if more detail is desired.

A matrix can be considered as a bounded linear operator over the vector space consisting of vectors of dimension $p-1$ over the complex numbers.

In this Appendix, $\mathbb{C}$ denotes the complex numbers and M_{p-1} refers to the set of all $p-1 \times p-1$ square matrices over the complex numbers. Therefore, all the matrices used in the following subsections are defined as square and of type $M_{p-1}(\mathbb{C})$, where p is the number of cells in the converter.

Theorem B.1. *For a $p-1 \times p-1$ square matrix $\mathbf{A}$, a nonzero vector $\mathbf{x}$ in $\mathbb{C}^{p-1}$ is called an* eigenvector *of $\mathbf{A}$ if $\mathbf{Ax}$ is a scalar multiple of $\mathbf{x}$, i.e.:*

$$\mathbf{Ax} = \varepsilon \mathbf{x} \tag{B.7}$$

The scalar ε is referred to as an eigenvalue *of $\mathbf{A}$ and the vector $\mathbf{x}$ is referred to as an* eigenvector *corresponding to ε. If $\mathbf{A}$ is an $p-1 \times p-1$ square matrix, then the following is true [1]:*

(a) *ε is an* eigenvalue *of $\mathbf{A}$.*

(b) *The system of equations $(\varepsilon \mathbf{I} - \mathbf{A})\,\mathbf{x} = \mathbf{0}$ has nontrivial solutions.*

(c) *There is a nonzero vector $\mathbf{x}$ in $\mathbb{C}^{p-1}$ such that $\mathbf{Ax} = \varepsilon \mathbf{x}$.*

(d) *ε is a real solution of the characteristic equation $\det(\varepsilon \mathbf{I} - \mathbf{A}) = 0$. This characteristic equation is a polynomial of degree $p-1$, where $p-1$ is the order of the matrix. According to the* Fundamental Theorem of Algebra *this equation has $p-1$ real/complex roots, $\varepsilon_1, \varepsilon_2, \ldots, \varepsilon_{p-1}$, i.e.:*

$$\det(\varepsilon \mathbf{I} - \mathbf{A}) = (\varepsilon - \varepsilon_1)(\varepsilon - \varepsilon_2) \cdots (\varepsilon - \varepsilon_{p-1}) \tag{B.8}$$

Some of the roots may however be repeated, resulting in the following:

$$\det(\varepsilon\mathbf{I}-\mathbf{A})=(\varepsilon-\varepsilon_1)^2\cdots(\varepsilon-\varepsilon_{p-1}) \tag{B.9}$$

The power of the root which was repeated is called the multiplicity *(algebraic multiplicity) of the* eigenvalue*.*

Definition B.1. *The spectrum of a* $p-1\times p-1$ *square matrix* $\mathbf{A}$ *is the set of all its* eigenvalues *and can be written as follows [10], [68]:*

$$\sigma(\mathbf{A})=\{\varepsilon_1,\varepsilon_2,\cdots,\varepsilon_{p-1}\} \tag{B.10}$$

Definition B.2. *The* spectral radius *of a* $p-1\times p-1$ *square matrix* $\mathbf{A}$ *can be defined as the largest absolute value of the* eigenvalues *and can be written as follows [3], [10], [12], [19], [68]:*

$$\rho(\mathbf{A})=\max_{1\leq l\leq p-1}|\varepsilon_l| \tag{B.11}$$

where ε_l *refers to the* l^{th} eigenvalue *of matrix* $\mathbf{A}$*.*

Theorem B.2. *For a* $p-1\times p-1$ *square matrix* $\mathbf{A}$*, the sum of the main diagonal entries is defined as the* trace *of the matrix* $\mathbf{A}$*, denoted as* $\mathrm{tr}(\mathbf{A})$*. The trace of a matrix* $\mathbf{A}$ *is also equal to the sum of its* $p-1$ eigenvalues *[18], [19]. This can be written as follows:*

$$\begin{aligned}\mathrm{tr}(\mathbf{A})&=\sum_{l=1}^{p-1}[\mathbf{A}]_{ll}\\&=\sum_{l=1}^{p-1}\varepsilon_l\end{aligned} \tag{B.12}$$

where $[\mathbf{A}]_{ll}$ *refers to the diagonal elements of matrix* $\mathbf{A}$ *and* ε_l *refers to the* l^{th} eigenvalue *of matrix* $\mathbf{A}$*. If* $\mathbf{A}$ *and* $\mathbf{B}$ *are matrices of type* $M_{p-1}(\mathbb{C})$ *and* a *is a constant, then the following properties are valid [1]:*

(a) $\mathrm{tr}(\mathbf{A}+\mathbf{B})=\mathrm{tr}(\mathbf{A})+\mathrm{tr}(\mathbf{B})$

(b) $\mathrm{tr}(a\mathbf{A})=a\,\mathrm{tr}(\mathbf{A})$

(c) $\mathrm{tr}(\mathbf{A^T})=\mathrm{tr}(\mathbf{A})$

(d) $\mathrm{tr}(\mathbf{AB})=\mathrm{tr}(\mathbf{BA})$

Theorem B.3. *The* Spectral Mapping Theorem for matrices *states that for a polynomial in* z*, where* z *is of* $\mathbb{C}$*:*

$$p(z)\;=\;a_{p-1}z^{p-1}\;+\;a_{p-2}z^{p-2}\;+\;\cdots\;+\;z_0I \tag{B.13}$$

the spectrum *of the polynomial of a matrix* $\mathbf{A}$ *can be written as follows [11], [12]:*

$$\sigma(p(\mathbf{A})) \quad = \quad p\left\{\sigma(\mathbf{A})\right\} \tag{B.14}$$

Theorem B.4. *For a square matrix* $\mathbf{A}$*, the* determinant*, denoted as* $\det(\mathbf{A})$*, is the product of the* eigenvalues *of* $\mathbf{A}$*. It can be defined as follows [18] (Theorem 268B):*

$$\det(\mathbf{A}) = \prod_{l=1}^{p-1} \varepsilon_l \tag{B.15}$$

where ε_l *refers to the* l^{th} eigenvalue *of matrix* $\mathbf{A}$*. The* determinant *of a matrix has the following properties:*

(a) $\det(\mathbf{A^T}) = \det(\mathbf{A})$

(b) $\det(\mathbf{AB}) = \det(\mathbf{A})\det(\mathbf{B}) = \det(\mathbf{BA})$

Theorem B.5. *For a matrix* $\mathbf{A}$*, the* norm*, denoted as* $\|\mathbf{A}\|$ *can be defined as follows [10], [12]:*

$$\|\mathbf{A}\| = \max_r \sum_{s=1}^{p-1} |[A]_{rs}| \tag{B.16}$$

where $[A]_{rs}$ *refers to the* rs^{th} *element of matrix* $\mathbf{A}$*. If the matrix* $\mathbf{A}$ *is a* diagonal matrix*, the above definition reduces to the following:*

$$\|\mathbf{A}\| = \max\left\{|\varepsilon_1|, |\varepsilon_2|, \ldots, |\varepsilon_{p-1}|\right\} \tag{B.17}$$

The matrix norm *has the following properties:*

(a) $\|0\| = 0$

(b) $\|\mathbf{A}\| > 0$ *if* $\mathbf{A} \neq 0$

(c) $\|a\mathbf{A}\| = |a|\,\|\mathbf{A}\|$

(d) $\|\mathbf{A} + \mathbf{B}\| \leq \|\mathbf{A}\| + \|\mathbf{B}\|$

(e) $\|\mathbf{AB}\| \leq \|\mathbf{A}\|\,\|\mathbf{B}\|$

where a *is a* scalar *and* $\mathbf{A}$ *and* $\mathbf{B}$ *are* $p-1 \times p-1$ *matrices of* $\mathbb{C}$*.*

Theorem B.6. *The* adjoint*,* involution *or* Hermitian transpose *of a matrix, denoted as* $\mathbf{A}^*$*, is the* conjugate transpose *of the matrix* $\mathbf{A}$ *and has the following properties [2], [3], [18]:*

(a) $(a\mathbf{A} + b\mathbf{B})^* = \overline{a}\mathbf{A}^* + \overline{b}\mathbf{B}^*$

(b) $\mathbf{I}^* = \mathbf{I}$

(c) $\mathbf{A}^{**} = \mathbf{A}$

(d) $(\mathbf{AB})^* = \mathbf{B}^*\mathbf{A}^*$

(e) $(\mathbf{A}^*)^{-1} = (\mathbf{A^{-1}})^*$

(f) $\|\mathbf{A}\| = \|\mathbf{A}^*\|$

(g) $\rho(\mathbf{AA}^*) = \|\mathbf{A}^*\|^2$

Theorem B.7. *"The principal* $p-1^{th}$ *root* ω *of unity, is a root satisfying the equations* $\omega^{p-1} = 1$ *and the following property holds:*

$$\sum_{r=0}^{p-2} \omega^{rs} = 0 \;\; \textit{for } s = 1, \cdots, p-1\text{"} \tag{B.18}$$

[4] p. 11, [7], [66] and [68].

Theorem B.8. *The union* $\mathbb{G}$ *of the* $p-1$ Gerschgorin circles *defined by the following:*

$$|z - [\mathbf{A}]_{rr}| \leq \delta_r \;\; \textit{where} \;\; \delta_r = \sum_{\substack{r=1 \\ s \neq r}}^{p-1} |[\mathbf{A}]_{rs}| \;\; \textit{where } r = 1, \ldots, p-1 \tag{B.19}$$

contains the eigenvalues *of the matrix* $\boldsymbol{A}$ *in* $\mathbb{C}^{p-1}$*. Thus, the* eigenvalues *of the matrix* $\mathbf{A}$ *lie within the circles centred at* $[\mathbf{A}]_{rr}$ *with radii* δ_r *determined by equation (B.19) [14].*

B.3 The 3-cell calculations

This section aims at calculating $\det(2Re\{\mathbf{\Lambda}\})$. The matrix $2Re\{\mathbf{\Lambda}\}$ was first encountered in Chapter 4, section 4.4. The Theorems and Definitions listed in section B.2 are used in this section as an introduction and is then used extensively in the sections that follow. The first step in the calculation process is to factor the matrices $\mathbf{\Lambda}$ and $\overline{\mathbf{\Lambda}}$

$$\begin{aligned}
\mathbf{\Lambda} &= \begin{bmatrix} \lambda_1 + \lambda_2 & e^{j\frac{2\pi}{3}}\lambda_1 + e^{-j\frac{2\pi}{3}}\lambda_2 \\ e^{-j\frac{2\pi}{3}}\lambda_1 + e^{j\frac{2\pi}{3}}\lambda_2 & \lambda_1 + \lambda_2 \end{bmatrix} \\
&= \begin{bmatrix} \lambda_1 & \lambda_2 \\ e^{-j\frac{2\pi}{3}}\lambda_1 & e^{j\frac{2\pi}{3}}\lambda_2 \end{bmatrix} \begin{bmatrix} 1 & e^{j\frac{2\pi}{3}} \\ 1 & e^{-j\frac{2\pi}{3}} \end{bmatrix} \\
&= \begin{bmatrix} 1 & 1 \\ e^{-j\frac{2\pi}{3}} & e^{j\frac{2\pi}{3}} \end{bmatrix} \begin{bmatrix} \lambda_1 & 0 \\ 0 & \lambda_2 \end{bmatrix} \begin{bmatrix} 1 & e^{j\frac{2\pi}{3}} \\ 1 & e^{-j\frac{2\pi}{3}} \end{bmatrix}
\end{aligned} \tag{B.20}$$

and

$$\begin{aligned}\overline{\mathbf{\Lambda}} &= \begin{bmatrix} \overline{\lambda_1}+\overline{\lambda_2} & e^{-j\frac{2\pi}{3}}\overline{\lambda_1}+e^{j\frac{2\pi}{3}}\overline{\lambda_2} \\ e^{j\frac{2\pi}{3}}\overline{\lambda_1}+e^{-j\frac{2\pi}{3}}\overline{\lambda_2} & \overline{\lambda_1}+\overline{\lambda_2} \end{bmatrix} \\ &= \begin{bmatrix} \overline{\lambda_2} & \overline{\lambda_1} \\ e^{-j\frac{2\pi}{3}}\overline{\lambda_2} & e^{j\frac{2\pi}{3}}\overline{\lambda_1} \end{bmatrix} \begin{bmatrix} 1 & e^{j\frac{2\pi}{3}} \\ 1 & e^{-j\frac{2\pi}{3}} \end{bmatrix} \\ &= \begin{bmatrix} 1 & 1 \\ e^{-j\frac{2\pi}{3}} & e^{j\frac{2\pi}{3}} \end{bmatrix} \begin{bmatrix} \overline{\lambda_2} & 0 \\ 0 & \overline{\lambda_1} \end{bmatrix} \begin{bmatrix} 1 & e^{j\frac{2\pi}{3}} \\ 1 & e^{-j\frac{2\pi}{3}} \end{bmatrix} \end{aligned} \tag{B.21}$$

Equations (B.20) and (B.21) can now be combined into the following:

$$\begin{aligned} 2Re\{\mathbf{\Lambda}\} &= \begin{bmatrix} 2Re\{\lambda_1+\lambda_2\} & 2Re\{e^{j\frac{2\pi}{3}}\lambda_1+e^{-j\frac{2\pi}{3}}\lambda_2\} \\ 2Re\{e^{-j\frac{2\pi}{3}}\lambda_1+e^{j\frac{2\pi}{3}}\lambda_2\} & 2Re\{\lambda_1+\lambda_2\} \end{bmatrix} \\ &= \mathbf{\Lambda}+\overline{\mathbf{\Lambda}} \\ &= \begin{bmatrix} 1 & 1 \\ e^{-j\frac{2\pi}{3}} & e^{j\frac{2\pi}{3}} \end{bmatrix} \begin{bmatrix} \lambda_1 & 0 \\ 0 & \lambda_2 \end{bmatrix} \begin{bmatrix} 1 & e^{j\frac{2\pi}{3}} \\ 1 & e^{-j\frac{2\pi}{3}} \end{bmatrix} + \\ &\quad \begin{bmatrix} 1 & 1 \\ e^{-j\frac{2\pi}{3}} & e^{j\frac{2\pi}{3}} \end{bmatrix} \begin{bmatrix} \overline{\lambda_2} & 0 \\ 0 & \overline{\lambda_1} \end{bmatrix} \begin{bmatrix} 1 & e^{j\frac{2\pi}{3}} \\ 1 & e^{-j\frac{2\pi}{3}} \end{bmatrix} \\ &= \begin{bmatrix} 1 & 1 \\ e^{-j\frac{2\pi}{3}} & e^{j\frac{2\pi}{3}} \end{bmatrix} \begin{bmatrix} \lambda_1+\overline{\lambda_2} & 0 \\ 0 & \lambda_2+\overline{\lambda_1} \end{bmatrix} \begin{bmatrix} 1 & e^{j\frac{2\pi}{3}} \\ 1 & e^{-j\frac{2\pi}{3}} \end{bmatrix} \\ &= \mathbf{BLC} \end{aligned} \tag{B.22}$$

where:

$$\mathbf{B} = \begin{bmatrix} 1 & 1 \\ e^{-j\frac{2\pi}{3}} & e^{j\frac{2\pi}{3}} \end{bmatrix} \tag{B.23}$$

$$\mathbf{L} = \begin{bmatrix} \lambda_1+\overline{\lambda_2} & 0 \\ 0 & \lambda_2+\overline{\lambda_1} \end{bmatrix} \tag{B.24}$$

$$\mathbf{C} = \begin{bmatrix} 1 & e^{j\frac{2\pi}{3}} \\ 1 & e^{-j\frac{2\pi}{3}} \end{bmatrix} \tag{B.25}$$

The inverse of the diagonal matrix $\mathbf{L}$ can be calculated directly as follows:

$$\mathbf{L^{-1}} = \begin{bmatrix} \frac{1}{\lambda_1+\overline{\lambda_2}} & 0 \\ 0 & \frac{1}{\lambda_2+\overline{\lambda_1}} \end{bmatrix} \tag{B.26}$$

The determinant of $\mathbf{L}$ is the product of its diagonal elements and can be written as follows:

$$\det(\mathbf{L}) = (\lambda_1+\overline{\lambda_2})(\lambda_2+\overline{\lambda_1}) \tag{B.27}$$

In equation (B.22), it can be seen that the matrices $\mathbf{B}$ and $\mathbf{C}$ are conjugate transposes of each other, resulting in the following:

$$\mathbf{C} = \mathbf{B}^* \tag{B.28}$$

which leads to the following:

$$2Re\{\mathbf{\Lambda}\} = \mathbf{BLB}^* \tag{B.29}$$

The determinant of $2Re\{\mathbf{\Lambda}\}$ can be obtained directly as follows:

$$\begin{aligned}\det(2Re\{\mathbf{\Lambda}\}) &= (\lambda_1 + \lambda_2 + \overline{\lambda_1} + \overline{\lambda_2})(\lambda_1 + \lambda_2 + \overline{\lambda_1} + \overline{\lambda_2}) - \\ &\quad (e^{j\frac{2\pi}{3}}\lambda_1 + e^{-j\frac{2\pi}{3}}\lambda_2 + e^{-j\frac{2\pi}{3}}\overline{\lambda_1} + e^{j\frac{2\pi}{3}}\overline{\lambda_2})(e^{-j\frac{2\pi}{3}}\lambda_1 + e^{j\frac{2\pi}{3}}\lambda_2 + e^{j\frac{2\pi}{3}}\overline{\lambda_1} + e^{-j\frac{2\pi}{3}}\overline{\lambda_2}) \\ &= \lambda_1^2 + \lambda_2^2 + \overline{\lambda_1}^2 + \overline{\lambda_2}^2 + 2\lambda_1\lambda_2 + 2\lambda_1\overline{\lambda_1} + 2\lambda_1\overline{\lambda_2} + 2\overline{\lambda_1}\lambda_2 + 2\lambda_2\overline{\lambda_2} + 2\overline{\lambda_1\lambda_2} - \\ &\quad (\lambda_1^2 + \lambda_2^2 + \overline{\lambda_1}^2 + \overline{\lambda_2}^2 + (e^{j\frac{4\pi}{3}} + e^{-j\frac{4\pi}{3}})\lambda_1\lambda_2 + (e^{j\frac{4\pi}{3}} + e^{-j\frac{4\pi}{3}})\lambda_1\overline{\lambda_1} + 2\lambda_1\overline{\lambda_2} + \\ &\quad 2\overline{\lambda_1}\lambda_2 + (e^{j\frac{4\pi}{3}} + e^{-j\frac{4\pi}{3}})\lambda_2\overline{\lambda_2} + (e^{j\frac{4\pi}{3}} + e^{-j\frac{4\pi}{3}})\overline{\lambda_1\lambda_2})\end{aligned} \tag{B.30}$$

Using Euler's Relations, $e^{j\frac{4\pi}{3}}$ and $e^{-j\frac{4\pi}{3}}$ can be expanded as follows:

$$e^{j\frac{4\pi}{3}} = \cos\left(\frac{4\pi}{3}\right) + j\sin\left(\frac{4\pi}{3}\right) = -\frac{1}{2} - j\frac{\sqrt{3}}{2} \tag{B.31}$$

$$e^{-j\frac{4\pi}{3}} = \cos\left(\frac{4\pi}{3}\right) - j\sin\left(\frac{4\pi}{3}\right) = -\frac{1}{2} + j\frac{\sqrt{3}}{2} \tag{B.32}$$

Adding the relations shown in equations (B.31) and (B.32) results in the following:

$$e^{j\frac{4\pi}{3}} + e^{-j\frac{4\pi}{3}} = -1 \tag{B.33}$$

Using equation (B.33), (B.30) can be simplified to the following:

$$\begin{aligned}\det(2Re\{\mathbf{\Lambda}\}) &= 3(\lambda_1\lambda_2 + \lambda_1\lambda_1 + \lambda_2\overline{\lambda_2} + \overline{\lambda_1\lambda_2}) \\ &= 3(\lambda_1 + \overline{\lambda_2})(\lambda_2 + \overline{\lambda_1})\end{aligned} \tag{B.34}$$

The determinant of $2Re\{\mathbf{\Lambda}\}$ can be obtained indirectly as well. This method will also be demonstrated here, as this method will be used for the cases where the number of cells, $p > 3$. This method uses Theorem B.4(b) and is as follows:

$$\begin{aligned}\det(2Re\{\mathbf{\Lambda}\}) &= \det(\mathbf{B})\det(\mathbf{L})\det(\mathbf{C}) \\ &= \det(\mathbf{B})\det(\mathbf{C})\det(\mathbf{L})\end{aligned}$$

$$= \det(\mathbf{BC}) \det(\mathbf{L}) \tag{B.35}$$

Let $\mathbf{D}$ be the following matrix:

$$\begin{aligned} \mathbf{D} &= \mathbf{BC} \\ &= \mathbf{BB}^* \\ &= \begin{bmatrix} 2 & -1 \\ -1 & 2 \end{bmatrix} \end{aligned} \tag{B.36}$$

The following procedure describes how the eigenvalues of $\mathbf{D}$ can be calculated indirectly. This procedure will be extended to accomodate the "p-cell" case, discussed in section B.5. The procedure is as follows:

Matrix $\mathbf{D}$ can be rewritten in another form:

$$\begin{aligned} \mathbf{D} &= \mathbf{X} + 3\mathbf{I} \\ &= \begin{bmatrix} -1 & -1 \\ -1 & -1 \end{bmatrix} + 3 \begin{bmatrix} 1 & 0 \\ 0 & 1 \end{bmatrix} \end{aligned} \tag{B.37}$$

where:

$$\mathbf{X} = \begin{bmatrix} -1 & -1 \\ -1 & -1 \end{bmatrix} \tag{B.38}$$

$$\mathbf{I} = \begin{bmatrix} 1 & 0 \\ 0 & 1 \end{bmatrix} \tag{B.39}$$

Now that the matrix $\mathbf{D}$ was written in a different form, the spectrum of $\mathbf{D}$ can be calculated using the Spectral Mapping Theorem (Theorem B.3) as follows:

$$\begin{aligned} \sigma(\mathbf{D}) &= \sigma(\mathbf{X}) + 3\sigma(\mathbf{I}) \\ &= \sigma(\mathbf{X}) + \{3\} \end{aligned} \tag{B.40}$$

Note that:

$$\begin{aligned} \mathbf{X}^2 + 2\mathbf{X} &= 0 \\ \mathbf{X}(\mathbf{X} + 2\mathbf{I}) &= 0 \end{aligned} \tag{B.41}$$

The solutions of equation (B.41), i.e. $\{0, -2\}$, are also the eigenvalues of $\mathbf{X}$, which means that $\sigma(\mathbf{X}) = \{0, -2\}$. The reason for the solutions of equation (B.41) also being the eigenvalues of $\mathbf{X}$, follows from the spectral mapping theorem [12]. These values can then be substituted back into equation (B.40) as follows:

$$\begin{aligned} \sigma(\mathbf{D}) &= \sigma(\mathbf{X}) + \{3\} \\ &\subseteq \{0, -2\} + \{3\} \end{aligned}$$

$$= \{1, 3\} \tag{B.42}$$

From the solutions in equation (B.42), the spectrum of $\mathbf{D}$ can be represented as follows:

$$\sigma(\mathbf{D}) \subseteq \{1, 3\} \tag{B.43}$$

The spectrum is the set of eigenvalues of $\mathbf{D}$. According to Theorem 268B of [18], the trace of matrix $\mathbf{D}$ can be used to determine the multiplicity of the eigenvalues. This method is however only valid for this special case and is not valid in general. As described in section B.2, the trace of matrix $\mathbf{D}$ can be calculated as follows:

$$\begin{aligned} \mathrm{tr}(\mathbf{D}) &= [\mathbf{D}]_{11} + [\mathbf{D}]_{22} \\ &= 2 + 2 \\ &= 4 \end{aligned} \tag{B.44}$$

As the eigenvalues have been calculated to be $\{1, 3\}$, a trace of 4 means that the multiplicity of the eigenvalue $\{3\}$ is 1, as the sum of the eigenvalues sums to the trace value of $\mathbf{D}$. This is the only possible solution that results in a trace of 4 for this case.

Therefore the determinant of $\mathbf{D}$ can be obtained as follows:

$$\begin{aligned} \det(\mathbf{D}) &= 1 \cdot 3^1 \\ &= 3 \end{aligned} \tag{B.45}$$

Having calculated the determinant of $\mathbf{D}$, it is possible to calculate the determinant of $2Re\{\mathbf{\Lambda}\}$ as follows:

$$\begin{aligned} \det(2Re\{\mathbf{\Lambda}\}) &= \det(\mathbf{D}) \det(\mathbf{L}) \\ &= 3(\lambda_1 + \overline{\lambda_2})(\lambda_2 + \overline{\lambda_1}) \end{aligned} \tag{B.46}$$

The inverse of $2Re\{\mathbf{\Lambda}\}$ can be calculated directly or its norm can be calculated indirectly. The direct approach is feasible up to 3×3 matrices, after which the calculation becomes complicated. The direct approach for the calculation of $(2Re\{\mathbf{\Lambda}\})^{-1}$ is as follows:

$$\begin{aligned} (2Re\{\mathbf{\Lambda}\})^{-1} &= (\mathbf{B}^*)^{-1}\mathbf{L}^{-1}\mathbf{B}^{-1} \\ &= \frac{1}{e^{j\frac{2\pi}{3}} - e^{-j\frac{2\pi}{3}}} \begin{bmatrix} e^{j\frac{2\pi}{3}} & -e^{-j\frac{2\pi}{3}} \\ -1 & 1 \end{bmatrix} \begin{bmatrix} \frac{1}{\lambda_1+\overline{\lambda_2}} & 0 \\ 0 & \frac{1}{\lambda_2+\overline{\lambda_1}} \end{bmatrix} \frac{1}{e^{-j\frac{2\pi}{3}} - e^{j\frac{2\pi}{3}}} \begin{bmatrix} e^{j\frac{2\pi}{3}} & -1 \\ -e^{-j\frac{2\pi}{3}} & 1 \end{bmatrix} \\ &= \begin{bmatrix} \frac{1}{3}\frac{(\lambda_1+\overline{\lambda_2})+(\lambda_2+\overline{\lambda_1})}{(\lambda_1+\overline{\lambda_2})(\lambda_2+\overline{\lambda_1})} & \frac{1}{6}\frac{(1-j\sqrt{3})(\lambda_1+\overline{\lambda_2})+(1+j\sqrt{3})(\lambda_2+\overline{\lambda_1})}{(\lambda_1+\overline{\lambda_2})(\lambda_2+\overline{\lambda_1})} \\ \frac{1}{6}\frac{(1+j\sqrt{3})(\lambda_1+\overline{\lambda_2})+(1-j\sqrt{3})(\lambda_2+\overline{\lambda_1})}{(\lambda_1+\overline{\lambda_2})(\lambda_2+\overline{\lambda_1})} & \frac{1}{3}\frac{(\lambda_1+\overline{\lambda_2})+(\lambda_2+\overline{\lambda_1})}{(\lambda_1+\overline{\lambda_2})(\lambda_2+\overline{\lambda_1})} \end{bmatrix} \end{aligned} \tag{B.47}$$

The indirect approach for the calculation of $\|(2Re\{\mathbf{\Lambda}\})^{-1}\|$ is based on the properties from [2] as repeated in section B.2 Theorem B.6 as follows:

$$(2Re\{\mathbf{\Lambda}\})^{-1} = (\mathbf{B}^*)^{-1}\mathbf{L^{-1}}\mathbf{B^{-1}} \tag{B.48}$$

An upper bound for the norm of $(2Re\{\mathbf{\Lambda}\})^{-1}$ can now be determined by using equation (B.48), as follows:

$$\left\|(2Re\{\mathbf{\Lambda}\})^{-1}\right\| \leq \left\|(\mathbf{B}^*)^{-1}\right\| \left\|\mathbf{L^{-1}}\right\| \left\|\mathbf{B^{-1}}\right\| \tag{B.49}$$

According to Theorem 6.2.1.(iv) from [2] as repeated in Theorem B.6, the following is true for $\|\mathbf{B^{-1}}\|^2$:

$$\begin{aligned}\left\|\mathbf{B^{-1}}\right\|^2 &= \rho\left(\mathbf{B^{-1}}(\mathbf{B^{-1}})^*\right) \\ &= \rho\left(\mathbf{B^{-1}}(\mathbf{B}^*)^{-1}\right) \text{ from Theorem 6.1.1. (iv) [2]} \\ &= \rho\left((\mathbf{B}^*\mathbf{B})^{-1}\right)\end{aligned} \tag{B.50}$$

The relation between $\sigma(\mathbf{BB}^*)$ and $\sigma(\mathbf{B}^*\mathbf{B})$ is described by Lemma 3.1.2 on p. 36 of [2]:

$$\sigma(\mathbf{BB}^*) \cup \{0\} = \sigma(\mathbf{B}^*\mathbf{B}) \cup \{0\} \tag{B.51}$$

From equations (B.36), (B.43) and (B.51), it can be seen that the spectrum of $\mathbf{BB}^*$ is the following:

$$\sigma(\mathbf{BB}^*) = \{1, 3\} \tag{B.52}$$

Using the spectral mapping theorem [12], the spectrum of $(\mathbf{BB}^*)^{-1}$ is the inverse of the spectrum of $\mathbf{BB}^*$ as follows:

$$\sigma\left((\mathbf{BB}^*)^{-1}\right) = \left\{\frac{1}{3}, 1\right\} \tag{B.53}$$

Using Theorem B.2, the spectral radius of $(\mathbf{BB}^*)^{-1}$ can be calculated as follows:

$$\begin{aligned}\rho\left((\mathbf{BB}^*)^{-1}\right) &= \max\left\{|\varepsilon| : \varepsilon \in \ \sigma\left((\mathbf{BB}^*)^{-1}\right)\right\} \\ &= |1| \\ &= 1\end{aligned} \tag{B.54}$$

Substituting the result of equation (B.54) back into equation (B.50) results in the following:

$$\begin{aligned}\left\|\mathbf{B^{-1}}\right\|^2 &= 1 \\ \left\|\mathbf{B^{-1}}\right\| &= 1\end{aligned} \tag{B.55}$$

When Theorem B.6(f) is applied to equation (B.55), the following is obtained:

$$\left\|\left(\mathbf{B^{-1}}\right)^{*}\right\| = \left\|\mathbf{B^{-1}}\right\| \tag{B.56}$$

Theorem B.6(e) can now be applied to obtain the following:

$$\left\|(\mathbf{B}^{*})^{-1}\right\| = \left\|\left(\mathbf{B^{-1}}\right)^{*}\right\| \tag{B.57}$$

Now, from equation (B.55), it follows that

$$\left\|(\mathbf{B}^{*})^{-1}\right\| = 1 \tag{B.58}$$

Substituting equations (B.56) and (B.58) back into equation (B.49) results in the following:

$$\begin{aligned}\left\|(2Re\{\mathbf{\Lambda}\})^{-1}\right\| &\leq \left\|\mathbf{L^{-1}}\right\| \\ &= \max\left\{\frac{1}{\left|\lambda_1 + \overline{\lambda_2}\right|}, \frac{1}{\left|\lambda_2 + \overline{\lambda_1}\right|}\right\}\end{aligned} \tag{B.59}$$

The same approach can also be used to determine the spectral radius of $2Re\{\mathbf{\Lambda}\}$ as follows:

$$\begin{aligned}\rho(2Re\{\mathbf{\Lambda}\}) &= \rho(\mathbf{BLB}^{*}) \\ &\leq \|\mathbf{B}\|\,\|\mathbf{L}\|\,\|\mathbf{B}^{*}\|\end{aligned} \tag{B.60}$$

According to Theorem 6.2.1.(iv) from [2] as repeated in Theorem B.6, the following is true for $\|\mathbf{B}\|^2$:

$$\|\mathbf{B}\|^2 = \rho\left(\mathbf{BB}^{*}\right) \tag{B.61}$$

Using Theorem B.2 and the result of equation (B.52), the spectral radius of $\mathbf{BB}^{*}$ can be calculated as follows:

$$\begin{aligned}\rho\left(\mathbf{BB}^{*}\right) &= \max\left\{|\varepsilon| : \varepsilon \in\ \sigma\left(\mathbf{BB}^{*}\right)\right\} \\ &= |3| \\ &= 3\end{aligned} \tag{B.62}$$

Substituting the result of equation (B.62) into equation (B.61) results in the following:

$$\begin{aligned}\|\mathbf{B}\|^2 &= 3 \\ \|\mathbf{B}\| &= \sqrt{3}\end{aligned} \tag{B.63}$$

When Theorem B.6(f) is applied to equation (B.63), the following is obtained:

$$\|(\mathbf{B})^{*}\| = \|\mathbf{B}\| = \sqrt{3} \tag{B.64}$$

Substituting the result obtained in equation (B.64) into equation (B.60) results in the following:

$$\begin{aligned}\rho(2Re\{\mathbf{\Lambda}\}) &\leq \|\mathbf{B}\|\,\|\mathbf{L}\|\,\|\mathbf{B}^*\| \\ &= \sqrt{3}\,\|\mathbf{L}\|\,\sqrt{3} \\ &= 3\max\left\{\left|\lambda_1+\overline{\lambda_2}\right|,\left|\lambda_2+\overline{\lambda_1}\right|\right\}\end{aligned} \tag{B.65}$$

The above results, equations (B.46), (B.59) and (B.65) are valid for the steady-state analysis in Chapter 4. The matrix $2Re\{\mathbf{\Lambda}\}$ is multiplied with a constant $-\frac{1}{C}$ for the time constant analysis of Chapter 5. The above results can be adjusted to accomodate this constant. Using the properties of the determinant of a matrix, equation (B.46) can be rewritten for the time constant analysis as follows:

$$\det\left(-\frac{1}{C}2Re\{\mathbf{\Lambda}\}\right) = \left(-\frac{1}{C}\right)^2 3(\lambda_1+\overline{\lambda_2})(\lambda_2+\overline{\lambda_1}) \tag{B.66}$$

Using Theorem B.5(c) equations (B.59) and (B.65) can be rewritten for the time constant analysis as follows:

$$\left\|\left(-\frac{1}{C}2Re\{\mathbf{\Lambda}\}\right)^{-1}\right\| \leq |C|\max\left\{\frac{1}{\left|\lambda_1+\overline{\lambda_2}\right|},\frac{1}{\left|\lambda_2+\overline{\lambda_1}\right|}\right\} \tag{B.67}$$

$$\rho\left(-\frac{1}{C}2Re\{\mathbf{\Lambda}\}\right) \leq \frac{3}{C}\max\left\{\left|\lambda_1+\overline{\lambda_2}\right|,\left|\lambda_2+\overline{\lambda_1}\right|\right\} \tag{B.68}$$

B.4 The 4-cell calculations

This section follows roughly the same method as the previous section and aims at calculating $\det(2Re\{\mathbf{\Lambda}\})$ for the 4-cell case. A variant of the matrix $2Re\{\mathbf{\Lambda}\}$, i.e. $-\frac{1}{C}2Re\{\mathbf{\Lambda}\}$ was encountered in the examples used in Chapter 5, section 5.4, where the time constant analysis of a p-cell multicell converter was treated. The Theorems and Definitions listed in section B.2 are again used extensively for this calculation.

$$\begin{aligned}\mathbf{\Lambda} &= \begin{bmatrix} \lambda_1+\lambda_2+\lambda_3 & e^{j\frac{\pi}{2}}\lambda_1+e^{j\pi}\lambda_2+e^{-j\frac{\pi}{2}}\lambda_3 & e^{-j\pi}\lambda_1+\lambda_2+e^{-j\pi}\lambda_3 \\ e^{-j\frac{\pi}{2}}\lambda_1+e^{-j\pi}\lambda_2+e^{j\frac{\pi}{2}}\lambda_3 & \lambda_1+\lambda_2+\lambda_3 & e^{j\frac{\pi}{2}}\lambda_1+e^{j\pi}\lambda_2+e^{-j\frac{\pi}{2}}\lambda_3 \\ e^{j\pi}\lambda_1+\lambda_2+e^{j\pi}\lambda_3 & e^{-j\frac{\pi}{2}}\lambda_1+e^{-j\pi}\lambda_2+e^{j\frac{\pi}{2}}\lambda_3 & \lambda_1+\lambda_2+\lambda_3 \end{bmatrix} \\ &= \begin{bmatrix} \lambda_1 & \lambda_2 & \lambda_3 \\ e^{-j\frac{\pi}{2}}\lambda_1 & e^{-j\pi}\lambda_2 & e^{j\frac{\pi}{2}}\lambda_3 \\ e^{j\pi}\lambda_1 & \lambda_2 & e^{-j\pi}\lambda_3 \end{bmatrix}\begin{bmatrix} 1 & e^{j\frac{\pi}{2}} & e^{-j\pi} \\ 1 & e^{j\pi} & 1 \\ 1 & e^{j\frac{\pi}{2}} & e^{-j\pi} \end{bmatrix} \\ &= \begin{bmatrix} 1 & 1 & 1 \\ -j & -1 & j \\ -1 & 1 & -1 \end{bmatrix}\begin{bmatrix} \lambda_1 & 0 & 0 \\ 0 & \lambda_2 & 0 \\ 0 & 0 & \lambda_3 \end{bmatrix}\begin{bmatrix} 1 & j & -1 \\ 1 & -1 & 1 \\ 1 & -j & -1 \end{bmatrix}\end{aligned} \tag{B.69}$$

and

$$\begin{aligned}\overline{\mathbf{\Lambda}} &= \begin{bmatrix} \overline{\lambda_1}+\overline{\lambda_2}+\overline{\lambda_3} & e^{-j\frac{\pi}{2}}\overline{\lambda_1}+e^{-j\pi}\overline{\lambda_2}+e^{j\frac{\pi}{2}}\overline{\lambda_3} & e^{j\pi}\overline{\lambda_1}+\overline{\lambda_2}+e^{j\pi}\overline{\lambda_3} \\ e^{j\frac{\pi}{2}}\overline{\lambda_1}+e^{j\pi}\overline{\lambda_2}+e^{-j\frac{\pi}{2}}\overline{\lambda_3} & \overline{\lambda_1}+\overline{\lambda_2}+\overline{\lambda_3} & e^{-j\frac{\pi}{2}}\overline{\lambda_1}+e^{-j\pi}\overline{\lambda_2}+e^{j\frac{\pi}{2}}\overline{\lambda_3} \\ e^{-j\pi}\overline{\lambda_1}+\overline{\lambda_2}+e^{-j\pi}\overline{\lambda_3} & e^{j\frac{\pi}{2}}\overline{\lambda_1}+e^{j\pi}\overline{\lambda_2}+e^{-j\frac{\pi}{2}}\overline{\lambda_3} & \overline{\lambda_1}+\overline{\lambda_2}+\overline{\lambda_3} \end{bmatrix} \\ &= \begin{bmatrix} \overline{\lambda_3} & \overline{\lambda_2} & \overline{\lambda_1} \\ e^{-j\frac{\pi}{2}}\overline{\lambda_3} & e^{-j\pi}\overline{\lambda_2} & e^{j\frac{\pi}{2}}\overline{\lambda_1} \\ e^{j\pi}\overline{\lambda_3} & \overline{\lambda_2} & e^{-j\pi}\overline{\lambda_1} \end{bmatrix} \begin{bmatrix} 1 & e^{j\frac{\pi}{2}} & e^{-j\pi} \\ 1 & e^{j\pi} & 1 \\ 1 & e^{j\frac{\pi}{2}} & e^{-j\pi} \end{bmatrix} \\ &= \begin{bmatrix} 1 & 1 & 1 \\ -j & -1 & j \\ -1 & 1 & -1 \end{bmatrix} \begin{bmatrix} \overline{\lambda_3} & 0 & 0 \\ 0 & \overline{\lambda_2} & 0 \\ 0 & 0 & \overline{\lambda_3} \end{bmatrix} \begin{bmatrix} 1 & j & -1 \\ 1 & -1 & 1 \\ 1 & -j & -1 \end{bmatrix} \end{aligned} \tag{B.70}$$

Equations (B.69) and (B.70) can now be combined into the following:

$$\begin{aligned} 2Re\{\mathbf{\Lambda}\} &= \begin{bmatrix} 1 & 1 & 1 \\ -j & -1 & j \\ -1 & 1 & -1 \end{bmatrix} \begin{bmatrix} \lambda_1 & 0 & 0 \\ 0 & \lambda_2 & 0 \\ 0 & 0 & \lambda_3 \end{bmatrix} \begin{bmatrix} 1 & j & -1 \\ 1 & -1 & 1 \\ 1 & -j & -1 \end{bmatrix} + \\ &\quad \begin{bmatrix} 1 & 1 & 1 \\ -j & -1 & j \\ -1 & 1 & -1 \end{bmatrix} \begin{bmatrix} \overline{\lambda_3} & 0 & 0 \\ 0 & \overline{\lambda_2} & 0 \\ 0 & 0 & \overline{\lambda_3} \end{bmatrix} \begin{bmatrix} 1 & j & -1 \\ 1 & -1 & 1 \\ 1 & -j & -1 \end{bmatrix} \\ &= \begin{bmatrix} 1 & 1 & 1 \\ -j & -1 & j \\ -1 & 1 & -1 \end{bmatrix} \begin{bmatrix} \lambda_1+\overline{\lambda_3} & 0 & 0 \\ 0 & \lambda_2+\overline{\lambda_2} & 0 \\ 0 & 0 & \lambda_3+\overline{\lambda_1} \end{bmatrix} \begin{bmatrix} 1 & j & -1 \\ 1 & -1 & 1 \\ 1 & -j & -1 \end{bmatrix} \\ &= \mathbf{BLC} \end{aligned} \tag{B.71}$$

where:

$$\mathbf{B} = \begin{bmatrix} 1 & 1 & 1 \\ -j & -1 & j \\ -1 & 1 & -1 \end{bmatrix} \tag{B.72}$$

$$\mathbf{L} = \begin{bmatrix} \lambda_1+\overline{\lambda_3} & 0 & 0 \\ 0 & \lambda_2+\overline{\lambda_2} & 0 \\ 0 & 0 & \lambda_3+\overline{\lambda_1} \end{bmatrix} \tag{B.73}$$

$$\mathbf{C} = \begin{bmatrix} 1 & j & -1 \\ 1 & -1 & 1 \\ 1 & -j & -1 \end{bmatrix} \tag{B.74}$$

The inverse of the diagonal matrix $\mathbf{L}$ can be calculated directly and can be written as follows:

$$\mathbf{L^{-1}} = \begin{bmatrix} \frac{1}{\lambda_1+\overline{\lambda_3}} & 0 & 0 \\ 0 & \frac{1}{\lambda_2+\overline{\lambda_2}} & 0 \\ 0 & 0 & \frac{1}{\lambda_3+\overline{\lambda_1}} \end{bmatrix} \tag{B.75}$$

The determinant of $\mathbf{L}$ is the product of its diagonal elements and can be written as follows:

$$\det(\mathbf{L}) = (\lambda_1 + \overline{\lambda_3})(\lambda_2 + \overline{\lambda_2})(\lambda_3 + \overline{\lambda_1}) \tag{B.76}$$

In equation B.69, it can be seen that the matrices $\mathbf{B}$ and $\mathbf{C}$ are conjugate transposes of each other, resulting in the following simplification:

$$\mathbf{C} = \mathbf{B}^* \tag{B.77}$$

which leads to the following:

$$2Re\{\mathbf{\Lambda}\} = \mathbf{BLB}^* \tag{B.78}$$

The determinant of $2Re\{\mathbf{\Lambda}\}$ will be calculated indirectly as follows:

$$\begin{aligned} \det(2Re\{\mathbf{\Lambda}\}) &= \det(\mathbf{B})\det(\mathbf{L})\det(\mathbf{C}) \\ &= \det(\mathbf{B})\det(\mathbf{C})\det(\mathbf{L}) \\ &= \det(\mathbf{BC})\det(\mathbf{L}) \end{aligned} \tag{B.79}$$

Let $\mathbf{D}$ be the following matrix:

$$\begin{aligned} \mathbf{D} &= \mathbf{BC} \\ &= \mathbf{BB}^* \\ &= \begin{bmatrix} 3 & -1 & -1 \\ -1 & 3 & -1 \\ -1 & -1 & 3 \end{bmatrix} \end{aligned} \tag{B.80}$$

The following procedure describes the indirect calculation of the eigenvalues of $\mathbf{D}$:
Matrix $\mathbf{D}$ can be rewritten in the following form:

$$\begin{aligned} \mathbf{D} &= \mathbf{X} + 4\mathbf{I} \\ &= \begin{bmatrix} -1 & -1 & -1 \\ -1 & -1 & -1 \\ -1 & -1 & -1 \end{bmatrix} + 4 \begin{bmatrix} 1 & 0 & 0 \\ 0 & 1 & 0 \\ 0 & 0 & 1 \end{bmatrix} \end{aligned} \tag{B.81}$$

where:

$$\mathbf{X} = \begin{bmatrix} -1 & -1 & -1 \\ -1 & -1 & -1 \\ -1 & -1 & -1 \end{bmatrix} \tag{B.82}$$

$$\mathbf{I} = \begin{bmatrix} 1 & 0 & 0 \\ 0 & 1 & 0 \\ 0 & 0 & 1 \end{bmatrix} \tag{B.83}$$

Now that the matrix $\mathbf{D}$ was written in a different form, the spectrum of equation (B.81) can be calculated as follows:

$$\begin{aligned} \sigma(\mathbf{D}) &= \sigma(\mathbf{X}) + 4\sigma(\mathbf{I}) \\ &= \sigma(\mathbf{X}) + \{4\} \end{aligned} \tag{B.84}$$

Again, using the spectral mapping theorem [12], equation (B.84) can be rewritten as follows:

$$\begin{aligned} \mathbf{X^2} + 3\mathbf{X} &= 0 \\ \mathbf{X}(\mathbf{X} + 3\mathbf{I}) &= 0 \end{aligned} \tag{B.85}$$

The solutions of equation (B.85), i.e. $\{0, -3\}$, are also the eigenvalues of $\mathbf{X}$, which means that $\sigma(\mathbf{X}) = \{0, -3\}$. The reason for the solutions of equation (B.85) also being the eigenvalues of $\mathbf{X}$, again follows from the spectral mapping theorem [12]. These values can then be substituted back into equation (B.84) as follows:

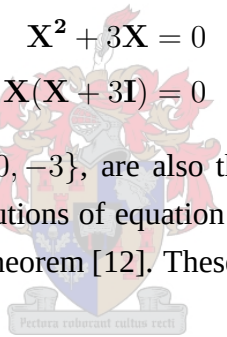

$$\begin{aligned} \sigma(\mathbf{D}) &= \sigma(\mathbf{X}) + \{4\} \\ &\subseteq \{0, -3\} + \{4\} \\ &= \{1, 4\} \end{aligned} \tag{B.86}$$

From the solutions in equation (B.86), the spectrum of $\mathbf{D}$ can be represented as follows:

$$\sigma(\mathbf{D}) \subseteq \{1, 4\} \tag{B.87}$$

The spectrum is the set of eigenvalues of $\mathbf{D}$. According to Theorem 268B of [18], the trace of matrix $\mathbf{D}$ can be used to determine the multiplicity of the eigenvalues. As described in section B.2, the trace of matrix $\mathbf{D}$ can be calculated as follows:

$$\begin{aligned} \mathrm{tr}(\mathbf{D}) &= [D]_{11} + [D]_{22} + [D]_{33} \\ &= 3 + 3 + 3 \\ &= 9 \end{aligned} \tag{B.88}$$

As the eigenvalues have been calculated to be $\{1, 4\}$, a trace of 9 means that the multiplicity of the eigenvalue $\{4\}$ is 2, as the sum of the eigenvalues sums to the trace value of $\mathbf{D}$. This is the only possible solution that results in a trace of 9 for this case.

Therefore the determinant of $\mathbf{D}$ can be obtained as follows:

$$\begin{aligned} \det(\mathbf{D}) &= 1 \cdot 4 \cdot 4 \\ &= 16 \end{aligned} \tag{B.89}$$

Having calculated the determinant of $\mathbf{D}$, it is possible to calculate the determinant of $2Re\{\mathbf{\Lambda}\}$ as follows:

$$\begin{aligned} \det(2Re\{\mathbf{\Lambda}\}) &= \det(\mathbf{D}) \det(\mathbf{L}) \\ &= 16(\lambda_1 + \overline{\lambda_3})(\lambda_2 + \overline{\lambda_2})(\lambda_3 + \overline{\lambda_1}) \end{aligned} \tag{B.90}$$

The indirect approach from the previous section is used again to calculate $\|(2Re\{\mathbf{\Lambda}\})^{-1}\|$ This approach is used as follows, from section B.2 [2]:

$$(2Re\{\mathbf{\Lambda}\})^{-1} = (\mathbf{B}^*)^{-1}\mathbf{L^{-1}}\mathbf{B^{-1}} \tag{B.91}$$

An upper bound for the norm of $(2Re\{\mathbf{\Lambda}\})^{-1}$ can now be determined by using equation (B.91), as follows:

$$\left\|(2Re\{\mathbf{\Lambda}\})^{-1}\right\| \leq \left\|(\mathbf{B}^*)^{-1}\right\| \left\|\mathbf{L^{-1}}\right\| \left\|\mathbf{B^{-1}}\right\| \tag{B.92}$$

According to Theorem 6.2.1.(iv) from [2] as repeated in B.2, the following is true for $\|\mathbf{B^{-1}}\|^2$:

$$\begin{aligned} \left\|\mathbf{B^{-1}}\right\|^2 &= \rho\left(\mathbf{B^{-1}}(\mathbf{B^{-1}})^*\right) \\ &= \rho\left(\mathbf{B^{-1}}(\mathbf{B}^*)^{-1}\right) \text{ from Theorem 6.1.1. (iv) [2]} \\ &= \rho\left((\mathbf{B}^*\mathbf{B})^{-1}\right) \end{aligned} \tag{B.93}$$

The relation between $\sigma(\mathbf{BB}^*)$ and $\sigma(\mathbf{B}^*\mathbf{B})$ is described by Lemma 3.1.2 on p. 36 of [2]:

$$\sigma(\mathbf{BB}^*) \cup \{0\} = \sigma(\mathbf{B}^*\mathbf{B}) \cup \{0\} \tag{B.94}$$

From equations (B.80), (B.86) and (B.94), it can be seen that the spectrum of $\mathbf{BB}^*$ is the following:

$$\sigma(\mathbf{BB}^*) = \{1, 4\} \tag{B.95}$$

Using the spectral mapping theorem [12], the spectrum of $(\mathbf{BB}^*)^{-1}$ is the inverse of the spectrum of $\mathbf{BB}^*$ as follows:

$$\sigma\left((\mathbf{BB}^*)^{-1}\right) = \left\{\frac{1}{4}, 1\right\} \tag{B.96}$$

Using Theorem B.2, the spectral radius of $(\mathbf{BB}^*)^{-1}$ can be calculated as follows:

$$\begin{aligned}\rho\left((\mathbf{BB}^*)^{-1}\right) &= \max\left\{|\varepsilon| : \varepsilon \in \ \sigma\left((\mathbf{BB}^*)^{-1}\right)\right\} \\ &= |1| \\ &= 1\end{aligned} \tag{B.97}$$

Substituting the result of equation (B.97) back into equation (B.93) results in the following:

$$\begin{aligned}\left\|\mathbf{B^{-1}}\right\|^2 &= 1 \\ \left\|\mathbf{B^{-1}}\right\| &= 1\end{aligned} \tag{B.98}$$

When Theorem B.6(f) is applied to equation (B.98), the following is obtained:

$$\left\|\left(\mathbf{B^{-1}}\right)^*\right\| = \left\|\mathbf{B^{-1}}\right\| \tag{B.99}$$

Theorem B.6(e) can now be applied to obtain the following:

$$\left\|(\mathbf{B}^*)^{-1}\right\| = \left\|\left(\mathbf{B^{-1}}\right)^*\right\| \tag{B.100}$$

Now, from equation (B.98), it follows that

$$\left\|(\mathbf{B}^*)^{-1}\right\| = 1 \tag{B.101}$$

Substituting equations (B.99) and (B.101) back into equation (B.92) results in the following:

$$\begin{aligned}\left\|(2Re\{\mathbf{\Lambda}\})^{-1}\right\| &\leq \left\|\mathbf{L^{-1}}\right\| \\ &= \max\left\{\frac{1}{\left|\lambda_1 + \overline{\lambda_3}\right|}, \frac{1}{\left|\lambda_2 + \overline{\lambda_2}\right|}, \frac{1}{\left|\lambda_3 + \overline{\lambda_1}\right|}\right\}\end{aligned} \tag{B.102}$$

The same approach can also be used to determine the spectral radius of $2Re\{\mathbf{\Lambda}\}$ as follows:

$$\begin{aligned}\rho(2Re\{\mathbf{\Lambda}\}) &= \rho(\mathbf{BLB}^*) \\ &\leq \|\mathbf{B}\|\,\|\mathbf{L}\|\,\|\mathbf{B}^*\|\end{aligned} \tag{B.103}$$

According to Theorem 6.2.1.(iv) from [2] as repeated in Theorem B.6, the following is true for $\|\mathbf{B}\|^2$:

$$\|\mathbf{B}\|^2 = \rho\left(\mathbf{B}\mathbf{B}^*\right) \tag{B.104}$$

Using Theorem B.2 and the result of equation (B.95), the spectral radius of $\mathbf{B}\mathbf{B}^*$ can be calculated as follows:

$$\begin{aligned}\rho\left(\mathbf{B}\mathbf{B}^*\right) &= \max\left\{|\varepsilon| : \varepsilon \in \ \sigma\left(\mathbf{B}\mathbf{B}^*\right)\right\} \\ &= |4| \\ &= 4\end{aligned} \tag{B.105}$$

Substituting the result of equation (B.105) into equation (B.104) results in the following:

$$\begin{aligned}\|\mathbf{B}\|^2 &= 4 \\ \|\mathbf{B}\| &= 2\end{aligned} \tag{B.106}$$

When Theorem B.6(f) is applied to equation (B.106), the following is obtained:

$$\|(\mathbf{B})^*\| = \|\mathbf{B}\| = 2 \tag{B.107}$$

Substituting the result obtained in equation (B.107) into equation (B.103) results in the following:

$$\begin{aligned}\rho(2Re\{\mathbf{\Lambda}\}) &\leq \|\mathbf{B}\|\,\|\mathbf{L}\|\,\|\mathbf{B}^*\| \\ &= 2\,\|\mathbf{L}\|\,2 \\ &= 4\max\left\{\left|\lambda_1+\overline{\lambda_3}\right|,\left|\lambda_2+\overline{\lambda_2}\right|,\left|\lambda_3+\overline{\lambda_1}\right|\right\}\end{aligned} \tag{B.108}$$

The above results, equations (B.90) and (B.102) are valid for the steady-state analysis in Chapter 4. The matrix $2Re\{\mathbf{\Lambda}\}$ is multiplied with a constant $-\frac{1}{C}$ for the time constant analysis of Chapter 5. The above results can be adjusted to accomodate this constant. Using the properties of the determinant of a matrix, equation (B.90) can be rewritten for the time constant analysis as follows:

$$\det\left(-\frac{1}{C}2Re\{\mathbf{\Lambda}\}\right) = \left(-\frac{1}{C}\right)^3 16\prod_{l=1}^{3}(\lambda_l+\overline{\lambda_{4-l}}) \tag{B.109}$$

Using Theorem B.5(c) equations (B.102) and (B.108) can be rewritten for the time constant analysis as follows:

$$\left\|\left(-\frac{1}{C}2Re\{\mathbf{\Lambda}\}\right)^{-1}\right\| \leq |C|\max\left\{\frac{1}{\left|\lambda_1+\overline{\lambda_3}\right|},\frac{1}{\left|\lambda_2+\overline{\lambda_2}\right|},\frac{1}{\left|\lambda_3+\overline{\lambda_1}\right|}\right\} \tag{B.110}$$

$$\rho\left(-\frac{1}{C}2Re\{\mathbf{\Lambda}\}\right) \leq \frac{4}{C}\max\left\{\left|\lambda_1+\overline{\lambda_3}\right|,\left|\lambda_2+\overline{\lambda_2}\right|,\left|\lambda_3+\overline{\lambda_1}\right|\right\} \tag{B.111}$$

B.5 The p-cell calculations

This section follows the same method as the previous section and aims at calculating $\det(2Re\{\mathbf{\Lambda}\})$. The matrix $2Re\{\mathbf{\Lambda}\}$ was encountered in Chapter 4, section 4.5, where the steady-state analysis of a p-cell multicell converter was treated. This is the final section of this appendix and will end with the results mentioned in the introduction.

$$
\begin{aligned}
\mathbf{\Lambda} &= \begin{bmatrix}
\sum_{l=1}^{p-1}\lambda_l & \sum_{l=1}^{p-1}e^{j\frac{2\pi l}{p}}\lambda_l & \dots & \sum_{l=1}^{p-1}e^{j\frac{2\pi l(p-2)}{p}}\lambda_l \\
\sum_{l=1}^{p-1}e^{j\frac{-2\pi l}{p}}\lambda_l & \sum_{l=1}^{p-1}\lambda_l & \dots & \sum_{l=1}^{p-1}e^{j\frac{2\pi l(p-3)}{p}}\lambda_l \\
\vdots & \vdots & \ddots & \vdots \\
\sum_{l=1}^{p-1}e^{j\frac{-2\pi l(p-2)}{p}}\lambda_l & \sum_{l=1}^{p-1}e^{j\frac{2\pi l(p-3)}{p}}\lambda_l & \dots & \sum_{l=1}^{p-1}\lambda_l
\end{bmatrix} \\
&= \begin{bmatrix}
\lambda_1 & \lambda_2 & \dots & \lambda_{p-1} \\
e^{-j\frac{2\pi}{p}}\lambda_1 & e^{-j\frac{4\pi}{p}}\lambda_2 & \dots & e^{-j\frac{2\pi(p-1)}{p}}\lambda_{p-1} \\
\vdots & \vdots & \vdots & \vdots \\
e^{-j\frac{2\pi(p-2)}{p}}\lambda_1 & e^{-j\frac{4\pi(p-2)}{p}}\lambda_2 & \dots & e^{-j\frac{2\pi(p-2)(p-1)}{p}}\lambda_{p-1}
\end{bmatrix}
\begin{bmatrix}
1 & e^{j\frac{2\pi}{p}} & \dots & e^{j\frac{2\pi(p-2)}{p}} \\
1 & e^{j\frac{4\pi}{p}} & \dots & e^{j\frac{4\pi(p-2)}{p}} \\
\vdots & \vdots & \vdots & \vdots \\
1 & e^{j\frac{2\pi(p-1)}{p}} & \dots & e^{j\frac{2\pi(p-2)(p-1)}{p}}
\end{bmatrix} \\
&= \begin{bmatrix}
1 & 1 & \dots & 1 \\
e^{-j\frac{2\pi}{p}} & e^{-j\frac{4\pi}{p}} & \dots & e^{-j\frac{2\pi(p-1)}{p}} \\
\vdots & \vdots & \vdots & \vdots \\
e^{-j\frac{2\pi(p-2)}{p}} & e^{-j\frac{4\pi(p-2)}{p}} & \dots & e^{-j\frac{2\pi(p-2)(p-1)}{p}}
\end{bmatrix}
\begin{bmatrix}
\lambda_1 & 0 & \dots & 0 \\
0 & \lambda_2 & \dots & 0 \\
\vdots & \vdots & \vdots & \vdots \\
0 & 0 & \dots & \lambda_{p-1}
\end{bmatrix} \\
&\quad \begin{bmatrix}
1 & e^{j\frac{2\pi}{p}} & \dots & e^{j\frac{2\pi(p-2)}{p}} \\
1 & e^{j\frac{4\pi}{p}} & \dots & e^{j\frac{4\pi(p-2)}{p}} \\
\vdots & \vdots & \vdots & \vdots \\
1 & e^{j\frac{2\pi(p-1)}{p}} & \dots & e^{j\frac{2\pi(p-2)(p-1)}{p}}
\end{bmatrix}
\end{aligned}
\tag{B.112}
$$

and

$$
\begin{aligned}
\overline{\mathbf{\Lambda}} &= \begin{bmatrix}
\sum_{l=1}^{p-1}\overline{\lambda_l} & \sum_{l=1}^{p-1}e^{-j\frac{2\pi l}{p}}\overline{\lambda_l} & \dots & \sum_{l=1}^{p-1}e^{-j\frac{2\pi l(p-2)}{p}}\overline{\lambda_l} \\
\sum_{l=1}^{p-1}e^{j\frac{2\pi l}{p}}\overline{\lambda_l} & \sum_{l=1}^{p-1}\overline{\lambda_l} & \dots & \sum_{l=1}^{p-1}e^{-j\frac{2\pi l(p-3)}{p}}\overline{\lambda_l} \\
\vdots & \vdots & \ddots & \vdots \\
\sum_{l=1}^{p-1}e^{j\frac{2\pi l(p-2)}{p}}\overline{\lambda_l} & \sum_{l=1}^{p-1}e^{-j\frac{2\pi l(p-3)}{p}}\overline{\lambda_l} & \dots & \sum_{l=1}^{p-1}\overline{\lambda_l}
\end{bmatrix} \\
&= \begin{bmatrix}
\overline{\lambda_{p-1}} & \overline{\lambda_{p-2}} & \dots & \overline{\lambda_1} \\
e^{-j\frac{2\pi}{p}}\overline{\lambda_{p-1}} & e^{-j\frac{4\pi}{p}}\overline{\lambda_{p-2}} & \dots & e^{-j\frac{2\pi(p-1)}{p}}\overline{\lambda_1} \\
\vdots & \vdots & \vdots & \vdots \\
e^{-j\frac{2\pi(p-2)}{p}}\overline{\lambda_{p-1}} & e^{-j\frac{4\pi(p-2)}{p}}\overline{\lambda_{p-2}} & \dots & e^{-j\frac{2\pi(p-2)(p-1)}{p}}\overline{\lambda_{p-1}}
\end{bmatrix}
\begin{bmatrix}
1 & e^{j\frac{2\pi}{p}} & \dots & e^{j\frac{2\pi(p-2)}{p}} \\
1 & e^{j\frac{4\pi}{p}} & \dots & e^{j\frac{4\pi(p-2)}{p}} \\
\vdots & \vdots & \vdots & \vdots \\
1 & e^{j\frac{2\pi(p-1)}{p}} & \dots & e^{j\frac{2\pi(p-2)(p-1)}{p}}
\end{bmatrix}
\end{aligned}
$$

$$= \begin{bmatrix} 1 & 1 & \dots & 1 \\ e^{-j\frac{2\pi}{p}} & e^{-j\frac{4\pi}{p}} & \dots & e^{-j\frac{2\pi(p-1)}{p}} \\ \vdots & \vdots & \vdots & \vdots \\ e^{-j\frac{2\pi(p-2)}{p}} & e^{-j\frac{4\pi(p-2)}{p}} & \dots & e^{-j\frac{2\pi(p-2)(p-1)}{p}} \end{bmatrix} \begin{bmatrix} \lambda_1 + \overline{\lambda_{p-1}} & 0 & \dots & 0 \\ 0 & \lambda_2 + \overline{\lambda_{p-2}} & \dots & 0 \\ \vdots & \vdots & \vdots & \vdots \\ 0 & 0 & \dots & \lambda_{p-1} + \overline{\lambda_1} \end{bmatrix} \begin{bmatrix} 1 & e^{j\frac{2\pi}{p}} & \dots & e^{j\frac{2\pi(p-2)}{p}} \\ 1 & e^{j\frac{4\pi}{p}} & \dots & e^{j\frac{4\pi(p-2)}{p}} \\ \vdots & \vdots & \vdots & \vdots \\ 1 & e^{j\frac{2\pi(p-1)}{p}} & \dots & e^{j\frac{2\pi(p-2)(p-1)}{p}} \end{bmatrix} \tag{B.113}$$

Equations (B.112) and (B.113) can now be combined into the following:

$$\begin{aligned} 2Re\{\mathbf{\Lambda}\} = & \begin{bmatrix} 1 & 1 & \dots & 1 \\ e^{-j\frac{2\pi}{p}} & e^{-j\frac{4\pi}{p}} & \dots & e^{-j\frac{2\pi(p-1)}{p}} \\ \vdots & \vdots & \vdots & \vdots \\ e^{-j\frac{2\pi(p-2)}{p}} & e^{-j\frac{4\pi(p-2)}{p}} & \dots & e^{-j\frac{2\pi(p-2)(p-1)}{p}} \end{bmatrix} \begin{bmatrix} \lambda_1 & 0 & \dots & 0 \\ 0 & \lambda_2 & \dots & 0 \\ \vdots & \vdots & \vdots & \vdots \\ 0 & 0 & \dots & \lambda_{p-1} \end{bmatrix} \\ & \begin{bmatrix} 1 & e^{j\frac{2\pi}{p}} & \dots & e^{j\frac{2\pi(p-2)}{p}} \\ 1 & e^{j\frac{4\pi}{p}} & \dots & e^{j\frac{4\pi(p-2)}{p}} \\ \vdots & \vdots & \vdots & \vdots \\ 1 & e^{j\frac{2\pi(p-1)}{p}} & \dots & e^{j\frac{2\pi(p-2)(p-1)}{p}} \end{bmatrix} + \begin{bmatrix} 1 & 1 & \dots & 1 \\ e^{-j\frac{2\pi}{p}} & e^{-j\frac{4\pi}{p}} & \dots & e^{-j\frac{2\pi(p-1)}{p}} \\ \vdots & \vdots & \vdots & \vdots \\ e^{-j\frac{2\pi(p-2)}{p}} & e^{-j\frac{4\pi(p-2)}{p}} & \dots & e^{-j\frac{2\pi(p-2)(p-1)}{p}} \end{bmatrix} \\ & \begin{bmatrix} \lambda_1 + \overline{\lambda_{p-1}} & 0 & \dots & 0 \\ 0 & \lambda_2 + \overline{\lambda_{p-2}} & \dots & 0 \\ \vdots & \vdots & \vdots & \vdots \\ 0 & 0 & \dots & \lambda_{p-1} + \overline{\lambda_1} \end{bmatrix} \begin{bmatrix} 1 & e^{j\frac{2\pi}{p}} & \dots & e^{j\frac{2\pi(p-2)}{p}} \\ 1 & e^{j\frac{4\pi}{p}} & \dots & e^{j\frac{4\pi(p-2)}{p}} \\ \vdots & \vdots & \vdots & \vdots \\ 1 & e^{j\frac{2\pi(p-1)}{p}} & \dots & e^{j\frac{2\pi(p-2)(p-1)}{p}} \end{bmatrix} \\ = & \mathbf{BLC} \end{aligned} \tag{B.114}$$

where:

$$\mathbf{B} = \begin{bmatrix} 1 & 1 & \dots & 1 \\ e^{-j\frac{2\pi}{p}} & e^{-j\frac{4\pi}{p}} & \dots & e^{-j\frac{2\pi(p-1)}{p}} \\ \vdots & \vdots & \vdots & \vdots \\ e^{-j\frac{2\pi(p-2)}{p}} & e^{-j\frac{4\pi(p-2)}{p}} & \dots & e^{-j\frac{2\pi(p-2)(p-1)}{p}} \end{bmatrix} \tag{B.115}$$

$$\mathbf{L} = \begin{bmatrix} \lambda_1 + \overline{\lambda_{p-1}} & 0 & \dots & 0 \\ 0 & \lambda_2 + \overline{\lambda_{p-2}} & \dots & 0 \\ \vdots & \vdots & \vdots & \vdots \\ 0 & 0 & \dots & \lambda_{p-1} + \overline{\lambda_1} \end{bmatrix} \tag{B.116}$$

$$\mathbf{C} = \begin{bmatrix} 1 & e^{j\frac{2\pi}{p}} & \dots & e^{j\frac{2\pi(p-2)}{p}} \\ 1 & e^{j\frac{4\pi}{p}} & \dots & e^{j\frac{4\pi(p-2)}{p}} \\ \vdots & \vdots & \vdots & \vdots \\ 1 & e^{j\frac{2\pi(p-1)}{p}} & \dots & e^{j\frac{2\pi(p-2)(p-1)}{p}} \end{bmatrix} \tag{B.117}$$

The inverse of the diagonal matrix $\mathbf{L}$ can be calculated directly as follows:

$$\mathbf{L^{-1}} = \begin{bmatrix} \frac{1}{\lambda_1+\overline{\lambda_{p-1}}} & 0 & \dots & 0 \\ 0 & \frac{1}{\lambda_2+\overline{\lambda_{p-2}}} & \dots & 0 \\ \vdots & \vdots & \vdots & \vdots \\ 0 & 0 & \dots & \frac{1}{\lambda_{p-1}+\overline{\lambda_1}} \end{bmatrix} \tag{B.118}$$

The determinant of $\mathbf{L}$ is the product of its diagonal elements and can be written as follows:

$$\det(\mathbf{L}) = (\lambda_1 + \overline{\lambda_{p-1}})(\lambda_2 + \overline{\lambda_{p-2}}) \cdots (\lambda_{p-1} + \overline{\lambda_1}) \tag{B.119}$$

For a $p-1 \times p-1$ square matrix $\mathbf{\Lambda}$, each element $[\mathbf{\Lambda}]_{rs}$ can be described by the following equation:

$$[\mathbf{\Lambda}]_{rs} = \sum_{l=1}^{p-1} e^{j\frac{2\pi l(s-r)}{p}} \lambda_l \tag{B.120}$$

For the $p-1 \times p-1$ square matrix $\overline{\mathbf{\Lambda}}$, each element $[\overline{\mathbf{\Lambda}}]_{rs}$ can be described by the following equation:

$$\left[\overline{\mathbf{\Lambda}}\right]_{rs} = \sum_{l=1}^{p-1} e^{j\frac{2\pi l(r-s)}{p}} \lambda_l \tag{B.121}$$

In equation (B.112), it can be seen that the matrices $\mathbf{B}$ and $\mathbf{C}$ are conjugate transposes of each other, resulting in the following:

$$\mathbf{C} = \mathbf{B}^* \tag{B.122}$$

which leads to the following:

$$2Re\{\mathbf{\Lambda}\} = \mathbf{BLB}^* \tag{B.123}$$

The determinant of $2Re\{\mathbf{\Lambda}\}$ can be obtained indirectly as follows:

$$\begin{aligned} \det(2Re\{\mathbf{\Lambda}\}) &= \det(\mathbf{B}) \det(\mathbf{L}) \det(\mathbf{C}) \\ &= \det(\mathbf{B}) \det(\mathbf{C}) \det(\mathbf{L}) \\ &= \det(\mathbf{BC}) \det(\mathbf{L}) \end{aligned} \tag{B.124}$$

Let $\mathbf{D}$ be the following matrix:

$$
\begin{aligned}
\mathbf{D} &= \mathbf{BC} \\
&= \mathbf{BB}^{*} \\
&= \begin{bmatrix}
p-1 & e^{j\frac{2\pi}{p}} + e^{j\frac{4\pi}{p}} + \ldots + e^{j\frac{2\pi(p-1)}{p}} \\
e^{-j\frac{2\pi}{p}} + e^{-j\frac{4\pi}{p}} + \ldots + e^{-j\frac{2\pi(p-1)}{p}} & p-1 \\
\vdots & \ddots \\
e^{-j\frac{2\pi(p-2)}{p}} + e^{-j\frac{4\pi(p-2)}{p}} + \ldots + e^{-j\frac{2\pi(p-2)(p-1)}{p}} & e^{-j\frac{2\pi(p-3)}{p}} + e^{-j\frac{4\pi(p-3)}{p}} + \ldots + e^{-j\frac{2\pi p(p-4)}{p}}
\end{bmatrix} \\
&\quad \begin{bmatrix}
\cdots & e^{j\frac{2\pi(p-2)}{p}} + e^{j\frac{4\pi(p-2)}{p}} + \ldots + e^{j\frac{2\pi(p-2)(p-1)}{p}} \\
\cdots & e^{j\frac{2\pi(p-3)}{p}} + e^{j\frac{4\pi(p-3)}{p}} + \ldots + e^{j\frac{2\pi p(p-4)}{p}} \\
\ddots & \vdots \\
\cdots & p-1
\end{bmatrix} \\
&= \begin{bmatrix}
p-1 & -1 & \cdots & -1 \\
-1 & p-1 & \cdots & -1 \\
\vdots & \ddots & \ddots & \vdots \\
-1 & -1 & \cdots & p-1
\end{bmatrix}
\end{aligned}
\tag{B.125}
$$

In equation (B.125), each element of the matrix $\mathbf{D}$ sums to -1. This results from the fact that each element, except the diagonal elements, contain all the $p-1$ roots of unity, except for 1. Therefore from equation (B.18), it follows that each element sums to -1. The following procedure describes the indirect calculation of the eigenvalues of $\mathbf{D}$:

Matrix $\mathbf{D}$ can now be rewritten in another form:

$$
\begin{aligned}
\mathbf{D} &= \mathbf{X} + p\mathbf{I} \\
&= \begin{bmatrix}
-1 & -1 & -1 & \cdots & -1 \\
-1 & -1 & -1 & \cdots & -1 \\
\vdots & \vdots & \vdots & \vdots & \vdots \\
-1 & -1 & -1 & \cdots & -1
\end{bmatrix} + p \begin{bmatrix}
1 & 0 & 0 & \cdots & 0 \\
0 & 1 & 0 & \cdots & 0 \\
\vdots & \ddots & \ddots & \ddots & \vdots \\
0 & 0 & 0 & \cdots & 1
\end{bmatrix}
\end{aligned}
\tag{B.126}
$$

where:

$$
\mathbf{X} = \begin{bmatrix}
-1 & -1 & -1 & \cdots & -1 \\
-1 & -1 & -1 & \cdots & -1 \\
\vdots & \vdots & \vdots & \vdots & \vdots \\
-1 & -1 & -1 & \cdots & -1
\end{bmatrix}
\tag{B.127}
$$

$$\mathbf{I} = \begin{bmatrix} 1 & 0 & 0 & \cdots & 0 \\ 0 & 1 & 0 & \cdots & 0 \\ \vdots & \ddots & \ddots & \ddots & \vdots \\ 0 & 0 & 0 & \cdots & 1 \end{bmatrix} \tag{B.128}$$

Now that the matrix $\mathbf{D}$ was written in a different form, the spectrum of equation (B.126) can be calculated as follows:

$$\begin{aligned} \sigma(\mathbf{D}) &= \sigma(\mathbf{X}) + p\sigma(\mathbf{I}) \\ &= \sigma(\mathbf{X}) + \{p\} \end{aligned} \tag{B.129}$$

Again, using the spectral mapping theorem [12], equation (B.129) can be rewritten again as follows:

$$\begin{aligned} \mathbf{X^2} + (p-1)\mathbf{X} &= 0 \\ \mathbf{X}(\mathbf{X} + (p-1)\mathbf{I}) &= 0 \end{aligned} \tag{B.130}$$

The solutions of equation (B.130), i.e. $\{0, -(p-1)\}$, are also the eigenvalues of $\mathbf{X}$, which means that $\sigma(\mathbf{X}) = \{0, -(p-1)\}$. The reason for the solutions of equation (B.130) also being the eigenvalues of $\mathbf{X}$, again follows from the spectral mapping theorem [12]. These values can then be substituted back into equation (B.129) as follows:

$$\begin{aligned} \sigma(\mathbf{D}) &= \sigma(\mathbf{X}) + \{p\} \\ &\subseteq \{0, -(p-1)\} + \{p\} \\ &= \{1, p\} \end{aligned} \tag{B.131}$$

From the solutions in equation (B.131), the spectrum of $\mathbf{D}$ can be represented as follows:

$$\sigma(\mathbf{D}) \subseteq \{1, p\} \tag{B.132}$$

The spectrum is the set of eigenvalues of $\mathbf{D}$. According to Theorem 268B of [18], the trace of matrix $\mathbf{D}$ can be used to determine the multiplicity of the eigenvalues. As described in section B.2, the trace of matrix $\mathbf{D}$ can be calculated as follows:

$$\begin{aligned} \mathrm{tr}(\mathbf{D}) &= [\mathbf{D}]_{11} + [\mathbf{D}]_{22} + \ldots + [\mathbf{D}]_{(p-1)(p-1)} \\ &= \sum_{l=1}^{p-1} [\mathbf{D}]_{ll} \\ &= (p-1)^2 \\ &= p^2 - 2p + 1 \end{aligned} \tag{B.133}$$

As the eigenvalues have been calculated to be $\{1, p\}$, the trace was calculated to be $p^2 - 2p + 1$. It is also known that the trace is the sum of the eigenvalues and the determinant the product of the eigenvalues, see section B.2. The multiplicity, γ, of the eigenvalue $\{p\}$ can then be solved from the following equation as follows:

$$\begin{aligned} 1 + \gamma \cdot p &= p^2 - 2p + 1 \\ \gamma &= p - 2 \end{aligned} \tag{B.134}$$

From the above it can be concluded that the determinant of $\mathbf{D}$ is as follows:

$$\det(\mathbf{D}) = 1 \cdot p^{p-2} \tag{B.135}$$

Knowing the determinant of $\mathbf{D}$, it is possible to calculate the determinant of $2Re\{\mathbf{\Lambda}\}$ as follows:

$$\begin{aligned} \det(2Re\{\mathbf{\Lambda}\}) &= \det(\mathbf{D}) \det(\mathbf{L}) \\ &= p^{p-2}(\lambda_1 + \overline{\lambda_{p-1}})(\lambda_2 + \overline{\lambda_{p-2}}) \dots (\lambda_{p-1} + \overline{\lambda_1}) \\ &= p^{p-2} \prod_{l=1}^{p-1} (\lambda_l + \overline{\lambda_{p-l}}) \end{aligned} \tag{B.136}$$

The indirect approach for the calculation of $\|(2Re\{\mathbf{\Lambda}\})^{-1}\|$ is the same approach as used in section B.3 with the difference that it is extended to p-cells. The properties from [2] as repeated in section B.2 are also used here as follows:

$$(2Re\{\mathbf{\Lambda}\})^{-1} = (\mathbf{B}^*)^{-1}\mathbf{L^{-1}}\mathbf{B^{-1}} \tag{B.137}$$

The norm of $(2Re\{\mathbf{\Lambda}\})^{-1}$ can now be determined by using equation (B.137), as follows:

$$\left\|(2Re\{\mathbf{\Lambda}\})^{-1}\right\| \leq \left\|(\mathbf{B}^*)^{-1}\right\| \left\|\mathbf{L^{-1}}\right\| \left\|\mathbf{B^{-1}}\right\| \tag{B.138}$$

According to Theorem 6.2.1.(iv) from [2] as repeated in section B.2, the following is true for $\|\mathbf{B^{-1}}\|^2$:

$$\begin{aligned} \left\|\mathbf{B^{-1}}\right\|^2 &= \rho\left(\mathbf{B^{-1}}(\mathbf{B^{-1}})^*\right) \\ &= \rho\left(\mathbf{B^{-1}}(\mathbf{B}^*)^{-1}\right) \text{ from Theorem 6.1.1. (iv) [2]} \\ &= \rho\left((\mathbf{B}^*\mathbf{B})^{-1}\right) \end{aligned} \tag{B.139}$$

The relation between $\sigma(\mathbf{B}\mathbf{B}^*)$ and $\sigma(\mathbf{B}^*\mathbf{B})$ is described by Lemma 3.1.2 on p. 36 of [2]:

$$\sigma(\mathbf{B}\mathbf{B}^*) \cup \{0\} = \sigma(\mathbf{B}^*\mathbf{B}) \cup \{0\} \tag{B.140}$$

From equations (B.125), (B.131) and (B.140), it can be seen that the spectrum of $\mathbf{BB}^*$ is the following:

$$\sigma(\mathbf{BB}^*) = \{1, p\} \tag{B.141}$$

Using the spectral mapping theorem [12], the spectrum of $(\mathbf{BB}^*)^{-1}$ is the inverse of the spectrum of $\mathbf{BB}^*$ as follows:

$$\sigma\left((\mathbf{BB}^*)^{-1}\right) = \left\{\frac{1}{p}, 1\right\} \tag{B.142}$$

Using Definition B.2, the spectral radius of $(\mathbf{BB}^*)^{-1}$ can be calculated as follows:

$$\begin{aligned}\rho\left((\mathbf{BB}^*)^{-1}\right) &= \max\left\{|\varepsilon| : \varepsilon \in \ \sigma\left((\mathbf{BB}^*)^{-1}\right)\right\} \\ &= |1| \\ &= 1\end{aligned} \tag{B.143}$$

Substituting the result of equation (B.143) back into equation (B.139) results in the following:

$$\begin{aligned}\left\|\mathbf{B^{-1}}\right\|^2 &= 1 \\ \left\|\mathbf{B^{-1}}\right\| &= 1\end{aligned} \tag{B.144}$$

When Theorem B.6(f) is applied to equation (B.144), the following is obtained:

$$\left\|\left(\mathbf{B^{-1}}\right)^*\right\| = \left\|\mathbf{B^{-1}}\right\| \tag{B.145}$$

Theorem B.6(e) can now be applied to obtain the following:

$$\left\|(\mathbf{B}^*)^{-1}\right\| = \left\|\left(\mathbf{B^{-1}}\right)^*\right\| \tag{B.146}$$

Now, from equation (B.144), it follows that

$$\left\|(\mathbf{B}^*)^{-1}\right\| = 1 \tag{B.147}$$

Substituting equations (B.145) and (B.147) back into equation (B.138) results in the following:

$$\begin{aligned}\left\|(2Re\{\mathbf{\Lambda}\})^{-1}\right\| &\leq \left\|\mathbf{L^{-1}}\right\| \\ &= \max\left\{\frac{1}{\left|\lambda_1 + \overline{\lambda_{p-1}}\right|}, \frac{1}{\left|\lambda_2 + \overline{\lambda_{p-2}}\right|}, \ldots, \frac{1}{\left|\lambda_{p-1} + \overline{\lambda_1}\right|}\right\}\end{aligned} \tag{B.148}$$

The same approach can also be used to determine the spectral radius of $2Re\{\mathbf{\Lambda}\}$ as follows:

$$\rho(2Re\{\mathbf{\Lambda}\}) = \rho(\mathbf{BLB}^*)$$

$$\leq \|\mathbf{B}\| \, \|\mathbf{L}\| \, \|\mathbf{B}^*\| \tag{B.149}$$

According to Theorem 6.2.1.(iv) from [2] as repeated in Theorem B.6, the following is true for $\|\mathbf{B}\|^2$:

$$\|\mathbf{B}\|^2 = \rho\left(\mathbf{B}\mathbf{B}^*\right) \tag{B.150}$$

Using Theorem B.2 and the result of equation (B.141), the spectral radius of $\mathbf{B}\mathbf{B}^*$ can be calculated as follows:

$$\begin{aligned} \rho\left(\mathbf{B}\mathbf{B}^*\right) &= \max\left\{|\varepsilon| : \varepsilon \in \ \sigma\left(\mathbf{B}\mathbf{B}^*\right)\right\} \\ &= |p| \\ &= p \end{aligned} \tag{B.151}$$

Substituting the result of equation (B.151) into equation (B.150) results in the following:

$$\begin{aligned} \|\mathbf{B}\|^2 &= p \\ \|\mathbf{B}\| &= \sqrt{p} \end{aligned} \tag{B.152}$$

When Theorem B.6(f) is applied to equation (B.152), the following is obtained:

$$\|(\mathbf{B})^*\| = \|\mathbf{B}\| = \sqrt{p} \tag{B.153}$$

Substituting the result obtained in equation (B.153) into equation (B.149) results in the following:

$$\begin{aligned} \rho(2Re\{\mathbf{\Lambda}\}) &\leq \|\mathbf{B}\| \, \|\mathbf{L}\| \, \|\mathbf{B}^*\| \\ &= \sqrt{p} \, \|\mathbf{L}\| \, \sqrt{p} \\ &= p \max\left\{\left|\lambda_1 + \overline{\lambda_{p-1}}\right|, \left|\lambda_2 + \overline{\lambda_{p-2}}\right|, \ldots, \left|\lambda_{p-1} + \overline{\lambda_1}\right|\right\} \end{aligned} \tag{B.154}$$

The above results, equations (B.136) and (B.148) are valid for the steady-state analysis in Chapter 4. The matrix $2Re\{\mathbf{\Lambda}\}$ is multiplied with a constant $-\frac{1}{C}$ for the time constant analysis of Chapter 5. The above results can be adjusted to accomodate this constant. Using the properties of the determinant of a matrix, equation (B.136) can be rewritten for the time constant analysis as follows:

$$\det\left(-\frac{1}{C}2Re\{\mathbf{\Lambda}\}\right) = \left(-\frac{1}{C}\right)^{p-1} p^{p-2} \prod_{l=1}^{p-1} (\lambda_l + \overline{\lambda_{p-l}}) \tag{B.155}$$

Using equation (B.17) and property (c) of Theorem B.5 equations (B.148) and (B.154) can be rewritten for the time constant analysis as follows:

$$\left\|(2Re\{\mathbf{\Lambda}\})^{-1}\right\| \leq |C| \max\left\{\frac{1}{\left|\lambda_1 + \overline{\lambda_{p-1}}\right|}, \frac{1}{\left|\lambda_2 + \overline{\lambda_{p-2}}\right|}, \ldots, \frac{1}{\left|\lambda_{p-1} + \overline{\lambda_1}\right|}\right\} \tag{B.156}$$

$$\rho\left(-\frac{1}{C}2Re\{\mathbf{\Lambda}\}\right) \leq \frac{p}{C}\max\left\{\left|\lambda_1+\overline{\lambda_{p-1}}\right|,\left|\lambda_2+\overline{\lambda_{p-2}}\right|,\ldots,\left|\lambda_{p-1}+\overline{\lambda_1}\right|\right\} \qquad \text{(B.157)}$$

B.6 Summary

The mathematical analysis included in this appendix proved to be useful in both the steady-state and time constant analyses of Chapters 4 and 5.

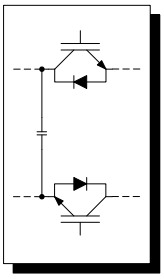

Appendix C

Converter design

The converter design discussed in this appendix is a summary of a paper written by the author and co-authors on this subject [57].

C.1 Generic Powercell

The idea behind the "Powercell" was to create a generic building block with which one can build a p-cell multicell converter. It was thought that the following specifications would meet the needs required for a converter for this topology:

- On-board isolated IGBT gate-drives with error feedback.
- Cell capacitor connections
- On-board optic-fibre gating signal interface
- Isolated power supply

A diagram of the proposed Powercell module is shown in Figure C-1.

C.2 Design considerations

The following considerations were taken into account with the design of the Powercell: power supply isolation, dv/dt limitations and gate-drives. The limiting factors were power supply isolation and dc-bus isolation.

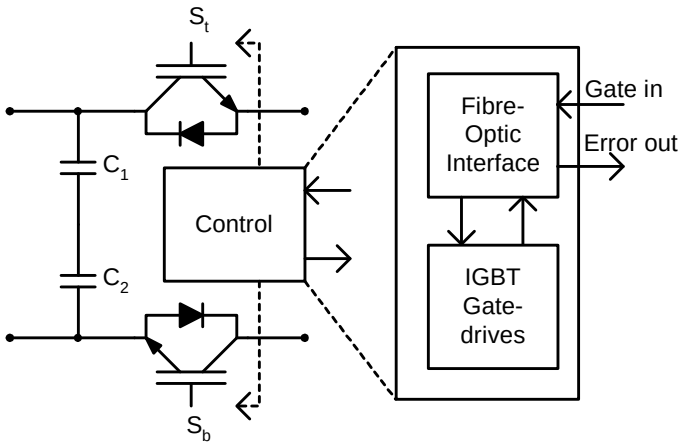

Figure C-1. *The Powercell module.*

C.2.1 Choosing a Ground reference

One of the first choices that had to be made concerning the Powercell was the ground reference of the control circuitry. Five possible options were identified and are shown in Figure C-2.

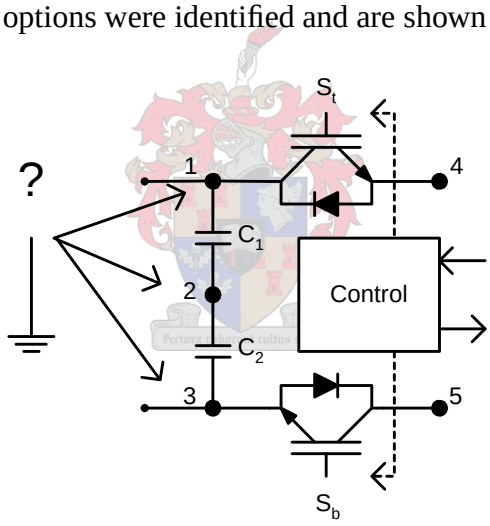

Figure C-2. *Choosing the Ground reference.*

The choice of ground would determine the isolation needed between the IGBTs and the control circuitry. In the case of this topology, the outermost cell's input voltage would determine the isolation of every subsequent cell. If an input voltage of $1.8\ kV$ is considered and each IGBT switches $600\ V$, the following voltage differences can be calculated for the cell shown in Figure C-2:

- v14=0/600 V (pulse)
- v24=-900 V + 0/600 V (pulse)
- v34=-1800 V + 0/600 V (pulse)

- v53=0/600 V (pulse)
- v52=-900 V + 0/600 V (pulse)
- v51=-1800 V + 0/600 V (pulse)

The above voltages are shown as dc isolation plus a dynamic voltage (caused by the switching devices). The different points require different types of signal isolation, e.g. dc voltage isolation and maximum dv/dt isolation. In order to isolate signals referred to these points, one would require opto-couplers or isolation transformers with characteristics that suit the needs. Commercially available opto-couplers usually possess one of two main characteristics: high dv/dt isolation or high dc isolation, but rarely both.

When looking at Figure C-2, the three most popular ground choices would be point 1, 2 or 3. Point 1 requires high dv/dt isolation for the S_t-switch and high dc isolation for the S_b-switch. Point 2 requires both high dv/dt and high dc isolation for the S_t-switch and high dc isolation for the S_b-switch. Point 3 also requires high dv/dt and high dc isolation for the S_t-switch. Isolation for the S_b-switch is not necessary for a single cell, but is required when cells are chained. From these characteristics, point 1 was the most feasible when using opto-couplers.

Due to the high opto-coupler specifications required, another solution was proposed, i.e. that of using optic fibre. The cost is roughly the same as that of opto-couplers, but the isolation is much higher and the dv/dt capability is sufficient.

The voltage differences between the different points were not the only consideration for the choice of ground point.

In the end, point 1 was used as the ground for the control circuitry because of the isolation needed.

C.2.2 Isolated IGBT gate-drives with error feedback

Two IGBT gate-drives were included on the Powercell, each with an isolated power supply. The gate-drives have error-detection, which is fed back via the fibre-optics to the controller.

C.2.3 Cell capacitor connections

Clip-on cell capacitor connections were made on the Powercell so that capacitors with different voltage ratings can be easily connected onto the Powercell. The cell capacitors have to be of a high quality because they have to carry the full load current. A high quality metallized polypropylene type was chosen. These capacitors are relatively compact and can be connected directly onto the Powercell.

C.2.4 On-board optic-fibre gate-signal interface

The on-board optic-fibre gate-signal interface consists of an optic fibre receiver and transmitter for each IGBT device. The receiver receives the gating signals which are fed to the gate-drives.

C.2.5 Isolated power supply

An isolated power supply was designed to supply the control circuit as well as the two gate-driving circuits with power. The isolation has to be more than the maximum input voltage of the outermost Powercell, i.e. Vd. Care must be taken to minimise capacitive coupling with the gate-drive power supplies.

In conclusion it has been shown that designing a generic Powercell is not trivial and depends on many design factors. It has also been shown that it is not possible to build a truly generic Powercell, i.e. that can be used in an p-cell multicell converter. The limiting factor is the voltage isolation and the maximum input voltage.

The main advantage of this modular approach is the ease of construction of a multicell converter and reconfiguration for a converter with a higher number of cells.

C.3 Schematic diagrams of Powercell

The schematics of the Powercell were designed and drawn in P-CAD 2000® and are spread over four sheets. These sheets correspond to the following design sections:

(a) Sheet 1: Full-bridge converter supplying both the low- and high sides of the cell with $\pm 24\ V$.

(b) Sheet 2: Full-bridge driver circuitry.

(c) Sheet 3: High-side IGBT driver and power circuitry.

(d) Sheet 4: Low-side IGBT driver and power circuitry.

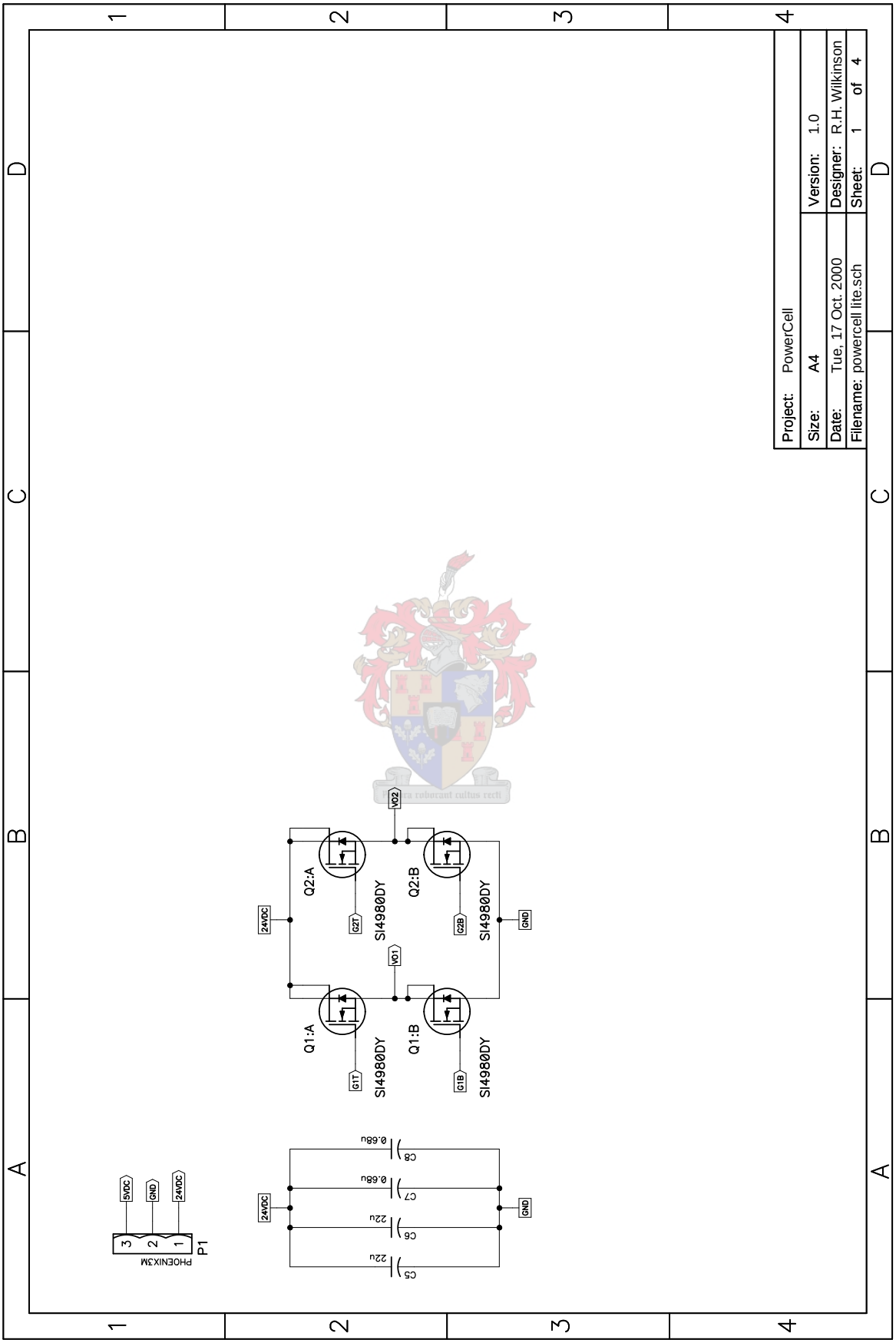
Project: PowerCell
Size: A4
Version: 1.0
Date: Tue, 17 Oct. 2000
Designer: R.H. Wilkinson
Filename: powercell lite.sch
Sheet: 1 of 4
5VDC
GND
24VDC
P1
PHOENIX3M
C5 22u
C6 22u
C7 0.68u
C8 0.68u
Q1:A
Q1:B
Q2:A
Q2:B
SI4980DY
G1T
G1B
G2T
G2B
VO1
VO2

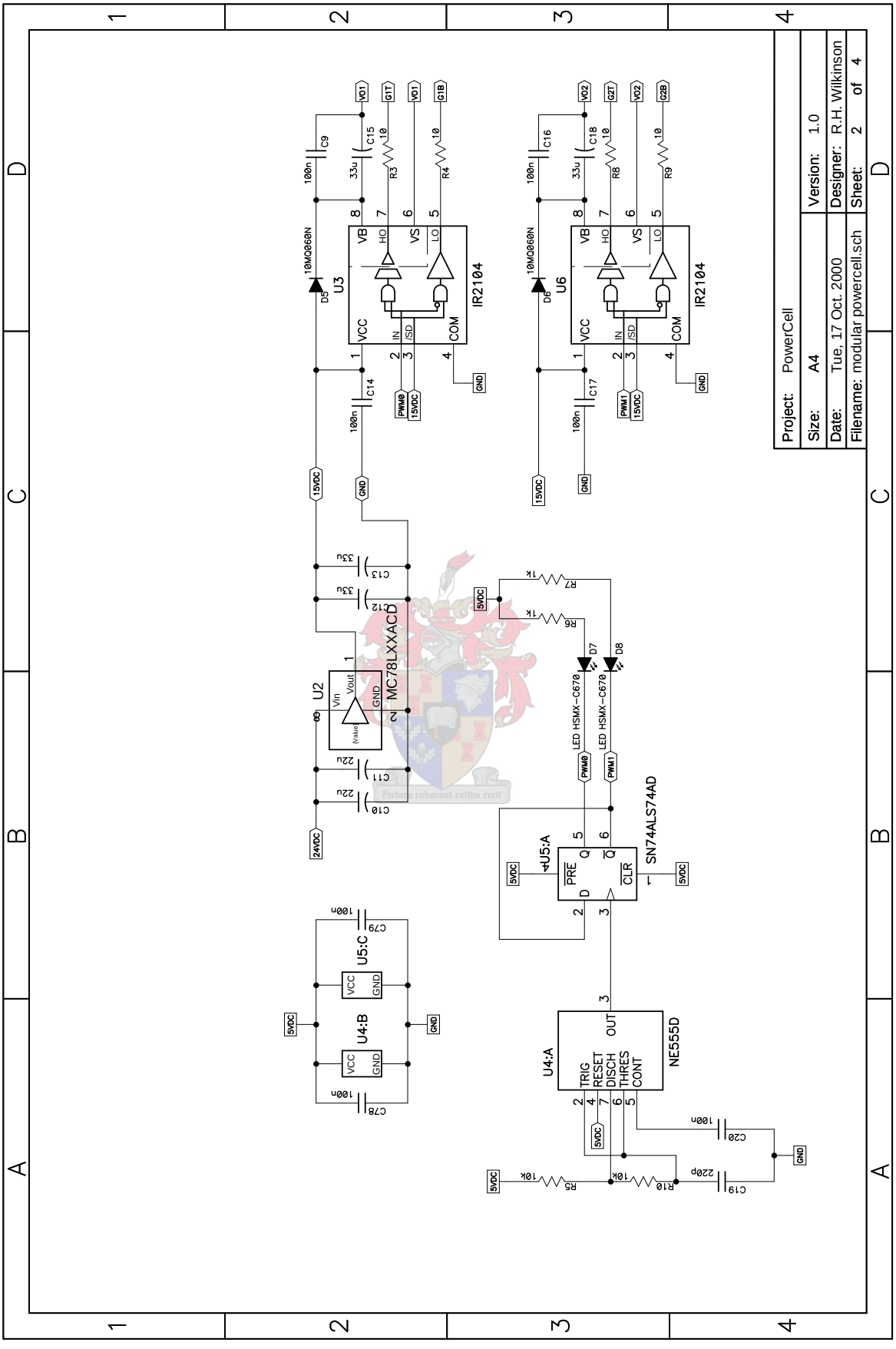
Project: PowerCell
Size: A4
Version: 1.0
Date: Tue, 17 Oct. 2000
Designer: R.H. Wilkinson
Filename: modular powercell.sch
Sheet: 2 of 4
U3
IR2104
U6
IR2104
U2
MC78LXXACD
U5:A
SN74ALS74AD
U5:C
U4:B
U4:A
NE555D
D5
D6
D7
D8
LED HSMX-C670
LED HSMX-C670
10MQ060N
10MQ060N
15VDC
5VDC
24VDC
GND
PWM0
PWM1
VO1
VO2
G1T
G1B
G2T
G2B
C9
C14
C15
C16
C17
C18
C13
C12
C11
C10
C79
C78
C20
C19
R3
R4
R8
R9
R7
R6
R5
R10
100n
33u
22u
1k
10k
10
220p

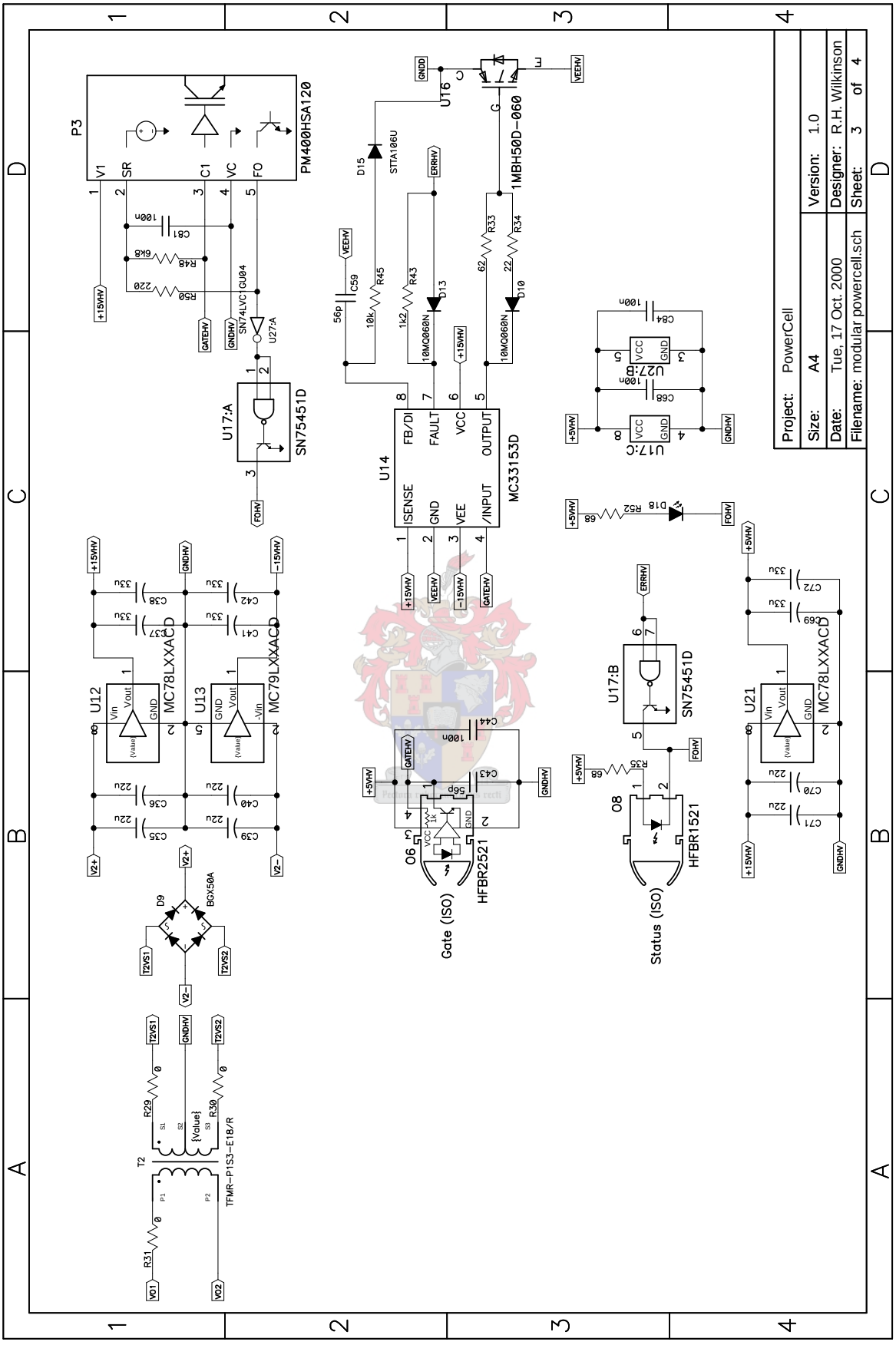
Project: PowerCell
Size: A4
Version: 1.0
Date: Tue, 17 Oct. 2000
Designer: R.H. Wilkinson
Filename: modular powercell.sch
Sheet: 3 of 4
P3
PM400HSA120
U16
1MBH50D-060
U14
MC33153D
SN75451D
HFBR2521
HFBR1521
Gate (ISO)
Status (ISO)
MC78LXXACD
MC79LXXACD
BGX50A
TFMR-P1S3-E18/R

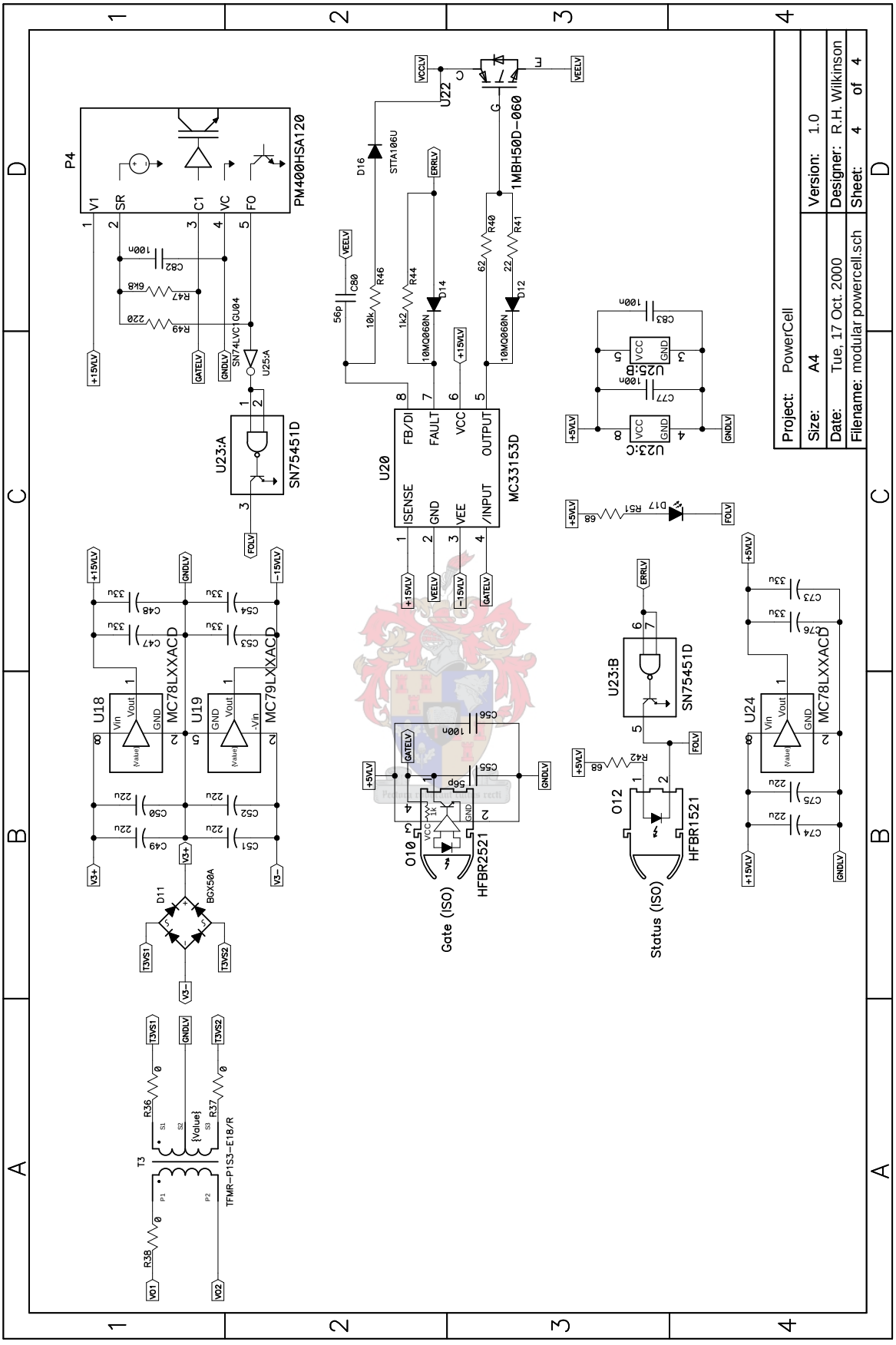
Project: PowerCell
Size: A4
Version: 1.0
Date: Tue, 17 Oct. 2000
Designer: R.H. Wilkinson
Filename: modular powercell.sch
Sheet: 4 of 4
P4
PM400HSA120
U22
1MBH50D-060
U20
MC33153D
U23:A
SN75451D
U23:B
SN75451D
U23:C
U25:A
SN74LVC1GU04
U25:B
U18
MC78LXXACD
U19
MC79LXXACD
U24
MC78LXXACD
D11
BGX50A
D16
STTA106U
D12
10MQ060N
D14
10MQ060N
D17
U10
HFBR2521
Gate (ISO)
U12
HFBR1521
Status (ISO)
T3
TFMR-P1S3-E18/R
R36
R37
R38
R40
R41
R42
R44
R46
R47
R49
R51
C47
C48
C49
C50
C51
C52
C53
C54
C55
C56
C73
C74
C75
C76
C77
C80
C82
C83
+15VLV
-15VLV
+5VLV
GNDLV
VEELV
VCCLV
ERRLV
GATELV
FOLV
T3VS1
T3VS2
V3+
V3-
V01
V02

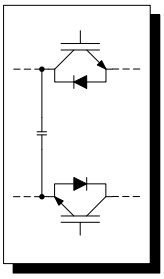

Appendix D

Matlab programs

The natural balance theory was implemented in a “Designtool” in Matlab®. This “Designtool” can be used to obtain harmonic information as well as information on the unbalance decay and the balance of the cell capacitor voltages.

An executable of this program is included on the CD-ROM accompanying this dissertation.

A screenshot of the “Designtool” interface is shown in Figure D-1.

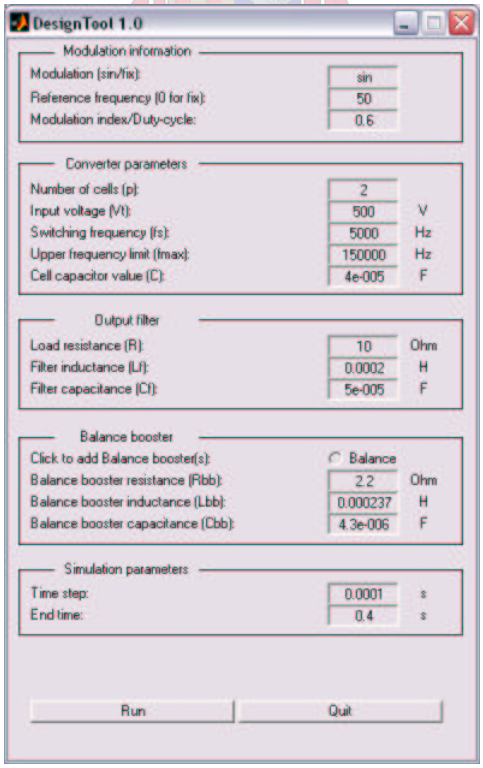

Figure D-1. *Screenshot of the “Designtool” interface.*

The “Designtool” program is in fact a graphic user interface which calls Matlab® procedures which are used in the calculation process of the results.

The main procedures are included on the CD-ROM accompanying this dissertation. These procedures are as follows:

- spectra.m
- loadimp.m
- timeconst.m

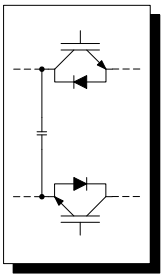

Appendix E

Meynard et al's multicell model

This Appendix is a brief summary of Meynard et al's multicell model published in [26]. The original notation as used in [26] was adapted to conform to the notation used in this dissertation.

A diagram of a p-cell multicell converter is shown in Figure E-1.

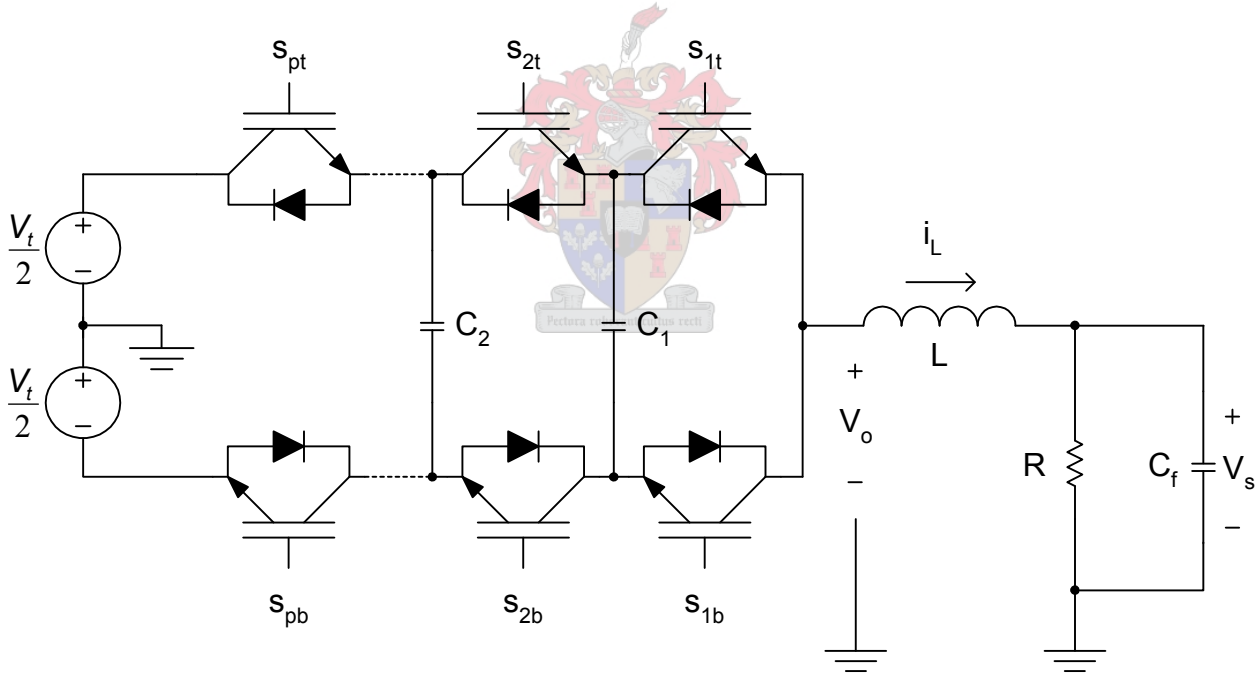

Figure E-1. *A p-cell multicell converter.*

The exponential Fourier series is given by the following equation:

$$f(t) = \sum_{-\infty}^{\infty} C_m e^{jm\theta} \tag{E.1}$$

Its coefficient, C_m is given by the following equation:

$$C_m = \frac{1}{2\pi}\int_0^{2\pi} f(t)e^{-jm\theta}d\theta \tag{E.2}$$

The exponential Fourier coefficients C_m of the waveform shown in Figure E-2 can be calculated as shown in the following calculation:

$$\begin{aligned}
C_m &= \frac{1}{2\pi}\int_0^{2\pi} 1\cdot e^{-jm\theta}d\theta \\
&= \frac{1}{2\pi}\int_{-\phi-D\pi}^{-\phi+D\pi} e^{-jm\theta}d\theta \\
&= \frac{1}{2\pi}\left(\frac{e^{-jm\theta}}{-jm}\right)\Big|_{-\phi-D\pi}^{-\phi+D\pi} \\
&= \frac{-1}{2jm\pi}\left(e^{-jm(-\phi+D\pi)} - e^{-jm(-\phi-D\pi)}\right) \\
&= \frac{j}{2m\pi}\left(e^{jm\phi-jmD\pi} - e^{jm\phi+jmD\pi}\right) \\
&= \frac{j}{2m\pi}\left(e^{jm\phi}e^{-jmD\pi} - e^{jm\phi}e^{jmD\pi}\right) \\
&= \frac{-j}{2m\pi}\left(e^{jm\phi}e^{jmD\pi} - e^{jm\phi}e^{-jmD\pi}\right) \\
&= \frac{-j}{2m\pi}\left(e^{jmD\pi} - e^{-jmD\pi}\right)e^{jm\phi} \\
&= \frac{(-j)(j)}{m\pi}\sin(mD\pi)e^{jm\phi} \\
&= \frac{1}{m\pi}\sin(mD\pi)e^{jm\phi}
\end{aligned} \tag{E.3}$$

The harmonic generated by a single cell with a supply voltage of $1\ V$ is represented by the following:

$$H_m = \frac{2}{m\pi}\sin(mD\pi)e^{jm\phi} \tag{E.4}$$

In a p-cell converter, the voltage across a conducting switch is zero and across a blocking switch is $V_{C_i} - V_{C_{i-1}}$. Consequently, V_s^m, the m^{th} harmonic of the chopped voltage is then as follows:

$$\begin{aligned}
V_s^m &= \sum_{i=1}^{p} H_m\left(V_{C_i} - V_{C_{i-1}}\right) \\
&= \sum_{i=1}^{p} \frac{2}{m\pi}\sin(mD\pi)\left(V_{C_i} - V_{C_{i-1}}\right)e^{jm\phi_i}
\end{aligned} \tag{E.5}$$

If a quantity, G_i^m (not to be confused with conductance) is defined as follows:

$$G_i^m = \frac{1}{m\pi}\sin(mD_i\pi)e^{jm\phi_i} \tag{E.6}$$

then equation (E.5) can be rewritten as follows:

$$\begin{aligned}
V_s^m &= 2\sum_{i=1}^{p} G_i^m \left(V_{C_i} - V_{C_{i-1}}\right) \\
&= 2\left[G_1^m \left(V_{C_1} - V_{C_0}\right) + G_2^m \left(V_{C_2} - V_{C_1}\right) + G_3^m \left(V_{C_3} - V_{C_2}\right) + \ldots\right. \\
&\quad \left. + G_{p-1}^m \left(V_{C_{p-1}} - V_{C_{p-2}}\right) + G_p^m \left(V_{C_p} - V_{C_{p-1}}\right)\right] \\
&= 2\left[G_1^m \left(V_{C_1}\right) + G_2^m \left(V_{C_2} - V_{C_1}\right) + G_3^m \left(V_{C_3} - V_{C_2}\right) + G_1^m \left(V_{C_1} - V_{C_0}\right) + \ldots\right. \\
&\quad \left. + G_{p-1}^m \left(V_{C_{p-1}} - V_{C_{p-2}}\right) + G_p^m \left(V_t - V_{C_p}\right)\right] \\
&= 2\begin{bmatrix} G_1^m - G_2^m & G_2^m - G_3^m & \ldots & G_{p-2}^m - G_{p-1}^m & G_{p-1}^m - G_p^m \end{bmatrix} \begin{bmatrix} V_{C_1} \\ V_{C_2} \\ \vdots \\ V_{C_{p-1}} \\ V_{C_p} \end{bmatrix} + 2G_p^m V_t
\end{aligned} \tag{E.7}$$

Then the m^{th} harmonic of the load current can be written as a function of Z^m, the impedance of the load at m times the switching frequency as follows:

$$\begin{aligned}
I^m &= \frac{V_s^m}{Z^m} \\
&= |I^m| \, e^{j\psi^m}
\end{aligned} \tag{E.8}$$

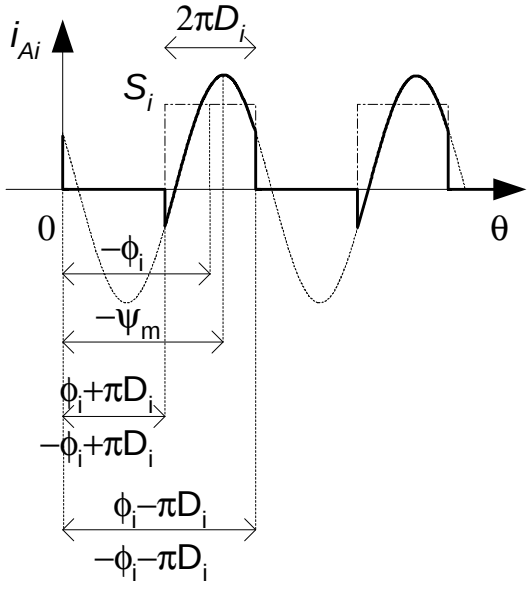

Figure E-2. *Waveform used in exponential Fourier series calculation.*

An example showing the first harmonic of the current associated with switch S_{it} is shown in Figure E-2.

The average current in switch S_{it} generated by the m^{th} harmonic of the load current can be calculated as follows:

$$\begin{aligned}
I^m_{S_{it}} &= \frac{1}{2\pi}\int_{-\phi_i-D_i\pi}^{-\phi_i+D_i\pi} |I^m|\cos(m\theta+\psi^m)d\theta \\
&= \frac{|I^m|}{2m\pi}\sin(m\theta+\psi^m)|_{-\phi_i-D_i\pi}^{-\phi_i+D_i\pi} \\
&= \frac{|I^m|}{2m\pi}\left[\sin(m(-\phi_i+D_i\pi)+\psi^m)-\sin(m(-\phi_i-D_i\pi)+\psi^m)\right] \\
&= \frac{|I^m|}{2m\pi}\left[\sin((-m)(-\phi_i)+mD_i\pi+\psi^m)-\sin(-m\phi_i-mD_i\pi+\psi^m)\right] \\
&= \frac{|I^m|}{2m\pi}2\cos\left(\frac{(-m)(-\phi_i)+mD_i\pi+\psi^m-m\phi_i-mD_i\pi+\psi^m}{2}\right) \\
&\quad \sin\left(\frac{(-m)(-\phi_i)+mD_i\pi+\psi^m+m\phi_i+mD_i\pi-\psi^m}{2}\right) \\
&= \frac{|I^m|}{m\pi}\cos(\psi^m-m\phi_i)\sin(mD_i\pi)
\end{aligned} \tag{E.9}$$

where ψ^m is phase of the m^{th} harmonic of the load current.

Starting with the following equation:

$$I^m_{S_{it}} = \frac{|I^m|}{m\pi}\sin(mD_i\pi)\cos(\psi^m-m\phi_i) \tag{E.10}$$

Equation (E.8) is repeated here for convenience as follows:

$$\begin{aligned}
I^m &= \frac{V^m_s}{Z^m} \\
&= |I^m|\,e^{j\psi^m}
\end{aligned} \tag{E.11}$$

Using Euler's relations, $e^{j\psi^m}$ and $e^{-jm\phi_i}$ can be written as follows:

$$e^{j\psi^m} = \cos\psi^m + j\sin\psi^m \tag{E.12}$$

and

$$e^{-jm\phi_i} = \cos(m\phi_i) + j\sin(m\phi_i) \tag{E.13}$$

then

$$\begin{aligned}
e^{j\psi^m}e^{-jm\phi_i} &= e^{j(\psi^m-m\phi_i)} \\
&= \cos(\psi^m-m\phi_i)+j\sin(\psi^m-m\phi_i)
\end{aligned} \tag{E.14}$$

It can now be seen that:

$$I_{S_{it}}^m = Re\left\{\frac{1}{m\pi}\sin(mD_i\pi)e^{-jm\phi_i}\left|I^m\right|e^{j\psi^m}\right\} \tag{E.15}$$

and

$$G_i^m = \frac{1}{m\pi}\sin(mD_i\pi)e^{jm\phi_i} \tag{E.16}$$

$$\overline{G_i^m} = \frac{1}{m\pi}\sin(mD_i\pi)e^{-jm\phi_i} \tag{E.17}$$

Thus:

$$I_{S_{it}}^m = Re\left\{\overline{G_i^m}I^m\right\} \tag{E.18}$$

and from the differential equation $i_C = C\frac{dv_C}{dt}$ it follows that:

$$\dot{V}_{C_i}^m = \frac{1}{C_i}I_{C_i}^m \tag{E.19}$$

where $\dot{V}_{C_i}^m$ is the variation of the cell capacitor voltage over one switching period and $I_{C_i}^m$ is the average cell capacitor current over one switching period.

Rewriting $I_{C_i}^m = I_{S_{(i+1)t}}^m - I_{S_{it}}^m$ the previous equation can be rewritten as the following:

$$\begin{aligned}\dot{V}_{C_i}^m &= \frac{1}{C_i}\left(I_{S_{(i+1)t}}^m - I_{S_{it}}^m\right)\\ &= \frac{1}{C_i}\left(Re\left\{\overline{G_{i+1}^m}I^m - \overline{G_i^m}I^m\right\}\right)\\ &= \frac{1}{C_i}Re\left\{\left(\overline{G_{i+1}^m} - \overline{G_i^m}\right)I^m\right\}\\ &= \frac{1}{C_i}Re\left\{\overline{G_{i+1}^m - G_i^m}I^m\right\}\end{aligned} \tag{E.20}$$

Expanding equation (E.20) the following is obtained:

$$\begin{bmatrix}\dot{V}_{C_1}^m\\ \vdots\\ \dot{V}_{C_{p-1}}^m\end{bmatrix} = Re\left\{\begin{bmatrix}\frac{1}{C_1}\overline{G_2^m - G_1^m}\\ \vdots\\ \frac{1}{C_{p-1}}\overline{G_p^m - G_{p-1}^m}\end{bmatrix}I^m\right\} \tag{E.21}$$

From $I^m = \frac{V_s^m}{Z^m}$ equation (E.21) can be rewritten as follows:

$$V_s^m = 2 \begin{bmatrix} G_1^m & \dots & G_p^m \end{bmatrix} \cdot \begin{bmatrix} V_{C_1} \\ \vdots \\ V_{C_{p-1}} \end{bmatrix} + 2G_p^m V_t \tag{E.22}$$

$$\begin{aligned} I^m &= \frac{V_s^m}{Z^m} \\ &= 2\left[G_i^m\right]\left[V_{C_i}^m\right]\frac{1}{Z^m} + 2G_p^m V_t \frac{1}{Z^m} \end{aligned} \tag{E.23}$$

$$\left[\dot{V}_{C_i}^m\right] = 2Re\left\{\left[\frac{1}{C_i}\overline{G_{i+1}^m - G_i^m}\right]\frac{1}{Z^m}\left(\left[\dots G_i^m - G_{i+1}^m \dots\right]\left[V_{C_i}^m\right] + G_p^m V_t\right)\right\} \tag{E.24}$$

Equation (E.24) can be rewritten in the general state-space form, e.g. $\dot{X} = AX + BU$ with the following:

$$X = V_{C_i}^m \tag{E.25}$$

$$U = V_t \tag{E.26}$$

$$A = Re\left\{\left[\frac{1}{C_i}\overline{G_{i+1}^m - G_i^m}\right]\frac{1}{Z^m}\left[\dots G_i^m - G_{i+1}^m \dots\right]\right\} \tag{E.27}$$

$$B = Re\left\{\left[\frac{1}{C_i}\overline{G_{i+1}^m - G_i^m}\right]\frac{1}{Z^m}G_p^m\right\} \tag{E.28}$$

Taking r harmonics into account:

$$\left[\dot{V}_{C_i}^m\right] = \sum_{m=1}^{r} 2Re\left\{\begin{bmatrix} \vdots \\ \frac{1}{C_i}\overline{G_{i+1}^m - G_i^m} \\ \vdots \end{bmatrix}\frac{1}{Z^m}\left(\left[\dots G_i^m - G_{i+1}^m \dots\right]\left[V_{C_i}^m\right] + G_p^m V_t\right)\right\} \tag{E.29}$$

Expanding equation (E.29) into the form $\dot{V}_{C_i} = A(D_i)V_{C_i} + B(D_i)V_t, \;\; i = 1, \dots, p-1$:

$$A = -2Re\left\{\begin{bmatrix} \frac{\overline{G_1^1 - G_2^1}}{C_1} & \dots & \frac{\overline{G_1^r - G_2^r}}{C_1} \\ \vdots & \ddots & \vdots \\ \frac{\overline{G_{p-1}^1 - G_p^1}}{C_{p-1}} & \dots & \frac{\overline{G_{p-1}^r - G_p^r}}{C_{p-1}} \end{bmatrix} \cdot \begin{bmatrix} \frac{G_1^1 - G_2^1}{Z^1} & \dots & \frac{G_{p-1}^1 - G_p^1}{Z^1} \\ \vdots & \ddots & \vdots \\ \frac{G_1^r - G_2^r}{Z^r} & \dots & \frac{G_{p-1}^r - G_p^r}{Z^r} \end{bmatrix}\right\} \tag{E.30}$$

$$B = 2Re\left\{\begin{bmatrix} \frac{\overline{G_1^1 - G_2^1}}{C_1} & \cdots & \frac{\overline{G_1^r - G_2^r}}{C_1} \\ \vdots & \ddots & \vdots \\ \frac{\overline{G_{p-1}^1 - G_p^1}}{C_{p-1}} & \cdots & \frac{\overline{G_{p-1}^r - G_p^r}}{C_{p-1}} \end{bmatrix} \cdot \begin{bmatrix} \frac{G_p^1}{Z^1} \\ \vdots \\ \frac{G_p^r}{Z^r} \end{bmatrix}\right\} \tag{E.31}$$

Index